Metal-Catalyzed Stereoselective C–H Functionalization Mediated Kinetic Resolution of Sulfoximines and Unsymmetrical Multiple C–H Annulations

A Thesis
Submitted for the Degree of
DOCTOR OF PHILOSOPHY
in
CHEMISTRY

By

Kallol Mukherjee

School of Chemistry
University of Hyderabad
Hyderabad 500 046
Telangana
India

June, 2021

To

My Family

&

Well-wishers

TABLE OF CONTENTS

DECLARATION

I hereby declare that the matter embodied in the thesis entitled **"Metal-Catalyzed Stereoselective C–H Functionalization Mediated Kinetic Resolution of Sulfoximines and Unsymmetrical Multiple C–H Annulations"** is the result of investigation carried out by me in the School of Chemistry, University of Hyderabad, Hyderabad, India, under the supervision of **Prof. Akhila Kumar Sahoo**.

In keeping with the general practice of reporting scientific observations, due acknowledgements have been made on the basis of the findings of other investigators. Any omission, which might have occurred by oversight or error, is regretted. This research work is free from Plagiarism. I hereby agree that my thesis can be deposited in Shodhganga/INFLIBNET. A report on plagiarism statistics from the University Librarian is enclosed.

Kallol Mukherjee

Kallol Mukherjee
(14CHPH23)

Akhila Ky. Sahoo 28/6/2021

Prof. Akhila Kumar Sahoo
(Supervisor)

Prof. AKHILA K. SAHOO
School of Chemistry
University of Hyderabad
Central University P.O.
Hyderabad, INDIA.

University of Hyderabad

June, 2021

CERTIFICATE

This is to certify that the thesis entitled **"Metal-Catalyzed Stereoselective C–H Functionalization Mediated Kinetic Resolution of Sulfoximines and Unsymmetrical Multiple C–H Annulations"** submitted by **Kallol Mukherjee** holding registration number **14CHPH23** in partial fulfilment of the requirements for award of Doctor of Philosophy in the School of Chemistry is a bonafide work carried out by him under my supervision and guidance.

This thesis is free from plagiarism and has not been submitted previously in part or in full to this or any other University or Institution for award of any degree or diploma.

Parts of the thesis have been:

A. Published in following publication

K. Mukherjee, M. Shankar, K. Ghosh and A. K. Sahoo* *Org. Lett.* **2018, *20,*** 1914.

K. Mukherjee, E Ramesh, K. Ghosh and A. K. Sahoo. *Asian J. Org. Chem.* **2018, 7,** 1380.

B. Presented in the following conferences

1. ChemFest-2017; **2.** ICCHD-2018; **3.** J-NOST Conference-2019; **4.** ChemFest-2020.

Further the student has passed the following courses towards fulfilment of course work requirement for Ph.D.

Course code	Name	Credits	Pass/Fail
CY-401	Basic Concepts and Coordination Chemistry	3	**Pass**
CY-452	Organic Reactions and Mechanisms	3	**Pass**
CY-801	Research Proposal	3	**Pass**
CY-805	Instrumental Methods A	3	**Pass**

Kumara Swamy 28/6/2021

Dean
School of Chemistry

Dean
School of Chemistry
University of Hyderabad
P.O. Central University
Gachibowli, Hyderabad-500 046.

Akhila K. Sahoo 28/6/2021

Prof. Akhila K. Sahoo
(Thesis Supervisor)

Prof. AKHILA K. SAHOO
School of Chemistry
University of Hyderabad
Central University P.O.
Hyderabad, INDIA.

Acknowledgements

I express my hearty gratitude and profound thanks to my supervisor **Prof. Akhila Kumar Sahoo** for his excellent guidance, encouragement, and the freedom that he gave to me in carrying out various research projects. His optimistic approach and patience towards every aspect was admirable and inspiring. Throughout my Ph.D tenure, he was always been approachable, helpful, and friendly. I am fortunate to be a part of his research group. He considered me as one of his family members.

I take this opportunity to thank Prof. K. C. Kumara Swamy, Dean, School of Chemistry for providing the facilities needed for our research. I sincerely thank my doctoral committee members Prof. R. Balamurugan and Prof. S. Pal for their guidance and encouragement. I extend my sincere thanks to the former Deans and all the faculty members of School of Chemistry for their cooperation and encouragement on various aspects.

I sincerely thank all the non-teaching staffs in School of Chemistry for their assistance on various occasions. I am thankful to all my colleagues in School of Chemistry for helping me in various aspects. I thank ACRHEM, DST and UGC for providing required instruments, chemicals and CSIR for followship.

From the bottom of my heart, I thank Dr. Koushik Ghosh, Dr. M. Ramu Yadav Dr. Raja. K. Rit, and Dr. Majji Shankar for being such generous co-worker, guide, and friend. A special thanks to Dr. Mallesh, Dr. Bhanu, Dr. Nayan, Dr. Sanatan, Dr. Sudheer, Dr. Nagarjuna, Dr. Tirumaleswararao and Dr. Arjit for their help & support. I value my association with my friends and labmates Dr. Ajijit, Dr. Prabagar, Dr. Suresh, Rajendra, Prasad, Balaraju, Srinivas, Shubham, Manash, Arghadip, Somratan, Koneti, Manoj, Aradhana and Avijit for their encouragement, helpful discussion, pleasant company, and cooperation during my Ph.D. tenure. I thank to all M.Sc and UGC networking project students for their help during my thesis work.

My hearty thanks to Prof. A. K. Sahoo's family, Madam (Rashmita Sahoo) and Sonu (Amlesh) for the support and hosting group dinner at their home.

I record my special thanks to my juniors Somratan, Debu and my political debate partner Arijit da for their time to time discussion and making my life enjoyable and memorable in the University of Hyderabad.

Without my parents (Bijoy and Jayashree) and brother (Kuntal Mukherjee) relentless support and love, I would have not reached at this position. I owe everything to them. I would like to express my sincere thanks to all my family members; Suprava (putu), Ami (masi), Tamal and Rinku for their close association with me.

It's my pleasure to thank my teachers (Prof. Pranab Sarkar, Prof. Adinath Majji, Dr. Alakananda Hazra and Subir), where I learned the importance of my life.

I am lucky to have friends like Prabakar, Suman, Sandip, Mou, Anif, Umamaheswara, Samitha, Shipra in HCU.

I express my gratitude and profound thanks to my best friends Saswata Dasgupta, Asif and Suman for their encouragement and support.

Lastly this acknowledgement would be incomplete without express my gratitude to my family members, lab mates, friends and teachers who have been a constant source of inspiration and support throughout my Ph.D tenure.

Kallol Mukherjee

University of Hyderabad

June, 2021

List of Abbreviations

AcOH	acetic acid
Ac	acetyl
Ar	aryl
	alpha
aq	aqueous
	beta
	butylated hydroxytoluene
BIPHEP	2,2'-bis(diphenylphosphino)-1,1'-biphenyl
Bn	benzyl
Boc	Tert-butyloxycarbonyl
BQ	1,4-benzoquinone
br	broad
^{n}Bu	n-butyl
^{t}Bu	*tert*-butyl
Bz	benzoyl
C	degree celsius
cat.	catalyst
calcd	calculated
^{13}C NMR	carbon-13 nuclear magnetic resonance spectroscopy
CH_3CN	acetonitrile
$CHCl_3$	chloroform
CMD	concerted metalation−deprotonation
m-CPBA	*m*-chloroperbenzoic acid
Cp	cyclopentadienyl
Co	cobalt
CCA	chiral carboxylic acid

d	doublet
DBU	1,8-diazabicyclo[5.4.0]undec-7-ene
1,2-DCE	1,2-dichloroethane
DCM	dichloromethane
DMAP	4-dimethylaminopyridine
dd	doublet of doublet
DG	directing group
DMF	*N*,*N*-dimethylformamide
DMSO	dimethyl sulfoxide
dt	doublet of triplet
δ	delta
ee	enantiomeric excess
EDC.HCl	1-ethyl-3-(3-dimethylaminopropyl)carbodiimide
equiv	equivalent
Et	ethyl
e.g.	exempli gratia
ESI	electron spray ionization
EWG	electron-withdrawing group
FT-IR	fourier transform infrared spectroscopy
E+	electrophile
g	gram
	gamma
h	hour
^{1}H NMR	proton nuclear magnetic resonance spectroscopy
HRMS	high-resolution mass spectroscopy
Hz	hertz
IPA	isopropyl alcohol
J	coupling constant in hertz
$K_2S_2O_8$	potassium persulfate

MeOH	methanol
MPAA	Mono protected amino acid
MPS	methyl phenyl sulfoximine
MPyS	methyl-2-pyridyl sulfoximine
mg	milligram
m.p.	melting point
mmol	millimole
mL	milliliter
NHC	N-heterocyclic carbene
N_2	nitrogen
Nu	nucleophile
Ns	o-Nitrobenzensulfonyl
Pd	palladium
$PhI(OAc)_2$	phenyl iodo diacetate
Piv	pivaloyl
^{n}Pr	n-propyl
rt	room temperature
Ru	ruthenium
Rh	rhodium
R_f	retention factor
TBHP	*tert*-butyl hydroperoxide
td	triplet of doublets
TEMPO	(2,2,6,6-tetramethylpiperidin-1-yl)oxy
THF	tetrahydrofuran
TLC	thin-layer Chromatography
TM	transition metals
TMS	trimethylsilyl
Ts	tosyl
m	micromolar

Chapter 1

Stereoselective C–H Bond Activation and Annulation: An Introduction

Abstract

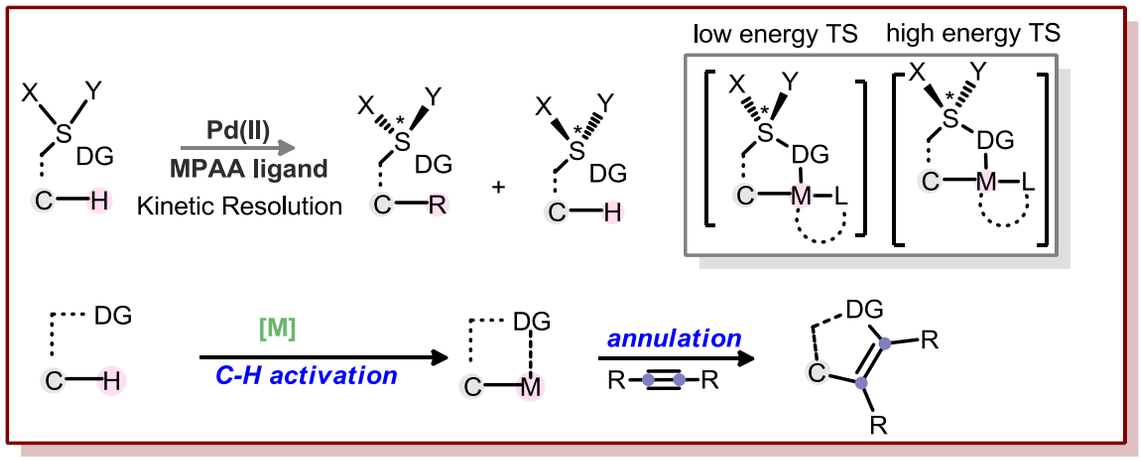

C–H activation strategy has been employed for the introduction of chirality in molecules as well as the construction of complex molecular scaffolds through unsymmetrical multiple C–H annulations. In the first part of this chapter, a brief introduction of C–H activation along with various mechanisms of C–H activation are discussed. The second part enumerates the concept of kinetic resolution of substrates through C–H functionalization. The origin of stereoselectivity and the use of chiral amino acid ligand in combination with transition metal catalyst is briefed. The coordination of sulfoximine pyridyl-motif with Pd(II)-catalyst and mono-protected chiral amino acid (MPAA) ligand for the enantio-determining C(aryl –H activation is narrated. The last part of this chapter covers unsymmetrical multiple annulations and hydroarylation 'in water' that involves C–H activation.

I.1. Introduction:

Inert C–H bonds are undoubtedly ubiquitous. Hence, direct conversion of C–H bonds to carbon-carbon (C–C), carbon-heteroatom (C–X) bonds has had a significant impact enriching the synthetic potential. Along this line, direct functionalization of C–H bond could reliably be used making complex molecular scaffolds with ease. Thus, the development of novel synthetic method linked to the functionalization of inert C–H bonds always appealing. The transition-metal (TM) catalyzed cross-coupling reactions offered a synthetically alternative plan for making diverse ranges of bond formations; however, these methods primarily require pre-functionalized precursors, which are prepared from readily available materials by multi-step synthesis, and generate a large amount of waste by-products during the reaction. In this connection, an unconventional TM-catalyzed activation and functionalization of inert C–H bond has provided a synthetically alternative greener pathway by not only discovering new reactions but also making novel chemical space with diversity. Despite the tremendous synthetic potential, selective activation of a particular C–H bond in organic molecules by combining the inherent stereo- and regio-selectivity issues is always challenging.

I.1.1. Transition metal-catalyzed cross-coupling reaction

Transition metal catalyzed cross-couplings are the trustworthy approaches for the introduction of complexity in the molecule.[1] In this case, an organometallic reagent (main group metal), in the presence of a group 8 or group 10 metal catalysts in combination with an organic electrophile allows making C–C and C–heteroatom bonds (**Scheme I.1**).[2] Since the early discoveries in this field by Kumada, Suzuki , Kochi, Corriu, and Murahashi; many organometallic reagents, such as organoboron, organosilicon, organotin, and organozinc have proved to be very useful coupling partner for cross-coupling reactions. Diversity of coupling partners and electrophiles made these process key tools for organic synthesis, resulting a plethora of synthetic methods towards pharmaceuticals and natural products.[3] The overall catalytic cycle of the cross-coupling reaction is depicted in **Scheme I.2**. In general, the cross-coupling

reaction mainly involves oxidative addition of electrophile to metal centre, followed by transmetalation, and finally, reductive elimination (**Scheme I.2**).

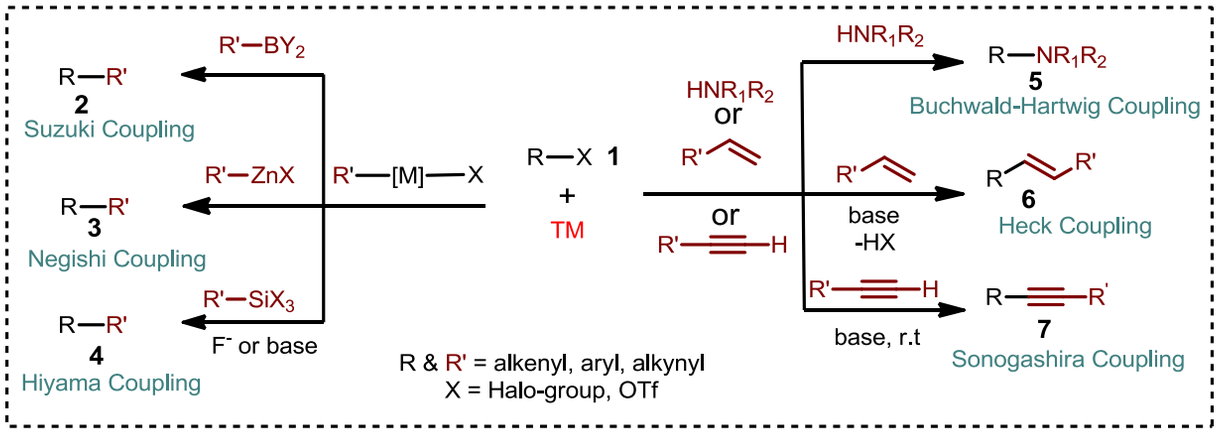

Scheme I.1: General overview of metal-catalyzed cross-coupling reaction

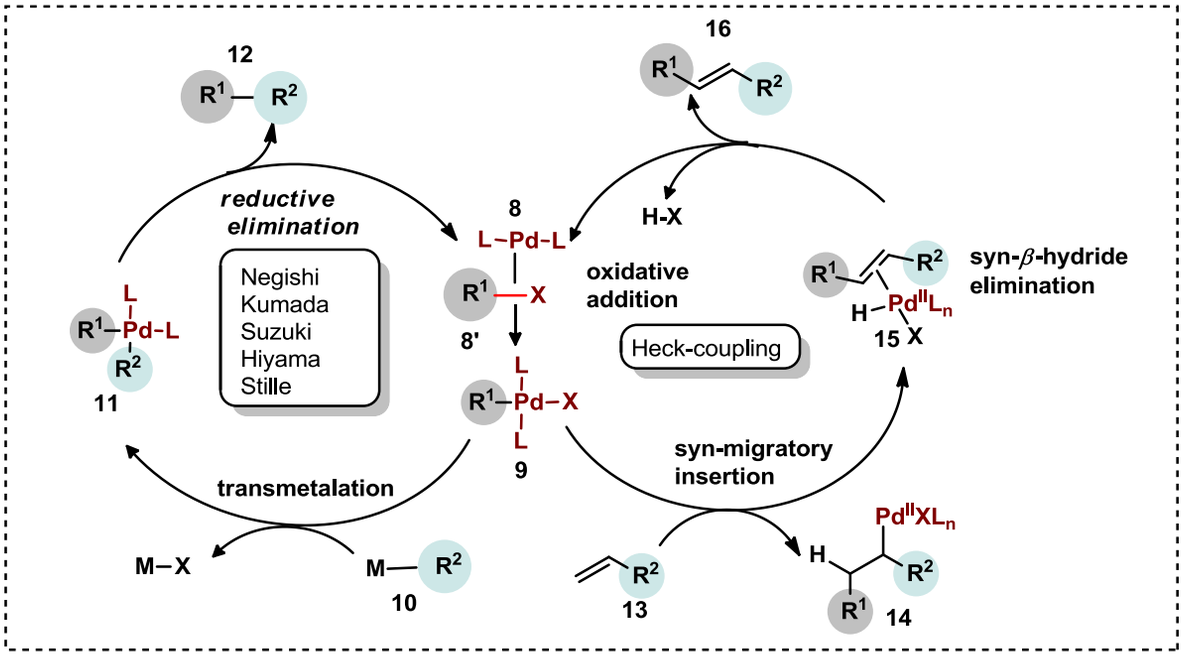

Scheme I.2: Pathways of various cross-coupling reactions

However, most of the cross-coupling reactions often associated with requirement of pre-functionalized starting materials (electrophiles, organometallic reagents, and nucleophiles), which make this process synthetically lengthy and cumbersome.[4]

Therefore, development of an alternate straightforward, atom-economical, and greener method for the synthesis of complex molecules from readily accessible precursors always draws significant attention to the synthetic community.

I.2. The C–H Bond Activation/ Functionalization

The C–H activation is a chemical process that functionalizes the inert C–H bond by increasing its reactivity. In organometallic point of view, C–H activation refers to a process where metal interacts with the inert C–H bond of **17** and directly forms a metal-carbon intermediate **18**. Next, interaction of an electrophile or nucleophile to **18** then makes C-C and C-heteroatom bonds in **19**.[5] The first step in generally a C–H activation and the second step is the functionalization. Thus, C–H activation can be termed as C-H functionalization, whereas C–H functionalization is not always considered as C–H activation. The formation of direct metal-carbon intermediate is the main feature of C–H activation (**Scheme I.3**).

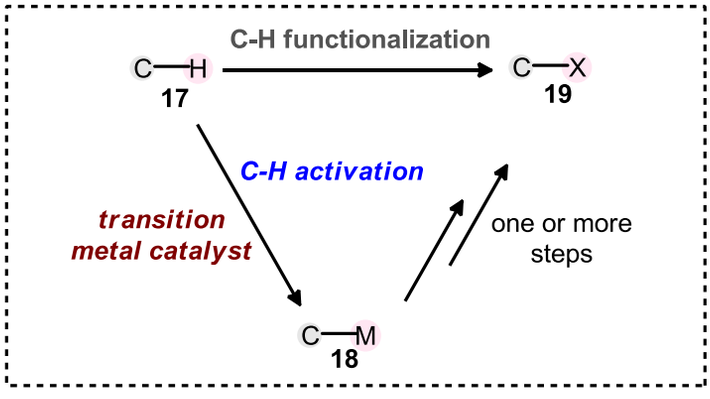

Scheme I.3: C–H bond activation/C–H functionalization

I.3. Mechanistic Pathway Overview of C–H Activation

The C–H activation or functionalization process occurs in two different ways. One involves outer-sphere mechanism, where C–H bond at first inserts into the ligated transition metal (TM) species (see **20**, **Scheme I.4**). While the other 'inner-sphere' mechanism encompasses a direct coordination of TM to the C–H bond that in-situ

forms a C–M or C–M–H intermediate (see **21**, **Scheme I.4**). Although "C-H functionalization" and "C-H activation" terminologies are often mixed up and created confusion in the chemical society, however, the term "C-H activation" is widely confined to inner-sphere mechanism.[6a]

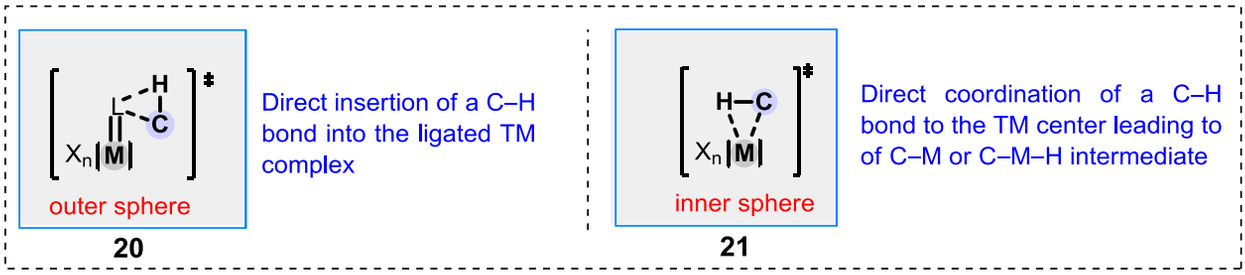

Scheme I.4: inner-sphere and outer-sphere mechanism

I.3.1. Insights of outer-sphere mechanism

In case of outer-sphere mechanism: no direct interaction of the C–H bond with the active metal catalyst occurs; instead, the ligand attached with the TM-species reacts with the C–H bond. The ligated-TM-species can either abstracts a hydrogen radical followed by recombination with organic radical or the ligand can directly insert into the inert C–H bond (**23** or **26**; **Scheme I.5**). Thus, the outer-sphere mechanism usually occurs with the insertion of high oxidation state metal containing reactive oxo, carbene, or nitrene species to the C–H bond.

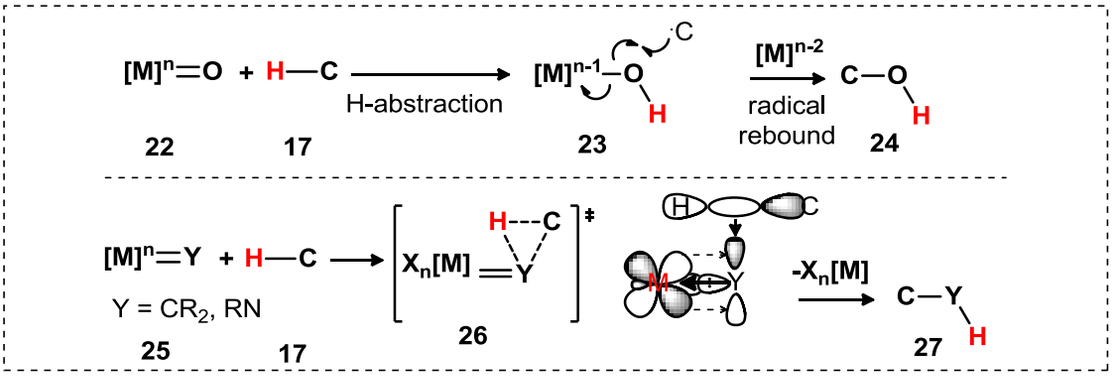

Scheme I.5: Outer-sphere mechanism

I.3.2. Insights of inner-sphere mechanism: nucleophilic vs electrophilic character [6]

Inner-sphere mechanism in C–H bond functionalization comprises with the coordination of C–H bond with the active metal complex to provide a metal-carbon intermediate. Thus, interaction of TM-coordinated aryl or alkyl species with the external electrophile/nucleophile or the ligand attached with the metal itself can trigger the functionalization. Based on the mechanistic insights, the inner-sphere mechanism occurs in three ways. They are typified as: (i) electrophilic activation, (ii) σ-bond metathesis, and (iii) oxidative addition. However, the exact pathways of inner sphere C–H activation has become so far unclear. With respect to the charge transfer direction, the inner-sphere C–H activation process is being simplified and broadly classified into two main categories: (i) reverse charge transfer from metal dπ orbital to the σ* orbital of the coordinated C–H bond and (ii) forward charge transfer (CT) from filled σ orbital of C–H bond to an empty dσ orbital of metal.[6b] The electron deficient metal complex as well as cationic late transition metal complex having low energy dπ and dσ orbitals participate in forward CT over reverse CT; the overall process is thus electrophilic (**Scheme I.6**, right). On the other hand, electron-rich transition metals having high energy dπ and dσ orbitals participate in reverse CT and therefore the pathway is nucleophilic (**Scheme I.6**, left).

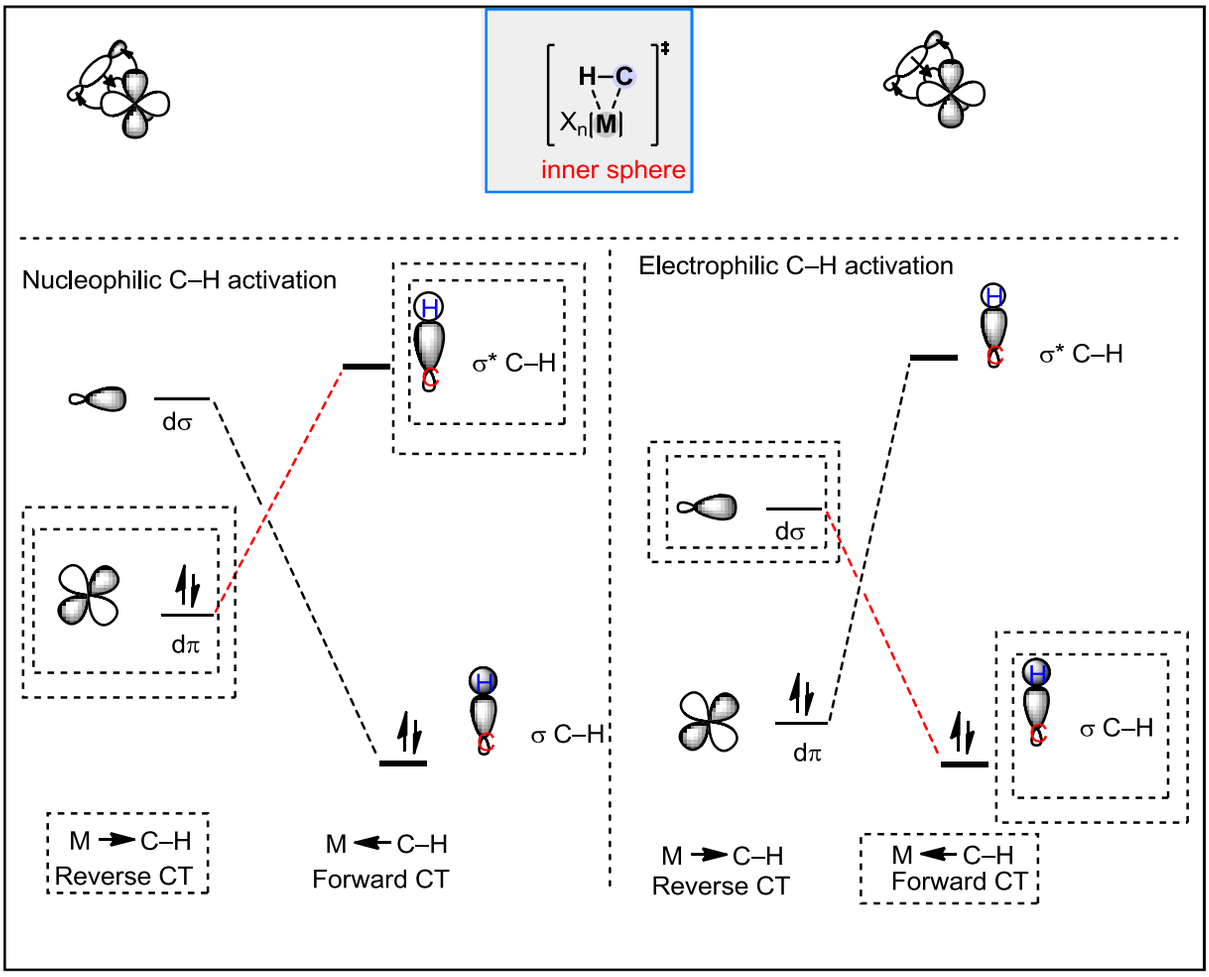

Scheme I.6: Nucleophilic vs electrophilic C–H activation

I.3.2.1. Oxidative addition

The electron-rich, nucleophilic, low-valent d^8 second- and third-row late transition metal complexes mostly involve oxidative addition pathways for the C–H activation. In this case, a balanced enthalpy change among C–H bond breakage and the M–C and M–H bonds formation is maintained. The transformation initiates with the metal coordination to C–H bond and then electron density transfer to the LUMO of C–H bond (

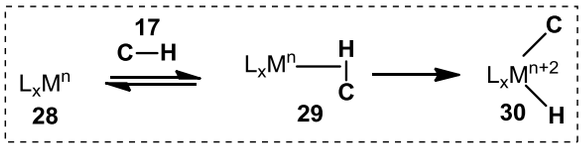

Scheme I.7: oxidative addition mechanism

The gradual accumulation of electron density in the LUMO could decrease the C–H bond order and therefore is ease to

cleave. Eventually oxidative addition of a nucleophilic moiety could increase the oxidation state of TM. To get a qualitative idea of oxidative addition, the respective molecular diagram is sketched in **Scheme 1.8**.

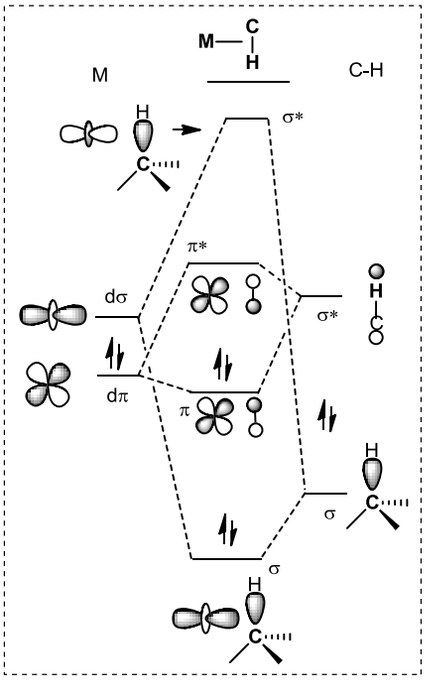

***Scheme I.8**: MO diagram of oxidative addition*

I.3.2.2. Sigma-bond metathesis

The early TM with d^0 electronic configuration and high oxidation state is not amenable to undergoing oxidative addition. Such species can react with a particular C–H bond via σ-bond metathesis (σ-BM). This mechanism involves four centered kite-like transition state **34** that takes place without changing oxidation state of the metal (**Scheme I.9**). Mainly, the group-III metals (scandium lanthanides and actinides) along with few group-IV and V TM are amenable to this mechanism.

A qualitative MO diagram for s-bond metathesis is shown in **Scheme I.10.** the absence of d-electrons thus precludes the -interaction.

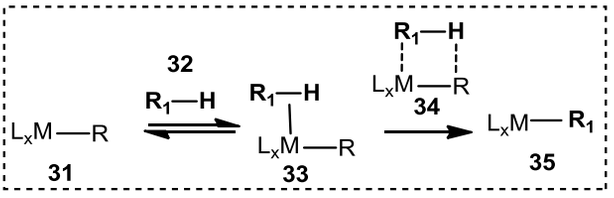

Scheme I.9: Sigma-bond metathesis mechanism

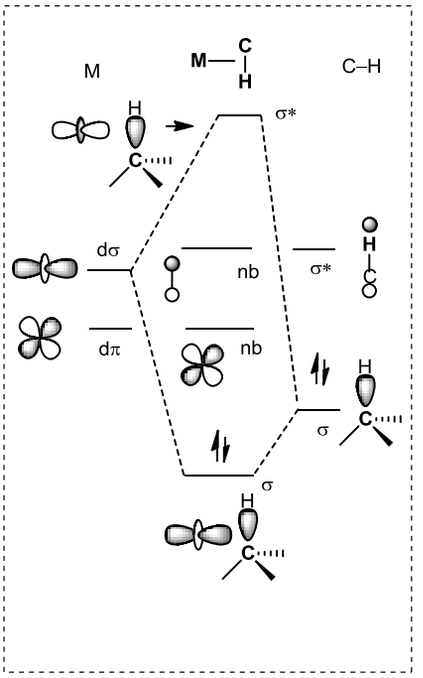

***Scheme I.10**: MO diagram of sigma-bond metathesis*

I.3.2.3. Electrophilic C–H activation:

The electron-deficient high oxidation state late transition metal complexes, such as Pd(II), Ru(II), Ir(III) and Pt(II) mostly participate in the electrophilic activation. In such cases, the coordination of C–H bond to metal complex starts with strong σ-donation and weak π-back-donation (**Scheme I.11 and Scheme I.12**). In case of aromatic system, electrophilic addition of TM species into the arene moiety at first forms a wheland type intermediate **36**. Next, the base mediated loss of proton forms a metal-carbon intermediate **37**.

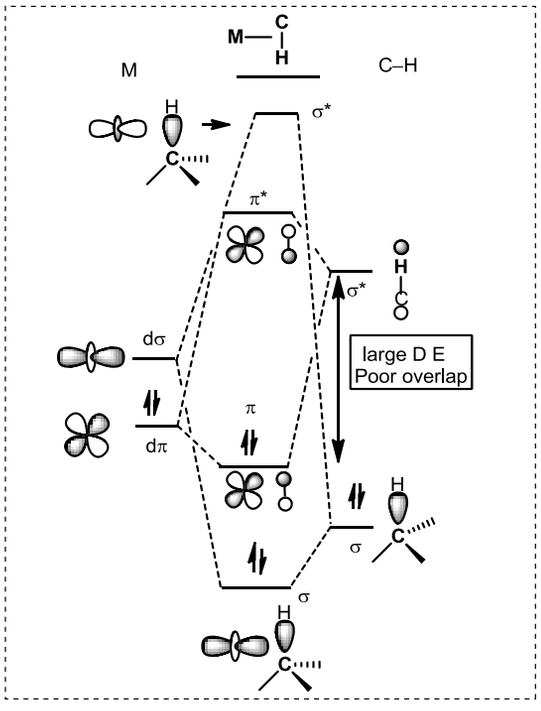

Scheme I.11 MO diagram of electrophilic C–H activation

A qualitative molecular orbital diagram is sketched in **Scheme I.11**. The mechanism involves an interaction of energetically viable TM d-orbital (d with the C–H bond ( ).

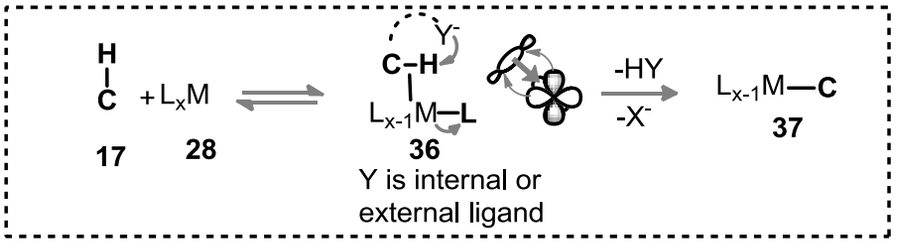

Scheme I.12 Electrophilic mechanism

I.3.2.4. Ambiphilic concerted mechanism: [7,8]

The inner-sphere mechanism that involves an intramolecular H–abstraction by an internal ligand, such as an alkoxy or an halide anion, or a bridging heteroatom based species (for example: carboxylate anion) via a concerted cyclic mechanism (**Scheme I.13)**. This mechanism can be classified as: internal electrophilic substitution (IES),

ambiphilic metal-ligand activation (AMLA), or concerted metalation deprotonation (CMD). In these cases, a significant H-bond between ligand lone pair with the corresponding C–H bond increases the electron density of C–H -bond, which eventually facilitates the agostic interaction(**38**→**40**→**37** or **39**→**41**→**37**) (**Scheme I.13**).

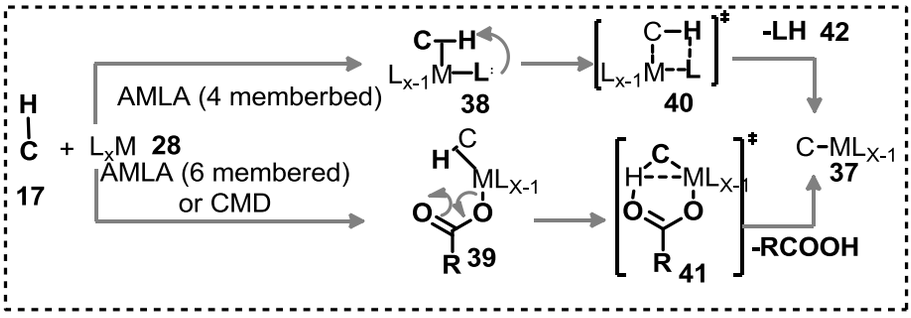

Scheme I.13 Ambiphilic concerted mechanism

I.3.2.5. 1,2-addition:

An alternate 1,2-addition involves a sigma bond metathesis of C–H bond **17** to the double bonded metal-nonmetal (M X) species **43** via a concerted four membered transition state **44**. The newly formed H–X species remain attached to the metal complex **45** (**Scheme I.14**).

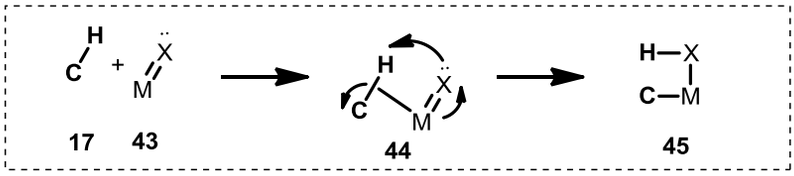

Scheme I.14 1,2-addition

I.4. Different Methods of C–H Functionalization

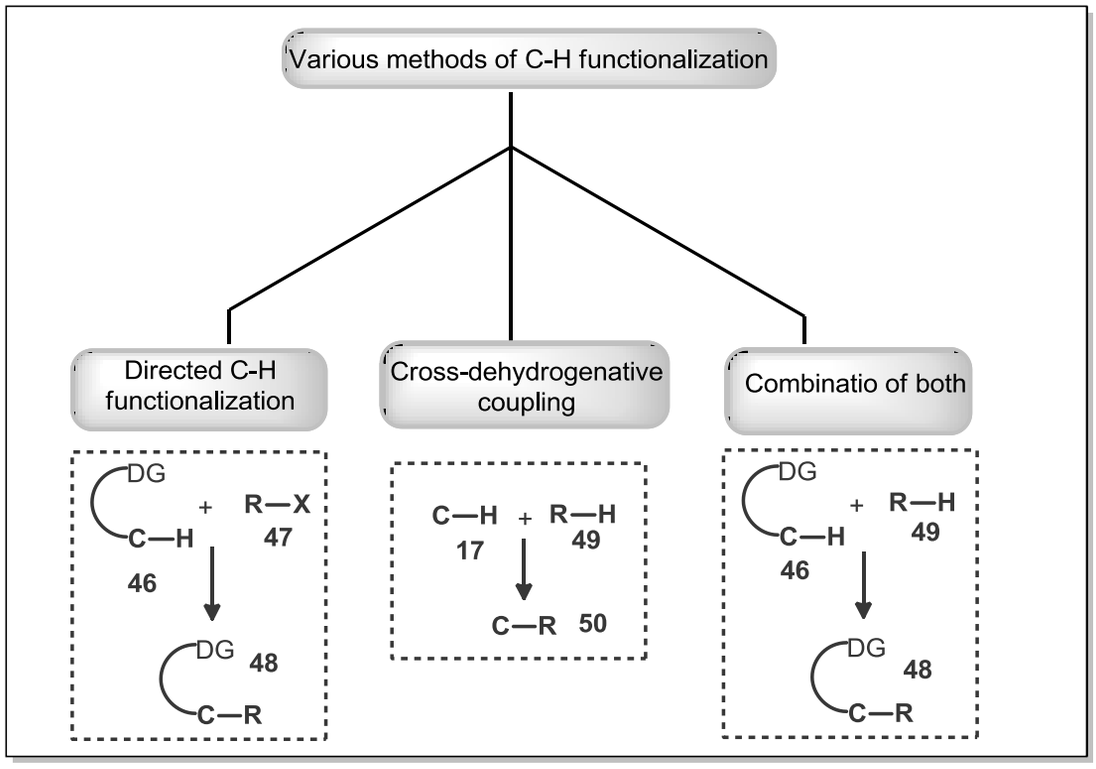

Scheme I.15 Different methods of C–H activation/functionalization

The transition-metal catalyzed C–H activation/functionalization can be categorised into three main classes (**Scheme I.15**):

1) **Directed activation**: The directing group (DG) assisted C–H activation initiates with the coordination of DG with the TM complex, which activates the C–H bond close proximity to the TM-species. The transformation is therefore highly regioselective. By tuning the DG, the C–H activation can be made –*ortho*, -*meta*, or –*para* selective.

2) **Cross-dehydrogenative or non-directed activation**: Cross-dehydrogenative C–H activation generally happens with the most acidic C–H bond. Thus, the process is non-regioselective.[13]

3) **DG assisted cross-dehydrogenative coupling**: This process involves the combination of the above two pathways.

This thesis primarily based on "Directing Group Assisted C-H Bond Activation" principle. The contents of this thesis aims in the development of TM catalyzed kinetic resolution of sulfoximine through C–H functionalization, synthesis of spiro-fused heterocycles through multiple C–H annulations, and hydroarylation 'in water'.

I.5. Transition Metal Catalyzed Stereoselective C–H Activation:

In the past few decade, the TM-catalyzed C−H bond functionalization has gained a great amount of attention for development of versatile synthetic methods that functionalizes inert C–H bonds to –OH, $–NH_2$, halide, and aryl or alkyl groups and the synthesis of complex molecules.[9] Among various TMs employed for the C–H activation domain, palladium (Pd) catalysts have been widely used as further functionalization of palladium−carbon intermediate is ease and well-studied.[10] Significant efforts on Pd-catalyzed C–H functionalization are mostly linked to racemic transformations. Moreover, ligands play significant in facilitating cleavage of C–H bond and enhancing the overall reactivity for the formation of C−C/C−X bonds.[3] The ligand coordination with Pd-species can lower energy barrier of elementary steps involved in C–H activation and also modulate facial selectivity (regio- as well stereoselectivity). [11]

In this section, a brief historical background in the development of bifunctional mono-N-protected amino acid (MPAA) ligands for discovering Pd-catalyzed stereoselective C–H functionalization is discussed. The conceptual imprints for the kinetic resolution of molecular scaffolds in presence of MPAA ligand and Pd-catalyst is also enumerated.

I.5.1 Historical background and discovery of MPAA ligand towards stereoselective C–H functionalization:

I.5.1.1 Background: In 1969 Werneke group has attempted performing cyclopalladation of (dimethylamino)methylferrocene **51** with K_2PdCl_4 but ended up with only amine ligation species **52** (**Scheme I.16)**.[12a]

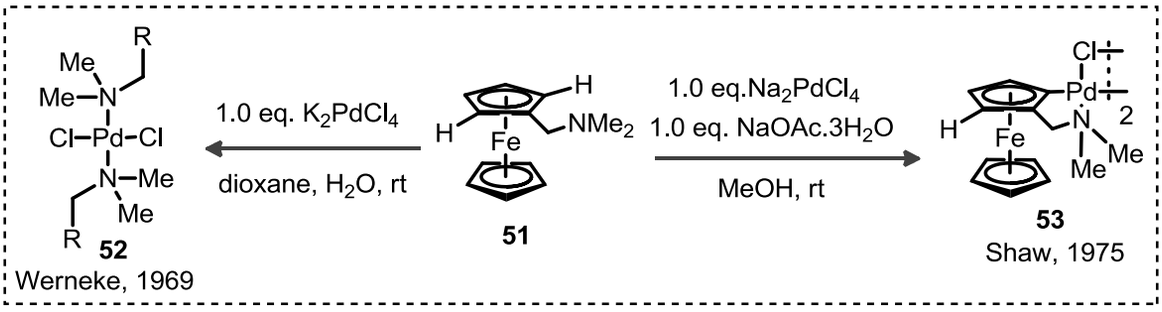

Scheme I.16: Acetate anion-mediated cyclopalladation

In 1975, the Shaw group successfully demonstrated the synthesis of desired cyclopalladation complex **53** from (dimethylamino)methylferrocene **51** when carried out in presence of stoichiometry amount sodium acetate (**Scheme I.16**).[12b] This is one of the earliest examples of acetate mediated cyclopalladation of C(sp^2)–H bond.[13]

In 1979, Sokolov proposed an alternate mechanism for the DG assisted acetate anion mediated C(aryl)−H deprotonation in combination with Pd(II) catalyst. The Pd–carbon bond formation occurs through a six-membered cyclic transition state **55** following concerted metalation deprotonation (CMD) pathway (**Scheme I.17**).[14]

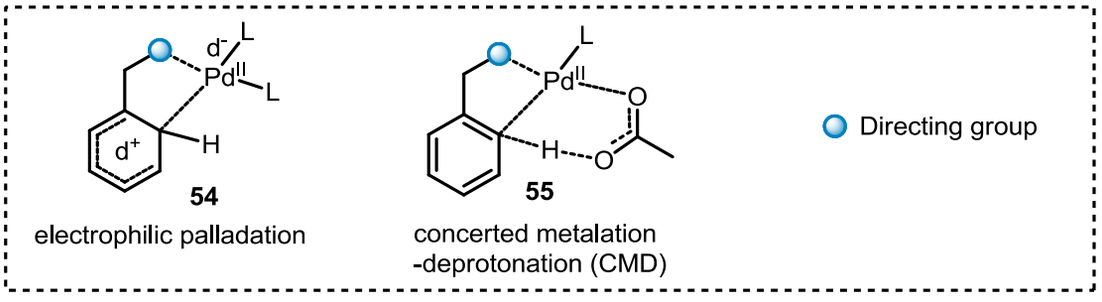

Scheme I.17: Topology of CMD process

One of the earliest reports on stereoselective cyclopalladation has been showcased by Sokolov in 1977. The reaction of a (dimethylamino)methylferrocene **56** containing α-amine chiral center with 1.0 equivalent of Na_2PdCl_4 and sodium acetate has led to a diastereoselective cyclopalladation (**57:58)** with d.r. 85:15 (**Scheme I.18**).[15]

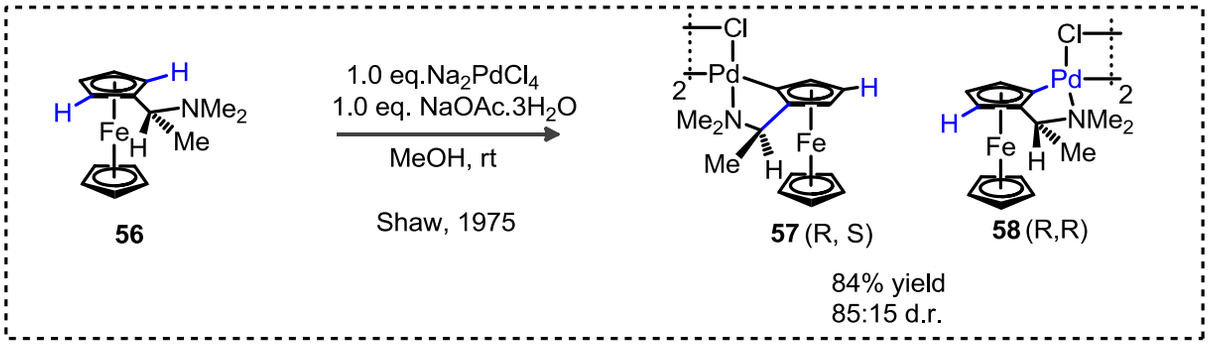

Scheme I.18: Substrate controlled diastereoselective cyclopalladation

I.5.1.2 Discovery of MPAA ligand:

In 1979, Sokolov hypothesized that instead achiral carboxylic acid in CMD mediated cyclopalladation, the use of chiral amino acid as carboxylate source **60** could bring chiral induction in cyclopalladation step from **59** to **61** (**Scheme I.19**).[14]

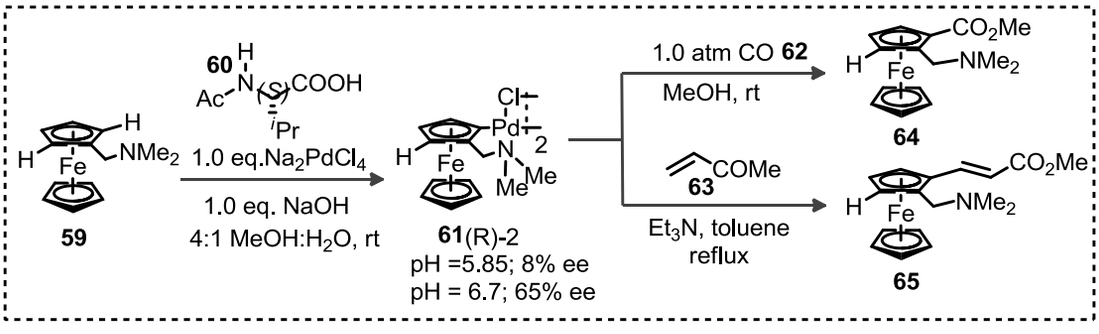

Scheme I.19: Ligand controlled diastereoselective cyclopalladation

I.5.2. Selective examples for the synthesis of C-stereogenic molecules via C(sp²)–H functionalization:

The Yu group developed Pd/MPAA catalyzed desymmetrization strategy for the construction of stereogenic C–C via C–alkylation/C–alkenylation and intramolecular C–O bond formation **66**–**68** (**Scheme I.20**). Identical strategy has been expanded further to the synthesis of various chiral amine derivatives **69**–**71** (**Scheme I.20**).[16,17]

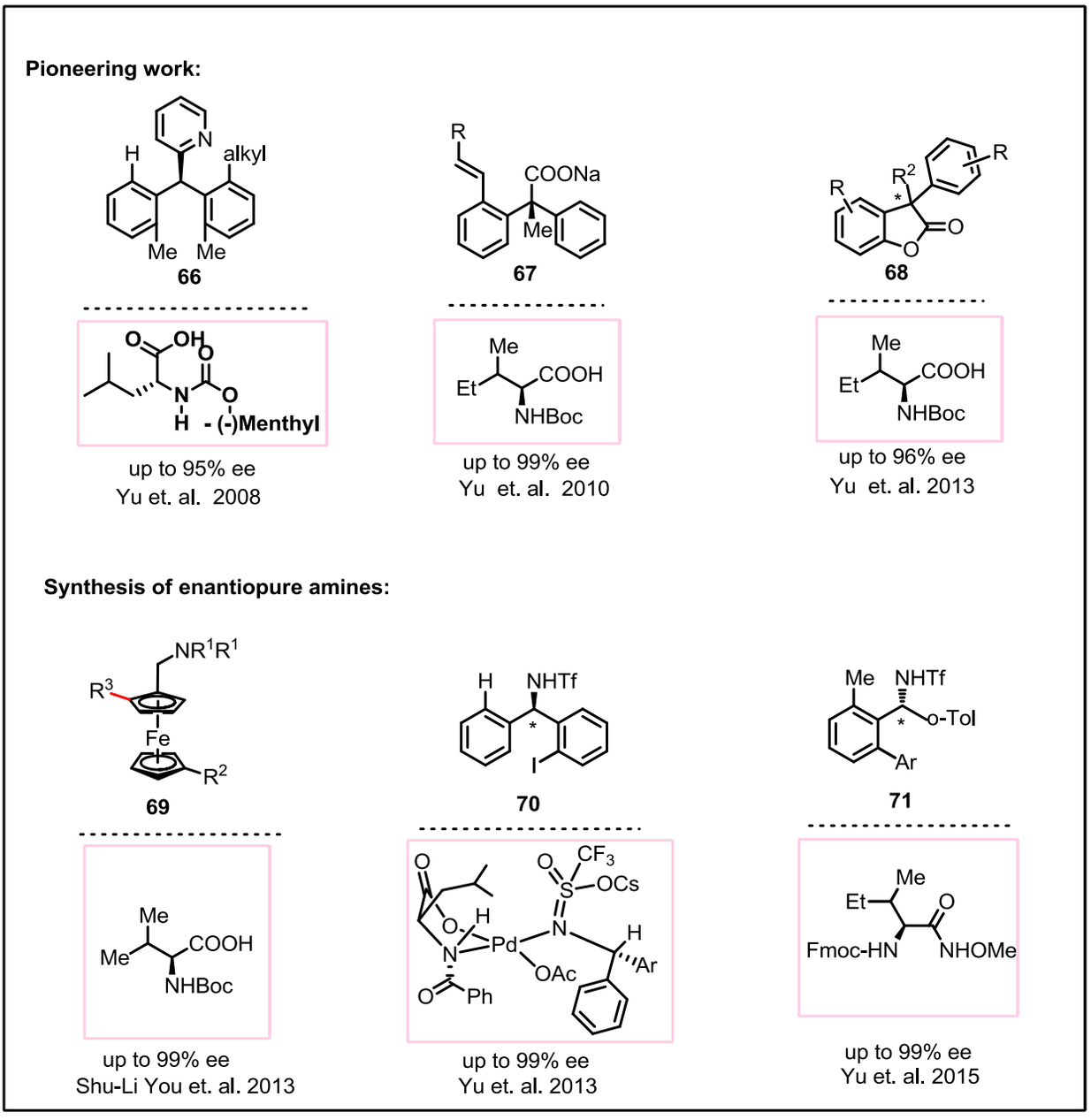

Scheme I.20: Synthesis of C-stereogenic molecules via C(sp^2 –H functionalization

I.5.3 Selective example of the synthesis of C-stereogenic molecules via C(sp^3)–H functionalization:

In **2014** and **2015**, Yu group revealed an early example of Pd/MPAA catalyzed enantioselective C(sp^3 –H arylation via desymmetrization of cyclobutyl (**72**), acyclic amide **73** and cyclopropyl **75** derivatives (**Scheme I.21**). [18a-b]

In **2016**, the same group reported the discovery of N-acetyl-protected chiral aminoethyl quinoline ligands enabled enantioselective functionalization of β-methylene C–H bonds for the generation of C-stereogenic aliphatic amides **74** with high enantioselectivity (**Scheme I.21**). [18c]

In continuation, the amino acid transient DG can facilitate enantioselective arylation of β-methylene C–H bonds of benzyl carbon of **76** (**Scheme I.21**).[18d]

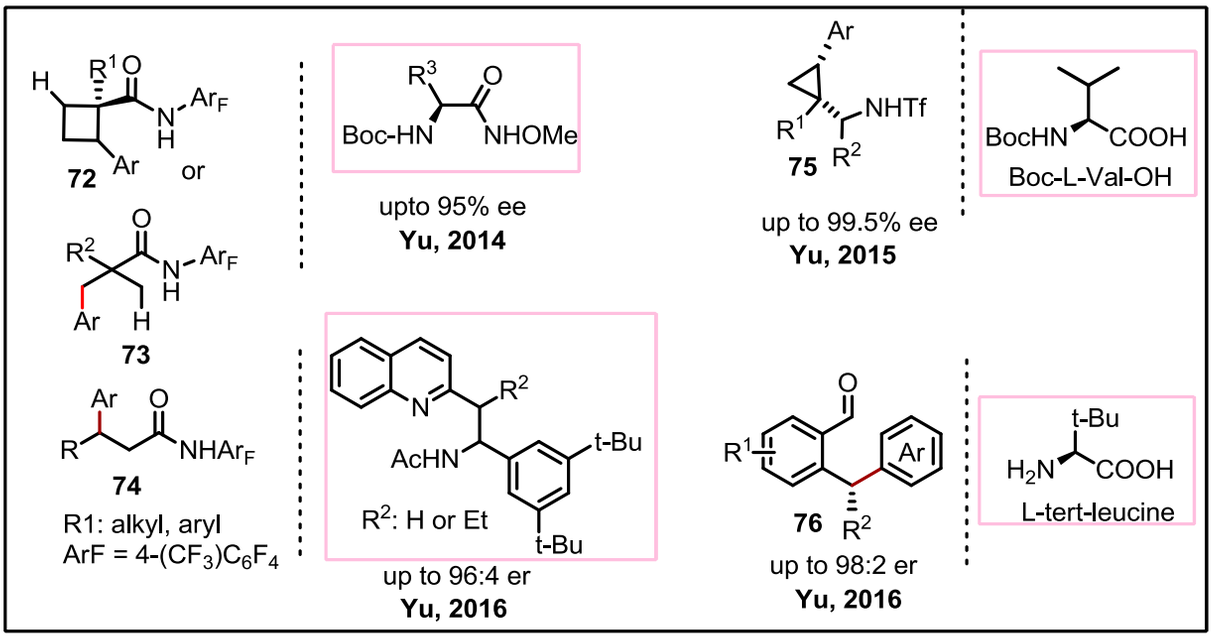

Scheme I.21: Selected example of C-stereogenic molecules via C(sp^3)–H functionalization

I.5.4 Synthesis of C-stereogenic molecules via *m*-selective C(sp^2)–H functionalization:

In **2018**, Yu group reported a challenging enantioselective *m*-C–H activation using a catalytic amount of chiral norbornene [(+)-NBE-CO2Me] transient mediator (**Scheme I.22**).[19] This method has been used for the enantioselective *meta*-C–H arylation of benzylamine derivatives **77**.

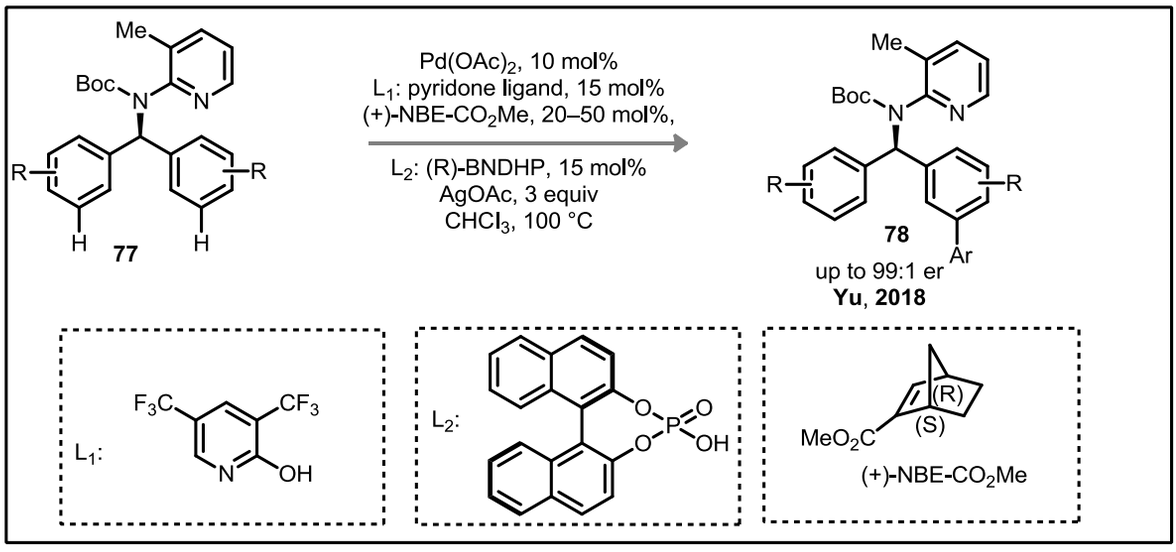

Scheme I.22: Desymmetrization via *meta*-selective functionalization

I.5.5 Synthesis of heteroatom centered stereogenic molecules via C(sp²)–H functionalization:

Related examples of Pd/Rh/Ir-catalyzed enantioselective C(sp² –H functionalization for the generation of stereogenic heteroatom center are listed in **Scheme I.23**.[20]

The Yu and Wang group independently reported Pd/MPAA catalyzed enantioselective C(sp²)–H functionalization for the construction of stereogenic P (**79**) and S-centered (**80**) molecules, respectively (**Scheme I.23**).

In **2017**, the Cramer group demonstrated chiral Rh/Ir catalyzed enantioselective C(sp² –H functionalization for the construction of stereogenic P-centered annulation product **81** and C–N bod forming compound **82**, respectively (**Scheme I.23**).[R]

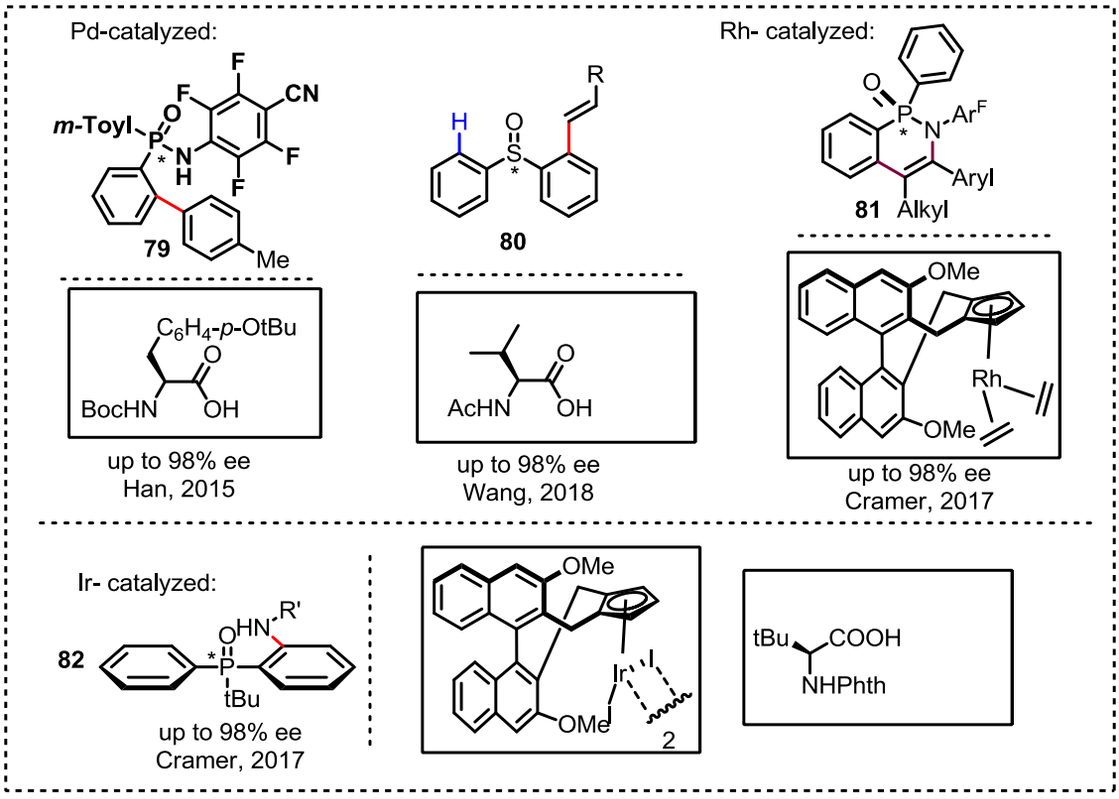

Scheme I.23: Selected example of metal catalyzed formation of stereo heteroatom center

I.5.6. Palladium Catalyzed Kinetic Resolution, Motivation, Hypothesis, and Planning

A notable effort has been made in the past decade in the enantioselective C–H functionalization by desymmetrization strategies and among these approaches, palladium catalyzed desymmetrization of prochiral C–H bond has been successfully implemented for the construction of stereogenic carbon, phosphorus and sulfur center. However, requirement of two enantiotropic group in the compound limits the desymmetrization method synthetically practical. At this point, the kinetic resolution (KR) method could easily address these inherent drawbacks. Thus, Yu's discovery on Pd-catalyzed KR of benzyl amine and aryl acetic acid via arylation and alkenylation is undoubtedly a breakthrough (**Scheme I.24A**). In spite of this success, the related strategy of Pd-catalyzed heteroatom centred KR of arenes remains unknown, although exceedingly appealing (**Scheme I.24B**).

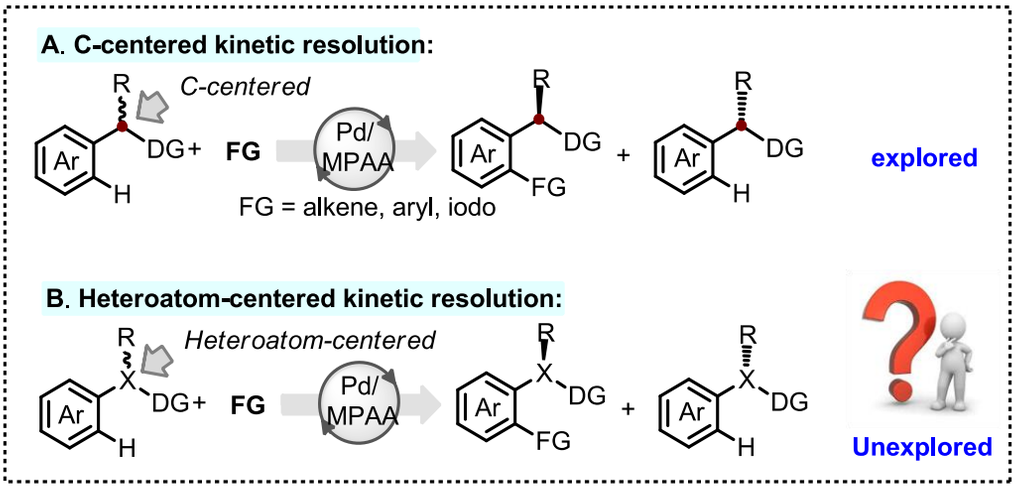

Scheme I.24: Palladium catalyzed kinetic resolution via C(sp² –H activation and motivation

With this intention, we devised a Pd-catalyzed KR of 2-pyridylaryl sulfoximines using a commercially available Pd(II) catalyst and a simple chiral amino acid (MPAA) ligand, via C(aryl)–H arylation and olefination (Fig 1B), which remains unexplored (**Scheme I.25**).[21] The concept relies on kinetically regulated CMD step of C(aryl)–H activation (k_1>>k_2, **Scheme I.25**) through preferred coordination of pyridine over imine to Pd-MPAA and ligand geometry **CMD$_{Pyr\text{-}DS}$** over **CMD$_{Pyr\text{-}DR}$** (**Scheme I.25**). *A transformation is therefore developed and discussed in Chapter II.*

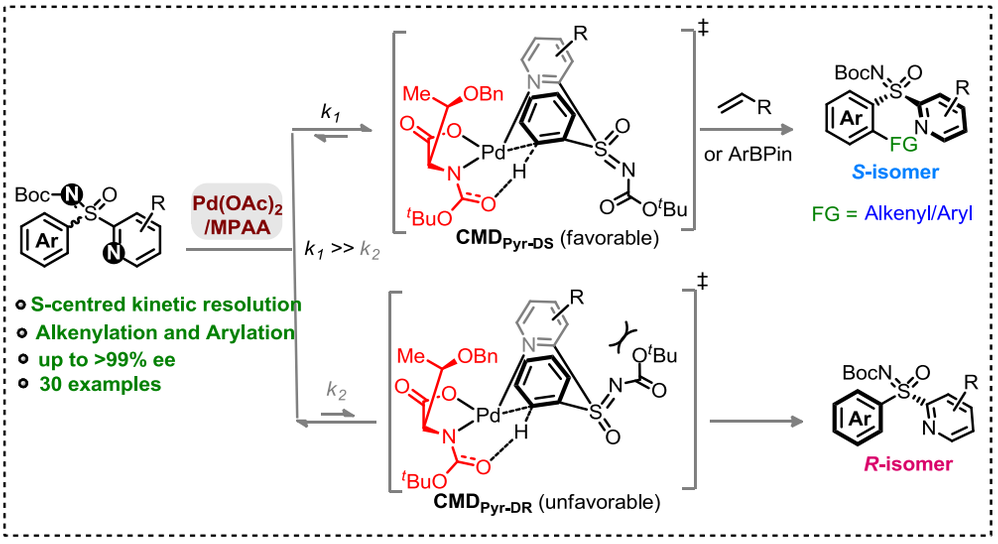

Scheme I.25: Kinetic resolution of phenyl pyridyl sulfoximine

I.6 Transition Metal Catalyzed Annulation Reaction

The TM-catalyzed annulation approaches have been widely implemented for the construction of variety of heterocyclic compounds. In 1991 and 1995, Larock group reported palladium catalyzed annulation of substituted aryl halides **93** with a wide range of internal alkynes **94** (**Scheme I.26**).[22] This method showed a straightforward pathway for the construction of benzofurans, indoles, benzopyrans, and isocoumarins. However, pre-functionalized precursors required in this process limits synthetic utility of this transformation. A probable solution to this would be TM-catalyzed annulation via direct C–H activation.

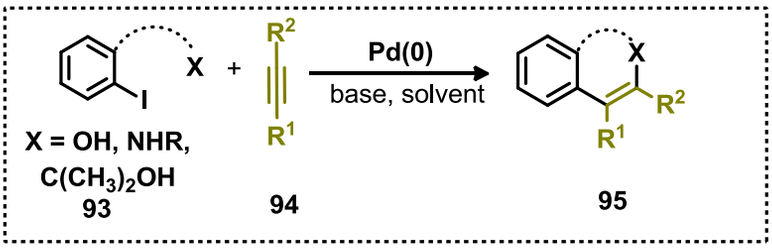

Scheme I.26: Larock annulation of aryl halide with alkynes

I.6.1 Transition metal-catalyzed oxidative annulation via C–H activation

The DG enabled TM-catalyzed oxidative annulation of aromatic C–H bond with alkenes/alkynes offers an atom-economical pathway for the construction of highly conjugated heteroarenes from readily accessible precursors.[23] Few the most recent demonstration of TM-catalyzed oxidative annulations are showcased in **Scheme I.27**. In 2007, Miura group showed a Rh(III)-catalyzed oxidative C–H annulation of easily accessible benzoic acids with alkyne derivatives for the synthesis of highly substituted lactones.[27] Subsequently, Rh(III), Ru(II), and Co(III) catalysts have been employed for the discovery of DG assisted annulations with alkynes and unsaturated systems for the synthesis of wide arrays of novel N/O-bearing heterocycles; a brief snapshots for the construction of new heterocycles is depicted in **Scheme I.27**.[23-27]

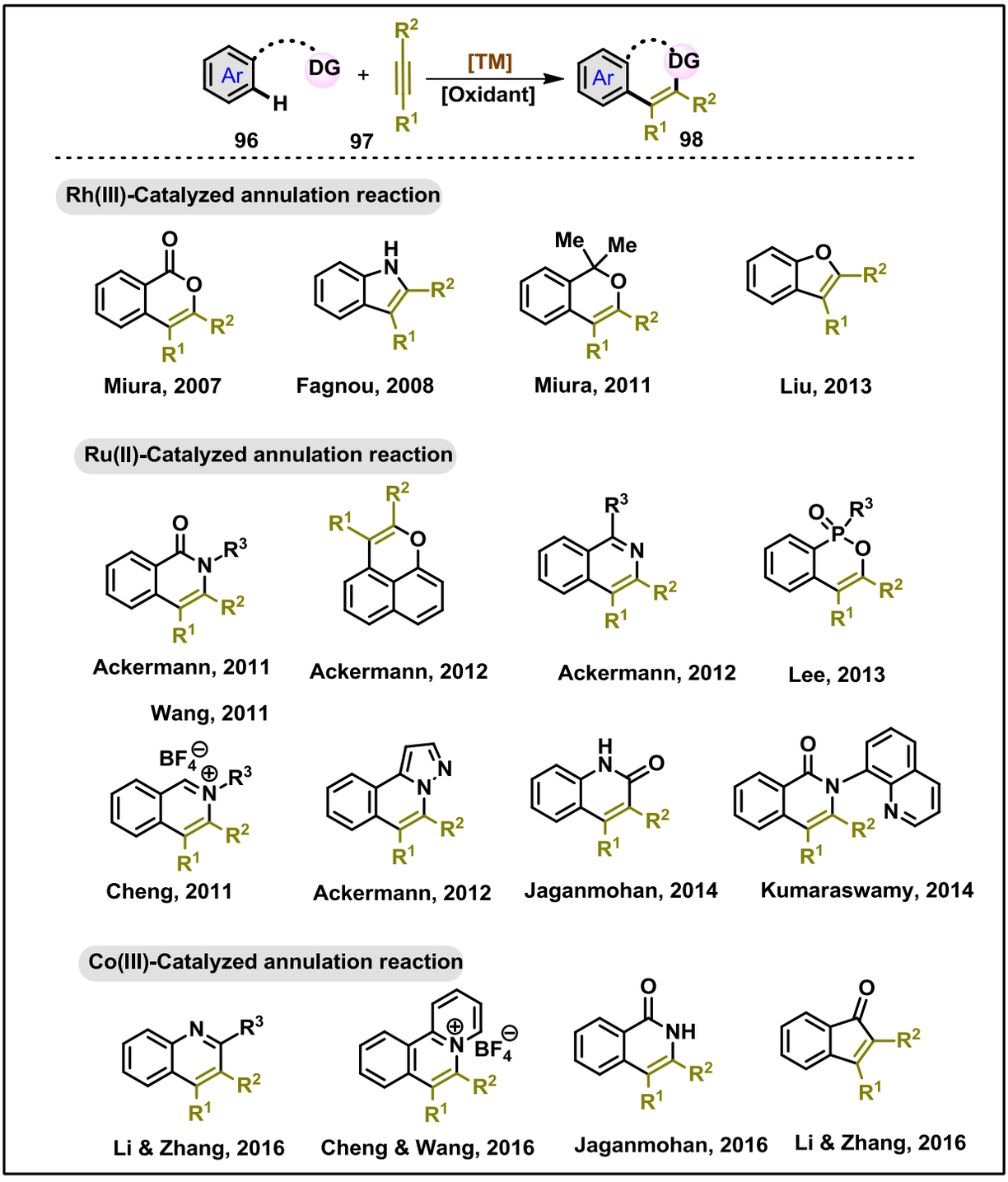

Scheme I.27: Selected examples of transition-metal catalyzed annulations

I.6.2 Mechanism of transition-metal catalyzed oxidative annulation

A representative mechanistic cycle for the DG mediated annulation reaction with alkyne is shown in **Scheme I.28** (Path-I: non-oxidizable DG; Path-II: Oxidizable DG). The transformation initiates with the coordination of TM with DG to form the respective metallacycle A or I.

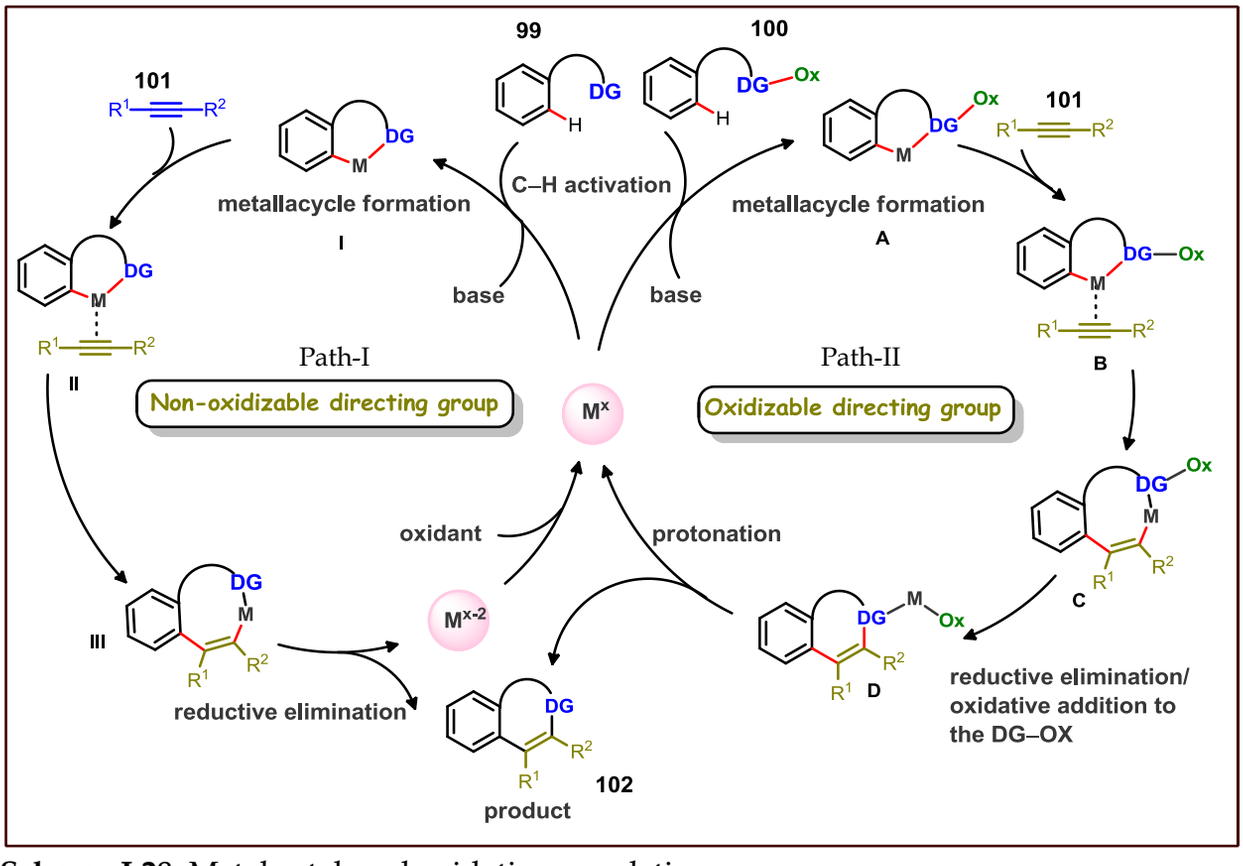

Scheme I.28: Metal catalyzed oxidative annulation

Next, the alkyne insertion to **A** or **I** give metallacycle **C** and **III** via **B** and **II**, respectively. The formation of 7-membered metallacycle **C**/**III** is quite common for both the methods (Path I and II). In case of Path-I, reductive elimination of **Int-III** delivers the corresponding mono-annulation product **102** with the reduction of TM species to M^{x-2}. Thus, external oxidant is necessary to re-oxidise the catalyst M^{x-2} to M^{x} for further reaction (**oxidant enabled; Path-I).** Whereas in Path-II, reductive elimination of **C** and simultaneous oxidative insertion of metal complex across the DG-Ox bond and protodemetalation of **D** delivers the annulation product **102** along with active catalyst M^{x} (**oxidant free; Path-II**).[26]

I.6.3. Transition metal-catalyzed multiple C–H activation

Over the time, numerous efforts have been devoted in the development of synthetic methods for the activation and functionalization of multiple C–H bonds. However, these transformations mostly dealt with mono-functionalized C–H bond followed by the introduction of second functional group in the other C–H bond. Simultaneous introduction of distinct functionalities in multiple C–H bonds remain challenging.

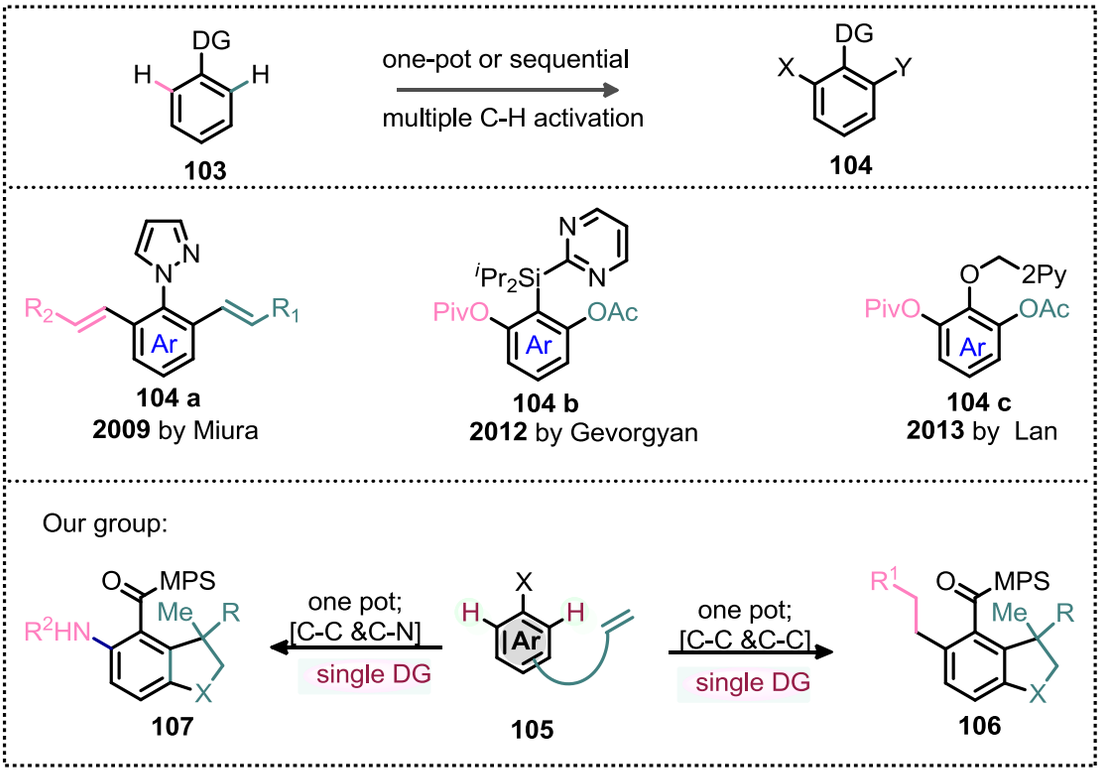

Scheme I.29: Selected examples of multiple C–H functionalization

In 2009, Miura and co-workers reported pyrazolyl group directed unsymmetrical di-alkenylation of arenes (**104a**; **Scheme I.29)**.[28]

In 2012, Gevorgyan group showcased a sequential acetoxylation followed by pivoxylation of two *ortho*-C(arene)–H bonds. The multiple unsymmetrical C–O bond formations were viable in one-pot in the presence of a pyrimidyl-DG (**104b**; **Scheme I.29**).[29]

Similar kind of sequential olefination of two ortho-C–H bonds was demonstrated by Lan and co-worker using 2-pyridylmethyl as a removable directing group. (**Scheme I.29**).

In 2012, our group demonstrated methylphenyl sulfoximine directed intramolecular *o*-C–H hydroarylation followed by intermolecular *o'*-C–N and C–C bond formation for the synthesis of peripheral substituted dihydrobenzofuran derivatives **(106, 107; Scheme I.29)**. Interestingly, both steps are performed in one-pot.[30]

I.7. Motivation, Hypothesis, and Planning

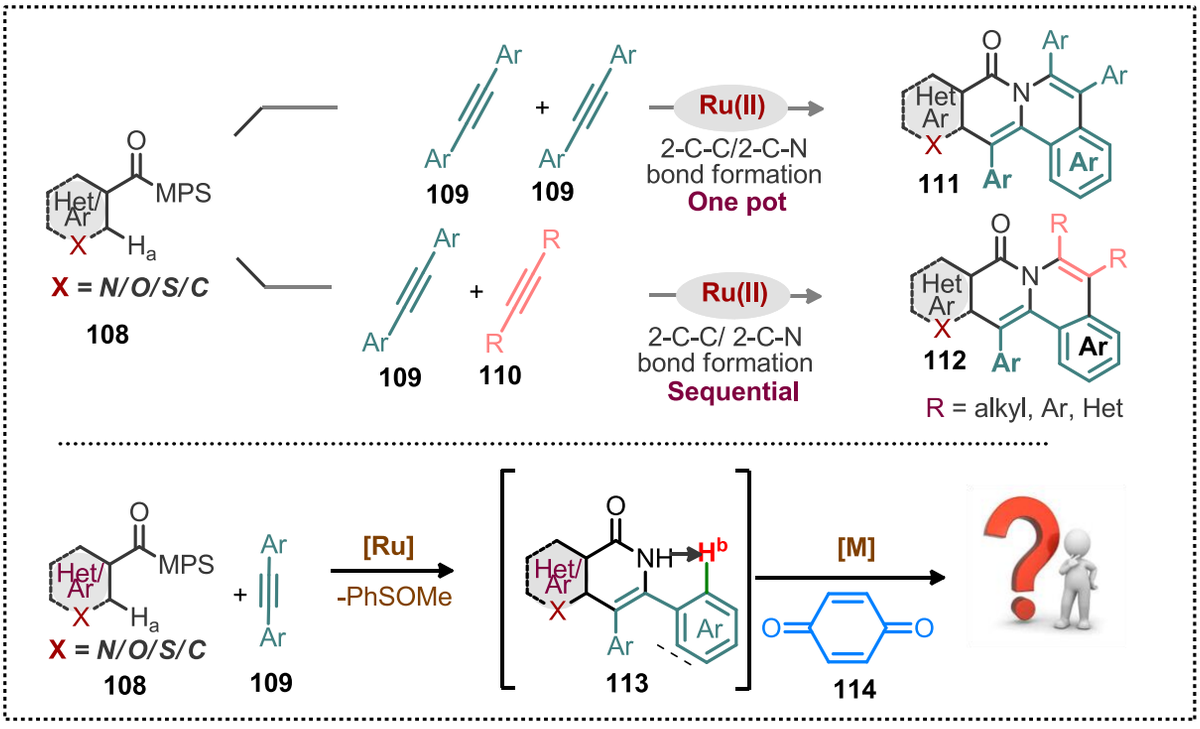

Scheme I.30: Motivation and hypothesis of multiple cyclization

Our group has recently showcased a Ru-catalyzed sulfoximine directed one-pot symmetrical double annulation of arenes with alkyne to construct -extended poly-fused heterocycles **111** (**Scheme I.30**). The identical transformation can also be applied for the two-pot unsymmetrical linear-type double annulations with different alkynes to make **112** (**Scheme I.30**).

Inspired from these demonstrations of double annulations, we envisaged performing a sequential double annulation with alkyne and a quinone moiety in an orchestrated manner. This process could lead to either a -extended poly-fused heterocycles **111** by stitching two molecules of alkyne or the annulation process could bind both alkyne and quinone simultaneously (**Scheme I.30**). *A transformation in this line is therefore developed and discussed in Chapter III.*

The TM-catalyzed DG enabled intramolecular hydroarylation of arenes with olefins have been well-studied (**Scheme I.31**).[30] The transformations are successful when carried out in organic solvents, such as: toluene, 1,2-dichloroethane, 1,4-dioxane etc (**Scheme I.31**). We hypothesized that the hydroarylation reaction may be possible in water medium instead of organic solvent. Thus, amide directed hydroarylation strategy in water medium is envisaged (**Scheme I.31**). *The Ru-catalyzed intramolecular hydroarylation transformation is therefore developed and discussed in Chapter IV.*

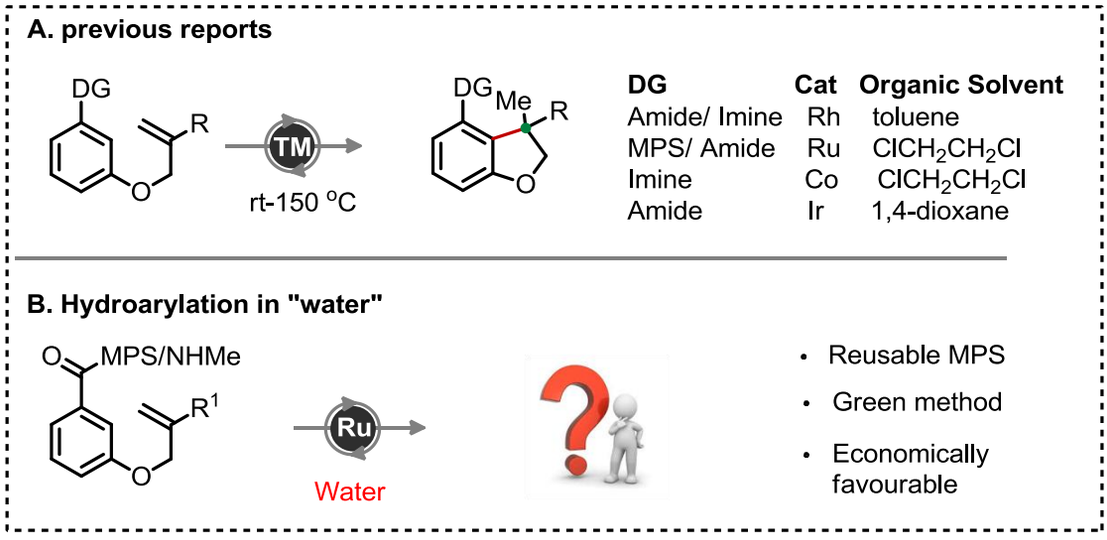

Scheme I.31: Intramolecular hydroarylation 'in water'

1.8. References

(1) *Metal-Catalyzed Cross-Coupling Reactions, 2nd ed.* A. De. Meijere, F. Diederich, *Wiley-VCH, Weinheim*, **2004**.

(2) For reviews, see: (a) J. K. Stille, *Angew. Chem. Int. Ed.* **1986**, *25*, 508. (b) R. F. Heck, in *Comprehensive Organic Synthesis, Vol. 4* (Eds.: B. M. Trost, I. Fleming), Pergamon Press, Oxford, **1991**, 833. (c) N. Miyaura, A. Suzuki, *Chem. Rev.* **1995**, *95*, 2457. (d) J. F. Hartwig, *Acc. Chem. Res.* **1998**, *31*, 852. (e) J. P. Wolfe, S. Wagaw, J. F. Marcoux, S. Buchwald, L. *Acc. Chem. Res.*, **1998**, *31*, 805. (f) T. Hiyama, *J. Organomet. Chem.* **2002**, *653*, 58. (g) E.-i. Negishi, Q. Hu, Z. Huang, M. Qian, G. Wang, *Aldrichimica Acta* **2005**, *38*, 71. (h) D. S. Surry, S. L. Buchwald, *Angew. Chem. Int. Ed.* **2008**, *47*, 6338. (i) J. F. Hartwig, *Nature* **2008**, *455*, 314. (j) S. E. Denmark, C. S. Regens, *Acc. Chem. Res.* **2008**, *41*, 1486.

(3) Cross-coupling reactions applications, see: (a) K. C. Nicolaou, S. A. Snyder, In *Classics in Total Synthesis II*, *VCH: Weinheim*, **2003**. (b) F. Naso, F. Babudri, G. M. Farinola, *Pure Appl. Chem.* **1999**, *71*, 1485. (c) C. Torborg, M. Beller, *Adv. Synth. Catal.* **2009**, *351*, 3027. (d) J. Magano, J. R. Dunetz, *Chem. Rev.* **2011**, *111*, 2177.

(4) (a) B. M. Trost, *Angew. Chem. Int. Ed.* **1995**, *34*, 259. (b) A. F. P. Biajoli, C. S. Schwalm, J. Limberger, T. S. Claudino, A. L. Monteiro, *J. Braz. Chem. Soc.* **2014**, 25, 2186.

(5) For reviews on C–H activation chemistry, see: (a) J. R. Lewis, R. G. Bergman, J. A. Ellman, *Acc. Chem. Res.* **2008**, *41*, 1013. (b) X. Chen, K. M. Engle, D. H. Wang, J. Q. Yu, *Angew. Chem. Int. Ed.* **2009**, *48*, 5094. (c) T. Newhouse, P. S. Baren, *Angew. Chem. Int. Ed.* **2011**, *50*, 3362. (d) S. R. Neufeldt, M. S. Sanford, *Acc. Chem. Res.* **2012**, *45*, 936.

(6) (a) F. Roudesly, J. Oble, G. Poli, *J. Mol. Catal. A*, **2017**, *426,* 275-296. (b) D. H. Ess, W. A. Goddard, III, R. A. Periana, *Organometallics* **2010**, *29*, 6459-6472.

(7) (a) L. Ackermann, *Chem. Rev.* **2011**, *111*, 1315. (b) S. I. Gorelsky, D. Lapointe, K. Fagnou, *J. Org. Chem.* **2012**, *77*, 658. (c) S. I. Gorelsky, D. Lapointe, K. Fagnou, *J. Am. Chem. Soc.* **2008**, *130*, 10848.

(8). J. Oxgaard, W. J. Tenn, R. J. Nielsen, R. A. Periana, W. Goddard, *Organometallics* **2007**, *26*, 1565.

(9). J. F. Hartwig, Acc. Chem. Res. **2017**, *50*, 549−555.

(10) (2) (a) X. Chen, K. M. Engle, D.-H. Wang, J.-Q. Yu, *Angew. Chem., Int. Ed*. **2009**, *48*, 5094−5115. (b) T. W. Lyons, M. S. Sanford, *Chem. Rev*. **2010**, *110*, 1147. (c) J. He, M. Wasa, K. S. L. Chan, Q. Shao, J.-Q. Yu, *Chem. Rev*. **2017**, *117*, 8754−8786.

(11) T. G. Saint-Denis, R.-Y. Zhu, G. Chen, Q.-F. Wu, J.-Q. Yu, *Science,* **2018**, 359, eaao4798.

(12) (a) E. B. Moynahan, F. D. Popp, M. F. Werneke, *J. Organomet. Chem*. **1969**, *19*, 229−232. (b) J. C. Gaunt, B. L. Shaw, *J. Organomet. Chem*. **1975**, *102*, 511−516.

(13) A. G. Constable, W. S. McDonald, L. C. Sawkins, B. L. Shaw, *J. Chem. Soc., Chem. Commun*. **1978**, 1061.

(14) V. I. Sokolov, L. L. Troitskaya, O. A. Reutov, *J. Organomet. Chem*. **1979**, *182*, 537−546.

(15) V. I. Sokolov, L. L. Troitskaya, O. A. Reutov, *J. Organomet. Chem*. **1977**, *133*, C28−C30.

(16) (a). B.-F. Shi, N. Maugel, Y.-H. Zhang, J.-Q. Yu, *Angew. Chem., Int. Ed*. **2008**, *47*, 4882. (b) B. F. Shi, Y. H. Zhang, J. K. Lam, D. H. Wang, J. Q. Yu, *J. Am. Chem. Soc.* **2010**, *132*, 460. (c) X. F. Cheng, Y. Li, Y. M. Su, F. Yin, J. Y. Wang, J. Sheng, H. U. Vora, X. S. Wang, J. Q. Yu, *J. Am. Chem. Soc.* **2013**, *135*, 1236.

(17) (a) D.-W. Gao, Y.-C. Shi, Q. Gu, Z.-L. Zhao, S.-L. You, *J. Am. Chem. Soc.* **2013**, *135*, 86. (b) L. Chu, X.-C. Wang, C. E. Moore, A. L. Rheingold, J.-Q. Yu, *J. Am. Chem. Soc.* **2013**, *135*, 16344, (c) B. N. Laforteza, K. S. Chan, J. Q. Yu, *Angew. Chem., Int. Ed.* **2015**, *54*, 11143.

(18). (a) K.-J. Xiao, D. W. Lin, M. Miura, R.-Y. Zhu, W. Gong, M. Wasa, J.-Q. Yu, *J. Am. Chem. Soc.* **2014**, *136*, 8138. (b) K. S. L. Chan, H.-Y. Fu,; J.-Q. Yu, *J. Am. Chem. Soc.* **2015**, *137*, 2042. (c) G. Chen, W. Gong, Z. Zhuang, M. S. Andrä, Y.-Q. Chen, X. Hong, Y.-F. Yang, T. Liu, K. N. Houk, J.-Q. Yu, *Science* **2016**, *353*, 1023. (d) F. L. Zhang, K. Hong, T. J. Li, H. Park, J. Q. Yu, *Science* **2016**, *351*, 252.

(19) H. Shi, A. N. Herron, Y. Shao, Q. Shao, J.-Q. Yu, *Nature* **2018**, *558*, 581.

(20) Z.-J. Du, J. Guan, G.-J. Wu, P. Xu, L.-X. Gao, F.-S. Han, *J. Am. Chem. Soc.* **2015**, *137*, 632, (b) Y.-C. Zhu, Y. Li, B.-C. Zhang, F.-X. Zhang, Y.-N. Yang, X.-S. Wang, *Angew. Chem., Int. Ed.* **2018**, *57*, 5129. (c) J. Diesel, N. Cramer, *ACS Catal.* **2019**, *9*, 9164.

(21) Q. Shao, K. Wu, Z. Zhuang, S. Qian, J.-Q. Yu, *Acc. Chem. Res.* **2020**, *53*, 833.

(22) G. Zeni, R. C. Larock, *Chem. Rev.* **2006**, *106*, 4644.

(23) Selected Rh, Ru and Co-catalyzed oxidative annulation reviews: (a) T. Satoh, M. Miura, *Chem. Eur. J.* **2010,** *16*, 11212. (b) J. Wencel-Delord, T. Dröge, F. Liu, F. Glorius, *Chem. Soc. Rev.* **2011**, *40*, 4740. (c) G. Song, F. Wang, X. Li, *Chem. Soc. Rev.* **2012**, *41*, 3651. (d) P. B. Arockiam, C. Bruneau, P. H. Dixneuf, *Chem. Rev*. **2012**, *112*, 5879. (e) L. Ackermann, *Acc. Chem. Res.* **2014**, *47,* 281. (f) M. Gulías, J. L. Mascareñas, *Angew. Chem. Int. Ed.* **2016**, *55*, 11000. (g) S. Prakash, R. Kuppusamy, C.-H. Cheng, *ChemCatChem* **2018**, *10*, 683.

(24) (a) X. Xu, Y. Liu, C.-M. Park, *Angew. Chem. Int. Ed.* **2012**, *51*, 9372. (b) P. Tao, Y. Jia, *Sci. China: Chem.* **2016**, *59*, 1109. (c) N. S. Upadhyay, J. Jayakumar, C.-H. Cheng, *Chem. commun.* **2017**, *53*, 2491. (d) J. Tang, S. Li, Z. Liu, Y. Zhao, Z. She, V. D. Kadam, G. Gao, J. Lan, J. You, *Org. Lett.* **2017**, *19*, 604. (e) L. Song, G. Tian, Y. He, E. V. Van der Eycken, *Chem. Commun.* **2017**, *53*, 12394. (f) A. Lerchen, T. Knecht, M. Koy, C. G. Daniliuc, F. Glorius, *Chem. -Eur. J.* **2017**, *23*, 12149. (g) C. Raji Reddy, K. Mallesh, *Org. Lett.* **2018**, *20*, 150.

(25) (a) L. Ackermann, A. V. Lygin, N. Hofmann, *Angew. Chem. Int. Ed.* **2011**, *50*, 6379. (b) Y. Yang, K. Li, Y. Cheng, D. Wan, M. Li, J. You, *Chem. Commun.* **2016**, *52*, 2872.

26) (a) J. Mo, L. Wang, Y. Liu, X. Cui, *Synthesis* **2015**, 47, 439. (b) Z. Wang, P. Xie, Y. Xia, *Chin. Chem. Lett.* **2018**, *29*, 47 (c) C. Zhu, C.-Q. Wang, C. Feng, *Tetrahedron Lett.* **2018**, *59*, 430.

(27) (a) K. Ueura, T. Satoh, M. Miura, *Org. Lett.* **2007**, *9*, 1407 (b) K. Ueura, T. Satoh, M. Miura, *J. Org. Chem.* **2007**, 72, 5362.

(28) N. Umeda, K. Hirano, T. Satoh, M. Miura, *J. Org. Chem.* **2009**, *74*, 7094–7099.

(29) A. V. Gulevich, F. S. Melkonyan, D. Sarkar, V. Gevorgyan, *J. Am. Chem. Soc.* **2012**, *134*, 5528–5531

(30) K. Ghosh, R. K. Rit, E. Ramesh, A. K. Sahoo, Angew. Chem., Int. Ed. **2016**, 55, 7821

Chapter II

Kinetic Resolution of Sulfur-Stereogenic Sulfoximines by Pd(II)-MPAA Catalyzed C–H Olefination and Arylation

Abstract

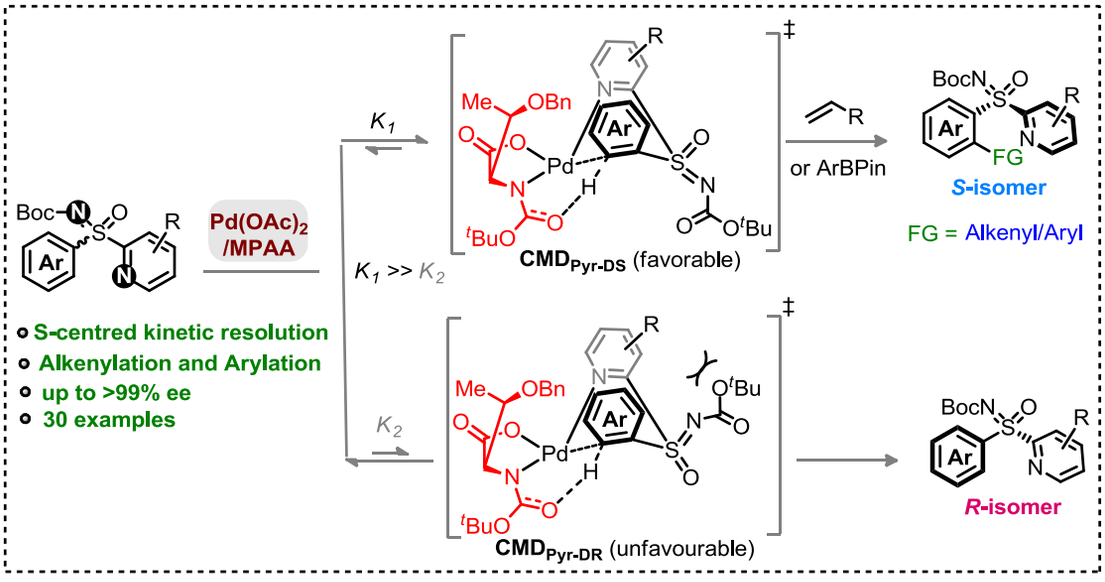

A direct Pd(II)-catalyzed kinetic resolution of heteroayl-enabled sulfoximines through an *ortho*-C–H alkenylation/arylation of arenes has been developed for the first time. The coordination of sulfoximine pyridyl-motif with Pd(II)-catalyst and chiral amino acid MPAA ligand helps the enantio-determining C(aryl)–H activation. This method provides access to a wide range of enantiomerically enriched aryl-pyridyl-sulfoximine precursors and the C(aryl)–H alkenylation/arylation adducts in good yields with high enantio-selectivity (up to >99% ee), and selectivity factor up to >200; which are otherwise inaccessible by the conventional methods. The directing group (DG) preference, ligand effect, geometry constraints, and the transient six-membered concerted-metalation-deprotonation (CMD) species displays indomitable resilience in the stereoselectivity origin; DFT studies validate this outcome.

Reference:

Kallol Mukherjee, Nicolas Grimblat, Somratan Sau, Koushik Ghosh, Majji Shankar, Vincent Gandon and Akhila K. Sahoo*

II.1. Introduction

The directing group (DG) assisted desymmetrization of prochiral C–H bond provides an impeccable entry to construct functionalized chiral molecules. This strategy has led to making stereogenic carbon, phosphorus, silicon and sulfur centered species through selective functionalization of prochiral C–H bonds.[1–3] However, essential requirements of two enantiotopic groups limits synthetic potential of desymmetrization processes. At this juncture, kinetic resolution (KR) of C–H bonds is undoubtedly an attractive alternative (**Scheme II.1A**). In this regard, the Yu's DG assisted chiral amino acid enabled palladium (Pd)-catalyzed carbon centred KR of arene C–H bonds through alkenylation, arylation, and/or iodination is undoubtedly a breakthrough constructing highly functionalized

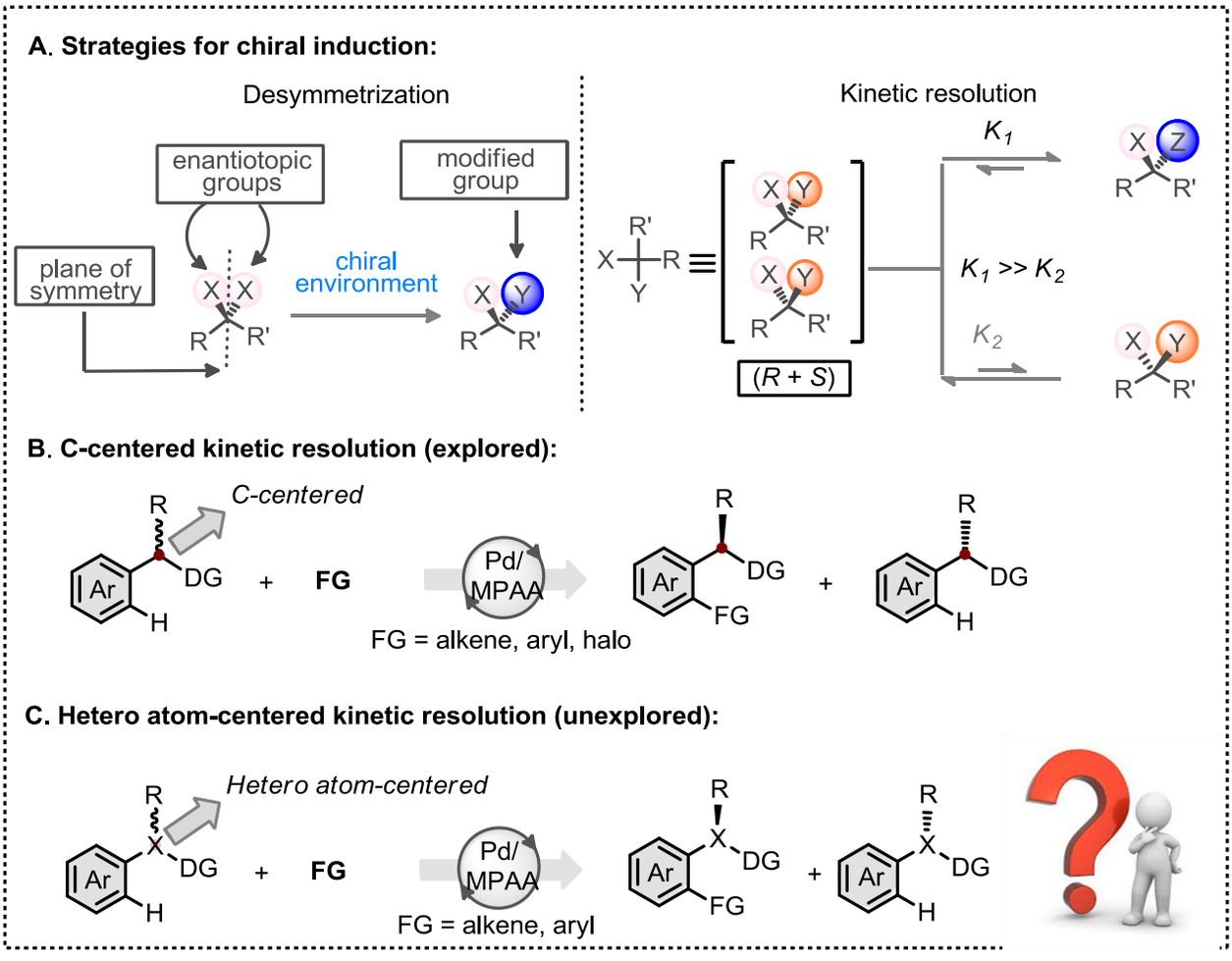

Scheme II.1: Kinetic resolution for the generation of stereogenic hetero atom centre chiral entities. (**Scheme II.1B**).[4] However, these strategies are limited to C-centred resolution while related strategy for heteroatom centered KR of arene is obscure (**Scheme II.1C**).

II.2. Previous strategies for Pd/MPAA catalyzed desymmetrization

In **2008**, Yu group reported a desymmetrization method for the Pd(II)/ monoprotected amino acids (MPAA)-catalyzed enantioselective activation of C(sp^2)–H bond. This process is successful for making chiral C-stereogenic centre. Monoprotected -amino acid ligands are found essential in this process. The mechanistic feature is sketched in **Scheme II.2**.[2a]

The transformation begins with the in-situ formation of Pd/MPAA-complex **3**. Next,

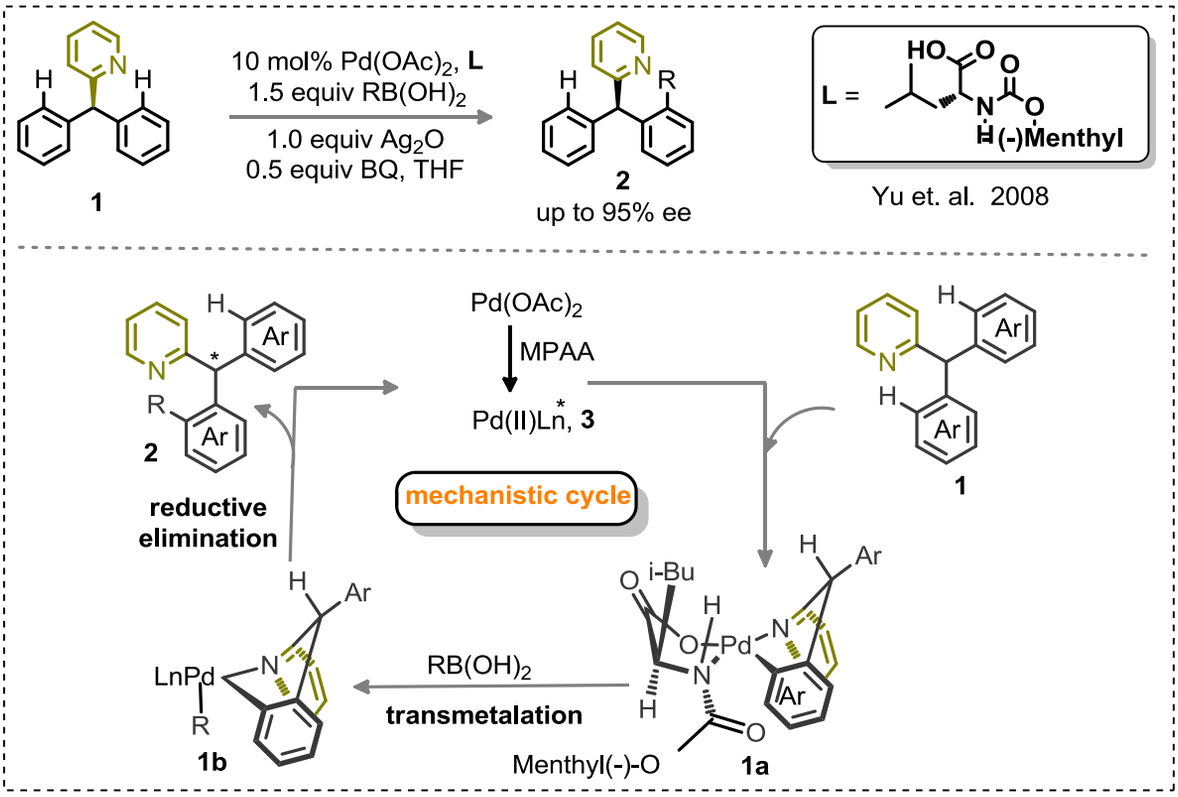

Scheme II.2: Pd(II)/MPAA-catalyzed enantioselective C(sp^2)–H functionalization via alkylation

the reaction of **3** with **1** proceeds with enantio-determining C–H activation to deliver 6-membered palladacycle **1a**. The transmetalation of **1a** with the boronic acid counterpart then provides **1b**. Finally, reductive elimination of **1b** gives the final product **2** (**Scheme II.2**).

In **2010**, the identical strategy has been extended for the enantioselective C−H activation of carboxylic acids **4**. Monoprotected α-amino acids are once again found effective for the enantio-determining C–H insertion of **4** to enable **4a** (**Scheme II.3**).[2c]

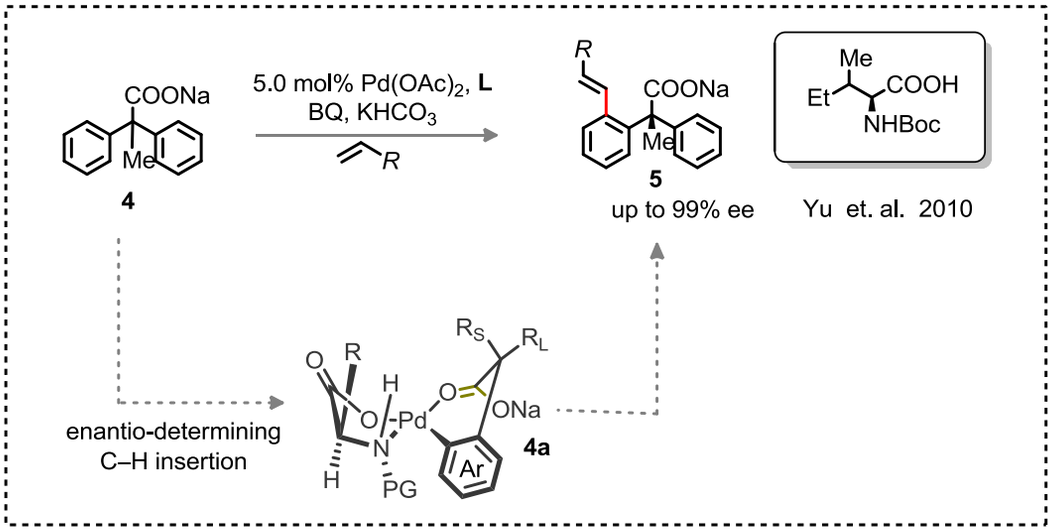

Scheme II.3: Enantioselective C−H activation reactions of carboxylic acid

In **2013**, the same group developed Pd(II)/MPAA catalyzed enantioselective C(sp²)–H activation and simultaneous intramolecular C–O bond formation to deliver chiral benzofuranones **7** with up to 96% ee. This is the first example of enantioselecctive C–H functionalization which involves Pd(II)/Pd(IV) catalysis (**Scheme II.4**).[2e]

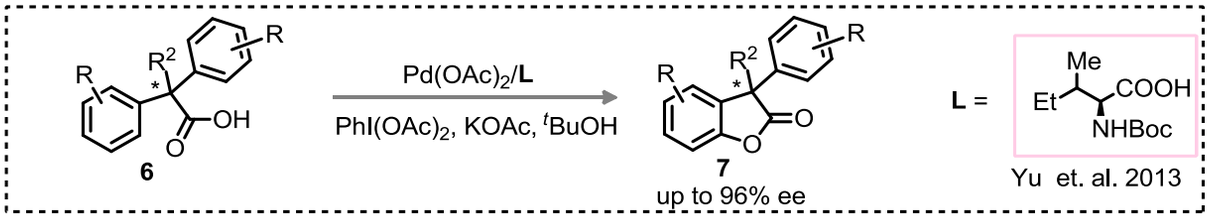

Scheme II. 4: Enantioselective C(sp²)–H activation and synthesis of chiral benzofuranones

In same year, the You group revealed Pd/MPAA catalyzed stereoselective C–H functionalization of aminomethylferrocene derivatives **8** for the construction of planar-chiral ferrocenes derivatives **9** with high enantioselectivity. Commercially available N-Boc-protected amino acids are being successfully used for the chiral induction. Moreover, the reaction occurs in the presence of air as external oxidant, which makes the current synthetic method practical (**Scheme II.5**).[2g]

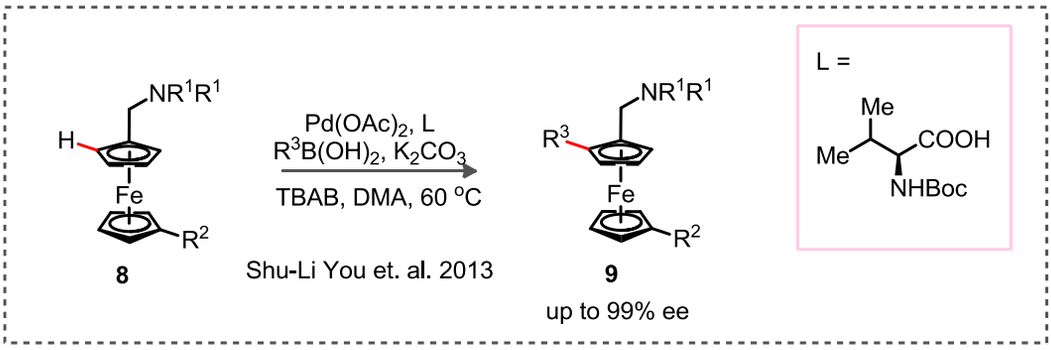

Scheme II.5: Stereoselective C–H functionalization of aminomethylferrocene

In **2013**, a first example of an Pd-catalyzed enantioselective C(sp²)−H iodination of (diarylmethyl)amine **10a** has been demonstrated by the Yu group. This strategy

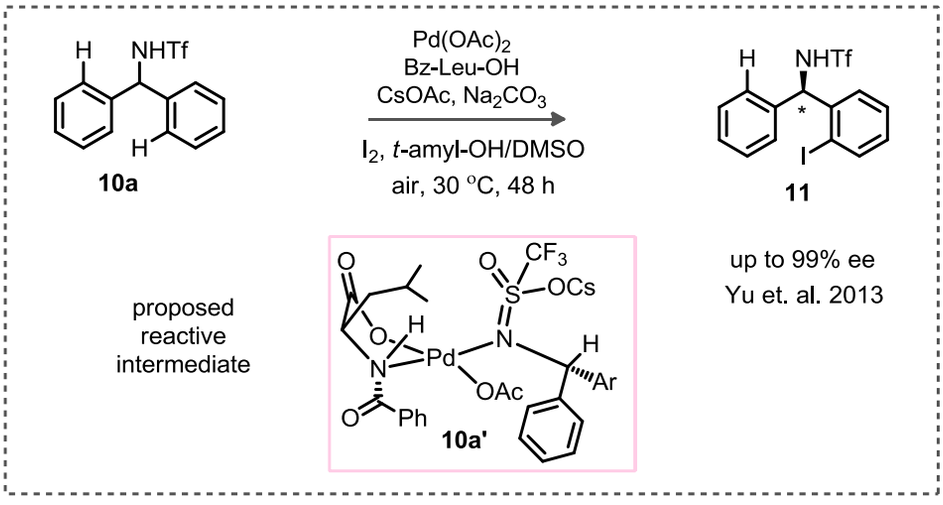

Scheme II.6: Pd(II)/MPAA-catalyzed enantioselective C(sp²)–H iodination

provides a useful access to functionalized chiral (diarylmethyl)amine derivatives **11**. The commercially available mono-N-protected amino acid ligand (MPAA) along with

the inexpensive halogenating agent I_2 are used in this transformation making the method synthetically workable (**Scheme II.6**).[2f] A neutral σ-donor directing group helps the formation of reactive intermediate **10a'**.

In **2015**, a stereoselective C(sp^2)–H functionalization of nosyl-protected diarylmethylamines **10b** with ArBpin has been developed by the the same group. Once again, the MPAA ligand has been found effective to deliver the respective arylated chiral diarylmethylamine derivatives **12** (**Scheme II.7**).[2i]

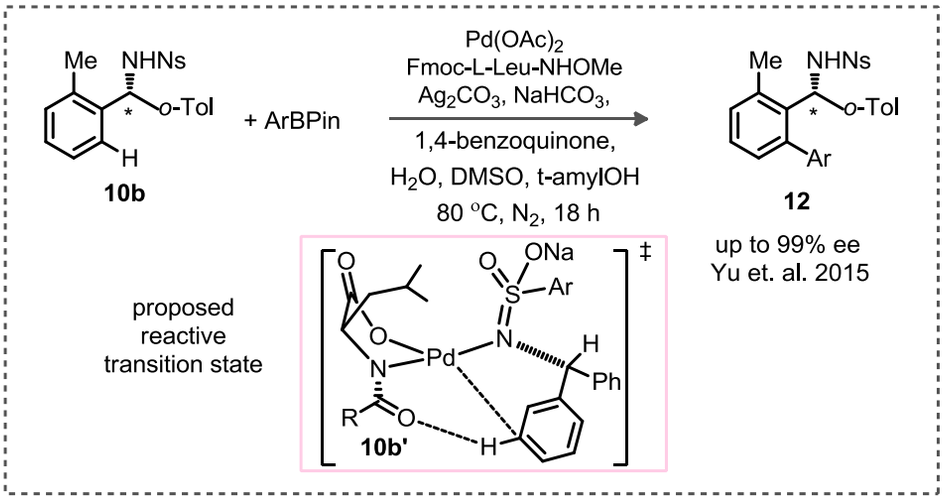

Scheme II.7: Pd(II)/MPAA-catalyzed enantioselective C(sp^2)-H functionalization via arylation

Although the known desymmetrization strategies are viable in making C–H functionalized chiral molecules, prochiral C–H bonds are essential for all these transformations.[2] While kinetic resolution (KR) of C–H bonds offers booming advantages for making functionalized chiral molecules.

II.3. Motivation and Design of Kinetic Resolution

In this regard, Yu's pioneering routes on DG assisted chiral amino acid enabled palladium (Pd)-catalyzed carbon centred KR of arene C–H bond through alkenylation, arylation, and/or iodination is undoubtedly a breakthrough (**Scheme II.8**).[4] Despite the

successes, related strategy for the *Pd-catalyzed heteroatom centered KR of arene* remains obscure although exceedingly appealing (**Scheme II.8**).

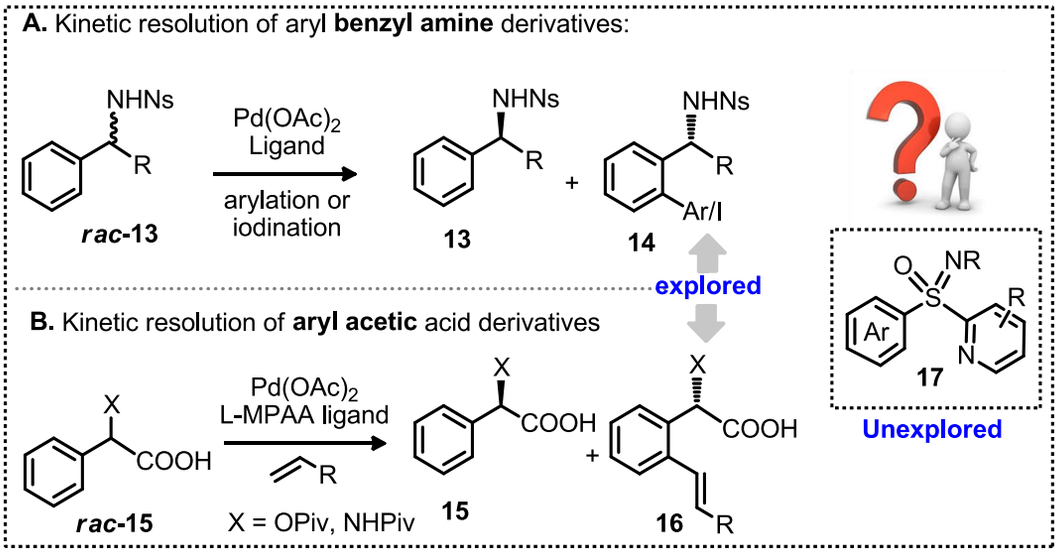

Scheme II.8: Kinetic resolution for the generation of stereogenic C-centre

On the other hand sulfoximines, configurationally stable motif with *S*-stereogenicity, have been found in the molecules of medicinal importance and agrochemicals.[5] Notably, sulfoximines have emerged as chiral auxiliary and DG for C–H functionalizations.[6] These benefits have enabled facile access to diverse range of sulfoximines. Whereas syntheses of enantioenriched sulfoximines have invariably rely on resolution techniques, stereoselective imination and oxidation.[7,8] Elegant enantioselective and KR routes to sulfoximines have been independently developed by Cramer and Li group, but all these approaches rely on Rh -catalyzed [4+2] annulation of diazoesters and aryl-sulfoximines in presence of specially designed ligands (**Scheme II.9**).[9] Mechanistically, this transformation proceeds with the coordination of the sulfoximine **18/19** to the Rh(III) center which initiates *ortho*-C–H activation via a CMD pathway. Then coordination and insertion of the diazo species **21** with **18b** leads to the formation of carbenoid intermediate **18c**, which in turn undergoes protonation to produce ketone **22**. Finally an off-cycle cyclocondensation offers desired product **20a** or **20b**.

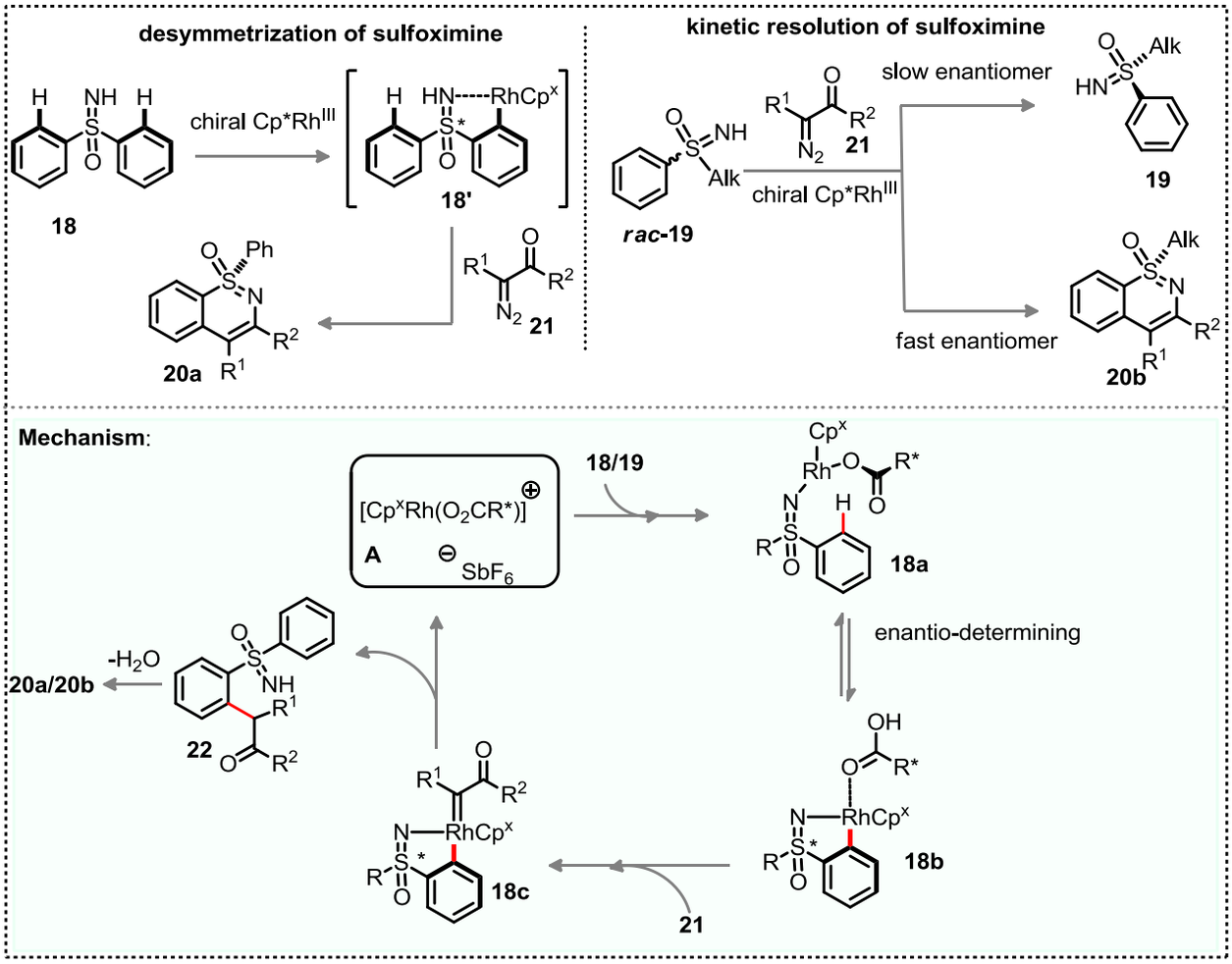

Scheme II.9: Desymmetrization and kinetic resolution of sulfoximines through annulation

To this end, we devised a Pd-catalyzed C–H functionalization method for KR of 2-pyridylaryl sulfoximine using commercially available Pd(II) catalyst and chiral amino acid (MPAA) ligand via C(aryl –H arylation and olefination (**Figure II.1A**), which is unexplored. The concept relies on kinetically regulated concerted-metalation-deprotonation (CMD) step of C(aryl –H activation (K_1>>K_2, **Figure II.1A**), coordination of pyridine over imine to Pd-MPAA and the ligand geometry $\mathbf{CMD_{Pyr\text{-}DS}}$ over $\mathbf{CMD_{Pyr\text{-}DR}}$ (**Figure II.1B**). These factors might influence the selectivity (*S* over *R*; **Figure II.1A**).

(Detailed explaination is given in section **II.4.7**) The transformation is general constructing wide arrays of enantiomerically enriched C-olefinated/arylated aryl-pyridyl-*S*-sulfoximines, which are otherwise inaccessible by other routes.

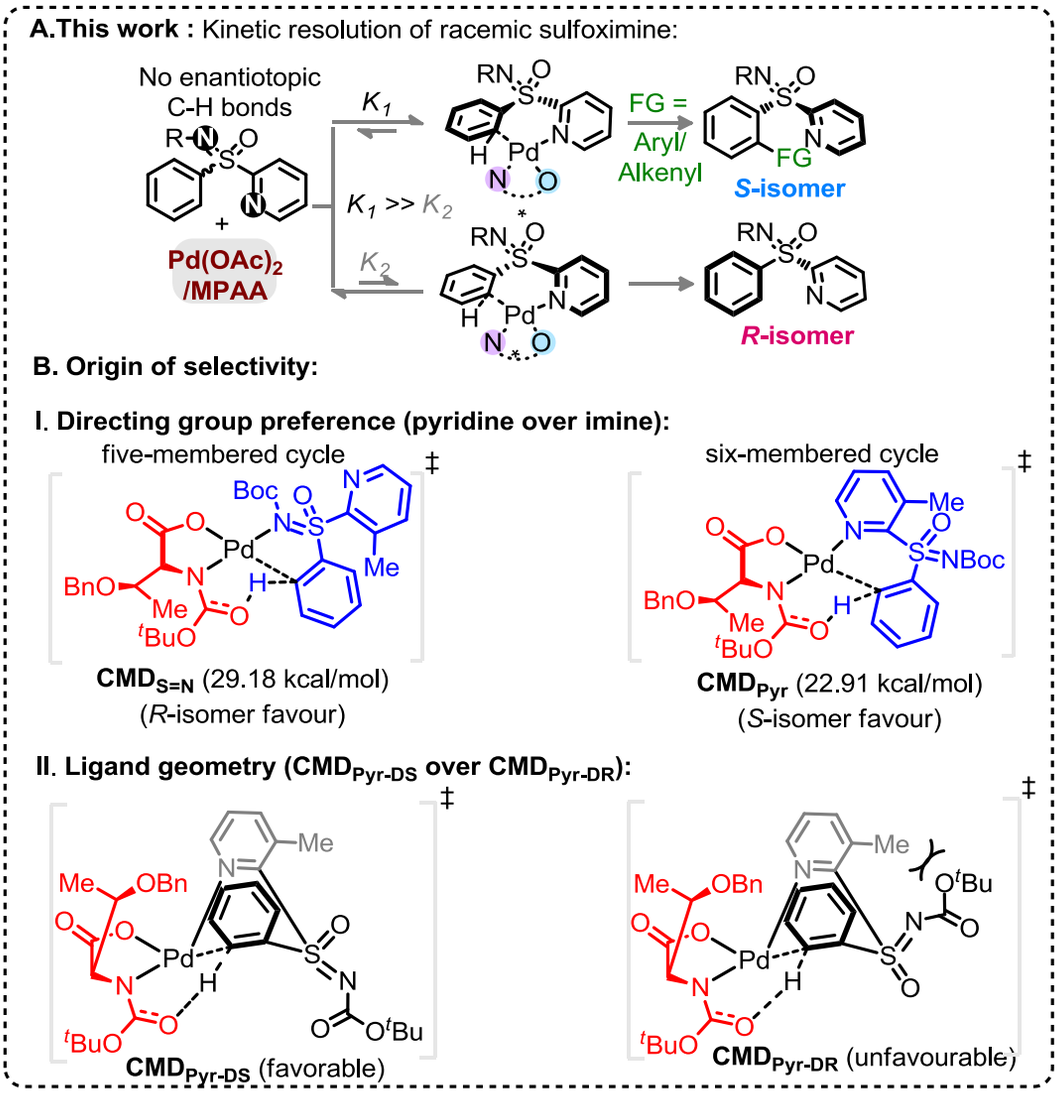

Figure II.1: Kinetic resolution of sulfoximine

II.4. Results and Discussion

II.4.1. Synthesis of precursors

General procedure for the synthesis of racemic (rac) 27a–27l (GP-1):[10]

To pursue our hypothesis, diverse range of N-Boc protected aryl-pyridyl-sulfoximine precursors are prepared using the known synthetic procedures. Coupling of thiols with pyridines followed by $PhI(OAc)_2$/$(NH_4)_2CO_3$ mediated imination and oxidation gives sulfoximine. Finally Boc-protection gives the N-Boc protected aryl-pyridyl-sulfoximine precursors (Detailed procedure is given in experimental section). A list of aryl-pyridyl-sulfoximine derivatives are shown in **Scheme II.10**.

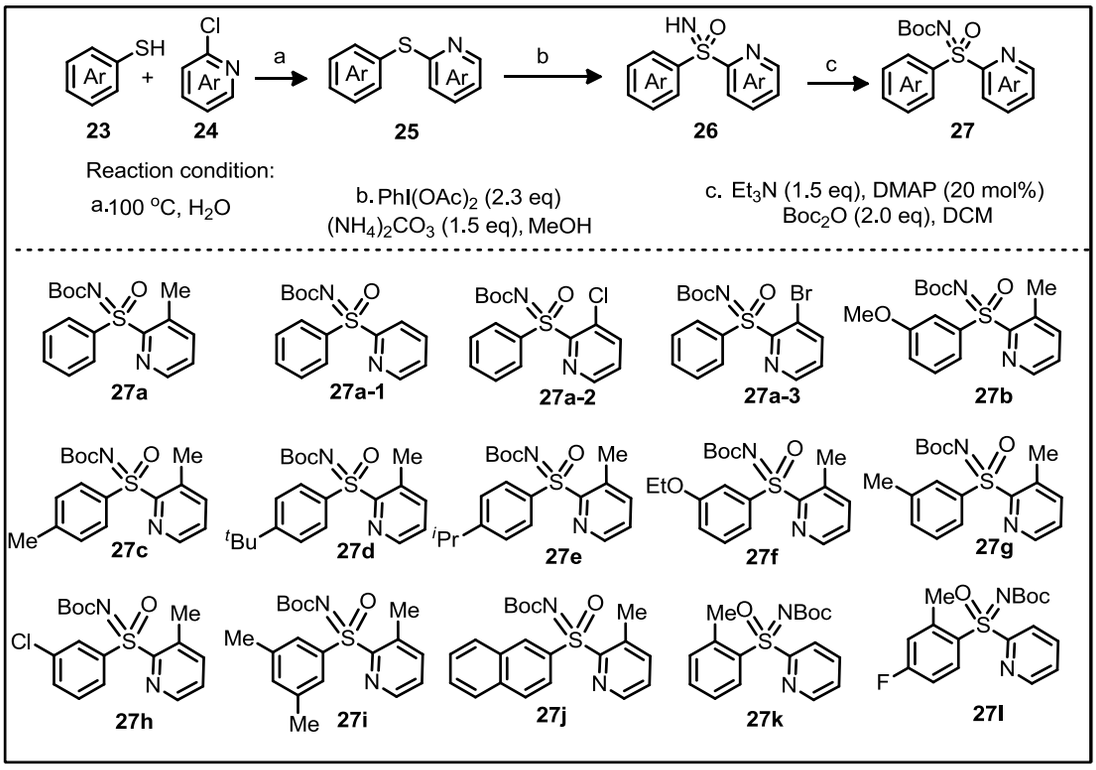

Scheme II.10: List of sulfoximine precursors synthesized

Thiols (**23**) and pyridines (**24**) are purchased from commercially available source and used; the molcules are listed in **Scheme II.11**.

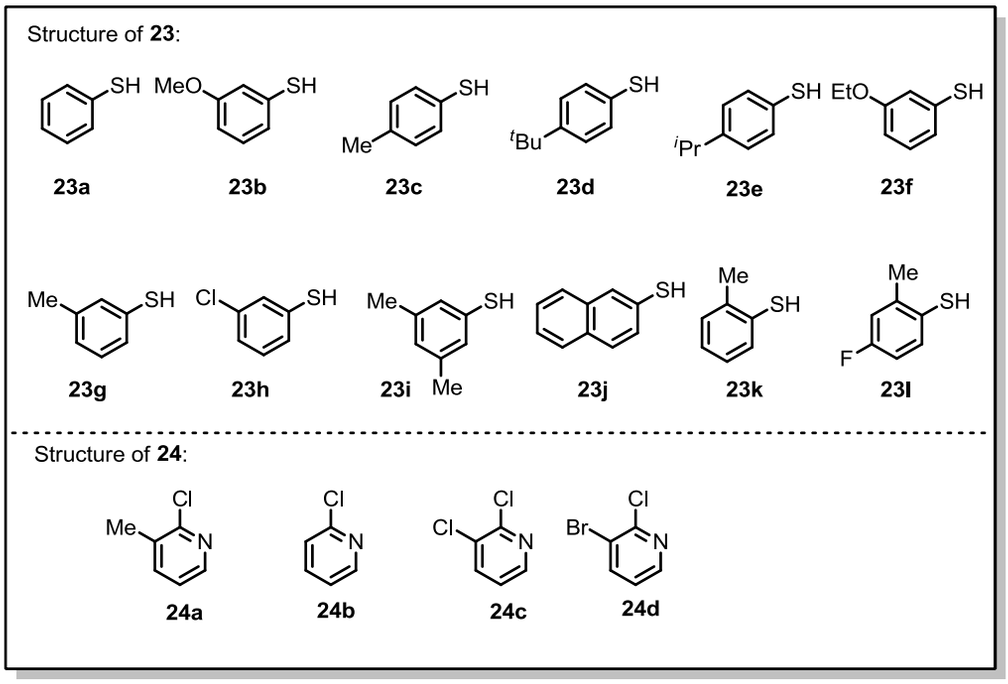

Scheme II.11: List of thiols and pyridines used for sulfoximine synthesis

II.4.2. Synthesis of Chiral Ligands (GP-2):[11]

All mono protected amino acids ligands **L1**–**L8** and **L11** were purchased from commercial sources or synthesized following the known procedures.[2] Ligands **L9** and **L10** are prepared and presented in **Scheme II.12**.

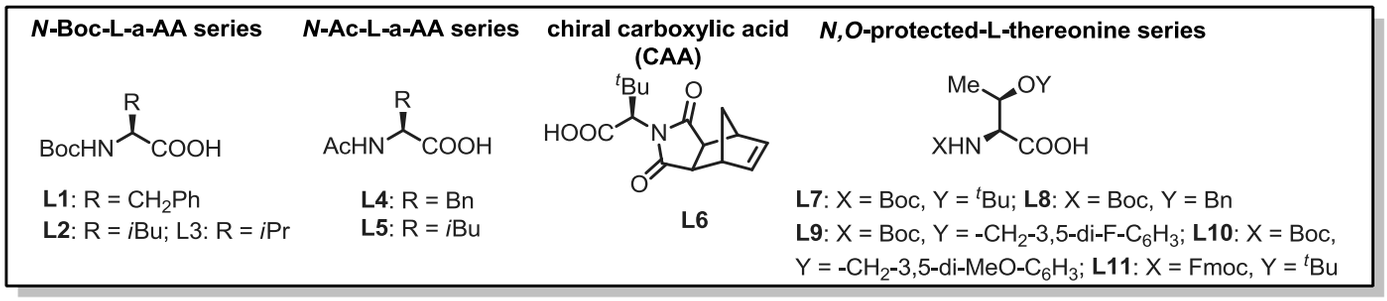

Scheme II.12: List of mono protected amino acid ligands for the kinetic resolution

II.4.3. Optimization studies

II.4.3.1. Optimization of reaction conditions for C–H alkenylative kinetic resolution:

The study was initiated in the non-substituted N-Boc-phenyl-2-pyridyl sulfoximine (*rac*-**27a-1**) with ethyl acrylate (**28a**; 0.6 equiv) in presence of $Pd(OAc)_2$ (10 mol%), Boc-L-Phe-OH (**L1**; 30 mol%), Ag_2CO_3 (2.0 equiv) in $ClCH_2CH_2Cl$ (1,2-DCE) at 75 °C (**Table II.1**). The desired C2-alkenylation product (*S*)-**29a-1** (18%, conversion after 3 days) along with

Table II.1. Ligands Screening [a]

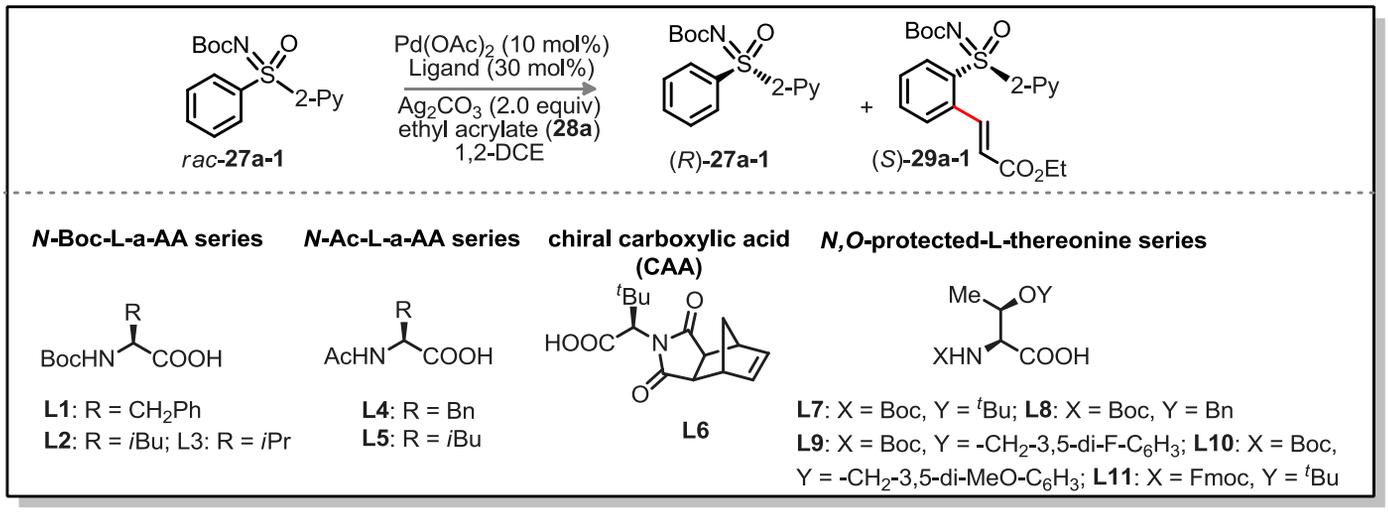

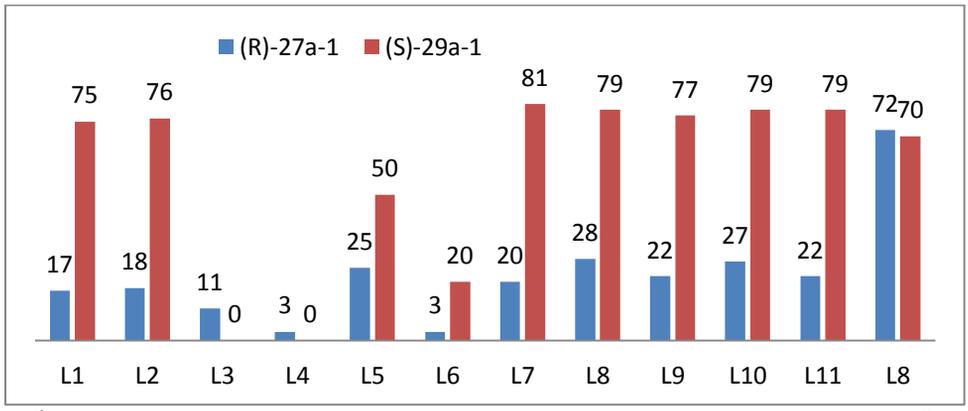

	L1	L2	L3	L4	L5	L6	L7	L8	L9	L10	L11	L8
s[d]	8	9	–	–	4	–	12	11	10	11	11	12[e]
c[c]	18	19	–	–	33	–	20	26	22	25	22	50[e]

[a]Reaction conditions: ***rac*-27a-1** (0.1 mmol), ethyl acrylate **28a** (0.6 equiv), $Pd(OAc)_2$ (10 mol%), ligand (30 mol%), Ag_2CO_3 (2.0 equiv), 1,2-DCE (1.0 mL), N_2, 75 °C, 3 days. [b]Calculated conversion, C = eeSM/(eeSM + eePR). [c]Determined by chiral HPLC analysis. [d]Selectivity factor (*s*) = ln[(1 − C)(1 − eeSM)]/ln[(1 − C)(1 + eeSM)]. [e]Ethyl acrylate (2.0 equiv) was used.

the precursor (*R*)-**27a-1** were obtained in 75% ee and 17% ee, respectively, exhibiting a low selectivity factor (*s*) of 8. This encouraging result unfolded our curiosity examining the effect of other ligands. None of the N-Boc-, N-acetyl-, and N-imide-protected commercially available -amino acid ligands (**L2**–**L6**) with distinct side chains were effective. Assuming the additional coordination ability of easily modifiable –OH group in threonine, various N, O-protected threonine ligands were tested.

The reaction *s* factor was improved a little for (*S*)-**29a-1** 81% ee and 79% ee, when Boc-L-Thr(*t*Bu)-OH (**L7**) and Boc-L-Thr(Bn)-OH (**L8**) were used, respectively. Electronic perturbation in O-benzyl moiety does not have any impact on enantioselectivity (**L9** and **L10**). The use of **28a** (2.0 equiv) in presence of ligand **L8** could found effective improving the conversion (50%) with (*S*)-**29a-1** (70% ee).

Table II.2. Solvent screening [a]

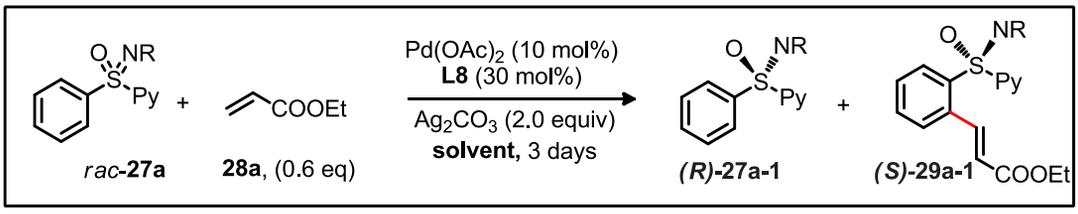

Entry	solvent	Conversion[b]	*ee* [%][c]		*s*[d]
			(R)-27a-1	*(S)*-29a-1	
1	THF	trace	–	–	–
2	CH_3CN	trace	–	–	–
3	1,4-dioxane	trace	–	–	–
4	HFIP	trace	–	–	–
5	toluene	12.76	12	82	11
6	TFT	24.78	28	85	16
7	2-chloro toluene	16.33	16	82	12
8	3-methoxy anisole	27.27	30	80	12
9	1,2-dimethoxy propane	9.9	09	82	11
10	4-Cl-TFT	17	17	83	13
11	TFE	trace	–	–	–
12	2-methoxy propane	trace	–	–	–
13	2-methyl anisole	20.75	24	84	14

[a]Reaction conditions: ***rac*-27a-1** (0.1 mmol), ethyl acrylate **28a** (0.6 equiv), $Pd(OAc)_2$ (10 mol%), **L8** (30 mol%), Ag_2CO_3 (2.0 equiv), solvent (1.0 mL), N_2, 75 °C, 3 days. [b]Calculated conversion, C = eeSM/(eeSM + eePR). [c]Determined by chiral HPLC analysis. [d]Selectivity factor (*s*) = ln[(1 − C)(1 − eeSM)]/ln[(1 − C)(1 + eeSM)].

A number of solvents were tested. None of them was found effective in increasing the conversion of the desired product **29a-1** (**Table II.2**).

To enhance sulfoximine resolution enantioselectivity by maintaining conversion (~50%; **Table II.1**), we scrutinized the co-oxidant effect (**Table II.3**). 2-chlorobenzoquinone (2-Cl-BQ) was found best providing 77% ee of (*S*)-**29a-1** (39% conversion, *s* factor of 13; entry-2, **Table II.3**).

Table II.3. Additive screening [a]

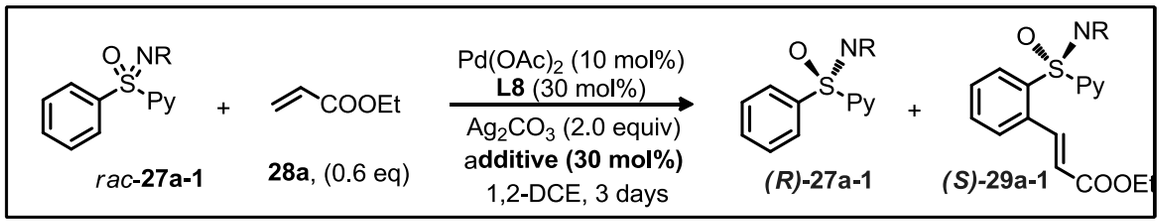

Entry	Additive	Conversion[b]	*ee* [%][c]		*s*[d]
			(*R*)-27a-1	(*S*)-29a-1	
1	BQ	18	17	78	10
2	2-chloro BQ	39	50	77	13
3	2, 5-dichloro BQ	35	40	75	10

[a]Reaction conditions: **rac-27a-1** (0.1 mmol), ethyl acrylate **28a** (0.6 equiv), $Pd(OAc)_2$ (10 mol%), L8 (30 mol%), Ag_2CO_3 (2.0 equiv), additives (0.3 equiv), 1,2-DCE (1.0 mL), N_2, 75 °C, 3 days. [b]Calculated conversion, C = eeSM/(eeSM + eePR). [c]Determined by chiral HPLC analysis. [d]Selectivity factor (*s*) = ln[(1 − C)(1 − eeSM)]/ln[(1 − C)(1 + eeSM)].

Next, we unravelled scrutinizing DG effect (**Table II.4**). Thus, various substituted 2-pyridyl containing sulfoximines were independently subjected to **2a**. Upon various trials, 3-methyl pyridyl DG was found superior affording alkenylation resolution species (S)-**29a** (96% ee) with s factor of 58, although conversion was confined to 17% (entry 1). While 3-Cl/Br substituted pyridyl DG were unsuccessful (entries 2 and 3). The reaction conversion was improved to 22% when **28a** (2.0 equiv) was employed

under the reaction shown in entry 4. The identical transformation with methyl acrylate (**28b**, 2.0 equiv) could enhance the conversion to 27% (entry 5). Finally, loading of 2-Cl-BQ 50 mol% led to (S)-**29b** (96% ee, s factor of 85 with 34% conversion; entry 6, **Table II.4**) and found optimum.

Table II.4. Directing group screening [a]

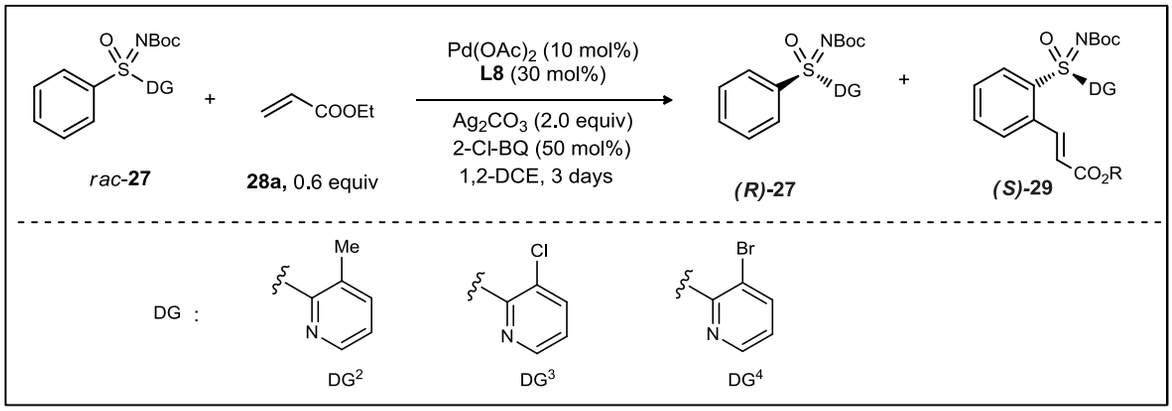

Entry	DG	Conversion[b]	*ee* [%][c]		*s*[d]
			(R)- 27	*(S)*-29	
1	DG^2	17	20	96	58
2	DG^3	nr	–	–	–
3	DG^4	nr	–	–	–
4[e]	DG^2	22	27	95	48
5[f]	DG^2	27			
6[f,g]	DG^2	34			

[a]Reaction conditions: **rac-27** (0.1 mmol), acrylate **28** (0.6 equiv), $Pd(OAc)_2$ (10 mol%), **L8** (30 mol%), Ag_2CO_3 (2.0 equiv), additives (0.3 equiv), 1,2-DCE (1.0 mL), N_2, 75 °C, 3 days. [b]Calculated conversion, C = eeSM/(eeSM + eePR). [c]Determined by chiral HPLC analysis. [d]Selectivity factor (*s*) = ln[(1 − C)(1 − eeSM)]/ln[(1 − C)(1 + eeSM)]. [e]Ethyl acrylate (2.0 equiv) was used. [f]Methyl acrylate instead ethyl acrylate. [g]2-Cl-BQ (50 mol%) was used.

II.4.3.2 Optimization of reaction conditions (arylation):

Next, we investigated the feasibility of Pd-catalyzed C–H arylative KR of sulfoximines (**Table II.5–Table II.8**). The reaction of N-Boc-3-methoxyphenyl-2-(3-methylpyridyl) sulfoximine (**27b**) with (4-CF_3)Ph-Bpin (**31a**; 2.0 equiv) was performed under the catalytic conditions of **Table II.5**. Pleasingly, the desired product (*S*)-**30a** was obtained

in 94% ee with *s* factor of 39 along with the recovery of (*R*)-**27b** in 20% ee and 18% conversion (entry 1, **Table II.5**). The oxidant Ag_2O played a vital role; conversion was increased to 51% (entry 2, **Table II.5**). Carrying out the reaction at 60 °C enhanced the *s* factor to 50 (entry 4, **Table II.5**). The s factor was raised to 64 with reaction conversion 41% and 94% ee of (*S*)-**30a**, when trifluorotoluene (TFT) was used (entry 1, **Table II.6**). Performing the reaction with 20 mol% of **L8** improved the outcome (entry 3, **Table II.7**). Importantly, reaction concentration from 0.1 M to 0.067 M led to (*S*)-**30a** (94% ee) and (*R*)-**27b** (88% ee) with 48% conversion and *s* factor of 95 (entry 3, **Table II.8**).

Table II.5. Oxidant screening[a]

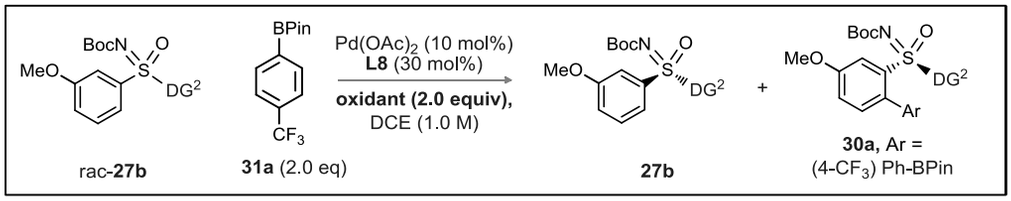

Entry	Oxidant	Conversion (c)[b]	*ee* [%][c]		*s*[d]
			(R)-1b	*(S)*-5a	
1	Ag_2CO_3	18	20	94	39
2	Ag_2O	51	88	86	38
3	AgOAc	12	12	90	21
4[e]	Ag_2O	43	70	92	50

[a]Reaction conditions: *rac*-**27b** (0.1 mmol), **31a** (2.0 equiv), $Pd(OAc)_2$ (10 mol%), **L8** (30 mol%), oxidant (2.0 equiv), 2-Cl-BQ (0.5 equiv), 1,2-DCE (1.0 mL), N_2, 75 °C, 3 days. [b]Calculated conversion, C = eeSM/(eeSM + eePR). [c]Determined by chiral HPLC analysis. [d]Selectivity factor (*s*) = ln[(1 − C)(1 − eeSM)]/ln[(1 − C)(1 + eeSM)]. [e]Reaction is performed in 60 °C.

Table II.6. Solvent screening[a]

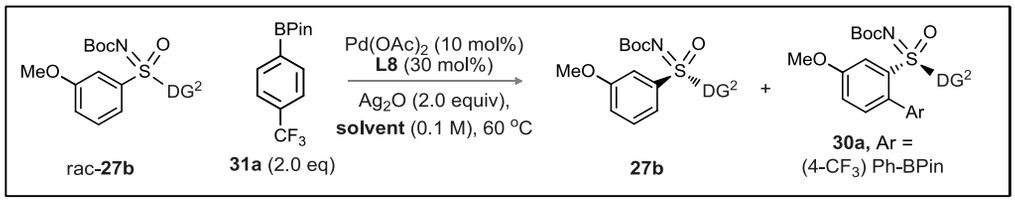

Entry	Solvent	Conversion	*ee* [%][c]	*s*[d]

		(c)[b]	*(R)*-1b	*(S)*-5a	
1	TFT	41	66	94	64
2	THF	31	44	96	75
3	*t*-Amyl-OH	36.0	54	96	84

[a]Reaction conditions: *rac*-**27b** (0.1 mmol), **31a** (2.0 equiv), $Pd(OAc)_2$ (10 mol%), **L8** (30 mol%), Ag_2O (2.0 equiv), 2-Cl-BQ (0.3 equiv), 1,2-DCE (1.0 mL), N_2, 75 °C, 3 days. [b]Calculated conversion, C = eeSM/(eeSM + eePR). [c]Determined by chiral HPLC analysis. [d]Selectivity factor (*s*) = ln[(1 − C)(1 − eeSM)]/ln[(1 − C)(1 + eeSM)].

Table II.7. Screening of ligand loading[a]

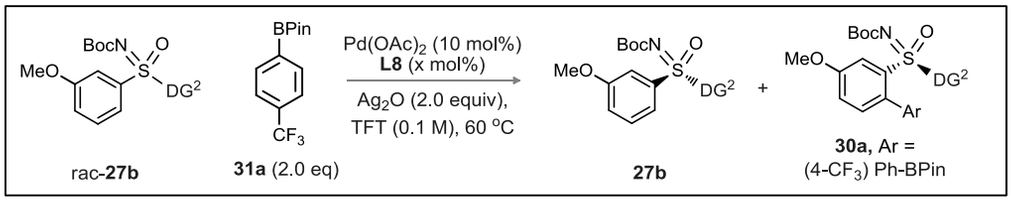

Entry	Ligand loading (x mol%)	Conversion (c)[b]	*ee* [%][c]		*s*[d]
			(R)-1b	*(S)*-5a	
1	10 mol%	41	64	94	62
2	15 mol%	42	68	94	66
3	20 mol%	46	80	94	79
4	40 mol%	40	62	94	61

[a]Reaction conditions: *rac*-**27b** (0.1 mmol), **31a** (2.0 equiv), $Pd(OAc)_2$ (10 mol%), **L8** (x mol%), Ag_2O (2.0 equiv), 2-Cl-BQ (0.3 equiv), 1,2-DCE (1.0 mL), N_2, 75 °C, 3 days. [b]Calculated conversion, C = eeSM/(eeSM + eePR). [c]Determined by chiral HPLC analysis. [d]Selectivity factor (*s*) = ln[(1 − C)(1 − eeSM)]/ln[(1 − C)(1 + eeSM)].

Table II.8. Screening of solvent loading[a]

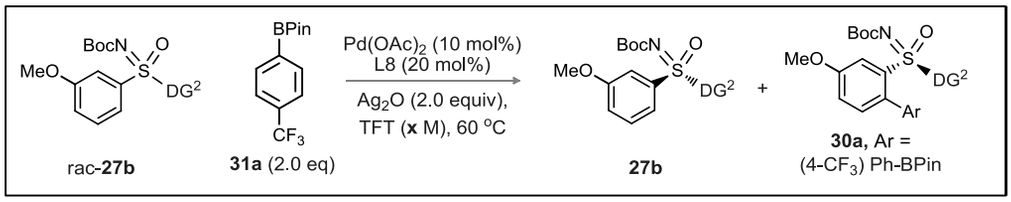

Entry	Molarity	Conversion	*ee* [%]c	s[d]

		(c)[b]	*(R)*-1b	*(S)*-5a	
1	0.2 M	41	64	94	62
2	0.13 M	41	66	94	64
3	0.067 M	48	88	94	95
4	0.05 M	47	84	94	86

[a]Reaction conditions: *rac*-**27b** (0.1 mmol), **31a** (2.0 equiv), $Pd(OAc)_2$ (10 mol%), **L8** (20 mol%), Ag_2O (2.0 equiv), 2-Cl-BQ (0.3 equiv), 1,2-DCE (x M), N_2, 75 °C, 3 days. [b]Calculated conversion, C = eeSM/(eeSM + eePR). [c]Determined by chiral HPLC analysis. [d]Selectivity factor (*s*) = ln[(1 − C)(1 − eeSM)]/ln[(1 − C)(1 + eeSM)].

II.4.4. Reaction scope-I

The reaction generality of Pd-catalyzed C–H alkenylative KR of sulfoximines was then surveyed (**Table** II.9).[10] Compound **29b** (98.2:1.8 er) was isolated in 26% yield. The alkenylation occurred at the less-hindered arene C–H bond and the chiral sulfoximines **29c** and **29d** were obtained with *s* factors of 162 and 140, respectively. The catalytic system was compatible with common functional groups, such as ketone, sulfone and phosphate in the alkene, providing access to **29e** (95.6:4.4 er), **29f** (94.6:5.4 er) and **29g** (97.6:2.4 er). *Notably, the reaction of methyl vinyl sulfone with* ***27b*** *displayed an exceptional s factor of >200 for compound* ***29h****.* The reaction of *p*-(Me/^{t}Bu/^{i}Pr)-substituted aryl sulfoximines with **28b/** vinyl-ketone (**28c**)/ vinyl-sulfone (**28f**) smoothly delivered **29i**–**m** in excellent enantioselectivity and *s* factor of 55 to >200. The *m*-substituted electron donating (OEt, Me) and chloro bearing aryl-sulfoximines underwent olefination with **28b** to give the desired products **29n**–**p** with *s* factor of 24 to 111. The low yield of **29p** (22%; 94.4:5.6 er) is justified by a conversion of 28%, which can be attributed to electron deactivation by the halo group and the possibility for the formation of cross-coupled side product. Even the sterically hindered *m*,*m*'-dimethyl substituted aryl sulfoximine **27i** reacted well, yielding **29q** (36%, 97.9:2.1 er, *s* factor of 107).

Table II.9. Scope of C–H alkenylative kinetic resolution of sulfoximines[a],[c]

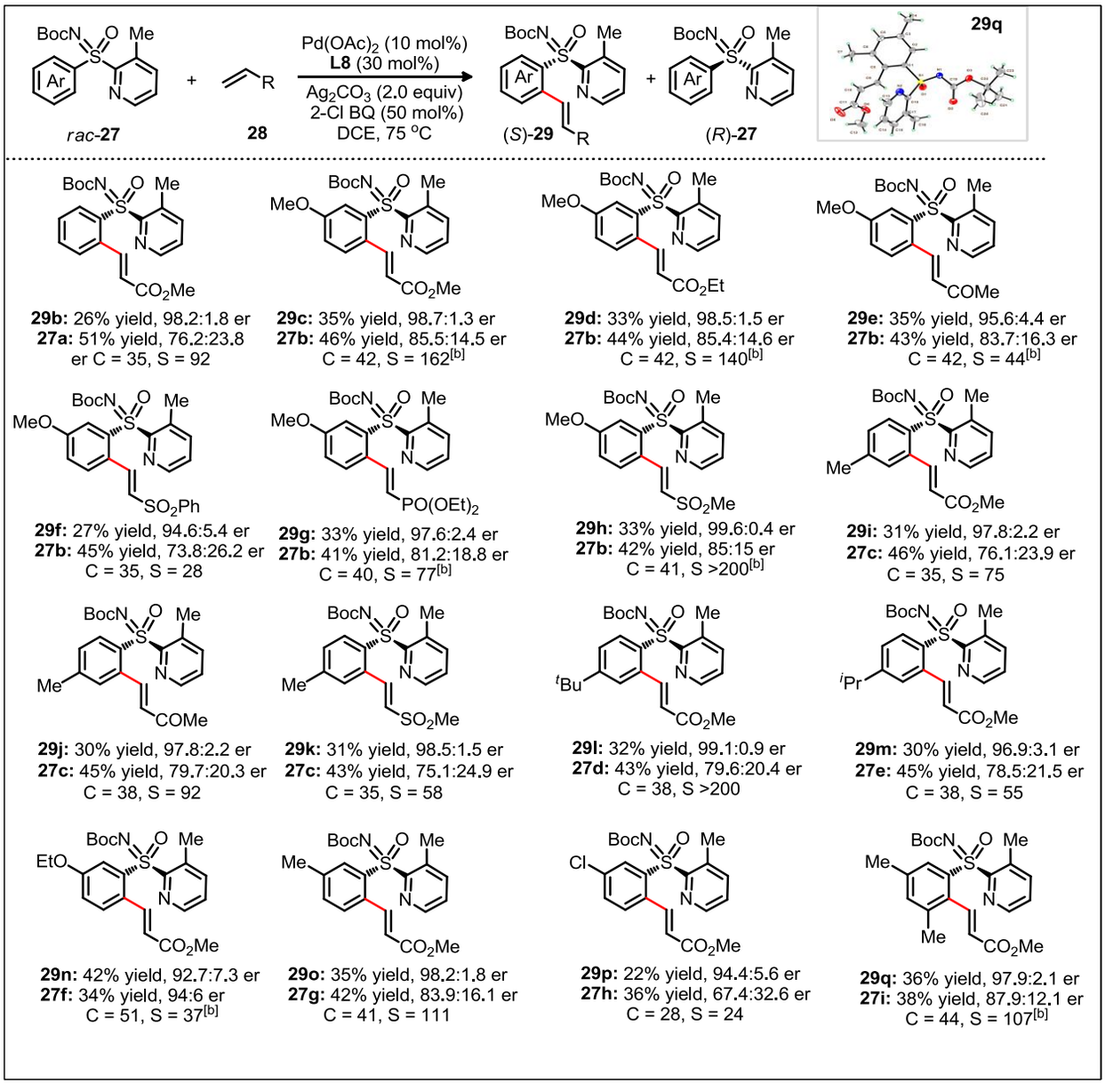

[a]Reaction conditions: *rac*-**27** (0.25 mmol), olefin (2.0 equiv), $Pd(OAc)_2$ (10 mol%), **L8** (30 mol%), Ag_2CO_3 (2.0 equiv), 2-Cl-BQ (0.5 equiv), 1,2-DCE (2.5 mL), 75 °C, 3 days. [b]Olefin (1.8 equiv) was used. [c]Yield of the isolated olefinated product. Calculated conversion, C = eeSM/(eeSM + eePR). enantiomeric ratio (er) was determined by chiral HPLC analysis. Selectivity factor (*s*) = ln[(1 − C)(1 − eeSM)]/ln[(1 − C)(1 + eeSM)].

II.4.5. Reaction scope-II

We next probe sulfoximines KR via enantioselective C−H arylation with arylpinacol boronate esters (**Table** II.10).

Table II.10. Scope of C–H arylative kinetic resolution of sulfoximines[a],[b]

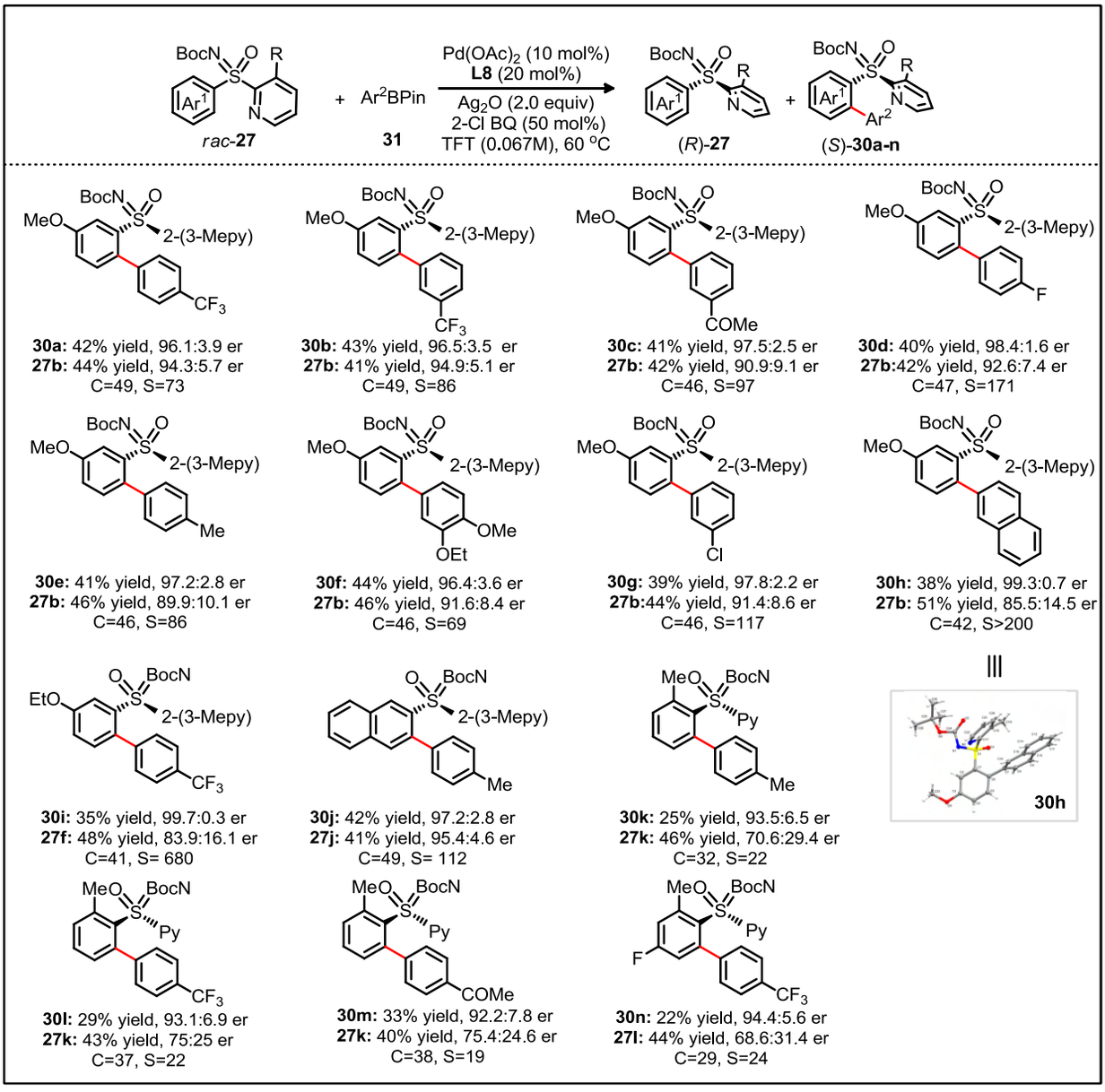

[a]Reaction conditions: *rac*- **17** (0.2 mmol), **31** (2.0 equiv), $Pd(OAc)_2$ (10 mol%), **L8** (20 mol%), Ag_2O (2.0 equiv), 2-Cl-BQ (0.5 equiv), TFT (3.0 mL), 60 °C, 3 days. [b]Yield of the isolated arylation product. Calculated conversion, C = eeSM/(eeSM + eePR); Enantiomeric ratio (er) was determined by chiral HPLC analysis;. Selectivity (s) = ln[(1 − C)(1 − eeSM)]/ln[(1 − C)(1 + eeSM)]

At first, the reaction of **17b** with various arylpinacol boronate esters having electron withdrawing groups [*p*-CF_3 (**31a**), *m*-CF_3 (**31b**), *m*-COMe (**31c**) and *p*-F (**31d**)], electron donating groups [*p*-Me (**31e**), and *p*-OMe-*m*-OEt (**31f**))] at the aryl motif independently

led to the arylative resolution products **30a** (96.1:3.9 er, 42%), **30b** (96.5:3.5 er, 43%), **30c** (97.5:2.5 er, 41%), **30d** (98.4:1.6 er, 40%), **30e** (97.2:2.8 er, 41%), and **30f** (96.4:3.6 er, 44%), respectively, with *s* factor of 69–171 and conversion 46–49%. Moreover, the precursor (*R*)-**17b** was isolated in 41–46% yield with good enantioselectivity. The labile –Cl group was tolerated under the Pd-catalytic system, making **30g** (97.8:2.2 er, 39%) with an *s* factor of 117. Notably, –conjugated naphthyl-enabled sulfoximine resolution product **30h** (99.0:1.0 er, *s* factor of >200) was reliably accessed. *The arylation of m-OEt-phenyl bearing sulfoximine* ***1c*** *with* ***31a*** *provided* ***30i*** *(>99% ee) with s factor of >200.* Likewise, **30j** (97.2:2.8 er, *s* factor of 112) was made from the arylation of 2-naphthyl containing sulfoximine **17j** with **31e**. The steric bulkiness in aryl-motifs exerts influence on C–H functionalizations. Despite the challenges, *o*-tolyl enabled sulfoximines, **17k** and **17l**, were successful in undergoing arylation with **31a**/**31c**/**31e** to afford **30k**–**n** in good enantioselectivity; the moderate *s* factor of 19–24 and conversion (*c* 29–38%) is considered suitable.

II.4.6. DFT studies

We performed a theoretical study to unveil the reaction mechanism (**Figure II.2**).[12,13] The MPAA ligand coordination to the metal center lowers the energy barrier of the CMD step, forming a semi planar five membered ring.[12] The coordination of both nitrogen atoms in sulfoximine **27a** forms **int-0** with the displacement of acetic acid, where the *S*-configuration at sulfur is 1.0 kcal/mol more stable than the *R* one. Prior to deprotonation, a *cis* coordination of aryl group to the *N*-protected moiety of the MPAA-ligated intermediate occurs. This assists the CMD process by establishing the absolute configuration of the sulfur motif. This calculation fully complies with the experimental observations of the resolution selectivity (calc. 98:2, exp. 98:2; **Figure II.2**a-III).

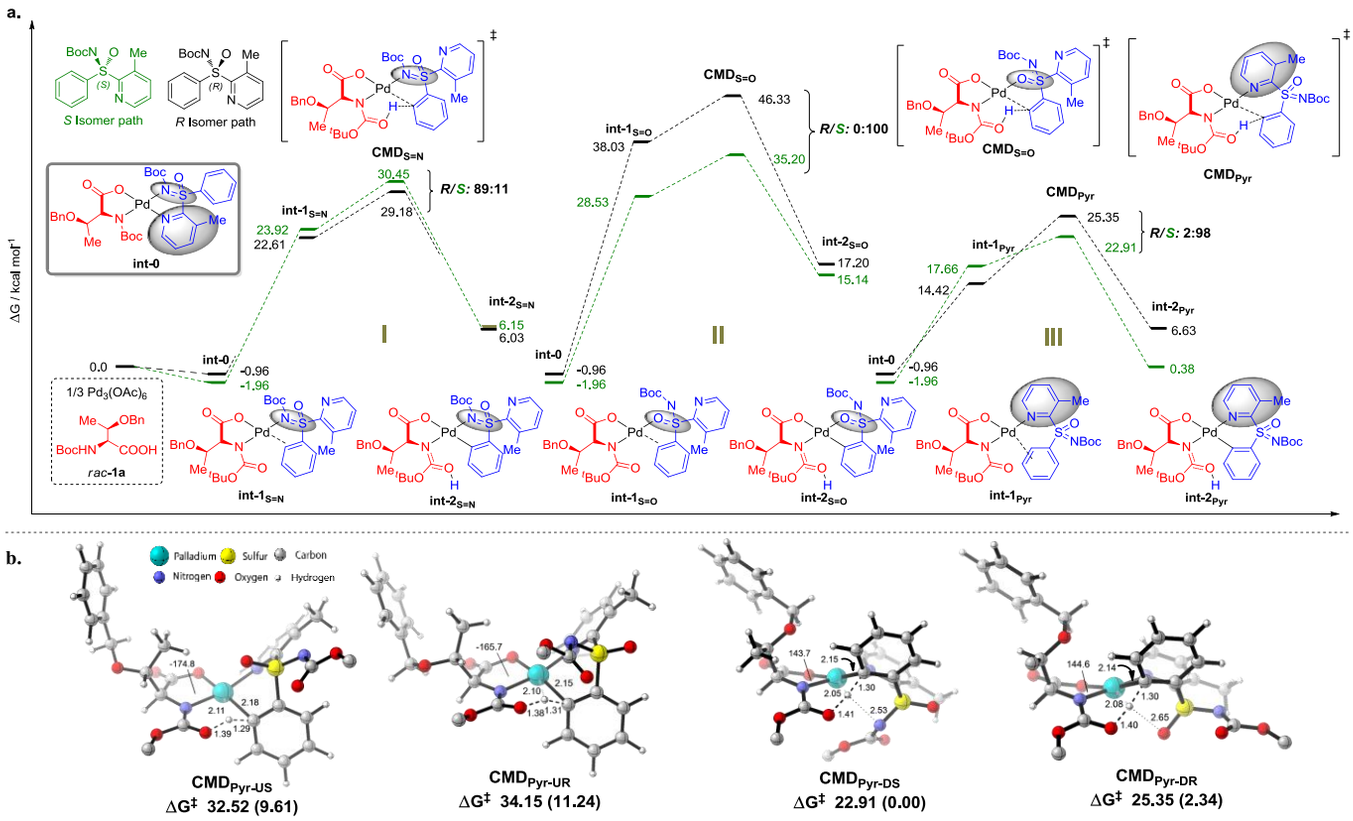

Figure II.2. [a]Free enegy profile, [b]Transition structures for each **CMD$_{Pyr}$** approach. *tert*-Butyl group from NBoc removed from all models to simplify visualization. Free energies in kcal/mol, distances in Å. Free energies at 343.15 K in DCE in kcal/mol. Relative free energies in parenthese.

Notably, the experimentally observed ***S*-int-2$_{Pyr}$** is thermodynamically favored over ***R*-int-2$_{Pyr}$** isomer by 6 kcal/mol. In retrospect, the CMD transition states of **int-1$_{S=N}$** (**Figure II.2a-I**) and **int-1$_{S=O}$** (**Figure II.2a-II**) lie much higher than **int-1$_{Pyr}$** (**Figure II.2a-III**), and their respective $G^{\neq}$ do not coincide with the experimental findings. We believe the CMD step could be responsible for the kinetic resolution. This hypothesis has been previously validated by Cheng *et al*, who also focused their study on the CMD as determining step.[12] Based on their findings, and considering the plane defined by the coordination of MPAA to the Pd, the bulky –side chain of the ligand (above the plane) pushes the N-Boc moiety down to avoid steric hindrance (**Figure II.2b** and **Figure II.1-B**). Thus, sulfoximine phenyl group coordination complex with Pd-MPAA can point upward (U) or downward (D) on the plane, with *R* or *S* configurations. This translates

to four possible CMDs: **CMD$_{Pyr\text{-}UR}$**, **CMD$_{Pyr\text{-}US}$**, **CMD$_{Pyr\text{-}DR}$** and **CMD$_{Pyr\text{-}DS}$**. The CMDs adopt a 6-membered palladacycle with twisted boat conformation. In case of upward phenyl group linkage (**CMD$_{Pyr\text{-}UR}$** and **CMD$_{Pyr\text{-}US}$**), the sulfur atom and its substituents are located above the plane; while these substituents are below the plane for **CMD$_{Pyr\text{-}DR}$** and **CMD$_{Pyr\text{-}DS}$**. In agreement with Cheng's observations,[12] the C1-N2-Pd-O3 dihedral angle for **CMD$_{Pyr\text{-}UR}$** and **CMD$_{Pyr\text{-}US}$** is *ca* 170°, which generates a high steric interaction when compared with the *ca* 140° for **CMD$_{Pyr\text{-}DR}$** and **CMD$_{Pyr\text{-}DS}$**. These latter are favored by hydrogen bond interactions, making the combination of steric and electronic effects accounting for a difference of nearly 10 kcal/mol in each enantiomer. The preference for the *S* configuration by ~2.5 kcal/mol over the *R* isomer, lies in a steric clash of the NBoc group with the methyl group from the pyridine moiety and in consequence with the phenyl group, causing an energetically demanding arrangement.

Based on the literature, which included experimental observations, it is known that insertion/elimination steps come right after the CMD.[12] To corroborate our selectivity findings, we studied the mechanism for the insertion step in the Pyr and N=O series. Analysis of the transition states revealed that, as in the CMD case, pyridine acting as a directing group provides the lowest energy barriers (24.28 kcal/mol for the *S* isomer and 28.67 kcal/mol for the *R* isomer). The study of this step confirms the selectivity observed at the CMD and shows the irreversibility of the reaction.

II.4.7. Application

The synthetic potential of chiral sulfoximine was next probed (**Scheme II.13**). The trifuloroacetic acid (TFA) mediated *N*-Boc deprotection of (*R*)-**27b** provided chiral sulfoximine (*R*)-**32** (95% ee). Next, reduction of (*R*)-**32** led to chiral sulfoxide (*R*)-**33** (90% ee) when exposed to *t*-BuNO_2 at rt for 2 h; chiral integrity of S-motif is preserved. The N-Boc deprotection and intramolecular Michael cyclization to the activated olefin-moiety of (*S*)-**29c** was smooth delivering **34** (as a single diastereomer) in 95% ee. A one-

pot TFA assisted N-Boc deprotection and oxidative intramolecular C–N bond formation of (*S*)-**30d** furnished (*S*)-**35** (93% ee, 62% yield).

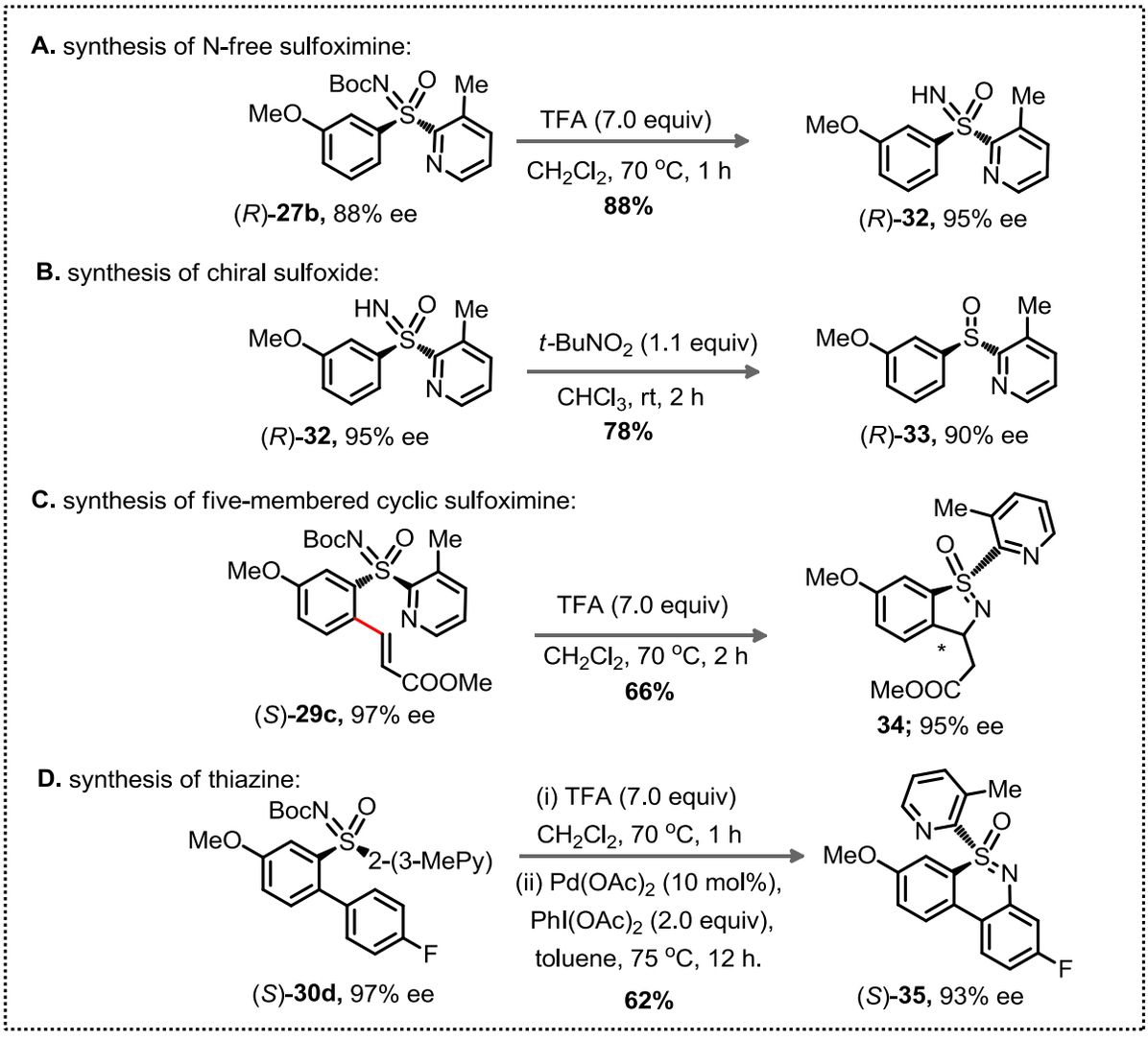

Scheme II.13: Derivatization of Chiral Product

II.5. Conclusion

In summary, a Pd(II)-catalyzed pyridyl substituted KR of sulfoximines through C(aryl –H alkenylation and arylation has been revealed for the first time. The transformation addresses the inherent challenges in the KR of coordinatively active pyridyl-enabled sulfoximines (highly susceptible to TM-catalyst quenching) with no

prochiral center in the presence of chiral amino acid MPAA ligands and Pd(II)-catalyst. The common functional groups were tolerated under Pd-catalysis exhibiting good substrate scope for C–H alkenylative and arylative sulfoximines KR products in high enantioselectivity with *s* factor up to >200. In-depth DFT studies uncover the salient features of coordination selectivity of pyridyl-group over sulfoximine imine.

II.6. Experimental

II.6.1. General Experimental Information:

All the reactions were performed in oven-dried screw capped tubes. Commercial grade solvents were distilled prior to use. Column chromatography was performed using either 100–200 Mesh or 230–400 Mesh silica gel. Thin layer chromatography (TLC) was performed on silica gel GF254 plates. Visualization of spots on TLC plates was accomplished with UV light (254 nm) and staining over I_2 chamber.

Proton, carbon, and fluorine nuclear magnetic resonance spectra (^{1}H NMR, ^{13}C NMR, and ^{19}F NMR) were recorded based on the resonating frequencies as follows:(^{1}H NMR, 400 MHz; ^{13}C NMR, 101 MHz; ^{19}F NMR, 376 MHz) and (^{1}H NMR, 500 MHz; ^{13}C NMR, 126 MHz; ^{19}F NMR, 470 MHz) having the solvent resonance as internal standard (^{1}H NMR, $CDCl_3$ at 7.26 ppm; ^{13}C NMR, $CDCl_3$ at 77.0 ppm). In few cases, tetramethylsilane (TMS) was used as reference standard at 0.00 ppm. Data for ^{1}H NMR are reported as follows: chemical shift (ppm), multiplicity (s singlet; bs broad singlet; d doublet; bd broad doublet, t triplet; bt broad triplet; q quartet; m multiplet), coupling constants, *J*, in (Hz), and integration. Data for ^{13}C NMR, ^{19}F NMR were reported in terms of chemical shift (ppm). IR spectra were reported in cm□1. LC–MS spectra were obtained with ionization voltage of 70 ev; data was reported in the form of *m/z* (intensity relative to base peak 100). Melting points were determined by electro–thermal heating and are uncorrected. High resolution mass spectra were obtained in ESI mode. X-ray data was collected at 298K using graphite monochromated Mo–K radiation (0.71073 Å).

Enantiomeric ratios (er) were determined on a Shimadzu LC-20AD HPLC system using commercially available chiral columns. All racemic products were prepared under the same procedure than the chiral products although with the employment of a racemic monoprotected amino acid ligand.

II.6.2. Materials

Unless otherwise noted, all the reagents and intermediates were obtained commercially and used without purification. Dichloromethane (DCM), 1,2-dichloroethane (DCE), and 1,4-dioxane were distilled over CaH_2. $Pd(OAc)_2$, trifluoro toluene (TFT), quinones, acrylates, boronic acids and amino acid ligands were purchased from Sigma Aldrich Ltd, and used as received. Analytical and spectral data of all the known compounds are exactly matching with reported values.

II.6.3. Experimental Procedures and Analytical Data:

II.6.3.1. General procedure for the synthesis of racemic (rac) 27a–27l (GP-1):[1]

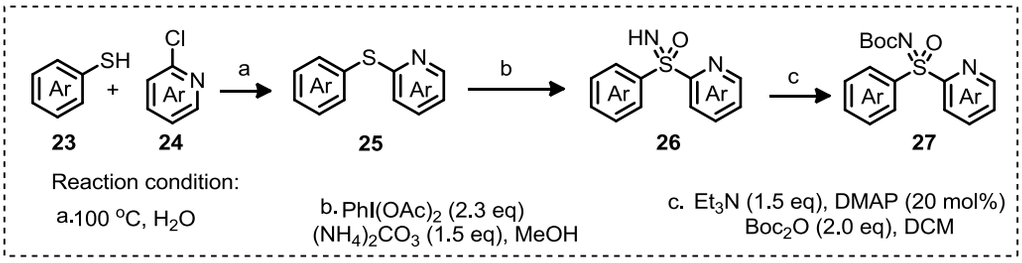

A suspension mixture of thiol **23** (5.5 mmol) and substituted-2-chloro pyridine **24** (5.0 mmol) in H_2O (5.0 mL) was taken in a 50 mL screw capped tube and stirred at 100 °C for 6 h. After reaction completion, the product was extracted with EtOAc (2 × 100 mL). Then the combined organic extracts were washed with $NaHCO_3$ solution (2 × 100 mL). Finally the organic layer was dried over Na_2SO_4. The solvent was removed under reduced pressure to give the crude sulfide product **25**, which was used for the next step without further purification.

To a stirred solution of sulfide **25** in MeOH (10 mL) was added $(NH_4)_2CO_3$ (0.72 g, 7.5 mmol). Subsequently, $PhI(OAc)_2$ (3.7 g, 11.5 mmol) was added and the resulting mixture was stirred at rt. Upon disappearance of sulfide (checked by TLC), the solvent was removed under reduced pressure. The phenyl iodide and other non polar impurities were eliminated though a short column filtration eluenting with hexane: ethyl acetate 90:10 mixture at first and then with 100% ethyl acetate. The crude sulfoximine product **26** was collected; which was used for the next step without further purification.

To a stirred solution of crude sulfoximine **26** in dry CH_2Cl_2 (100 mL) was added triethylamine (10 mmol) and 4-N,N-dimethylamino pyridine (DMAP; 1.0 mol %). The reaction mixture was stirred for 30 min at 0 °C. Next, a solution of Boc_2O (10 mmol) in dry CH_2Cl_2 (50 mL) was added. The solution was warmed to rt and stirred for 5 h. Evaporation of organic solvent and purification by column chromatography eluting with hexane: ethyl acetate 3:2 mixture gave the corresponding N-Boc protected aryl-2-pyridyl sulfoximine products **27a**, **27a-1**, **27a–2**, **27a–3**, and **27b–27l**.

N-Boc-protected 3-methyl-2-(phenylsulfonimidoyl)pyridine (27a):

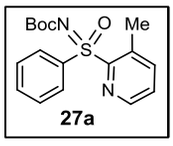

27a

27a (864 mg, 52%) as colorless solid; ^{1}H NMR (400 MHz, $CDCl_3$) δ d, J 4.8 Hz, 1H), 8.10–8.04 (m, 2H), 7.63–7.55 (m, 2H), 7.54–7.46 (m, 2H), 7.32–7.24 (m, 1H), 2.74 (s, 3H), 1.31 (s, 9H); ^{13}C NMR (101 MHz, $CDCl_3$) δ 157.4, 155.1, 146.4, 141.7, 136.9, 135.0, 133.5, 129.2, 128.8, 126.5, 80.3, 27.8, 19.1; IR (KBr) $_{max}$ 2918, 2850, 1734, 1464, 1261, 1150, 804 cm^{-1}; **HRMS (ESI)** for $C_{17}H_{20}N_2NaO_3S$ $(M+Na)^+$: calcd. 355.1087, found 355.1096.

N-Boc-protected 2-(phenylsulfonimidoyl)pyridine (27a-1):

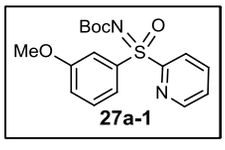

27a-1

27a-1 (860 mg, 54%) as colorless solid; ^{1}H NMR (500 MHz, $CDCl_3$) δ – m, 1H), 8.35–8.29 (m, 1H), 8.15– 08 (m, 2H), 7.91 (t, J 7.75 Hz, 1H), 7.61–7.54 (m, 1H), 7.50 (t, J 7.5 Hz, 2H), 7.45–7.39 (m, 1H),

1.31 (s, 9H); ^{13}C NMR (126 MHz, $CDCl_3$) δ157.9, 157.3, 150.2, 138.1, 136.7, 133.6, 129.04, 129.00, 126.6, 123.4, 80.6, 27.8; IR (KBr) $_{max}$ 2976, 1677, 1451, 1238, 911 cm^{-1}; **HRMS (ESI)** for $C_{16}H_{18}N_2NaO_3S^+$(M+H)$^+$: calcd. 341.0930, found 341.0944.

N-Boc-protected 3-chloro-2-(phenylsulfonimidoyl)pyridine (27a-2):

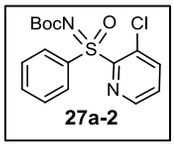

27a-2

27a-2 (864 mg, 49%) as pale-yellow solid; ^{1}H NMR (500 MHz, $CDCl_3$) δ 8.61–8.55 (m, 1H), 8.17–8.11 (m, 2H), dt, *J* 8.0, 1.2 Hz, 1H), 7.64–7.57 (m, 1H), 7.54–7.47 (m, 2H), dd, *J* 8.0, 4.5 Hz, 1H), 1.34 (s, 9H); ^{13}C NMR (126 MHz, $CDCl_3$) δ156.9, 153.3, 147.2, 140.7, 135.8, 134.0, 130.8, 129.4, 129.0, 127.7, 80.7, 27.8; IR (KBr) $_{max}$ 2977, 2923, 1738, 1700, 1246, 1151, 1084 cm^{-1}.

N-Boc-protected 3-bromo-2-(phenylsulfonimidoyl)pyridine (27a-3):

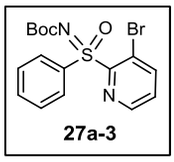

27a-3

27a-3 (1.05 g, 53%) as yellow solid; ^{1}H NMR (500 MHz, $CDCl_3$) δ dd, *J* 4.5, 1.0 Hz, 1H), 8.21–8.16 (m, 2H), dd, *J* 7.75, 0.75 Hz, 1H), t, *J* 7.5 Hz, 1H), t, *J* 8.0 Hz, 2H), dd, *J* 8.0, 4.5 Hz, 1H), 1.37 (s, 9H); ^{13}C NMR (126 MHz, $CDCl_3$) δ156.9, 154.8, 147.7, 144.3, 135.9, 134.0, 129.6, 129.0, 127.5, 118.6, 80.8, 27.9; IR (KBr) $_{max}$ 2980, 2926, 1665, 1273, 1247, 1153 cm^{-1}.

N-Boc-protected 2-(3-methoxyphenylsulfonimidoyl)-3-methylpyridine (27b):

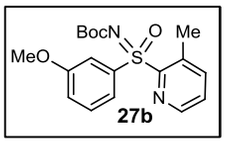

27b

27b (761 mg, 42%) as colorless solid. ^{1}H NMR (500 MHz, $CDCl_3$) δ d, *J* 4.5 Hz, 1H), 7.67–7.59 (m, 2H), 7.58 (t, *J* 2.25 Hz, 1H), 7.41 (t, *J* 8.0 Hz, 1H), 7.30 (dd, *J* 7.5, 4.5 Hz, 1H), 7.14–7.08 (m, 1H), 3.82 (s, 3H), 2.75 (s, 3H), 1.33 (s, 9H); ^{13}C NMR (126 MHz, $CDCl_3$) δ159.7, 157.4, 155.2, 146.4, 141.7, 138.3, 134.9, 129.7, 126.5, 121.5, 120.1, 113.7, 80.3, 55.7, 27.9, 19.1; IR (KBr) $_{max}$ 2970, 2926, 1739, 1649, 1367, 1241, 1038 cm^{-1}; **HRMS (ESI)** for $C_{18}H_{22}N_2NaO_4S^+$ (M+Na)$^+$: calcd. 385.1192, found 385.1202.

N-Boc-protected 3-methyl-2-(4-methylphenylsulfonimidoyl)pyridine (27c):

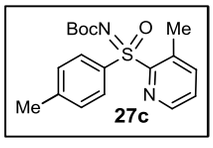

27c

27c (831 mg, 48%) as colorless solid. ^{1}H NMR (400 MHz, $CDCl_3$) δ (d, *J* 4.0 Hz, 1H), 7.97–7.91 (m, 2H), 7.59 (d, *J* 7.2 Hz, 1H), 7.32–7.24 (m, 3H), 2.72 (s, 3H), 2.38 (s, 3H), 1.31 (s, 9H); ^{13}C NMR (101 MHz, $CDCl_3$) δ157.5, 155.3, 146.3, 144.5, 141.6, 134.7, 133.7, 129.4, 129.1, 126.4, 80.2, 27.8, 21.5, 19.1; IR

(KBr) $_{max}$ 2980, 2923, 2847, 1664, 1272, 1152, 1090 cm^{-1}; **HRMS (ESI)** for $C_{18}H_{22}N_2NaO_3S^+$ $(M+Na)^+$: calcd. 369.1243, found 369.1258.

N-Boc-protected 2-(4-(tert-butyl)phenylsulfonimidoyl)-3-methylpyridine (27d):

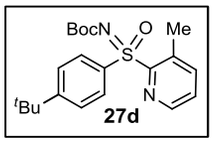

27d (1.01 g, 52%) as colorless solid; ^{1}H NMR (400 MHz, $CDCl_3$) δ d, J 4.4 Hz, 1H), 8.04–7.97 (m, 2H), 7.62 (d, J 7.6 Hz, 1H), 7.56–7.50 (m, 2H), 7.31 (dd, J z, 1H), 2.76 (s, 3H), 1.34 (s, 9H), 1.32 (s, 9H); ^{13}C NMR (101 MHz, $CDCl_3$) δ157.6, 157.4, 155.5, 146.5, 141.6, 134.9, 133.9, 129.1, 126.4, 125.9, 80.3, 35.2, 31.0, 27.9, 19.3; IR (KBr) $_{max}$ 2968, 1699, 1239, 1223, 1148, 1069, 909 cm^{-1}; **HRMS (ESI)** for $C_{21}H_{28}N_2NaO_3S^+$ $(M+Na)^+$: calcd. 411.1713, found 411.1724.

N-Boc-protected 2-(4-isopropylphenylsulfonimidoyl)-3-methylpyridine (27e):

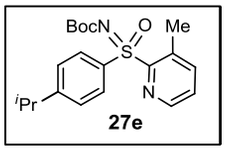

27e (1.05 g, 56%) as light red solid; ^{1}H NMR (400 MHz, $CDCl_3$) δ d, J 4.4 Hz, 1H), 8.03–7.96 (m, 2H), 7.61 (d, J 7.6 Hz, 1H), 7.37 (d, J 8.8 Hz, 2H), 7.30 (dd, J 7.8, 4.6 Hz, 1H), 3.03–2.89 (m, 1H), 2.75 (s, 3H), 1.34 (s, 9H), 1.24 (d, J 7.2 Hz, 6H); ^{13}C NMR (101 MHz, $CDCl_3$) δ157.6, 155.5, 155.1, 146.5, 141.6, 134.9, 134.2, 129.4, 127.0, 126.4, 80.3, 34.2, 27.9, 23.5, 19.3; IR (KBr) $_{max}$ 2970, 1663, 1269, 1245, 1151, 1093, 896 cm^{-1}; **HRMS (ESI)** for $C_{20}H_{27}N_2O_3S^+$ $(M+H)^+$: calcd. 375.1737, found 375.1747.

N-Boc protected 2-(3-ethoxyphenylsulfonimidoyl)-3-methylpyridine (27f):

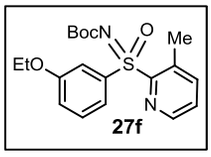

27f (866 mg, 46%) as yellow solid; ^{1}H NMR (400 MHz, $CDCl_3$) δ –8.35 (m, 1H), 7.67–7.55 (m, 3H), 7.44–7.36 (m, 1H), 7.34–7.27 (m, 1H), 7.14–7.07 (m, 1H), 4.05 (q, J 7.07 Hz, 2H), 2.75 (s, 3H), 1.38 (t, J 7.0 Hz, 3H), 1.33 (s, 9H); ^{13}C NMR (101 MHz, $CDCl_3$) δ159.1, 157.4, 155.2, 146.4, 141.7, 138.1, 134.9, 129.7, 126.5, 121.3, 120.6, 114.3, 80.3, 64.0, 27.9, 19.2, 14.5; IR (KBr) $_{max}$ 2980, 2929, 1671, 1598, 1471, 1245, 1154 cm^{-1}; **HRMS (ESI)** for $C_{19}H_{24}N_2NaO_4S^+$ $(M+Na)^+$: calcd. 399.1349, found 399.1358.

N-Boc protected 3-methyl-2-(3-methylphenylsulfonimidoyl)pyridine (27g):

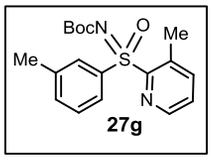

27g (883 mg, 51%) as colorless solid; ^{1}H NMR (500 MHz, $CDCl_3$) δ d, J 4.0 Hz, 1H), 7.93–7.84 (m, 2H), 7.61 (d, J 7.5 Hz, 1H), 7.42–7.37 (m, 2H), 7.33–7.27 (m, 1H), 2.75 (s, 3H), 2.39 (s, 3H), 1.33 (s, 9H); ^{13}C NMR (126 MHz, $CDCl_3$) δ157.6, 155.2, 146.5, 141.7, 139.1, 136.8, 135.0, 134.4, 129.4, 128.6, 126.5, 126.3, 80.3, 27.9, 21.3, 19.2; IR (KBr) $_{max}$ 2974, 1671, 1264, 1244, 1145, 1095, 894 cm^{-1}; **HRMS (ESI)** for $C_{18}H_{22}N_2NaO_3S^+$ $(M+Na)^+$: calcd. 369.1243, found 369.1259.

N-Boc protected 2-(3-chlorophenylsulfonimidoyl)-3-methylpyridine (27h):

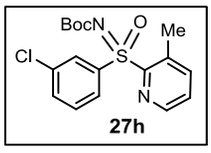

27h (899 mg, 49%) as yellow solid; ^{1}H NMR (500 MHz, $CDCl_3$) δ d, J 5.0 Hz, 1H), 8.12–8.07 (m, 1H), 8.00–7.94 (m, 1H), 7.64 (d, J 8.0 Hz, 1H),7.60–7.54 (m, 1H), 7.47 (t, J 8.0 Hz, 1H), 7.32 (dd, J 7.5 Hz, 1H), 2.79 (s, 3H), 1.34 (s, 9H); ^{13}C NMR (126 MHz, $CDCl_3$) δ157.2, 154.9, 146.4, 141.8, 139.0, 135.3, 135.1, 133.6, 129.9, 129.4, 127.6, 126.7, 80.7, 27.9, 19.1; IR (KBr) $_{max}$ 2977, 2926, 1699, 1666, 1271, 1235, 1147 cm^{-1}; **HRMS (ESI)** for $C_{17}H_{19}ClN_2NaO_3S^+$ $(M+Na)^+$: calcd. 389.0697, found 389.0709.

N-Boc protected 2-(3,5-dimethylphenylsulfonimidoyl)-3-methylpyridine (27i):

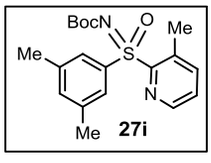

27i (1.03 g, 57%) as colorless solid; ^{1}H NMR (500 MHz, $CDCl_3$) δ d, J 4.5 Hz, 1H), 7.69 (bs, 2H), 7.61 (d, J 7.0 Hz, 1H), 7.30 (dd, J 7.5, 4.5 Hz, 1H), 7.20 (bs, 1H), 2.75 (s, 3H), 2.35 (s, 6H), 1.34 (s, 9H); ^{13}C NMR (126 MHz, $CDCl_3$) δ157.7, 155.3, 146.6, 141.7, 138.9, 136.6, 135.4, 135.0, 126.5, 126.4, 80.3, 27.9, 21.2, 19.3; IR (KBr) $_{max}$ 2977, 2929, 2850, 1741, 1700, 1666, 1273, 1157 cm^{-1}; **HRMS (ESI)** for $C_{19}H_{24}N_2NaO_3S^+$ $(M+Na)^+$: calcd. 383.1400, found 383.1409.

N-Boc protected 3-methyl-2-(naphthalene-2-sulfonimidoyl)pyridine (27j):

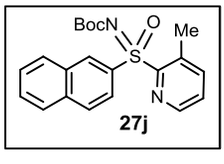

27j (1.16 g, 61%) as colorless solid; ^{1}H NMR (500 MHz, $CDCl_3$) δ s, 1H), 8.37–8.32 (m, 1H), 8.06–8.01 (m, 1H), 8.00–7.91 (m, 2H), 7.90–7.86 (m, 1H), 7.67–7.55 (m, 3H), 7.32–7.26 (m, 1H), 2.82 (s, 3H), 1.35 (s, 9H); ^{13}C NMR (126 MHz, $CDCl_3$) δ157.6, 155.5, 146.4, 141.7, 135.2, 135.1, 134.1, 132.1, 131.0, 129.5, 129.2, 128.9, 127.8, 127.4, 126.4, 124.1, 80.4, 27.9, 19.2; IR (KBr) $_{max}$ 3012, 2970,

2929, 1744, 1662, 1062, 857 cm^{-1}; **HRMS (ESI)** for $C_{21}H_{22}N_2NaO_3S^+$ $(M+Na)^+$: calcd. 405.1243, found 405.1251.

N-Boc-protected 2-(2-methylphenylsulfonimidoyl)pyridine (27k):

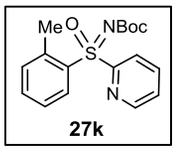

27k

27k (864 mg, 52%) as colorless solid.; ^{1}H NMR (400 MHz, $CDCl_3$) δ d, *J* 4.8 Hz, 1H), 8.44 (d, *J* = 8.0 Hz, 1H), 8.37 (d, *J* 8.0 Hz, 1H), 7.94 (td, *J* 7.8, 1.9 Hz, 1H), 7.52–7.37 (m, 3H), 7.22 (d, *J* 7.6 Hz, 1H), 2.42 (s, 3H), 1.30 (s, 9H); ^{13}C NMR (101 MHz, $CDCl_3$) δ157.4, 156.8, 150.1, 138.4, 137.8, 135.0, 133.7, 132.7, 131.4, 126.8, 126.5, 123.8, 80.5, 27.8, 20.5; IR (KBr) $_{max}$ 2973, 2929, 1666, 1450, 1232, 1142, 752 cm^{-1}.

N-Boc-protected 2-(4-fluoro-2-methylphenylsulfonimidoyl)pyridine (27l):

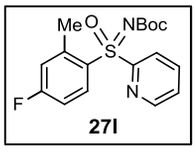

27l

27l (823 mg, 47%) as colorless solid.; ^{1}H NMR (400 MHz, $CDCl_3$) δ bd, *J* 4.8 Hz, 1H), 8.42–8.32 (m, 2H), 7.94 (td, *J* 7.8, 1.7 Hz, 1H), 7.49–7.42 (m, 1H), 7.10–7.01 (m, 1H), 6.91 (dd, *J* 9.2, 2.4 Hz, 1H), 2.39 (s, 3H), 1.29 (s, 9H); ^{13}C NMR (101 MHz, $CDCl_3$) δ165.4 (d, *J* 258 Hz), 157.2, 156.6, 150.1, 141.8 (d, *J* 9.1 Hz), 137.9, 134.3 (d, *J* 10 Hz), 130.6, 126.9, 123.6, 119.5 (d, *J* 22 Hz), 113.6 (d, *J* 22 Hz), 80.5, 27.7, 20.5; ^{19}F NMR (225 MHz, $CDCl_3$) δ ppm: –104.9 (s). IR (KBr) $_{max}$ 2981, 1660, 1576, 1276, 1144, 1118, 856 cm^{-1}.

II.6.3.2. Synthesis of L9 and L10 ligands (GP-2):[2]

To a solution of L-Boc-Thr-OH (5.0 g, 22 mmol) in DMF (80 mL) was added sodium hydride (55% dispersion in mineral oil, 2.1 g, 48 mmol) at –20 °C. After being stirred for 2 h, benzyl bromide derivatives (24 mmol) was added to the reaction. The resulting mixture was stirred at room temperature for 5 h and then quenched with saturated NH_4Cl solution. The reaction mixture was poured into water (100 mL) and washed with diethyl ether (2 × 25 mL). The aqueous solution was acidified with citric acid and extracted with EtOAc (3 × 50 mL). The combined extracts were washed with brine (3 × 30 mL), and then dried over anhydrous Na_2SO_4. The solution was concentrated in reduced pressure and was purified by flash chromatography using a mixture of hexane and EtOAc (2 : 1 v/v) to give a thick colorless syrupy liquid.

2-((*tert*-Butoxycarbonyl)amino)-3-((3,5-difluorobenzyl)oxy)butanoic acid (L9):

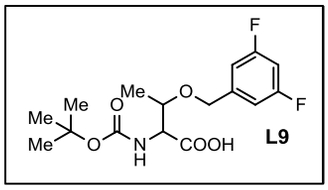

L9: 5.2 g, 68% yield, colorless viscous liquid, **^{1}H NMR (400 MHz, $CDCl_3$)** δ 9.71 (s, 1H), 6.78–6.61 (m, 3H), 5.31 (d, *J* 9.6 Hz, 1H), 4.53 (d, *J* 12.4 Hz, 1H), 4.43–4.33 (m, 1H), 4.20–4.10 (m, 1H), 1.45 (s, 9H), 1.26 (d, *J* = 6.0 Hz, 3H); **^{13}C NMR (101 MHz, $CDCl_3$)** δ 175.8, 162.9 (dd, *J* 249, 12 Hz), 156.2, 141.9 (t, *J* 9.1 Hz), 109.8 (dd, *J* 19, 7.1 Hz), 102.8 (t, *J* 26 Hz), 80.4, 75.2, 69.8, 57.9, 28.2, 16.1; ^{19}F NMR (471 MHz, $CDCl_3$) δ –109.8 (s). IR (KBr) $_{max}$ 2979, 1712, 1627, 1597, 1160, 1115, 847 cm^{-1}; **HRMS (ESI)** for $C_{16}H_{21}F_2NNaO_5^+$ $(M+Na)^+$: calcd. 368.1280, 368.1288.

2-((*tert*-Butoxycarbonyl)amino)-3-((3,5-dimethoxybenzyl)oxy)butanoic acid (L10):

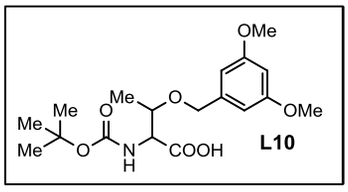

L10: 5.5 g, 68% yield, brown solid, **^{1}H NMR (500 MHz, $CDCl_3$)** δ 6.42 (bd, *J* 2.0 Hz, 2H), 6.35 (s, 1H), 5.36 (d, *J* 9.0 Hz, 1H), 4.50 (d, *J* 12.0 Hz, 1H), 4.38 (d, *J* 12.0 Hz, 1H), 4.33 (d, *J* 9.5 Hz, 1H), 4.20–4.15 (m, 1H), 3.74 (s, 6H), 1.44 (s, 9H), 1.24 (d, *J* = 5.2 Hz, 3H); **^{13}C NMR (101 MHz, $CDCl_3$)** δ 175.2, 160.7, 156.2, 140.1, 105.4, 99.7, 80.1, 74.5, 71.0, 58.0, 55.3, 28.3, 16.2; IR (KBr) $_{max}$ 3433, 2936, 1680, 1597, 1519, 1152, 1053 cm^{-1}; **HRMS (ESI)** for $C_{18}H_{27}NNaO_7^+$ $(M+Na)^+$: calcd. 392.1680, found 392.1689.

II.6.3.3. General procedures for kinetic resolution via Pd-catalyzed C(sp²)–H olefination (GP-3):

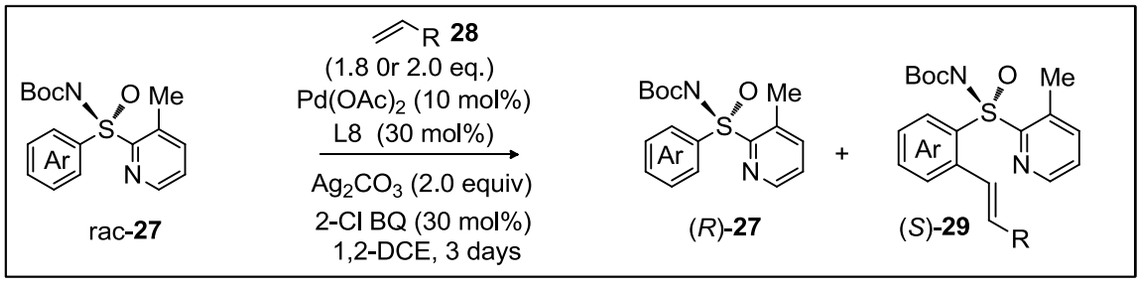

To an oven-dried 10 mL screw-capped vial was added $Pd(OAc)_2$ (0.025 mmol) **L8** (0.075 mmol) and 1,2-DCE (2.5 mL). The mixture was stired for 2 h at 50 °C. The reaction mixture was cooled to rt. The substrate **27** (0.25 mmol), olefin (0.45– 5 mmol), 2-

chlorobenzoquinone (0.075–0.125 mmol), Ag_2CO_3 (0.5 mmol) was then added. The mixture was stirred for 48–72 h at 70 °C. The resulting mixture was then cooled to rt and filtered through a small pad of Celite and concentrated in vacuo. The residue was purified by preparative TLC using hexane/EtOAc as the eluent to afford the chiral product.

_N_-Boc protected (_S,E_)-methyl 3-(2-(3-methylpyridine-2-sulfonimidoyl)phenyl)acrylate (29b):

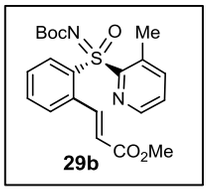

29b: 27 mg, 26% yield, 96% ee, colorless solid, $[\alpha]_D^{25}$ c 0.01, $CHCl_3$); **^{1}H NMR (500 MHz, $CDCl_3$)** δ 8.40 (d, *J* 8.0 Hz, 1H), 8.31–8.23 (m, 2H), 7.65 (t, *J* 7.5 Hz, 2H), 7.60 (t, *J* 8.0 Hz, 2H), 7.31 (dd, *J* 7.5, 5.0 Hz, 1H), 6.11 (d, *J* 15.5 Hz, 1H), 3.74 (s, 3H), 2.86 (s, 3H), 1.33 (s, 9H); **^{13}C NMR (126 MHz, $CDCl_3$)** δ 166.2, 157.0, 155.0, 146.0, 141.8, 141.7, 136.3, 136.2, 135.8, 133.7, 131.0, 129.6, 128.8, 126.6, 122.0, 80.5, 51.8, 27.9, 19.0; IR (KBr) $_{max}$ 3021, 2926, 2853, 1738, 1367, 1216 cm^{-1}; **HRMS (ESI)** for $C_{21}H_{25}N_2O_5S^+$ $(M+H)^+$: calcd. 417.1479, found 417.1487; **HPLC condition**: Daicel IG-3, *i*-PrOH, Flow rate = 0.3 mL/min, UV = 254 nm, tR = 18.6 min (major) and tR = 22.8 min (minor).

_N_-Boc protected (_R_)-3-methyl-2-(phenylsulfonimidoyl)pyridine (27a):

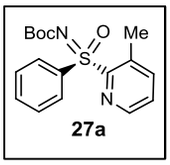

27a: 42 mg, 51% yield, 52% ee; $[\alpha]_D^{25}$ –17.5 (c 0.016, $CHCl_3$); **HPLC condition**: Daicel IG-3, *i*-PrOH, Flow rate = 0.3 mL/min, UV = 254 nm, tR = 22.0 min (major) and tR = 20.3 min (minor).

_N_-Boc protected (_S,E_)-methyl 3-(4-methoxy-2-(3-methylpyridine-2- sulfonimidoyl) phenyl) acrylate (29c):

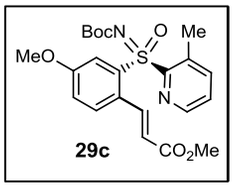

3c: 39 mg, 35% yield, 97% ee, colorless solid, $[\alpha]_D^{25}$ +55.3 (c 0.13, $CHCl_3$); **^{1}H NMR (500 MHz, $CDCl_3$)** δ 8.25 (dd, *J* 4.75, 1.25 Hz, 1H), 8.19 (d, *J* 16.0, 1H), 7.90 (d, *J* 3.0 Hz, 1H), 7.66 (dd, *J* 7.75, 0.75 Hz, 1H), 7.55 (d, *J* 8.5 Hz, 1H), 7.31 (dd, *J* 7.75, 4.75 Hz, 1H), 7.13 (dd, *J* 8.5, 2.5 Hz, 1H), 6.05 (d, *J* 16.0 Hz, 1H), 3.90 (s, 3H), 3.71 (s, 3H), 2.85 (s, 3H), 1.33 (s, 9H); **^{13}C NMR (126 MHz, CDCl3)** δ 166.4, 160.5, 157.0, 154.9, 146.0, 141.7, 141.2, 137.5, 135.6,

130.0, 128.1, 126.6, 120.0, 119.9, 115.6, 80.5, 55.8, 51.6, 27.9, 18.9; IR (KBr) $_{max}$ 2970, 2923, 1720, 1272, 1232, 1155, 1035 cm^{-1}; **HRMS (ESI)** for $C_{22}H_{26}N_2NaO_6S^+$ $(M+Na)^+$: calcd. 469.1404, found 469.1413; **HPLC condition**: Phenomenex Chiralpak cellulose-2, n-hexane/i-PrOH =60/40, Flow rate = 0.4 mL/min, UV = 254 nm, tR = 57.7 min (major) and tR = 50.9 min (minor).

***N*-Boc protected (*R*)-2-(3-methoxyphenylsulfonimidoyl)-3-methylpyridine (27b):**

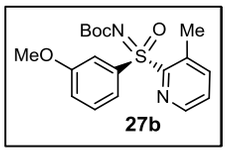

27b: 42 mg, 46% yield, 71% ee $[\alpha]_D^{25}$ –41.5 (c = 0.378, $CHCl_3$); **HPLC condition**: Daicel IG-3, MeOH, Flow rate = 0.5 mL/min, UV = 254 nm, tR = 14.5 min (major) and tR = 10.2 min (minor).

***N*-Boc protected (*S,E*)-ethyl 3-(4-methoxy-2-(3-methylpyridine-2-sulfonimidoyl)phenyl) acrylate (29d):**

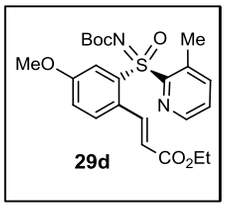

29d: 38 mg, 33% yield, 97% ee, colorless solid, $[\alpha]_D^{25}$ +25.2 (c 0.138, $CHCl_3$); **1H NMR (400 MHz, CDCl3)** δ 8.27 (d, *J* 4.8 Hz, 1H), 8.17 (d, *J* 15.6 Hz, 1H), 7.94 (d, *J* 2.8 Hz, 1H), 7.66 (d, *J* 8.0 Hz, 1H), 7.54 (d, *J* 8.4 Hz, 1H), 7.34–7.28 (m, 1H), 7.17–7.10 (m, 1H), 6.04 (d, *J* 15.6 Hz, 1H), 4.19 (q, *J* 7.2 Hz, 2H), 3.92 (s, 3H), 2.87 (s, 3H), 1.35 (s, 9H), 1.28 (t, *J* = 7.0 Hz, 3H); **13C NMR (101 MHz, CDCl3)** δ 166.0, 160.4, 157.0, 155.0, 146.1, 141.6, 140.8, 137.6, 135.8, 130.0, 128.1, 126.6, 120.5, 119.9, 115.5, 80.5, 60.4, 55.9, 27.9, 19.1, 14.3; IR (KBr) $_{max}$ 2969, 1738, 1366, 1229, 1216, 1156 cm^{-1}; **HRMS (ESI)** for $C_{23}H_{28}N_2NaO_6S^+$ $(M+Na)^+$: calcd. 483.1560, found 483.1571; **HPLC condition**: Daicel IG-3, MeOH, Flow rate = 0.2 mL/min, UV = 254 nm, tR = 25.5 min (major) and tR = 36.8 min (minor).

***N*-Boc protected (*R*)-2-(3-methoxyphenylsulfonimidoyl)-3-methylpyridine (27b):**

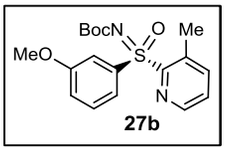

27b: 40 mg, 44% yield, 70% ee; $[\alpha]_D^{25}$ –29.8 (c = 0.12, $CHCl_3$); **HPLC condition**: Daicel IG-3, MeOH, Flow rate = 0.2 mL/min, UV 254 nm, tR 36.0 min (major) and tR 25.1 min (minor).

***N*-Boc protected (*S,E*)-4-(4-methoxy-2-(3-methylpyridine-2-sulfonimidoyl)phenyl)but-3-en-2-one (29e):**

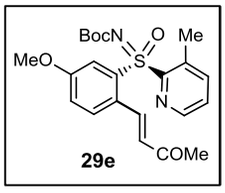

29e: 37 mg, 35% yield, 91% ee, colorless foam, $[\alpha]_D^{25}$ = +97 (c = 0.06, $CHCl_3$); **1H NMR (500 MHz, $CDCl_3$)** δ 8.46 (d, *J* 16.5, 1H), 8.33 (dd, *J*

4.5, 1.0 Hz, 1H), 7.87 (d, *J* = 3.0 Hz, 1H), 7.67 (d, *J* = 7.0 Hz, 1H), 7.63 (d, *J* 8.5 Hz, 1H), 7.36 (dd, *J* 8.0, 4.5 Hz, 1H), 7.15 (dd, *J* 8.75, 2.75 Hz, 1H), 6.30 (d, *J* 16.5 Hz, 1H), 3.91 (s, 3H), 2.75 (s, 3H), 2.35 (s, 3H), 1.34 (s, 9H); **^{13}C NMR (126 MHz, CDCl3)** δ 199.1, 160.8, 157.0, 154.8, 145.9, 142.0, 141.3, 137.5, 135.3, 129.9, 129.4, 128.1, 127.0, 119.8, 115.9, 80.6, 55.9, 27.9, 26.1, 19.0; IR (KBr) $_{max}$ 2974, 2923, 2363, 1738, 1668, 1366, 1232, 1152 cm^{-1}; **HRMS (ESI)** for $C_{22}H_{27}N_2O_5S^+$ $(M+H)^+$: calcd. 431.1635, found 431.1641; **HPLC condition**: Daicel OT (+), n-hexane/i-PrOH =70/30, Flow rate = 0.2 mL/min, UV = 254 nm, tR = 45.1 min (major) and tR = 39.9 min (minor).

***N*-Boc protected (R)-2-(3-methoxyphenylsulfonimidoyl)-3-methylpyridine(27b):**

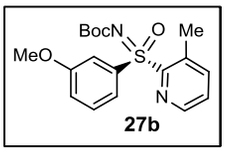

27b

27b: 39 mg, 43% yield, 67 % ee; $[\alpha]_D^{25}$ = –28.0 (c = 0.114, $CHCl_3$); **HPLC condition**: Daicel IG-3, MeOH, Flow rate = 0.5 mL/min, UV = 254 nm, tR = 14.6 min (major) and tR = 10.1 min (minor).

***N*-Boc protected (*S*,*E*)-2-(5-methoxy-2-(2-(phenylsulfonyl)vinyl)phenylsulfonimidoyl)-3-methyl pyridine (29f):**

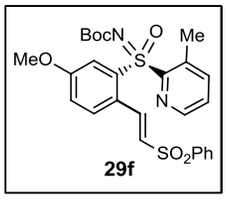

29f

29f: 35.7 mg, 27% yield, 89% ee, colorless foam, $[\alpha]_D^{25}$ = +12.42 (c = 1.0, $CHCl_3$); **^{1}H NMR (500 MHz, CDCl$_3$)** δ 8.28 (d, *J* 15.0 Hz, 1H), 8.24 (dd, *J* 4.5, 1.0 Hz, 1H), 7.91– (m, 3H), 7.69 (dd, *J* = 7.75, 0.75 Hz, 1H), 7.60–7.53 (m, 1H), 7.52–7.45 (m, 3H), 7.33 (dd, *J* = 7.5, 4.5 Hz, 1H), 7.10 (dd, *J* = 8.75, 2.75 Hz, 1H), 6.57 (d, *J* = 15.0 Hz, 1H), 3.89 (s, 3H), 2.87 (s, 3H), 1.33 (s, 9H); **^{13}C NMR (126 MHz, CDCl3)** δ 161.1, 156.7, 154.6, 146.1, 141.9, 140.2, 139.3, 138.4, 135.7, 133.2, 130.3, 129.2, 128.6, 127.8, 126.8, 125.6, 119.5, 116.1, 80.6, 55.9, 27.9, 19.0; IR (KBr) $_{max}$ 2969, 2927, 1738, 1246, 1145, 1083, 733 cm^{-1}; **HRMS (ESI)** for $C_{26}H_{28}N_2NaO_6S_2^+$ $(M+H)^+$: calcd. 551.1281, found 551.1292; **HPLC condition**: Daicel ODH, n-hexane/i-PrOH =50/50, Flow rate = 0.5 mL/min, UV = 254 nm, tR = 20.7 min (major) and tR = 18.9 min (minor).

***N*-Boc protected (*R*)-2-(3-methoxyphenylsulfonimidoyl)-3-methylpyridine (27b):**

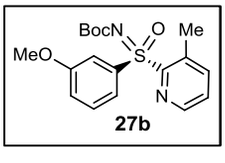

27b

27b: 41 mg, 45% yield, 48% ee; $[\alpha]_D^{25}$ –18.8 (c = 0.258, $CHCl_3$); HPLC condition: Daicel ODH, *n*-hexane/**i**-PrOH =50/50, Flow rate = 0.5 mL/min, UV = 254 nm, tR = 10.1 min (major) and tR = 8.6 min (minor).

_N_-Boc protected (_S_,_E_)-diethyl 4-methoxy-2-(3-methylpyridine-2-sulfonimidoyl)styrylphosphonate (29g):

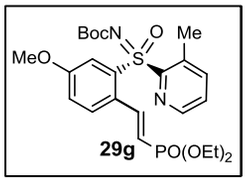

29g: 43 mg, 33% yield, 95% ee, colorless solid, $[\alpha]_D^{25}$ 14.1 (c 0.058, $CHCl_3$); **^{1}H NMR (500 MHz, $CDCl_3$)** δ 8.29 (dd, *J* 4.75, 1.25 Hz, 1H), 7.96–7.84 (m, 2H), 7.67 (d, *J* 7.5 Hz, 1H), 7.57 (d, *J* 8.5 Hz, 1H), 7.32 (dd, *J* 7.75, 4.75 Hz, 1H), 7.14 (dd, *J* 8.5, 2.5 Hz, 1H), 6.01–5.90 (m, 1H), 4.10–3.98 (m, 4H), 3.91 (s, 3H), 2.83 (s, 3H), 1.33 (s, 9H), 1.31–1.22 (m, 6H); **^{13}C NMR (126 MHz, CDCl3)** δ 160.4, 156.8, 154.8, 146.0, 143.7 (*J* 8.8 Hz), 141.8, 137.2, 135.5, 129.9, 128.5 (d, *J* 25.2 Hz), 126.7, 119.8, 116.6 (d, *J* 191.5 Hz), 115.5, 80.5, 62.03 (d, *J* 6.3 Hz), 62.01 (d, *J* 5.0 Hz), 55.9, 27.9, 19.0, 16.34, 16.3; IR (KBr) $_{max}$ 2969, 2920, 2850, 1738, 1366, 1228, 1216 cm^{-1}; **HRMS (ESI)** for $C_{24}H_{33}N_2NaO_7PS^+$ $(M+Na)^+$: calcd. 547.1638, found 546.2053; **HPLC condition**: Daicel IC-3, MeOH, Flow rate = 0.3 mL/min, UV = 254 nm, t_R = 16.7 min (major) and t_R = 15.8 min (minor).

***N*-Boc protected (*R*)-2-(3-methoxyphenylsulfonimidoyl)-3-methylpyridine (27b):**

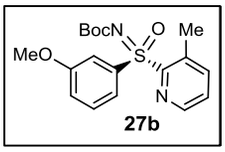

27b: 37 mg, 41% yield, 62% ee; $[\alpha]_D^{25}$ –21.0 (c 0.348, $CHCl_3$); **HPLC condition**: Daicel IG-3, MeOH, Flow rate 0.5 mL/min, UV 254 nm, tR = 14.8 min (major) and tR 10.2 min (minor).

***N*-Boc protected (*S*,*E*)-2-(5-methoxy-2-(2-(methylsulfonyl)vinyl)phenylsulfonimidoyl)-3-methyl pyridine (29h):**

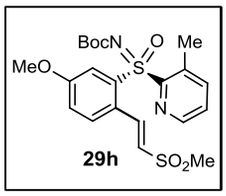

29h: 38 mg, 33%, 99% ee, colorless solid, $[\alpha]_D^{25}$ +16.9 (c 0.16, $CHCl_3$); **^{1}H NMR (400 MHz, CDCl3)** δ 8.35–8.26 (m, 2H), 7.84 (d, *J* 2.4 Hz, 1H), 7.70 (dd, *J* 7.6, 0.8 Hz, 1H), 7.53 (d, *J* 8.8 Hz, 1H), 7.36 (dd, *J* 7.6, 4.4 Hz, 1H), 7.16 (dd, *J* 8.6, 2.6 Hz, 1H), 6.60 (d, *J* 15.2 Hz, 1H), 3.91 (s, 3H), 3.03 (s, 3H), 2.83 (s, 3H), 1.31 (s, 9H); **^{13}C NMR (101 MHz, $CDCl_3$)** δ 161.2, 156.5, 154.6, 146.2, 142.15, 142.09, 138.3, 135.5, 130.5, 128.3, 127.0, 126.0, 119.6, 116.2, 80.8, 56.0, 43.0, 27.9, 19.0; IR (KBr) $_{max}$ 2977, 2932, 2367, 1738, 1242, 1153, 1127 cm^{-1}; **HRMS (ESI)** for $C_{21}H_{26}N_2NaO_6S_2^+$ $(M+H)^+$: calcd. 489.1124, found 489.1134; **HPLC condition**: Daicel IC-3, i-PrOH, Flow rate = 0.5 mL/min, UV = 254 nm, tR = 52.9 min (major) and tR = 36.8 min (minor).

N-Boc protected (*R*)-2-(3-methoxyphenylsulfonimidoyl)-3-methylpyridine (27b):

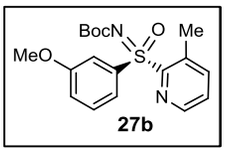

27b: 38 mg, 42% yield, 70% ee; $[\alpha]_D^{25}$ = –44.56 (c 0.364, $CHCl_3$); **HPLC condition**: Daicel IG-3, MeOH, Flow rate 0.5 mL/min, UV = 254 nm, tR = 13.9 min (major) and tR 10.2 min (minor).

N-Boc protected (*S,E*)-methyl 3-(5-methyl-2-(3-methylpyridine-2-sulfonimidoyl)phenyl) acrylate (29i):

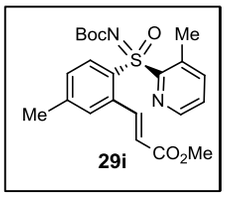

29i: 33 mg, 31% yield, 96% ee, colorless viscous liquid, $[\alpha]_D^{25}$ +29.4 (c 0.108, $CHCl_3$); **^{1}H NMR (500 MHz, $CDCl_3$)** δ 8.29–8.20 (m, 3H), 7.64 (dd, *J* 7.75, 0.75 Hz, 1H), 7.41–7.36 (m, 2H), 7.29 (dd, *J* 7.75, 4.75 Hz, 1H), 6.09 (d, *J* 15.5 Hz, 1H), 3.73 (s, 3H), 2.83 (s, 3H), 2.44 (s, 3H), 1.33 (s, 9H); **^{13}C NMR (126 MHz, $CDCl_3$)** δ 166.2, 157.1, 155.1, 145.9, 144.7, 141.9, 141.6, 136.1, 135.6, 133.1, 131.1, 130.3, 129.5, 126.5, 121.7, 80.3, 51.7, 27.9, 21.5, 19.0; IR (KBr) $_{max}$ 2969, 2923, 1722, 1366, 1273, 1226, 1154 cm^{-1}; **HRMS (ESI)** for $C_{22}H_{27}N_2O_5S^+$ $(M+H)^+$: calcd. 431.1635, found 431.1646; **HPLC condition**: Daicel ODH, n-hexane/i-PrOH 70/30, Flow rate 0.3 mL/min, UV 254 nm, tR 22.8 min (major) and tR 25.5 min (minor).

N-Boc protected (*R*)-3-methyl-2-(4-methylphenylsulfonimidoyl)pyridine (27c):

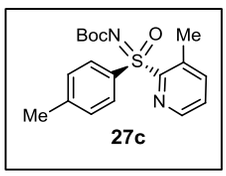

27c: 40 mg, 46% yield, 52% ee; $[\alpha]_D^{25}$ –22.3 (c 0.182, $CHCl_3$); **HPLC condition**: Daicel IG-3, MeOH, Flow rate 0.5 mL/min, UV 254 nm, tR 19.2 min (major) and tR 10.6 min (minor).

N-Boc protected (*S,E*)-4-(5-methyl-2-(3-methylpyridine-2-sulfonimidoyl)phenyl)but-3-en-2-one (29j):

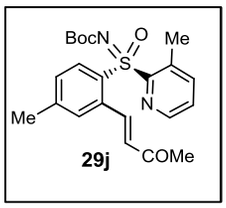

29j: 31 mg, 30% yield, 96% ee, colorless solid, $[\alpha]_D^{25}$ 96.2 (c 0.08, $CHCl_3$); **^{1}H NMR (500 MHz, $CDCl_3$)** δ 8.49 (d, *J* 16.5 Hz, 1H), 8.32 (d, *J* 4.5 Hz, 1H), 8.22 (d, *J* 8.0 Hz, 1H), 7.65 (d, *J* 7.5 Hz, 1H), 7.45 (bs, 1H), 7.39 (d, *J* 8.0 Hz, 1H), 7.34 (dd, *J* 8.0, 4.5 Hz, 1H), 6.32 (d, *J* 16.5 Hz, 1H), 2.72 (s, 3H), 2.44 (s, 3H), 2.37 (s, 3H), 1.34 (s, 9H); **^{13}C NMR (126 MHz, $CDCl_3$)** δ 199.1, 157.2, 154.9, 145.8, 145.0, 141.9, 141.8, 136.0, 135.2, 132.9, 131.00, 130.97, 130.5, 129.3, 126.9, 80.5, 27.9, 26.2, 21.5, 19.0; IR (KBr) $_{max}$ 2969, 2922, 1738, 1671, 1228, 1154

cm^{-1}; **HRMS (ESI)** for $C_{22}H_{27}N_2O_4S^+$ $(M+H)^+$: calcd. 415.1686, found 415.1694; **HPLC condition**: Daicel IG-3, MeOH, Flow rate 0.5 mL/min, UV 254 nm, tR 26.0 min (major) and tR 29.9 min (minor).

***N*-Boc protected (*R*)-3-methyl-2-(4-methylphenylsulfonimidoyl)pyridine (27c):**

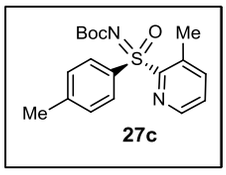

27c: 39 mg, 45% yield, 59% ee; $[\alpha]_D^{25}$ –35.6 (c 0.114, $CHCl_3$); **HPLC condition**: Daicel IG-3, MeOH, Flow rate 0.5 mL/min, UV 254 nm, tR 19.5 min (major) and tR 10.9 min (minor).

***N*-Boc protected (*S,E*)-3-methyl-2-(4-methyl-2-(2-(methylsulfonyl)vinyl)phenyl sulfonimidoyl) pyridine (29k):**

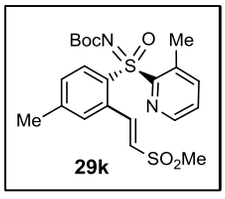

29k: 35 mg, 31% yield, 94% ee, colorless solid, $[\alpha]_D^{25}$ +67.2 (c 0.136, $CHCl_3$); **^{1}H NMR (500 MHz, $CDCl_3$)** δ 8.37 (d, *J* 15.5 Hz, 1H), 8.31 (d, *J* 3.5 Hz, 1H), 8.16 (d, *J* 8.0 Hz, 1H), 7.67 (d, *J* 7.0 Hz, 1H), 7.42 (d, *J* 8.0 Hz, 1H), 7.39–7.30 (m, 2H), 6.65 (d, *J* 15.0 Hz, 1H), 3.04 (s, 3H), 2.79 (s, 3H), 2.45 (s, 3H), 1.29 (s, 9H); **^{13}C NMR (101 MHz, $CDCl_3$)** δ 156.6, 154.8, 146.2, 145.1, 142.9, 142.0, 135.4, 134.2, 133.6, 131.0, 130.9, 130.0, 126.9, 80.6, 42.9, 27.8, 21.4, 19.0 (1 carbon overlap); IR (KBr) $_{max}$ 2969, 2932, 1739, 1228 cm^{-1}; **HRMS (ESI)** for $C_{21}H_{26}N_2NaO_5S_2^+$ $(M+H)^+$: calcd. 473.1175, found 473.1181; **HPLC condition**: Daicel IG-3, MeOH, Flow rate 0.5 mL/min, UV 254 nm, tR 12.6 min (major) and tR 18.0 min (minor).

***N*-Boc protected (*R*)-3-methyl-2-(4-methylphenylsulfonimidoyl)pyridine (27c):**

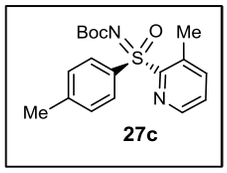

27c: 37 mg, 43% yield, 50% ee; $[\alpha]_D^{25}$ –17.3 (c 0.252, $CHCl_3$); **HPLC condition**: Daicel IG-3, MeOH, Flow rate 0.5 mL/min, UV 254 nm, tR = 18.3 min (major) and tR 10.5 min (minor).

***N*-Boc protected (*S,E*)-methyl 3-(5-(tert-butyl)-2-(3-methylpyridine-2-sulfonimidoyl) phenyl) acrylate (29l):**

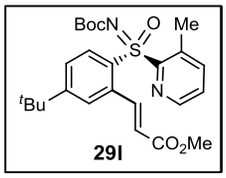

29l: 38 mg, 32% yield, 98% ee, colorless foam, $[\alpha]_D^{25}$ +41.9 (c 0.16, $CHCl_3$); **^{1}H NMR (400 MHz, CDCl3)** δ 8.32–8.29 (d, *J* 2.0 Hz, 1H), 8.28–8.24 (m, 2H), 7.64 (d, *J* 7.6 Hz, 1H), 7.61–7.53 (m, 2H), 7.29 (dd, *J*

7.6, 4.4 Hz, 1H), 6.10 (d, *J* 15.6 Hz, 1H), 3.74 (s, 3H), 2.83 (s, 3H), 1.35 (s, 9H), 1.32 (s, 9H); **^{13}C NMR (101 MHz, $CDCl_3$)** δ 166.2, 157.5, 157.0, 155.2, 146.0, 142.4, 141.6, 135.8, 135.6, 133.2, 130.9, 126.8, 126.5, 126.0, 121.6, 80.3, 51.7, 35.2, 30.9, 27.9, 19.0; IR (KBr) $_{max}$ 2968, 2360, 1721, 1366, 1271, 1249, 1154 cm^{-1}; **HRMS (ESI)** for $C_{25}H_{32}N_2NaO_5S^+$ $(M+Na)^+$: calcd. 495.1924, found 495.1937; **HPLC condition**: cellulose-2, n-hexane/i-PrOH 50/50, Flow rate 0.5 mL/min, UV 254 nm, tR 20.1 min (major) and tR 32.2 min (minor).

***N*-Boc protected (*R*)-2-(4-(tert-butyl)phenylsulfonimidoyl)-3-methylpyridine (27d):**

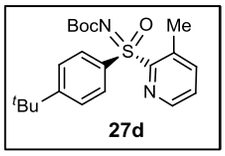

27d: 42 mg, 43% yield, 59% ee; , $[\alpha]_D^{25}$ +33.3 (c 0.1, $CHCl_3$); **HPLC condition**: Daicel IG-3, MeOH, Flow rate 0.5 mL/min, UV 254 nm, tR 31.5 min (major) and tR 12.2 min (minor).

***N*-Boc protected (*S,E*)-methyl 3-(5-isopropyl-2-(3-methylpyridine-2-sulfonimidoyl)phenyl) acrylate (29m):**

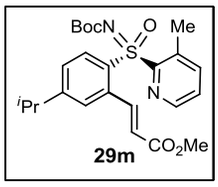

29m: 34 mg, 30% yield, 94% ee, colorless solid, $[\alpha]_D^{25}$ +27.6 (c 0.55, $CHCl_3$); **^{1}H NMR (400 MHz, $CDCl_3$)** δ 8.32–8.23 (m, 3H), 7.65 (d, *J* 7.6 Hz, 1H), 7.46–7.39 (m, 2H), 7.30 (dd, *J* 7.6, 4.4 Hz, 1H), 6.11 (d, *J* 15.6 Hz, 1H), 3.75 (s, 3H), 3.07–2.94 (m, 1H), 2.84 (s, 3H), 1.33 (s, 9H), 1.29 (d, *J* 6.8 Hz, 6H); **^{13}C NMR (101 MHz, $CDCl_3$)** δ 166.2, 157.1, 155.2, 146.0, 142.2, 141.6, 136.2, 135.6, 133.5, 131.2, 127.8, 127.1, 126.5, 121.7, 80.3, 51.7, 34.1, 27.9, 23.53, 23.46, 19.0 (1 carbon is overlapped); IR (KBr) $_{max}$ 2986, 1720, 1666, 1267, 1247, 1151, 1041 cm^{-1}; **HRMS (ESI)** for $C_{24}H_{31}N_2O_5S^+$ $(M+H)^+$: calcd. 459.1948, found 459.1959; **HPLC condition**: Daicel IG-3, *i*-PrOH, Flow rate 0.5 mL/min, UV 254 nm, tR 30.1 min (major) and tR 57.6 min (minor).

***N*-Boc protected (*R*)-2-(4-isopropylphenylsulfonimidoyl)-3-methylpyridine (27e):**

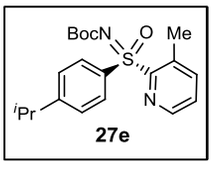

27e: 42 mg, 45% yield, 57% ee; $[\alpha]_D^{25}$ –28.9 (c 0.588, $CHCl_3$); **HPLC condition**: Daicel IG-3, MeOH, Flow rate 0.5 mL/min, UV 254 nm, tR 23.4 min (major) and tR 12.0 min (minor).

_N_-Boc protected (_S,E_)-methyl 3-(4-ethoxy-2-(3-methylpyridine-2-sulfonimidoyl)phenyl) acrylate (29n):

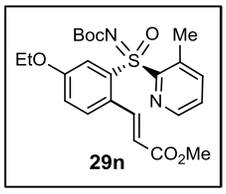

29n: 48 mg, 42% yield, 85% ee, colorless foam, $[\alpha]_D^{25}$ +50.1 (c 0.11, $CHCl_3$); **1H NMR (500 MHz, $CDCl_3$)** δ 8.26 (dd, *J* 4.5, 0.75 Hz, 1H), 8.19 (d, *J* 16.0 Hz, 1H), 7.89 (d, *J* 3.0 Hz, 1H), 7.68–7.62 (m, 1H), 7.53 (d, *J* 8.5 Hz, 1H), 7.30 (dd, *J* 8.0, 4.5 Hz, 1H), 7.11 (dd, *J* 8.5, 2.5 Hz, 1H), 6.04 (d, *J* 15.5 Hz, 1H), 4.13 (q, *J* 6.83 Hz, 2H), 3.71 (s, 3H), 2.84 (s, 3H), 1.42 (t, *J* 7.0 Hz, 3H), 1.33 (s, 9H); **13C NMR (126 MHz, CDCl3)** δ 166.5, 159.9, 156.9, 155.0, 146.0, 141.6, 141.2, 137.5, 135.6, 129.9, 127.8, 126.6, 120.1, 119.8, 116.3, 80.4, 64.3, 51.6, 27.9, 18.9, 14.5; IR (KBr) $_{max}$ 2921, 2850, 1737, 1366, 1230, 1156 cm^{-1}; **HRMS (ESI)** for $C_{23}H_{29}N_2O_6S^+$ $(M+H)^+$: calcd. 461.1741, found 489.1749; **HPLC condition**: Daicel IC-3, *i*-PrOH, Flow rate 0.5 mL/min, UV 254 nm, tR 37.7 min (major) and tR 28.6 min (minor).

_N_-Boc protected (_R_)-2-(3-ethoxyphenylsulfonimidoyl)-3-methylpyridine (27f):

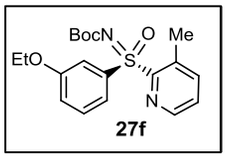

27f: 32 mg, 34% yield, 88% ee; $[\alpha]_D^{25}$ – 8 (c 0.258, $CHCl_3$); **HPLC condition**: Daicel IG-3, MeOH, Flow rate = 0.5 mL/min, UV = 254 nm, tR 34.1 min (major) and tR 16.8 min (minor).

_N_-Boc protected (_S,E_)-methyl 3-(4-methyl-2-(3-methylpyridine-2-sulfonimidoyl)phenyl) acrylate (29o):

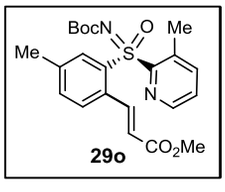

29o: 38 mg, 35% yield, 96% ee, colorless foam, $[\alpha]_D^{25}$ +29.7 (c 0.03, $CHCl_3$); **1H NMR (500 MHz, $CDCl_3$)** δ 8.26 (d, *J* 3.5 Hz, 1H), 8.25–8.18 (m, 2H), 7.66 (d, *J* 8.0 Hz, 1H), 7.49 (d, *J* 7.5 Hz, 1H), 7.43 (d, *J* 8.5 Hz, 1H), 7.30 (dd, *J* 8.0, 4.5 Hz, 1H), 6.08 (d, *J* 16.0 Hz, 1H), 3.73 (s, 3H), 2.87 (s, 3H), 2.47 (s, 3H), 1.34 (s, 9H); **^{13}C NMR (126 MHz, $CDCl_3$)** δ 166.3, 157.1, 155.2, 146.0, 141.62, 141.60, 140.4, 136.1, 135.9, 134.5, 133.3, 131.3, 128.7, 126.5, 121.2, 80.4, 51.7, 27.9, 21.3, 19.0; IR (KBr) $_{max}$ 2969, 2853, 1738, 1366, 1228, 1216, 1156 cm^{-1}; **HRMS (ESI)** for $C_{22}H_{26}N_2NaO_5S^+$ $(M+Na)^+$: calcd. 453.1455, found 453.1469; **HPLC condition**: Cellulose-1, n-hexane/i-PrOH 70/30, Flow rate 0.3 mL/min, UV 254 nm, tR 28.0 min (major) and tR 24.1 min (minor).

N-Boc protected (*R*)-3-methyl-2-(3-methylphenylsulfonimidoyl)pyridine (27g):

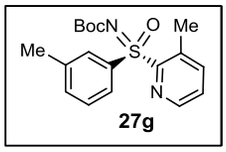

27g: 36 mg, 42% yield, 68% ee; $[\alpha]_D^{25}$ –66.7 (c 0.006, $CHCl_3$); **HPLC condition**: Daicel IG-3, MeOH, Flow rate 0.3 mL/min, UV 254 nm, tR 18.2 min (major) and tR 16.4 min (minor).

N-Boc protected (*S,E*)-methyl 3-(4-chloro-2-(3-methylpyridine-2-sulfonimidoyl)phenyl) acrylate (29p):

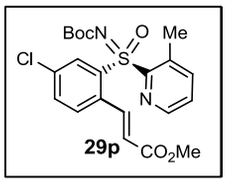

29p: 25 mg, 22% yield, 89% ee, colorless foam, , $[\alpha]_D^{25}$ 32.1 (c 0.07, $CHCl_3$); **1H NMR (500 MHz, $CDCl_3$)** δ 8.37 (d, *J* 2.0 Hz, 1H), 8.24 (dd, *J* 4.5, 1.0 Hz, 1H), 8.18 (d, *J* 15.5 Hz, 1H), 7.69 (dd, *J* 7.75, 0.75 Hz, 1H), 7.61 (dd, *J* 8.25, 2.25 Hz, 1H), 7.53 (d, *J* 8.5 Hz, 1H), 7.33 (dd, *J* 7.75, 4.75 Hz, 1H), 6.11 (d, *J* 16 Hz, 1H), 3.74 (s, 3H), 2.88 (s, 3H), 1.34 (s, 9H); **^{13}C NMR (126 MHz, $CDCl_3$)** δ 166.0, 156.8, 154.7, 146.0, 141.8, 140.7, 137.8, 136.1, 135.9, 134.7, 133.8, 131.0, 129.9, 126.8, 122.3, 80.8, 51.9, 27.9, 18.9; IR (KBr) $_{max}$ 2969, 2851, 1727, 1221, 1208, 1100 cm^{-1}; **HRMS (ESI)** for $C_{21}H_{23}ClN_2NaO_5S^+$ $(M+Na)^+$: calcd. 473.0908, found 473.0919; **HPLC condition**: Daicel IG-3, MeOH, Flow rate 0.2 mL/min, UV 254 nm, tR = 23.1 min (major) and tR 22.0 min (minor).

N-Boc protected (*R*)-2-(3-chlorophenylsulfonimidoyl)-3-methylpyridine (27h):

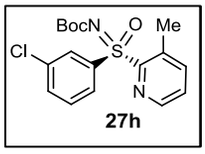

27h: 33 mg, 36% yield, 35% ee; $[\alpha]_D^{25}$ –46 (c 0.05, $CHCl_3$); **HPLC condition**: Daicel IG-3, MeOH, Flow rate 0.2 mL/min, UV 254 nm, tR 32.4 min (major) and tR 24.3 min (minor).

***N*-Boc protected (*S,E*)-methyl 3-(2,4-dimethyl-6-(3-methylpyridine-2-sulfonimidoyl) phenyl) acrylate (29q):**

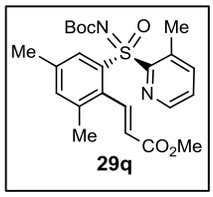

29q: 40 mg, 36% yield, 96% ee, colorless foam, $[\alpha]_D^{25}$ 8.3 (c 0.1, $CHCl_3$); **^{1}H NMR (400 MHz, $CDCl_3$)** δ 8.25 (dd, *J* 4.6, 1.0 Hz, 1H), 8.18 (bs, 1H), 7.76 (d, *J* 16.4 Hz, 1H), 7.58 (dd, *J* 7.6, 0.8 Hz, 1H), 7.33–7.27 (m, 2H), 5.48 (d, *J* 16.4 Hz, 1H), 3.72 (s, 3H), 2.78 (s, 3H), 2.42 (s, 3H), 2.25 (s, 3H), 1.36 (s, 9H); **^{13}C NMR (101 MHz, $CDCl_3$)** δ 165.8, 157.3, 155.3, 146.0, 141.3, 141.2, 138.3, 137.4, 136.7, 136.5, 136.4, 132.5, 128.9, 126.4, 125.1, 80.3, 51.6, 28.0, 21.1, 20.8, 19.1; IR (KBr) $_{max}$

2966, 2920, 2851, 1725, 1258, 1154, 1014 cm^{-1}; **HRMS (ESI)** for $C_{23}H_{29}N_2O_5S^+$ $(M+H)^+$: calcd. 445.1792, found 445.1799; **HPLC condition**: Daicel IC-3, i-PrOH, Flow rate 0.5 mL/min, UV 254 nm, tR 44.2 min (major) and tR 57.5 min (minor).

N-Boc protected (*R*)-2-(3,5-dimethylphenylsulfonimidoyl)-3-methylpyridine (27i):

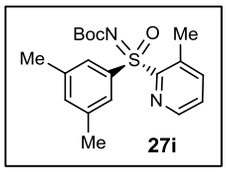

27i: 34 mg, 38% yield, 76% ee; $[\alpha]_D^{25}$ –29.3 (c 0.028, $CHCl_3$); **HPLC condition**: Daicel IG-3, MeOH, Flow rate 0.5 mL/min, UV 254 nm, tR 14.1 min (major) and tR 10.1 min (minor).

II.6.3.4. General procedures for kinetic resolution via Pd-catalyzed C(sp^2)–H arylation (GP-4):

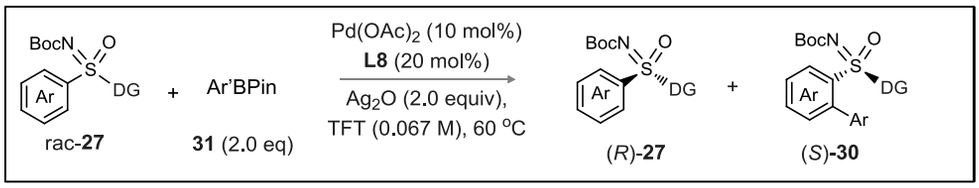

To an oven-dried 10 mL screw-capped vial was added substrate (0.2 mmol), ArBPin (0.4 mmol), $Pd(OAc)_2$ (4.6 mg, 0.02 mmol), L8 (0.04 mmol), Ag_2O (56 mg, 0.4 mmol), 2-chloro benzoquinone (0.1 mmol), TFT (3.0 mL). The mixture was stirred for 72 h at 60 °C. The resulting mixture was then cooled to rt and filtered through a small pad of Celite and concentrated in vacuo. The residue was purified by silica gel column chromatography using hexane/EtOAc as eluent to afford the chiral product and chiral starting material.

(S)-N-Boc protected 2-(4-methoxy-4'-(trifluoromethyl)-[1,1'-biphenyl]-2-sulfonimidoyl)-3-methyl-pyridine (30a):

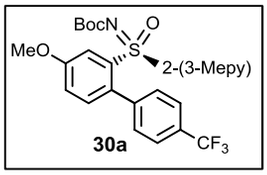

30a: 42 mg, 42% yield, 92% ee, colorless solid, $[\alpha]_D^{25}$ 9.7 (c 0.216, $CHCl_3$); **^{1}H NMR (400 MHz, $CDCl_3$)** δ 8.23–8.18 (m, 2H), 7.37–7.30 (m, 3H), 7.20 (dd, *J* 7.8, 4.6 Hz, 1H), 7.15– m, 1H), 7.12–6.95 (m, 3H), 3.96 (s, 3H), 2.29 (s, 3H), 1.32 (s, 9H); **^{13}C NMR (101 MHz, $CDCl_3$)** δ 159.1, 157.0, 154.9, 146.0, 141.8, 140.9, 138.0, 136.6, 133.3, 132.9, 130.2, 129.4 (q, *J* 32 Hz), 126.3, 124.00 (q, *J* 274 Hz), 124 (q, *J* 4.0 Hz), 119.5, 114.7, 80.3, 55.9, 27.9, 18.8; **^{19}F NMR (471 MHz,**

$CDCl_3$) δ – 62.76, IR (KBr) $_{max}$ 2969, 1663, 1600, 1322, 1106, 822, 800 cm^{-1}; **HPLC condition**: Daicel Chiralpak IG-3, MeOH /*i*-PrOH 95/5, Flow rate = 0.3 mL/min, UV = 254 nm, tR 17.2 min (major) and tR = 14.5 min (minor).

(*R*)-N-Boc protected 2-(3-methoxyphenylsulfonimidoyl)-3-methylpyridine (27b):

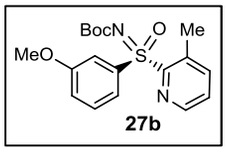

27b: 32 mg, 44% yield, 89% ee; $[\alpha]_D^{25}$ –35.7 (c 0.172, $CHCl_3$); **HPLC condition**: Daicel IG-3, MeOH, Flow rate = 0.7 mL/min, UV 254 nm, tR 7.3 min (minor) and tR 10.3 min (major).

(*S*)-N-Boc protected 2-(4-methoxy-3'-(trifluoromethyl)-[1,1'-biphenyl]-2-sulfonimidoyl)-3-methyl-pyridine (30b):

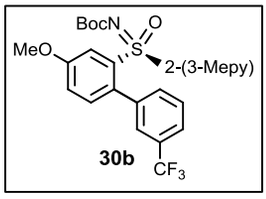

30b: 43 mg, 43% yield, 93% ee, colorless foam, $[\alpha]_D^{25}$ = (c = 0.06, $CHCl_3$); **^{1}H NMR (400 MHz, $CDCl_3$)** δ – (m, 2H), 7.45 (d, *J* 7.2 Hz, 1H), 7.37–7.29 (m, 3H), 7.20 (dd, *J* 7.6, 4.4 Hz, 1H), 7.19–7.12 (m, 1H), 7.11–7.06 (m, 1H), 6.93–6.82 (m, 1H), 3.98 (s, 3H), 2.28 (s, 3H), 1.34 (s, 9H); **^{13}C NMR (101 MHz, $CDCl_3$)** δ 159.0, 157.1, 154.7, 146.0, 141.0, 138.8, 138.0, 136.6, 133.9, 133.6, 132.7, 129.5 (q, *J* 32 Hz), 127.7, 126.5, 125.8, 124.2 (q, *J* 4.0 Hz), 123.7 (q, *J* 274 Hz), 119.5, 114.7, 80.3, 55.9, 27.9, 18.8; **^{19}F NMR (471 MHz, $CDCl_3$)** δ – 62.49; IR (KBr) $_{max}$ 2985, 1645, 1276, 1246, 1158, 1119, 901 cm^{-1}; **HPLC condition**: Daicel Chiralpak AS-H, n-hexane/*i*-PrOH 90/10, Flow rate 1.00 mL/min, UV 254 nm, tR = 13.3 min (major) and tR 15.5 min (minor).

(*R*)-N-Boc protected 2-(3-methoxyphenylsulfonimidoyl)-3-methylpyridine (27b):

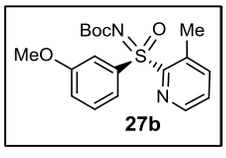

27b: 30 mg, 41% yield, 90% ee; $[\alpha]_D^{25}$ – 9 (c = 0.129, $CHCl_3$); **HPLC condition**: Daicel IG-3, MeOH, Flow rate 0.5 mL/min, UV 254 nm, tR 15.4 min (major).and tR 10.7 min (minor).

(*S*)-N-Boc protected 1-(4'-methoxy-2'-(3-methylpyridine-2-sulfonimidoyl)-[1,1'-biphenyl]-3-yl)-ethanone (30c):

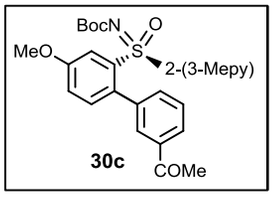

30c: 39 mg, 41% yield, 95% ee, colorless foam, $[\alpha]_D^{25}$ 0 (c 0.01, $CHCl_3$); **^{1}H NMR (500 MHz, $CDCl_3$)** δ 8.24–8.16 (m, 2H), 7.78 (d, *J* 7.5 Hz, 1H), 7.45–7.37 (m, 1H), 7.31 (d, *J* 7.5 Hz, 1H), 7.25–7.07 (m, 5H), 3.95 (s, 3H), 2.46 (s, 3H), 2.25 (s, 3H), 1.32 (s, 9H); **^{13}C NMR (126 MHz, $CDCl_3$)** δ 197.5,

159.0, 157.0, 154.9, 146.0, 140.8, 138.5, 138.0, 136.4, 136.0, 134.5, 133.6, 133.3, 129.9, 127.6, 127.0, 126.2, 119.5, 114.8, 80.2, 55.9, 27.9, 26.5, 18.8; IR (KBr) $_{max}$ 2969, 2926, 1738, 1365, 1275, 1229, 1156 cm^{-1}; **HRMS (ESI)** for $C_{26}H_{28}N_2NaO_5S^+$ $(M+Na)^+$: calcd. 503.1611, found 503.1619; **HPLC condition**: Daicel IG-3, MeOH, Flow rate = 0.3 mL/min, UV = 254 nm, tR = 20.1 min (major) and tR 25.4 min (minor).

(*R*)-N-Boc protected 2-(3-methoxyphenylsulfonimidoyl)-3-methylpyridine (27b):

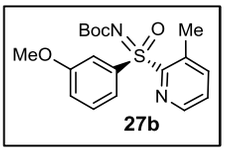

27b: 30 mg, 42% yield, 82% ee; $[\alpha]_D^{25}$ –62 (c = 0.01, $CHCl_3$); **HPLC condition**: Daicel IG-3, MeOH, Flow rate 0.3 mL/min, UV 254 nm, tR 24.7 min (major) and tR 17.1 min (minor).

(*S*)-N-Boc protected 2-(4'-fluoro-4-methoxy-[1,1'-biphenyl]-2-sulfonimidoyl)-3-methylpyridine (30d):

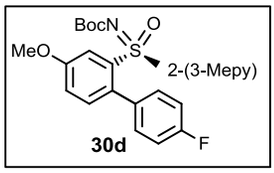

30d: 36 mg, 40% yield, 97% ee, colorless solid, $[\alpha]_D^{25}$ 61 (c 0.22, $CHCl_3$); **^{1}H NMR (500 MHz, $CDCl_3$)** δ 8.25–8.20 (m, 1H), 8.20 (d, *J* 3.0 Hz, 1H), 7.37 (d, *J* 7.5 Hz, 1H), 7.20 (dd, *J* 7.5, 4.5 Hz, 1H), 7.15– m, 1H), 7.08–7.03 (m, 1H), 6.78–6.73 (m, 4H), 3.94 (s, 3H), 2.33 (s, 3H), 1.32 (s, 9H); **^{13}C NMR (126 MHz, $CDCl_3$)** δ 162.1 (d, *J* 248 Hz), 158.8, 157.0, 155.0, 145.9, 140.9, 138.1, 136.6, 134.0, 133.9, 133.5, 131.5, 126.2, 119.5, 114.6, 114.0 (d, *J* 21 Hz), 80.2, 55.8, 27.9, 18.9; IR (KBr) $_{max}$ 2969, 1663, 1600, 1322, 1106, 822, 800 cm^{-1}; **^{19}F NMR (376 MHz, $CDCl_3$)** δ – 114.76; **HPLC condition**: Daicel Chiralpak IH-3, *i*-PrOH, Flow rate = 0.4 mL/min, UV = 254 nm, tR = 13.5 min (major) and tR 15.4 min (minor).

(*R*)-N-Boc protected 2-(3-methoxyphenylsulfonimidoyl)-3-methylpyridine (27b):

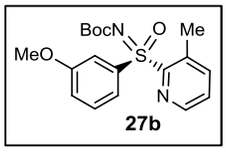

27b: 30 mg, 42% yield, 85% ee; $[\alpha]_D^{25}$ –56 (c = 0.025, $CHCl_3$); **HPLC condition**: Daicel IG-3, MeOH, Flow rate 0.5 mL/min, UV 254 nm, tR 15.7 min (major) and tR 11.1 min (minor).

(*S*)-N-Boc protected 2-(4-methoxy-4'-methyl-[1,1'-biphenyl]-2-sulfonimidoyl)-3-methylpyridine (30e):

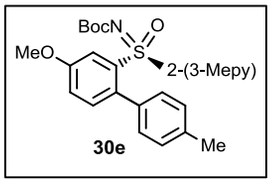

30e: 37 mg, 41% yield, 94% ee, colorless foam, $[\alpha]_D^{25}$ (c 0.122, $CHCl_3$); **^{1}H NMR (500 MHz, $CDCl_3$)** δ 8.20 (d, *J* 2.5 Hz, 2H),

7.31 (d, *J* 7.5 Hz, 1H), 7.20–7.14 (m, 1H), 7.13–7.09 (m, 1H), 7.08–7.04 (m, 1H), 6.95–6.70 (m, 4H), 3.95 (s, 3H), 2.28 (s, 6H), 1.32 (s, 9H); **^{13}C NMR (101 MHz, $CDCl_3$)** δ 158.5, 157.1 155.1, 145.9, 140.7, 138.0, 136.9, 136.8, 135.1, 134.7, 133.9, 129.6, 127.8, 126.0, 119.6, 114.2, 80.1, 55.9, 27.9, 21.1, 18.9; IR (KBr) $_{max}$ 2974, 2924, 1658, 1268, 1245, 1155, 1032 cm^{-1}; **HPLC condition**: Daicel Chiralpak IG-3, MeOH /i-PrOH =95/5, Flow rate = 0.3 mL/min, UV = 254 nm, tR = 17.9 min (minor).and tR = 19.6 min (major).

(*R*)-N-Boc protected 2-(3-methoxyphenylsulfonimidoyl)-3-methylpyridine (27b):

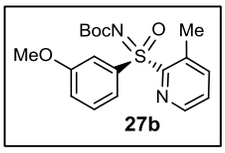

27b: 33 mg, 46% yield, 80% ee; $[\alpha]_D^{25}$ = –34.75 (c = 0.175, $CHCl_3$); **HPLC condition**: Daicel IG-3, MeOH, Flow rate = 0.7 mL/min, UV = 254 nm, tR = 7.3 min (minor) and tR = 10.3 min (major).

(*S*)-N-Boc protected 2-(3'-ethoxy-4,4'-dimethoxy-[1,1'-biphenyl]-2-sulfonimidoyl)-3-methyl-pyridine (30f):

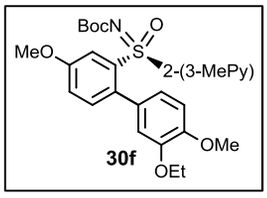

30f: 45 mg, 44% yield, 93% ee, colorless solid, $[\alpha]_D^{25}$ 4 (c 0.01, $CHCl_3$); **^{1}H NMR (500 MHz, $CDCl_3$)** δ 8.21–8.17 (m, 2H), 7.30 (d, *J* 7.5 Hz, 1H), 7.13 (dd, *J* 7.5, 4.5 Hz, 1H), 7.10–7.04 (m, 2H), 6.85–6.10 (m, 3H), 3.92 (s, 3H), 3 –3.80 (m, 2H), 3.79 (s, 3H), 2.30 (s, 3H), 1.36 (t, *J* 7.0 Hz, 3H), 1.30 (s, 9H); **^{13}C NMR (126 MHz, $CDCl_3$)** δ 158.4, 157.1, 154.9, 148.3, 146.7, 145.7, 140.5, 138.3, 136.7, 134.1, 133.9, 130.3, 125.8, 122.0, 119.4, 114.4, 114.0, 110.2, 79.9, 63.8, 55.9, 55.8, 27.8, 18.8, 14.6; IR (KBr) $_{max}$ 3028, 2974, 2850, 1738, 1366, 1228, 1216 cm^{-1}; **HRMS (ESI)** for $C_{27}H_{33}N_2O_6S^+$ $(M+H)^+$: calcd. 513.2054, found 513.2062; **HPLC condition**: Daicel IG-3, MeOH, Flow rate = 0.3 mL/min, UV = 254 nm, tR = 20.4 min (major) and tR = 18.4 min (minor).

(R)-N-Boc protected 2-(3-methoxyphenylsulfonimidoyl)-3-methylpyridine (27b):

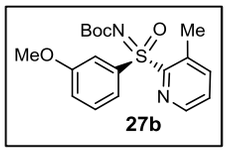

27b: 33 mg, 46% yield, 83% ee; $[\alpha]_D^{25}$ = –68.0 (c = 0.01, $CHCl_3$); **HPLC condition**: Daicel IG-3, MeOH, Flow rate = 0.3 mL/min, UV = 254 nm, tR = 24.6 min (major) and tR = 17.1 min (minor).

(*S*)-N-Boc protected 2-(3'-chloro-4-methoxy-[1,1'-biphenyl]-2-sulfonimidoyl)-3-methyl pyridine (30g):

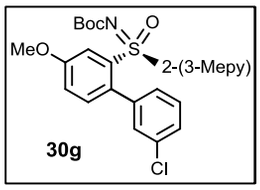

30g: 37 mg, 39% yield, 96% ee, colorless foam, $[\alpha]_D^{25}$ (c 0.01, $CHCl_3$); **^{1}H NMR (400 MHz, $CDCl_3$)** δ 8.25 (d, *J* 4.8 Hz, 1H), 8.22 (d, *J* 2.8 Hz, 1H), 7.38 (d, *J* 7.6 Hz, 1H), 7.26–7.20 (m, 2H), 7.19–7.09 (m, 3H), 7.09–7.03 (m, 2H), 3.96 (s, 3H), 2.33 (s, 3H), 1.34 (s, 9H); **^{13}C NMR (126 MHz, $CDCl_3$)** δ 159.0, 157.1, 154.9, 146.0, 140.9, 139.8, 138.2, 136.9, 133.5, 132.9, 132.8, 128.5, 127.5, 126.2, 119.5, 114.6, 80.2, 55.9, 28.0, 19.0 (2 carbons missing); **HRMS (ESI)** for $C_{24}H_{26}ClN_2O_4S^+$ $(M+H)^+$: calcd. 473.1296, found 473.1305; **HPLC condition**: Daicel IG-3, MeOH, Flow rate = 0.3 mL/min, UV = 254 nm, tR = 18.1 min (major) and tR = 20.0 min (minor).

(*R*)-N-Boc protected 2-(3-methoxyphenylsulfonimidoyl)-3-methylpyridine (27b):

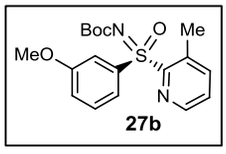

27b: 32 mg, 44% yield, 83% ee; $[\alpha]_D^{25}$ = –70.0 (c = 0.01, $CHCl_3$); **HPLC condition**: Daicel IG-3, MeOH, Flow rate = 0.3 mL/min, UV = 254 nm, tR = 24.2 min (major) and tR = 16.9 min (minor).

(*S*)-N-Boc protected 2-(5-methoxy-2-(naphthalen-1-yl)phenylsulfonimidoyl)-3-methylpyridine (30h):

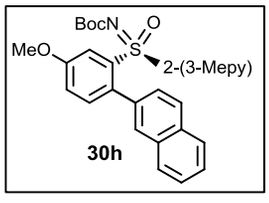

30h: 37 mg, 38% yield, 98% ee, colorless foam, $[\alpha]_D^{25}$ (c 0.029, $CHCl_3$); **^{1}H NMR (500 MHz, $CDCl_3$)** δ 8.30–8.26 (m, 1H), 8.22–8.17 (m, 1H), 7.76 (d, *J* 8.0 Hz, 1H), 7.65–7.38 (m, 5H), 7.20–7.14 (m, 3H), 7.12–7.06 (m, 1H), 7.06–7.02 (m, 1H), 3.99 (s, 3H), 1.96 (s, 3H), 1.31 (s, 9H); **^{13}C NMR (126 MHz, $CDCl_3$)** δ 158.7, 157.1, 155.1, 145.9, 140.6, 138.3, 137.0, 135.5, 134.5, 133.8, 132.3, 132.2, 128.0, 127.4, 126.6, 126.1, 126.0, 125.9, 119.5, 114.4, 80.1, 55.9, 27.9, 18.5; IR (KBr) $_{max}$ 2974, 2931, 1662, 1452, 1366, 1247, 1148 cm^{-1}; **HPLC condition**: Phenomenex Chiralpak Amylose2, n-hexane/i-PrOH =50/50, Flow rate 0.7 mL/min, UV 254 nm, tR 11.7 min (major) and tR 16.7 min (minor).

(*R*)-N-Boc protected 2-(3-methoxyphenylsulfonimidoyl)-3-methylpyridine (27b):

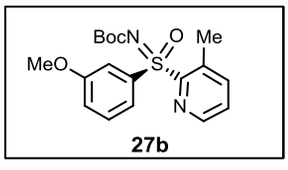

27b: 37 mg, 51% yield, 71% ee; $[\alpha]_D^{25}$ = –31.28 (c = 0.186, $CHCl_3$); **HPLC condition**: Daicel IG-3, MeOH, Flow rate = 0.5 mL/min, UV = 254 nm, tR = 10.7 min (major) and tR = 15.4 min (minor).

(*S*)-N-Boc protected 2-(4-ethoxy-4'-(trifluoromethyl)-[1,1'-biphenyl]-2-sulfonimidoyl)-3-methylpyridine (30i):

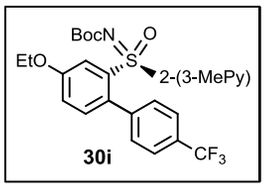

30i: 36 mg, 35% yield, 99% ee, colorless foam, $[\alpha]_D^{25}$ 6.23 (c 0.334, $CHCl_3$); **^{1}H NMR (500 MHz, $CDCl_3$)** δ –8.18 (m, 2H), 7.39–7.30 (m, 3H), 7.20 (dd, *J* 7.5, 4.5 Hz, 1H), 7.14 (dd, *J* 8.25, 2.75 Hz, 1H), 7.10–6.70 (m, 3H), 4.20 (q, *J* 7.0 Hz, 2H), 2.29 (s, 3H), 1.47 (t, *J* 7.0 Hz, 3H), 1.32 (s, 9H); **^{13}C NMR (126 MHz, $CDCl_3$)** δ 158.5, 157.0, 154.9, 146.0, 141.9, 140.9, 138.0, 136.5, 133.3, 132.7, 130.3, 129.4 (q, *J* 32 Hz), 126.3, 124.03 (q, *J* = 274 Hz), 123.97 (q, *J* 6.0 Hz), 119.7, 115.5, 80.3, 64.3, 27.9, 18.8, 14.7; **^{19}F NMR (471 MHz, $CDCl_3$)** δ –62.7; IR (KBr) $_{max}$ 2974, 1662, 1325, 1270, 1246, 1072, 1042 cm^{-1}; **HPLC condition**: Phenomenex Chiralpak Amylose2, n-hexane/i-PrOH = 85/15, Flow rate 0.4 mL/min, UV = 254 nm, tR = 21.4 min (major) and tR = 35.0 min (minor).

(*R*)-N-Boc protected 2-(3-ethoxyphenylsulfonimidoyl)-3-methylpyridine (27f):

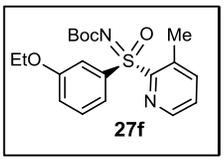

27f: 36 mg, 48% yield, 68% ee; $[\alpha]_D^{25}$ = – 8 (c 0.221, $CHCl_3$); **HPLC condition**: Daicel IG-3, MeOH, Flow rate = 0.5 mL/min, UV = 254 nm, tR = 13.2 min (minor) and tR = 26.5 min (major).

(*S*)-N-Boc protected 3-methyl-2-(3-(*p*-tolyl)naphthalene-2-sulfonimidoyl)pyridine (30j):

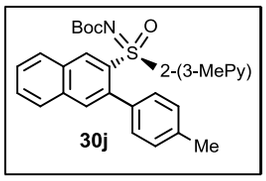

30j: 40 mg, 42% yield, 94% ee, colorless foam, $[\alpha]_D^{25}$ = (c 0.006, $CHCl_3$); **^{1}H NMR (400 MHz, $CDCl_3$)** δ 9.33 (s, 1H), 8.18 (dd, *J* 4.4, 1.2 Hz, 1H), 8.12 (d, *J* 7.2 Hz, 1H), 7.80 (d, *J* 7.6 Hz, 1H), 7.68–7.57 (m, 3H), 7.35–7.29 (m, 1H), 7.17 (dd, *J* 7.8, 4.6 Hz, 1H), 7.00–6.65 (m, 4H), 2.32 (s, 3H), 2.28 (s, 3H), 1.35 (s, 9H); **^{13}C NMR (101 MHz, $CDCl_3$)** δ 157.2, 155.0, 145.9, 140.7, 137.4, 137.3, 137.0, 135.3, 134.7, 134.6, 132.10, 132.07, 131.0, 129.7, 129.4, 127.7, 127.34, 127.27, 126.0, 80.1, 28.0, 21.1, 18.9 (1 carbon overlapped); IR (KBr) $_{max}$ 2971, 1662, 1275, 1248, 1151, 1060, 890 cm^{-1}; **HPLC condition**: YMC Amylose C-neo, n-hexane/i-PrOH 70/30, Flow rate 0.4 mL/min, UV 254 nm, tR 21.8 min (minor) and tR 24.3 min (major).

(*R*)-N-Boc protected 3-methyl-2-(naphthalene-2-sulfonimidoyl)pyridine (27j):

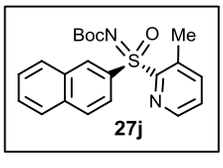

27j: 31 mg, 41% yield, 91% ee; $[\alpha]_D^{25}$ = –35.90 (c = 0.078, $CHCl_3$); **HPLC condition**: Daicel IG-3, MeOH, Flow rate = 0.7 mL/min, UV = 254 nm, tR = 9.6 min (minor). and tR = 29.4 min (major).

(*S*)-N-Boc protected 2-(3,4'-dimethyl-[1,1'-biphenyl]-2-sulfonimidoyl)pyridine (30k):

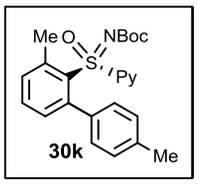

30k: 21 mg, 25% yield, 87% ee, colorless foam, $[\alpha]_D^{25}$ –17.31 (c 0.35, $CHCl_3$); **^{1}H NMR (500 MHz, $CDCl_3$)** δ 8.53 (d, *J* 5.0 Hz, 1H), 7.66 (d, *J* 8.0 Hz, 1H), 7.53– 46 (m, 1H), 7.41 (t, *J* 7.75 Hz, 1H), 7.37–7.28 (m, 2H), 7.15 (d, *J* 7.0 Hz, 1H), 7.07 (d, *J* 7.5 Hz, 1H), 6.97 (d, *J* 7.5 Hz, 1H), 6.64 (d, *J* 7.5 Hz, 1H), 6.27 (d, *J* 7.5 Hz, 1H), 2.93 (s, 3H), 2.30 (m, 3H), 1.41 (s, 9H); **^{13}C NMR (101 MHz, $CDCl_3$)** δ 158.3, 156.8, 149.6, 143.1, 142.8, 137.04, 136.96, 136.7, 135.0, 132.8, 131.8, 131.2, 130.0, 128.3, 127.9, 127.6, 126.3, 123.0, 80.3, 28.1, 23.5, 21.1; **HPLC condition**: Phenomenex Chiralpak Amylose2, n-hexane/*i*-PrOH 85/15, Flow rate = 0.7 mL/min, UV = 254 nm, tR 24.8 min (minor) and tR 29.2 min (major)

(*R*)-N-Boc protected 2-(2-methylphenylsulfonimidoyl) pyridine (27k):

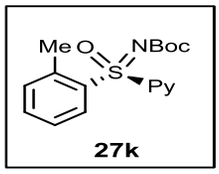

27k: 30 mg, 46% yield, 41% ee; $[\alpha]_D^{25}$ = 8.0 (c = 0.166, $CHCl_3$); **HPLC condition**: Daicel IG-3, MeOH, Flow rate 0.5 mL/min, UV 254 nm, tR 10.5 min (major) and tR 14.1 min (minor).

(*S*)-N-Boc protected 2-(3-methyl-4'-(trifluoromethyl)-[1,1'-biphenyl]-2-sulfonimidoyl) pyridine (30l):

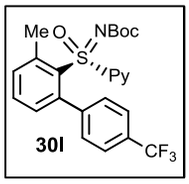

30l: 28 mg, 29% yield, 86% ee, colorless foam, $[\alpha]_D^{25}$ –81.68 (c 0.214, $CHCl_3$); **^{1}H NMR (500 MHz, $CDCl_3$)** δ 8.56 (d, *J* 4.0 Hz, 1H), 7.83 (d, *J* 8.0 Hz, 1H), 7.64–7.57 (m, 1H), 7.56–7.51 (m, 1H), 7.50–7.43 (m, 2H), 7.42–7.35 (m, 2H), 7.21 (d, *J* 8.0 Hz, 1H), 7.0 (d, *J* 7.5 Hz, 1H), 6.79 (d, *J* 8.0 Hz, 1H), 2.81 (s, 3H), 1.39 (s, 9H); ^{19}F NMR (376 MHz, $CDCl_3$) δ – 62.49; **^{13}C NMR (101 MHz, $CDCl_3$)** δ 158.0, 156.7, 149.8, 144.0, 142.2, 142.1, 137.5, 134.4, 133.4, 132.0, 130.8, 130.0, 129.0 (q, *J* 32 Hz), 128.9, 126.8, 124.0 (q, *J* 272 Hz), 123.8 (q, *J* 3.8 Hz), 122.8, 80.5, 28.0, 23.1 (one peak missing); IR (KBr) $_{max}$ 2979, 2938, 1660, 1279, 1243, 1156, 1120 cm^{-1}; **HPLC condition**: Phenomenex Chiralpak Amylose2, n-hexane/i-PrOH =90/10, Flow rate = 0.6 mL/min, UV 254 nm, tR 23.7 min (minor) and tR 27.8 min (major).

(*R*)-N-Boc protected 2-(2-methylphenylsulfonimidoyl) pyridine (27k):

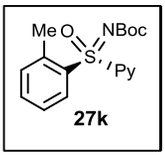

27k: 33mg, 49% yield, 50% ee; $[\alpha]_D^{25}$ (c 0.41, $CHCl_3$); **HPLC condition**: Daicel IG-3, MeOH, Flow rate = 0.3 mL/min, UV 254 nm, tR 10.4 min (major) and tR 14.0 min (minor).

(*S*)-N-Boc protected 1-(3'-methyl-2'-(pyridine-2-sulfonimidoyl)-[1,1'-biphenyl]-4-yl) ethanone (30m):

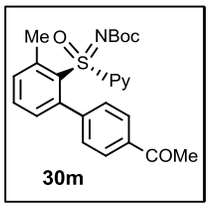

30m: 30 mg, 33% yield, 84% ee, colorless foam, $[\alpha]_D^{25}$ –22.91 (c = 0.213, $CHCl_3$); **^{1}H NMR (500 MHz, $CDCl_3$)** δ 8.59-8.53 (m, 1H), 7.91–7.82 (m, 2H), 7.65–7.56 (m, 2H), 7.49–7.33 (m, 4H), 7.03–6.97 (m, 1H), 6.83–6.77 (m, 1H), 2.77 (s, 3H), 2.58 (s, 3H), 1.38 (s, 9H); **^{13}C NMR (126 MHz, $CDCl_3$)** δ 197.7, 158.2, 156.6, 149.8, 145.5, 142.9, 141.9, 137.5, 135.5, 134.4, 133.2, 132.0, 130.7, 129.8, 128.8, 127.0, 126.9, 126.8, 122.8, 80.4, 28.0, 26.6, 23.0; IR (KBr) $_{max}$ 2974, 1673, 1646, 1280, 1237, 1111, 890 cm^{-1}; **HPLC condition**: YMC Amylose C-neo, n-hexane/i-PrOH 50/50, Flow rate = 0.5 mL/min, UV 254 nm, tR 9.7 min (minor) and tR 11.8 min (major).

(*R*)-N-Boc protected 2-(2-methylphenylsulfonimidoyl)pyridine(27k):

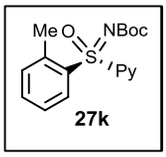

27k: 32 mg, 48% yield, 51% ee; $[\alpha]_D^{25}$ (c 0.45, $CHCl_3$); **HPLC condition**: Daicel IG-3, MeOH, Flow rate 0.5 mL/min, UV 254 nm, tR 10.9 min (major) and tR 14.5 min (minor).

(*S*)-N-Boc protected 2-(5-fluoro-3-methyl-4'-(trifluoromethyl)-[1,1'-biphenyl]-2-sulfonimidoyl)-pyridine (30n):

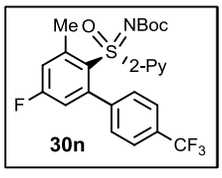

30n: 22 mg, 22% yield, 89% ee, colorless foam, $[\alpha]_D^{25}$ = –79.78 (c = 0.275, $CHCl_3$); **^{1}H NMR (400 MHz, $CDCl_3$)** δ 8.56 (dd, *J* 4.2, 0.6 Hz, 1H), 7.83 (d, *J* 8.0 Hz, 1H), 7.63 (td, *J* 7.8, 1.7 Hz, 1H), 7.57–7.52 (m, 1H), 7.45–7.43 (m, 1H), 7.43–7.37 (m, 1H), 7.23 (d, *J* 8.0 Hz, 1H), 7.09 (dd, *J* 8.8, 2.8 Hz, 1H), 6.81 (d, *J* 8.0 Hz, 1H), 6.74 (dd, *J* 8.4, 2.8 Hz, 1H), 2.79 (s, 3H), 1.41 (s, 9H); **^{13}C NMR (101 MHz, $CDCl_3$)** δ 164.6, 162.1, 157.9, 156.7, 149.8, 145.9, 145.8, 145.3, 145.2, 143.0, 137.6, 134.9, 130.4, 130.37, 130.0, 129.7, 129.67, 129.3, 129.0, 128.7, 128.0, 126.9, 125.3, 124.2,

124.0, 123.97, 123.9, 122.8, 122.6, 120.0, 119.9, 119.8, 118.0, 117.7, 80.6, 28.0, 24.8, 23.4; IR (KBr) $_{max}$ 3070, 2931, 1657, 1581, 1322, 1282, 1126 cm^{-1}; **^{19}F NMR (376 MHz, $CDCl_3$)** δ – 62.59, –106.89; **HPLC condition**: Phenomenex Chiralpak Amylose2, n-hexane/i-PrOH 90/10, Flow rate 0.7 mL/min, UV 254 nm, tR 16.1 min (minor) and tR 18.8 min (major).

(*R*)-N-Boc protected 2-(4-fluoro-2-methylphenylsulfonimidoyl)pyridine(27l):

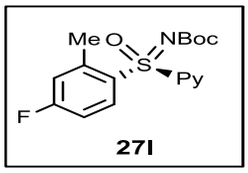

27l

27l: 36 mg, 51% yield, 37% ee; $[\alpha]_D^{25}$ c 0.088, $CHCl_3$); **HPLC condition**: Daicel IG-3, MeOH, Flow rate 0.5 mL/min, UV 254 nm, tR 10.2 min (major) and tR 12.9 min (minor).

II.6.3.5. Synthesis of chiral sulfoximine 32 (GP-5):

Chiral (*R*)-**27b** (0.2 mmol, 1.0 equiv) was dissolved in CH_2Cl_2 (2.0 mL) and TFA (10.0 equiv) was added. The mixture was stirred at 70 °C for 3 h. After concentration, the resulting residue was purified by flash column using hexane/EtOAc as the eluent to afford the desired product **32**.

(R)-2-(3-Methoxyphenylsulfonimidoyl)pyridine (32):

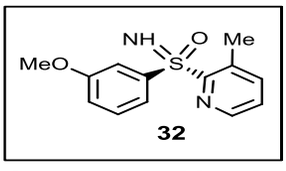

32

32: 46 mg, 88% yield, 95% ee, colorless highly viscous liquid, $[\alpha]_D^{25}$ –42.2 (c = 0.14, $CHCl_3$); **^{1}H NMR (500 MHz, $CDCl_3$)** δ 8.48 (d, *J* 4.5 Hz, 1H), 7.62–7.56 (m, 2H), 7.52 (t, *J* 2.25 Hz, 1H), 7.40 (d, *J* 8.0 Hz, 1H), 7.39–7.32 (m, 1H), 7.10 (dd, *J* 8.25, 2.25 Hz, 1H), 3.83 (s, 3H), 2.53 (s, 3H); **^{13}C NMR (126 MHz, $CDCl_3$)** δ 158.7, 156.0, 145.2, 140.9, 140.5, 132.2, 128.7, 125.8, 120.5, 118.6, 112.6, 54.7, 18.2; IR (KBr) $_{max}$ 3028, 2969, 1738, 1366, 1229, 1216 cm^{-1}; **HRMS (ESI)** for $C_{13}H_{15}N_2O_2S^+$ $(M+H)^+$: calcd. 263.0849, found 263.0858; **HPLC condition**: IH-3, MeOH/DEA 99.9/0.1, Flow rate = 0.5 mL/min, UV 254 nm, tR 9.4 min (major) and tR 10.2 min (minor).

II.6.3.6. Synthesis of chiral sulfoxide 33 (GP-6):

Chiral (*R*)-32 (0.2 mmol, 1.0 equiv) was dissolved in $CHCl_3$ (2.0 mL) under air and ^{t}BuONO (1.1 equiv) was added. The mixture was stirred at rt for 2 h. After

concentration, the resulting residue was purified by preparative TLC using hexane/EtOAc as the eluent to afford the desired product **33**.

(*R*)- 2-((3-Methoxyphenyl)sulfinyl)pyridine (33):

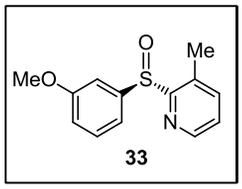

33

33: 39 mg, 78% yield, 90% ee, colorless highly viscous liquid, $[\alpha]_D^{25}$ –63 (c 0.13, $CHCl_3$); **^{1}H NMR (500 MHz, $CDCl_3$)** δ 8.47–8.40 (m, 1H), 7.25–7.18 (m, 2H), 7.18–7.08 (m, 2H), 6.88–7.80 (m, 1H), 3.68 (s, 3H), 2.37 (s, 3H); **^{13}C NMR (126 MHz, $CDCl_3$)** δ 160.5, 159.9, 147.5, 144.3, 139.8, 132.9, 129.7, 125.0, 117.04, 116.97, 109.4, 55.2, 16.5; IR (KBr) $_{max}$ 3456, 2925, 1592, 1479, 1283, 1245, 1038 cm^{-1}; **HRMS (ESI)** for $C_{13}H_{13}NNaO_2S^+$ $(M+Na)^+$: calcd. 270.0559, found 270.0570; **HPLC condition**: IC-3, MeOH, Flow rate = 0.5 mL/min, UV 254 nm, tR 14.0 min (major) and tR 14.8 min (minor).

II.6.3.5. Synthesis of Michael product 34 (GP-7):

Chiral (*R*)-**29c** (0.2 mmol, 1.0 equiv) was dissolved in CH_2Cl_2 (2.0 mL) and TFA (10.0 equiv) was added. The mixture was stirred at 70 °C for 3 h. After concentration, the resulting residue was purified by flash column using hexane/EtOAc as the eluent to afford the desired product **8**.

Methyl 2-((1S)-6-methoxy-1-(3-methylpyridin-2-yl)-1-oxidobenzo[d]isothiazol-3-yl)acetate (34):

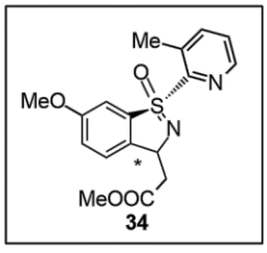

34

34: 46 mg, 66% yield, 95% ee , colorless highly viscous liquid. $[\alpha]_D^{25}$ 47.3 (c = 0.114, $CHCl_3$); ^{1}H NMR (500 MHz, $CDCl_3$) – m, (dd, *J* 7.75, 0.75 Hz, 1H), 7.40 (d, *J* 8.0 Hz, 1H), 7.28 (dd, *J* 7.5, 4.5 Hz, 1H), 7.18–7.12 (m, 2H), 5.29 (t, *J* 1.5 Hz, 1H), 3.80 (s, 3H), 3.71 (s, 3H), 2.89 (dd, *J* 6.75, 3.25 Hz, 2H), 2.66 (s, 3H); ^{13}C NMR (126 MHz, $CDCl_3$) δ 171.7, 160.2, 156.9, 146.2, 141.4, 141.1, 137.9, 133.1, 126.0, 124.1, 121.0, 106.5, 65.3, 55.8, 51.7, 43.1, 18.9; IR (KBr) $_{max}$ 2969, 2360, 2340, 1736, 1264, 1231, 1039 cm^{-1}; **HRMS (ESI)** for $C_{17}H_{19}N_2O_4S^+$ $(M+H)^+$: calcd. 347.1060, found 347.1070; **HPLC condition**: IG-3, MeOH, Flow rate 0.3 mL/min, UV 254 nm, tR 22.8 min (major) and tR 30.4 min (minor).

II.6.3.5. Synthesis of thiazine 35 (GP-8):

Chiral (*R*)-**30d** (0.2 mmol, 1.0 equiv) was dissolved in CH_2Cl_2 (2.0 mL) and TFA (10.0 equiv) was added. The mixture was stirred at 70 °C for 1 h. After basic work-up followed by concentration, it was further subjected to $Pd(OAc)_2$ (10 mol%), $PhI(OAc)_2$ (2.0 equiv) in toluene at 75 °C for 12 h. Next the crude was purified by flash column using hexane/EtOAc as the eluent to afford the desired product **9**.

(S)-8-Fluoro-3-methoxy-5-(3-methylpyridin-2-yl)dibenzo[c,e][1,2]thiazine 5-oxide (9):

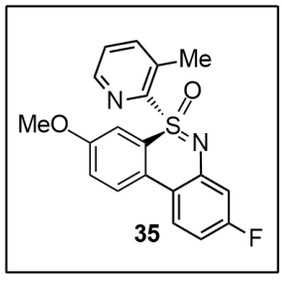

35: 44 mg, 62% yield, 93% ee, colorless highly viscous liquid. $[\alpha]_D^{25}$ 63.1 (c = 0.014, $CHCl_3$); ^{1}H NMR (500 MHz, $CDCl_3$) 8.50 (d, *J* = 4.5 Hz, 1H), 8.08 (d, *J* 9.0 Hz, 1H), 7.93 (dd, *J* 9.0, 6.0 Hz, 1H), 7.66 (d, *J* 7.5 Hz, 1H), 7.39 (dd, *J* 7.5, 4.5 Hz, 1H), 7.30 (dd, *J* 9.0, 2.5 Hz, 1H), 6.99 (d, *J* 2.5 Hz, 1H), 6.92 (dd, *J* 0.5, 2.5 Hz, 1H), 6.83–6.75 (m, 1H), 3.76 (s, 3H), 2.38 (s, 3H); ^{13}C NMR (101 MHz, $CDCl_3$) δ 63.5 (d, *J* 47 Hz), 158.7, 155.1, 146.5, 143.7 (d, *J* 12 Hz), 141.9, 134.3, 128.4, 127.0, 124.8, 124.4 (d, *J* 10 Hz), 123.2, 122.0, 113.5, 110.7 (d, *J* 3 Hz), 108.7 (d, *J* 22 Hz), 108.3, 55.7, 19.0; IR (KBr) $_{max}$ 2940, 2350, 2230, 1213, 1201, 1019 cm^{-1}; **^{19}F NMR (471 MHz, $CDCl_3$)** δ – 111.99; **HPLC condition**: IH-3, MeOH, Flow rate 0.4 mL/min, UV 254 nm, tR 15.1 min (major) and tR 15.8 min (minor).

II.7. References

[1] For recent reviews on enantioselective C–H functionalization, see: a) J. Wencel-Delord, F. Colobert, *Chem. Eur.J.* **2013**, *19*, 14010; b) C.Zheng, S.-L. You, *RSC Adv*. **2014**, *4*, 6173; c) T. G. Saint-Denis, R.-Y. Zhu, G. Chen, Q.-F. Wu, J.-Q. Yu, *Science* **2018**, 359, 759. C) J. Diesel, N. Cramer, *ACS Catal*. **2019**, *9*, 9164.

[2] a) B.-F. Shi, N. Maugel, Y.-H. Zhang, J.-Q. Yu, *Angew. Chem. Int. Ed*. **2008**, *47*, 4882; b) M. R. Albicker, N. Cramer, *Angew. Chem. Int. Ed*. **2009**, *48*, 9139; c) B.-F. Shi, Y.-H. Zhang, J. K. Lam, D.-H. Wang, J.-Q. Yu, *J. Am. Chem. Soc.* **2010**, *132*, 460; d) T. Saget, N. Cramer, *Angew. Chem. Int. Ed.* **2013**, *52*, 7865; e) X. F. Cheng, Y. Li, Y. M. Su, F. Yin, J. Y. Wang, J. Sheng, H. U. Vora, X. S. Wang, J. Q. Yu, *J. Am. Chem. Soc.* **2013**, *135*, 1236; f) L.

Chu, X. C. Wang, C. E. Moore, A. L. Rheingold, J. Q. Yu, *J. Am. Chem. Soc*. **2013**, *135*, 16344; g) Gao, D.-W.; Shi, Y.-C.; Gu, Q.; Zhao, Z.-L.; You, S.-L. *J. Am. Chem. Soc*. **2013**, *135*, 86– 89; h) T. Lee, T. W. Wilson, R. Berg, P. Ryberg, J. F. Hartwig, *J. Am. Chem. Soc*. **2015**, *137*, 6742; i) B. N. Laforteza, K. S. L. Chan, J. Q. Yu, Angew. Chem. Int. Ed. **2015**, *54*, 11143; j) D. Grosheva, N. Cramer, *ACS Catal*. **2017**, *7*, 7417; k) J. Wang, D.-W. Gao, J. Huang, S. Tang, Z. Xiong, H. Zu, S.-L. You, Q. Zhu, ACS Catal. **2017**, *7*, 3832; l) H. Shi, A. N. Herron, Y. Shao, Q. Shao, J.-Q. Yu, *Nature* **2018**, *558*, 581; m) L. Yang, M. Neuburger, O. Baudoin, *Angew. Chem. Int. Ed*. **2018**, *57*, 1394; n) L. Lin, S. Fukagawa, D. Sekine, E. Tomita, T. Yoshino, S. Matsunaga, *Angew. Chem. Int. Ed*. **2018**, *57*, 12048; o) N. Cramer, D. Grosheva, Angew. Chem. Int. Ed. **2018**, *57*, 13644;

[3] a) D. Gwon, S. Park, S. Chang, Tetrahedron **2015**, *71*, 4504; b) Z.- Q. Lin, W.-Z. Wang, S.-B. Yan, W.-L. Duan, *Angew. Chem. Int. Ed.* **2015**, *54*, 6265; c) L. Liu, A.- A. Zhang, Y. Wang, F. Zhang, Z. Zuo, W.-X. Zhao, C.-L. Feng, W. Ma, *Org. Lett*. **2015**, *17*, 2046; d) G. Xu, M. Li, S. Wang, W. Tang, *Org. Chem. Front.* **2015**, *2*, 1342; e) Z.-J. Du, J. Guan, G.-J. Wu, P. Xu, L.-X. Gao, F.-S. Han, *J. Am. Chem. Soc.* **2015**, *137*, 632; f) Y. Sun, N. Cramer, *Angew. Chem. Int. Ed*. **2017**, *56*, 364; g) S.-X. Li, Y.-N. Ma, S.-D. Yang, *Org. Lett*. **2017**, *19*, 1842; h) Y.-S. Jang, M. Dieckmann, N. Cramer, *Angew. Chem. Int. Ed.* **2017**, *56*, 15088; i) Z. Wang, T. Hayashi, *Angew. Chem. Int. Ed.* **2018**, 57, 1702; j) Y.-S. Jang, Ł. Woz´niak, J. Pedroni, N. Cramer, Angew. Chem. Int. Ed. **2018**, *57*, 12901; K) Y.-C. Zhu, Y. Li, B.-C. Zhang, F.-X. Zhang, Y.-N. Yang, X.-S. Wang, *Angew. Chem. Int. Ed*. **2018**, *57*, 5129. l) W. Liu, W. Yang, J. Zhu, Y. Guo, N. Wang, J. Ke, P. Yu, C. He, *ACS Catal*. **2020**, *10*, 7207.

[4] a) K.-J. Xiao, L. Chu, G. Chen, J.-Q. Yu, *J. Am. Chem. Soc*. **2016**, *138*, 7796; b) K.- J. Xiao, L. Chu, J.-Q. Yu, *Angew. Chem. Int.* Ed. **2016**, *55*, 2856; c) L. Chu, K.-J. Xiao, J.-Q. Yu, *Science* **2014**, *346*, 451.

[5] a) J. A. Sirvent, U. Lgcking, ChemMedChem **2017**, *12*, 476; b) M. Frings, C. Bolm, A. Blum, C. Gnamm, *Eur. J. Med. Chem*. **2017**, *126*, 225.

[6] a) K. Mukherjee, M. Shankar, K. Ghosh, A. K. Sahoo, *Org. Lett*. **2018**, *20*, 1914; b) M. Shankar, A. Saha, S. Sau, A. Ghosh, V. Gandon, and A. K. Sahoo, *Chem. Sci.* **2021**, *12*, 6393.

[7] J. Wang, M. Frings, C. Bolm, *Angew. Chem. Int. Ed*. **2013**, *52*, 8661; b) J. Legros, C. Bolm, *Angew. Chem. Int. Ed*. **2003**, *42*, 5487.

[8] a) S. Dong, M. Frings, H. Cheng, J. Wen, D. Zhang, G. Raabe, C. Bolm, *J. Am. Chem. Soc.* **2016**, *138*, 2166; b) J. Wang, M. Frings, C. Bolm, *Chem. Eur. J.* **2014**, *20*, 966.

[9] a) Y. Sun, N. Cramer, *Angew. Chem. Int. Ed.* **2018**, *57*, 15539; b) B. Shen, B. Wan, X. Li, *Angew. Chem. Int. Ed.* **2018**, *57*, 15534; c) T. Zhou, P.-F. Qian, J.-Y. Li, Y.-B. Zhou, H.-C. Li, H.-Y. Chen, and B.-F. Shi, *J. Am. Chem. Soc.* **2021**, *143*, 6810.

[10] (a) B. Sreedhar, P. S. Reddy, M. A. Reddy. *Synthesis,* **2009**, *10*, 1732-1738. (b) Y. Xie, B. Zhou, S. Zhou, S. Zhou, W. Wei, J. Liu, Y. Zhan, D. Cheng, M. Chen, Y. Li, B. Wang, X.-s. Xue, Z. Li, *ChemistrySelect,* **2017**, *2*, 1620-1624. (c) J. In, S. Hwang, C. Kim, J. H. Seo, S. Kim, *Eur. J. Org. Chem.* **2012**, *2013*, 965-971.

[11] N. Yutaka, H. Miki, T. Kenji, Y. Yasuchika, S. Chung-gi, *Bull Chem Soc Jpn*., **1995**, *68*, 1369-1377.

[12] G. J. Cheng, P. Chen, T. Y. Sun, X. Zhang, J. Q. Yu, Y. D. Wu, *Chem. - A Eur. J.* **2015**, *21*, 11180.

[13] G.-J. J. Cheng, Y.-F. F. Yang, P. Liu, P. Chen, T.-Y. Y. Sun, G. Li, X. Zhang, K. N. Houk, J.-Q. Yu, Y.-D. D. Wu, *J. Am. Chem. Soc.* **2014**, *136*, 894.

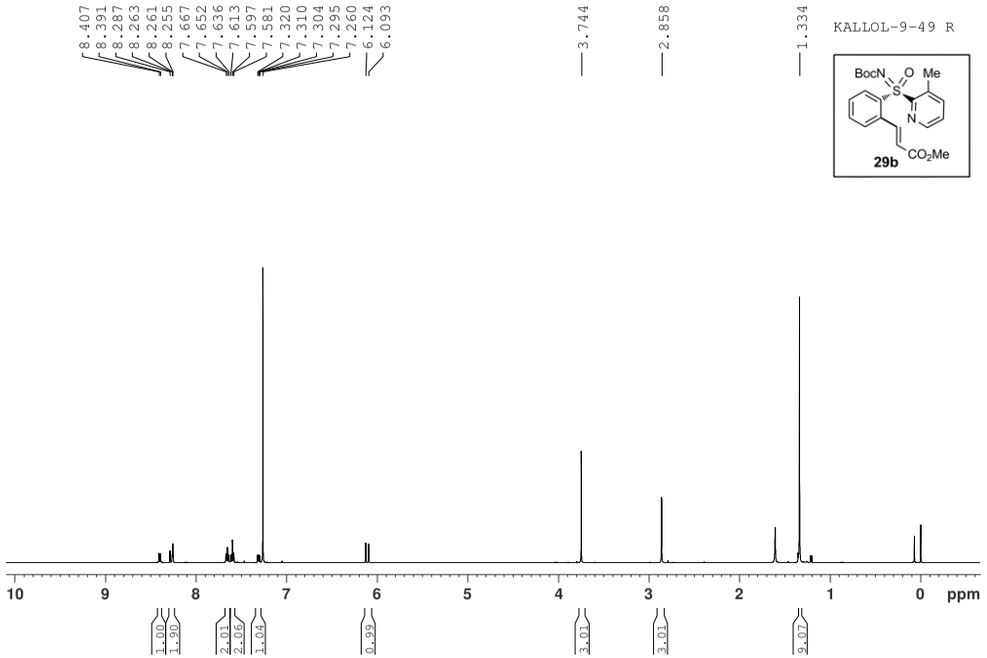
KALLOL-9-49 R
8.407
8.391
8.287
8.263
8.261
8.255
7.667
7.652
7.636
7.613
7.597
7.581
7.320
7.310
7.304
7.295
7.260
6.124
6.093
3.744
2.858
1.334
BocN
O
Me
CO2Me
29b
1.00
1.90
2.01
2.06
1.04
0.99
3.01
3.01
9.07
10 9 8 7 6 5 4 3 2 1 0 ppm

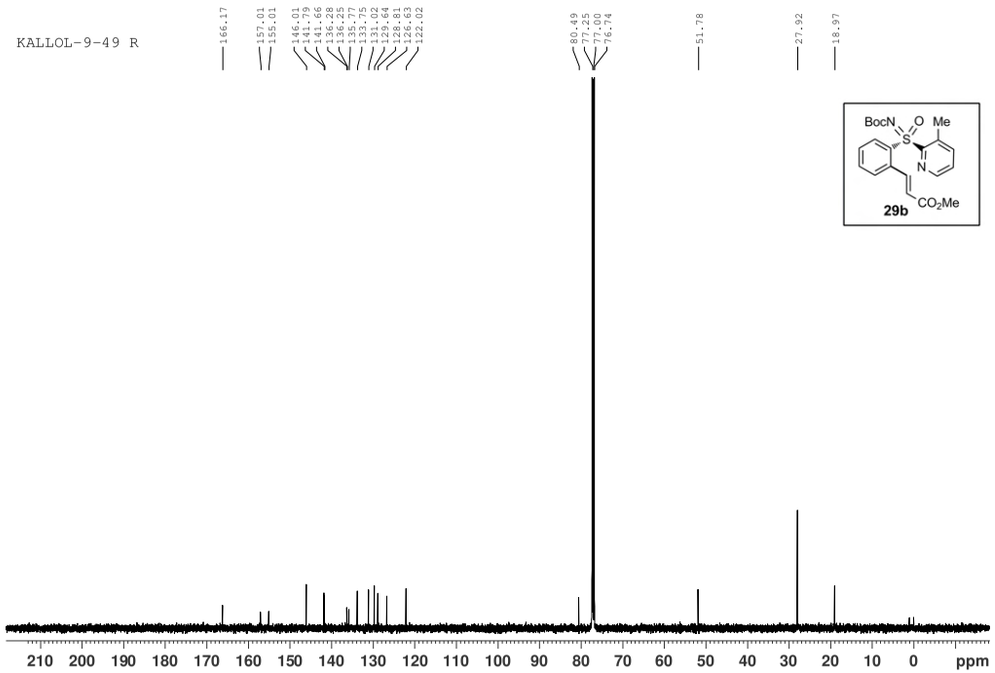
KALLOL-9-49 R
166.17
157.01
155.01
146.01
141.79
141.66
136.28
136.25
135.77
135.75
131.02
129.64
128.81
126.63
122.02
80.49
77.25
77.00
76.74
51.78
27.92
18.97
BocN
O
Me
CO2Me
29b
210 200 190 180 170 160 150 140 130 120 110 100 90 80 70 60 50 40 30 20 10 0 ppm

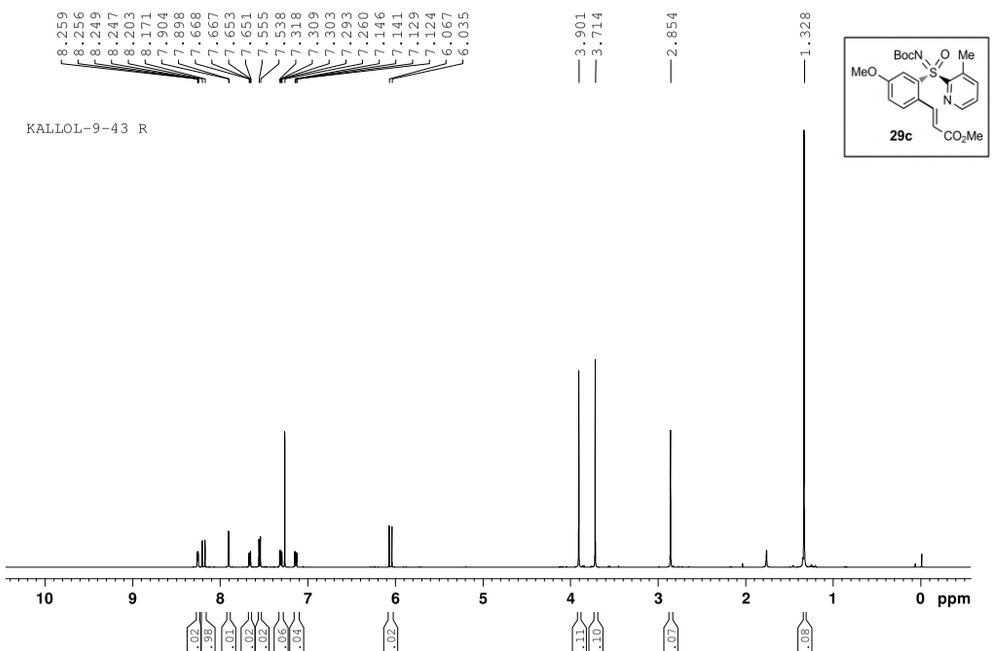
KALLOL-9-43 R
8.259
8.256
8.249
8.247
8.203
8.171
7.904
7.898
7.668
7.667
7.653
7.651
7.555
7.538
7.318
7.309
7.303
7.293
7.260
7.146
7.141
7.129
7.124
6.067
6.035
3.901
3.714
2.854
1.328
BocN
O
Me
MeO
CO2Me
29c
1.02
2.98
1.01
1.02
1.02
1.06
1.04
1.02
3.11
3.10
2.07
9.08
10 9 8 7 6 5 4 3 2 1 0 ppm

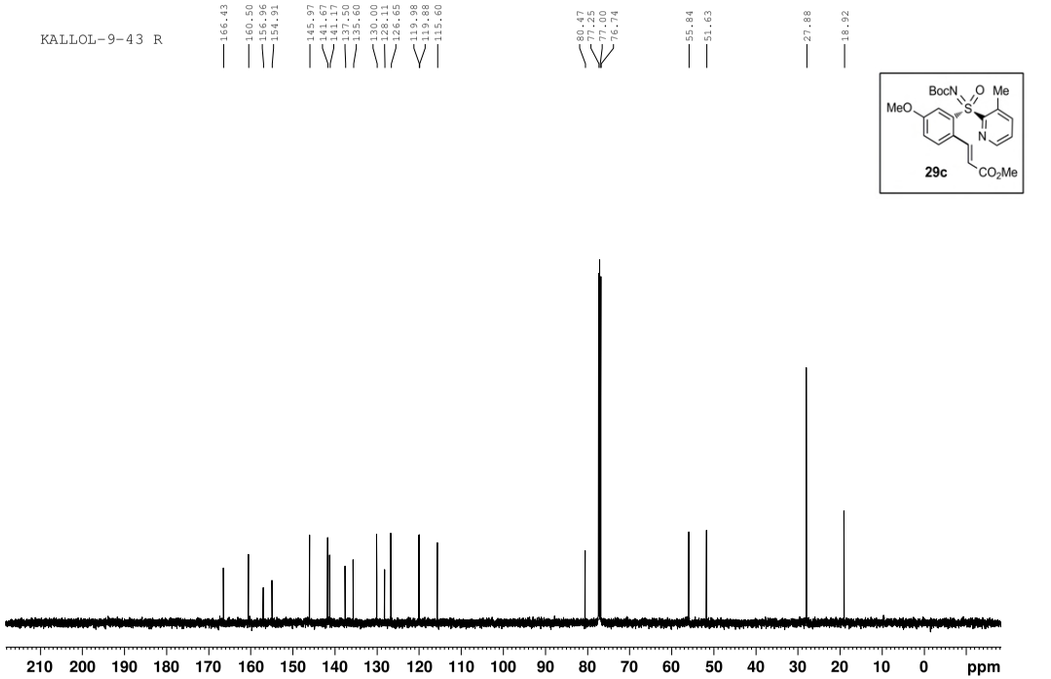
KALLOL-9-43 R
166.43
160.50
156.96
154.91
145.97
141.67
141.17
137.50
135.60
130.00
128.11
126.65
119.98
119.88
115.60
80.47
77.25
77.00
76.74
55.84
51.63
27.88
18.92
BocN
O
Me
MeO
CO2Me
29c
210 200 190 180 170 160 150 140 130 120 110 100 90 80 70 60 50 40 30 20 10 0 ppm

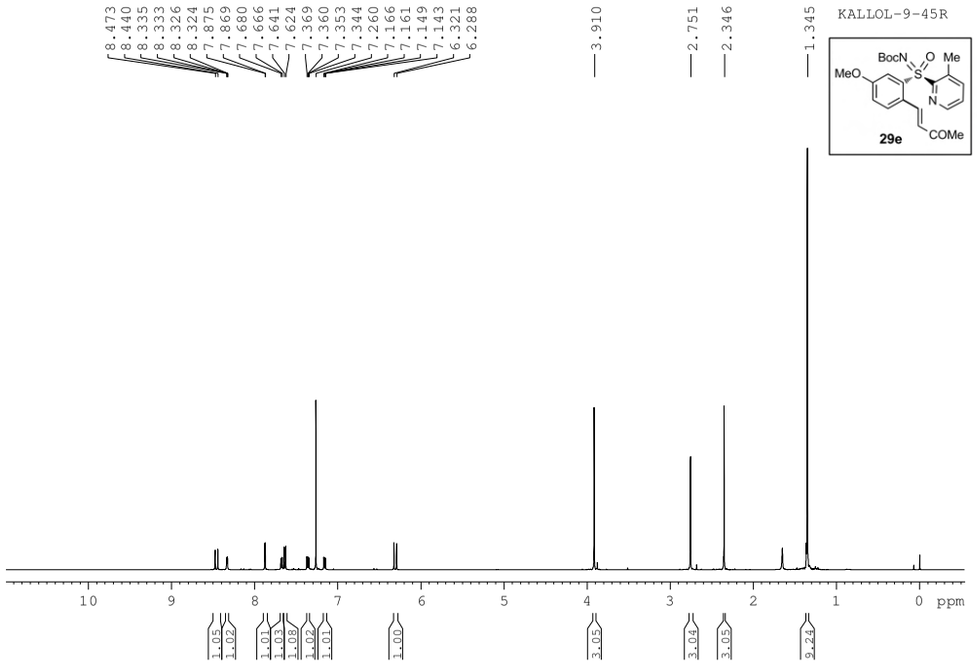
KALLOL-9-45R
8.473
8.440
8.335
8.333
8.326
8.324
7.875
7.869
7.680
7.666
7.641
7.624
7.369
7.360
7.353
7.344
7.260
7.166
7.161
7.149
7.143
6.321
6.288
3.910
2.751
2.346
1.345
BocN
O
Me
MeO
S
N
COMe
29e
10 9 8 7 6 5 4 3 2 1 0 ppm
1.05 1.02 1.01 1.03 1.08 1.02 1.01 1.00 3.05 3.04 3.05 9.24

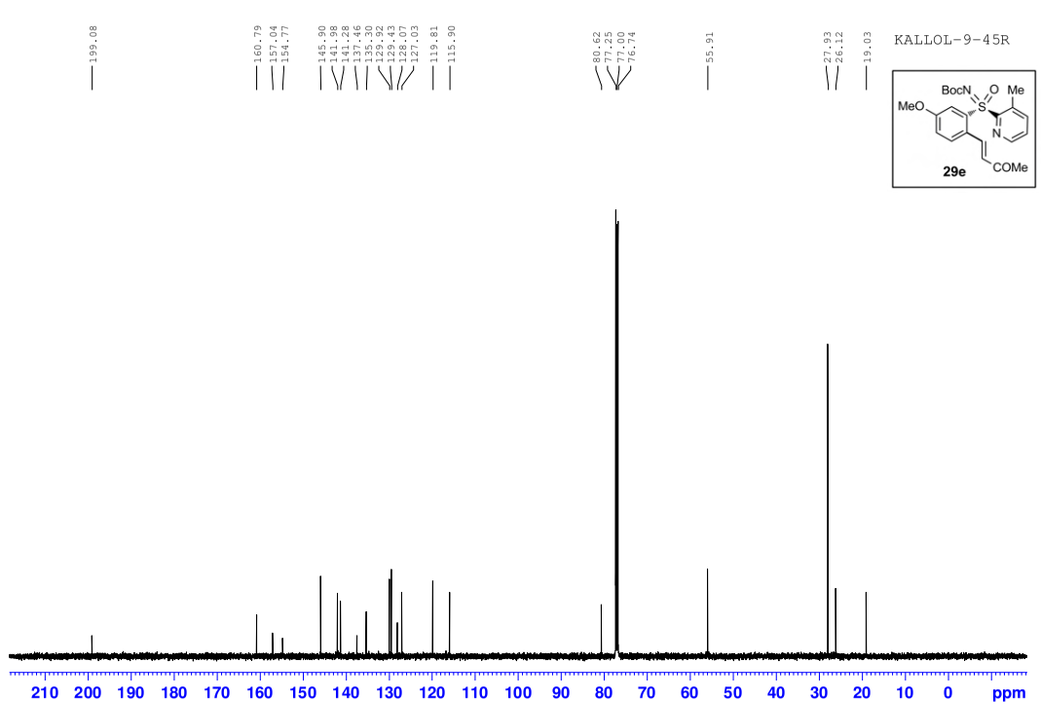
KALLOL-9-45R
199.08
160.79
157.04
154.77
145.90
141.98
141.28
137.46
135.30
129.92
129.43
128.07
127.03
119.81
115.90
80.62
77.25
77.00
76.74
55.91
27.93
26.12
19.03
BocN
O
Me
MeO
S
N
COMe
29e
210 200 190 180 170 160 150 140 130 120 110 100 90 80 70 60 50 40 30 20 10 0 ppm

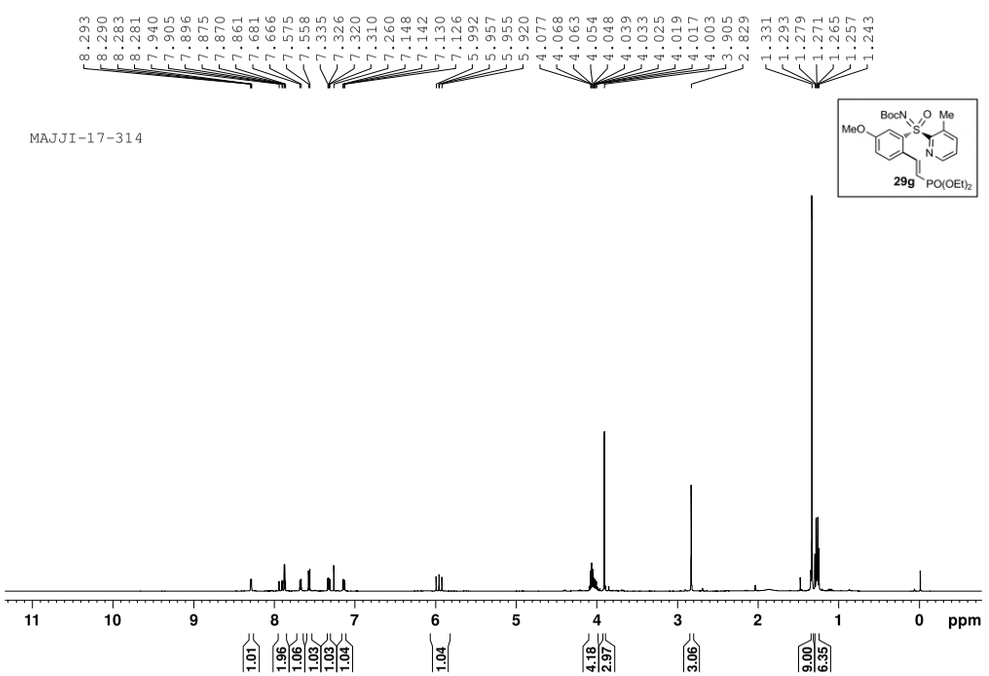
MAJJI-17-314
8.293
8.290
8.283
8.281
7.940
7.905
7.896
7.875
7.870
7.861
7.681
7.666
7.575
7.558
7.335
7.326
7.320
7.310
7.260
7.148
7.142
7.130
7.126
5.992
5.957
5.955
5.920
4.077
4.068
4.063
4.054
4.048
4.039
4.033
4.025
4.019
4.017
4.003
3.905
2.829
1.331
1.293
1.279
1.271
1.265
1.257
1.243
BocN
O
Me
MeO
S
N
29g
PO(OEt)2
11 10 9 8 7 6 5 4 3 2 1 0 ppm
1.01 1.96 1.06 1.03 1.03 1.04 1.04 4.18 2.97 3.06 9.00 6.35

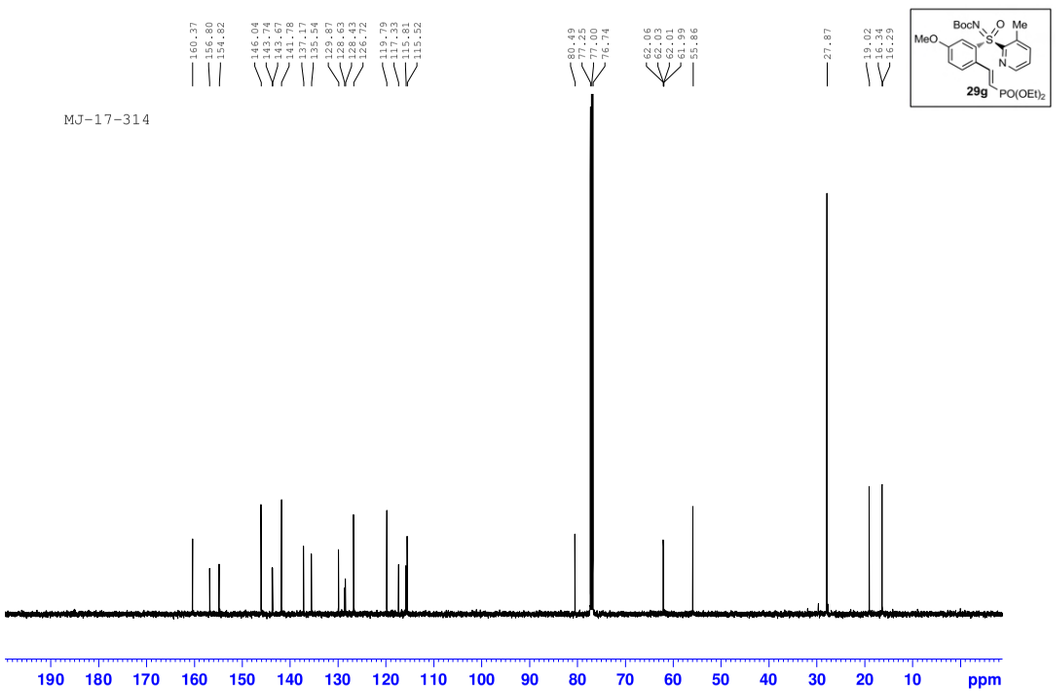
MJ-17-314
160.37
156.80
154.82
146.04
143.74
143.67
141.78
137.17
135.54
129.87
128.63
128.43
126.72
119.79
117.33
115.81
115.52
80.49
77.25
77.00
76.74
62.06
62.03
62.01
61.99
55.86
27.87
19.02
16.34
16.29
BocN
O
Me
MeO
S
N
29g
PO(OEt)2
190 180 170 160 150 140 130 120 110 100 90 80 70 60 50 40 30 20 10 ppm

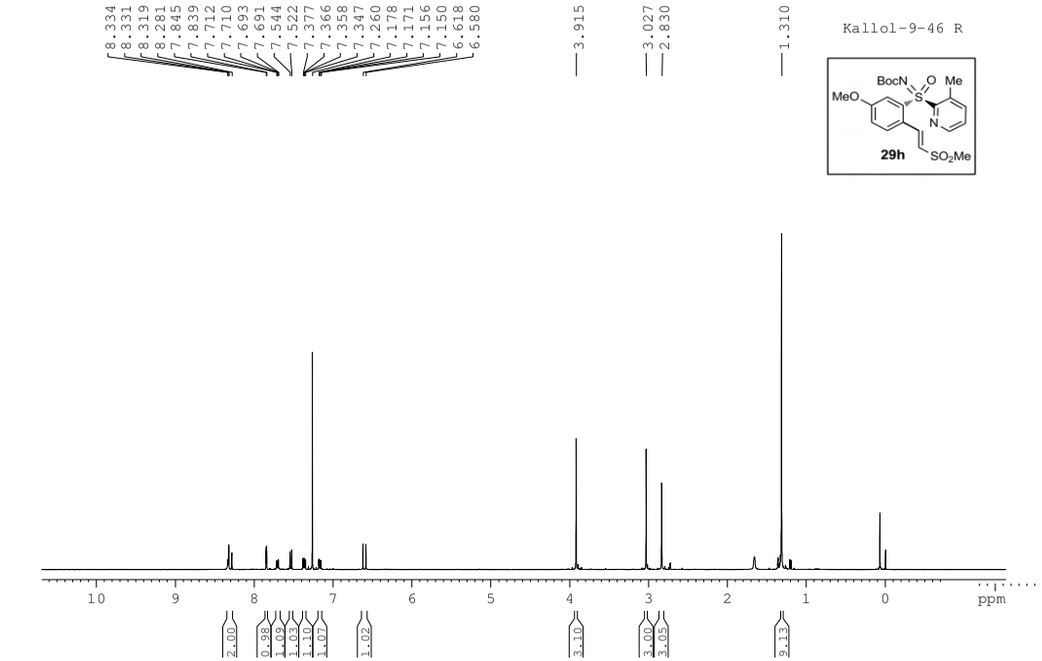
8.334
8.331
8.319
8.281
7.845
7.839
7.712
7.710
7.693
7.691
7.544
7.522
7.377
7.366
7.358
7.347
7.260
7.178
7.171
7.156
7.150
6.618
6.580
3.915
3.027
2.830
1.310
Kallol-9-46 R
BocN
O
Me
MeO
N
29h
SO2Me
2.00
0.98
1.09
1.03
1.10
1.07
1.02
3.10
3.00
3.05
9.13
ppm

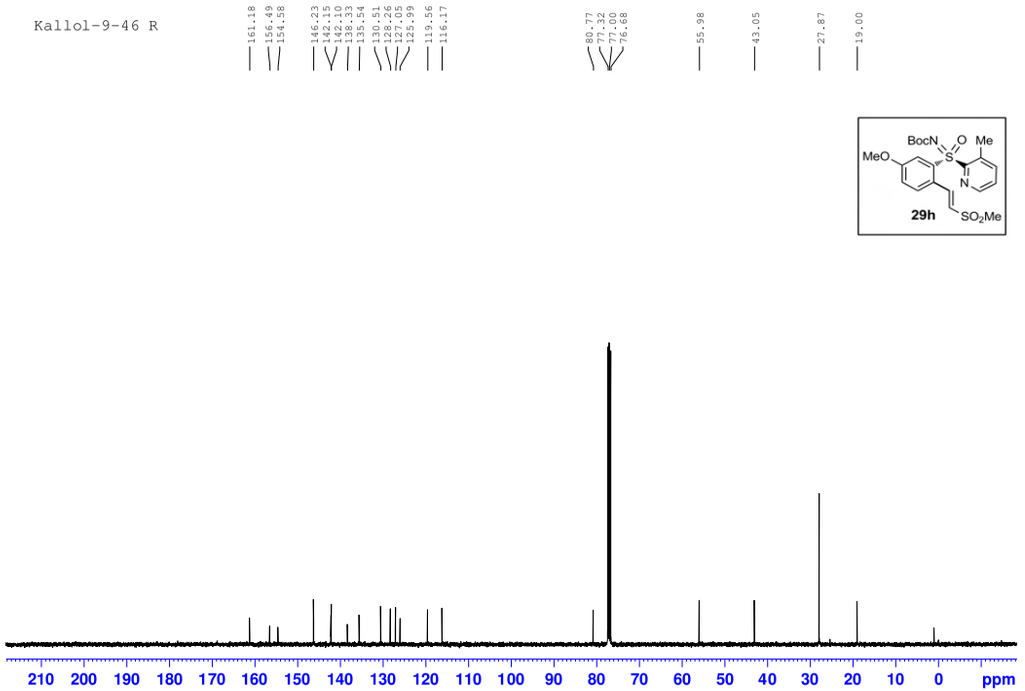
Kallol-9-46 R
161.18
156.49
154.58
146.23
142.15
141.00
138.33
135.54
130.51
128.26
127.05
125.99
119.56
116.17
80.77
77.32
77.00
76.68
55.98
43.05
27.87
19.00
BocN
O
Me
MeO
N
29h
SO2Me
210 200 190 180 170 160 150 140 130 120 110 100 90 80 70 60 50 40 30 20 10 0 ppm

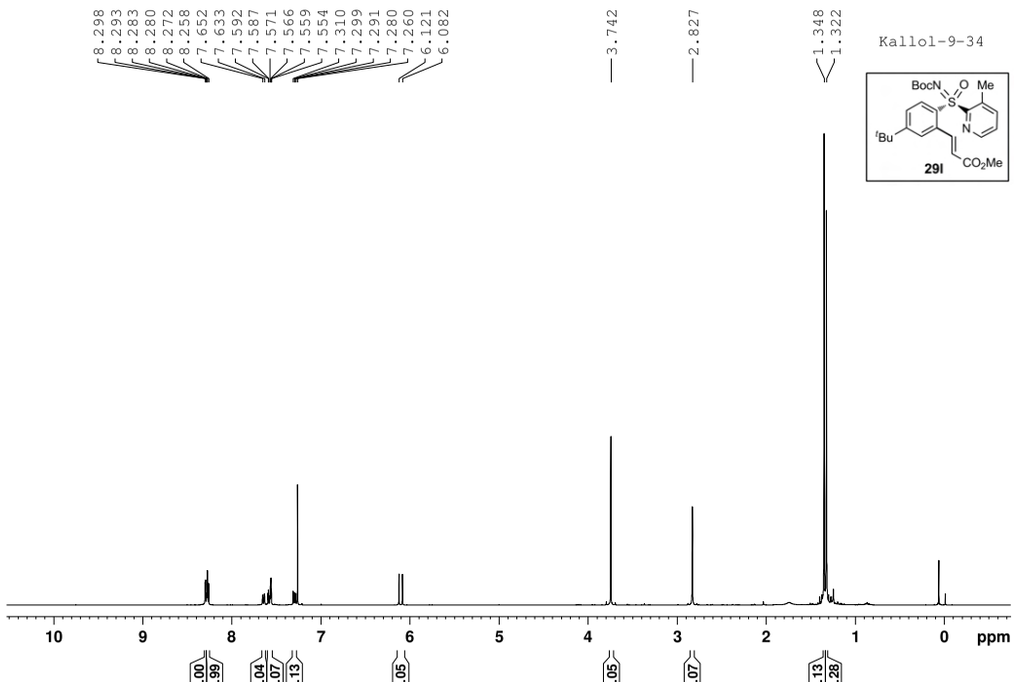
8.298
8.293
8.283
8.280
8.272
8.258
7.652
7.633
7.592
7.587
7.571
7.566
7.559
7.554
7.310
7.299
7.291
7.280
7.260
6.121
6.082
3.742
2.827
1.348
1.322
Kallol-9-34
BocN
O
Me
tBu
N
29l
CO2Me
10 9 8 7 6 5 4 3 2 1 0 ppm

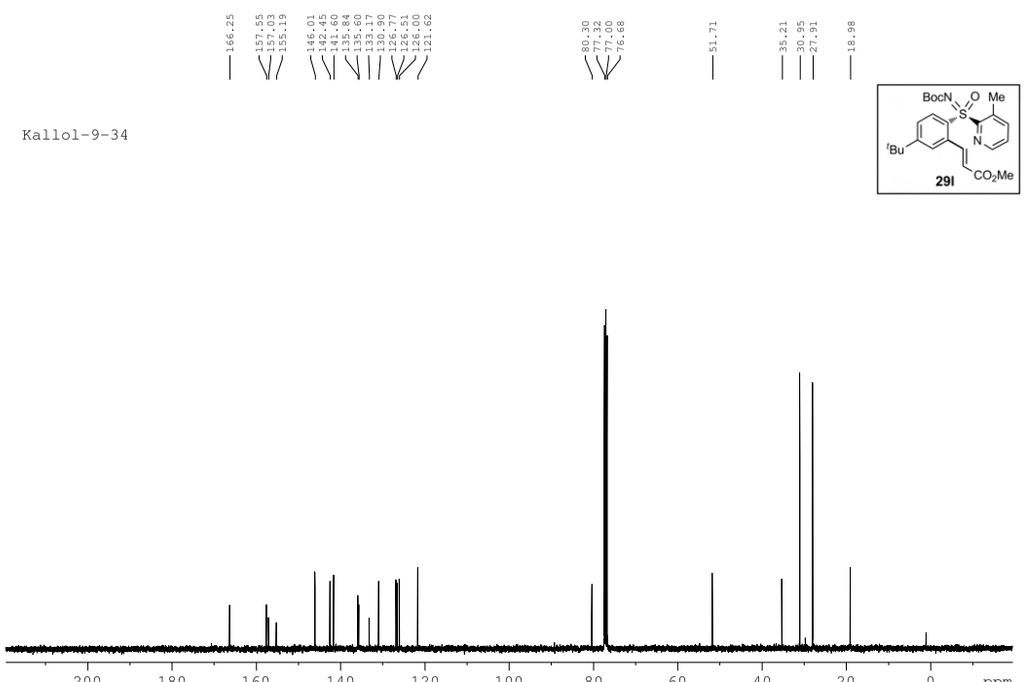
Kallol-9-34
166.25
157.55
157.03
155.19
146.01
142.45
141.60
135.84
135.60
130.17
130.00
126.77
126.51
126.00
121.62
80.30
77.32
77.00
76.68
51.71
35.21
30.95
27.91
18.98
BocN
O
Me
tBu
N
29l
CO2Me

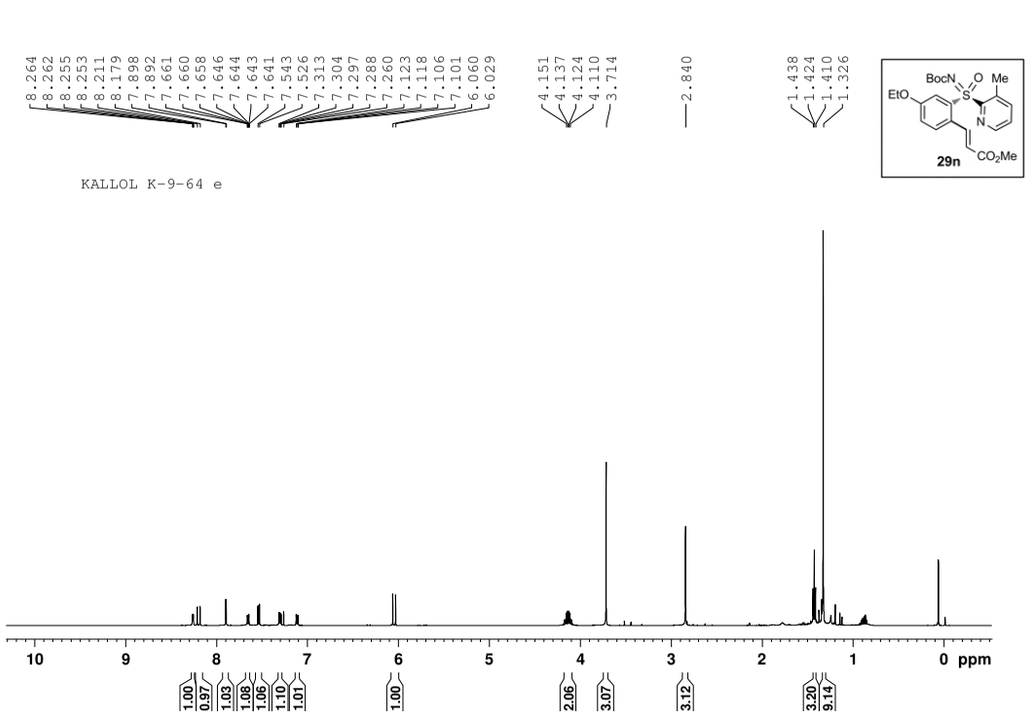
KALLOL K-9-64 e
29n

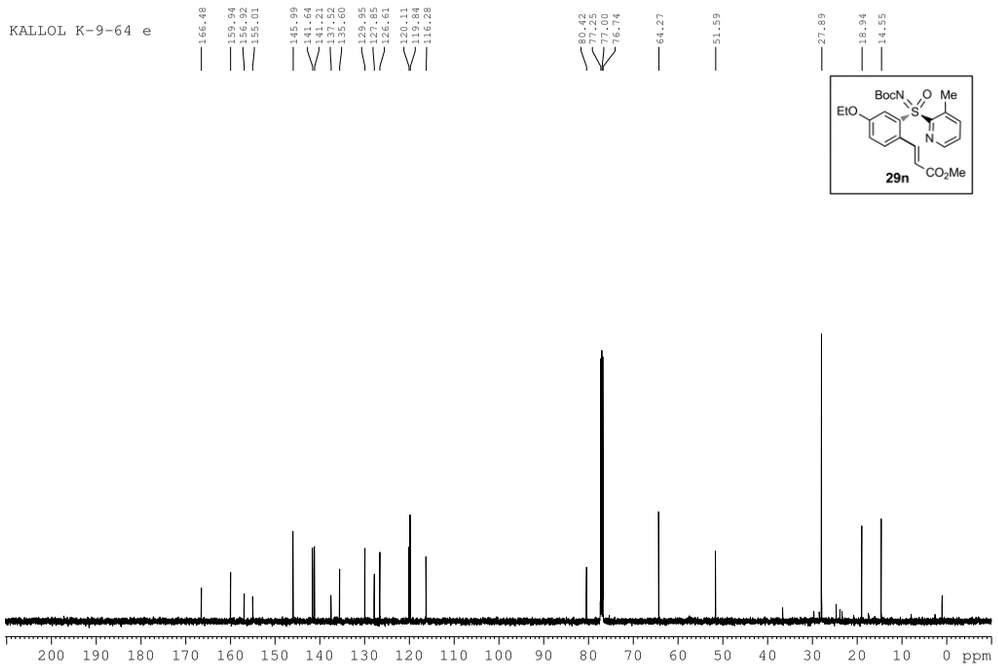
KALLOL K-9-64 e
29n

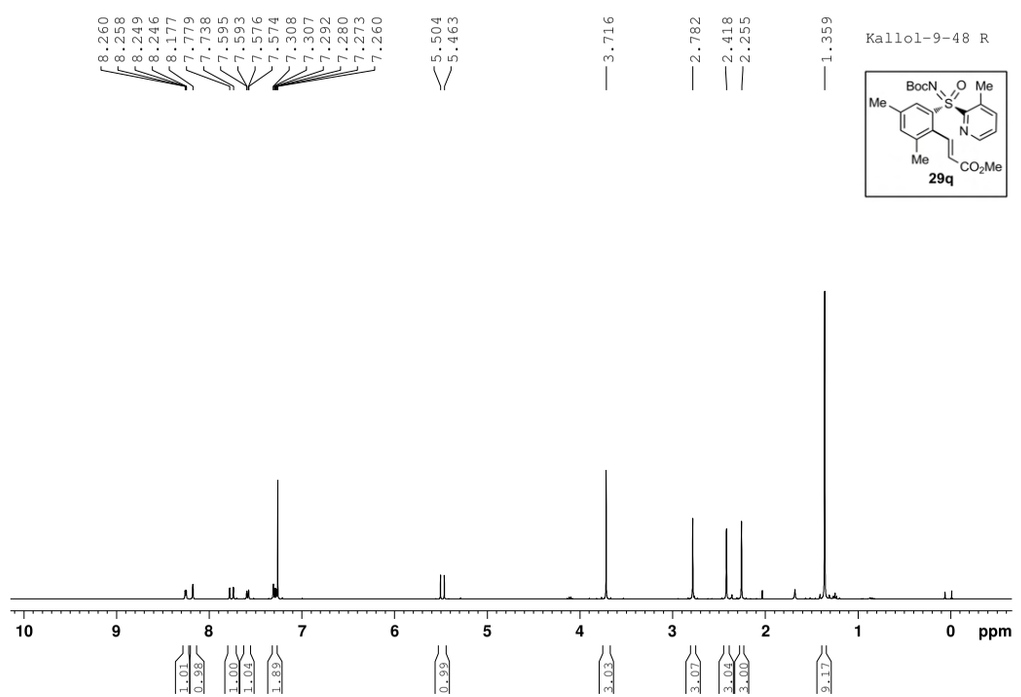
Kallol-9-48 R
29q

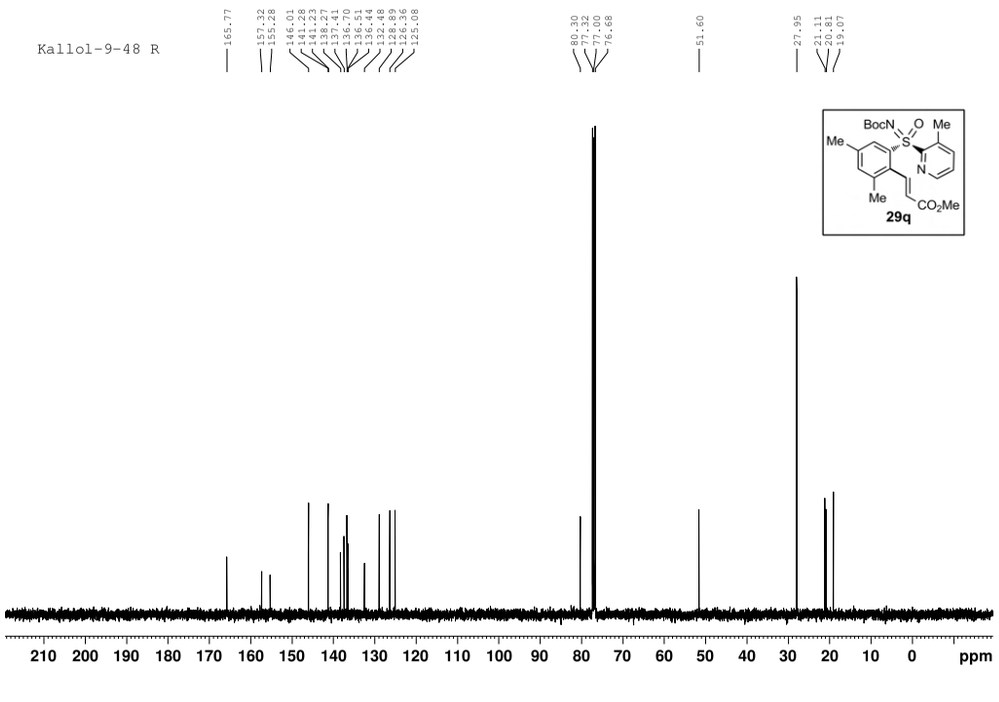
Kallol-9-48 R
29q

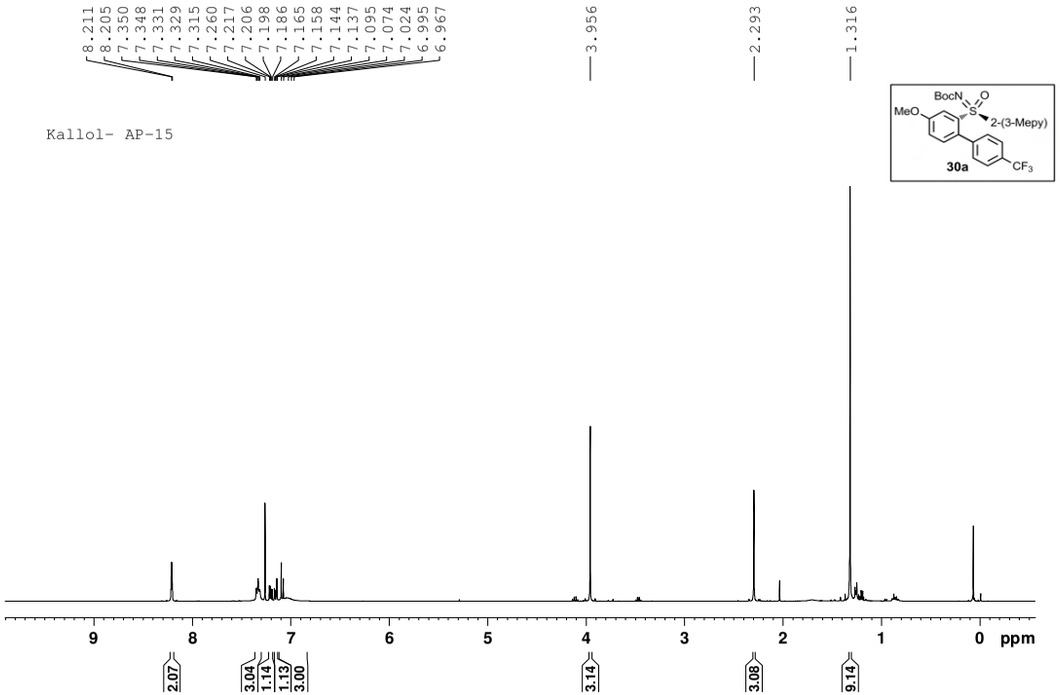
8.211
8.205
7.350
7.348
7.331
7.329
7.315
7.260
7.217
7.206
7.198
7.186
7.165
7.158
7.144
7.137
7.095
7.074
7.024
6.995
6.967
3.956
2.293
1.316
Kallol- AP-15
BocN
O
S
MeO
2-(3-Mepy)
CF3
30a
9 8 7 6 5 4 3 2 1 0 ppm
2.07
3.04
1.14
1.13
3.00
3.14
3.08
9.14

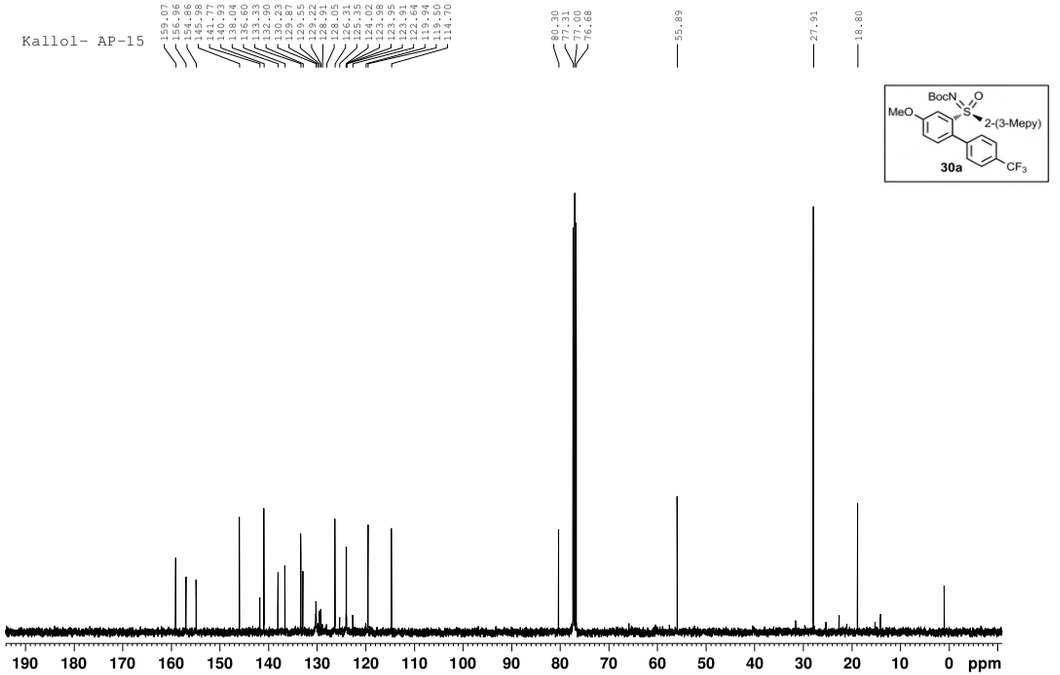
Kallol- AP-15
159.07
156.96
154.86
145.98
141.77
140.93
138.04
136.60
133.33
132.90
130.23
129.87
129.55
129.22
128.91
128.05
126.31
125.30
124.02
123.98
123.95
122.91
122.64
119.94
119.50
114.70
80.30
77.31
77.00
76.68
55.89
27.91
18.80
BocN
O
S
MeO
2-(3-Mepy)
CF3
30a
190 180 170 160 150 140 130 120 110 100 90 80 70 60 50 40 30 20 10 0 ppm

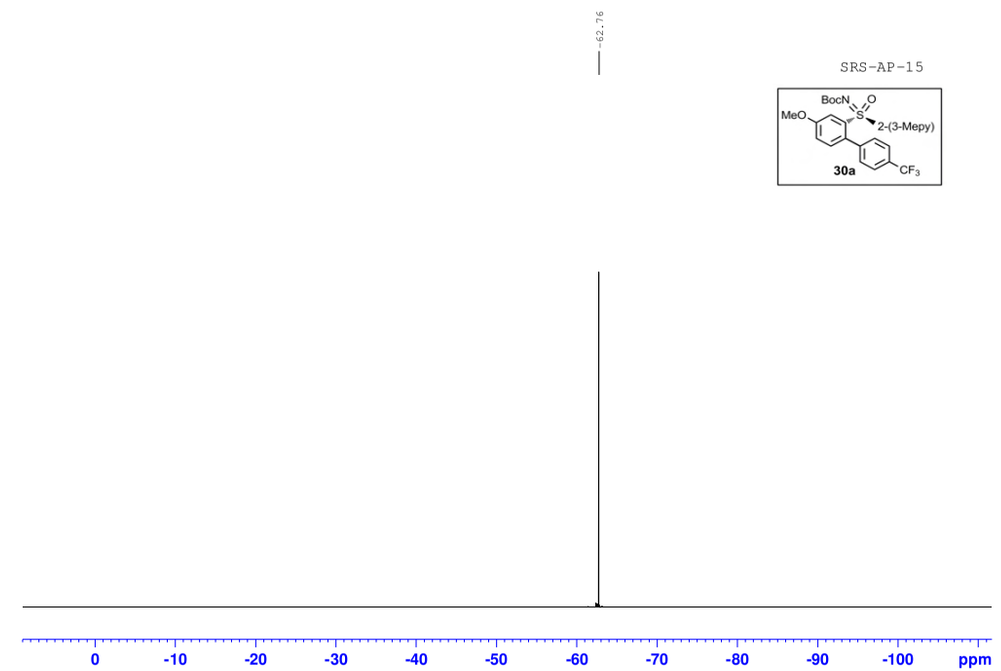
-62.76
SRS-AP-15
BocN
O
S
MeO
2-(3-Mepy)
CF3
30a
0 -10 -20 -30 -40 -50 -60 -70 -80 -90 -100 ppm

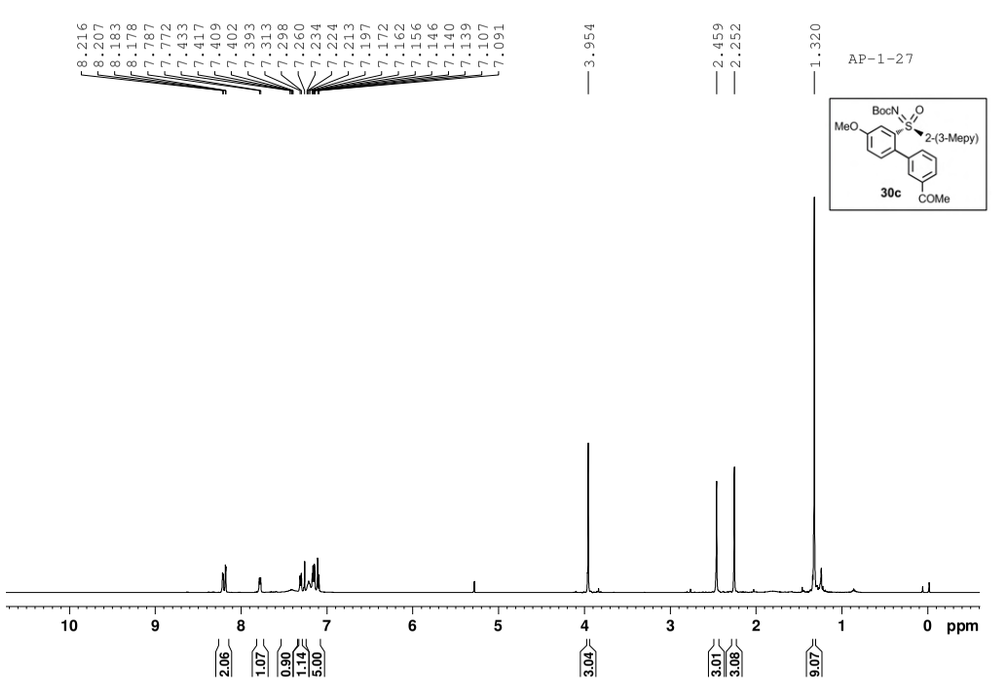
8.216
8.207
8.183
8.178
7.787
7.772
7.433
7.417
7.409
7.402
7.393
7.313
7.298
7.260
7.234
7.224
7.213
7.197
7.172
7.162
7.156
7.146
7.140
7.139
7.107
7.091
3.954
2.459
2.252
1.320
AP-1-27
BocN
O
S
MeO
2-(3-Mepy)
30c
COMe
10 9 8 7 6 5 4 3 2 1 0 ppm
2.06
1.07
0.90
1.14
5.00
3.04
3.01
3.08
9.07

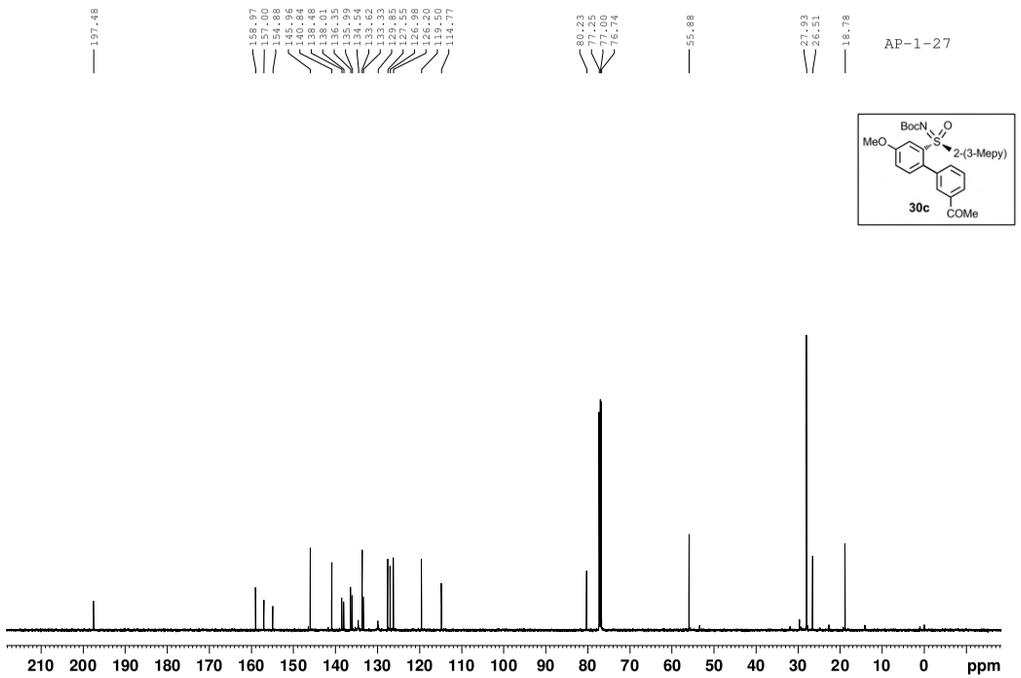
AP-1-27
30c
2-(3-Mepy)
BocN
MeO
COMe

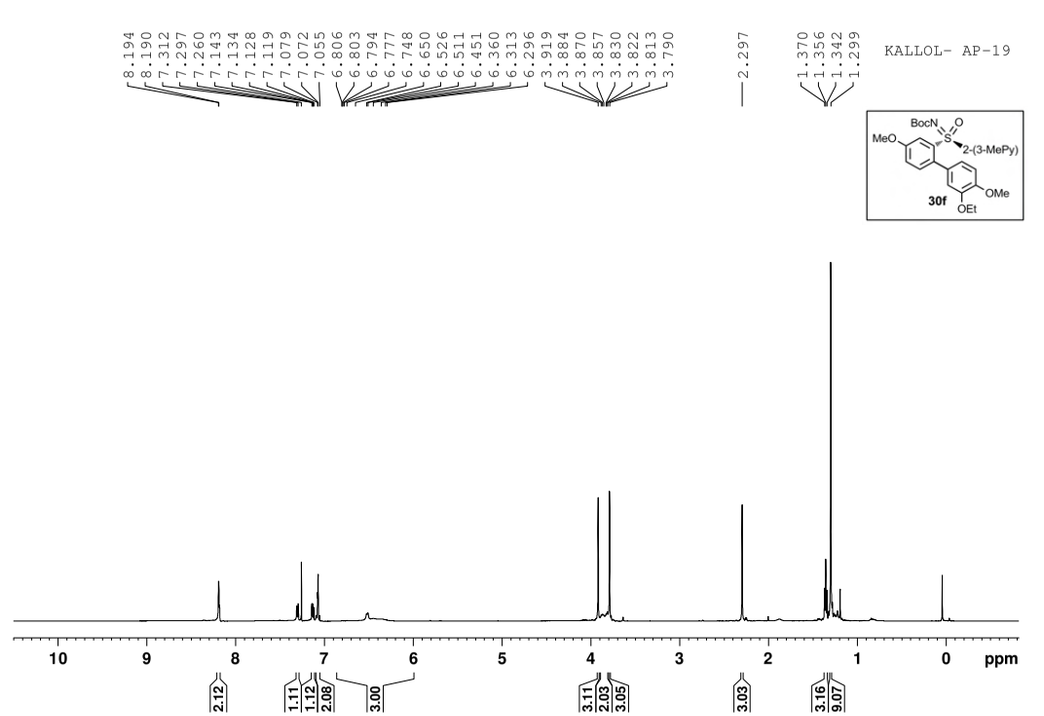
KALLOL- AP-19
30f
2-(3-MePy)
BocN
MeO
OMe
OEt

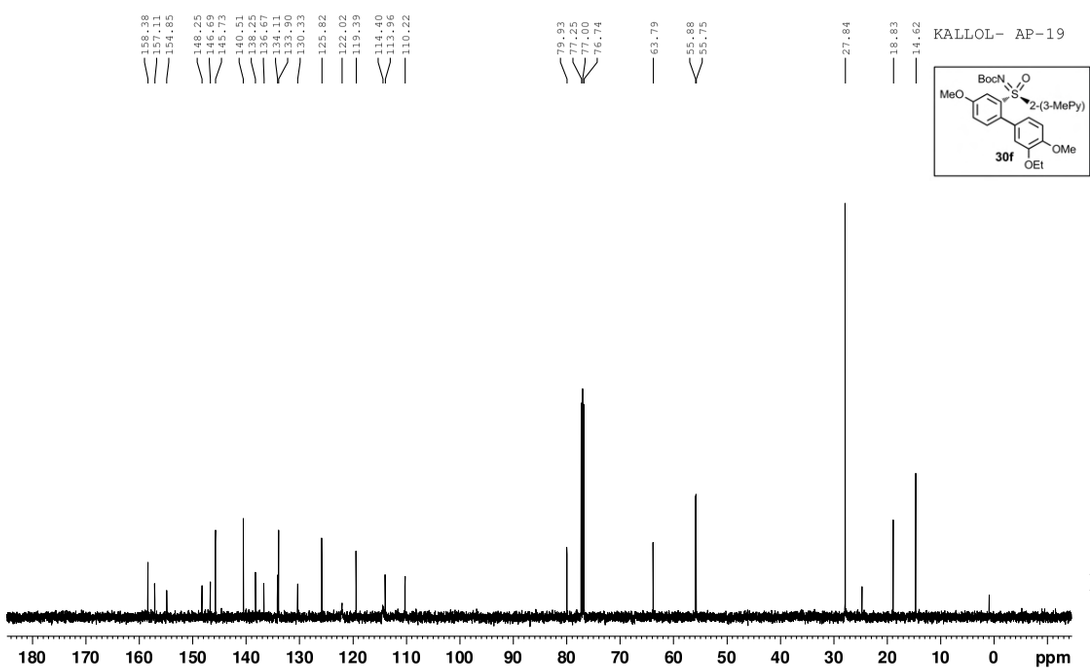
KALLOL- AP-19
30f
2-(3-MePy)
BocN
MeO
OMe
OEt

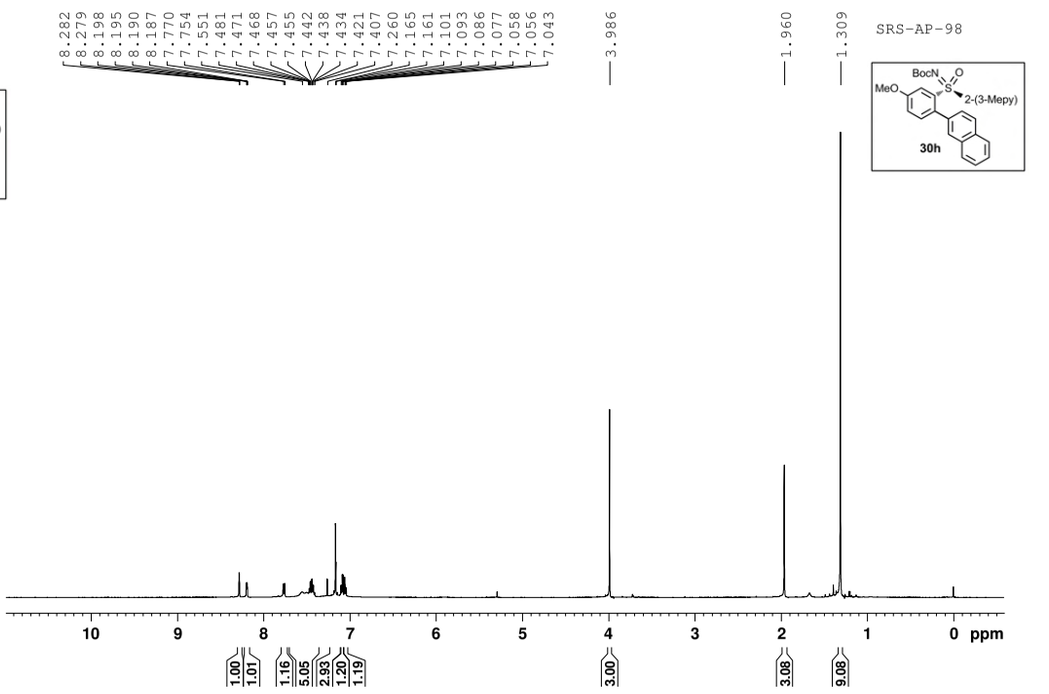
SRS-AP-98
30h
2-(3-Mepy)
BocN
MeO

SRS-AP-98

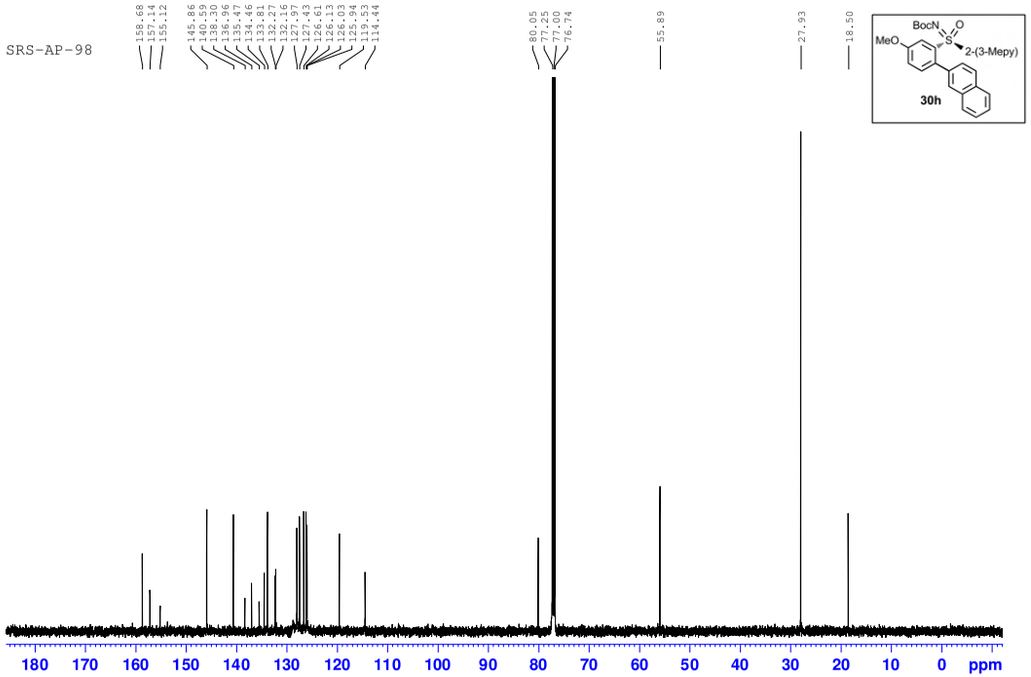

SRS-2-345

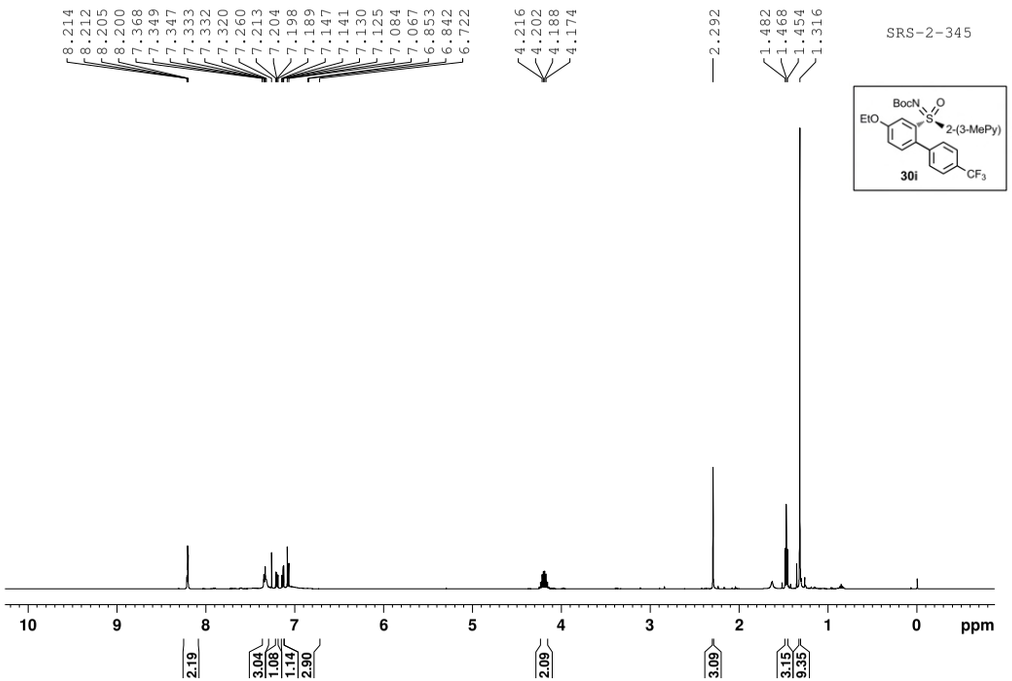

SRS-2-345

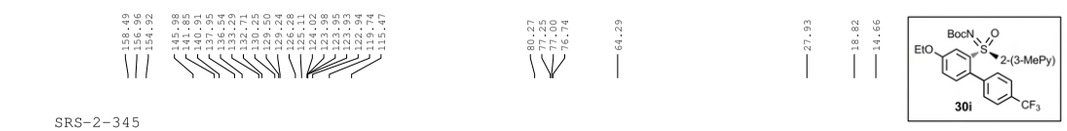

SRS-2-345

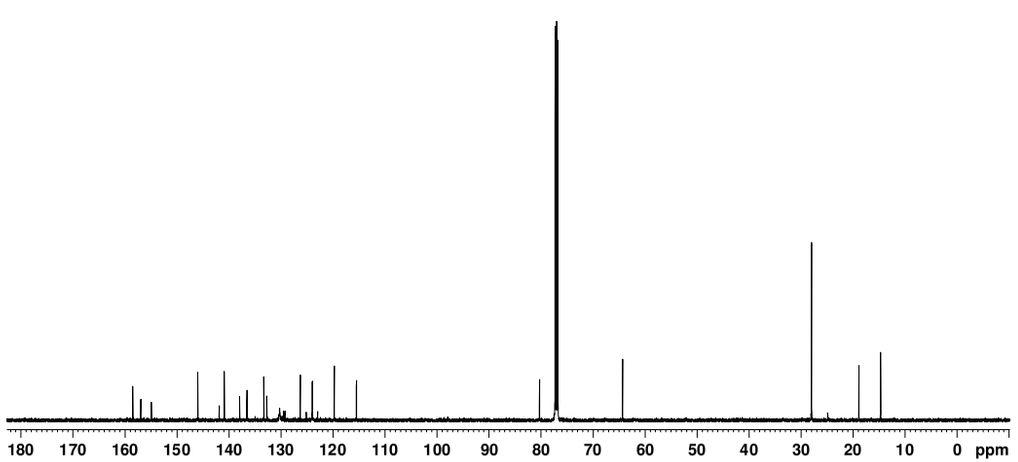

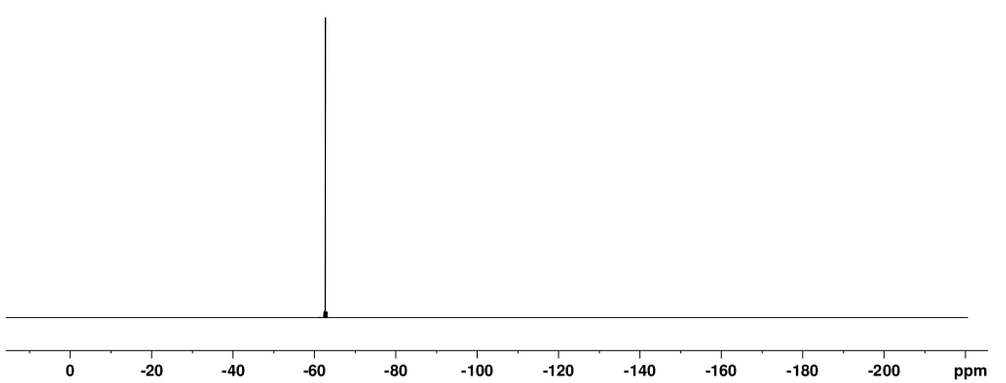

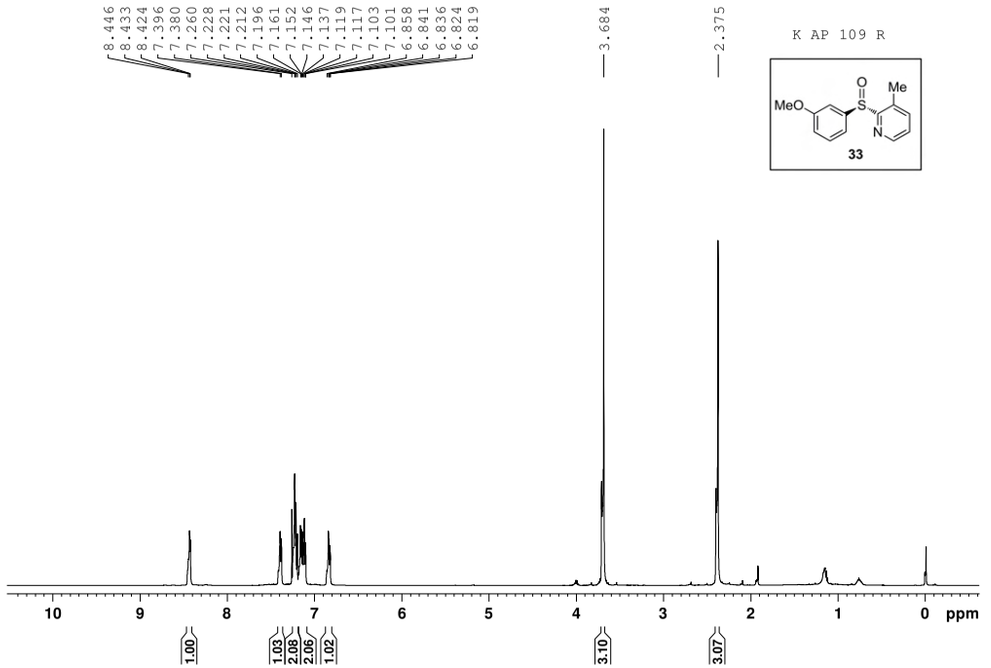
8.446
8.433
8.424
7.396
7.380
7.260
7.228
7.221
7.212
7.196
7.161
7.152
7.146
7.137
7.119
7.117
7.103
7.101
6.858
6.841
6.836
6.824
6.819
3.684
2.375
K AP 109 R
MeO
Me
33
10 9 8 7 6 5 4 3 2 1 0 ppm
1.00
1.03
2.08
2.06
1.02
3.10
3.07

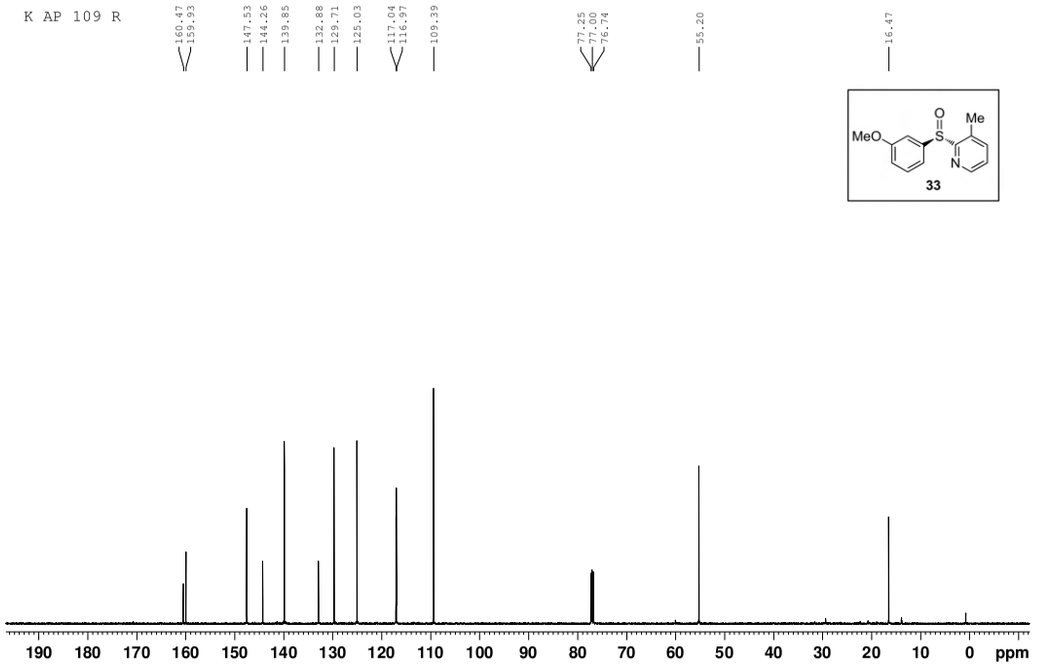
K AP 109 R
160.47
159.93
147.53
144.26
139.85
132.88
129.71
125.03
117.04
116.97
109.39
77.25
77.00
76.74
55.20
16.47
MeO
Me
33
190 180 170 160 150 140 130 120 110 100 90 80 70 60 50 40 30 20 10 0 ppm

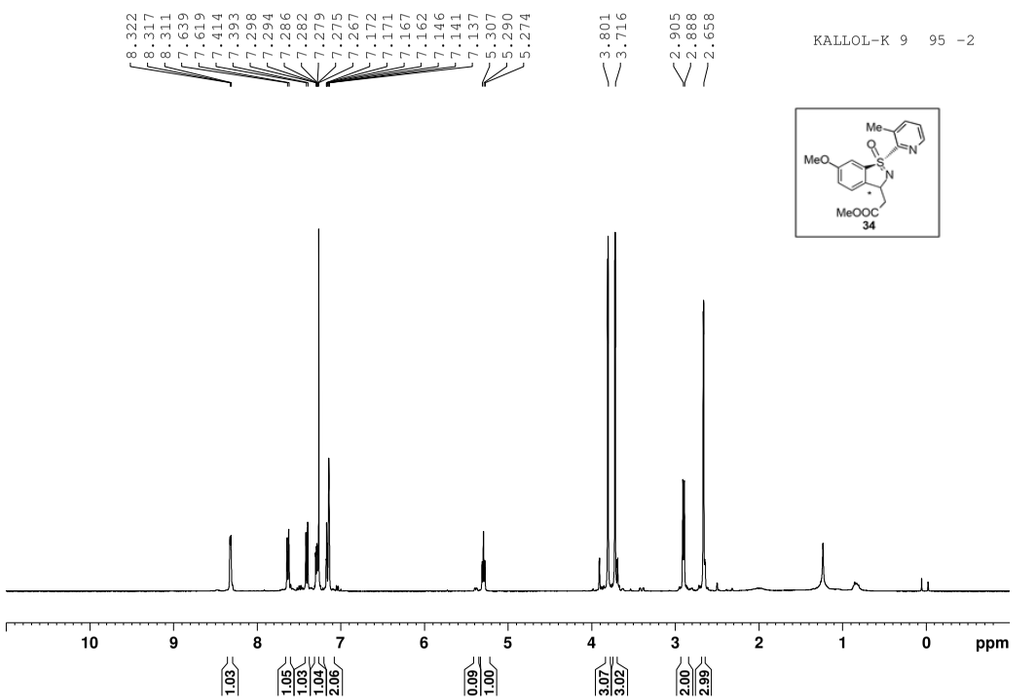
8.322
8.317
8.311
7.639
7.619
7.414
7.393
7.298
7.294
7.286
7.282
7.279
7.275
7.267
7.172
7.171
7.167
7.162
7.146
7.141
7.137
5.307
5.290
5.274
3.801
3.716
2.905
2.888
2.658
KALLOL-K 9 95 -2
MeO
Me
MeOOC
34
10 9 8 7 6 5 4 3 2 1 0 ppm
1.03
1.05
1.03
1.04
2.06
0.09
1.00
3.07
3.02
2.00
2.99

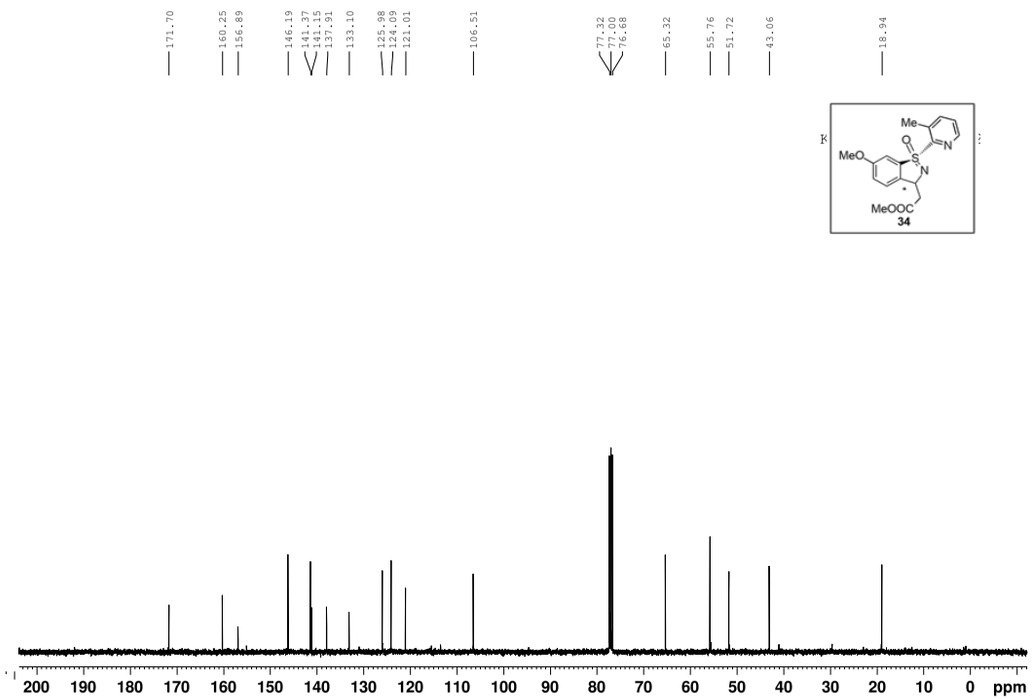
171.70
160.25
156.89
146.19
141.37
141.15
137.91
133.10
125.98
124.09
121.01
106.51
77.32
77.00
76.68
65.32
55.76
51.72
43.06
18.94
MeO
Me
MeOOC
34
200 190 180 170 160 150 140 130 120 110 100 90 80 70 60 50 40 30 20 10 0 ppm

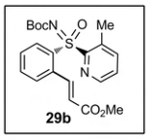

<Chromatogram>

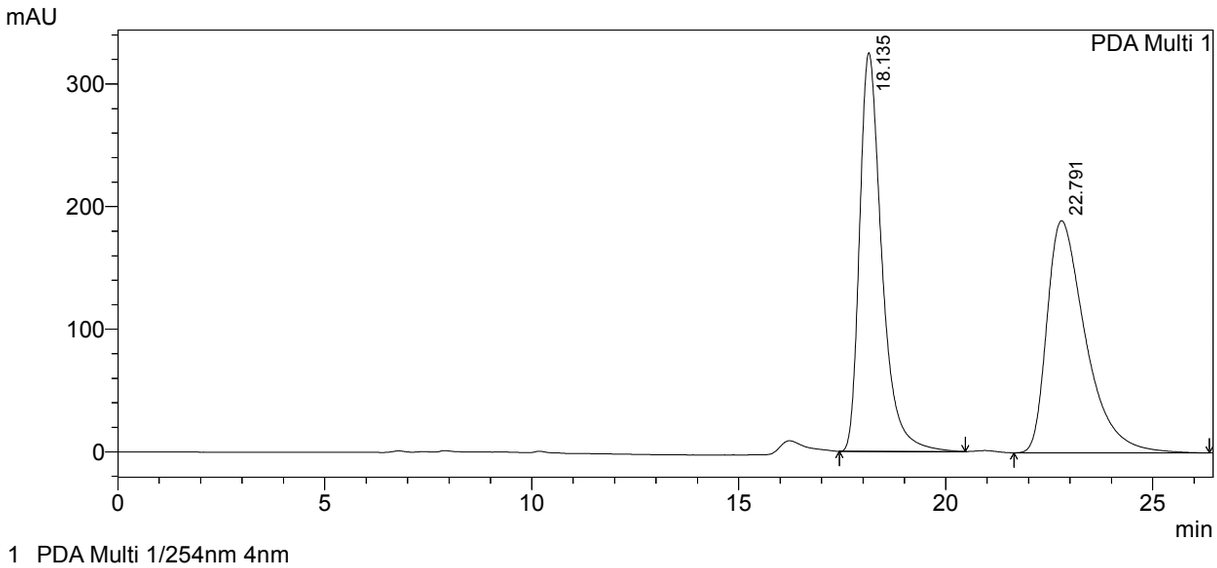

1 PDA Multi 1/254nm 4nm

PeakTable

PDA Ch1 254nm 4nm

Peak#	Ret. Time	Area	Height	Area %	Height %
1	18.135	12140347	325359	49.728	63.208
2	22.791	12273309	189387	50.272	36.792
Total		24413656	514746	100.000	100.000

<Chromatogram>

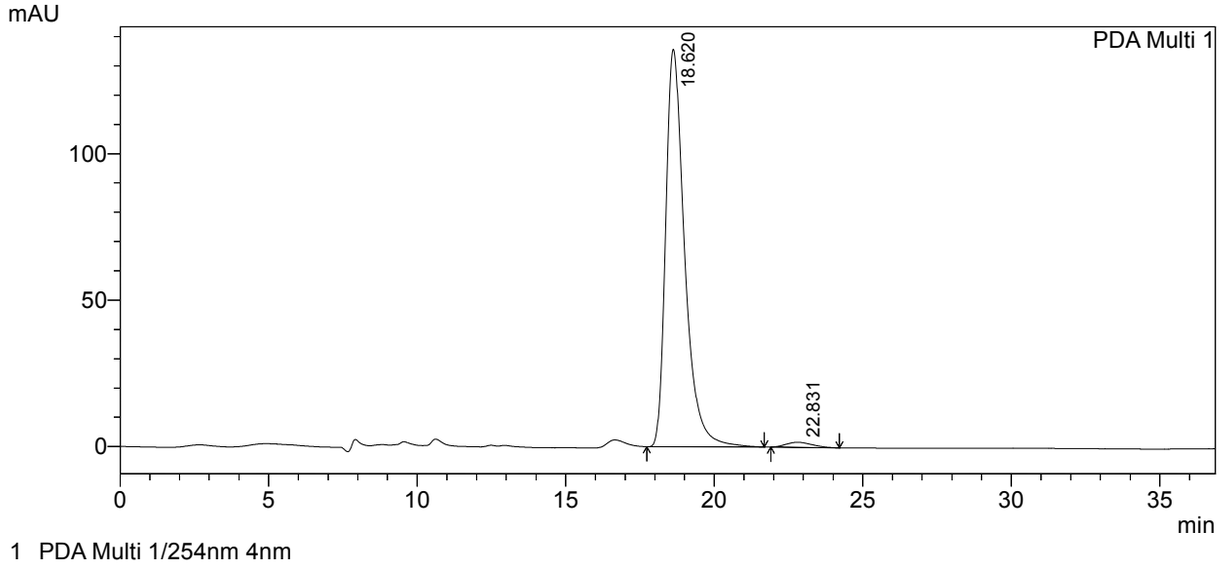

1 PDA Multi 1/254nm 4nm

PeakTable

PDA Ch1 254nm 4nm

Peak#	Ret. Time	Area	Height	Area %	Height %
1	18.620	6030335	135858	98.226	98.712
2	22.831	108928	1773	1.774	1.288
Total		6139263	137631	100.000	100.000

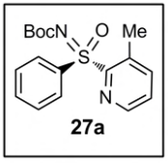

27a

<Chromatogram>

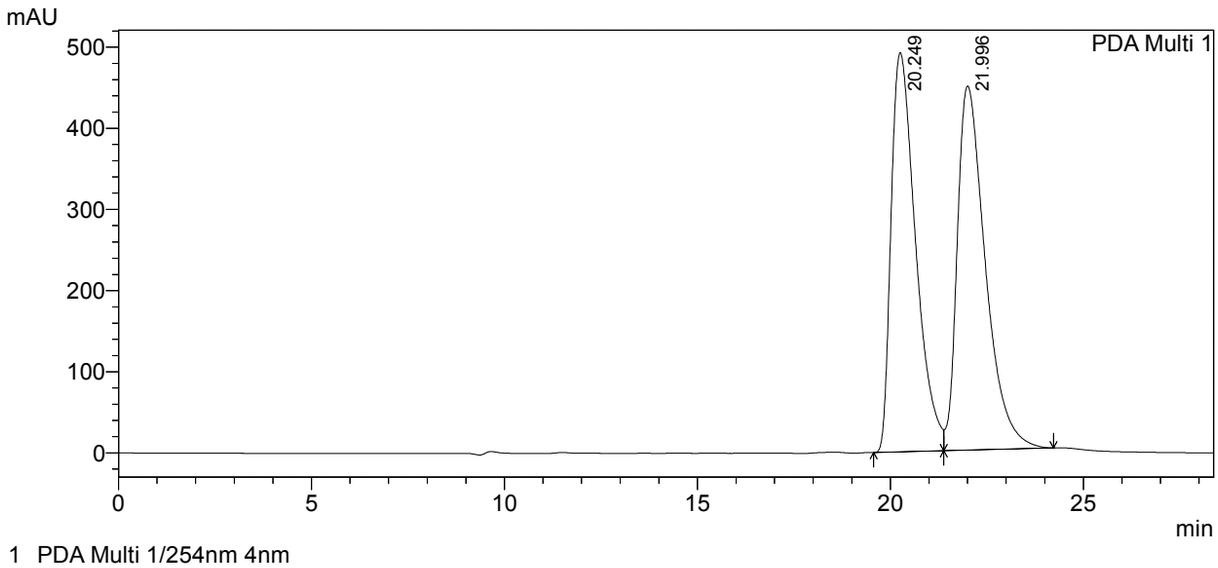

1 PDA Multi 1/254nm 4nm

PeakTable

PDA Ch1 254nm 4nm

Peak#	Ret. Time	Area	Height	Area %	Height %
1	20.249	21759605	492183	48.883	52.303
2	21.996	22753619	448841	51.117	47.697
Total		44513224	941024	100.000	100.000

<Chromatogram>

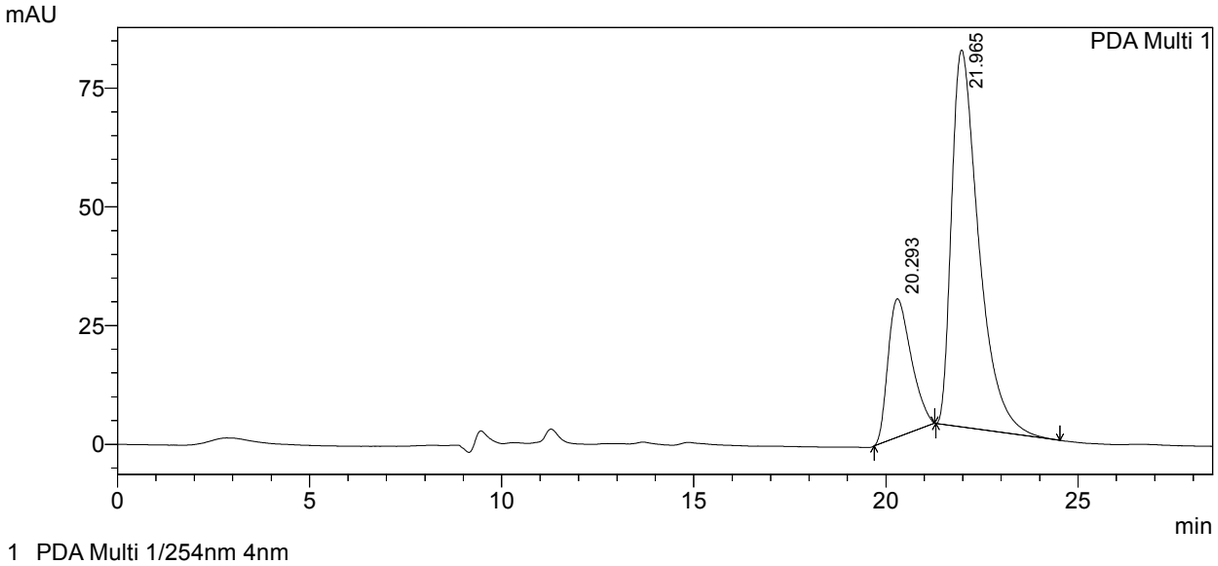

1 PDA Multi 1/254nm 4nm

PeakTable

PDA Ch1 254nm 4nm

Peak#	Ret. Time	Area	Height	Area %	Height %
1	20.293	1222975	29183	23.816	26.872
2	21.965	3912044	79417	76.184	73.128
Total		5135019	108600	100.000	100.000

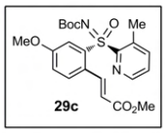

<Chromatogram>

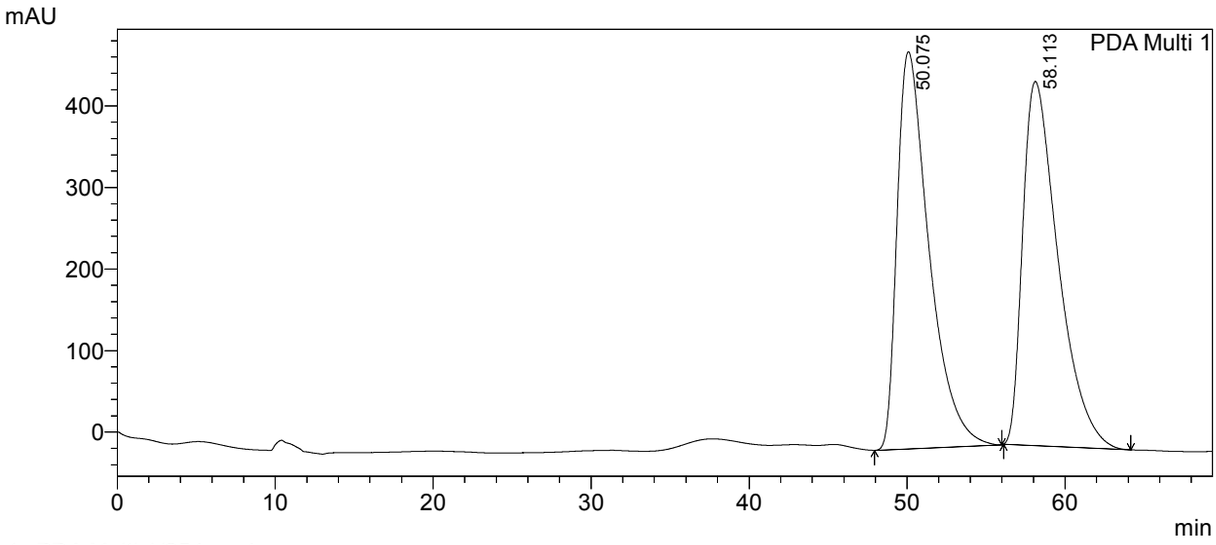

1 PDA Multi 1/254nm 4nm

PeakTable

PDA Ch1 254nm 4nm

Peak#	Ret. Time	Area	Height	Area %	Height %
1	50.075	68565966	487104	49.593	52.170
2	58.113	69690288	446578	50.407	47.830
Total		138256255	933682	100.000	100.000

<Chromatogram>

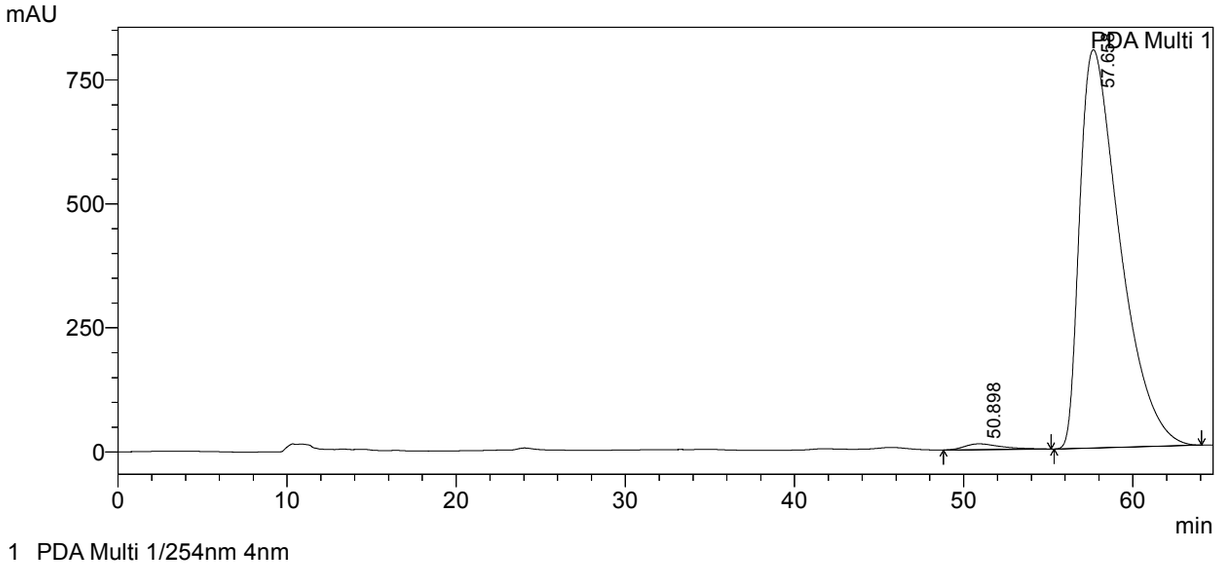

1 PDA Multi 1/254nm 4nm

PeakTable

PDA Ch1 254nm 4nm

Peak#	Ret. Time	Area	Height	Area %	Height %
1	50.898	1758161	11717	1.308	1.439
2	57.658	132678713	802741	98.692	98.561
Total		134436874	814458	100.000	100.000

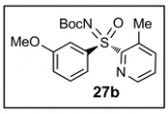

<Chromatogram>

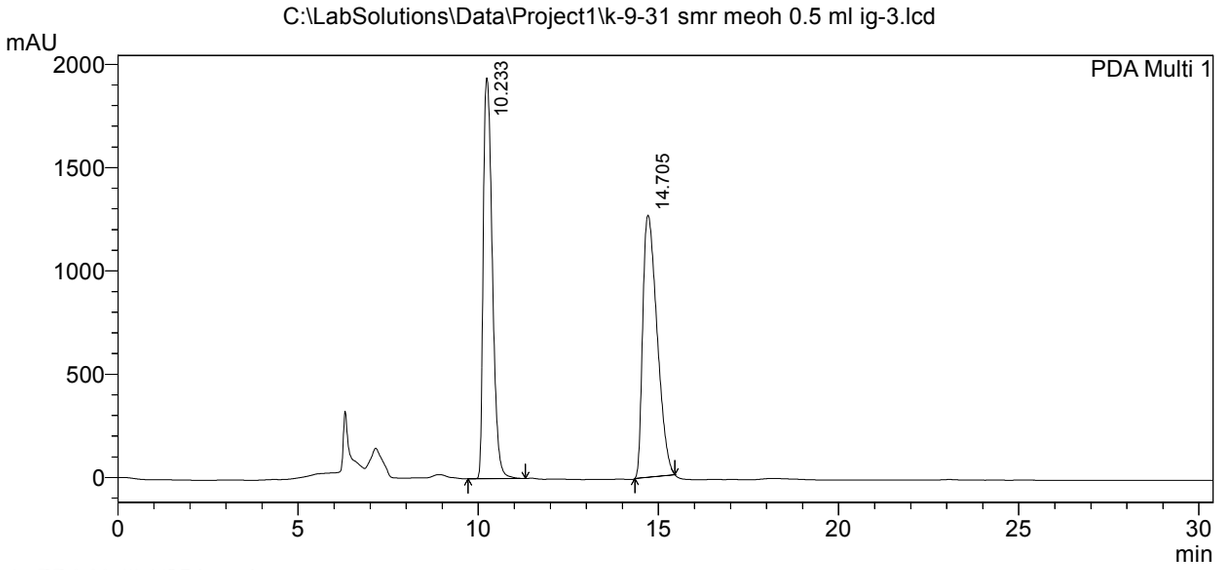

1 PDA Multi 1/254nm 4nm

PeakTable

PDA Ch1 254nm 4nm

Peak#	Ret. Time	Area	Height	Area %	Height %
1	10.233	33982048	1940394	49.174	60.456
2	14.705	35123078	1269225	50.826	39.544
Total		69105126	3209619	100.000	100.000

<Chromatogram>

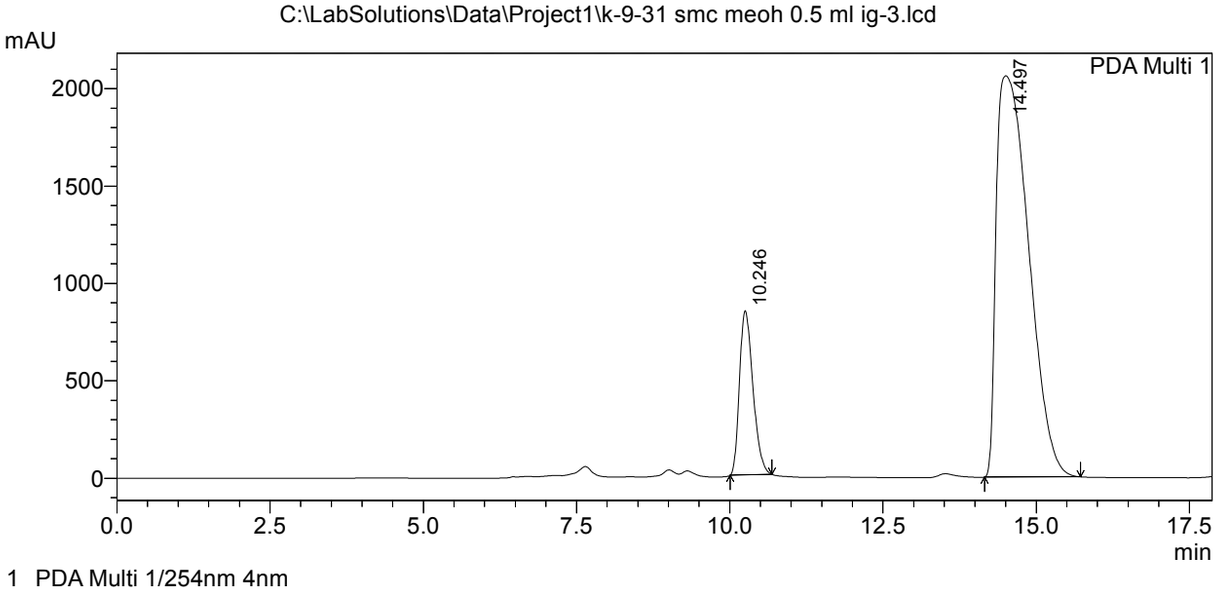

1 PDA Multi 1/254nm 4nm

PeakTable

PDA Ch1 254nm 4nm

Peak#	Ret. Time	Area	Height	Area %	Height %
1	10.246	12888462	843097	14.534	29.044
2	14.497	75787225	2059744	85.466	70.956
Total		88675687	2902841	100.000	100.000

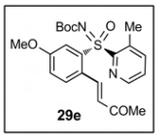

<Chromatogram>

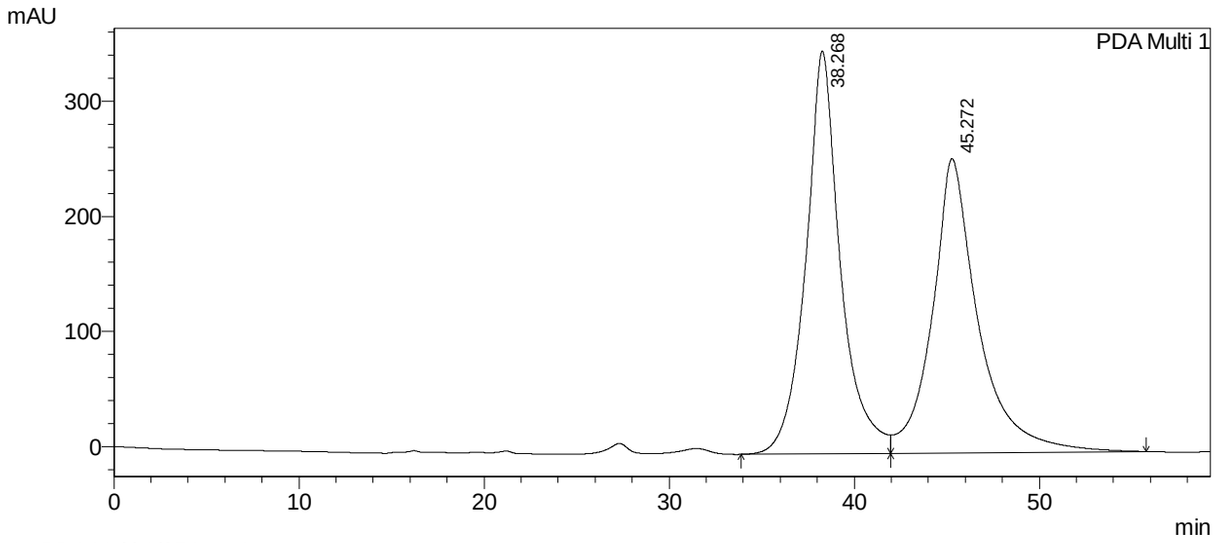

1 PDA Multi 1/254nm 4nm

PeakTable

PDA Ch1 254nm 4nm

Peak#	Ret. Time	Area	Height	Area %	Height %
1	38.268	45546152	350035	50.773	57.781
2	45.272	44158452	255761	49.227	42.219
Total		89704604	605796	100.000	100.000

<Chromatogram>

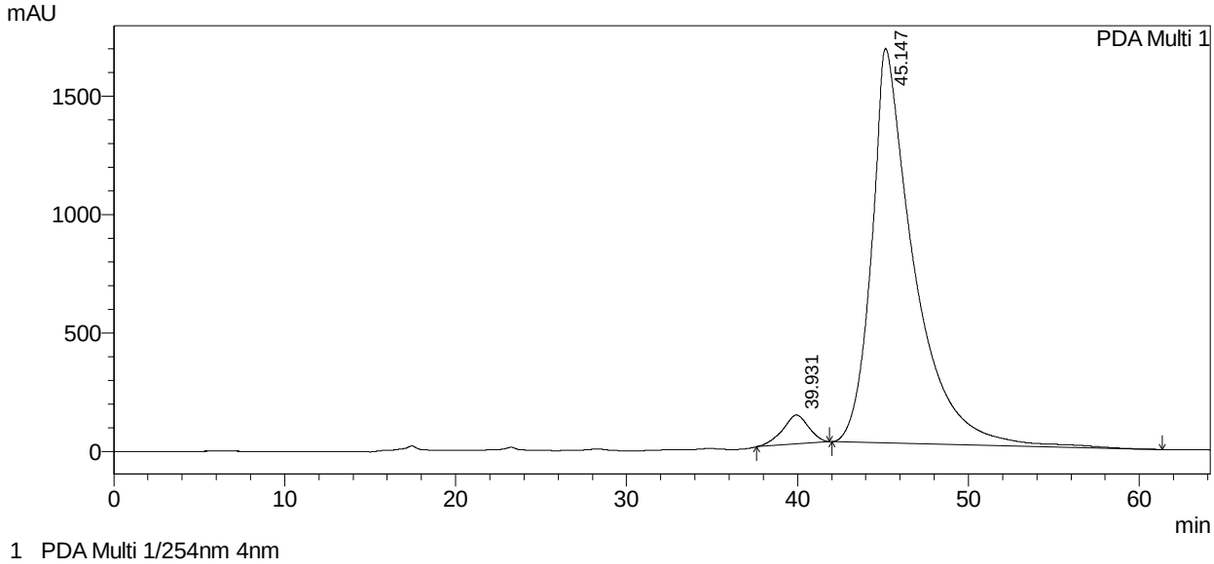

1 PDA Multi 1/254nm 4nm

PeakTable

PDA Ch1 254nm 4nm

Peak#	Ret. Time	Area	Height	Area %	Height %
1	39.931	13106862	123021	4.367	6.873
2	45.147	287054445	1667001	95.633	93.127
Total		300161307	1790022	100.000	100.000

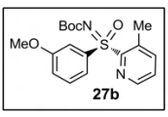

<Chromatogram>

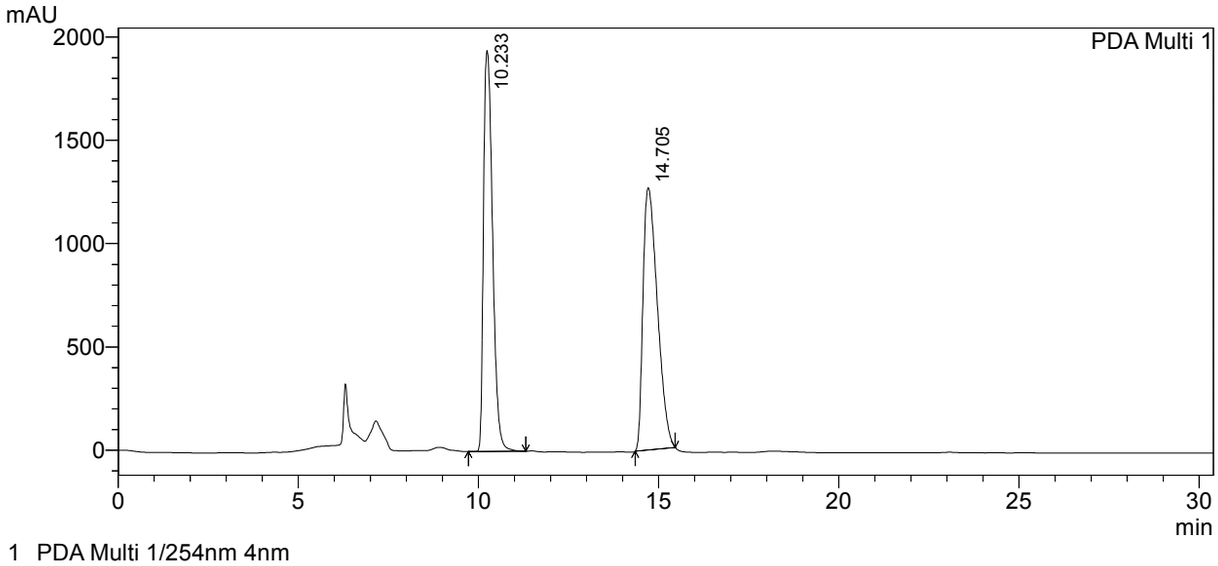

1 PDA Multi 1/254nm 4nm

PeakTable

PDA Ch1 254nm 4nm

Peak#	Ret. Time	Area	Height	Area %	Height %
1	10.233	33982048	1940394	49.174	60.456
2	14.705	35123078	1269225	50.826	39.544
Total		69105126	3209619	100.000	100.000

<Chromatogram>

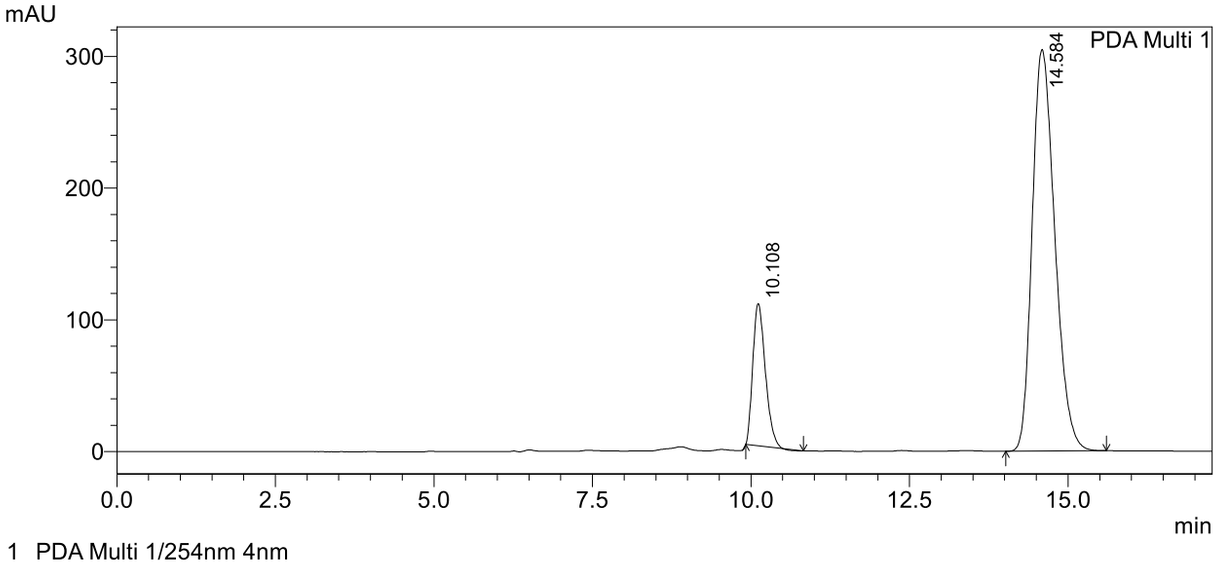

1 PDA Multi 1/254nm 4nm

PeakTable

PDA Ch1 254nm 4nm

Peak#	Ret. Time	Area	Height	Area %	Height %
1	10.108	1471807	107846	16.268	26.129
2	14.584	7575264	304904	83.732	73.871
Total		9047071	412751	100.000	100.000

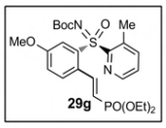

<Chromatogram>

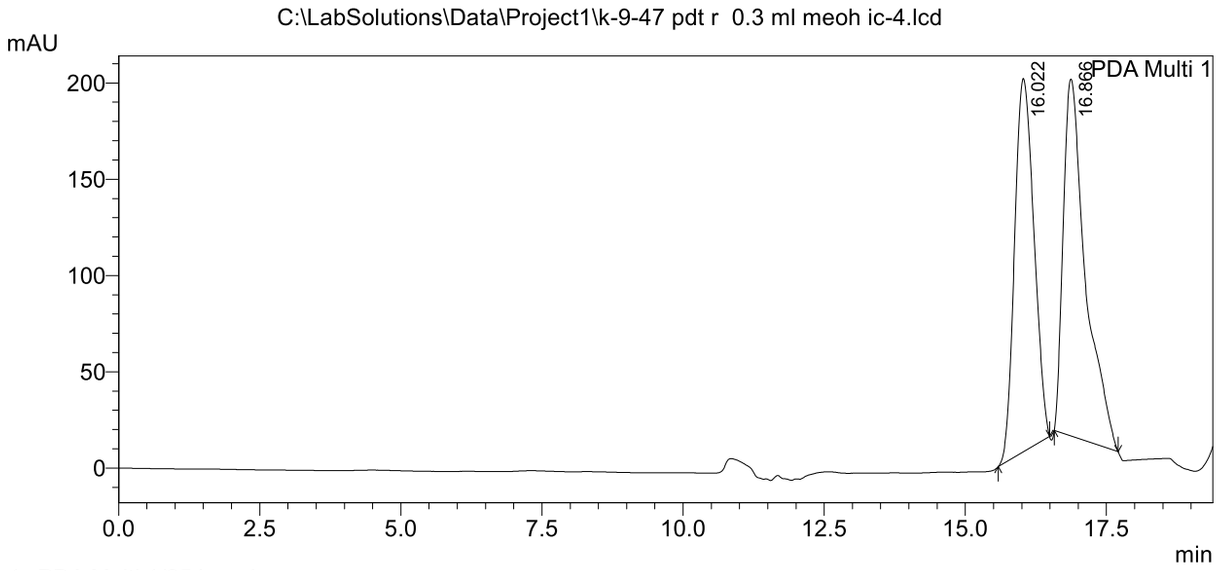

1 PDA Multi 1/254nm 4nm

PeakTable

PDA Ch1 254nm 4nm

Peak#	Ret. Time	Area	Height	Area %	Height %
1	16.022	4618687	194015	47.677	51.124
2	16.866	5068703	185482	52.323	48.876
Total		9687390	379497	100.000	100.000

<Chromatogram>

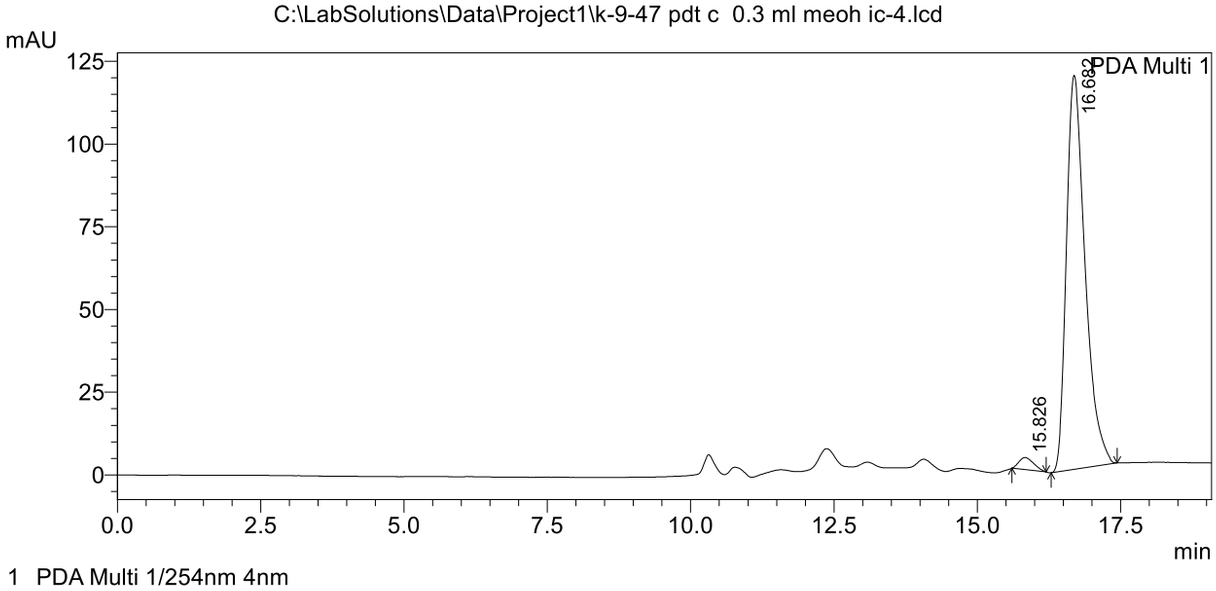

1 PDA Multi 1/254nm 4nm

PeakTable

PDA Ch1 254nm 4nm

Peak#	Ret. Time	Area	Height	Area %	Height %
1	15.826	66458	3673	2.404	2.992
2	16.682	2698595	119086	97.596	97.008
Total		2765053	122759	100.000	100.000

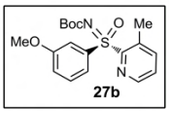

<Chromatogram>

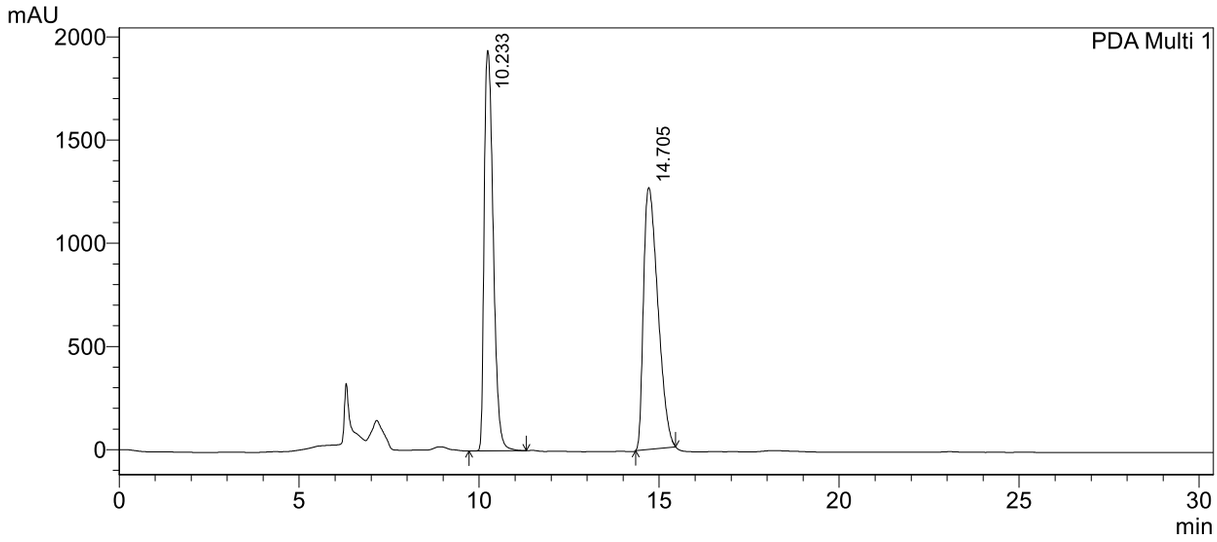

1 PDA Multi 1/254nm 4nm

PeakTable

PDA Ch1 254nm 4nm

Peak#	Ret. Time	Area	Height	Area %	Height %
1	10.233	33982048	1940394	49.174	60.456
2	14.705	35123078	1269225	50.826	39.544
Total		69105126	3209619	100.000	100.000

<Chromatogram>

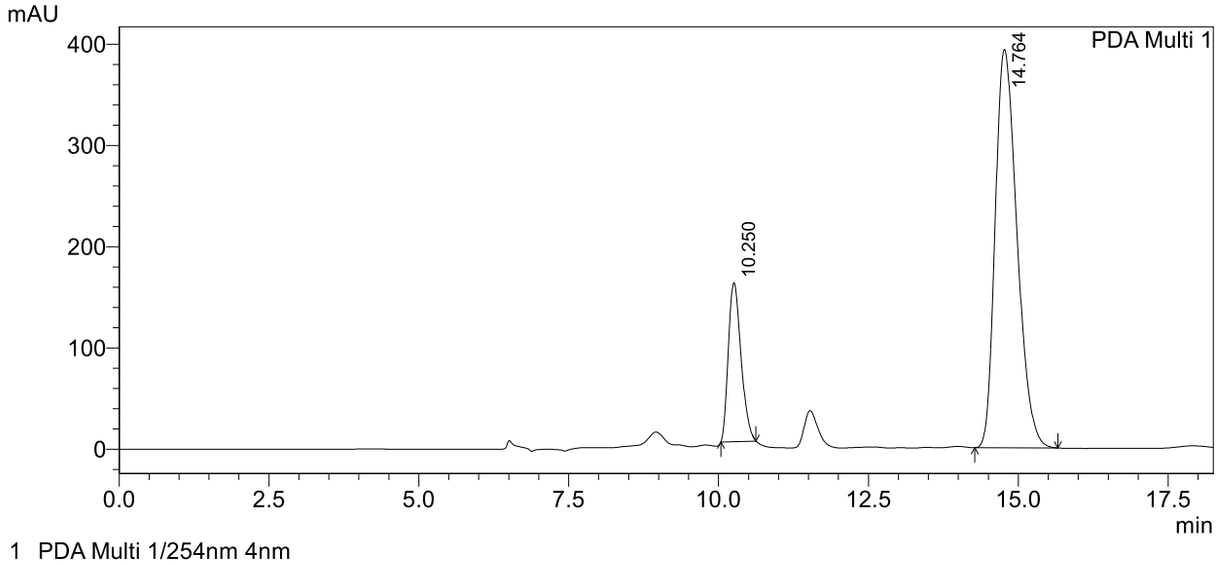

1 PDA Multi 1/254nm 4nm

PeakTable

PDA Ch1 254nm 4nm

Peak#	Ret. Time	Area	Height	Area %	Height %
1	10.250	2314939	157128	18.838	28.522
2	14.764	9973493	393781	81.162	71.478
Total		12288432	550909	100.000	100.000

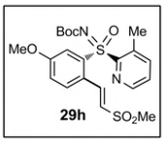

<Chromatogram>

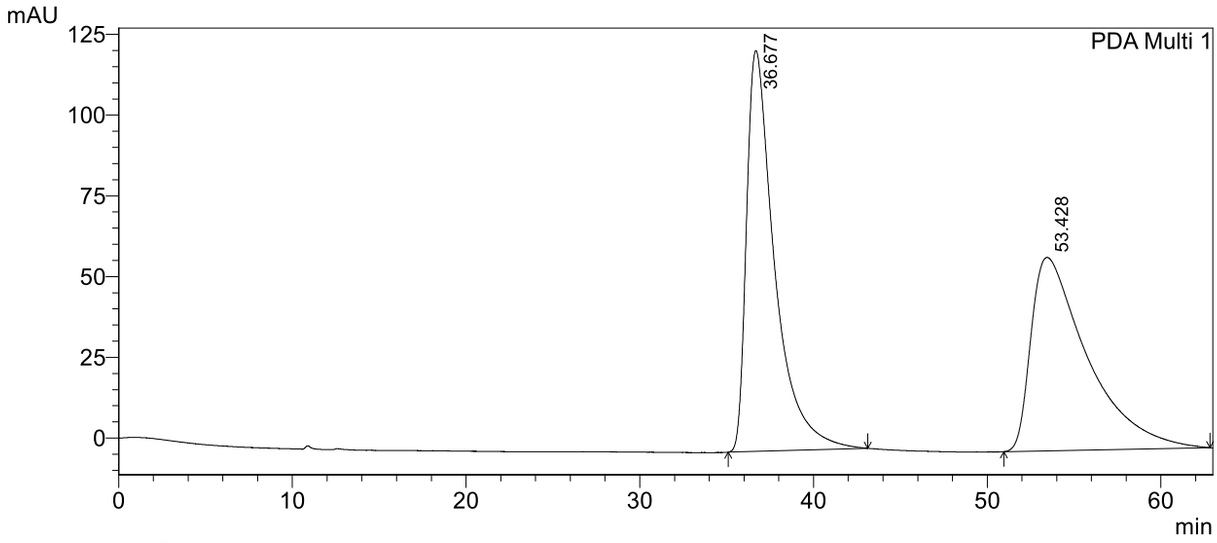

1 PDA Multi 1/254nm 4nm

PeakTable

PDA Ch1 254nm 4nm

Peak#	Ret. Time	Area	Height	Area %	Height %
1	36.677	13955896	124115	50.822	67.463
2	53.428	13504214	59859	49.178	32.537
Total		27460110	183974	100.000	100.000

<Chromatogram>

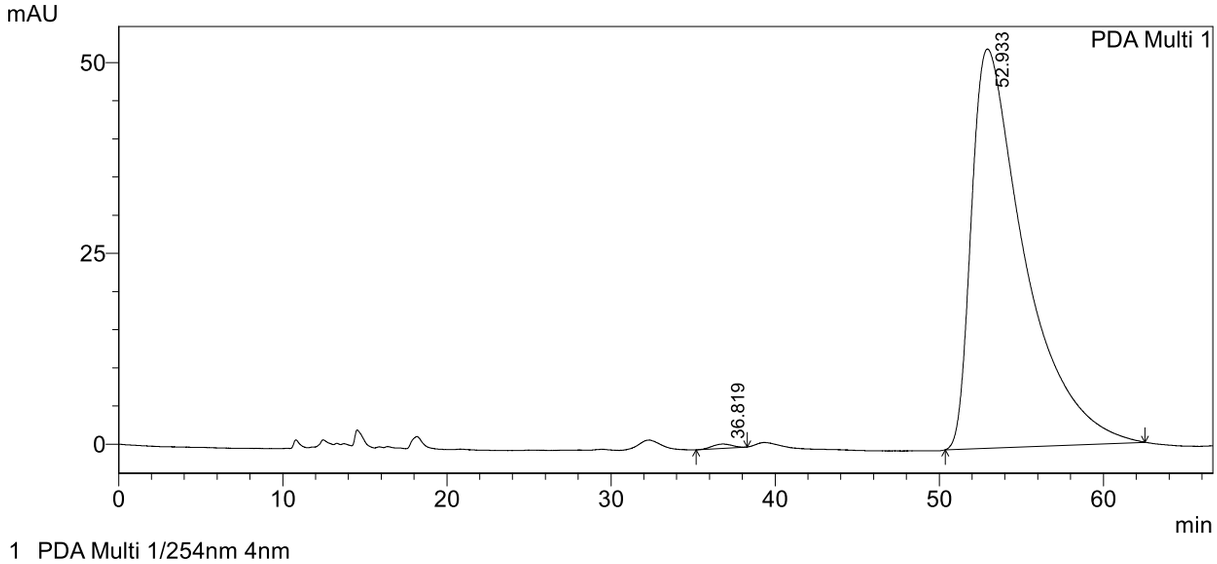

1 PDA Multi 1/254nm 4nm

PeakTable

PDA Ch1 254nm 4nm

Peak#	Ret. Time	Area	Height	Area %	Height %
1	36.819	46161	571	0.389	1.081
2	52.933	11817784	52305	99.611	98.919
Total		11863945	52876	100.000	100.000

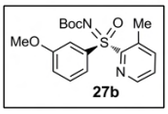

<Chromatogram>

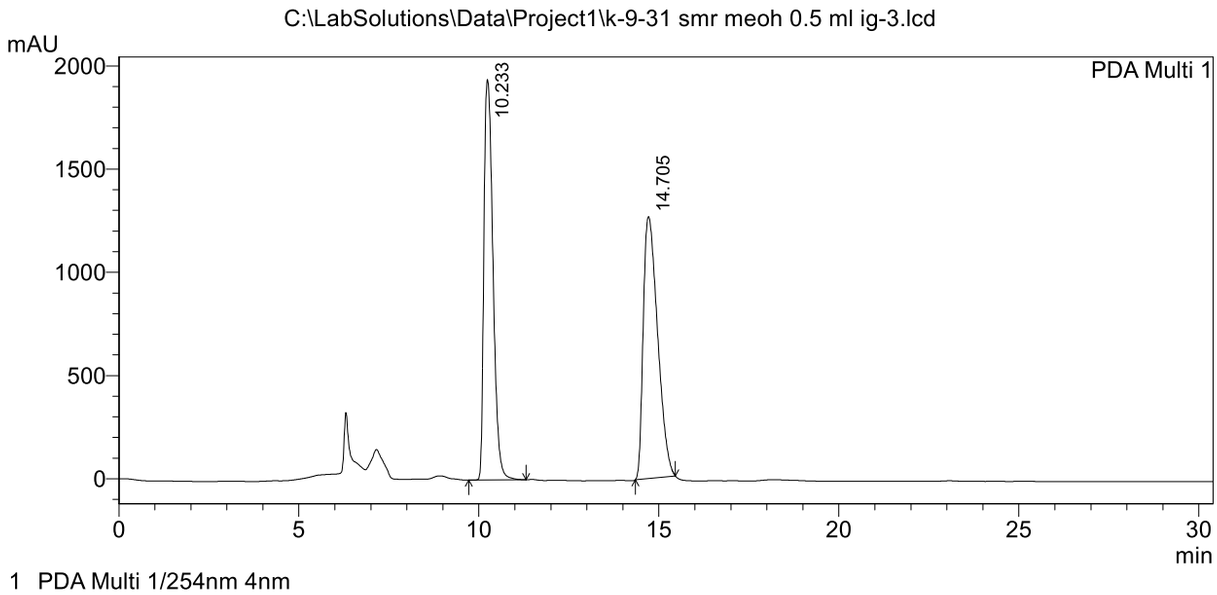

1 PDA Multi 1/254nm 4nm

PeakTable

PDA Ch1 254nm 4nm

Peak#	Ret. Time	Area	Height	Area %	Height %
1	10.233	33982048	1940394	49.174	60.456
2	14.705	35123078	1269225	50.826	39.544
Total		69105126	3209619	100.000	100.000

<Chromatogram>

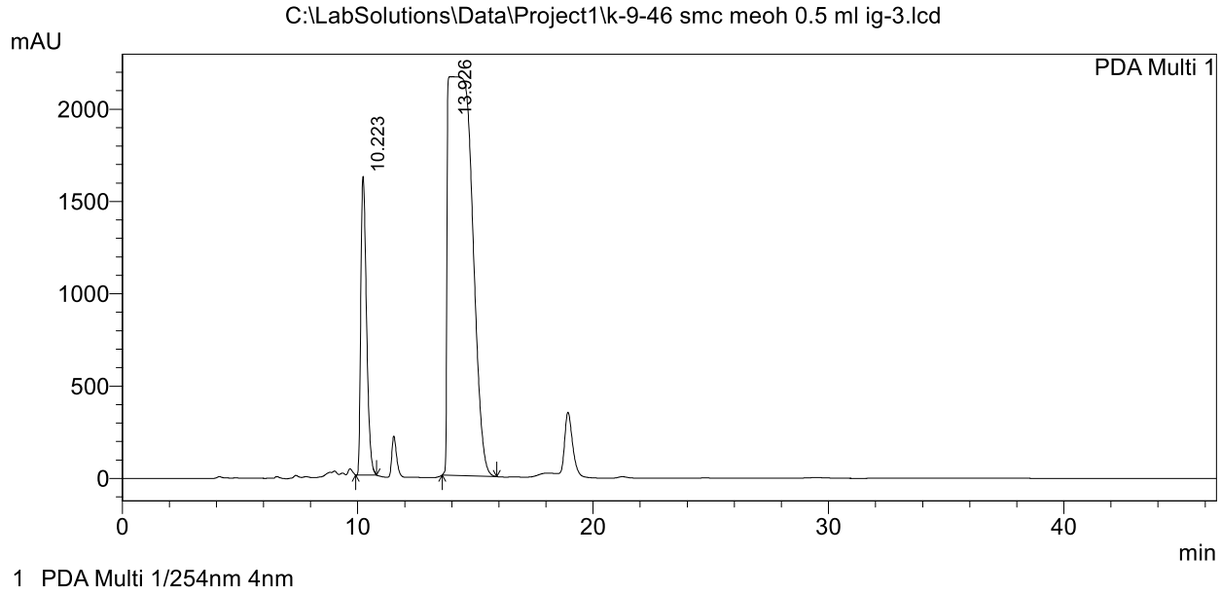

1 PDA Multi 1/254nm 4nm

PeakTable

PDA Ch1 254nm 4nm

Peak#	Ret. Time	Area	Height	Area %	Height %
1	10.223	27274631	1619262	14.961	42.860
2	13.926	155033052	2158732	85.039	57.140
Total		182307683	3777995	100.000	100.000

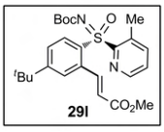

<Chromatogram>

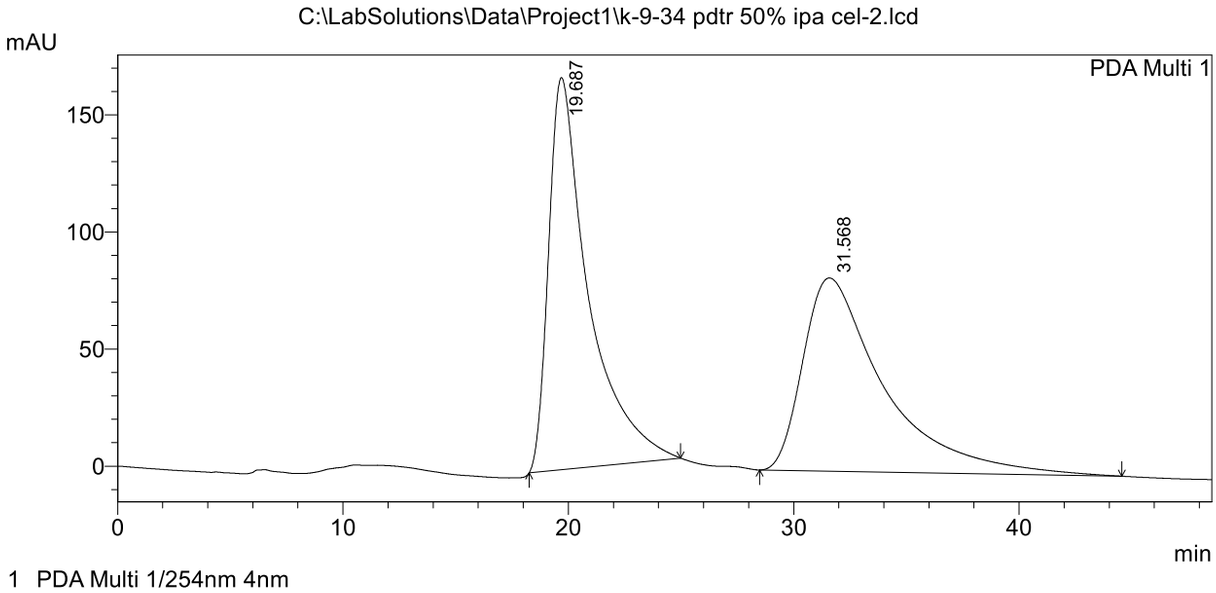

1 PDA Multi 1/254nm 4nm

PeakTable

PDA Ch1 254nm 4nm

Peak#	Ret. Time	Area	Height	Area %	Height %
1	19.687	20535896	167438	49.966	66.985
2	31.568	20563652	82527	50.034	33.015
Total		41099548	249965	100.000	100.000

<Chromatogram>

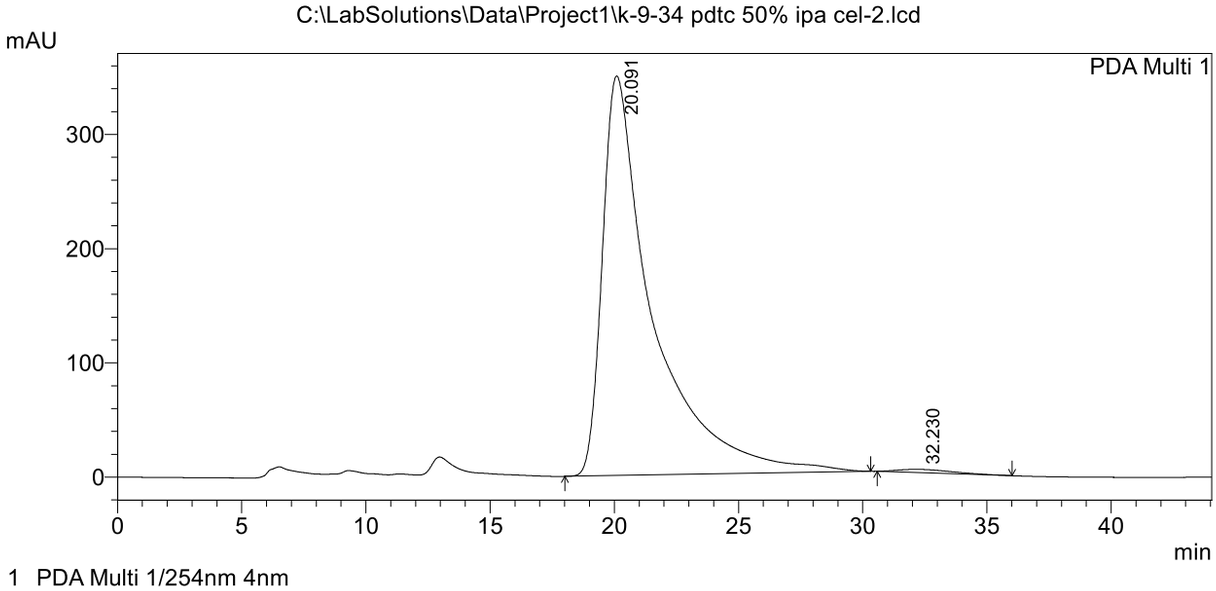

1 PDA Multi 1/254nm 4nm

PeakTable

PDA Ch1 254nm 4nm

Peak#	Ret. Time	Area	Height	Area %	Height %
1	20.091	49270866	349792	99.090	99.178
2	32.230	452604	2898	0.910	0.822
Total		49723471	352691	100.000	100.000

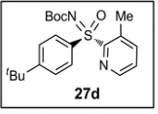

<Chromatogram>

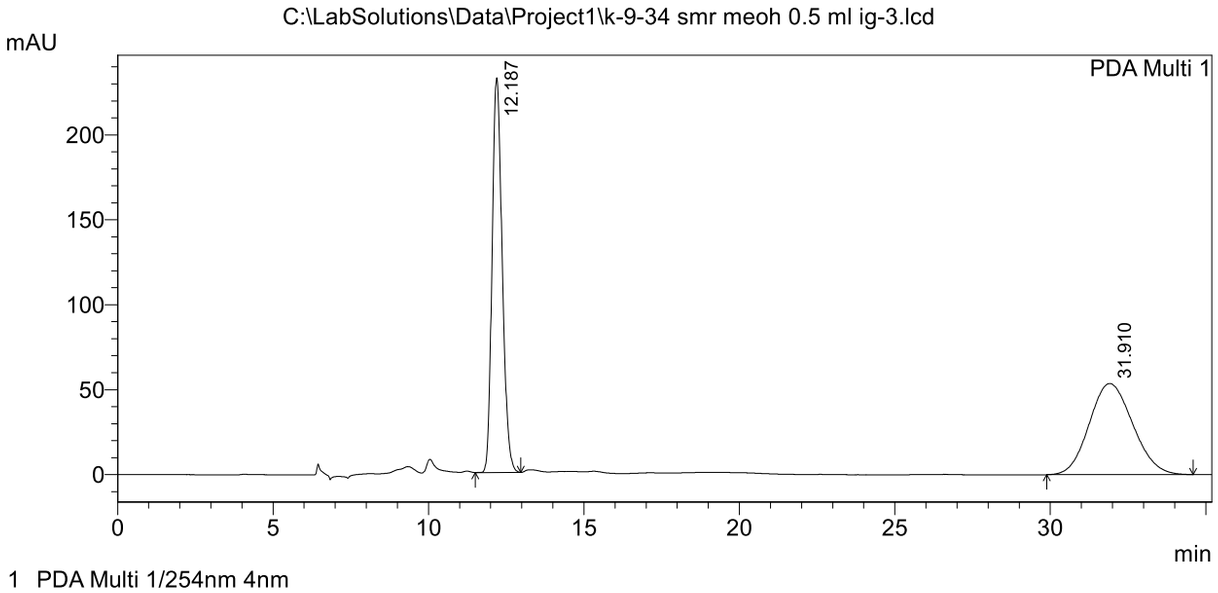

1 PDA Multi 1/254nm 4nm

PeakTable

PDA Ch1 254nm 4nm

Peak#	Ret. Time	Area	Height	Area %	Height %
1	12.187	5258040	232387	50.172	81.240
2	31.910	5222016	53663	49.828	18.760
Total		10480056	286050	100.000	100.000

<Chromatogram>

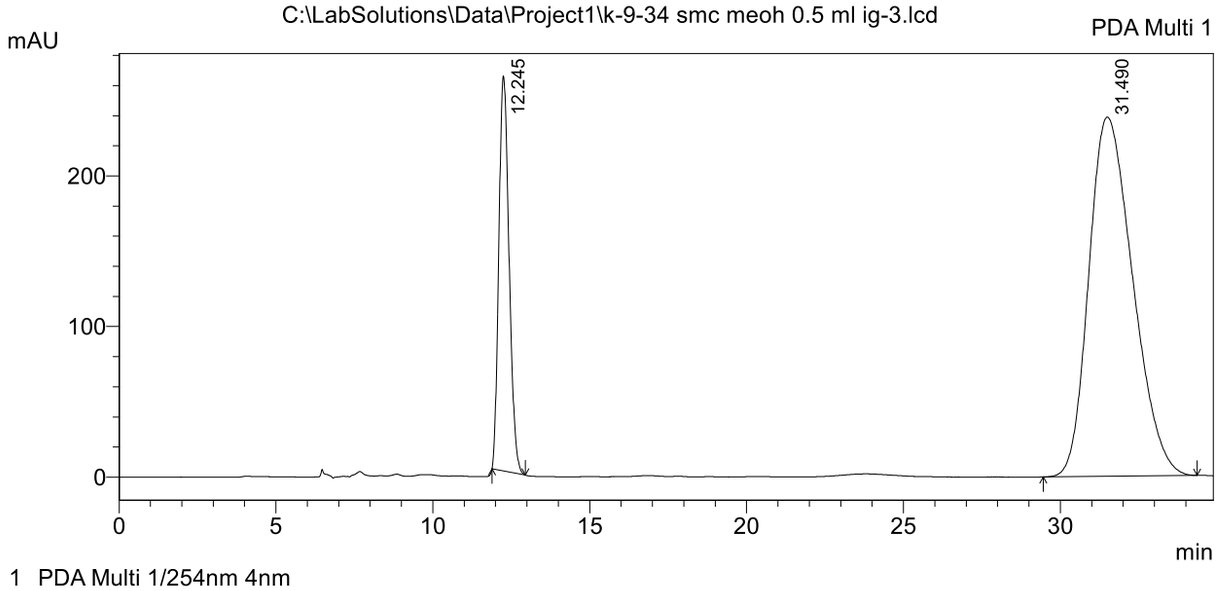

1 PDA Multi 1/254nm 4nm

PeakTable

PDA Ch1 254nm 4nm

Peak#	Ret. Time	Area	Height	Area %	Height %
1	12.245	5957283	262219	20.443	52.364
2	31.490	23183972	238538	79.557	47.636
Total		29141255	500757	100.000	100.000

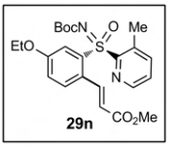

<Chromatogram>

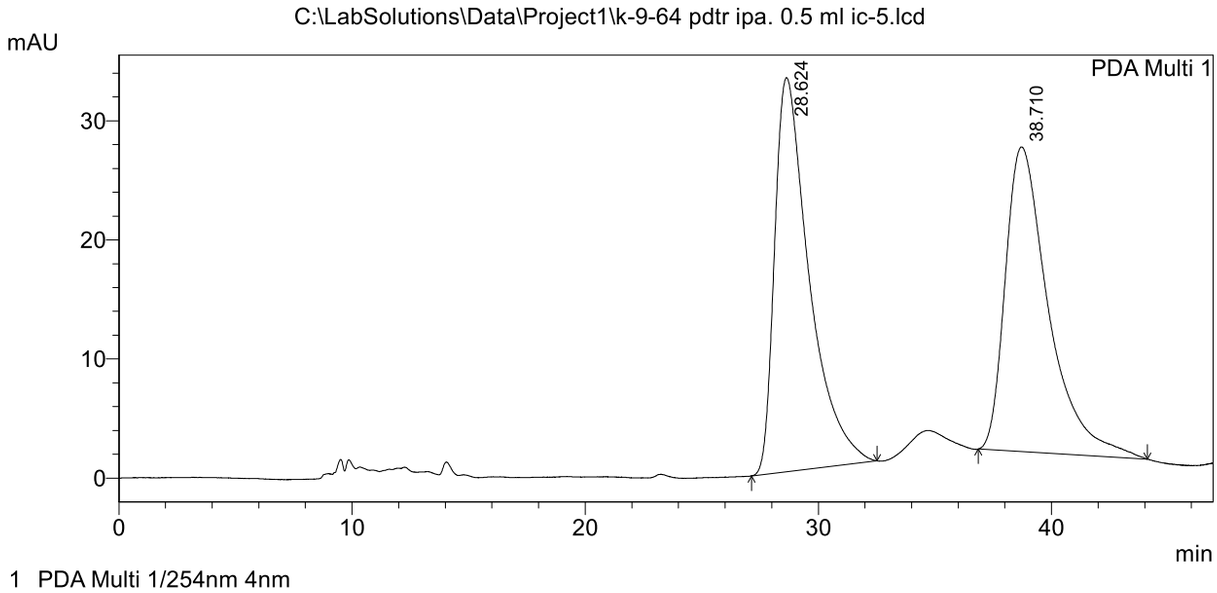

1 PDA Multi 1/254nm 4nm

PeakTable

PDA Ch1 254nm 4nm

Peak#	Ret. Time	Area	Height	Area %	Height %
1	28.624	3412946	33092	50.934	56.394
2	38.710	3287803	25588	49.066	43.606
Total		6700749	58681	100.000	100.000

<Chromatogram>

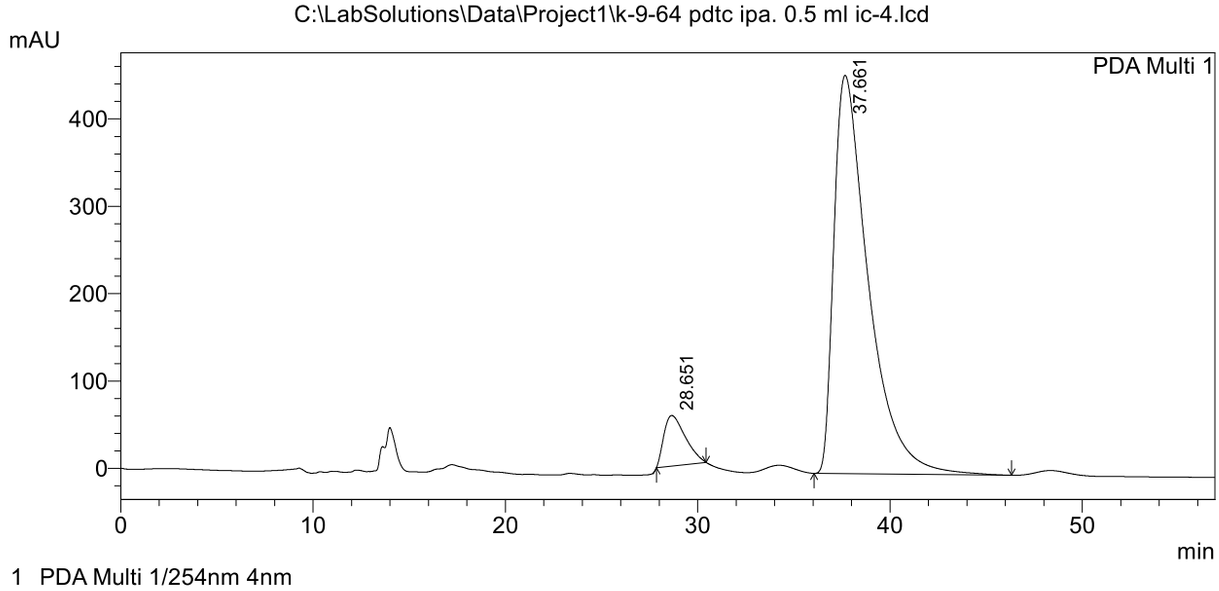

1 PDA Multi 1/254nm 4nm

PeakTable

PDA Ch1 254nm 4nm

Peak#	Ret. Time	Area	Height	Area %	Height %
1	28.651	4464027	57867	7.273	11.259
2	37.661	56912944	456077	92.727	88.741
Total		61376971	513944	100.000	100.000

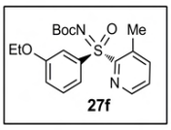

<Chromatogram>

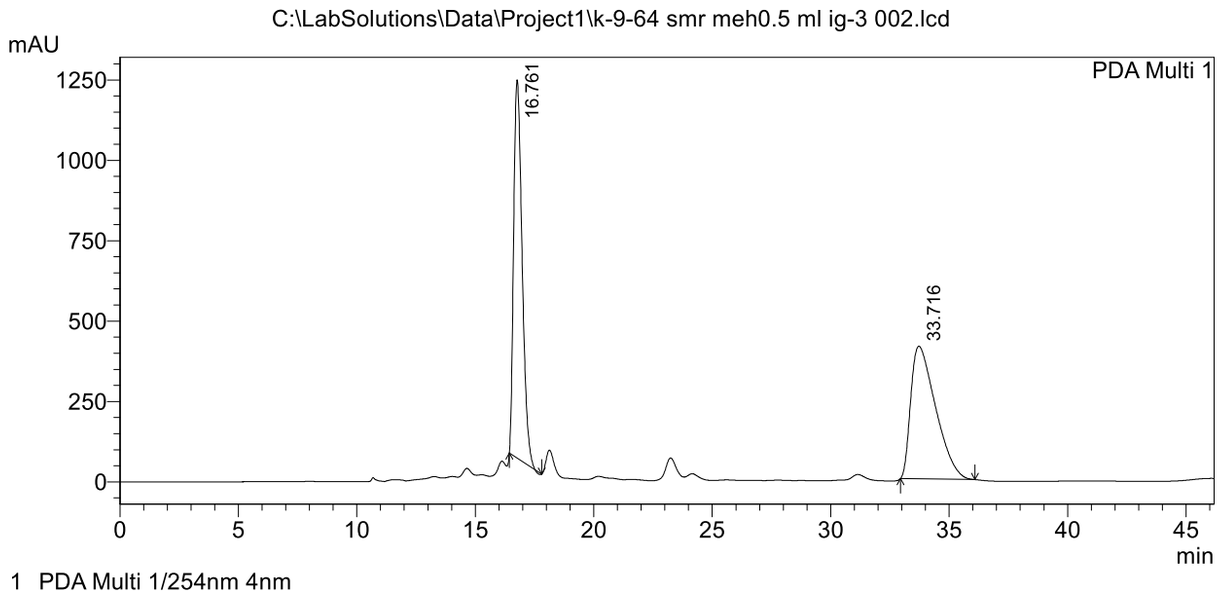

1 PDA Multi 1/254nm 4nm

PeakTable

PDA Ch1 254nm 4nm

Peak#	Ret. Time	Area	Height	Area %	Height %
1	16.761	29212575	1175965	49.290	74.038
2	33.716	30053593	412369	50.710	25.962
Total		59266167	1588335	100.000	100.000

<Chromatogram>

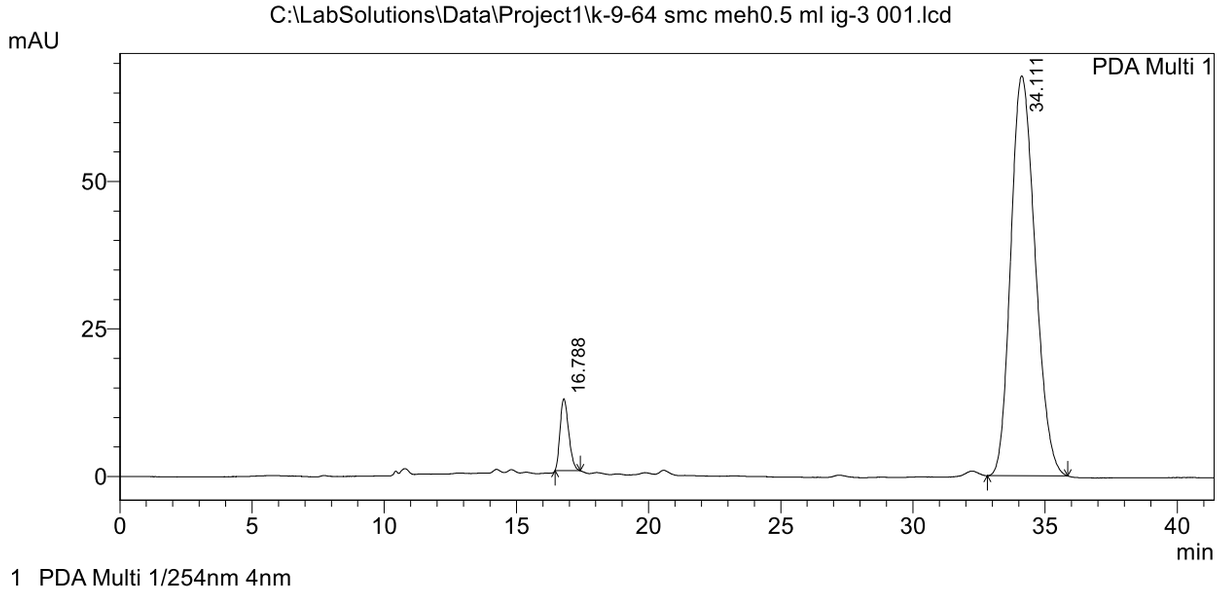

1 PDA Multi 1/254nm 4nm

PeakTable

PDA Ch1 254nm 4nm

Peak#	Ret. Time	Area	Height	Area %	Height %
1	16.788	276605	12214	5.975	15.269
2	34.111	4352747	67782	94.025	84.731
Total		4629352	79996	100.000	100.000

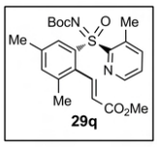

<Chromatogram>

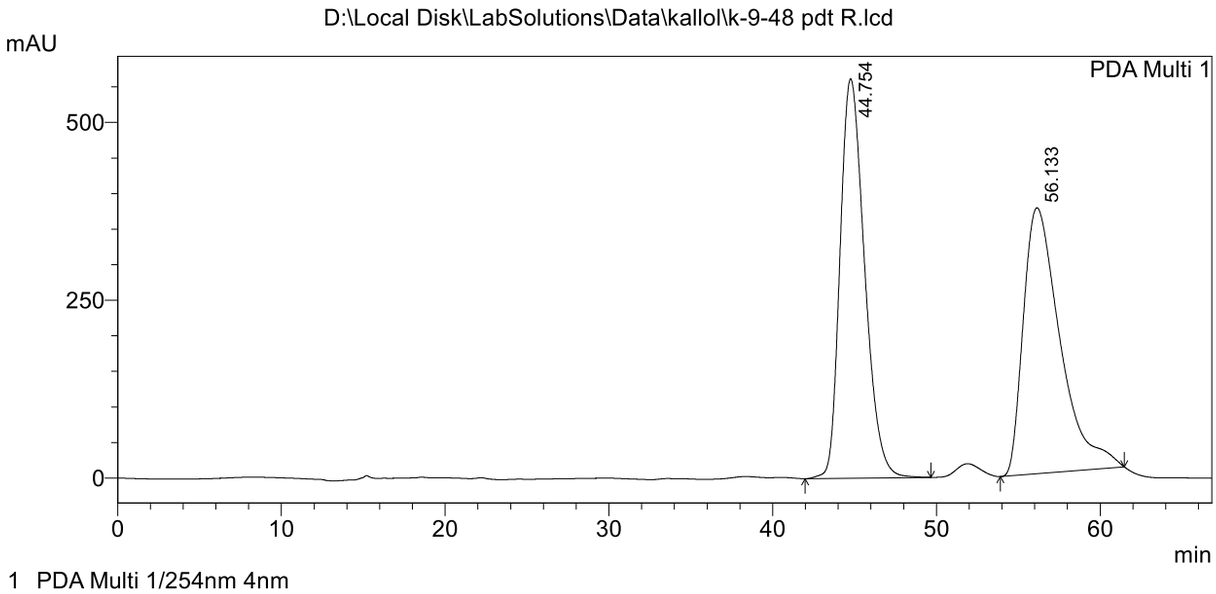

1 PDA Multi 1/254nm 4nm

PeakTable

PDA Ch1 254nm 4nm

Peak#	Ret. Time	Area	Height	Area %	Height %
1	44.754	58479508	561698	50.036	60.021
2	56.133	58395815	374143	49.964	39.979
Total		116875323	935842	100.000	100.000

<Chromatogram>

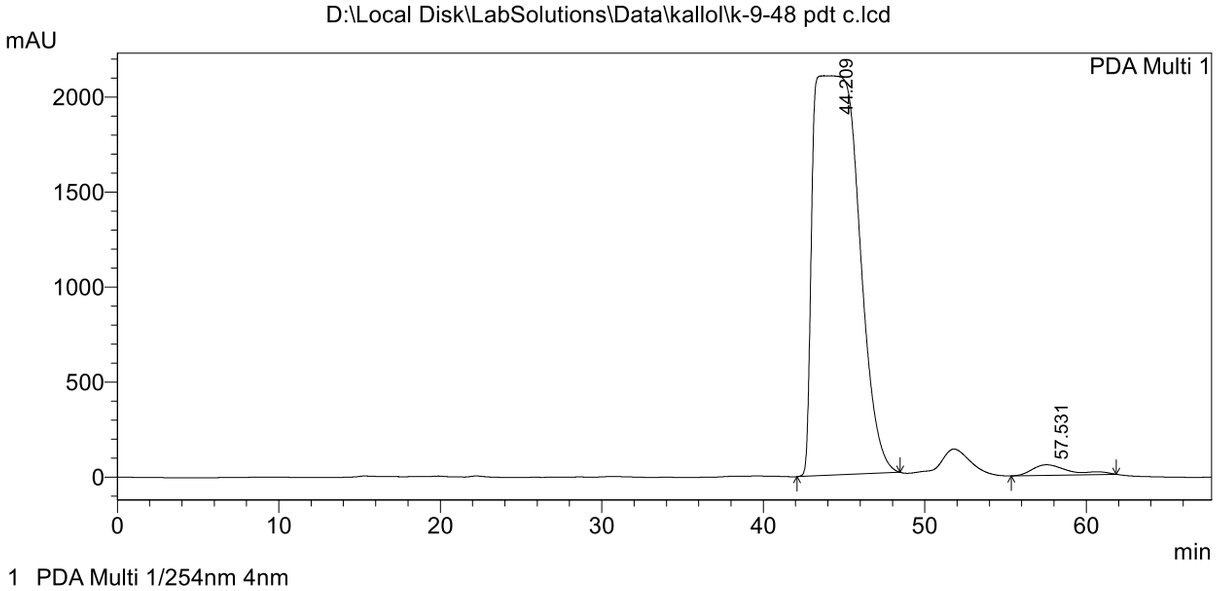

1 PDA Multi 1/254nm 4nm

PeakTable

PDA Ch1 254nm 4nm

Peak#	Ret. Time	Area	Height	Area %	Height %
1	44.209	413011528	2102714	97.890	97.424
2	57.531	8904257	55596	2.110	2.576
Total		421915785	2158311	100.000	100.000

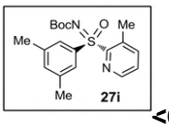

<Chromatogram>

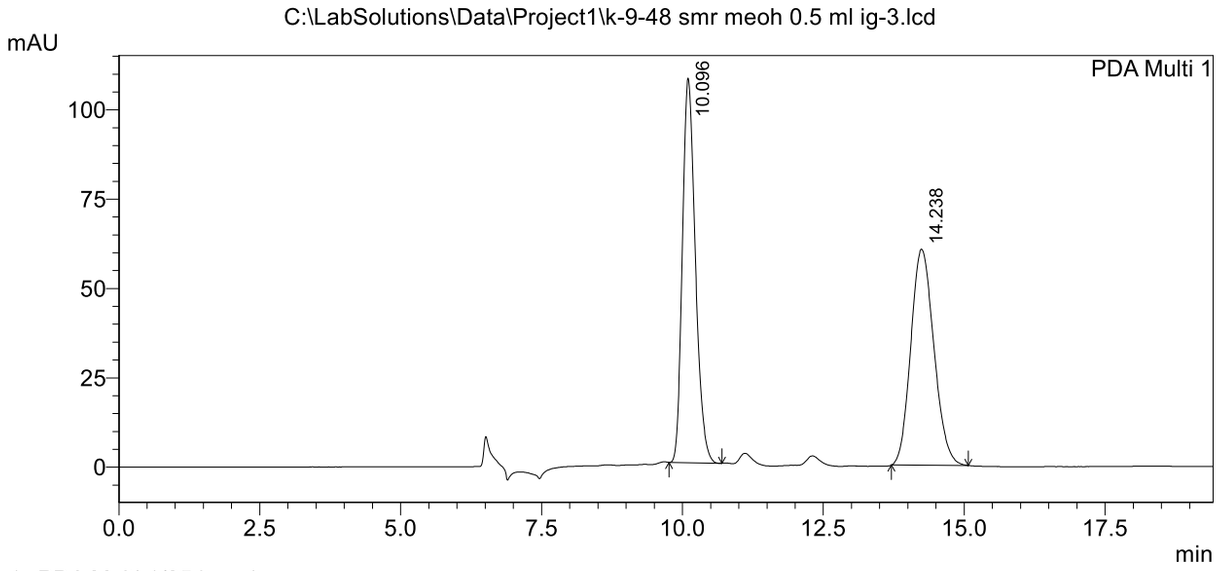

1 PDA Multi 1/254nm 4nm

PeakTable

PDA Ch1 254nm 4nm

Peak#	Ret. Time	Area	Height	Area %	Height %
1	10.096	1724157	107620	50.002	64.029
2	14.238	1723998	60460	49.998	35.971
Total		3448155	168080	100.000	100.000

<Chromatogram>

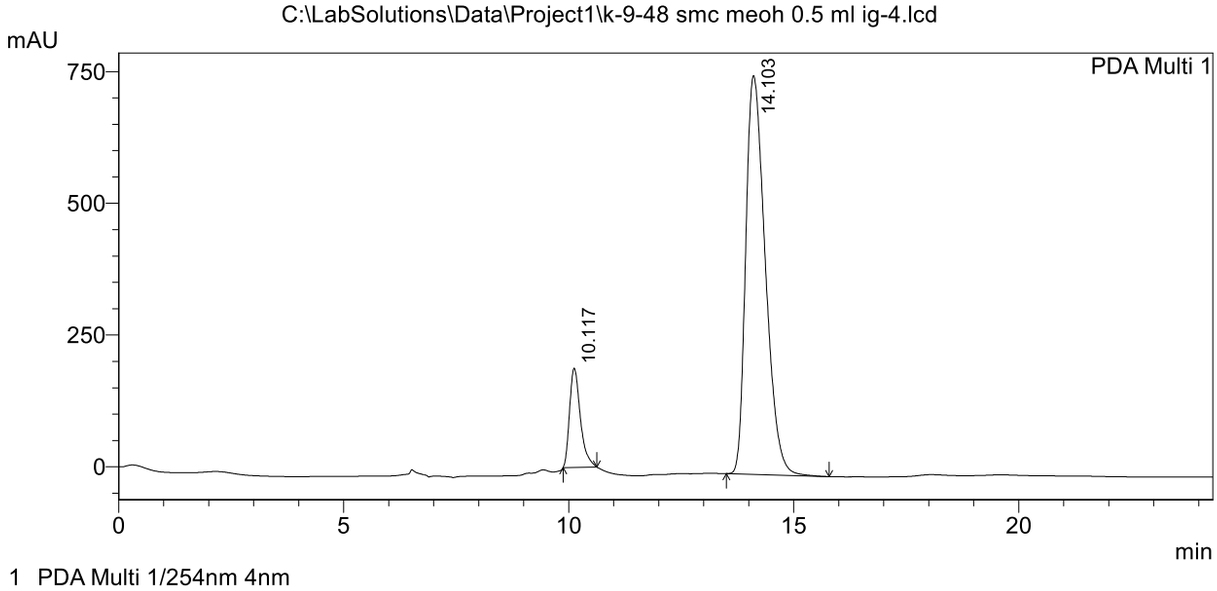

1 PDA Multi 1/254nm 4nm

PeakTable

PDA Ch1 254nm 4nm

Peak#	Ret. Time	Area	Height	Area %	Height %
1	10.117	3138475	188434	12.089	19.932
2	14.103	22823996	756968	87.911	80.068
Total		25962471	945403	100.000	100.000

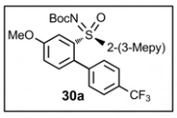

<Chromatogram>

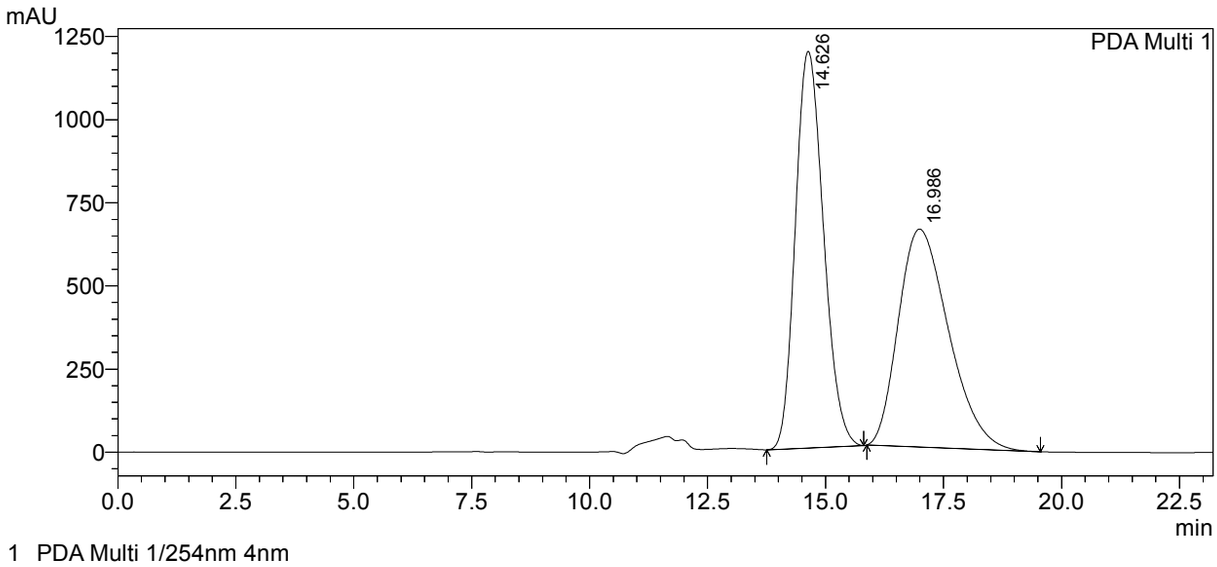

1 PDA Multi 1/254nm 4nm

PeakTable

PDA Ch1 254nm 4nm

Peak#	Ret. Time	Area	Height	Area %	Height %
1	14.626	49645651	1193604	50.530	64.535
2	16.986	48603974	655930	49.470	35.465
Total		98249625	1849534	100.000	100.000

<Chromatogram>

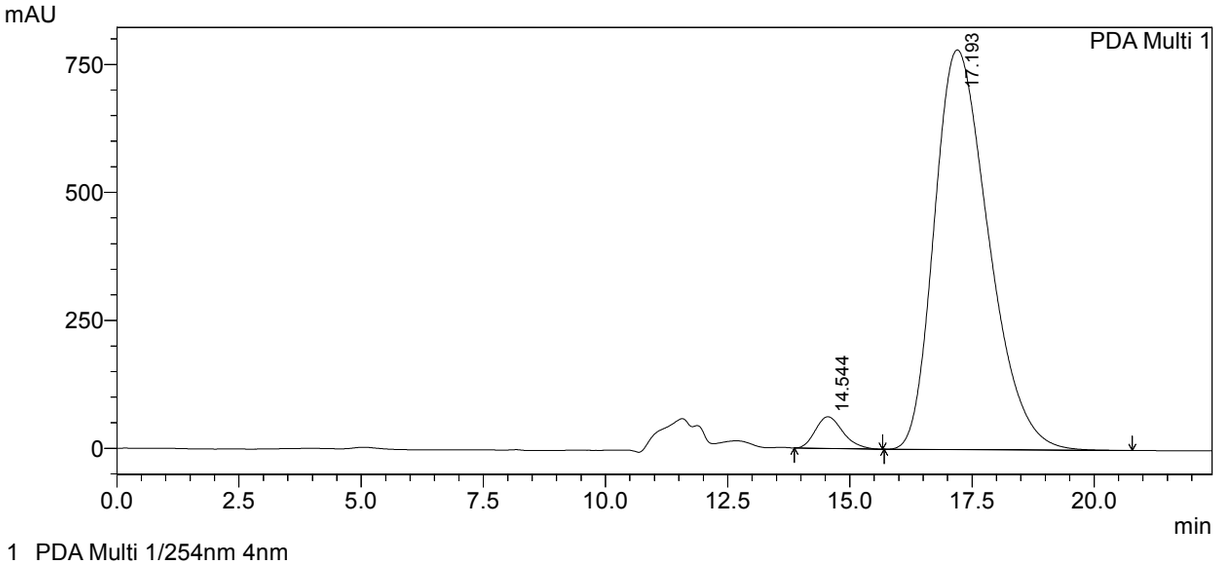

1 PDA Multi 1/254nm 4nm

PeakTable

PDA Ch1 254nm 4nm

Peak#	Ret. Time	Area	Height	Area %	Height %
1	14.544	2433157	61887	3.872	7.340
2	17.193	60402967	781272	96.128	92.660
Total		62836124	843158	100.000	100.000

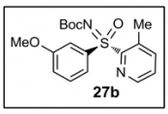

<Chromatogram>

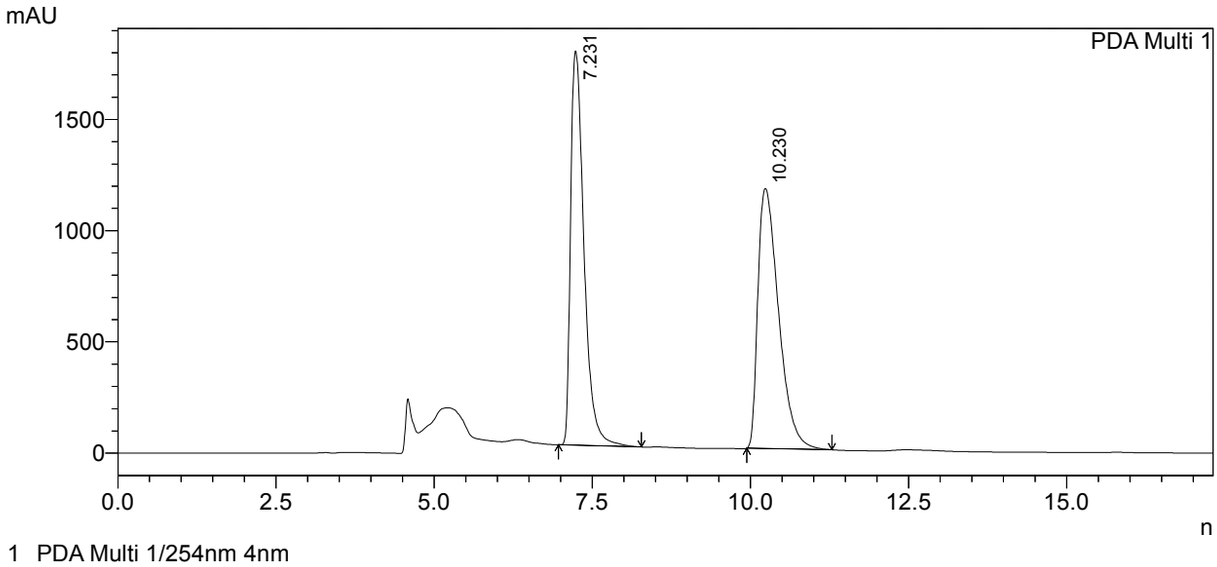

1 PDA Multi 1/254nm 4nm

PeakTable

PDA Ch1 254nm 4nm

Peak#	Ret. Time	Area	Height	Area %	Height %
1	7.231	26089270	1772445	49.517	60.253
2	10.230	26598037	1169216	50.483	39.747
Total		52687308	2941662	100.000	100.000

<Chromatogram>

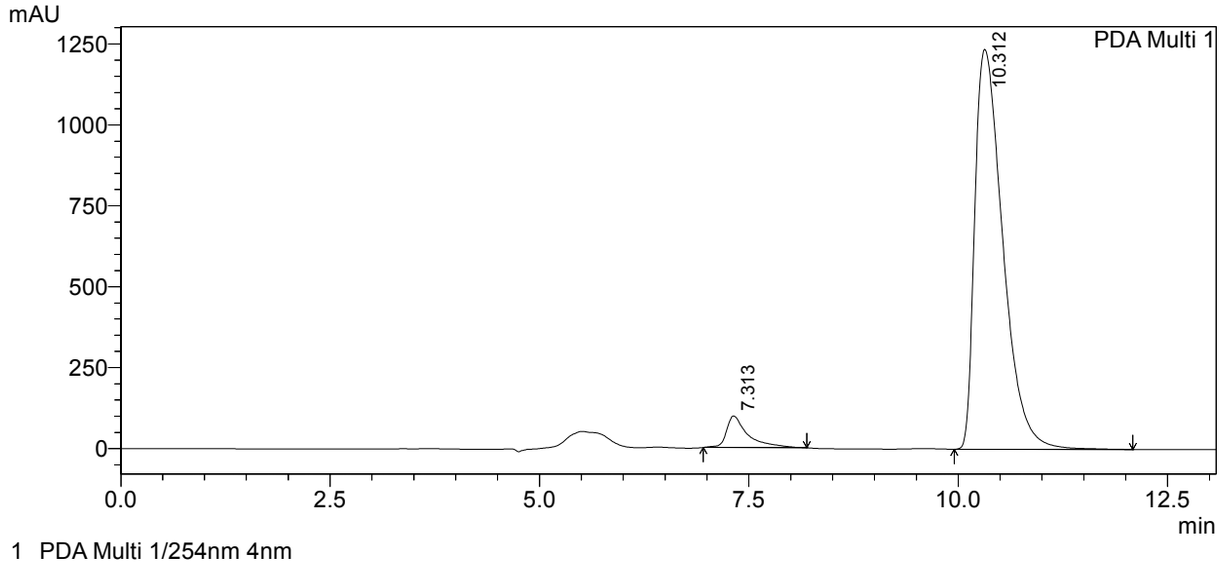

1 PDA Multi 1/254nm 4nm

PeakTable

PDA Ch1 254nm 4nm

Peak#	Ret. Time	Area	Height	Area %	Height %
1	7.313	1742706	97838	5.713	7.337
2	10.312	28763911	1235626	94.287	92.663
Total		30506617	1333464	100.000	100.000

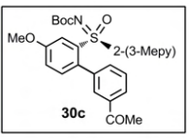

<Chromatogram>

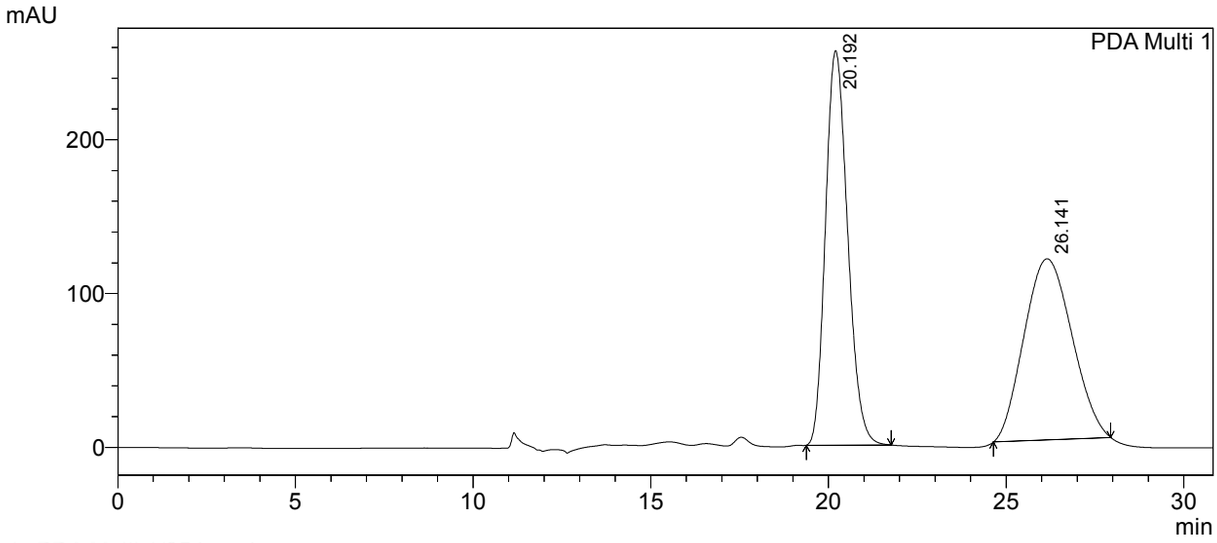

1 PDA Multi 1/254nm 4nm

PeakTable

PDA Ch1 254nm 4nm

Peak#	Ret. Time	Area	Height	Area %	Height %
1	20.192	11131465	256491	50.235	68.529
2	26.141	11027220	117787	49.765	31.471
Total		22158685	374279	100.000	100.000

<Chromatogram>

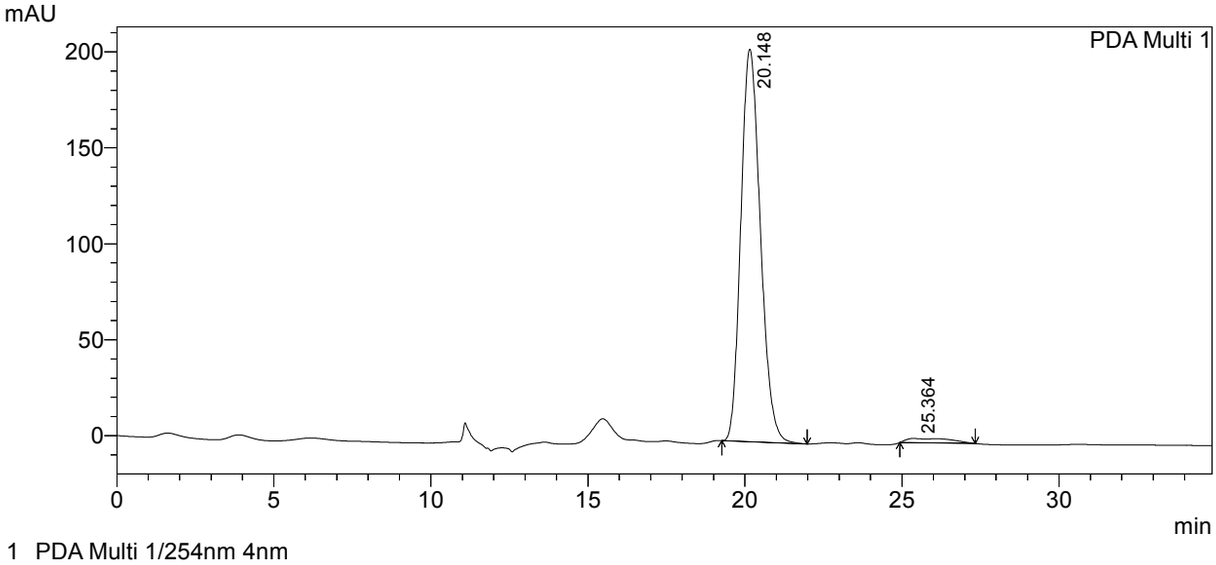

1 PDA Multi 1/254nm 4nm

PeakTable

PDA Ch1 254nm 4nm

Peak#	Ret. Time	Area	Height	Area %	Height %
1	20.148	8855069	204455	97.517	98.914
2	25.364	225464	2245	2.483	1.086
Total		9080533	206699	100.000	100.000

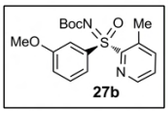

<Chromatogram>

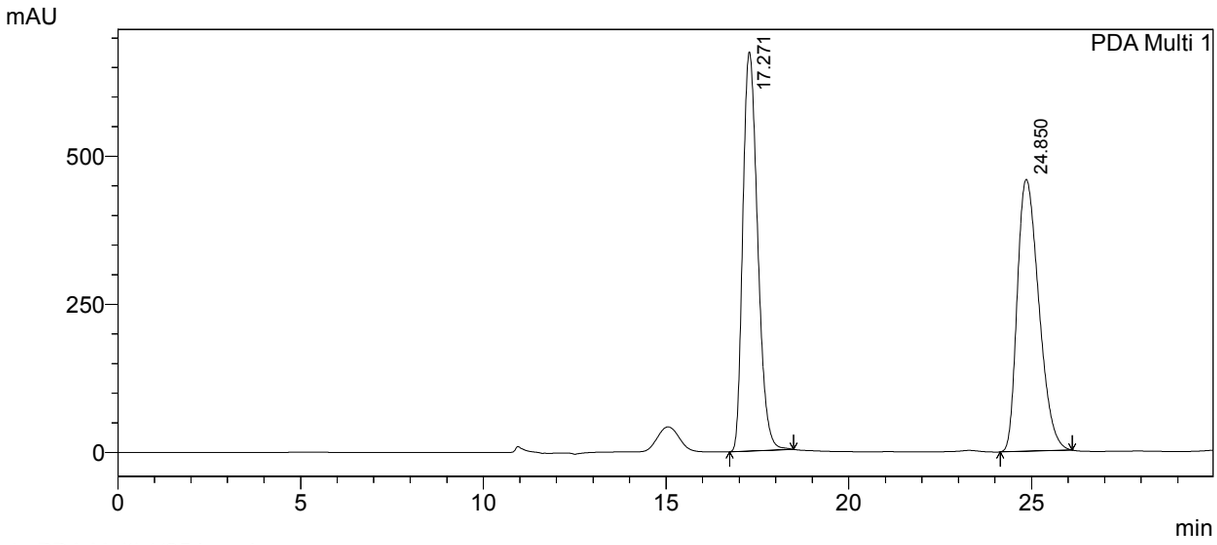

1 PDA Multi 1/254nm 4nm

PeakTable

PDA Ch1 254nm 4nm

Peak#	Ret. Time	Area	Height	Area %	Height %
1	17.271	18958640	674279	50.127	59.478
2	24.850	18862778	459374	49.873	40.522
Total		37821418	1133653	100.000	100.000

<Chromatogram>

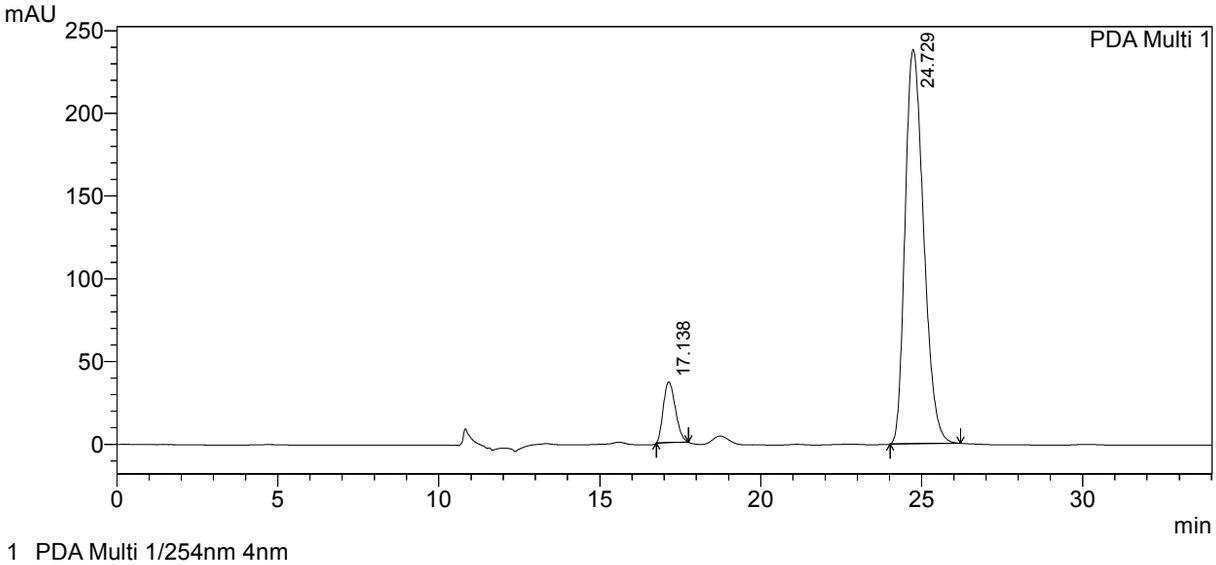

1 PDA Multi 1/254nm 4nm

PeakTable

PDA Ch1 254nm 4nm

Peak#	Ret. Time	Area	Height	Area %	Height %
1	17.138	954272	36682	9.086	13.334
2	24.729	9548608	238425	90.914	86.666
Total		10502880	275107	100.000	100.000

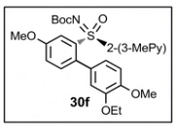

<Chromatogram>

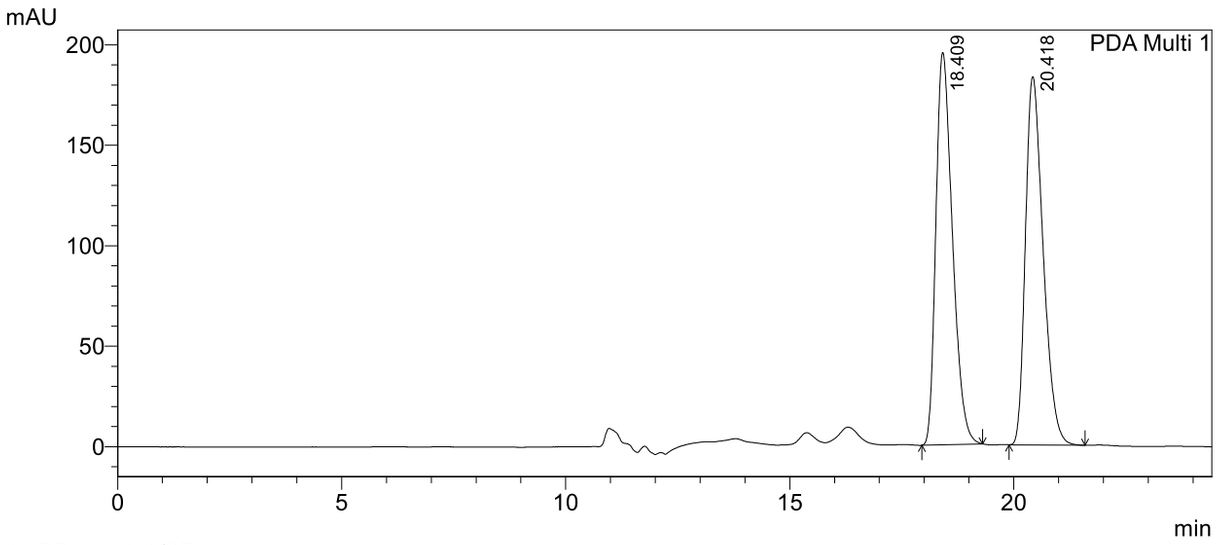

1 PDA Multi 1/254nm 4nm

PeakTable

PDA Ch1 254nm 4nm

Peak#	Ret. Time	Area	Height	Area %	Height %
1	18.409	5013677	195249	49.904	51.579
2	20.418	5033050	183297	50.096	48.421
Total		10046727	378546	100.000	100.000

<Chromatogram>

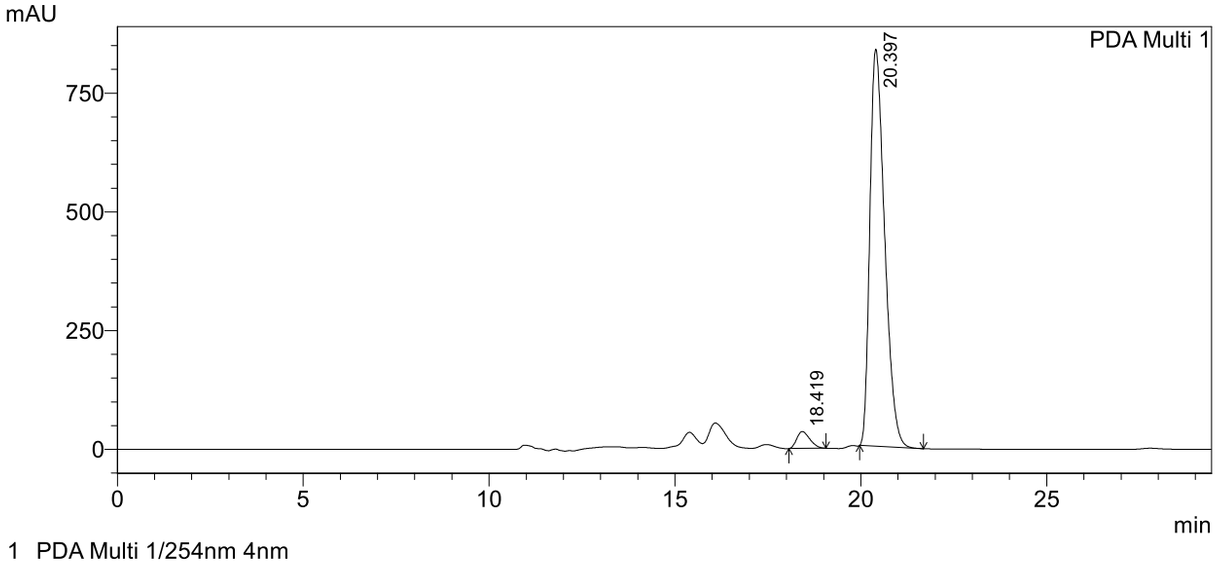

1 PDA Multi 1/254nm 4nm

PeakTable

PDA Ch1 254nm 4nm

Peak#	Ret. Time	Area	Height	Area %	Height %
1	18.419	870514	35639	3.627	4.088
2	20.397	23129703	836137	96.373	95.912
Total		24000218	871776	100.000	100.000

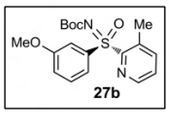

<Chromatogram>

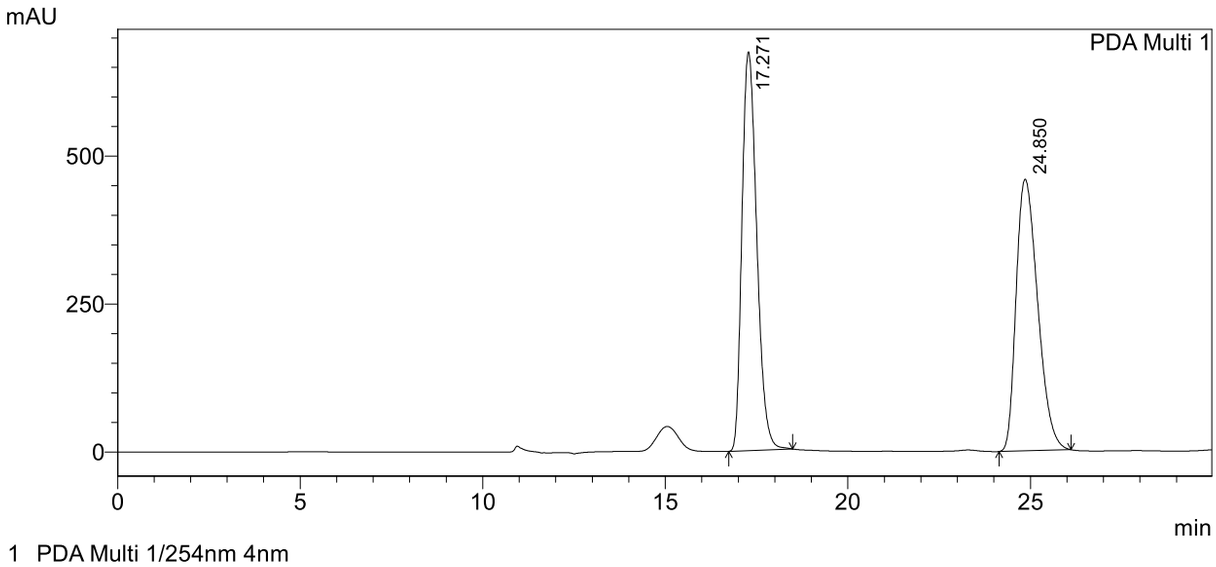

1 PDA Multi 1/254nm 4nm

PeakTable

PDA Ch1 254nm 4nm

Peak#	Ret. Time	Area	Height	Area %	Height %
1	17.271	18958640	674279	50.127	59.478
2	24.850	18862778	459374	49.873	40.522
Total		37821418	1133653	100.000	100.000

<Chromatogram>

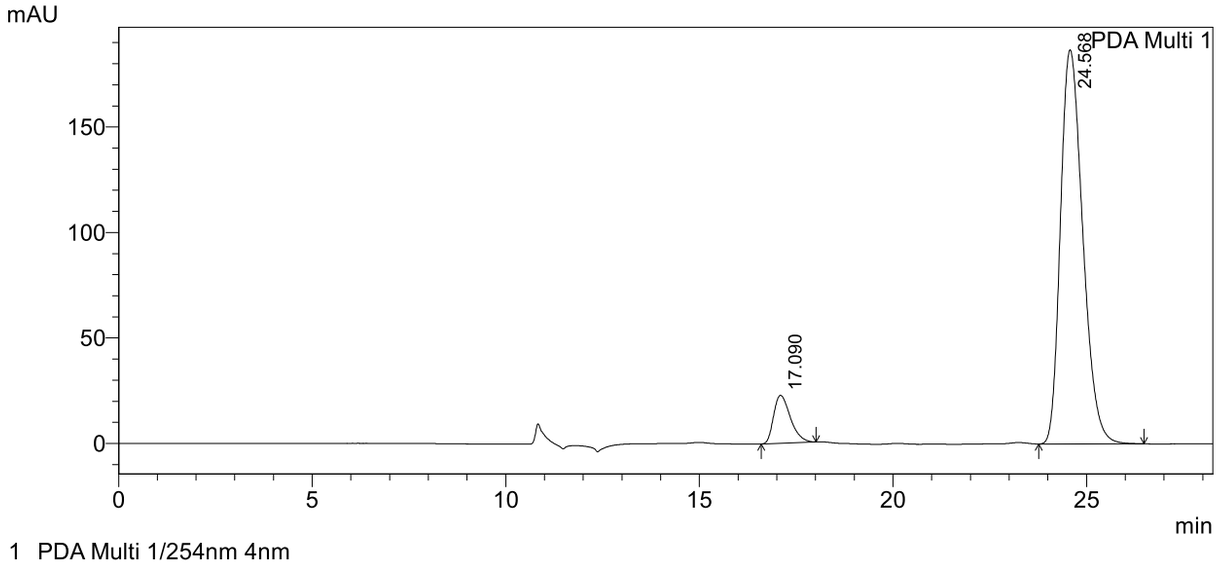

1 PDA Multi 1/254nm 4nm

PeakTable

PDA Ch1 254nm 4nm

Peak#	Ret. Time	Area	Height	Area %	Height %
1	17.090	686679	22760	8.408	10.858
2	24.568	7479913	186858	91.592	89.142
Total		8166592	209618	100.000	100.000

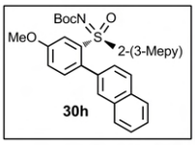

<Chromatogram>

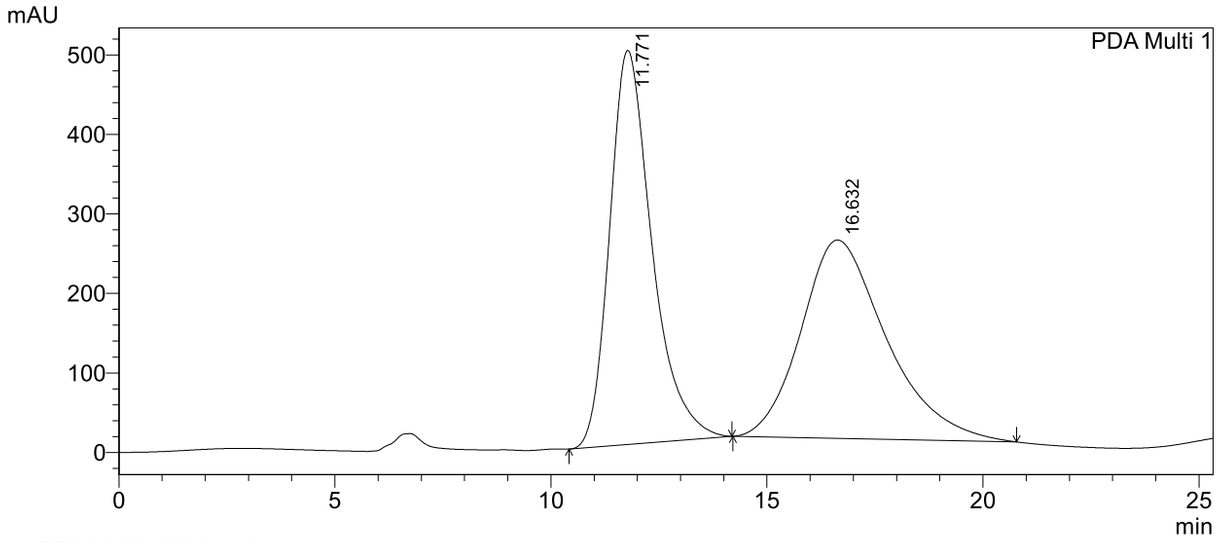

1 PDA Multi 1/254nm 4nm

PeakTable

PDA Ch1 254nm 4nm

Peak#	Ret. Time	Area	Height	Area %	Height %
1	11.771	33787977	495700	49.659	66.527
2	16.632	34251614	249415	50.341	33.473
Total		68039591	745115	100.000	100.000

<Chromatogram>

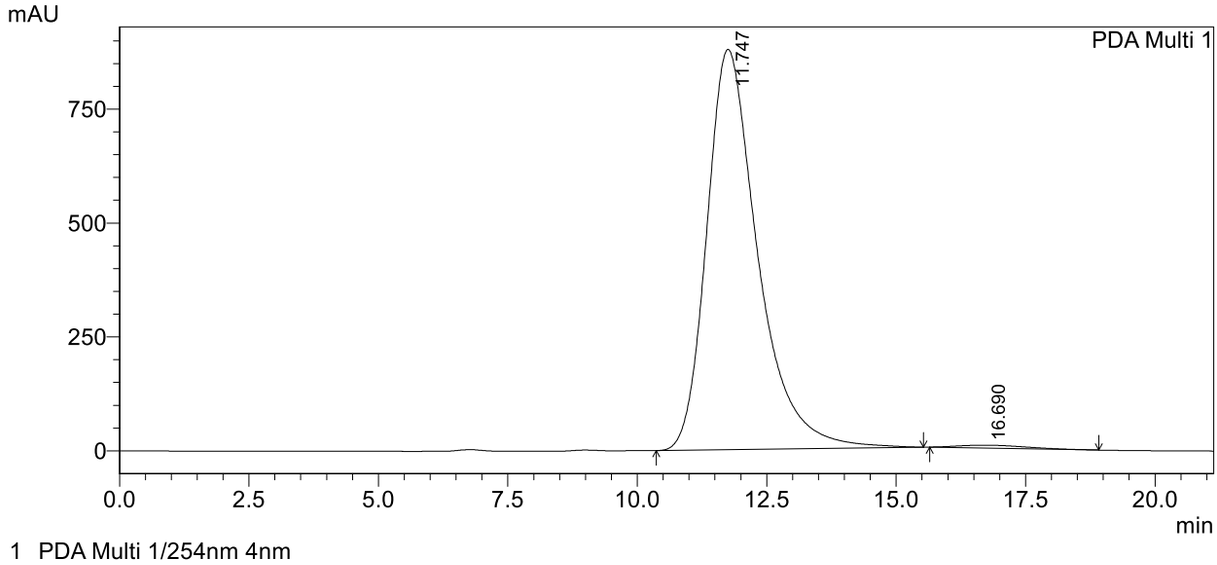

1 PDA Multi 1/254nm 4nm

PeakTable

PDA Ch1 254nm 4nm

Peak#	Ret. Time	Area	Height	Area %	Height %
1	11.747	60303928	878479	99.033	99.283
2	16.690	589082	6340	0.967	0.717
Total		60893009	884820	100.000	100.000

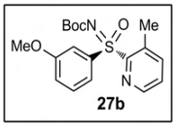

<Chromatogram>

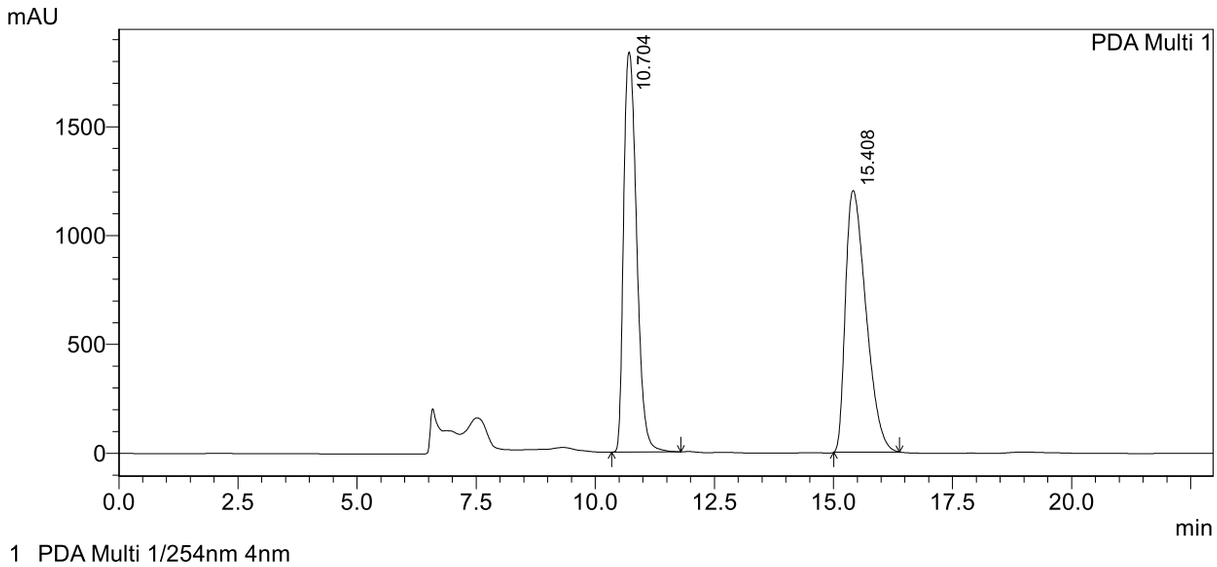

1 PDA Multi 1/254nm 4nm

PeakTable

PDA Ch1 254nm 4nm

Peak#	Ret. Time	Area	Height	Area %	Height %
1	10.704	34869126	1837706	49.194	60.452
2	15.408	36011188	1202230	50.806	39.548
Total		70880313	3039935	100.000	100.000

<Chromatogram>

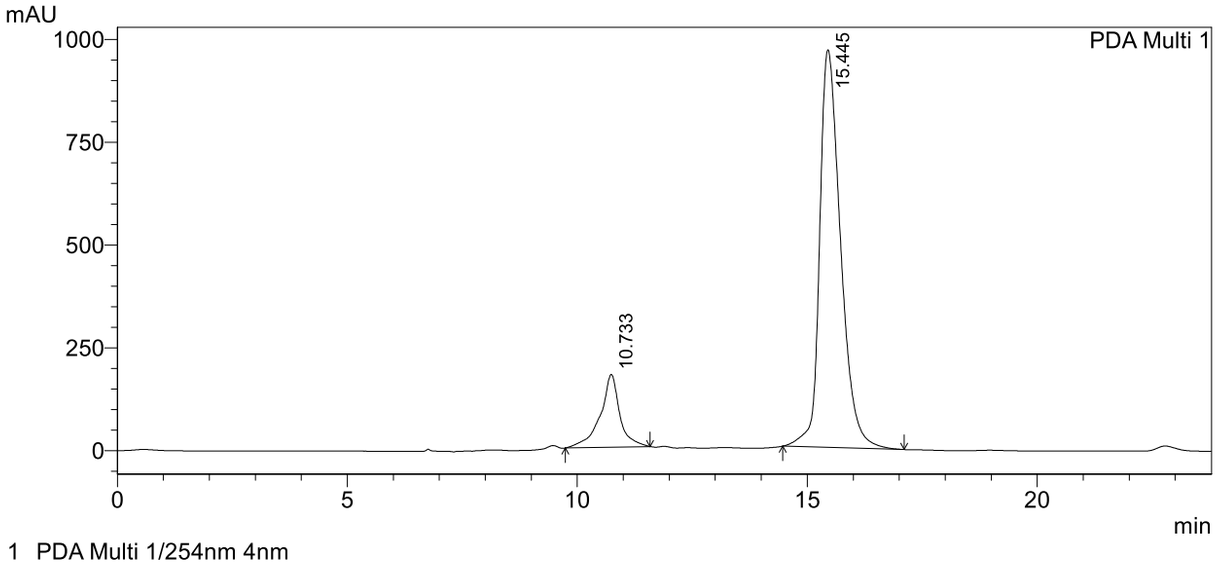

1 PDA Multi 1/254nm 4nm

PeakTable

PDA Ch1 254nm 4nm

Peak#	Ret. Time	Area	Height	Area %	Height %
1	10.733	5222002	177377	14.533	15.493
2	15.445	30708885	967512	85.467	84.507
Total		35930888	1144889	100.000	100.000

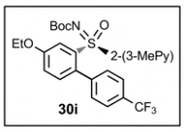

<Chromatogram>

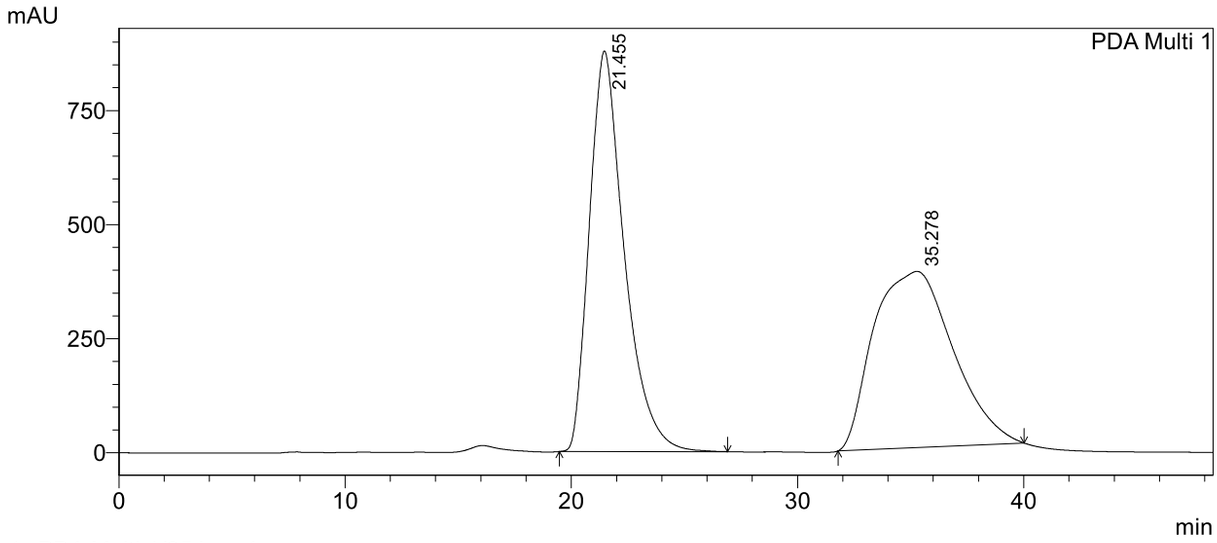

1 PDA Multi 1/254nm 4nm

PeakTable

PDA Ch1 254nm 4nm

Peak#	Ret. Time	Area	Height	Area %	Height %
1	21.455	94365214	877835	49.988	69.465
2	35.278	94410770	385869	50.012	30.535
Total		188775984	1263704	100.000	100.000

<Chromatogram>

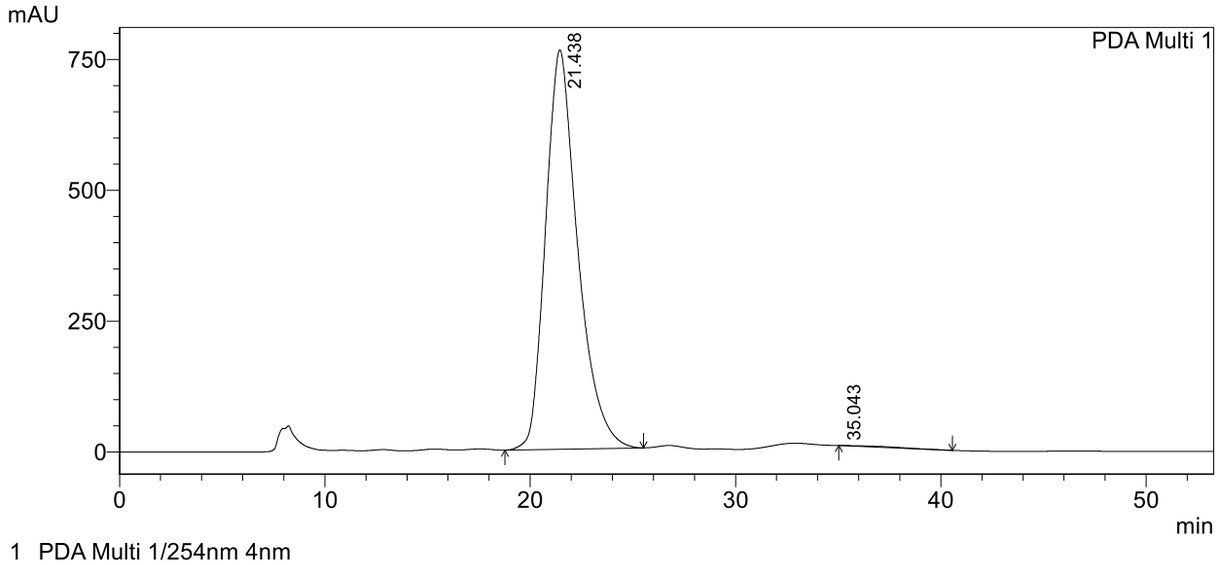

1 PDA Multi 1/254nm 4nm

PeakTable

PDA Ch1 254nm 4nm

Peak#	Ret. Time	Area	Height	Area %	Height %
1	21.438	83256759	763282	99.716	99.998
2	35.043	237325	13	0.284	0.002
Total		83494084	763295	100.000	100.000

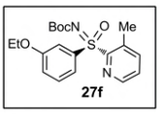

<Chromatogram>

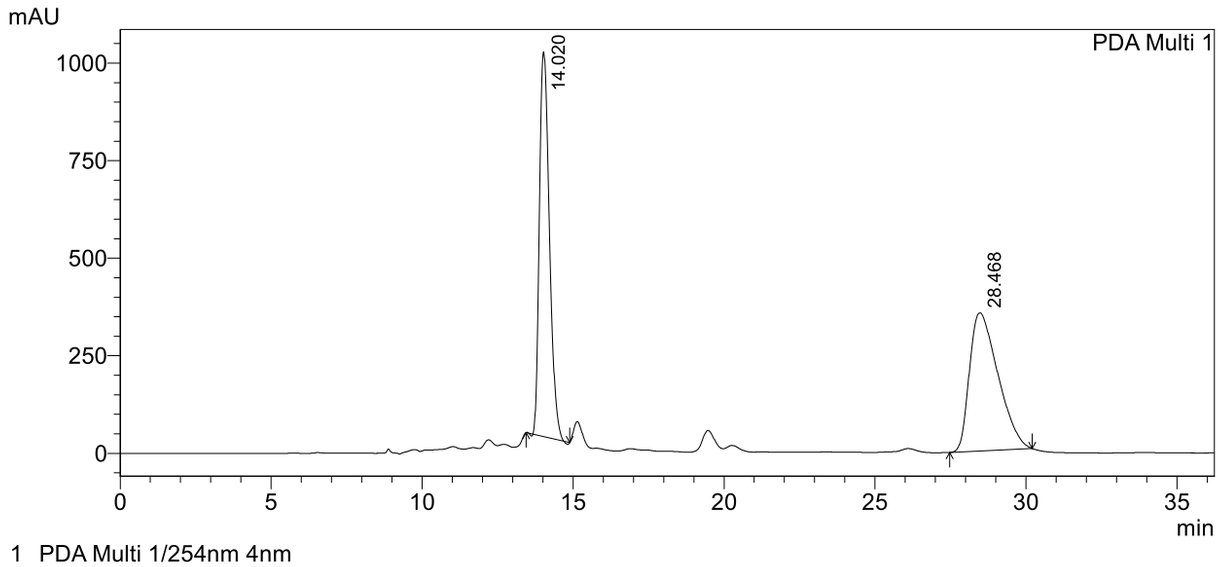

1 PDA Multi 1/254nm 4nm

PeakTable

PDA Ch1 254nm 4nm

Peak#	Ret. Time	Area	Height	Area %	Height %
1	14.020	22748450	985525	49.482	73.558
2	28.468	23224648	354266	50.518	26.442
Total		45973098	1339792	100.000	100.000

<Chromatogram>

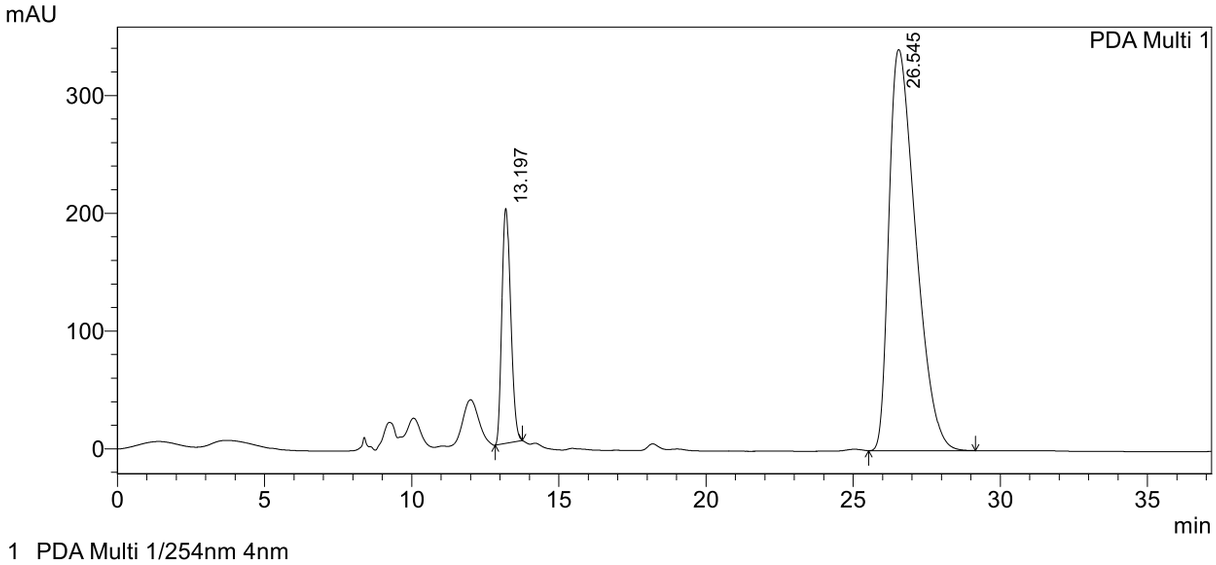

1 PDA Multi 1/254nm 4nm

PeakTable

PDA Ch1 254nm 4nm

Peak#	Ret. Time	Area	Height	Area %	Height %
1	13.197	4111421	199464	16.067	36.937
2	26.545	21478532	340553	83.933	63.063
Total		25589953	540017	100.000	100.000

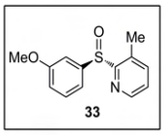

<Chromatogram>

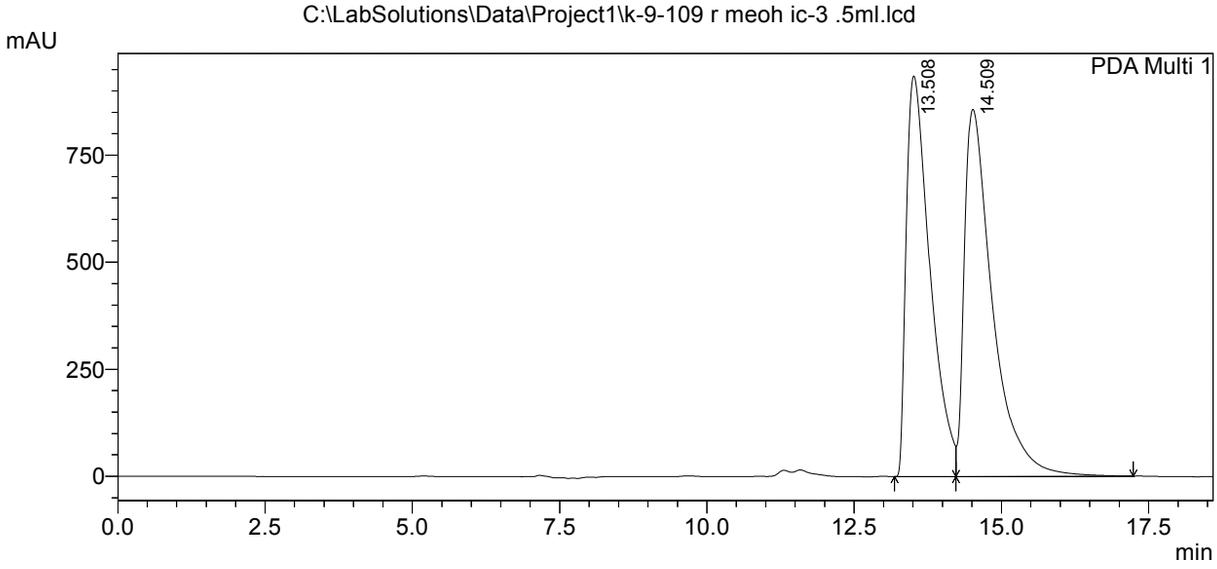

1 PDA Multi 1/254nm 4nm

PeakTable

PDA Ch1 254nm 4nm

Peak#	Ret. Time	Area	Height	Area %	Height %
1	13.508	26248588	935689	47.985	52.173
2	14.509	28452965	857757	52.015	47.827
Total		54701554	1793446	100.000	100.000

<Chromatogram>

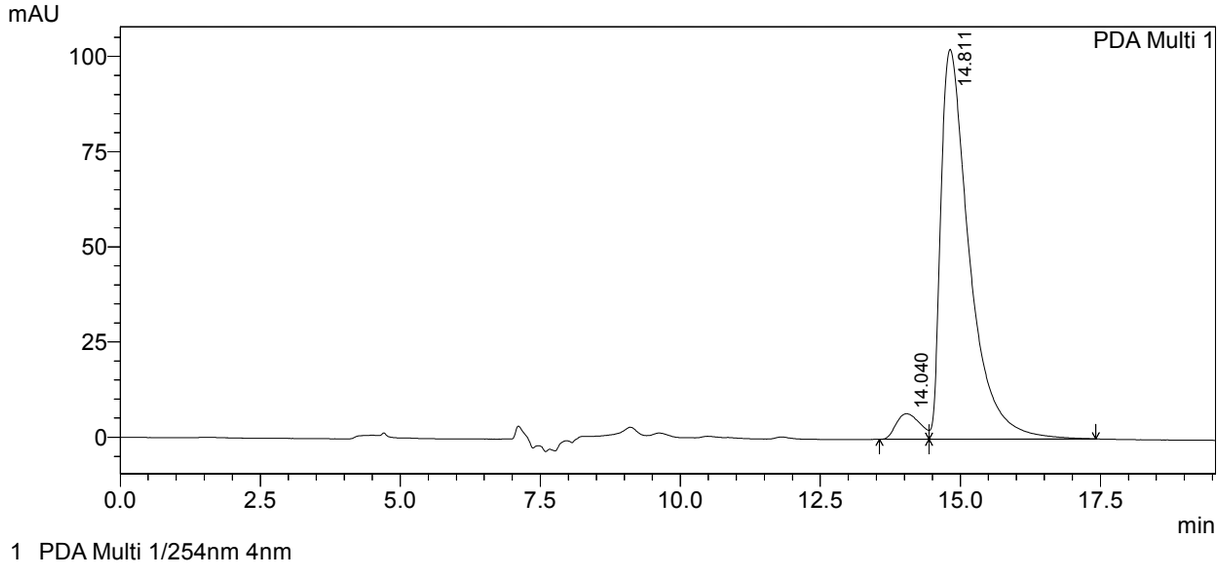

1 PDA Multi 1/254nm 4nm

PeakTable

PDA Ch1 254nm 4nm

Peak#	Ret. Time	Area	Height	Area %	Height %
1	14.040	198773	6698	5.192	6.139
2	14.811	3629324	102416	94.808	93.861
Total		3828097	109114	100.000	100.000

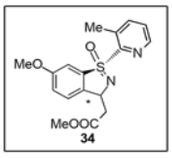

<Chromatogram>

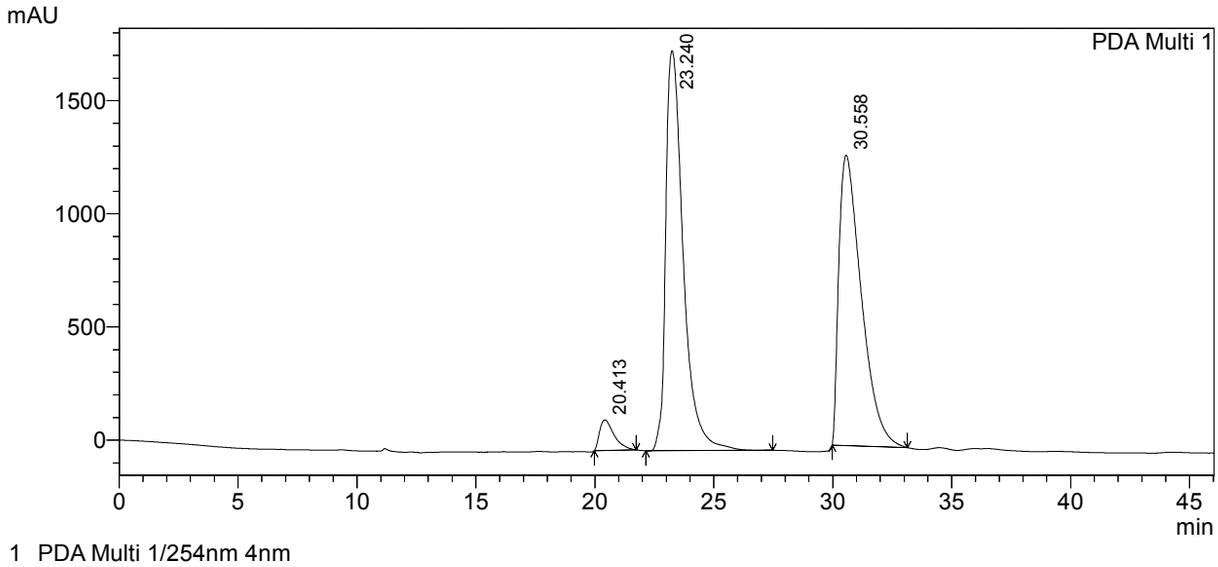

1 PDA Multi 1/254nm 4nm

PeakTable

PDA Ch1 254nm 4nm

Peak#	Ret. Time	Area	Height	Area %	Height %
1	20.413	5714931	134883	3.172	4.234
2	23.240	90191223	1767086	50.066	55.467
3	30.558	84238011	1283869	46.761	40.299
Total		180144165	3185837	100.000	100.000

<Chromatogram>

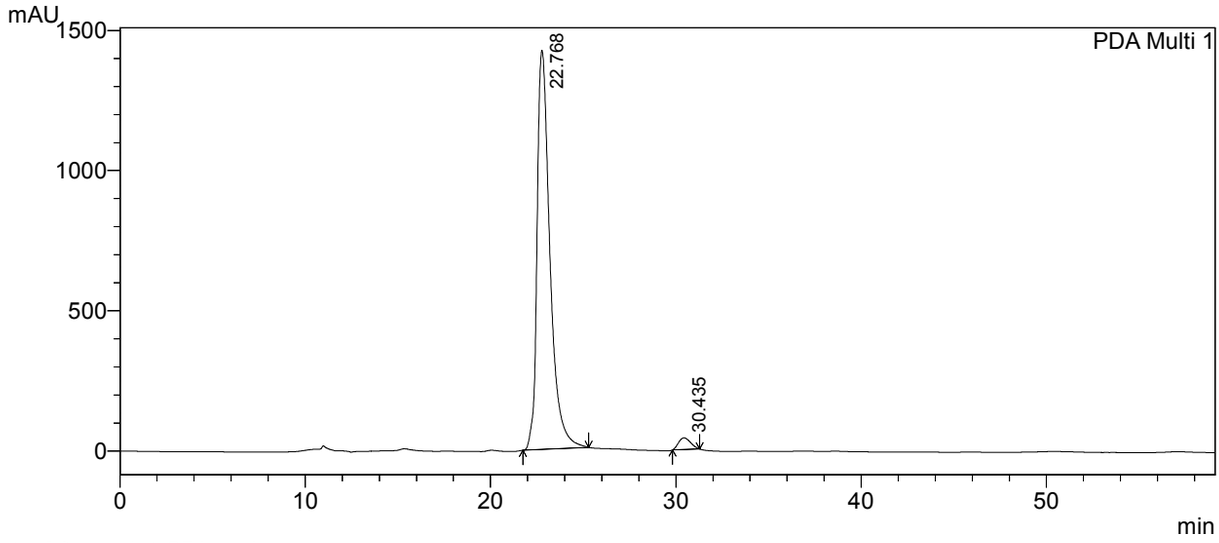

1 PDA Multi 1/254nm 4nm

PeakTable

PDA Ch1 254nm 4nm

Peak#	Ret. Time	Area	Height	Area %	Height %
1	22.768	68670177	1424000	97.307	97.136
2	30.435	1900279	41990	2.693	2.864
Total		70570456	1465990	100.000	100.000

Chapter III

Unsymmetrical Annulation of C(sp²)–H Bonds with Alkynes and Quinones: Access to Spiro-Isoquinolones

Abstract

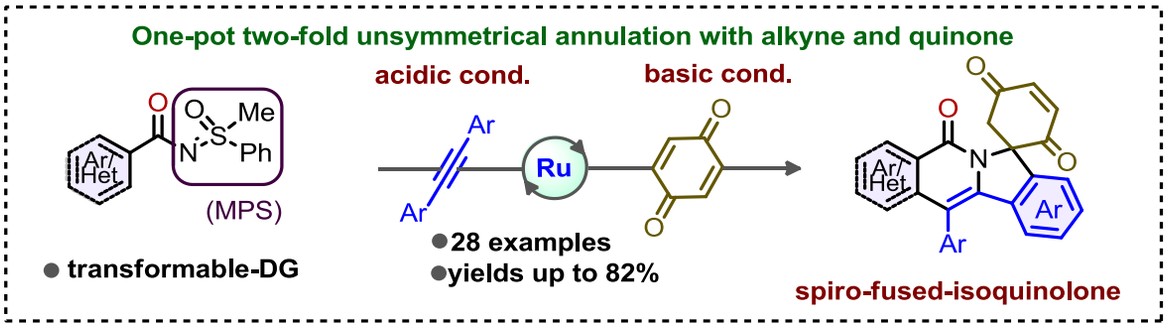

A non-trivial Ru-catalyzed one-pot sequential oxidative coupling of a (hetero)arene/vinylic/chromene system with alkyne and quinone is presented; the methyl phenyl sulfoximine (MPS) directing group is vital. This cyclization forms four (two C–C and two C–N) bonds in a single operation and produces unusual spiro-fused-isoquinolones with a broad scope. The release of phenyl methyl sulfoxide makes the MPS group transformable. A deuterium scrambling study sheds light on the reaction path.

Reference:

Kallol Mukherjee, Majji Shankar, Koushik Ghosh, and Akhila K. Sahoo
Org. Lett. **2018**, *20*, 1914–1917.

III.1. Introduction

The synthetically validated annulation tool has had a profound impact in chemistry, as this method reliably transforms the readily accessible less-functionalized compounds to structurally complex molecules.[1] In this regard, the transition-metal (TM)-catalyzed and directing group (DG) supported activation, functionalization, and annulation of inert C–H bonds are incomparable.[2–5] Obviously, the functionalization of environmentally different C–H bonds with distinct coupling partners results in structurally diverse molecular scaffolds.[6] A viable synthetic example of this is the directed double functionalization of proximal C–H bonds with identical functional groups.[7] By contrast, the chelation-assisted unsymmetrical functionalization of C–H bonds is often nonselective, uncontrolled, and unproductive;[8] however, a sequential two-step synthetic process under divergent DGs and/or different catalytic conditions is implemented for the construction of novel molecular scaffolds.[9]

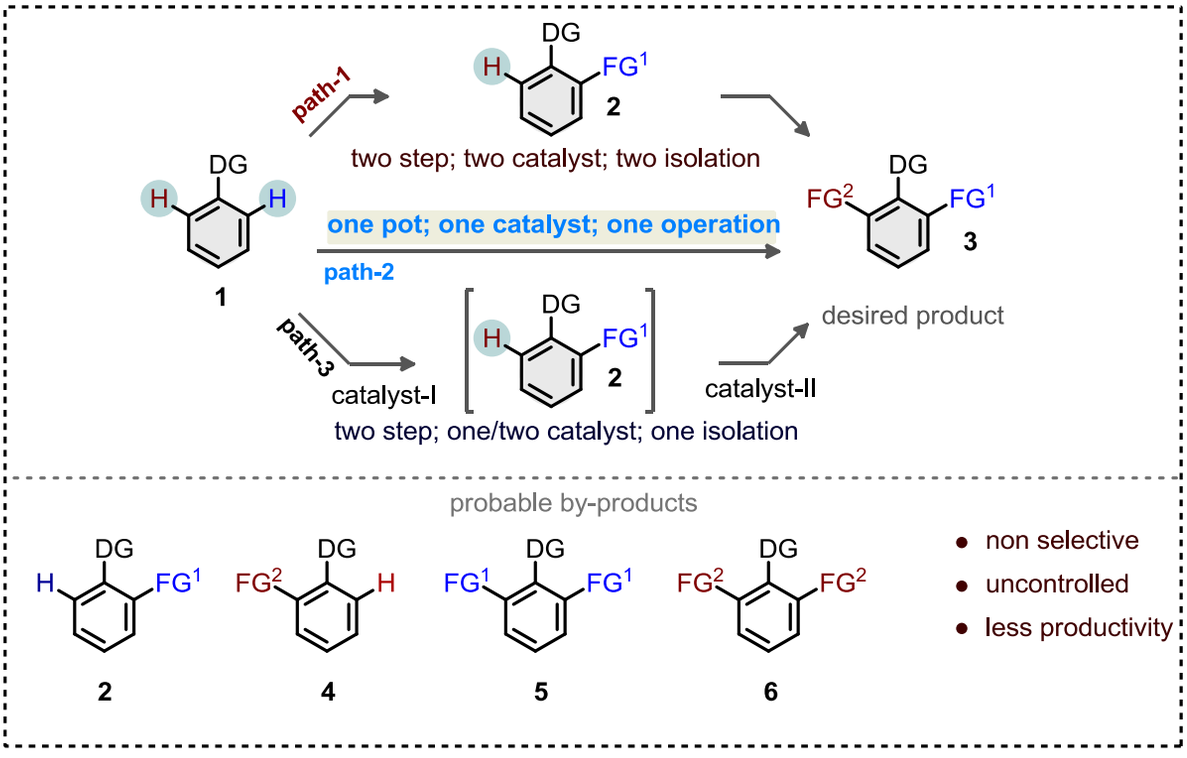

Scheme III.1: Multiple C–H functionalization and challenges

III.2. Previous strategies for annulation

III.2.1. Previous strategies of Ru-catalyzed mono-annulation:

In 2010 Ackermann group reported oxidative mono-annulation strategy for N–Me benzamide derivatives **7** with internal alkyne **8** for the synthesis of isoquinoline moieties **10** (**eq 1**, **Scheme III.2**). This method involves the inexpensive and air stable Ru(II) catalyst. The functionalization of N-Me benzamide dervivatives essentially requires an external oxidant. The external oxidant re-oxidizes the catalyst at the end of the cycle and makes the catalytic system active. Later the same protocol has been extended towards N–OMe benzamide substrate **9** (**eq 2**, **Scheme III.2**).[10, 11] The N–OMe moiety acts as an internal oxidant and thus, the synthetic method does not need external oxidant. Thus, the synthetic method is atom-economic and green. The mechanistic features of both the methods have been sketched in **Scheme III.2**.

Mechanistic cycles starts with the in-situ formation of active Ru(II)-complex [RuL$(OAc)_2$] **A**. The reaction of **A** with **7** or **9** provides 5-membered ruthenacycle **7a or 9a** via simultaneous N–H and C–H bond activation. Next, the alkyne insertion to **7a** or **9a** intermediate gives a 7-membered metallacycle **7b** or **9b.** Formation of 7-membered metalycycle is common for both the methods. Next, reductive elimination of **7b** delivers the corresponding mono-annulation product **10** along with the formation of inactive Ru(0) system. External oxidant is therefore necessary to re-oxidize Ru(0) to Ru(II) catalytic system, which helps the reaction to proceed further; thus, the transformation is ***oxidant enabled*** (**Scheme III.2**). While in case of **9b**, reductive elimination followed by oxidative insertion of Ru(II) complex across the N–OMe bond and protodemetalation of **9c** delivers isoquinoline derivative **11** along with active catalyst; thus, the transformation is ***oxidant free*** (**Scheme III.2**).

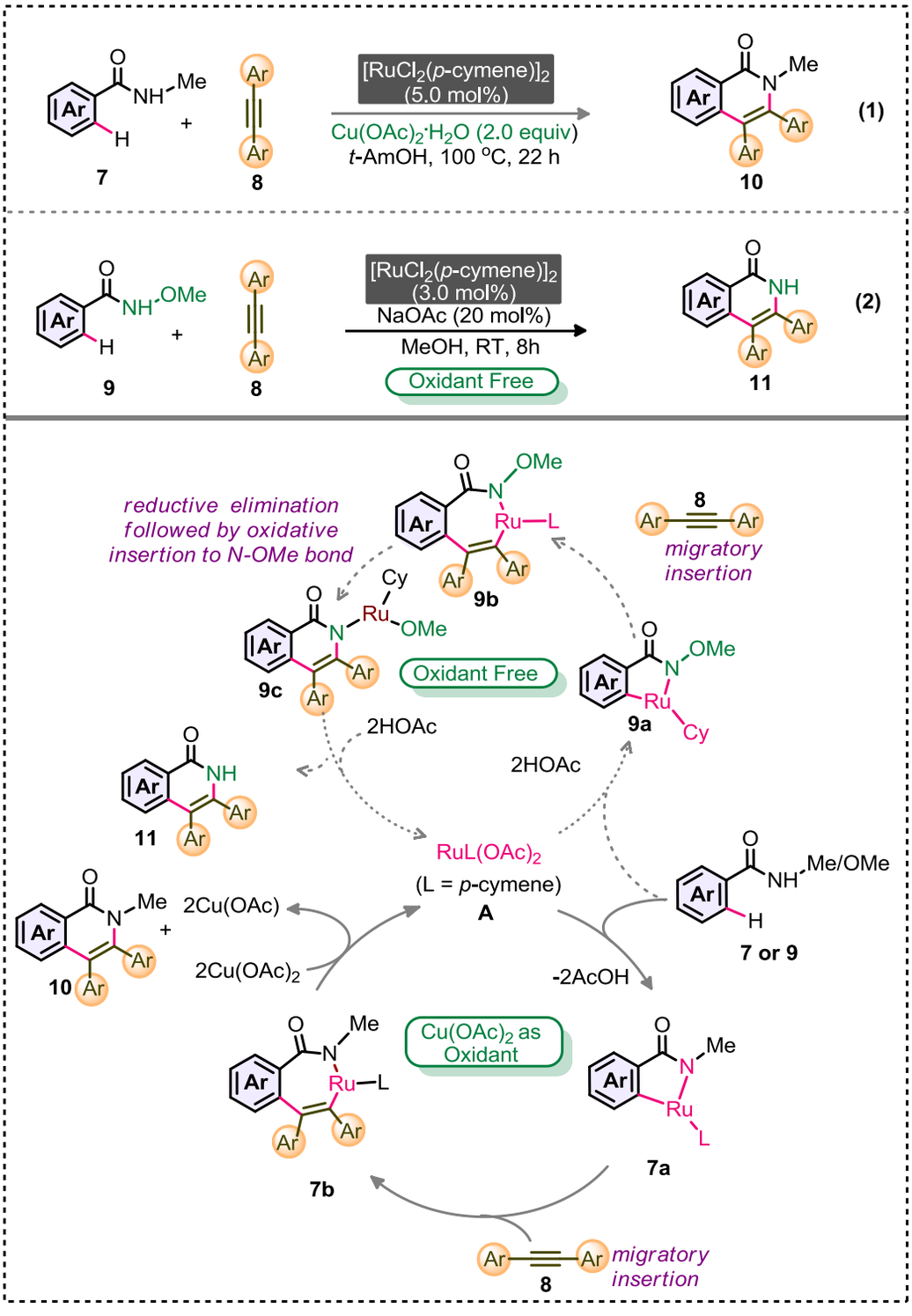

Scheme III.2: Ru(II)-catalyzed annulation of N–Me benzamide and N-OMe with alkyne and plausible mechanism

In 2011, identical strategy has been further extended for the construction of bio-active isoquinolones motifs in water medium (**Scheme III.3**). The N-methoxybenzamides **9** and/or hydroxymic acid derivatives **12** have been successfully employed for the reaction. Interestingly, Ru(II)-carboxylate, obtained in-situ from $[RuCl_2(p\text{-cymene})]_2$ and $MesCO_2K$ was essential for the reaction chemoselectivity.[12,13]

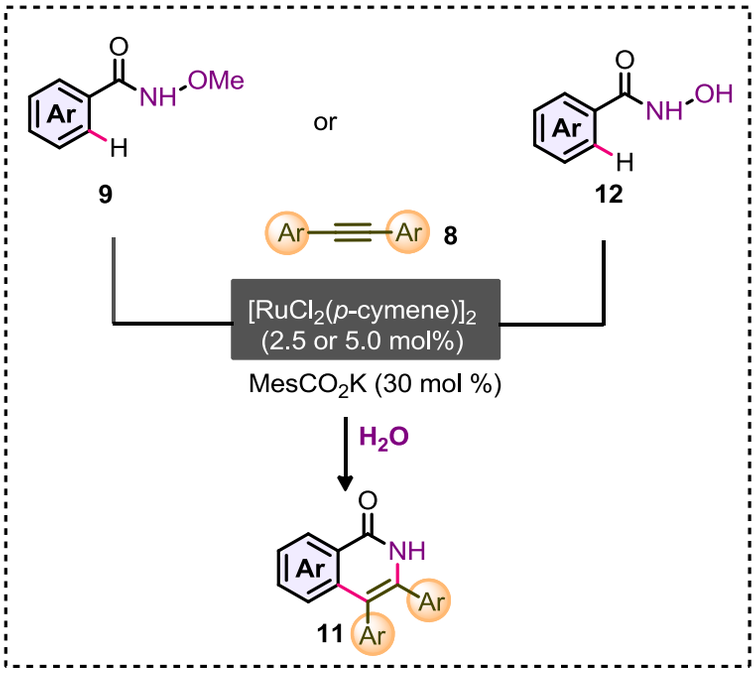

Scheme III.3: Ru(II)-catalyzed oxidative annulation in water medium

In **2014**, our group showcased a sulfoximine directing group assisted oxidative mono-annulation of MPS-coupled carboxylate **13** with internal alkyne. The sulfoximine moiety behave as an internal oxidant. The reaction proceeds without any external oxidant as sulfur (+6) of sulfoximine moiety is reduced to sulfoxide (+4; **14**) and Ru(0) gets reoxidized to Ru(II) (**Scheme III.4**).[14]

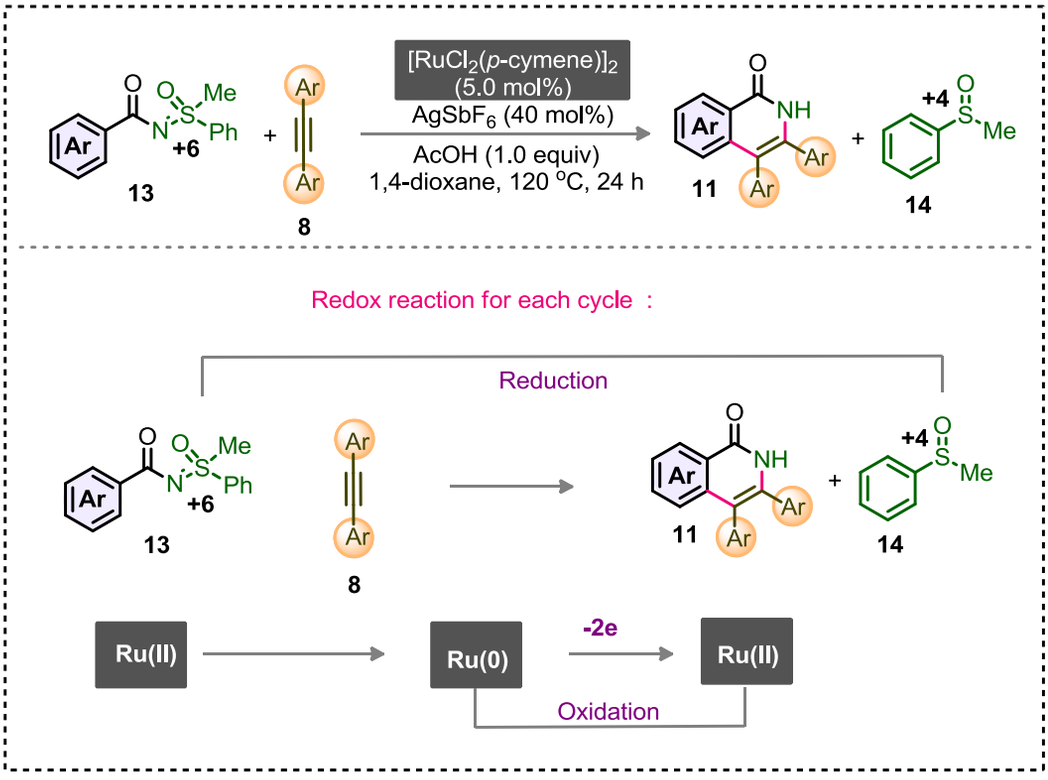

Scheme III.4: MPS directed Ru(II) catalyzed oxidative annulation of arenes

III.2.2. Known strategies of metal-catalyzed mono to di-annulation reactions:

The mono-annulation product isoquinolones **11** has been further used for the oxidative annulation with alkynes to form C–C and C–N bonds. This process leads to highly -conjugated dibenzo[a,g]quinolizin-8-one derivatives with broad substrate scope. (**Scheme III.5**).[15]

The key intermediates **11a**, **11b**, and **11c** are isolated and the structures are determined by X-ray crystallographic analysis. These informations provide insights in understanding the mechanistic details of the reaction. Thus, the mechanistic cycle involves a Ru(II)-Ru(0)-Ru(II) catalytic system (**Scheme III.5**). The sandwich Ru(0) complex **11c** can be reoxidized by external oxidant $Cu(OAc)_2$.

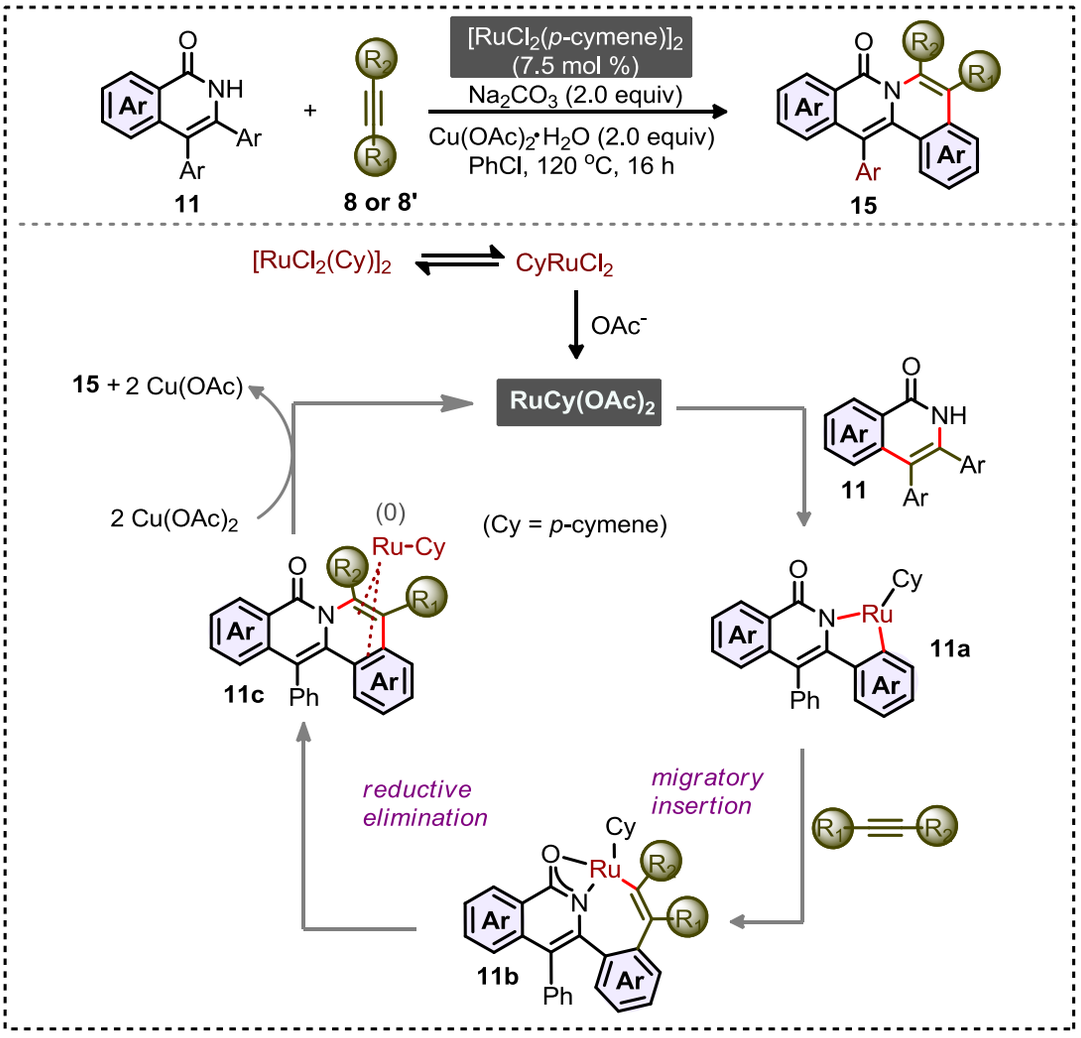

Scheme III. 5: Mechanism for the formation of polycyclic amides

In 2015, Wang group revealed an interesting Ir-catalyzed oxidative coupling of quinone with isoquinolones **11**. This process leads to the structurally complex spiro-derivatives. (**Scheme III.6**).[16a] In the same year Miura group developed Cu-catalyzed spirocyclization of benzamide with maleimide to make spiro-fused product **19** (**Scheme III.6**).[16b]

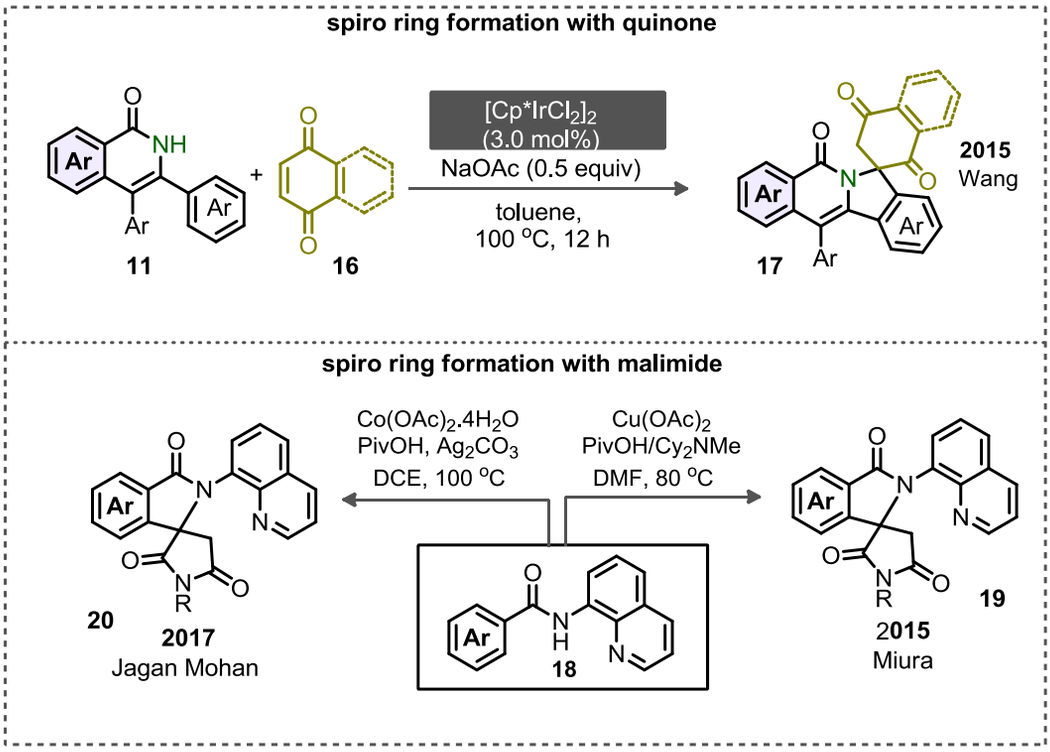

Scheme III.6: Ir(III)-catalyzed mono-annulation with quinone

In 2017 the same methodology was further extended for the Co-catalyzed annulation of **18** with succinimide for the synthesis of isoindolone spirosuccinimides **20** (**Scheme III.6**)[16c].

III.2.3. TM-Catalyzed of (One-pot/two-pot) symmectrical and un-symmetrical di-annulation.

In 2010, Miura and Satoh reported a Rh-catalyzed one-pot symmetrical di-annulation of benzamide derivatives when reacted with two molecules of alkyne.[17] At first, coupling of benzamide with one molecule alkyne leads to mono-annulation product **11**. Next, second C–H activation of the arene motif, proximity to the isoquinolone to provide **Int-B**. Finally, insertion of alkyne to **Int-B** leads to the symmetrical di-annulation product **15**. The same kind of di-annulation strategy were also revealed by Li group to access -conjugated scaffolds.[18] The overall process involves two C–C & C–N bond formation in one pot (**Scheme III.7**).

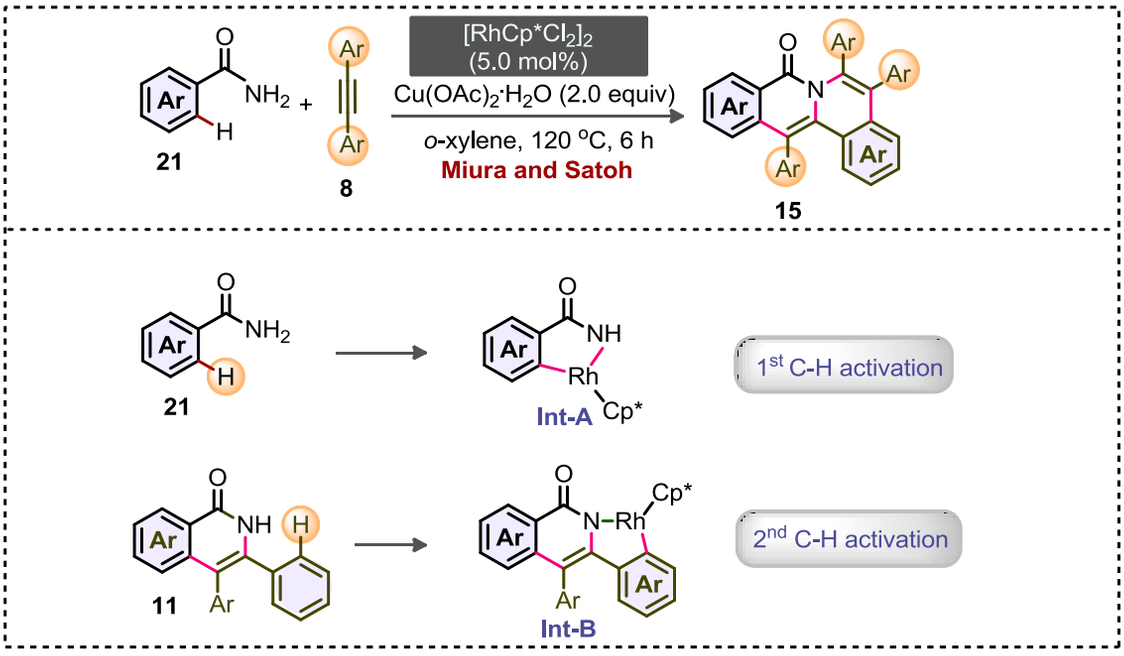

Scheme III.7: Symmetrical di-annulation between benzamides and alkynes

Later, Ru-catalysts have been used for the development of identical strategy. Thus, Dong group demonstrated a Ru-catalyzed one-pot symmetrical di-annulation of benzamide **21** derivatives with two alkyne molecules. However, the limited substrate scope and poor products yield of the diannulation products are the major drawbacks (**Scheme III.8**).[19]

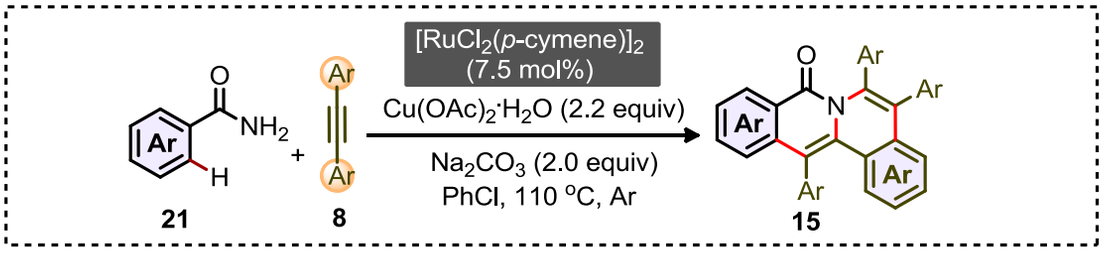

Scheme III.8: Double annulation between benzamides and diphenyl acetylene

In 2016, our group disclosed an interesting Ru-catalyzed symmetrical di-annulation of methyl phenyl sulfoximine (MPS) coupled heteroarenes **13** with two molecules of similar alkynes to deliver **15** (**Scheme III.9**). Next, the identical strategy has been used for the unsymmetrical difunctionalization of arenes with two distinct alkynes to afford **15′** (**Scheme III.9**).[20]

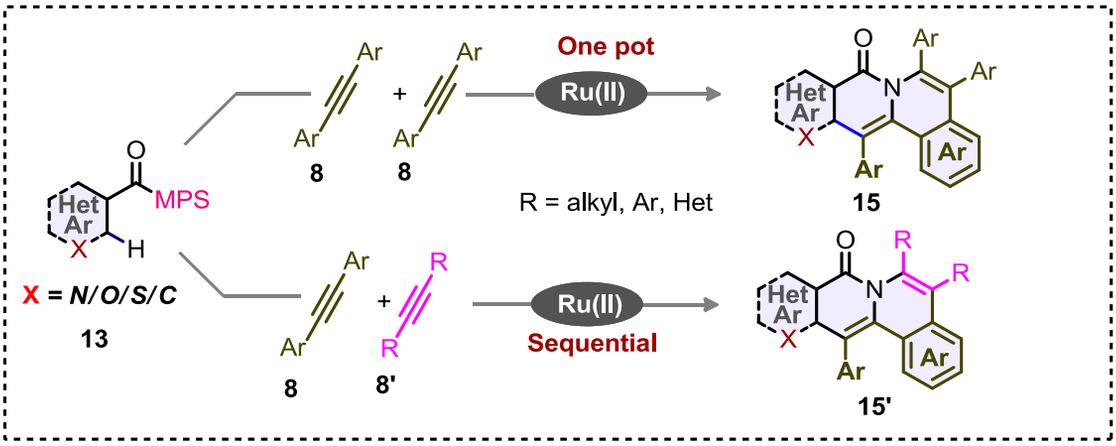

Scheme III.9: Double annulations of MPS-enabled (hetero)arenes

III.3. Motivation and Design for Unsymmertical Double Annulation

A one-pot, single DG-enabled unsymmetrical tandem *o*-C–H di-functionalization of arenes has recently been presented via the intramolecular *o*-C–H hydroarylation and intermolecular *o* -C–C/C–N bond formations,[21a] and also, the *o*-C–H alkylation and *o* -C–H amidation of *N*-phenoxyacetamide.[21b]

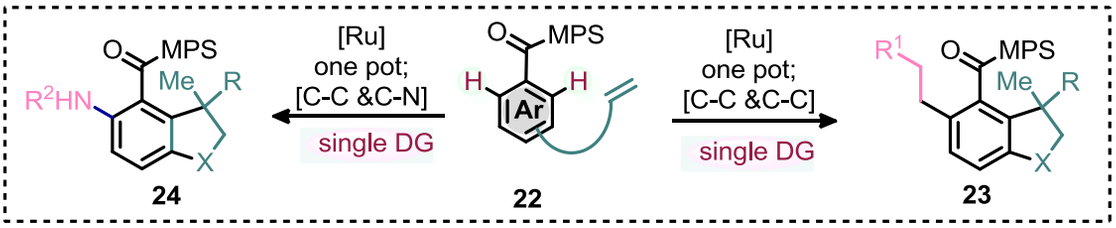

Scheme III.10: One-pot intermolecular hydroarylation and intermolecular *o* -C–C/C–N bond formations

Two synthetic steps are essential to realize a cascade two-fold annulation of arenes with different coupling partners; hence, stitching of distinct functional groups (FG^1/FG^2) requires different catalytic conditions (**Scheme III.11**).[9b-c]

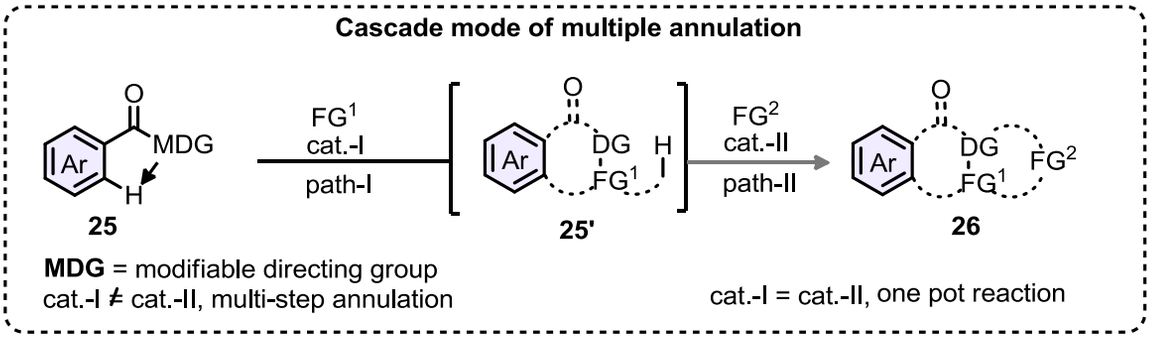

Scheme III.11: Mutiple annulation

We have recently demonstrated a direct double annulation of transformable methylphenyl sulfoximine (MPS)-DG-aided C(sp^2)–H bonds with different alkynes.[22] Thus, the one-pot, two-fold unsymmetrical C–H di-annulation of (hetero)arenes with distinct coupling partners (alkyne and olefin) in the presence of a single DG under single catalytic conditions is a worthwhile endeavor, which has so far not been reported. We propose that alkyne over olefin can undergo multiple annulation with C(sp^2)–H bonds and generate **11** (mono-annulation) and **15** (di-annulation) products,[22a] which eventually obstructs the formation of the projected unsymmetrical di-annulation compound **27/17** (**Scheme III.12**).

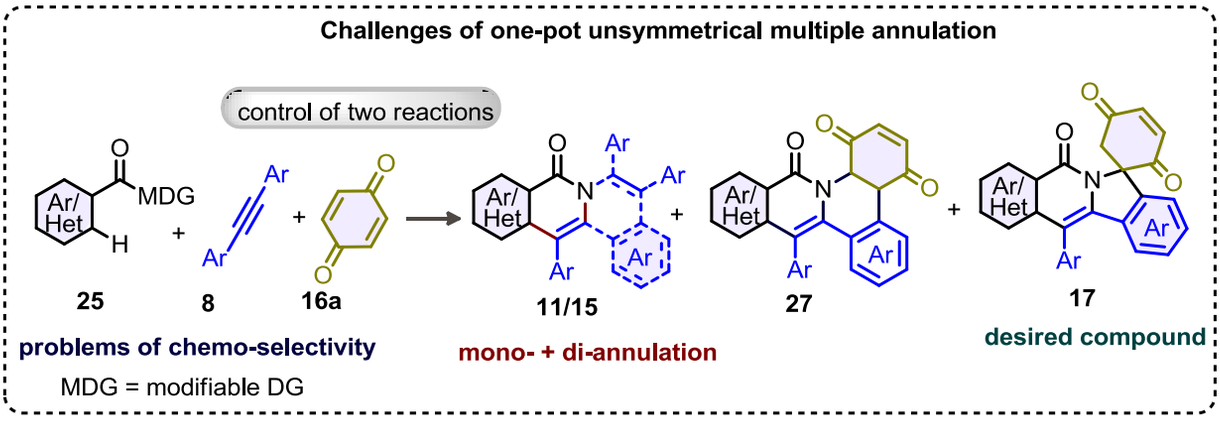

Scheme III.12: Challenges of mutiple annulation

Moreover, the quinone moiety is an effective Michael acceptor and is susceptible to Heck coupling; thus, -difunctionalization of the quinone motif to install a spiro-

skeleton is possible, although challenging.[23] However, the Ir-catalyzed oxidative coupling of isoquinolone with benzoquinone is feasible for constructing novel spiro-fused heteroarenes.[16a] Thus far, there have been no reports on the respective one-pot unsymmetrical multiple annulations of heteroarene/vinylic system from a simple carboxylate precursor.

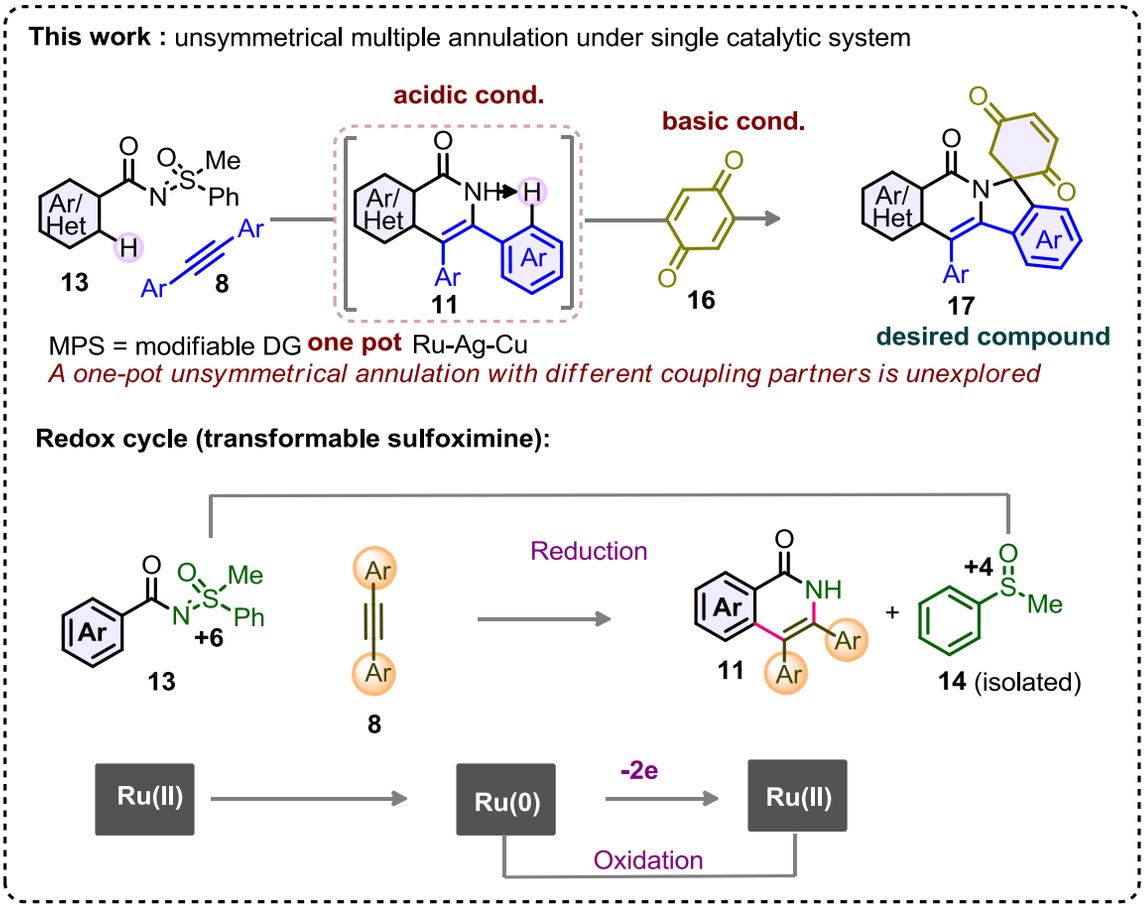

Scheme III.13: Orchestrated annulation of C(sp²)–H bonds with alkyne and quinone

On the basis of our preliminary understanding of the MPS-DG assisted annulation of hetero(arene)/vinylic systems, we herein invent a tunable one-step synthetic technique for the divergent annulation of C(sp²)–H bonds with alkyne and quinone (**Scheme III.13**). The strategy involves mono-annulation of proximal C–H bond of MPS-DG bearing amide and alkyne under cost-effective, air-stable Ru catalyst in presence of acid source.[24] The in-situ formation of isoquinolone/pyridone through protodemetalation restrict further di-annulation with alkyne and the oxidizable MPS-DG helps

regeneration of active catalyst. Next, the base-promoted annulation with quinone delivers the synthetically promising unusual spiro-fused-isoquinolones of pharmaceutical and material importance.[25] The isolation of methylphenyl sulfoxide, the sole precursor of MPS, endorses MPS-DG as transformable (**Scheme III.13**).[26]

(draw separately about the concept)

III.4. Results and Discussion

III.4.1. Synthesis of precursors

For achieving the goal, a library of starting materials has been synthesized using the known synthetic procedure and shown in **Scheme III.14.** [20,27]

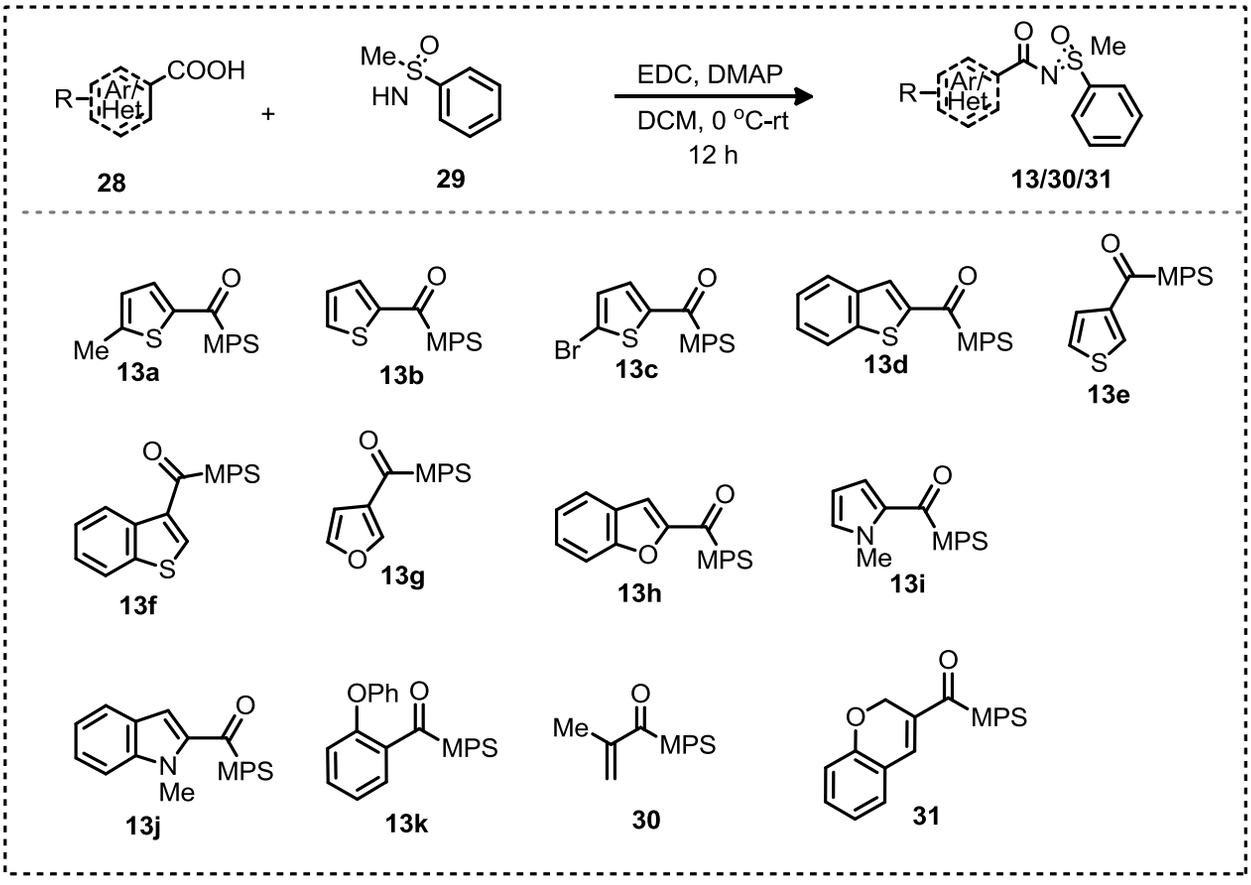

Scheme III.14: Preparation of N-heteroaroyl sulfoximine derivatives

Symmetrical and unsymmetrical alkynes were synthesized following the reported procedure.[28] Analytical and spectral data of these compounds are exactly matching with the reported values.

The symmetrical alkynes **8a**, **8b**, **8c**, **8d**, **8e**, **8f** and **8h** were prepared (**Scheme III.15**).[28] Diphenyl acetylene (**8a**) and phenyl N-butyl acetylene (**8g**) were purchased from comercially available source and used.

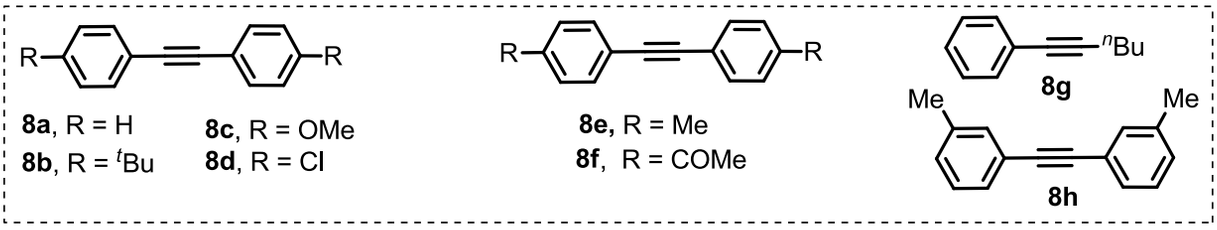

Scheme III.15: List prepared of symmetrical and unsymmetrical alkynes

Benzoquinone (BQ; **16a**), naphthaquinone (**16b**), and chloroquinone (**16c**) were purchased from commercially available source and used.

III.4.2. Optimization studies

The feasibility of the one-pot three component cascade annulations (envisaged in **Scheme III.13**) is probed by subjecting MPS coupled 5-methyl-thiophene-2-carboxylate (**13a**) with diphenylacetylene (**8a**) and benzoquinone (**16a**) in the presence of Ru-catalysts (Table III.1). Pleasingly, the predicted product **17a** (20%) and di-annulation compound **15** (35%; from **13a** and **8a**) formed when the reaction was executed under the catalytic conditions [Ru-catalyst (10 mol %), $AgSbF_6$ (40 mol %), and $Cu(OAc)_2 \cdot H_2O$ (1.0 equiv) in 1,2-dichloroethane (DCE) at 120 ^oC for 10 h] (entry 1). This result is particularly noteworthy; as MPS-bearing heteroarenes and alkynes are amenable to annulation, which occurs even at 60 C.[22a]

To realize better turnout of **17a**, the annulation episode among **13a**, **8a**, and **16a** was conducted at 60 ^oC (where alkyne undergoes cyclization) and 120 ^oC (where quinone

commences annulation) in a single pot under one catalytic condition; pleasingly, **17a** was isolated in 35% yield (entry 2). This information encouraged us to survey the reaction by turn wise addition of **8a** and **16a**. Thus, the entire transformation was performed accordingly [the reaction was at first carried out at 60 °C in presence of 1.2 equiv of **8a** for 10 h, subsequently **16a** was introduced and the mixture was then heated at 120 °C for 10 h]; this process resulted 45% of **17a** along with the diannulation product

Table III.1: Optimization of reaction conditions

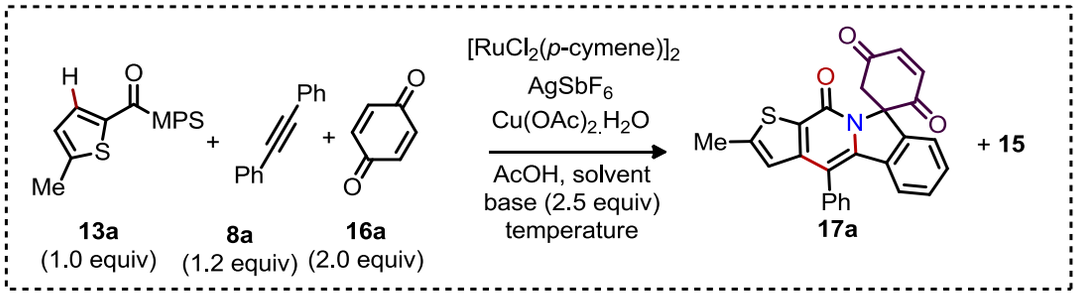

Entry	additive (2.0 equiv)	base (2.5 equiv)	temperature (°C)	yield of **17a** (%)
1	–	–	120	20 (35)[b,c]
2	–		60/120	35 (21)[b,c]
3	–		60/120	45 (18)
4	AcOH	_	90/120	26 (11)
5	AcOH	$NaHCO_3$	90/120	62 (07)
6	AcOH	Na_2CO_3	90/120	40 (10)
7	AcOH	K_2CO_3	90/120	39 (10)
8	AcOH	K_3PO_4	90/120	61 (06)
9	AcOH	KH_2PO_4	90/120	66 (05)
10	AcOH	KH_2PO_4	90/120	50 (15)[d]
11	AcOH	KH_2PO_4	90/120	72 (04)[e]
12	AcOH	KH_2PO_4	90/120	35 (40)[f,g]
13	AcOH	KH_2PO_4	90/120	39 (16)[h]
14	AcOH	KH_2PO_4	90/120	35 (0)[i]

[a]Reaction conditions: [a]Conditions: **13a** (0.18 mmol, 1.0 equiv), **8a** (1.2 equiv), Ru-catalyst (10 mol %), $AgSbF_6$ (40 mol %), $Cu(OAc)_2 \cdot H_2O$ (1.0 equiv), additive (2.0 equiv), DCE (1.5 mL) at 90 °C for 10 h; then BQ (2.0 equiv), base (2.5 equiv) and 1,4-dioxane (1.5 mL), at 120 C for 10 h; yield

of **15** (di-annulation with alkyne) is shown in the parenthesis. [b]All the reactants in one-pot. [c]**8a** (1.0 equiv). [d]1,4-dioxane instead of DCE. [e]Addition of 1,4-dioxane (1.5 mL) after first cyclization. [f]In the absence of $Cu(OAc)_2 \cdot H_2O$. [g]Yield of **11** (mono-annulation with alkyne) is shown in the parenthesis. [h]O_2 as oxidant. [i]$CuBr_2$ as oxidant.

15 (18%) (entry 3). Interestingly, annulation between **13a** and **8a** in presence of 2 equiv AcOH restricted the formation of **15** to 11%; meanwhile, delivery of **17a** was affected (entry 4), a consequence of ineffective binding of Ru to the NH-moiety of mono-annulation product in acid medium. Interestingly, addition of $NaHCO_3$ base, along with **16a** helped the production of **17a** (62%), endorsing the requirement of base after first cyclization (entry 5). Encouraged by the observation, various bases (Na_2CO_3, K_2CO_3, K_3PO_4, and KH_2PO_4) were screened (entries 6–9); KH_2PO_4 was found optimum yielding 66% of **17a** (entry 9). Although the overall reaction in 1,2-DCE was better over 1,4-dioxane (entries 9 and 10), the use of mixture of solvents in this two-fold cyclization strategy [1,2-DCE for the first annulation and subsequent addition of 1,4-dioxane in the second annulation] led to 72% **17a** (entry 11). This transformation in the absence of $Cu(OAc)_2 \cdot H_2O$ provided **17a** in only 35% yield, along with 40% of the mono-annulation compound **11** (entry 12) suggesting the oxidant indispensable; as it helps the regeneration of active catalyst after second annulation. Moreover, the reactions in presence of oxidant O_2 or $CuBr_2$ were not effective (entry 13 and entry 14). Thus, the one-pot synthetic avenue for the unsymmetrical annulation of **13a** with **8a** and **16a** under the optimized catalytic conditions (entry 11, **Table III.1**) smoothly provided unusual spiro-fused isoquinolone **17a**.

III.4.3. Reaction scope-I

The synthetic generality of this unprecedented two successive unsymmetrical annulation is validated by examining MPS-assisted cyclization of $C(sp^2)$–H bonds of challenging heteroarene/vinylic/chromene systems with alkynes and quinones (Scheme III.16). Thus, the MPS-coupled thiophene-2-/benzothiophene-2-carboxylate

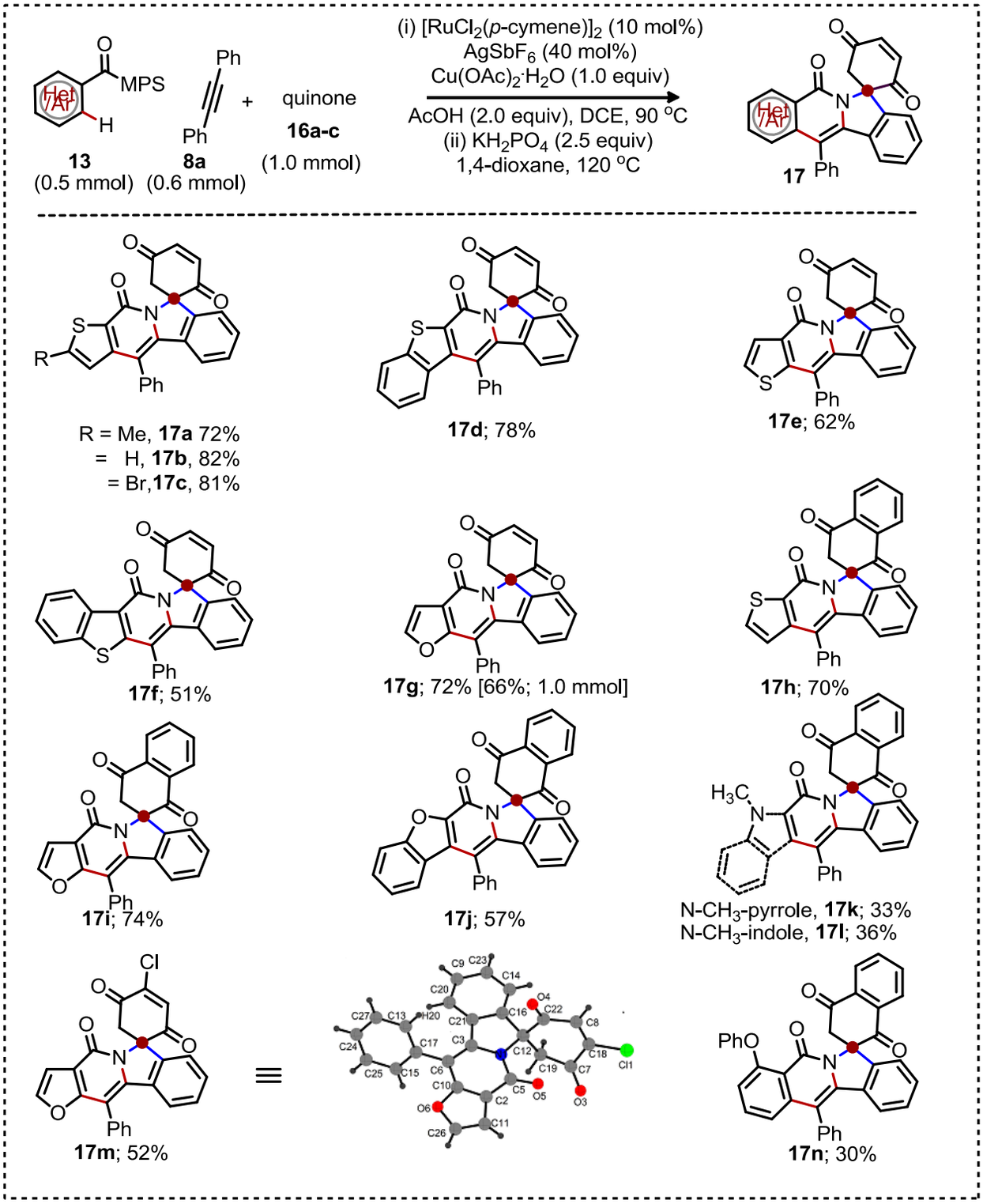

Scheme III.16: Cascade annulation of heteroaryls **13** with **8a** and quinone **16**

(**13a**–**d**) were reacted with **8a** and **16a** to afford the desired spiro-products **17a**–**17d** (72–82%); the modifiable Br-group survived to provide **17c**. The thiophene-3-

/benzothiophene-3-carboxylates were also participated, delivering **17e** (62%) and **17f** (51%). Likewise, the spiro-product from oxygen bearing heteroarene **17g** (72%) was readily isolated from the cyclization cascade of MPS-bearing furan-3-carboxylate (**13g**) with **8a** and **16a**.

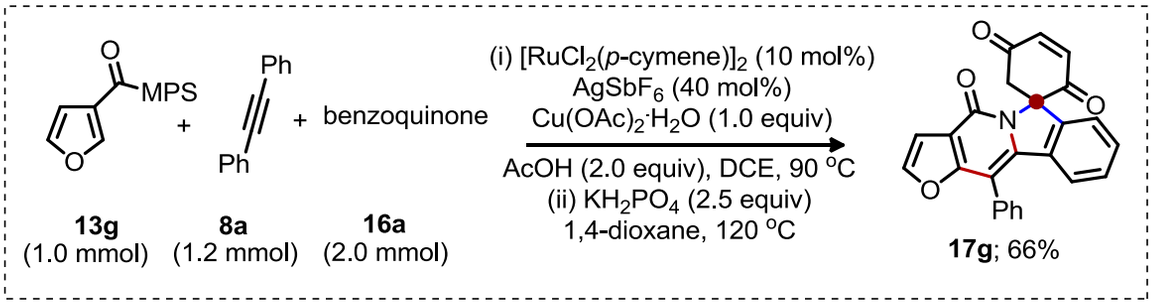

Scheme III.17: 1 mmol scale reaction

The identical reaction in 1.0 mmol scale; resulted 66% of **17g (Scheme III.17)**. The naphthaquinone (**16b**) also took part in the cascade cyclization episode with **13b**/**13g**/**13h** and **8a** to deliver **17h** (70%), **17i** (74%), and **17j** (57%), respectively (**Scheme III.16**). Moreover, the N-bearing heterocycles pyrrole and indole skeleton were stitched with **8a** and **16b** accessing the poly-fused spiro-skeletons **17k** and **17l**, albeit in moderate yield. The product **17m** was isolated from the annulations of **13g** with **8a** and 2-chloro-benzoquinone (**16c**); X-ray analysis confirms the structure **17m**. Annulations of challenging *o*-substituted arene motif with **8a** and **16b** delivered **17n**.

III.4.4. Reaction scope-II

We next probed the alkyne scope in this one-pot two-successive annulation of MPS-bearing heteroarene and quinone (**Scheme III.18**). Pleasingly, 1,2-diarylacetylenes {having *para*-substituents on the arene moiety, electron-donating [-^{t}Bu (**8b**)/-OMe (**8c**)] or -Cl (**8d**) group} smoothly reacted with **13b** and **16a** under the optimized procedure to afford spiro-fused enlarged isoquinolones **17o** (75%), **17p** (67%), and **17q** (69%). Likewise, the furan-enabled spiro-isoquinolone products **17r** (68%), **17s** (66%), and **17t**

(67%) were undeniably accessed when **13g** coupled with **8e** (*p*-Me-)/**8c** (*p*-MeO-) /electron-withdrawing (*p*-COMe) group containing alkyne (**8f**) and **16a**, respectively.

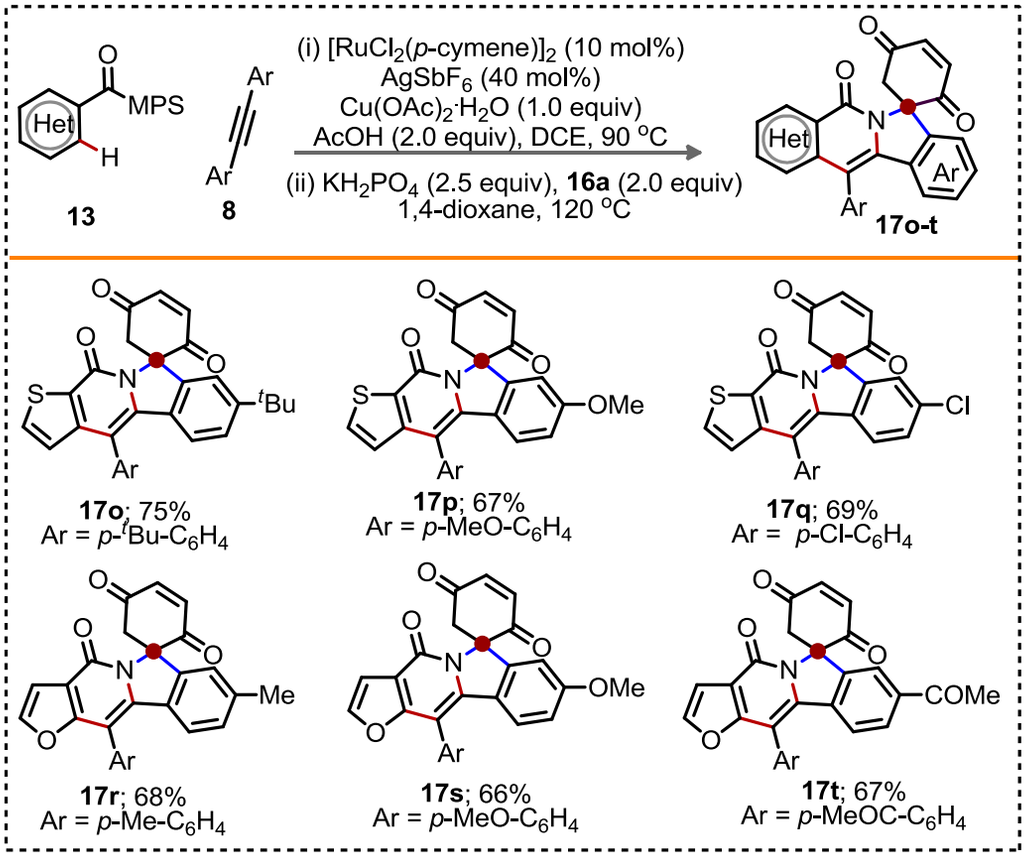

Scheme III.18: Cascade annulation of heteroaryls **13** with alkynes (**8**) and **16a**

III.4.5. Reaction scope-III

Inspired from the unsymmetrical di-annulation of heteroaryls with alkynes and quinones (**Scheme III.16** and **Scheme III.18**), the identical reaction in the challenging vinylic system was next surveyed (**Scheme III.19**); as vinylic systems tend to polymerize under the oxidative conditions and also are effective Michael acceptors.[18] Gratifyingly, the reaction of *N*-(methacryloyl)-MPS (**30**) with **8a** and **16b** under the optimized catalytic conditions in entry 11, **Table III.1** delivered **32a** in 62% yield. To further authenticate the synthetic viability of this two-fold annulations of acrylamides,

the reaction between **30**, the electron-rich (Me/^{t}Bu/OMe) group containing *para*-substituted 1,2-diarylacetylenes, and **16b** delivered the desired spiro-fused novel heterocycle manifolds **32b** (61%), **32c** (70%), and **32d** (62%).

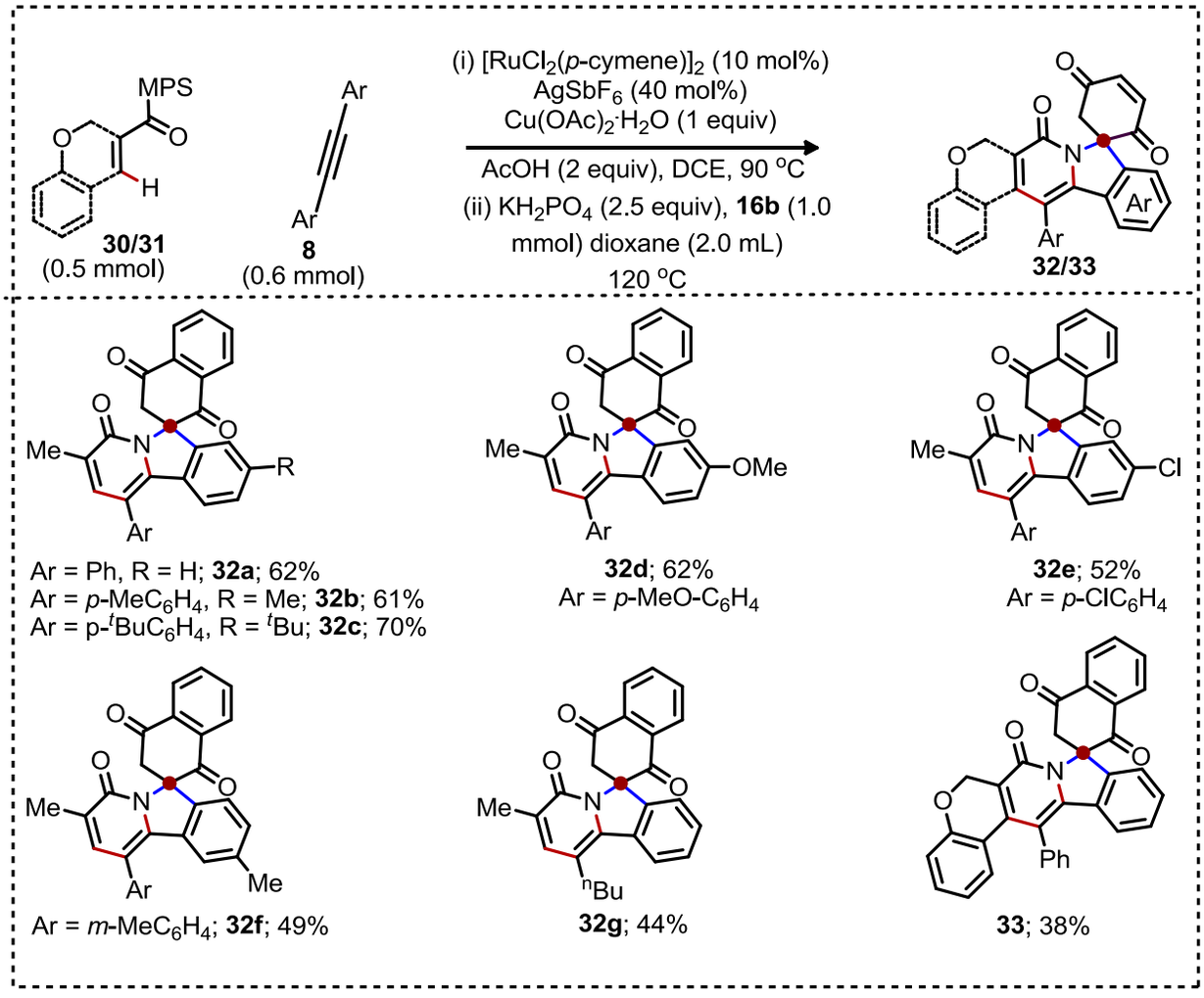

Scheme III.19: Cascade annulation of vinyl/chromenes **30/31** with alkynes (**8**) and **16b**

The product **32e** with the labile chloro group in the periphery was also constructed. The *meta*-Me bearing 1,2-diarylalkyne participated in the cascade annulation, accessing **32f**. The spiro compound **32g** was isolated from the annulation of **30**, unsymmetrical *n*-butyl-phenyl alkyne **8g**, and **16b**; the regioselective mono-annulation of **30** with **8g** makes this process feasible. The 2H-chromene-3-carboxylate derivative **31** successfully

underwent annulations with **8a** and **16b** to deliver the conjugated spiro species **33** in 38% yield.

III.4.6. Control Experiments

To understand the possible reaction pathway, a few control experiments have been performed (**Scheme III.20**). The reaction in the absence of oxidant $Cu(OAc)_2$ led to mono-annulation product (69%); the reductive cleavage of MPS group herein helps oxidation of Ru-catalyst and keeps the catalytic cycle active (eq 1). However, the reaction of **11b** with benzoquinone under the optimized condition led to 35% of the desired product **17b** (eq 1).

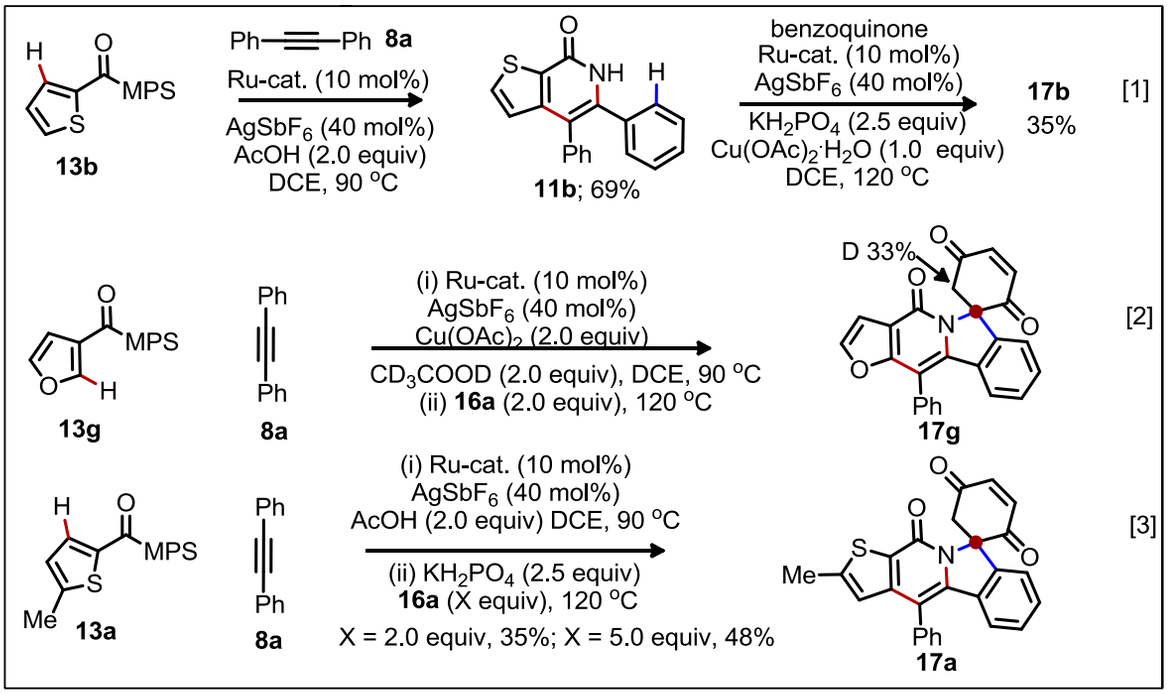

Scheme III.20. Control Experiments

Product **17g** with 33% deuterium incorporation in the quinone moiety was detected when the reaction exhibited in CD_3CO_2D (eq 2), reflecting the occurrence of protodemetalation in the transformation.[19] Hence, formation of the desired spiro-product is possible through the metalation of acidic $C(sp^3)$–H bond, followed by C–N reductive elimination (see the Mechanistic Cycle in **Scheme III.21**). Interestingly, the reaction in presence of 2.0 and 5.0 equiv of BQ produced 35% and 48% of **17a**,

respectively (eq 3); thus, the weak oxidant BQ is incapable in carrying out the transformation. Consequently, the oxidant $Cu(OAc)_2$ plays vital retaining the catalytic cycle alive via revival of active Ru(II) species.[5]

III.4.7. Mechanistic Cycle

Based on the precedence and the current observation, the plausible reaction pathway is outlined in **Scheme III.21**.[3,5] The reaction initiates with the coordination of MPS to the active Ru-species forming the ruthenacycle **13-I** via chelation-assisted C−H metalation.

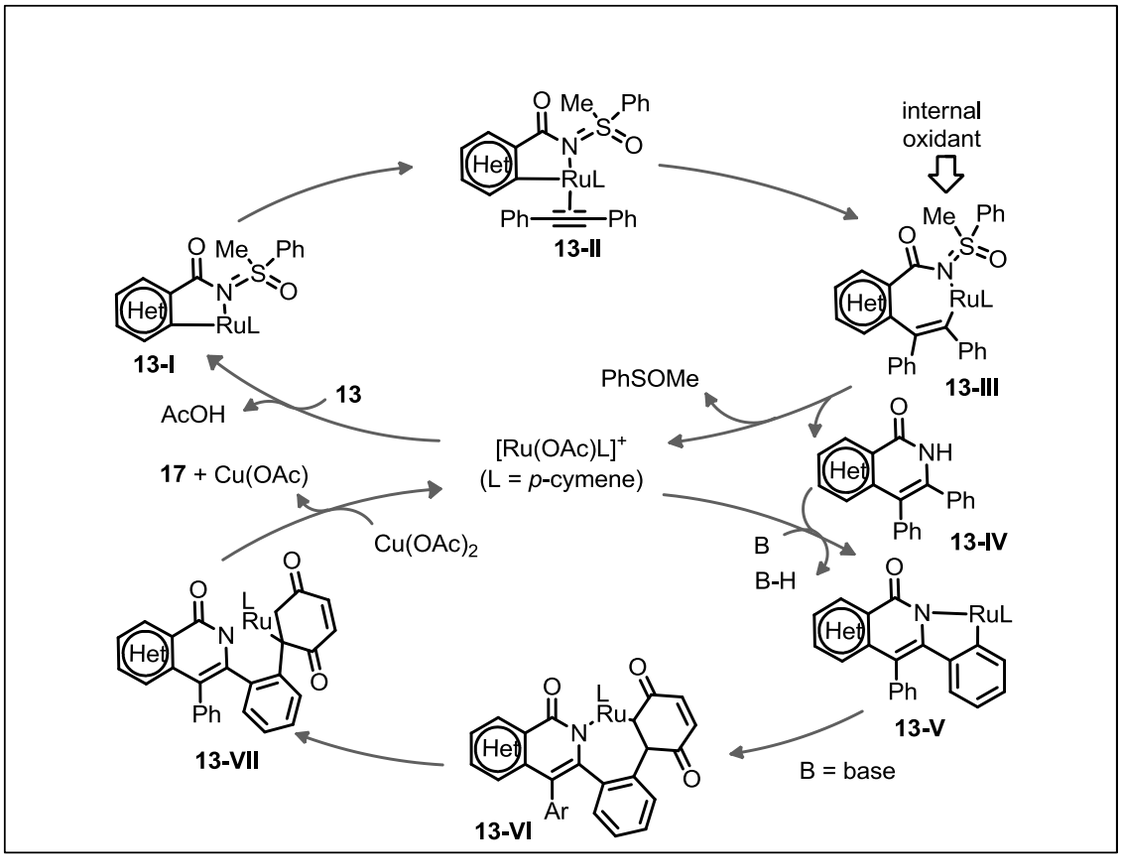

Scheme III.21: Proposed mechanistic profile

Subsequent alkyne coordination-insertion to **13-I** provides seven membered ruthenacycle **13-III** through **13-II**. Next, synergistic C−N reductive elimination and N−S cleavage affords **13-IV** in-situ, which simultaneously undergoes proximal C−H metalation to deliver **13-V**. Insertion of benzoquinone to **13-V** gives 7-membered ruthenacycle **13-VI**; protodemetalation of **13-VI** (eq 2, **Scheme III.20**) followed by

metalation of acidic C(sp^3)–H generates more stable 6-memberd ruthenacycle **13-VII**. Reductive elimination of **13-VII** finally leads to spiro-fused-isoquinolone **17**. The $Cu(OAc)_2$ helps regenerating the active Ru-catalyst.[29]

III.4.8. Application

The synthetic manipulation of peripheral olefin moiety in the spiro-isoquinolone scaffold was further elaborated by performing [4+2] cycloaddition of **17g** with cyclopentadiene resulting in complex molecular entity **34** (**Scheme III.22**).

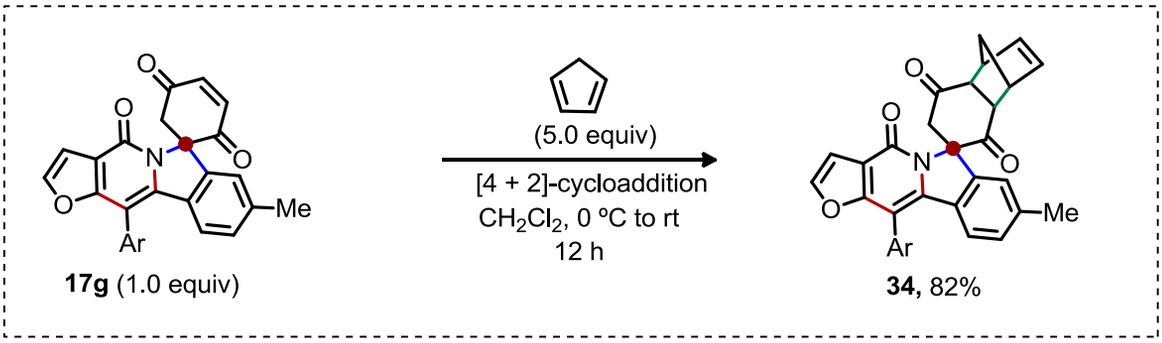

Scheme III.22. Application

III.5. Conclusion

In summary, we have revealed for the first time a Ru-catalyzed MPS-assisted two-fold unsymmetrical cyclization of heteroarenes/vinylic systems with different coupling partners (first with the alkynes and then with the quinones); both these annulations are realized via one-pot synthesis resulting in four bonds (two C–C and two C–N). These highly orchestrated cyclization techniques are largely suitable for the fabrication of un-natural spiro-isoquinolinones.

Recently, Ru-catalyzed C–H annulation strategy has been implemented for the synthesis of various spiro-fused heterocycles shown in **Scheme III.23.**

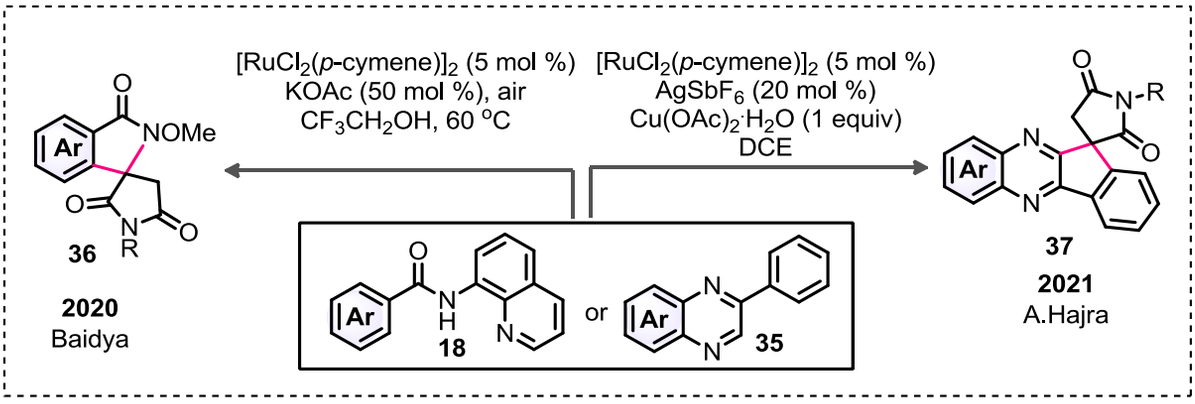

Scheme III.23: Synthesis of spiro-fused heterocycles

III.6. Experimental

III.6.1. General Experimental Information

All the reactions were performed in an oven-dried screw-capped tube/Schlenk flask. Commercial grade solvents were distilled prior to use. Column chromatography was performed using either 100–200 Mesh or 230–400 Mesh silica gel. Thin layer chromatography (TLC) was performed on silica gel GF254 plates. Visualization of spots on TLC plate was accomplished with UV light (254 nm) and staining over I_2 chamber.

Proton, carbon, and fluorine nuclear magnetic resonance spectra (^{1}H NMR, ^{13}C NMR, and ^{19}F NMR) were recorded based on the resonating frequencies as follows: (^{1}H NMR, 400 MHz; ^{13}C NMR, 101 MHz; ^{19}F NMR, 376 MHz) and (^{1}H NMR, 500 MHz; ^{13}C NMR, 126 MHz; ^{19}F NMR, 470 MHz) having the solvent resonance as internal standard (^{1}H NMR, $CDCl_3$ at 7.26 ppm; ^{13}C NMR, $CDCl_3$ at 77.0 ppm). Few cases tetramethylsilane (TMS) at 0.00 ppm was used as reference standard. Data for ^{1}H NMR are reported as follows: chemical shift (ppm), multiplicity (s singlet; bs broad singlet; d doublet; bd broad doublet, t triplet; bt broad triplet; q quartet; m multiplet), coupling constants, *J*, in (Hz), and integration. Data for ^{13}C NMR, ^{19}F NMR were reported in terms of chemical shift (ppm). IR spectra were reported in cm^{-1}. LC–MS spectra were obtained with ionization voltage of 70ev; data was reported in the form of *m/z* (intensity relative to base peak 100). Melting points were determined by electro–thermal heating and are uncorrected. High resolution mass spectra were obtained in ESI mode. X-ray

data was collected at 298K using graphite monochromated Mo–K radiation (0.71073 Å).

III.6.2. Materials

Unless otherwise noted, all the reagents and intermediates were obtained commercially and used without purification. Dichloromethane (DCM), 1,2-dichloroethane (DCE), and 1,4-dioxane were distilled over CaH_2. $[Ru(p\text{-cymene})Cl_2]_2$, $AgSbF_6$, $AgBF_4$, and KPF_6 were purchased from Sigma Aldrich Ltd, and used as received. Bases such as $Cu(OAc)_2{\cdot}H_2O$, KH_2PO_4, NaOAc, AgOAc, $NaHCO_3$, and K_3PO_4 were commercially available and used as received. Analytical and spectral data of all the known compounds are exactly matching with reported values.

III.6.3. General procedure for the sequential oxidative coupling of N-heteroaroylated methyl phenyl sulfoximines with alkynes and quinones:

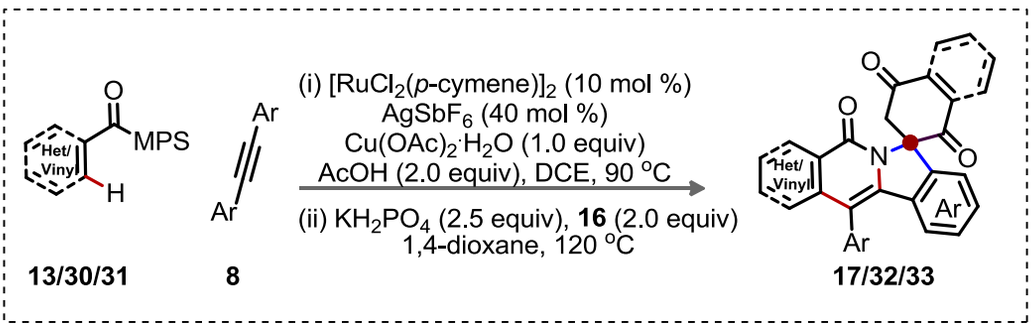

The annulation reactions were carried out in a 25 mL screw capped tube. The tube was charged with *N*-[hetero(aroylated)/acryloyl]-MPS (**13/30**) or MPS protected 2H-chromene-3-carboxylic acids (**31**) (0.5 mmol), alkyne (**8**, 0.6 mmol), $[RuCl_2(p\text{-cymene})]_2$ (31 mg, 10 mol %), and $Cu(OAc)_2{\cdot}H_2O$ (100 mg, 0.75 mmol). Subsequently, $AgSbF_6$ (69 mg, 40 mol %) was introduced in to the tube in a glovebox. The solvent 1,2-dichloroethane (DCE; 1.5 mL) and AcOH (60 L, 2.0 equiv) were added to the mixture and the resulting mixture was stirred at 90 C for 10 h. The reaction mixture was cooled to ambient temperature, and then KH_2PO_4 (170 mg, 2.5 equiv), quinones (**16**) (2.0 equiv), and subsequently 1,4-dioxane (1.5 mL) were added. The resulting mixture was then heated at 120 °C and continued for 10 h. Finally, the reaction mixture was cooled to

ambient temperature, filtered through a small plug of Celite and then washed with dichloromethane (3 × 10 mL). The solvents were evaporated under reduced pressure and the crude material was purified using column chromatography on silica gel (20–30% *n*–hexane/EtOAc eluent) to give the desired product **17/32/33**.

2'–Methyl–4'–phenyl–11'*H*–spiro[cyclohex[3]ene–1,9'–thieno[3',2':4,5]pyrido[2,1–a]isoindole]–2,5,11'–trione (17a):

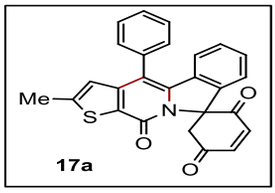

17a (153 mg, 72%) as yellow solid. m.p. 291–293 C; R_f 0.33 (7:3 hexane/EtOAc); ^{1}H NMR (400 MHz, $CDCl_3$) δ –7.53 (m, 3H), 7.51–7.42 (m, 2H), 7.30–7.23 (m, 1H), 7.22–7.09 (m, 4H), 6.64 (d, J 8.0 Hz, 1H), 6.56 (bs, 1H), 4.98 (d, J 16 Hz, 1H), 2.95 (d, J 16 Hz, 1H), 2.54 (s, 3H); ^{13}C NMR (101 MHz, $CDCl_3$) δ 195.1, 189.0, 156.0, 149.4, 148.8, 142.8, 141.3, 140.0, 138.8, 135.0, 133.1, 130.3, 130.1, 129.62, 129.60, 129.4, 129.2, 128.6, 127.1, 124.3, 122.6, 121.0, 113.9, 74.4, 45.7, 16.4; IR (KBr) $_{max}$ 1697, 1646, 1587, 1261, 1153, 1076, 698 cm^{-1}; **HRMS (ESI)** for $C_{26}H_{18}NO_3S$ $(M+H)^+$: calcd. 424.1007, found 424.1007.

4'–Phenyl–11'*H*–spiro[cyclohex[3]ene–1,9'–thieno[3',2':4,5]pyrido[2,1–a]isoindole]–2,5,11'–trione (17b):

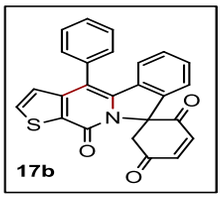

17b (168 mg, 82%) as yellow solid. m.p. 325–329 C; R_f 0.47 (3:7 hexane/EtOAc); ^{1}H NMR (400 MHz, $CDCl_3$) δ 7.67 (d, J 5.2 Hz, 1H), 7.61–7.54 (m, 3H), 7.52–7.44 (m, 2H), 7.31–7.26 (m, 1H), 7.23–7.10 (m, 4H), 6.91 (d, J 5.2 Hz, 1H), 6.67 (d, J 7.6 Hz, 1H), 4.98 (d, J 16 Hz, 1H), 2.96 (d, J 16 Hz, 1H); ^{13}C NMR (101 MHz, $CDCl_3$) δ 195.0, 188.9, 156.4, 148.2, 142.8, 141.3, 140.0, 138.8, 134.7, 133.7, 133.0, 130.3, 130.1, 129.8, 129.7, 129.4, 129.3, 128.7, 128.6, 124.5, 124.4, 121.0, 114.2, 74.5, 45.7; IR (Neat) $_{max}$ 1691, 1655, 1587, 1510, 1267, 1092, 916 cm^{-1}; **HRMS (ESI)** for $C_{25}H_{16}NO_3S$ $(M+H)^+$: calcd. 410.0851, found 410.0850.

2'–Bromo–4'–phenyl–11'*H*–spiro[cyclohex[3]ene–1,9'–thieno[3',2':4,5]pyrido[2,1–a]isoindole]-2,5,11'–trione (17c):

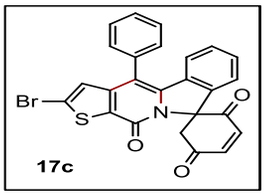

17c (198 mg, 81%) as yellow solid. m.p. 321–326 C; R_f 0.42 (7:3 hexane/EtOAc); ^{1}H NMR (400 MHz, $CDCl_3$) δ 7.61–7.54 (m, 3H), 7.50–7.41 (m, 2H), 7.29 (td, J 7.6, 0.8 Hz, 1H), 7.23–7.18 (m, 1H), 7.17–7.11 (m, 3H), 6.88 (bs, 1H), 6.65 (d, J 8.0 Hz, 1H), 4.93 (d, J 16 Hz, 1H), 2.95 (d, J 16 Hz, 1H); ^{13}C NMR (101 MHz, $CDCl_3$) δ 194.7, 188.6, 155.2, 148.3, 142.9, 141.2, 139.9, 139.5, 134.2, 132.7, 130.2, 130.1, 130.0, 129.8, 129.6, 129.4, 129.0, 127.3, 124.5, 123.0, 121.1, 113.3, 74.7, 45.5; IR (Neat) $_{max}$ 2922, 2852, 1698, 1650, 1469, 1218, 1080 cm^{-1}; **HRMS (ESI)** for $C_{25}H_{15}BrNO_3S$ $(M+H)^+$: calcd. 487.9956, found 487.9952.

13–Phenyl–6*H*–spiro[benzo[4',5']thieno[3',2':4,5]pyrido[2,1–a]isoindole–8,1'–cyclohex[3]ene]–2',5',6–trione (17d):

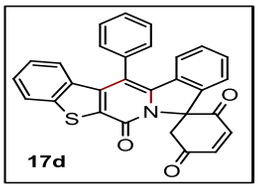

17d (179 mg, 78%) as yellow solid. m.p. 309–314 C; R_f 0.33 (7:3 hexane/EtOAc); ^{1}H NMR (400 MHz, $CDCl_3$) δ 7.91 (d, J 8.0 Hz, 1H), 7.72–7.64 (m, 3H), 7.60–7.54 (m, 2H), 7.42 (t, J 7.6 Hz, 1H), 7.31–7.19 (m, 2H), 7.18–7.05 (m, 4H), 6.78 (d, J 8.0 Hz, 1H), 6.36 (d, J 8.0 Hz, 1H), 5.04 (d, J = 16 Hz, 1H), 2.99 (d, J = 16 Hz, 1H); ^{13}C NMR (101 MHz, $CDCl_3$) δ 194.8, 188.6, 156.7, 142.9, 141.7, 141.3, 139.9, 139.6, 135.6, 134.8, 133.2, 130.5, 130.4, 130.1, 129.9, 129.81, 129.76, 129.3, 127.5, 125.6, 124.7,124.5, 123.4, 121.0, 114.9, 74.7, 45.4; IR (Neat) $_{max}$ 3055, 2920, 1698, 1647, 1586, 1266, 1081, 751, 733 cm^{-1}; **HRMS (ESI)** for $C_{29}H_{18}NO_3S$ $(M+H)^+$: calcd. 460.1007, found 460.1006.

11'–Phenyl–4'*H*–spiro[cyclohex[3]ene–1,6'–thieno[2',3':4,5]pyrido[2,1–a]isoindole]–2,4',5–trione (17e):

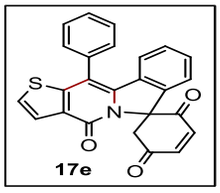

17e (127 mg, 62%) as yellow solid, R_f 0.37 (6:4 hexane/EtOAc); ^{1}H NMR (500 MHz, $CDCl_3$) δ (d, J 5.5 Hz, 1H), 7.62–7.53 (m, 4H), 7.53–7.49 (m, 1H), 7.32 (d, J 5.5 Hz, 1H), 7.28 (td, J 7.5, 0.8 Hz, 1H), 7.23–7.19 (m, 1H), 7.18–7.11 (m, 3H), 6.71 (d, J 8.0 Hz, 2H), 4.96 (d, J 16 Hz, 1H), 2.94 (d, J 16 Hz, 1H); ^{13}C NMR (126 MHz, $CDCl_3$) δ 195.0, 188.9, 156.8, 153.0, 142.8, 141.3, 140.4, 137.4, 134.5, 132.7, 129.93, 129.87, 129.8, 129.7, 129.6, 129.5, 129.3, 126.1, 125.1,

124.3, 121.1, 113.5, 74.5, 45.6; IR (Neat) $_{max}$ 3057, 2923, 1697, 1646, 1267 cm^{-1}; **HRMS (ESI)** for $C_{25}H_{15}NNaO_3S$ $(M+Na)^+$: calcd. 432.0670, found 432.0678.

6–phenyl–13*H*–spiro[benzo[4',5']thieno[2',3':4,5]pyrido[2,1–a]isoindole–11,1'–cyclohex[3]ene]–2',5',13–trione (17f):

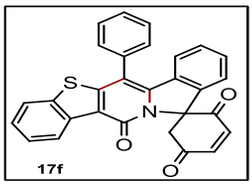

17f (117 mg, 51%) as yellow solid, m.p. 306–307 C; R_f 0.35 (7:3 hexane/EtOAc); ^{1}H NMR (400 MHz, $CDCl_3$) δ (d, J 8.0 Hz, 1H), 7.77 (d, J = 8.0 Hz, 1H), 7.65–7.58 (m, 3H), 7.58–7.52 (m, 1H), 7.51 (td, J 7.6, 1.2 Hz, 1H), 7.43 (td, J 7.6, 1.1 Hz, 1H), 7.33 (td, J 7.5, 0.8 Hz, 1H), 7.24 (s, 1H), 7.21 (s, 2H), 7.20–7.15 (m, 1H), 7.75 (d, J 8.0 Hz, 1H), 5.08 (d, J 16 Hz, 1H), 2.99 (d, J 16 Hz, 1H); ^{13}C NMR (101 MHz, $CDCl_3$) δ 194.9, 188.8, 156.9, 154.7, 142.9, 141.4, 140.9, 139.3, 138.5, 136.5, 134.4, 132.6, 130.3, 130.1, 130.0, 129.8, 129.7, 129.6, 129.4, 128.8, 125.9, 125.6, 125.0, 124.7, 121.8, 121.1, 113.5, 74.8, 45.5; IR (KBr) $_{max}$ 3057, 2923, 2851, 1635, 1439, 1219, 747 cm^{-1}; **HRMS (ESI)** for $C_{29}H_{17}NNaO_3S$ $(M+Na)^+$: calcd. 482.0827, found 482.0829.

11'–Phenyl–4'*H*–spiro[cyclohex[3]ene–1,6'–furo[2',3':4,5]pyrido[2,1–a]isoindole]–2,4',5–trione (17g):

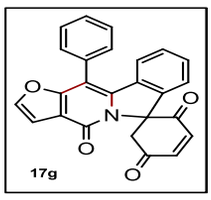

17g (142 mg, 72%) as pale yellow solid. m.p. 289–292 C; R_f 0.50 (5:5 hexane/EtOAc); ^{1}H NMR (400 MHz, $CDCl_3$) δ 7.62–7.49 (m, 6H), 7.33–7.27 (m, 1H), 7.23–7.19 (m, 1H), 7.18–7.14 (m, 3H),7.04 (d, J 2.0 Hz, 1H), 6.88 (d, J 8.0 Hz, 1H),4.96 (d, J 16 Hz, 1H), 2.94 (d, J 16 Hz, 1H); ^{13}C NMR (101 MHz, $CDCl_3$) δ 195.0, 188.9, 160.1, 157.0, 144.6, 142.8, 141.3, 140.4, 139.7, 132.6, 130.6, 130.5, 130.4, 130.0, 129.7, 129.3, 129.15, 129.12, 124.4, 121.0, 115.5, 107.9, 107.6,74.5, 45.6; IR (KBr) $_{max}$ 1691, 1660, 1546, 1267, 1081, 735 cm^{-1}; **HRMS (ESI)** for $C_{25}H_{16}NO_4(M+H)^+$: calcd. 394.1079, found 394.1074.

4'–Phenyl–1*H*,11'*H*–spiro[naphthalene–2,9'–thieno[3',2':4,5]pyrido[2,1–a]isoindole]–1,4,11'(3H)–trione (17h):

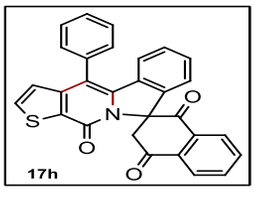

17h (161 mg, 70%) as yellolw solid. m.p. 320–326 C; R_f 0.35 (7:3 hexane/EtOAc); ^{1}H NMR (400 MHz, $CDCl_3$) δ 8.28 (dt, J = 7.6, 1.6 Hz,

2H), 7.91 (td, *J* 1.3 Hz, 1H), 7.84 (td, *J* 1.3 Hz, 1H), 7.67 (d, *J* 5.2 Hz, 1H), 7.62–7.54 (m, 3H), 7.54–7.47 (m, 2H), 7.18–7.06 (m, 2H), 6.92 (d, *J* 5.2 Hz, 1H), 6.91–6.87 (m, 1H), 6.67 (d, *J* 7.2 Hz, 1H), 5.25 (d, *J* 15.6 Hz, 1H), 3.14 (d, *J* 16 Hz, 1H); ^{13}C NMR (101 MHz, $CDCl_3$) δ193.5, 188.0, 156.6, 148.2, 140.4, 139.0, 136.3, 135.1, 134.9, 134.7, 134.1, 133.6, 133.1, 130.3, 130.2, 129.6, 129.4, 129.3, 129.1, 128.9, 128.7, 126.8, 124.5, 124.3, 121.5, 114.1, 75.4, 46.1; IR (Neat) $_{max}$ 2924, 1699, 1650, 1590, 1286, 1256 cm^{-1}; **HRMS (ESI)** for $C_{29}H_{17}NNaO_3S$ $(M+Na)^+$: calcd. 482.0827, found 482.0829.

11–Phenyl–1'*H*,4*H*–spiro[furo[2',3':4,5]pyrido[2,1–a]isoindole–6,2'–naphthalene]–1',4,4'(3'H)–trione(17i):

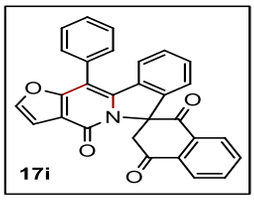

17i (164 mg, 74%) as yellow solid. m.p. 294–295 C; R_f 0.36 (6:4 hexane/EtOAc); ^{1}H NMR (400 MHz, $CDCl_3$) δ8.30–8.24 (m, 2H), 7.90 (td, *J* 9.4, 1.8 Hz, 1H), 7.83 (td, *J* 9.5, 1.5 Hz, 1H), 7.61–7.54 (m, 5H), 7.51 (d, *J* 2.0 Hz, 1H), 7.19–7.07 (m, 2H), 7.04 (d, *J* 2.0 Hz, 1H), 6.93–6.86 (m, 2H), 5.24 (d, *J* 16 Hz, 1H), 3.12 (d, *J* 15.6 Hz, 1H); ^{13}C NMR (101 MHz, $CDCl_3$) δ 193.5, 188.0, 160.1, 157.2, 144.5, 140.8, 139.8, 136.2, 135.1, 134.6, 134.0, 132.7, 130.7, 130.52, 130.46, 129.9, 129.4, 129.2, 129.1, 129.02, 129.0, 126.8, 124.2, 121.4, 115.5, 107.7, 107.6, 75.4, 45.9; IR (Neat) $_{max}$ 3049, 2920, 1699, 1593, 1547, 1255, 1159, 802, 735 cm^{-1}; **HRMS (ESI)** for $C_{29}H_{17}NNaO_4$ $(M+Na)^+$: calcd. 466.1055, found 466.1058.

13–Phenyl–1'*H*,6*H*–spiro[benzofuro[3',2':4,5]pyrido[2,1–a]isoindole–8,2'–naphthalene]–1',4',6(3'H)–trione (17j):

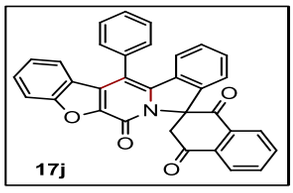

17j (140 mg, 57%) as pale yellow solid. m.p. 261–262 C; R_f 0.25 (7:3 hexane/EtOAc); ^{1}H NMR (500 MHz, $CDCl_3$) δ 8.29 (d, *J* 7.75 Hz, 2H), 7.92 (td, *J* 7.6, 1.3 Hz, 1H), 7.85 (td, *J* 7.6, 1.3 Hz, 1H), 7.69–7.63 (m, 4H), 7.63–7.58 (m, 2H), 7.51–7.44 (m, 1H), 7.17–7.07 (m, 3H), 6.94–6.88 (m, 1H), 6.80 (d, *J* 8.0 Hz, 1H), 6.73 (d, *J* 7.0 Hz, 1H), 5.36 (d, *J* 15.5 Hz, 1H), 3.16 (d, *J* 16 Hz, 1H); ^{13}C NMR (126 MHz, $CDCl_3$) δ193.4, 187.6, 157.4, 152.4, 143.2, 140.6, 138.6, 136.3, 135.2, 134.8, 134.2, 134.0, 133.0, 130.9, 130.3, 130.2, 129.8, 129.7, 129.6, 129.5, 129.2, 129.17, 128.8, 127.0, 124.1, 123.5, 123.4, 122.9, 121.6, 112.8, 112.0, 45.7;

IR (KBr) $_{max}$ 3056, 2909, 1667, 1254, 1205 cm^{-1}; **MS (EI)**(m/z) (%) 492 (M^{-} 100); Anal. Calcd. Value for $C_{25}H_{16}NO_4$: calcd. C, 80.31; H, 3.88; N, 2.84 found C, 80.23; H, 3.92; N, 2.81.

1'–Methyl–4'–phenyl–1*H*–spiro[naphthalene–2,9'–pyrrolo[3',2':4,5]pyrido[2,1–a]isoindole]–1,4,11'(1'H,3H)–trione (17k):

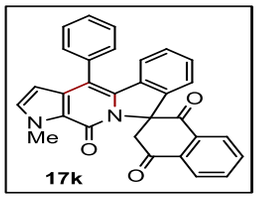

17k (75 mg, 33%) as dark brown solid. m.p. 249–253 C; R_f 0.2 (7:3 hexane/EtOAc); ^{1}H NMR (400 MHz, $CDCl_3$) δ 8.33–8.23 (m, 2H), 7.92–7.78 (m, 2H), 7.56–7.48 (m, 5H), 7.08–7.01 (m, 2H), 6.99 (d, *J* 2.8 Hz, 1H), 6.87–6.81 (m, 1H), 6.79–6.73 (m, 1H), 6.03 (d, *J* 2.4 Hz, 1H), 5.24 (d, *J* Hz, 1H), 4.16 (s, 3H), 3.13 (d, *J* 16 Hz, 1H); ^{13}C NMR (101 MHz, $CDCl_3$) δ 193.9, 188.9, 153.8, 140.0, 136.3, 135.2, 134.9, 134.7, 134.5, 134.2, 134.0, 133.8, 132.0, 130.15, 130.06, 129.12, 129.08, 129.0, 128.9, 128.3, 128.1, 126.7, 123.4, 122.2, 121.2, 113.3, 102.5, 74.8, 46.6, 65.8 cm^{-1}; IR (KBr) $_{max}$ 2960, 2919, 1700, 1650, 1588, 1246, 1014 cm^{-1}; **HRMS (ESI)** for $C_{30}H_{21}N_2O_3$ $(M+H)^+$: calcd. 457.1552, found 457.1552.

5–Methyl–13–phenyl–1'*H*–spiro[benzo[1,2]indolizino[6,7–b]indole–8,2'–naphthalene]–1',4',6(3'H,5H)–trione (17l):

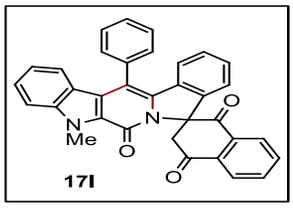

17l (91 mg, 36%) as yellow solid. m.p. 299–300 C; R_f 0.35 (7:3 hexane/EtOAc); ^{1}H NMR (400 MHz, $CDCl_3$) δ 8.35–8.27 (m, 2H), 7.95–7.81 (m, 2H), 7.68–7.62 (m, 3H), 7.64–7.58 (m, 2H), 7.48–7.38 (m, 2H), 7.09–7.03 (m, 2H), 7.00–6.92 (m, 1H), 6.91–6.85 (m, 1H), 6.78 (d, *J* = 8 Hz, 1H), 6.58–6.53 (m, 1H), 5.32 (d, *J* = 16 Hz, 1H), 4.35 (bs, 3H), 3.19 (d, *J* = 16 Hz, 1H); ^{13}C NMR (101 MHz, $CDCl_3$) δ 193.8, 188.5, 154.4, 141.5, 139.7, 136.3, 135.4, 135.0, 134.6, 134.2, 134.0, 133.8, 130.3, 130.2, 129.6, 129.5, 129.4, 129.1, 128.7, 128.3, 126.8, 126.7, 126.4, 126.2, 123.3, 122.7, 121.9, 121.2, 114.2, 109.9, 75.4, 46.2, 31.4; IR (KBr) $_{max}$ 3065, 2919, 1698, 1650, 1462, 1255, 1156 cm^{-1}; **HRMS (ESI)** for $C_{34}H_{23}N_2O_3$ $(M+H)^+$: calcd. 507.1709, found 507.1709.

4–Chloro–11'–phenyl–4'*H*–spiro[cyclohex[3]ene–1,6'–furo[2',3':4,5]pyrido[2,1–a]isoindole]–2,4',5–trione (17m):

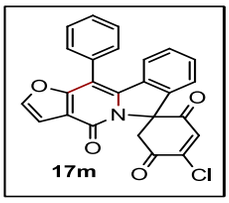

17m (111 mg, 52%) as yellow solid. m.p. 279–281 C; R_f 0.35 (7:3 hexane/EtOAc); ^{1}H NMR (400 MHz, $CDCl_3$) δ 7.61–7.50 (m, 6H), 7.42 (s, 1H), 7.32 (td, *J* 7.6, 0.8 Hz, 1H), 7.23–7.15 (m, 1H), 7.14 (d, *J* 8.0 Hz, 1H), 7.03 (d 2.0 Hz, 1H), 6.88 (d, *J* 8.0 Hz, 1H), 4.99 (d, *J* 16.4 Hz, 1H), 3.11 (d, *J* 16 Hz, 1H); ^{13}C NMR (101 MHz, $CDCl_3$) δ 160.2, 157.1, 150.2, 144.7, 140.0, 139.5, 138.6, 132.7, 130.5, 130.41, 130.38, 130.2, 129.9, 129.3, 129.2, 124.5, 120.9, 115.5, 108.1, 107.6, 74.6, 44.8; IR (Neat) $_{max}$ 3052, 2915, 1695, 1666, 1591, 1231, 1024 cm^{-1}; **HRMS (ESI)** for $C_{25}H_{15}ClNO_4(M+H)^+$: calcd. 428.0690, found 428.0683.

1–Phenoxy–12–phenyl–1'*H*,5*H*–spiro[isoindolo[2,1–b]isoquinoline–7,2'–naphthalene]–1', 4',5(3'H)–trione (17n):

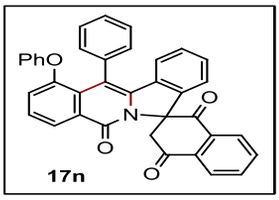

17n (81 mg, 30%) as brown solid. m.p. 276–279 C; R_f 0.36 (7:3 hexane/EtOAc); ^{1}H NMR (400 MHz, $CDCl_3$) δ 8.28–8.19 (m, 2H), 7.84 (t, *J* 7.2 Hz, 1H), 7.79 (*J* 7.4 Hz, 1H), 7.65–7.56 (m, 3H), 7.51–7.44 (m, 2H), 7.39 (t, *J* 8.2 Hz, 1H), 7.37–7.29 (m, 2H), 7.17–7.02 (m, 5H), 6.95–6.86 (m, 2H), 6.83 (d, *J* Hz, 1H); 6.36 (d, *J* Hz, 1H), 5.22 (d, *J* Hz, 1H) 3.11 (d, *J* Hz, 1H); ^{13}C NMR (101 MHz, $CDCl_3$) δ 193.9, 187.9, 159.1, 158.4, 156.6, 141.9, 140.8, 138.0, 136.1, 135.0, 134.8, 134.5, 134.1, 133.2, 132.8, 131.0, 130.9, 129.74,129.66, 129.5, 129.3, 129.1, 128.6, 126.6, 124.9, 123.6, 121.2, 120.3, 119.9, 116.6, 116.1, 114.2, 75.3, 46.0; IR: 2916, 2357, 1654, 1592, 1208 cm^{-1}; **HRMS (ESI)** for $C_{37}H_{23}NaNO_4$ $(M+Na)^+$: calcd. 568.1525, found 568.1525.

7'–(*tert*– utyl)–4'–(4–(*tert*–butyl)phenyl)–11'*H*–spiro[cyclohex[3]ene–1,9'–thieno[3',2':4,5] pyrido[2,1–a]isoindole]–2,5,11'–trione *(*17o):

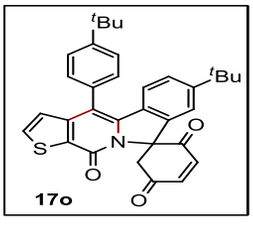

17o (196 mg, 75%) as yellow solid. m.p. 279–282 C; R_f 0.42 (7:3 hexane/EtOAc); ^{1}H NMR (400 MHz, $CDCl_3$) δ 7.63 (d, *J* 5.2 Hz, 1H), 7.59–7.53 (m, 2H), 7.38 (td, *J* 8.8, 2.4 Hz, 2H), 7.23–7.14 (m, 4H), 6.93 (d, *J* 5.2 Hz, 1H), 6.65 (d, *J* 8.4 Hz, 1H), 4.96 (d, *J* 16 Hz, 1H), 2.96 (d, *J* 16 Hz, 1H), 1.43 (s, 9H), 1.21 (s, 9H); ^{13}C NMR (101 MHz, $CDCl_3$) δ 195.2, 189.2, 156.5, 153.6, 151.6, 148.5, 142.7, 141.4, 140.0, 139.0, 133.4, 131.7, 130.3, 129.8, 129.7, 128.2,

127.2, 126.2, 126.0, 124.7, 124.0, 117.4, 113.6, 74.5, 45.8, 35.0, 34.8, 31.4, 31.0; IR (Neat) $_{max}$ 2956, 1696, 1655, 1262, 1081, 895, 787, 730 cm^{-1}; **HRMS (ESI)** for $C_{33}H_{32}NO_3S$ $(M+H)^+$: calcd. 522.2103, found 522.2107.

7'–Methoxy–4'–(4–methoxyphenyl)–11'*H*–spiro[cyclohex[3]ene–1,9'–thieno[3',2':4,5]pyrido[2,1–a]isoindole]–2,5,11'–trione (17p):

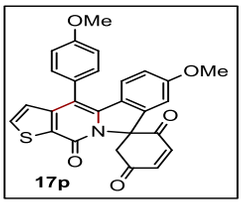

17p (157 mg, 67%) as yellow solid. m.p. 269–270 C; R_f 0.46 (1:1 hexane/EtOAc); ^{1}H NMR (400 MHz, $CDCl_3$) δ 7.63 (d, J 5.2 Hz, 1H), 7.42–7.32 (m, 2H), 7.15 (bs, 2H), 7.11–7.05 (m, 2H), 6.90 (d, J 5.2 Hz, 1H), 6.73–6.63 (d, 3H), 4.93 (d, J 16 Hz, 1H), 3.92 (s, 3H), 3.73 (s, 3H), 2.95 (d, J 16 HZ, 1H); ^{13}C NMR (101 MHz, $CDCl_3$) δ 195.0, 188.9, 160.8, 159.7, 156.5, 148.8, 142.7, 141.8, 141.3, 139.2, 133.5, 131.5, 131.4, 127.4, 126.9, 125.7, 125.5, 124.4, 115.2, 114.7, 112.3, 106.9, 74.2, 55.6, 55.3, 45.7; IR (Neat) $_{max}$ 2933, 2918, 1697, 1651, 1323, 1200, 1079 cm^{-1}; **HRMS (ESI)** for $C_{27}H_{20}NO_5S$ $(M+H)^+$: calcd. 470.1062, found 470.1062.

6'–Chloro–4'–(4–chlorophenyl)–11'*H*–spiro[cyclohex[3]ene–1,9'–thieno[3',2':4,5]pyrido[2,1–a]isoindole]–2,5,11'–trione (17q):

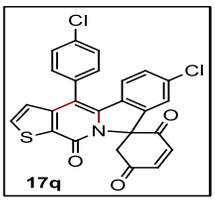

17q (165 mg, 69%) as yellow solid. m.p. 295–298 C; R_f 0.40 (7:3 hexane/EtOAc); ^{1}H NMR (400 MHz, $CDCl_3$) δ 7.70 (d, J 5.2 Hz, 1H), 7.60–7.54 (m, 2H), 7.46–7.38 (m, 2H), 7.20–7.14 (m, 4H), 6.88 (d, J 5.2 Hz, 1H), 6.64 (d, J 9.2 Hz, 1H), 4.93 (d, J = 16.4 Hz, 1H), 2.97 (d, J = 16.4 Hz, 1H); ^{13}C NMR (101 MHz, $CDCl_3$) δ 194.3, 188.3, 156.2, 147.8, 143.0, 141.5, 141.1, 138.0, 136.0, 135.1, 134.2, 132.9, 131.6, 131.5, 131.2, 130.3, 129.9, 129.8, 128.9, 125.2, 124.2, 121.6, 112.9, 74.1, 45.3; IR (KBr) $_{max}$ 2922, 1697, 1651, 1467, 1270, 1089 cm^{-1}; **HRMS (ESI)** for $C_{25}H_{13}Cl_2NNaO_3S$ $(M+Na)^+$: calcd. 499.9891, found 499.9897.

9'–Methyl–11'–(*p*–tolyl)–4'*H*–spiro[cyclohex[3]ene–1,6'–furo[2',3':4,5]pyrido[2,1–a]isoindole]–2,4',5–trione (17r):

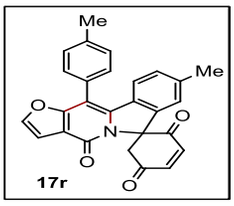

17r (143 mg, 68%) as yellow solid. m.p. 302–305 C; R_f 0.31 (6:4 hexane/EtOAc); ^{1}H NMR (400 MHz, $CDCl_3$) δ (d, J 2.0 Hz, 1H), 7.47–7.41 (m, 1H), 7.41–7.35 (m, 3H), 7.16 (bs, 2H), 7.02 (d, J 2.0 Hz,

1H), 7.01–6.96 (m, 2H), 6.83 (d, *J* 8.0 Hz, 1H), 4.94 (d, *J* 16 Hz, 1H), 2.92 (d, *J* 16 Hz, 1H), 2.49 (s, 3H), 2.30 (s, 3H); ^{13}C NMR (101 MHz, $CDCl_3$) δ 195.2, 189.1, 160.5, 157.1, 144.4, 142.8, 141.4, 140.8, 139.9, 139.0, 130.7, 130.4, 130.3, 130.04, 130.00, 129.8, 127.6, 124.2, 121.4, 115.0, 107.5, 107.3, 74.3, 45.6, 21.7, 21.5; IR (Neat) $_{max}$ 2921, 1698, 1665, 1269, 1081 cm^{-1}; **HRMS (ESI)** for $C_{27}H_{20}NO_4$ $(M+H)^+$: calcd. 422.1392, found 422.1384.

8'-Methoxy–11'–(4-methoxyphenyl)–4'*H*–spiro[cyclohex[3]ene–1,6'–furo[2',3':4,5]pyrido [2,1–a]isoindole]–2,4',5–trione (17s):

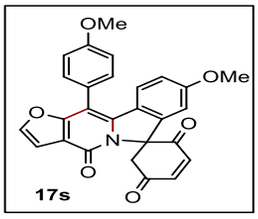

17s (150 mg, 66%) as yellow solid. m.p. 230–232 C; R_f 0.39 (1:1 hexane/EtOAc); ^{1}H NMR (400 MHz, $CDCl_3$) δ 7.50–7.40 (m, 3H), 7.15 (bs, 2H), 7.12–7.07 (m, 2H), 7.00 (d, *J* 2.0 Hz, 1H), 6.87 (d, *J* 8.8 Hz, 1H), 6.72 (dd, *J* 8.8, 2.4 Hz, 1H), 6.67 (d, *J* 2.4 Hz, 1H), 4.92 (d, *J* 16.4 Hz, 1H), 3.92 (s, 3H), 3.74 (s, 3H), 2.93 (d, *J* 16 Hz, 1H); ^{13}C NMR (101 MHz, $CDCl_3$) δ 195.0, 188.9, 161.1, 160.7, 160.0, 157.1, 144.1, 142.7, 142.3, 141.3, 140.0, 131.8, 131.7, 125.7, 125.1, 122.7, 115.3, 114.6, 114.3, 107.5, 107.0, 106.0, 74.2, 55.6, 55.3, 45.6; IR (KBr) $_{max}$ 1696, 1655, 1613, 1515, 1365, 1288, 1241 cm^{-1}; **HRMS (ESI)** for $C_{27}H_{20}NO_6$ $(M+H)^+$: calcd. 454.1291, found 454.1292.

8'–Acetyl–11'–(4–acetylphenyl)–4'*H*–spiro[cyclohex[3]ene–1,6'–furo[2',3':4,5]pyrido[2,1–a]isoindole]–2,4',5–trione (17t):

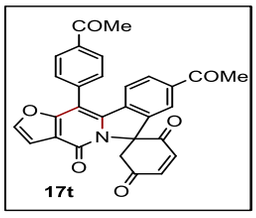

17t (160 mg, 67%) as yellow solid. m.p. 289–293 C; R_f 0.27 (1:1 hexane/EtOAc); ^{1}H NMR (400 MHz, $CDCl_3$) δ 8.18 (d, *J* 8.4 Hz, 2H), 7.79–7.65 (m, 4H), 7.56 (d, *J* 2.0 Hz, 1H), 7.25–7.20 (m, 1H), 7.19–7.14 (m, 1H), 7.06 (d, *J* 2.4 Hz, 1H), 6.99 (d, *J* 8.0 Hz, 1H), 4.89 (d, *J* 16 Hz, 1H), 2.97 (d, *J* 16.4, 1H), 2.72 (s, 3H), 2.51 (s, 3H); ^{13}C NMR (101 MHz, $CDCl_3$) δ 197.4, 195.7, 194.1, 188.5, 159.3, 156.8, 145.4, 143.2, 141.2, 141.0, 138.5, 138.1, 137.7, 136.2, 135.2, 130.9, 130.8, 130.2, 129.3, 129.1, 124.1, 120.6, 116.7, 108.2, 107.9, 74.4, 45.3, 26.7, 26.6; IR (KBr) $_{max}$ 3733, 1684, 1602, 1422, 1358, 1265; **HRMS (ESI)** for $C_{29}H_{19}NNaO_6$ $(M+Na)^+$: calcd. 500.1110, found 500.1110.

3'–Methyl–1'–phenyl–1H,4'H–spiro[naphthalene–2,6'–pyrido[2,1–a]isoindole]–1,4,4'(3H)–trione (32a):

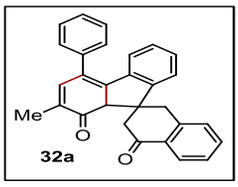

32a (130 mg, 62%) as yellow solid. m.p. 298–299 C; R_f 0.4 (7:3 hexane/EtOAc); ^{1}H NMR (500 MHz, $CDCl_3$) δ – (m, 2H), 7.89 (td, J 7.5, 1.3 Hz, 1H), 7.83 (td, J 7.6, 1.3 Hz, 1H), 7.53–7.44 (m, 5H), 7.35 (bd, J 1.0 Hz, 1H), 7.19–7.08 (m, 2H), 6.95 (dd, J 7.2, 1.2 Hz, 1H), 6.90 (dd, J 7.0 , 1.0 Hz, 1H), 5.21 (d, J 16 Hz, 1H), 3.05 (d, J 15.5 Hz, 1H), 2.24 (s, 3H); ^{13}C NMR (126 MHz, $CDCl_3$) δ193.6, 187.7, 160.8, 141.5, 140.6, 140.4, 136.8, 136.2, 135.0, 134.6, 134.2, 133.1, 129.8, 129.5, 129.3, 129.1, 129.0, 128.6, 128.3, 126.8, 124.1, 121.4, 117.2, 75.9, 45.4, 16.2; ^{13}C dept NMR (101 MHz, $CDCl_3$) 141.6, 135.1, 134.6, 129.9, 129.5, 129.4, 129.1, 128.3, 126.8, 124.1, 121.4, 45.4 (–CH_2), 16.2; IR (Neat) $_{max}$ 2914, 1698, 1651, 1594, 1548, 1287 cm^{-1}; **HRMS (ESI)** for $C_{28}H_{20}NO_3$ $(M+H)^+$: calcd. 418.1443, found 418.1446.

3',8'–Dimethyl–1'–(*p*–tolyl)–1H,4'H–spiro[naphthalene–2,6'–pyrido[2,1–a]isoindole]–1,4,4'(3H)–trione (32b):

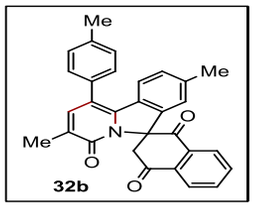

32b (137 mg, 61%) as yellow solid. m.p. 317–321 C; R_f 0.34 (7:3 hexane/EtOAc); ^{1}H NMR (500 MHz, $CDCl_3$) δ 8.30–8.23 (m, 2H), 7.89 (td, J 7.5, 2.0 Hz, 1H), 7.84 (td, J 7.5, 1.5 Hz, 1H), 7.36–7.27 (m, 5H), 6.96–6.88 (m, 2H), 6.66 (bs, 1H), 5.17 (d, J 15.5 Hz, 1H), 3.04 (d, J 15.5 Hz, 1H), 2.45 (s, 3H), 2.21 (s, 3H), 2.16 (s, 3H); ^{13}C NMR (101 MHz, $CDCl_3$) δ193.7, 188.0, 160.8, 141.8, 141.0, 140.6, 140.5, 137.9, 136.2, 135.0, 134.6, 134.2, 133.9, 130.6, 130.3, 129.6, 129.4, 129.0, 127.8, 126.8, 123.9, 121.7, 116.6, 75.6, 45.5, 21.6, 21.3, 16.2; IR (Neat) $_{max}$ 2918, 1698, 1650, 1596, 1513, 1257, 1014 cm^{-1}; **HRMS (ESI)** for $C_{30}H_{24}NO_3$ $(M+H)^+$: calcd. 446.1756, found 446.1759.

8'–(*tert*–Butyl)–1'–(4–(tert–butyl)phenyl)–3'–methyl–1H,4'H–spiro[naphthalene–2,6'–pyrido[2,1–a]isoindole]–1,4,4'(3H)–trione (32c):

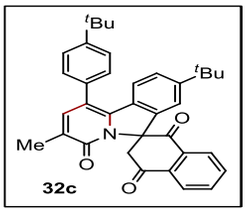

32c (184 mg, 70%) as yellowis white solid. m.p. 307–313 C; R_f 0.38 (7:3 hexane/EtOAc); ^{1}H NMR (400 MHz, $CDCl_3$) δ 8.27 (dd, J 7.8 & 1 Hz, 2H), 7.89 (td, J 7.5, 1.3 Hz, 1H), 7.83 (td, J 7.5, 1.5 Hz, 1H), 7.50

(bd, J = 8.4 Hz, 2H), 7.38 (bd, J = 8.0 Hz, 2H), 7.34 (d, J = 0.8 Hz, 1H), 7.18 (dd, *J* 8.4 & 1.6 Hz, 1H), 6.97 (d, *J* 8.4 Hz, 1H), 6.85 (d, J = 1.6 Hz, 1H), 5.19 (d, J = 16 Hz, 3H), 3.05 (d, J = 15.6 Hz, 1H), 2.22 (s, 3H), 1.40 (s, 9H), 1.05 (s, 9H); ^{13}C NMR (101 MHz, $CDCl_3$) δ193.7, 188.0, 160.9, 153.7, 151.2, 141.8, 140.54, 140.52, 136.2, 135.0, 134.5, 134.2, 133.8, 130.5, 129.1, 129.0, 127.8, 126.9, 126.5, 125.7, 123.7, 117.9, 116.7, 75.9, 45.5, 34.9, 34.7, 31.4, 30.8, 16.2; IR (Neat) $_{max}$ 2906, 1699, 1651, 1596, 1283, 1258 cm^{-1}; **HRMS (ESI)** for $C_{36}H_{35}NNaO_3$ $(M+Na)^+$: calcd. 552.2515, found 552.2515

8'–Methoxy–1'–(4–methoxyphenyl)–3'–methyl–1H,4'H–spiro[naphthalene–2,6'–pyrido[2, 1–a]isoindole]–1,4,4'(3H)–trione (32d):

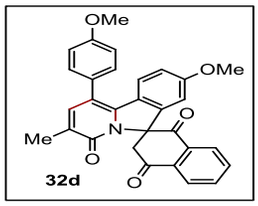

32d (148 mg, 62%) as yellow solid. m.p. 261–262 C; R_f 0.33 (3:2 hexane/EtOAc); ^{1}H NMR (400 MHz, $CDCl_3$) δ 8.29–8.21 (m, 2H), 7.91–7.77 (m, 2H), 7.35 (bd, *J* 7.6 Hz, 2H), 7.30 (d, *J* 0.8 Hz, 1H), 7.01 (d, *J* 8.8 Hz, 2H), 6.93 (d, *J* 8.8 Hz, 1H), 6.66 (dd, *J* 8.8, 2.4 Hz, 1H), 6.36 (d, *J* 2.4 Hz, 1H), 5.16 (d, *J* 16 Hz, 1H), 3.88 (s, 3H), 3.58 (s, 3H), 3.04 (d, *J* 16 Hz, 1H), 2.20 (s, 3H); ^{13}C NMR (101 MHz, $CDCl_3$) δ 193.5, 187.7, 160.81, 160.79, 159.4, 142.4, 142.0, 140.6, 136.0, 135.0, 134.6, 134.1, 130.7, 129.0, 126.8, 126.7, 125.7, 125.3, 115.4, 114.6, 114.3, 107.5, 75.5, 55.4, 55.3, 45.4, 16.1; IR (Neat) $_{max}$ 2937, 2837, 1651, 1512, 1291, 1246, 1029 cm^{-1}; **HRMS (ESI)** for $C_{31}H_{24}NO_5$ $(M+H)^+$: calcd. 478.1654, found 478.1653.

8'–Chloro–1'–(4–chlorophenyl)–3'–methyl–1H,4'H–spiro[naphthalene–2,6'–pyrido[2,1–a] isoindole]–1,4,4'(3H)–trione (32e):

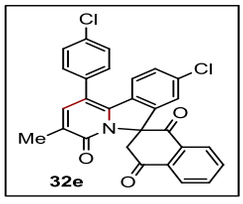

32e (126 mg, 52%) as yellow solid. m.p. 324–326 C; R_f 0.25 (7:3 hexane/EtOAc); ^{1}H NMR (400 MHz, $CDCl_3$) δ 8.27 (dd, *J* 7.8, 0.6 Hz, 2H), 7.96–7.82 (m, 2H), 7.49 (bd, *J* 8.8 Hz, 2H), 7.42–7.36 (m, 2H), 7.30 (d, *J* 0.8 Hz, 1H), 7.14 (dd, *J* 8.6, 1.8 Hz, 1H), 6.90 (d, *J* 8.4 Hz, 1H), 6.85 (d, *J* 1.6 Hz, 1H), 5.13 (d, *J* 16 Hz, 1H), 3.05 (d, *J* 15.6 Hz, 1H), 2.22 (s, 3H); ^{13}C NMR (101 MHz, $CDCl_3$) δ192.9, 187.2, 160.6, 142.2, 141.2, 139.5, 136.1, 135.9, 135.4, 134.9, 134.8, 134.5, 133.7, 131.4, 130.8, 130.0, 129.5, 129.3, 129.23, 129.17, 127.0, 124.8, 121.9, 116.0, 75.5, 45.1, 16.3; IR (KBr) $_{max}$ 2917, 1699, 1652, 1607, 1292, 1257, 1087 cm^{-1}; **HRMS (ESI)** for $C_{28}H_{17}Cl_2NNaO_3$ $(M+Na)^+$: calcd. 508.0483, found 508.0495.

3',9'–Dimethyl–1'–(*m*–tolyl)–1H,4'H–spiro[naphthalene–2,6'–pyrido[2,1–a]isoindole]–1,4,4'(3H)–trione (32f):

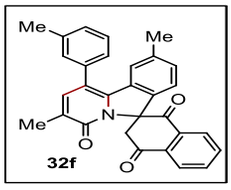

32f (109 mg, 49%) as brown solid. m.p. 292–293 C; R_f 0.30 (7:3 hexane/EtOAc); ^{1}H NMR (400 MHz, $CDCl_3$) δ 8.25 (dt, J 7.6, 1.6 Hz, 2H), 7.88 (td, J 7.5, 1.1 Hz, 1H), 7.86–7.78 (m, 1H), 7.38 (t, J 7.6 Hz, 1H), 7.34 (bd, J 1.2 Hz, 1H), 7.31–7.23 (m, 3H), 6.95 (dd, J 7.8, 0.6 Hz, 1H), 6.80 (bs, 1H), 6.76 (d, J 7.6 Hz, 1H), 5.20 (d, J Hz, 1H), 3.02 (d, J 18 Hz, 1H), 2.43 (s, 3H), 2.23 (s, 3H), 2.11 (s, 3H); ^{13}C NMR (101 MHz, $CDCl_3$) δ 193.7, 187.8, 160.8, 141.6, 140.4, 139.4, 137.9, 136.6, 136.1, 134.9, 134.5, 134.1, 133.2, 130.7, 130.1, 129.0, 128.9, 128.2, 126.7, 126.5, 124.6, 121.0, 117.2, 75.6, 45.5, 21.4, 21.3, 16.2; IR (KBr) $_{max}$ 3012, 2918, 1650, 1594, 1285, 1259 cm^{-1}; **HRMS (ESI)** for $C_{30}H_{24}NO_3$ $(M+H)^+$: calcd. 446.1756, found 446.1756.

1'–Butyl–3'–methyl–1H,4'H–spiro[naphthalene–2,6'–pyrido[2,1–a]isoindole]–1,4,4'(3H)–trione (32g):

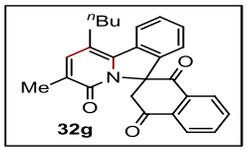

32g (87 mg, 44%) as yellow solid. m.p. 210–211 C; R_f 0.24 (7:3 hexane/EtOAc); ^{1}H NMR (500 MHz, $CDCl_3$) δ 8.23 (d, J 8.0 Hz, 2H), 7.87 (t, J 7.5 Hz, 1H), 7.84–7.75 (m, 2H), 7.43 (t, J 7.7 Hz, 1H), 7.28 (bs, 1H), 7.22 (t, J 7.5 Hz, 1H), 6.94 (d, J 8.0 Hz, 1H), 5.17 (d, J 15.5 Hz, 1H), 2.97 (d, J Hz, 1H), 2.88–2.73 (m, 2H), 2.19 (s, 3H), 1.72–1.62 (m, 2H), 1.55–1.43 (m, 2H), 0.99 (t, J 7.5 Hz, 3H); ^{13}C NMR (126 MHz, $CDCl_3$) δ 193.7, 187.9, 160.6, 142.0, 140.6, 140.1, 136.2, 134.9, 134.5, 134.1, 133.6, 129.8, 129.3, 129.0, 128.7, 126.7, 123.9, 121.6, 116.8, 75.6, 45.4, 31.9, 30.5, 22.6, 16.2, 13.9; IR (KBr) $_{max}$ 2956, 2928, 1697, 1650, 1594, 1064 cm^{-1}; **HRMS (ESI)** for $C_{26}H_{23}NNaO_3$ $(M+Na)^+$: calcd. 420.1576, found 420.1576.

14–Phenyl–1'H–spiro[chromeno[4',3':4,5]pyrido[2,1–a]isoindole–9,2'–naphthalene]–1',4',7(3'H,6H)–trione (33):

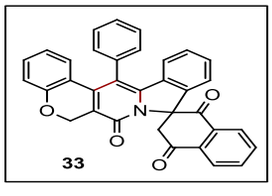

33 (96 mg, 38%) as brown solid. m.p. 323–328 C; R_f 0.30 (7:3 hexane/EtOAc); ^{1}H NMR (400 MHz, $CDCl_3$) δ 8.27 (d, J 8.0 Hz, 2H), 7.91 (td, J 7.6, 1.0 Hz, 1H), 7.84 (td, J 7.6, 1.2 Hz, 1H), 7.60–7.50

(m, 3H), 7.46–7.39 (m, 2H), 7.20–7.11 (m, 2H), 7.06 (t, *J* 7.4 Hz, 1H), 7.02 (dd, *J* 8.8, 1.0 Hz, 1H), 6.91 (d, *J* Hz, 1H), 6.67 (dd, *J* 8.0, 1.2 Hz, 1H), 6.56 (td, *J* 6.8, 1.0 Hz, 1H), 6.24 (d, *J* 7.6 Hz, 1H), 5.22 (d, *J* 5.6 Hz, 1H), 5.18 (d, *J* 4.0 Hz, 1H), 5.09 (d, *J* 14 Hz, 1H), 3.09 (d, *J* 16 Hz, 1H); ^{13}C NMR (101 MHz, $CDCl_3$) δ 193.2, 187.4, 157.6, 157.3, 143.0, 140.8, 140.7, 136.1, 135.9, 135.2, 134.7, 133.9, 133.2, 131.0, 130.9, 130.8, 130.1, 129.9, 129.7, 129.5, 129.1, 128.9, 128.4, 126.8, 125.3, 121.30, 121.27, 120.9, 117.5, 115.0, 63.4, 45.4; IR (KBr) $_{max}$ 2920, 2850, 1692, 1637, 1592, 1254, 1013 cm^{-1}; **HRMS (ESI)** for $C_{34}H_{22}NO_4$ $(M+H)^+$: calcd. 508.1549, found 508.1549.

III.6.4. General procedure for the sequential oxidative coupling with different equivalent of quinones:

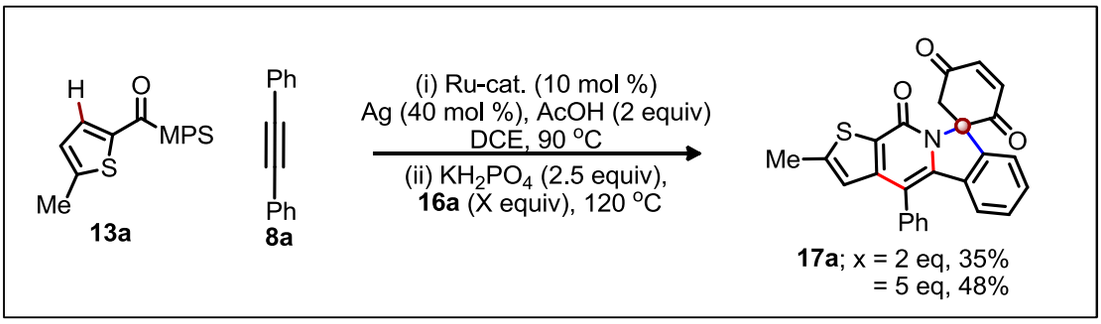

The annulation reactions were carried out in a 50 mL Schlenk tube having high pressure valve and side arm. The tube was charged with *N*-heteroaroylated-MPS (**13a**, 0.5 mmol), alkyne (**8a**, 0.6 mmol), $[RuCl_2(p\text{-cymene})]_2$ (31 mg, 10 mol %) and $AgSbF_6$ (69 mg, 40 mol %) was introduced in to the flask in a glovebox. The solvent 1,2-dichloroethane (DCE; 1.5 mL) and AcOH (60 L, 2.0 equiv) were added to the mixture and the resulting mixture was stirred at 90 C for 10 h. The reaction mixture was cooled to ambient temperature, and then KH_2PO_4 (170 mg, 2.5 equiv), **16a** (2.0 or 5.0 equiv) was added. The resulting mixture was then heated at 120 °C and the reaction was continued for 10 h. Finally, the reaction mixture was cooled to ambient temperature, filtered through a small plug of Celite and then washed with dichloromethane (3 × 10 mL). The solvents were evaporated under reduced pressure and the crude material was purified using

column chromatography on silica gel (20–30% *n*–hexane/EtOAc eluent) to give the desired product **17a**.

III.6.5 Deuterium study:

The annulation reactions were carried out in a 10 mL screw capped tube. The tube was charged with *N*-heteroaroylated-MPS (**13g**, 0.5 mmol), alkyne (**8a**, 0.6 mmol), $[RuCl_2(p\text{-cymene})]_2$ (31 mg, 10 mol %), and $Cu(OAc)_2$ (90 mg, 0.5 mmol). Subsequently, $AgSbF_6$ (69 mg, 40 mol %) was introduced in to the tube in a glovebox. The solvent 1,2-dichloroethane (DCE; 1.5 mL) and CD_3COOD (57 L, 2.0 equivalent) were added to the mixture and the resulting mixture was stirred at 90 °C for 10 h. The reaction mixture was cooled to ambient temperature, and then BQ (**16a**; 2.0 equiv) was added. The resulting mixture was then heated at 120 C and the reaction was continued for 10 h. Finally, the reaction mixture was cooled to ambient temperature, filtered through a small plug of Celite and then washed with dichloromethane (3 × 10 mL). The solvents were evaporated under reduced pressure and the crude material was purified using column chromatography on silica gel (20–30% *n*–hexane/EtOAc eluent) to give the desired product **17g**.

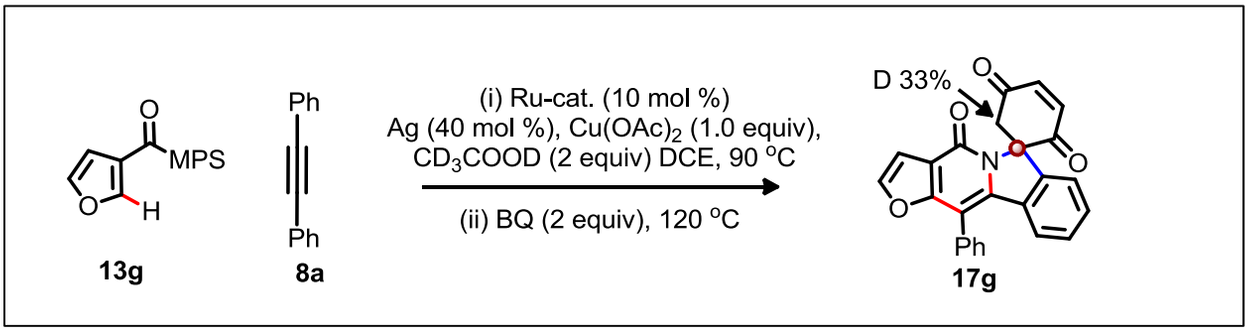

III.6.6 [4+2]-Cycloaddition:

The cycloaddition reactions were carried out in a 50 mL Schlenk tube having high pressure valve and side arm. The tube was charged with **17g** (0.2 mmol). Then dichloromethane was added. The reaction mixture was cooled to 0 °C and freshly distilled cyclopentadiene was added dropwise. Next the reaction was continued for 12

h. Finally, the reaction mixture was filtered through a small plug of Celite and then washed with dichloromethane (3 × 10 mL). The solvent was evaporated under reduced pressure and the crude material was purified using column chromatography on silica gel (20–30% *n*–hexane/EtOAc eluent) to give the desired product **34**.

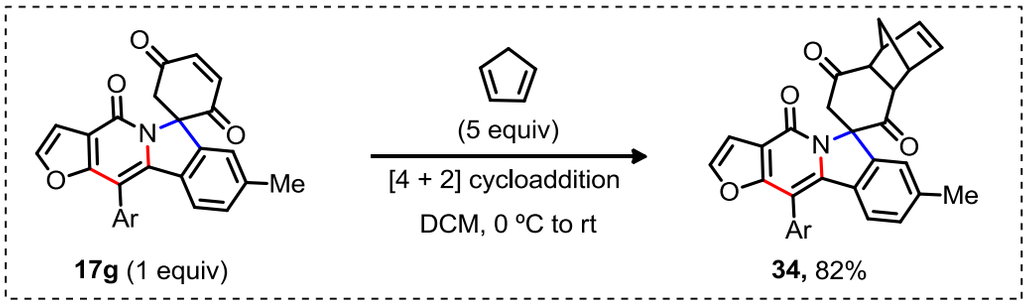

(1R,4S,4aS,8aR –8'–Methyl–11'– p–tolyl –4,4a–dihydro–1H,4'H–spiro[1,4–methanonaphthalene–6,6'–furo[2',3':4,5]pyrido[2,1–a]isoindole –4',5,8(7H,8aH –trione) (**34**):

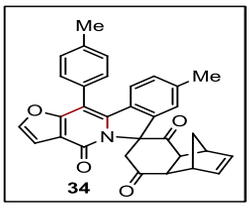

34 (80 mg, 82%) as yellow solid. m.p. 296–298 C; R_f 0.15 (7:3 hexane/EtOAc); ^{1}H NMR (400 MHz, $CDCl_3$) δ 7.45 (d, *J* 2.0 Hz, 1H), 7.44–7.37 (m, 2H), 7.37–7.32 (m, 2H), 7.04 (bs, 1H), 7.02 (d, *J* 2 Hz, 1H), 6.96 (dd, *J* 8.2 & 0.6 Hz, 1H), 6.82-6.76 (m, 1H), 6.76 (d, *J* = 8.4 Hz, 1H), 6.36 (dd, *J* 5.6 & 2.4 Hz, 1H), 4.6 (d, *J* Hz, 1H), 3.79 (s, 1H), 3.64–3.57 (m, 2H), 3.15 (dd, *J* 9.0 Hz & 3.8, 1H), 2.56 (dd, J 15.6 & 1.6, 1H), 2.48 (s, 3H), 2.33 (s, 3H), 1.65 (d, *J* Hz, 1H) 1.55 (d, *J* Hz, 1H); ^{13}C NMR (101 MHz, $CDCl_3$) δ 208.8, 198.5, 160.1, 157.2, 144.2, 140.6, 140.5, 139.7, 139.3, 138.8, 133.5, 130.40, 130.37, 130.3, 130.0, 129.9, 127.8, 124.1, 121.7, 115.0, 107.5, 106.9, 53.0, 50.6, 50.1, 49.8, 49.1, 45.7, 29.7, 21.8, 21.4 cm^{-1}; IR (KBr) $_{max}$ 3393, 2918, 2848, 1659, 1647, 1242, 1015 cm^{-1}; HRMS (ESI) for $C_{32}H_{26}NO_4$ $(M+H)^+$: calcd. 488.1862, found 488.1866.

III.6.7 Sequential oxidative coupling of MPS-bearing furan-3-carboxylate (13g) (1.0 mmol) with diphenyl acetylene (8a) and benzoquinone (16a):

The annulation reactions were carried out in a 25 mL screw capped tube. The tube was charged with MPS-bearing furan-3-carboxylate **13g** (249 mg, 1 mmol), **8a** (214 mg, 1.2 mmol), $[RuCl_2(p\text{-cymene})]_2$ (62 mg, 10 mol %), and $Cu(OAc)_2 \cdot H_2O$ (200 mg, 1.0 mmol). Subsequently, $AgSbF_6$ (137 mg, 40 mol %) was introduced in to the tube in a glovebox. The solvent 1,2-dichloroethane (DCE; 2 mL) and AcOH (120 L, 2.0 mmol) were added to the mixture and the resulting mixture was stirred at 90 C for 10 h. The reaction mixture was cooled to ambient temperature, and then KH_2PO_4 (340 mg, 2.5 mmol), BQ (**16a**; 216 mg, 2.0 mmol), and subsequently 1,4-dioxane (2.0 mL) were added. The resulting mixture was then heated at 120 C and continued for 10 h. Finally, the reaction mixture was cooled to ambient temperature, filtered through a small plug of Celite and then washed with dichloromethane (3 × 10 mL). The solvents were evaporated under reduced pressure and the crude material was purified using column chromatography on silica gel (20–30% *n*–hexane/EtOAc eluent) to give the desired product.

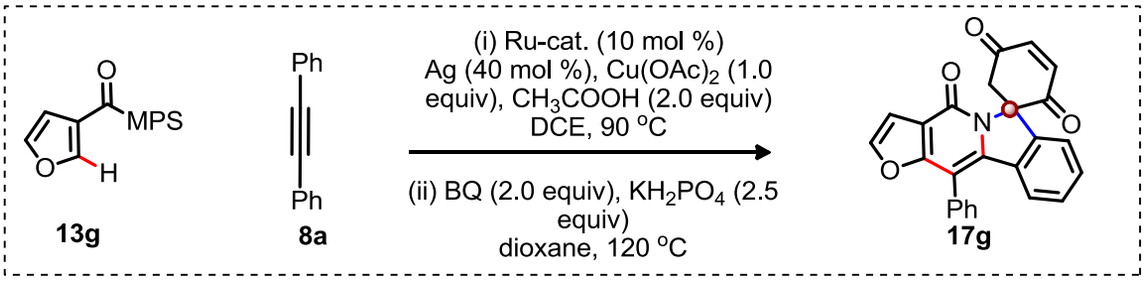

III.7. References

(1) (a) D. Y. K. Chen, S. W. Youn, *Chem. Eur. J.* **2012**, *18*, 9452. (b) P.-P. Zhang, Z.-M. Yan, Y.-H. Li, J.-X. Gong, Z. Yang, *J. Am. Chem. Soc.* **2017**, *139*, 13989.

(2) (a) E. F. Flegeau, C. Bruneau, P. H. Dixneuf, A. Jutand, *J. Am. Chem. Soc.* **2011**,*133*, 10161. (b) M. R. Yadav, R. K. Rit, M. Shankar, A. K. Sahoo, *Asian. J. Org. Chem.* **2015**, *4*, 846. (c) R.-Y. Zhu, M. E. Farmer, Y.-Q. Chen, J.-Q. Yu, *Angew. Chem., Int. Ed.* **2016**, *55*, 10578. (d) K. Korvorapun, N. Kaplaneris, T. Rogge, S. Warratz, A. C. Stückl, L. Ackermann, *ACS Catal.* **2018**, *8*, 886

(3) (a) T. Satoh, M. Miura, *Chem. Eur.J.* **2010**, *16*, 11212. (b) J. Wencel-Delord, T. Dröge, F. Liu, F. Glorius, *Chem. Soc. Rev*. **2011**, *40*, 4740. (c) G. Song, F. Wang, X. Li, *Chem. Soc. Rev.* **2012**, *41*, 3651. (d) L. Ackermann, *Acc. Chem. Res.* **2014**, *47,* 281. (e) M. Gulías, *J. L.* Mascareñas, *Angew. Chem. Int. Ed*. **2016**, *55*, 11000. (f) Y. Qin, L. Zhu, S. Luo, *Chem. Rev*. **2017**, *117*, 9433.

(4) (a) T. Fukutani, N. Umeda, K. Hirano, T. Satoh, M. Miura, *Chem. Commun*. **2009**, 5141. (b) K. Morimoto, K. Hirano, T. Satoh, M. Miura, *Org. Lett*. **2010**, *12*, 2068. (c) N. Guimond, C. Gouliaras, K. Fagnou, *J. Am. Chem. Soc.* **2010**,*132*, 6908. (d) X. Wei, M. Zhao, Z. Du, X. Li, *Org. Lett*. **2011,** *13*, 4636. (e) F. Wang, G. Song, X. Li, *J. Org. Chem.* **2011**, *76*, 2926

(5) (a) L. Ackermann, A. V. Lygin, N. Hofmann, *Angew. Chem., Int. Ed*. **2011**, *50*, 6379. (b) B. Li, H. Feng, S. Xu, B. Wang, *Chem. Eur. J.* **2011**, *17*, 12573. (c) L. Ackermann, S. Fenner, *Org. Lett.* **2011**, *13*, 6548. (d) L. Ackermann, J. Pospech, K. Graczyk, K. Rauch, *Org. Lett.* **2012**, *14*, 930. (e) K. Parthasarathy, N. Senthilkumar, J. Jayakumar, C.-H. Cheng, *Org. Lett*. **2012**, *14*, 3478. (f) J. Li, M. John, L. Ackermann, *Chem. Eur. J*. **2014**, *20*, 5403. (g) M. R. Yadav, R. K. Rit, M. Shankar, A. K. Sahoo, *J. Org. Chem.* **2014**, *79*, 6123.

(6) W. Yang, S. Ye, D. Fanning, T. Coon, Y. Schmidt, P. Krenitsky, D. Stamos, J.-Q. Yu, *Angew. Chem. Int. Ed*. **2015**, *54*, 2501.

(7) (a) G. Song, D. Chen, C.-L.Pan, R. H. Crabtree, X. Li, *J. Org. Chem*. **2010**, *75*, 7487. (b) S. Mochida, N. Umeda, K. Hirano, T. Satoh, M. Miura, *Chem. Lett.* **2010**, *39*, 744. (c) M. R. Yadav, R. K. Rit, A. K. Sahoo, *Chem. - Eur. J.* **2012**, *18*, 5541. (d) J. Jayakumar, K. Parthasarathy, Y.-H. Chen, T.-H. Lee, S.-C. Chuang, C.-H. Cheng, *Angew.Chem., Int. Ed.* **2014**, 53, 9889. (e) Q. Ge, Y. Hu, B. Li, B. Wang. *Org. Lett*. **2016**, *18*, 2483. (f) S. Peng, S. Liu, S. Zhang, S. Cao, J. Sun, *Org. Lett*. **2015**, *17*, 5032.

(8) K. M. Engle, D.-H. Wang, J.-Q. Yu,. *Angew. Chem., Int. Ed.* **2010**, *49,* 6169.

(9) (a) N. Umeda, K. Hirano, T. Satoh, M. Miura, *J. Org. Chem*. **2009**, *74*, 7094. (b) D. Sarkar, F. S. Melkonyan, A. V. Gulevich, V. Gevorgyan, *Angew. Chem., Int. Ed.* **2013**, *52,* 10800. (c) H. J. Kim, M. J. Ajitha, Y. Lee, J. Ryu, J. Kim, Y. Lee, Y. Jung, S. Chang, *J. Am. Chem. Soc.* **2014**, *136*, 1132. *(d)* M. R. Yadav, M. Shankar, E. Ramesh, K. Ghosh, A. K.

Sahoo, *Org. Lett*. **2015**, *17*, 1886 (e) D. Sarkar, A. V. Gulevich, F. S. Melkonyan, V. Gevorgyan, *ACS Catal*. **2015**, *5*, 6792. *(f)* K. Korvorapun, N. Kaplaneris, T. Rogge, S. Warratz, A. C. Stückl, L. **A**ckermann, *ACS Catal*. **2018**, *8*, 886. (g) J. Li, K. Korvorapun, S. D. Sarkar, T. Rogge, D. J. Burns, S. Warratz, L. Ackermann, *Nature Commun*. **2017**, *8*, 15430. (h) B. Li, C. B. Bheeter, C. Darcel, P. H. Dixneuf, *ACS Catal*. **2011**, *1*, 1221 (i) L. Ackermann, R. Born, P. Alvarez-Bercedo, *Angew.Chem.Int. Ed*. **2007**, *46*, 6364.

(10) L. Ackermann, A. V. Lygin, N. Hofmann, *Angew. Chem. Int. Ed*. **2011**, *50*, 6379.

(11) B. Li, H. Feng, S. Xu,B. Wang, *Chem. Eur. J*. **2011**, *17*, 12573

(12) L. Ackermann, S. Fenner, *Org. Lett*. **2011**, *13*, 6548.

(13) F.Yang, L. Ackermann, *J. Org. Chem*. **2014**, *79*, 12070.

(14) M. R. Yadav, R. K. Rit, M. Shankar,A.K.Sahoo, *J. Org. Chem*. **2014**, 79, 6123.

(15) (a) B. Li, H. Feng, N. Wang, J. Ma, H. Song, S. Xu, B. Wang, *Chem. Eur.J*. **2012**, *18*, 12873. (b) N. Wang, B. Li, H. Song, S. Xu, B. Wang, *Chem. Eur. J*. **2013**, *19*, 358.

(16) (a) T. Zhou, L. Li, B. Li, H. Song, B. Wang, *Org. Lett*. **2015**, *17*,4204. (b) W. Miura, K. Hirano, M. Miura, *Org. Lett*. **2015**, *17*, 4034. (c) R. Manoharan, M. Jeganmohan, *Org. Lett*. **2017**, *19*, 5884.

(17) S. Mochida, N. Umeda, K. Hirano, T. Satoh, M. Miura, *Chem. Lett*. **2010**, *39*, 744.

(18) G. Song, D. Chen, C. L. Pan, R. H. Crabtree, X. Li, *J. Org. Chem*. **2010**, 75, 7487.

(19) H. Lin, S. -S. Li, L. Dong, *Org. Biomol. Chem*. **2015**, *13*, 11228.

(20) M. Shankar, K. Ghosh, K. Mukherjee, R. K. Rit, *Org. Lett*. **2016** , *18*, 6416–6419.

(21) (a) K. Ghosh, R. K. Rit, E. Ramesh, A. K. Sahoo, *Angew. Chem. Int. Ed*. **2016**, *55*, 7821. (b) Y. Wu, Z. Chen, Y. Yang, W. Zhu, B. Zhou, *J. Am. Chem. Soc*. **2018**, *140*, 42.

(22) (a) M. Shankar**,** K. Ghosh**,** K. Mukherjee**,** R. K. Rit, and A. K. Sahoo, *Org. Lett.* **2016**, *18,* 6416. (b) M. Shankar, T. Guntreddi, E. Ramesh, A. K. Sahoo, *Org. Lett*. **2017**, *19*, 5665.

(23) (a) The Chemistry of the Quinonoid Compounds, Vol. 2; S. Patai, Z. Rappoport, *Wiley: New York*, **1988**; Part 1 and 2. (b) Y. Fujiwara, V. Domingo, I. B. Seiple, R. Gianatassio, M. D. Bel, P. S. Baran, *J. Am. Chem. Soc*. **2011**, *133*, 3292.

(24) P. B. Arockiam, C. Bruneau, P. H. Dixneuf, *Chem. Rev*. **2012**, *112*, 5879.;

(25) (a) M. C. Wilson, S.-J. Nam, T. A. M. Gulder, C. A. Kauffman, P. R. Jensen, W. Fenical, B. S. Moore, *J. Am. Chem. Soc*. **2011**, *133*, 1971. (b) P. D. O'Connor, L. N. Mander, M. M. W. McLachlan, *Org. Lett*. **2004**, 6, 703.

(26) (a) H. Okamura, C. Bolm, *Org. Lett*. **2004**, *6*, 1305.

(27) (a) M. R. Yadav, R. K. Rit, M. Shankar, A. K. Sahoo, *J.Org. Chem*. **2014**, *79*, 6123–6134. (b) M. R. Yadav, M. Shankar, E. Ramesh, K. Ghosh, A. K. Sahoo, *Org. Lett*. **2015**, *17*, 1886 –1889. (c) M. Shankar, T. Guntreddi, E. Ramesh, A. K. Sahoo, *Org. Lett*. **2017**, *19*, 5665 –5668.

(28) (a) M. J. Mio, L. C. Kopel, J. B. Braun, T. L. Gadzikwa, K. L. Hull, R. G. Brisbois, C. J. Markworth, P. A. Grieco, *Org.Lett*. **2002**, *4*, 3199 –3202. (b) K. Park, G. Bae, J. Moon, J. Choe, K. H. Song, S. Lee, *J. Org. Chem*. **2010**, *75*, 6244–6251

(29) L. Ackermann, Chem. Rev. **2011**, 111, 1315 – 1345.

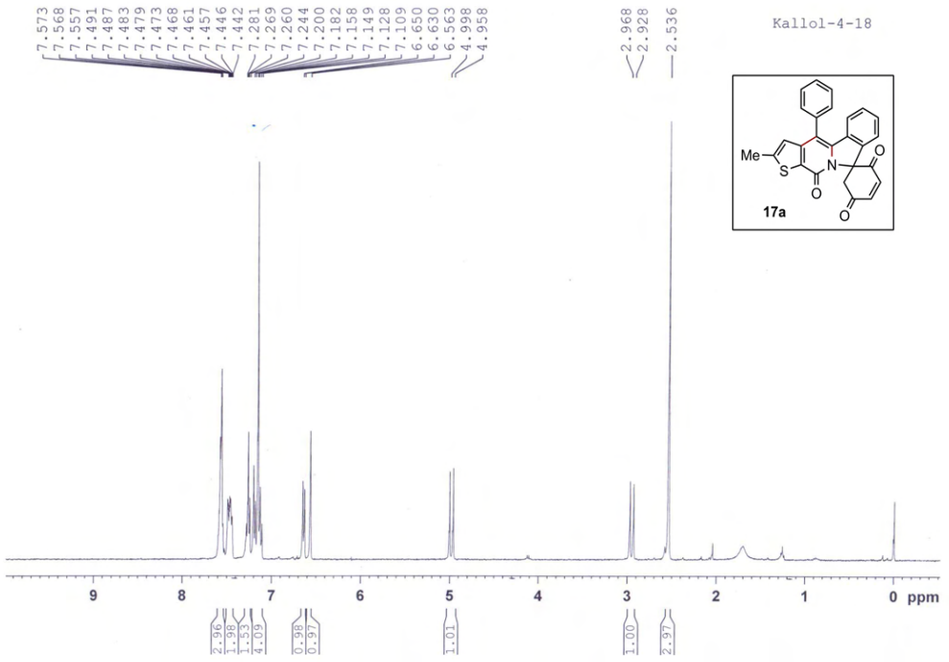
Kallol-4-18
17a

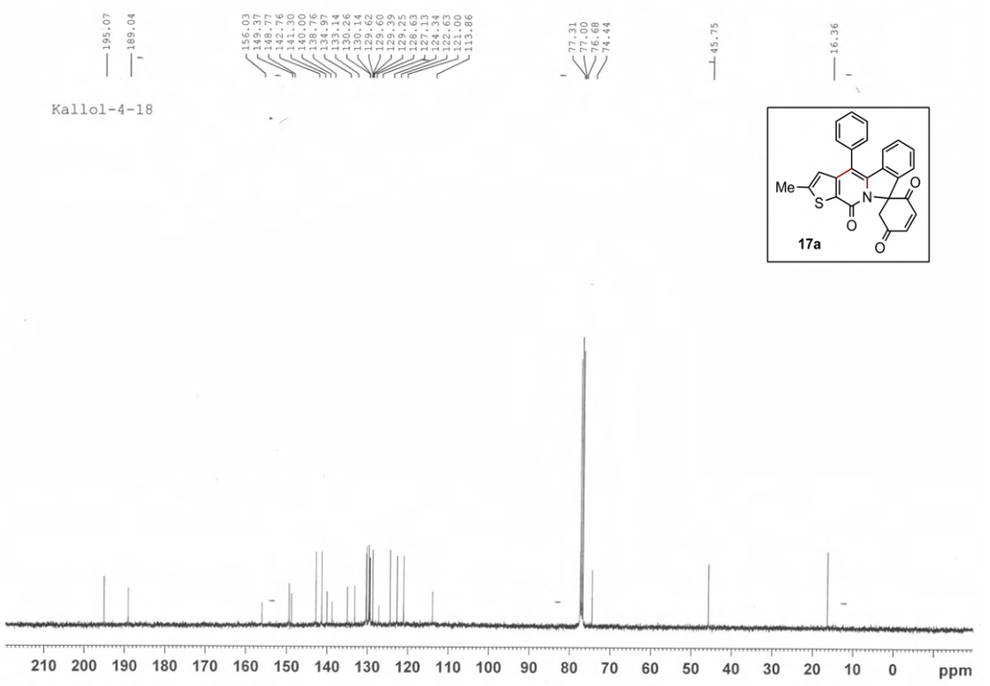
Kallol-4-18
17a

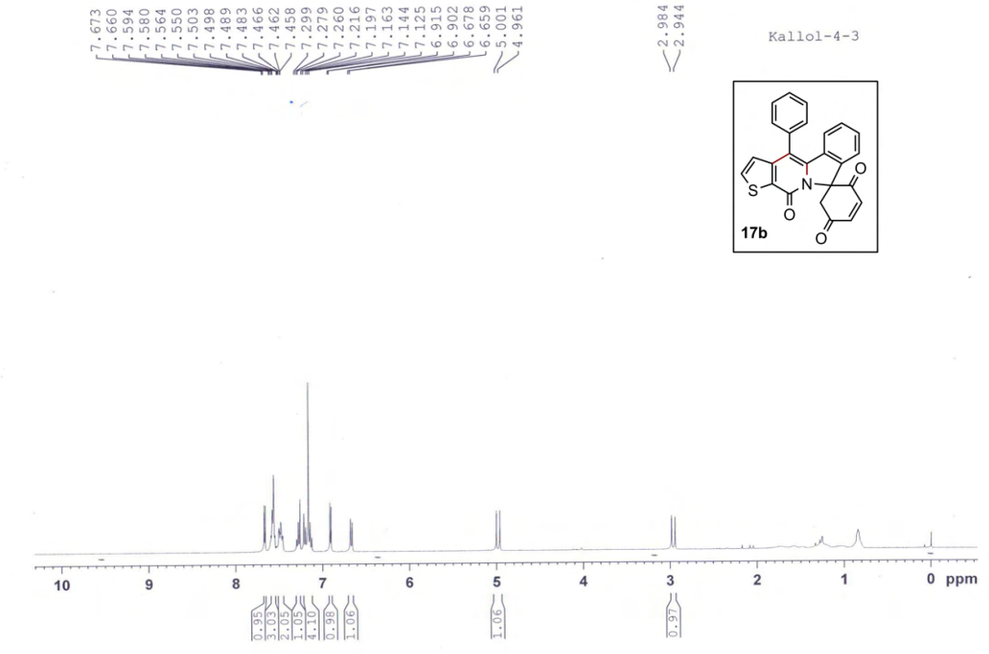
Kallol-4-3
17b

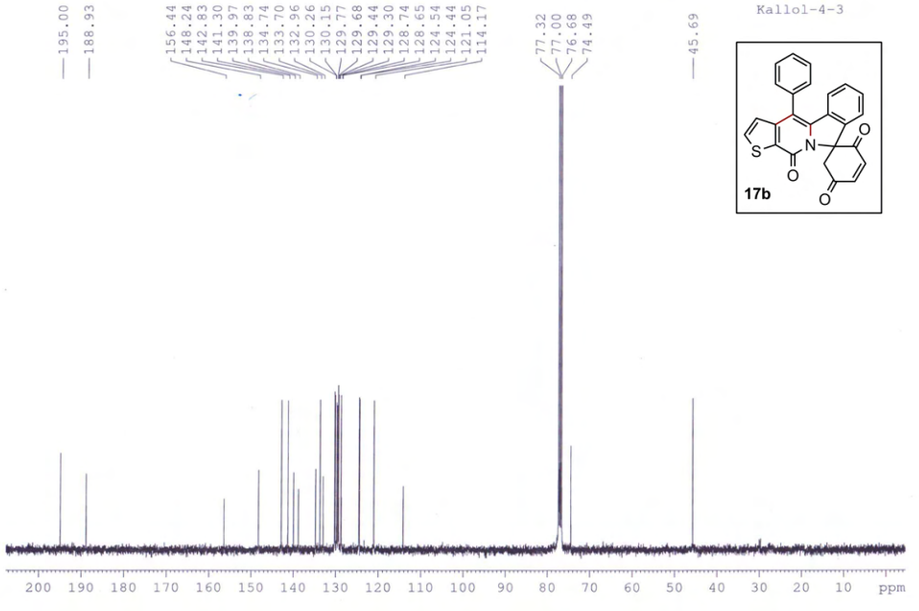
Kallol-4-3
17b

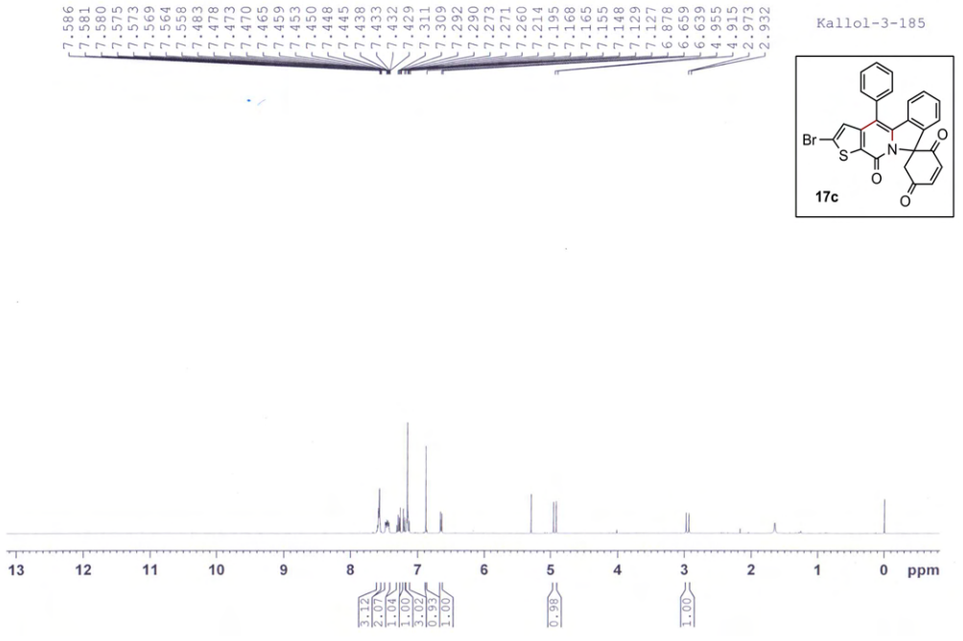
Kallol-3-185
17c
Br
S
N
O
O
O
13 12 11 10 9 8 7 6 5 4 3 2 1 0 ppm

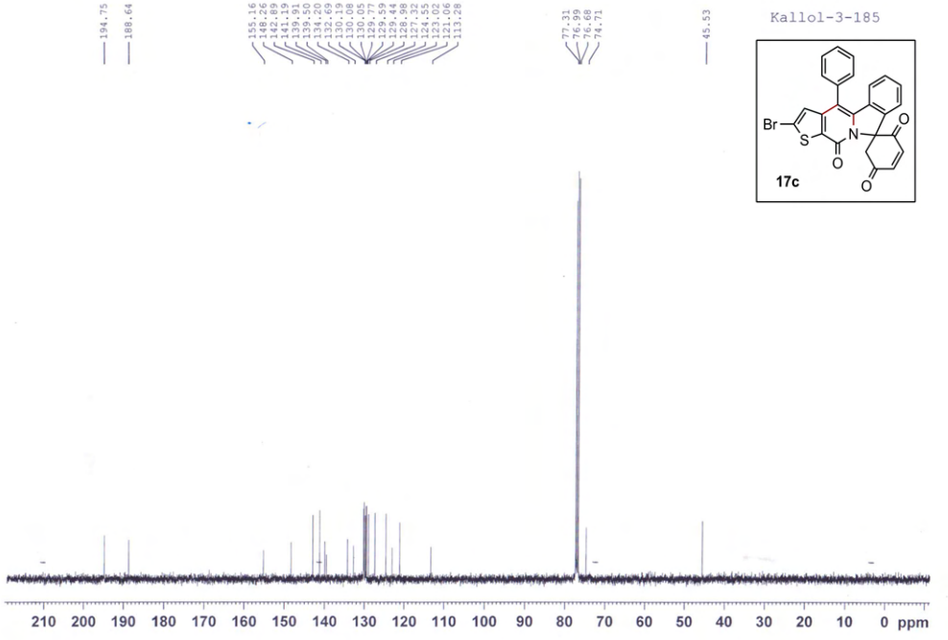
Kallol-3-185
17c
Br
S
N
O
O
O
210 200 190 180 170 160 150 140 130 120 110 100 90 80 70 60 50 40 30 20 10 0 ppm

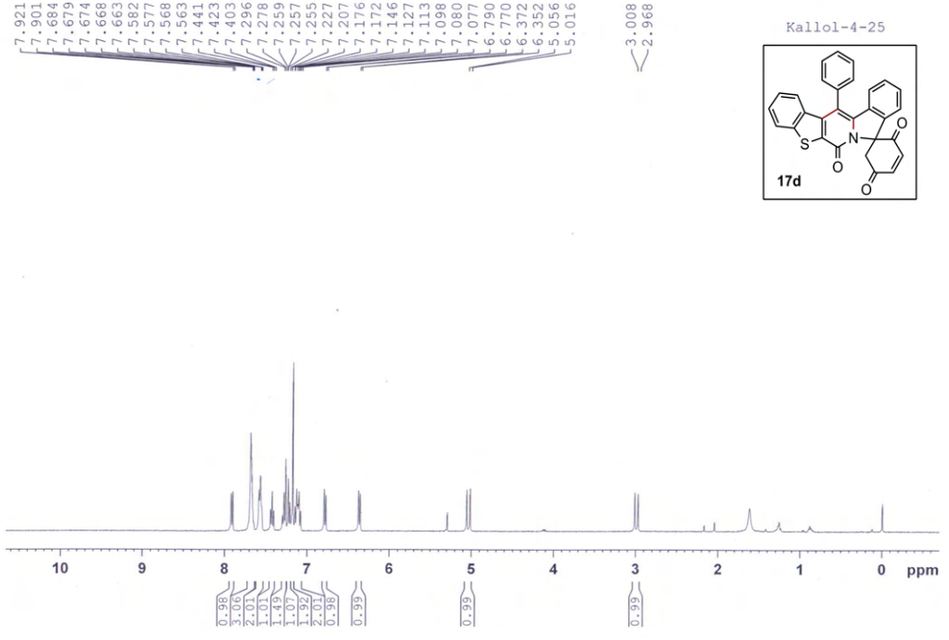
Kallol-4-25
17d
S
N
O
O
O
10 9 8 7 6 5 4 3 2 1 0 ppm

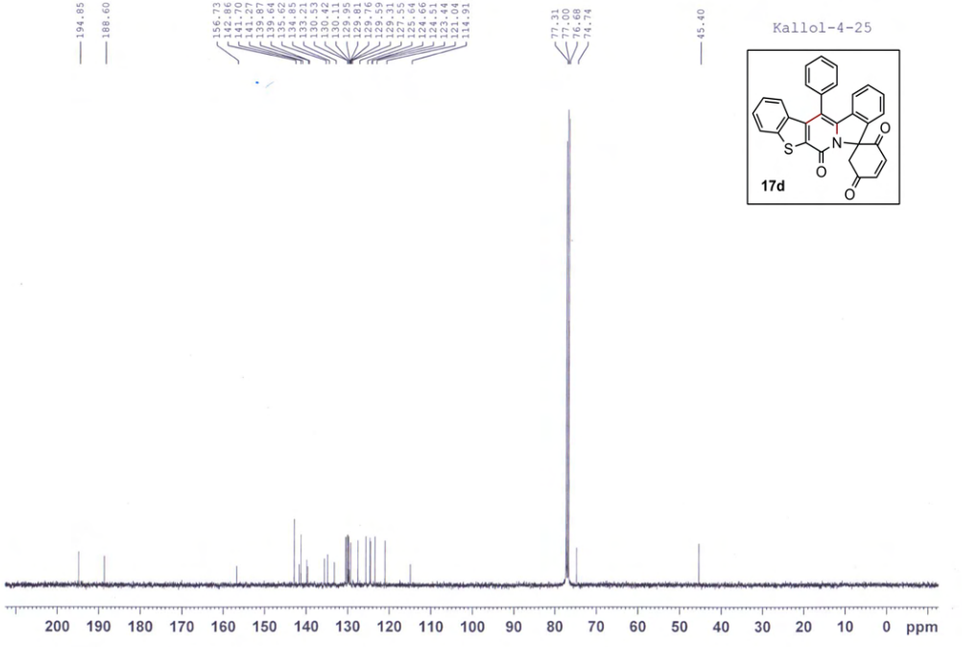
Kallol-4-25
17d
S
N
O
O
O
200 190 180 170 160 150 140 130 120 110 100 90 80 70 60 50 40 30 20 10 0 ppm

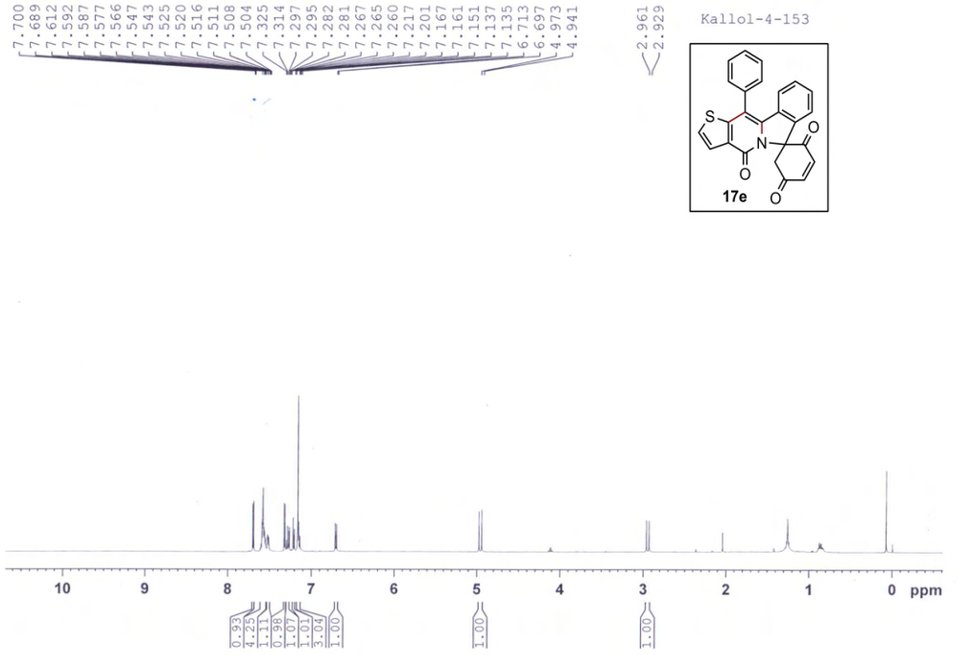
Kallol-4-153
17e

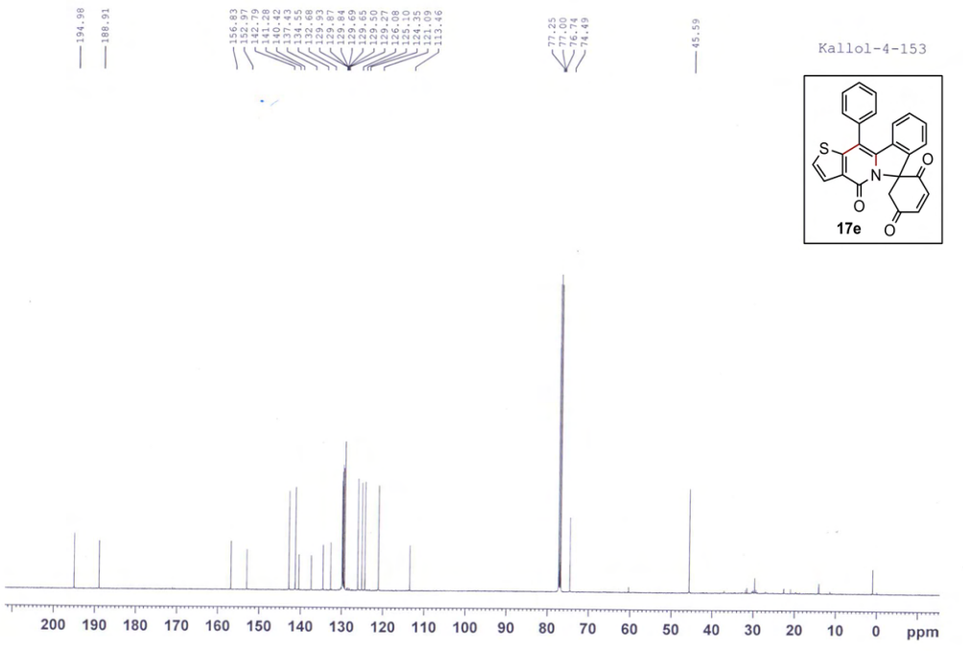
Kallol-4-153
17e

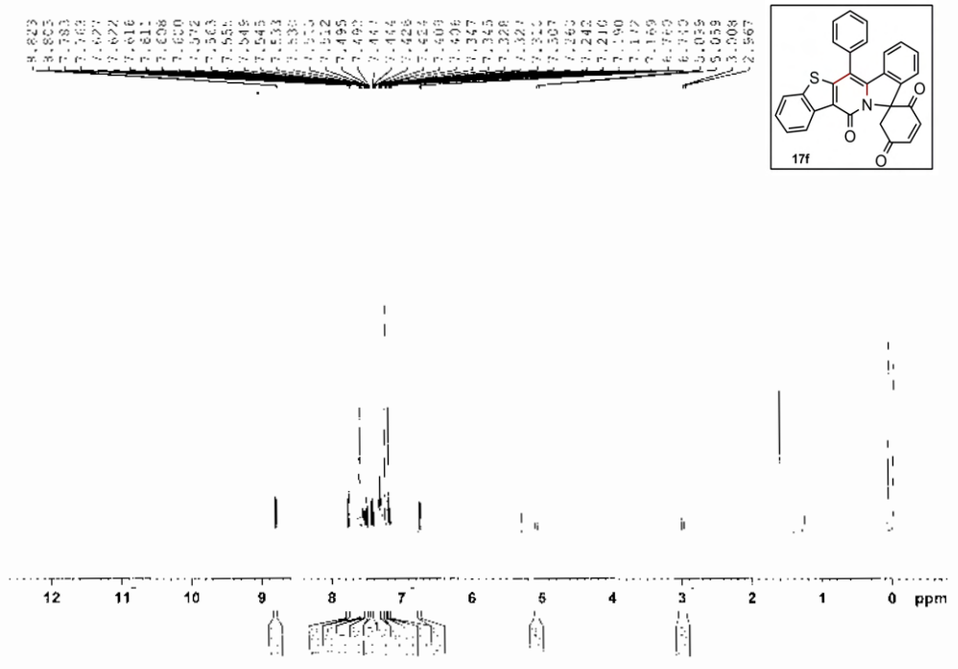
17f

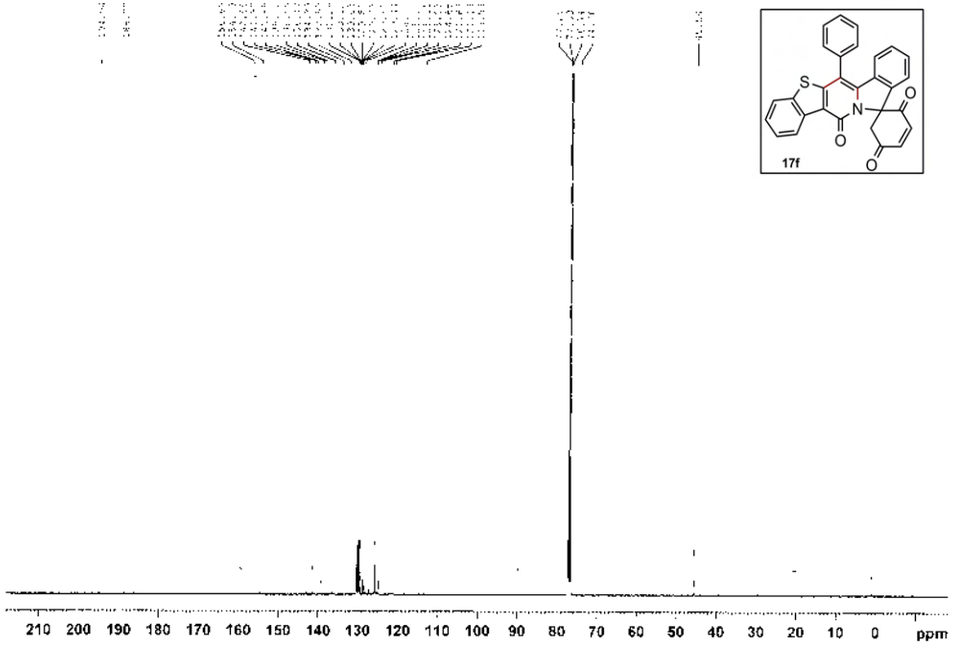
17f

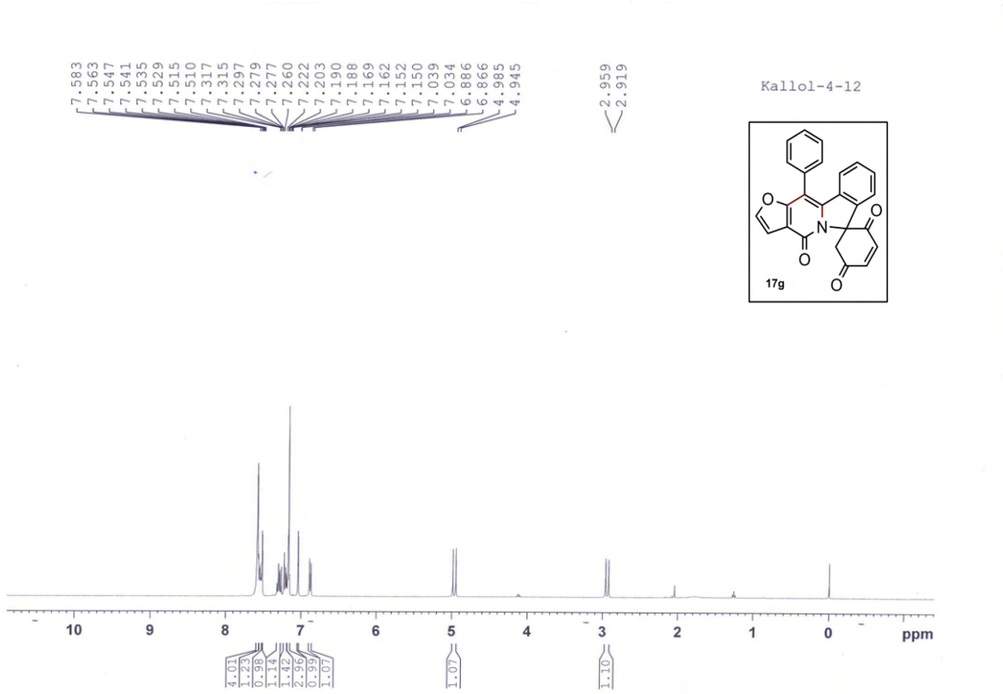
7.583
7.563
7.547
7.541
7.535
7.529
7.515
7.510
7.317
7.315
7.297
7.279
7.277
7.260
7.222
7.203
7.190
7.188
7.169
7.162
7.152
7.150
7.039
7.034
6.886
6.866
4.985
4.945
2.959
2.919
Kallol-4-12
17g
10 9 8 7 6 5 4 3 2 1 0 ppm
4.01
1.23
0.98
1.14
1.42
2.36
0.99
1.07
1.10

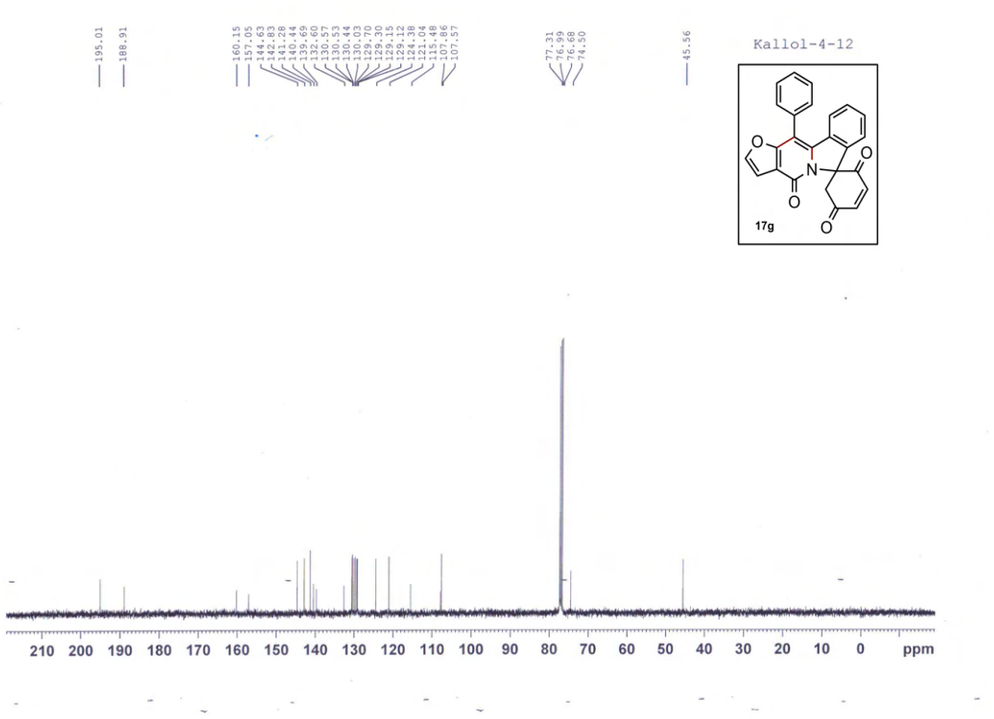
195.01
188.91
160.15
157.05
144.63
142.83
141.28
140.44
139.69
132.60
130.57
130.53
130.44
130.03
129.70
129.30
129.15
129.12
124.38
121.04
115.48
107.86
107.57
77.31
76.99
76.68
74.50
45.56
Kallol-4-12
17g
210 200 190 180 170 160 150 140 130 120 110 100 90 80 70 60 50 40 30 20 10 0 ppm

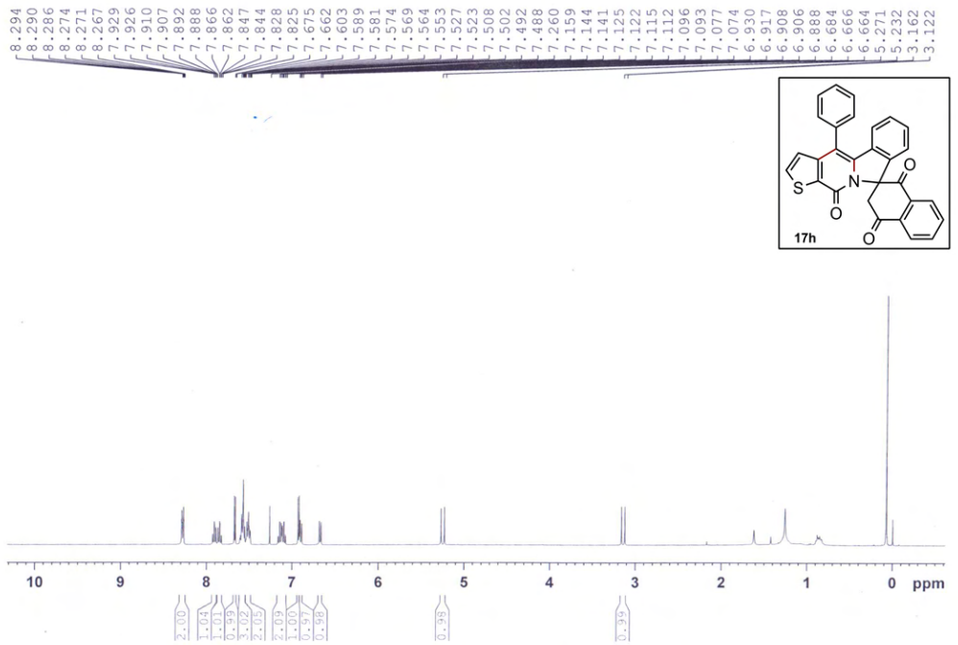
8.294
8.290
8.286
8.274
8.271
8.267
7.929
7.926
7.910
7.907
7.892
7.888
7.866
7.862
7.847
7.844
7.828
7.825
7.675
7.662
7.603
7.589
7.581
7.574
7.569
7.564
7.553
7.527
7.523
7.508
7.502
7.492
7.488
7.260
7.159
7.144
7.141
7.125
7.122
7.115
7.112
7.096
7.093
7.077
7.074
6.930
6.917
6.908
6.906
6.888
6.684
6.666
6.664
5.271
5.232
3.162
3.122
17h
10 9 8 7 6 5 4 3 2 1 0 ppm
2.00
1.04
1.01
0.99
3.02
2.05
2.09
1.00
0.97
0.98
0.99
0.99

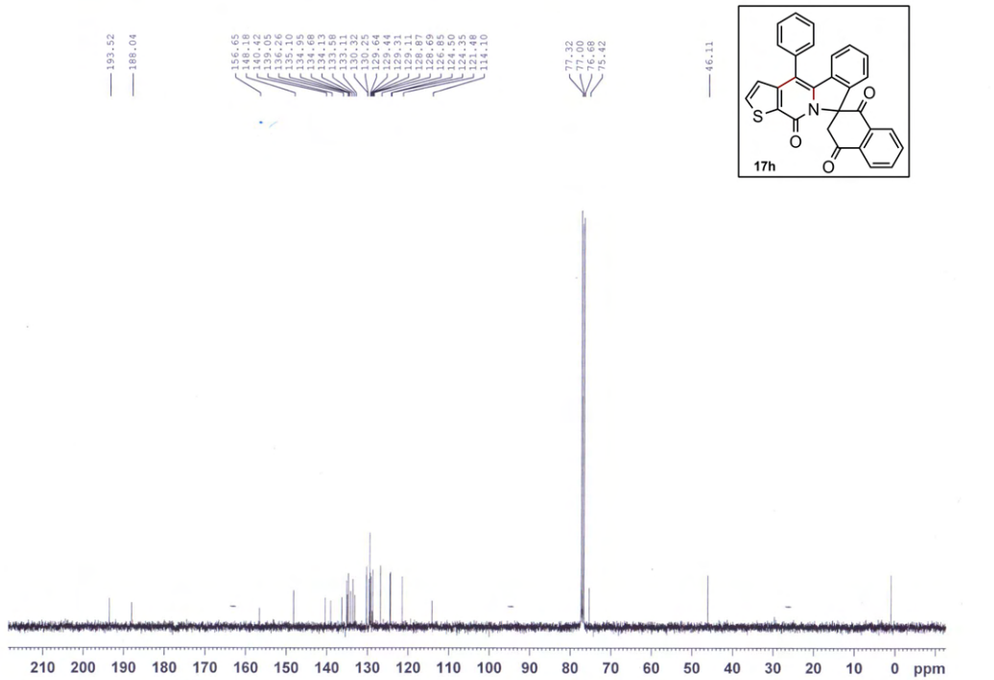
193.52
188.04
156.65
148.18
140.42
139.05
135.26
135.10
134.95
134.68
133.13
133.10
133.11
130.32
130.25
129.44
129.44
129.31
129.11
128.87
128.69
126.85
124.50
124.35
121.45
114.10
77.32
77.00
76.68
75.42
46.11
17h
210 200 190 180 170 160 150 140 130 120 110 100 90 80 70 60 50 40 30 20 10 0 ppm

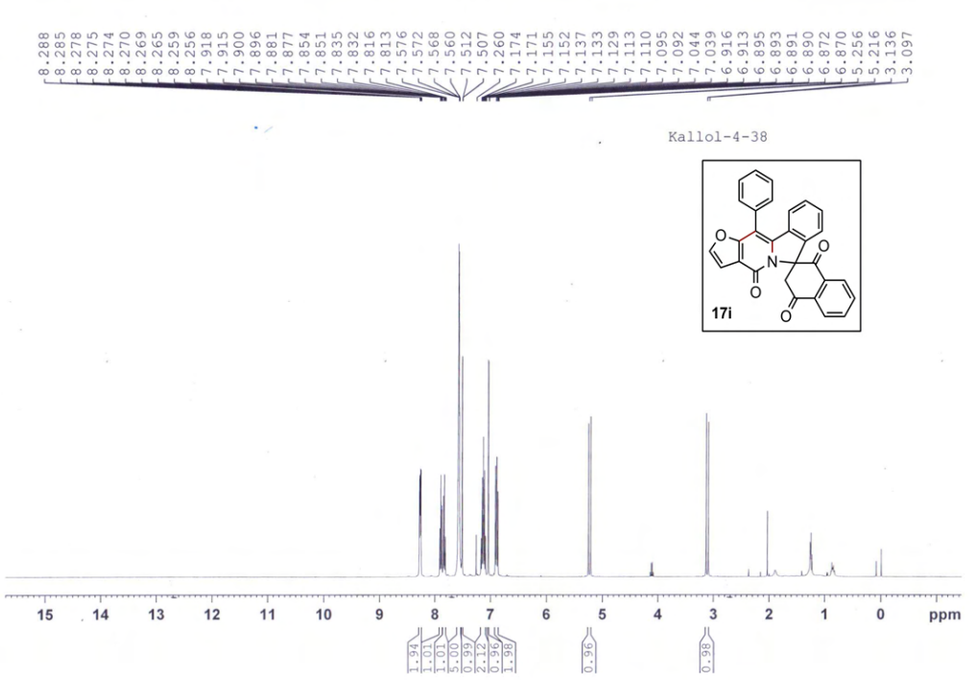
Kallol-4-38
17i

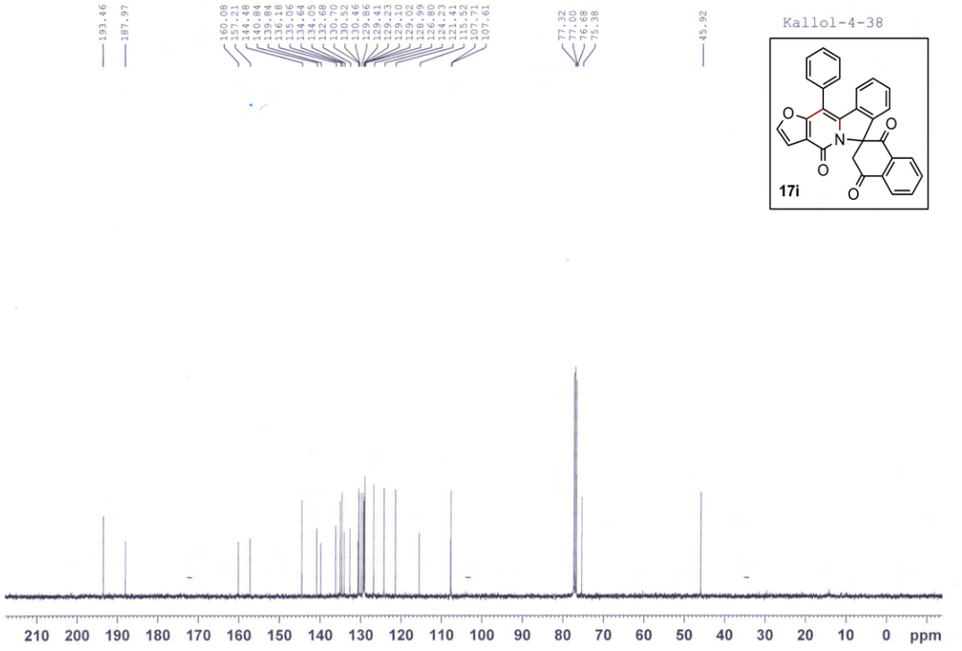
Kallol-4-38
17i

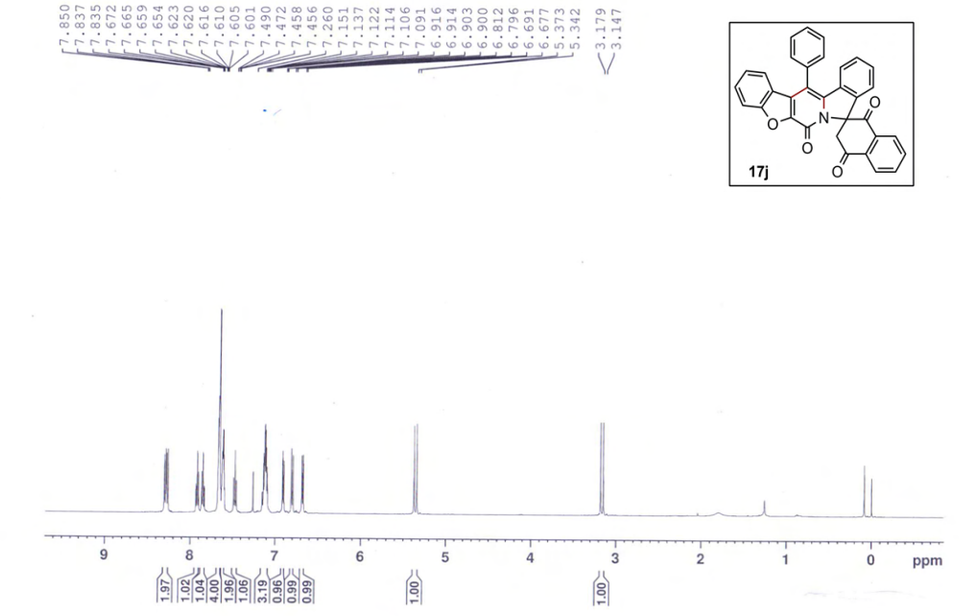
17j

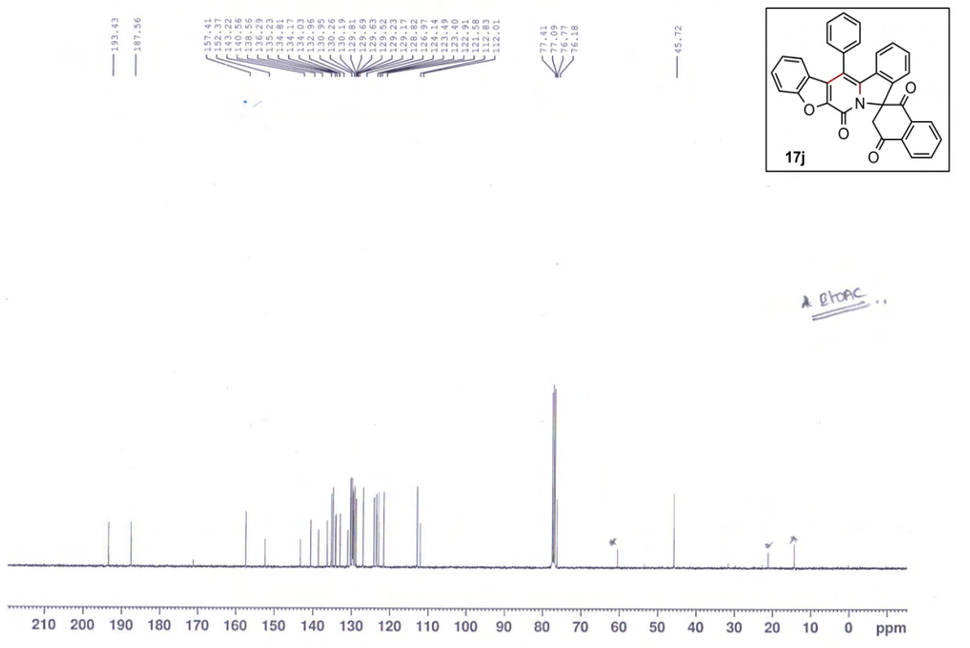
17j
A. EtOAc

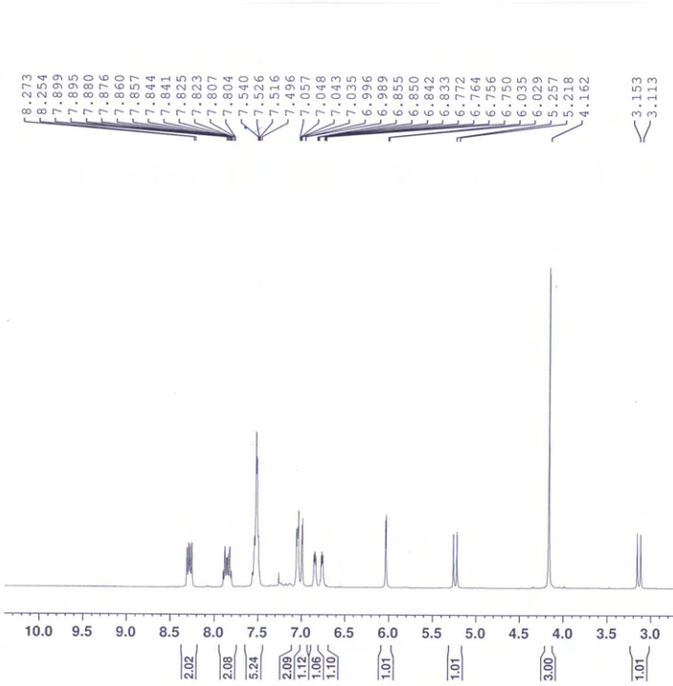
17k
ppm

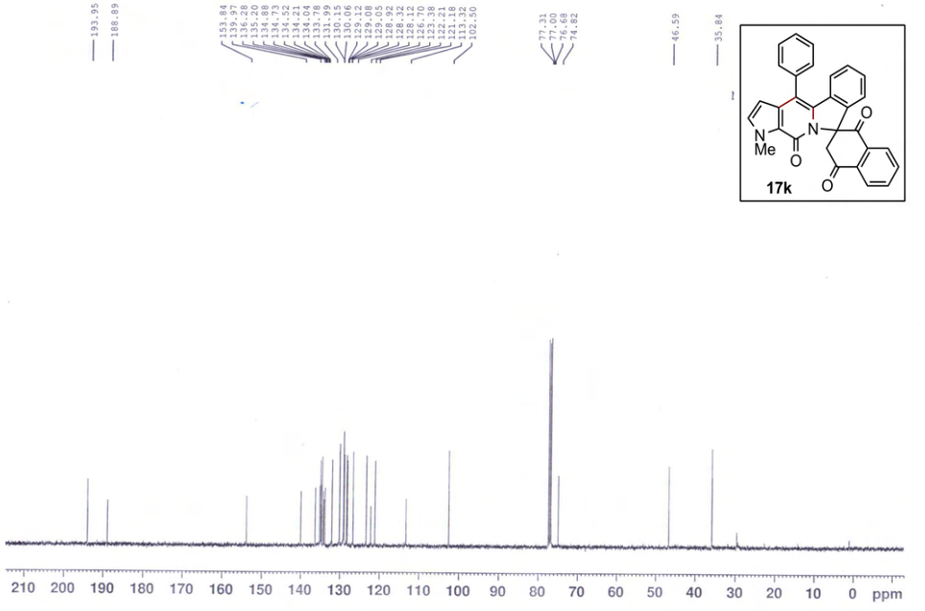
17k
ppm

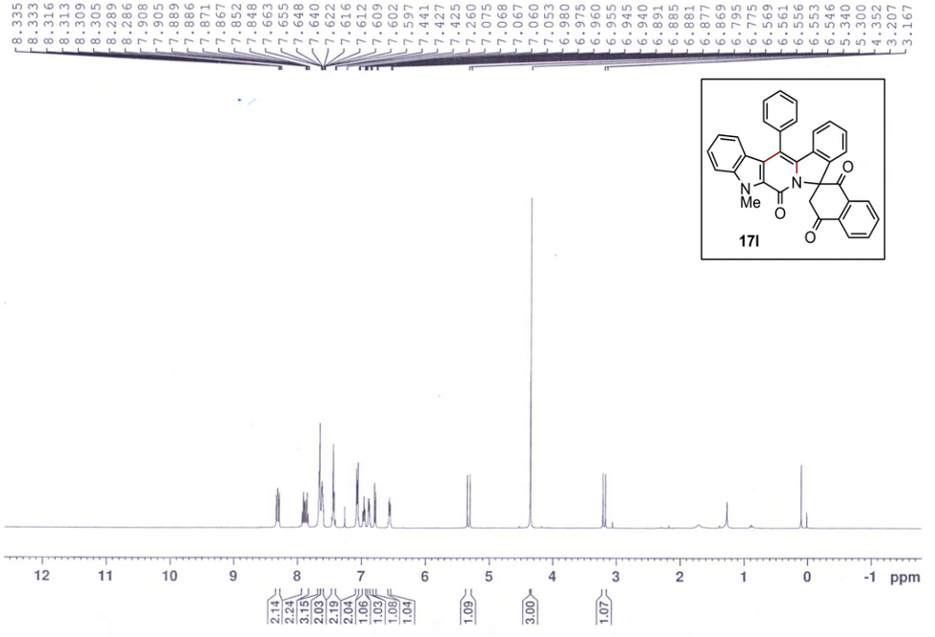
17l
ppm

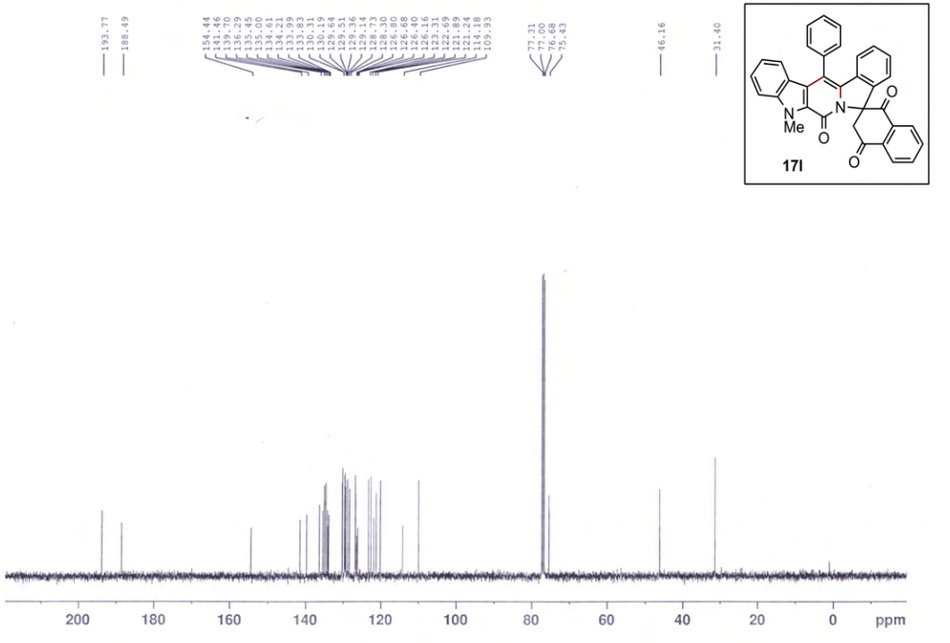
17l
ppm

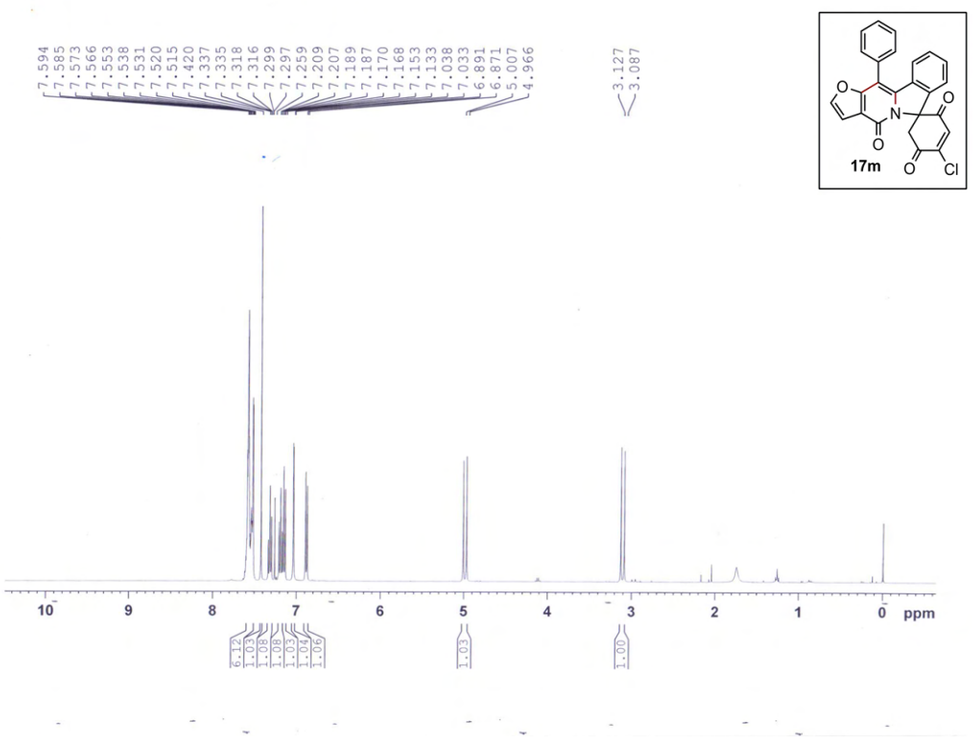
7.594
7.585
7.573
7.566
7.553
7.538
7.531
7.520
7.515
7.420
7.337
7.335
7.318
7.316
7.299
7.297
7.259
7.209
7.207
7.189
7.187
7.170
7.168
7.153
7.133
7.038
7.033
6.891
6.871
5.007
4.966
3.127
3.087
17m
O
Cl
10 9 8 7 6 5 4 3 2 1 0 ppm
6.12
1.03
1.08
1.08
1.08
1.03
1.04
1.06
1.03
1.00

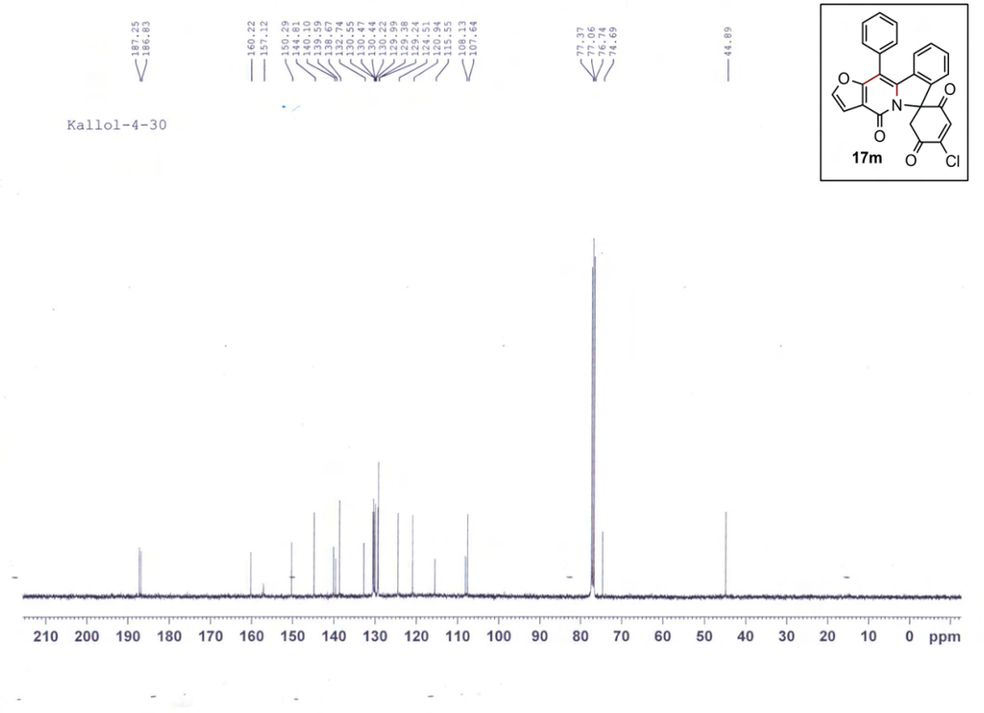
Kallol-4-30
187.25
186.83
160.22
157.12
150.29
144.81
140.10
139.59
138.67
134.74
130.55
130.47
130.44
130.22
129.99
129.38
129.24
129.11
128.94
125.55
108.13
107.64
77.37
77.06
76.74
74.69
44.89
17m
O
Cl
210 200 190 180 170 160 150 140 130 120 110 100 90 80 70 60 50 40 30 20 10 0 ppm

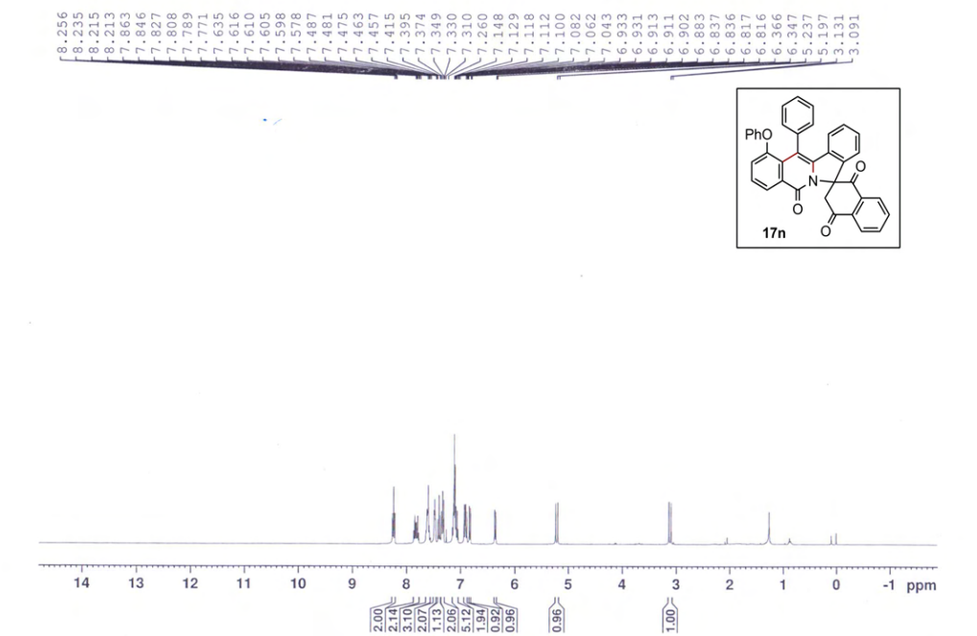
8.256
8.235
8.215
8.213
7.863
7.846
7.827
7.808
7.789
7.771
7.635
7.616
7.610
7.605
7.598
7.578
7.487
7.481
7.475
7.463
7.457
7.415
7.395
7.374
7.349
7.330
7.310
7.260
7.148
7.129
7.118
7.112
7.100
7.082
7.062
7.043
6.933
6.931
6.913
6.911
6.902
6.883
6.837
6.836
6.817
6.816
6.366
6.347
5.237
5.197
3.131
3.091
PhO
17n
O
14 13 12 11 10 9 8 7 6 5 4 3 2 1 0 -1 ppm
2.00
2.14
3.10
2.07
1.13
2.06
5.12
1.94
0.92
0.96
0.96
1.00

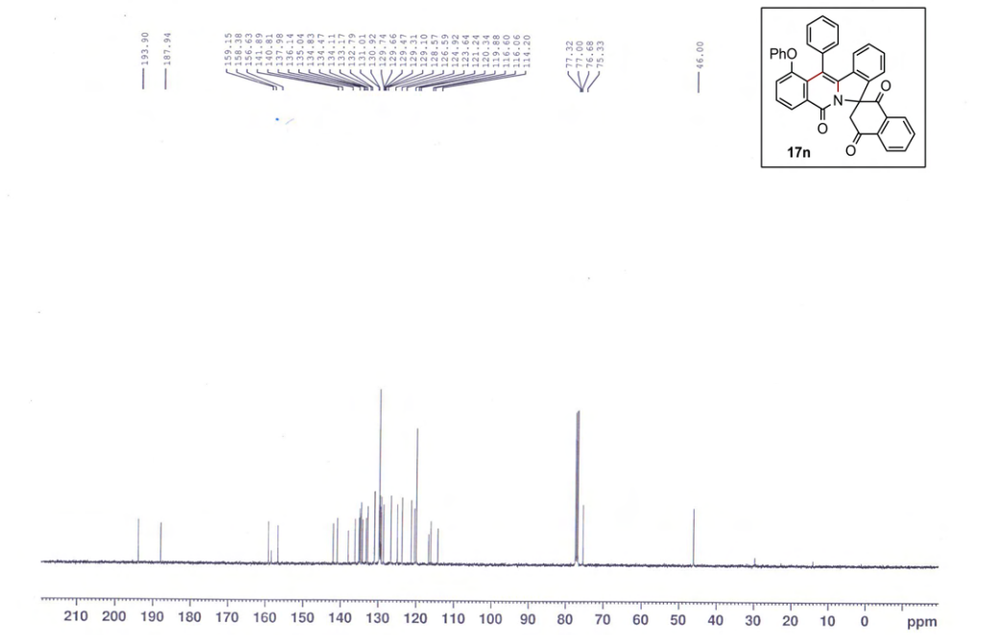
193.90
187.94
159.15
158.38
156.63
140.89
140.81
137.98
136.14
135.64
134.83
134.47
134.11
133.77
132.79
131.01
130.92
130.76
129.66
129.47
129.31
129.10
128.57
126.59
124.92
124.64
121.24
120.34
118.88
116.60
116.06
114.20
77.32
77.00
76.68
75.33
46.00
PhO
17n
O
210 200 190 180 170 160 150 140 130 120 110 100 90 80 70 60 50 40 30 20 10 0 ppm

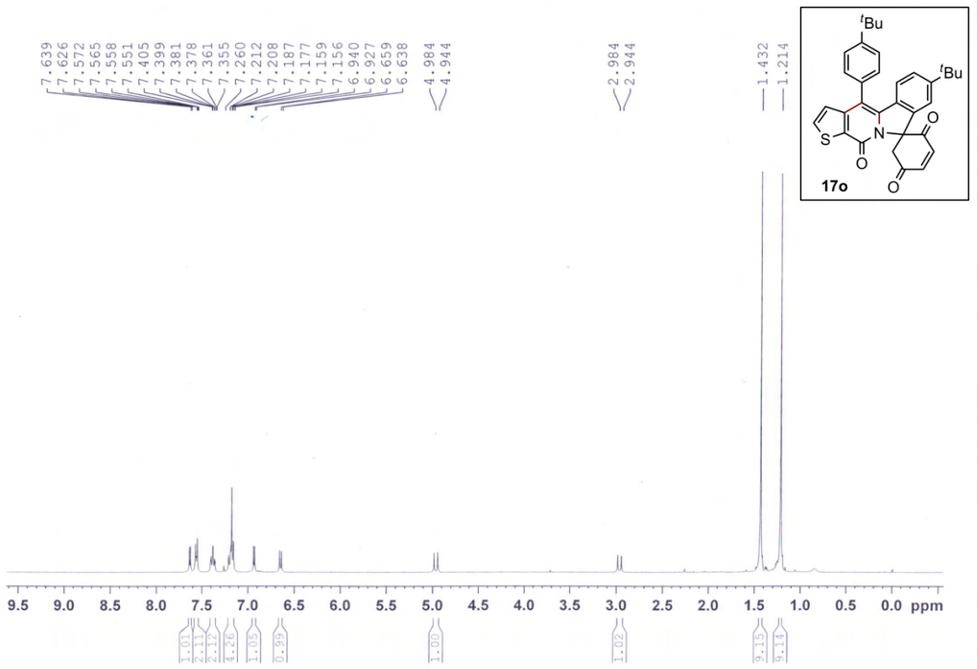
7.639
7.626
7.572
7.565
7.558
7.551
7.405
7.399
7.381
7.378
7.361
7.355
7.260
7.212
7.208
7.187
7.177
7.159
7.156
6.940
6.927
6.659
6.638
4.984
4.944
2.984
2.944
1.432
1.214
tBu
tBu
17o
9.5 9.0 8.5 8.0 7.5 7.0 6.5 6.0 5.5 5.0 4.5 4.0 3.5 3.0 2.5 2.0 1.5 1.0 0.5 0.0 ppm
1.01
2.11
2.12
4.46
1.05
0.99
1.00
1.02
9.15
9.14

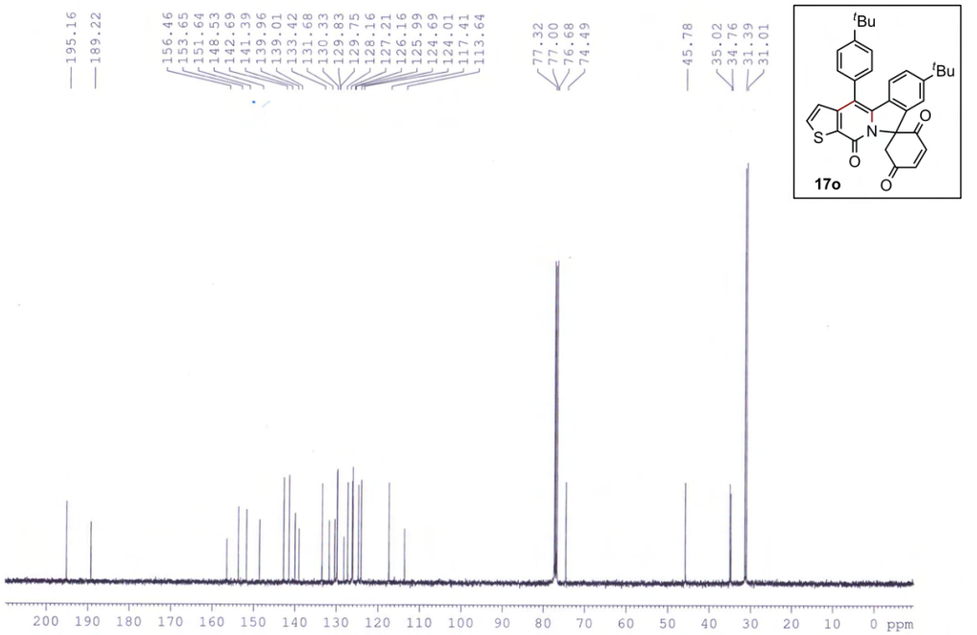
195.16
189.22
156.46
153.65
151.64
148.53
142.69
141.39
139.96
139.01
133.42
131.68
130.33
129.83
129.75
128.16
127.21
126.16
125.99
124.69
124.01
117.41
113.64
77.32
77.00
76.68
74.49
45.78
35.02
34.76
31.39
31.01
tBu
tBu
17o
200 190 180 170 160 150 140 130 120 110 100 90 80 70 60 50 40 30 20 10 0 ppm

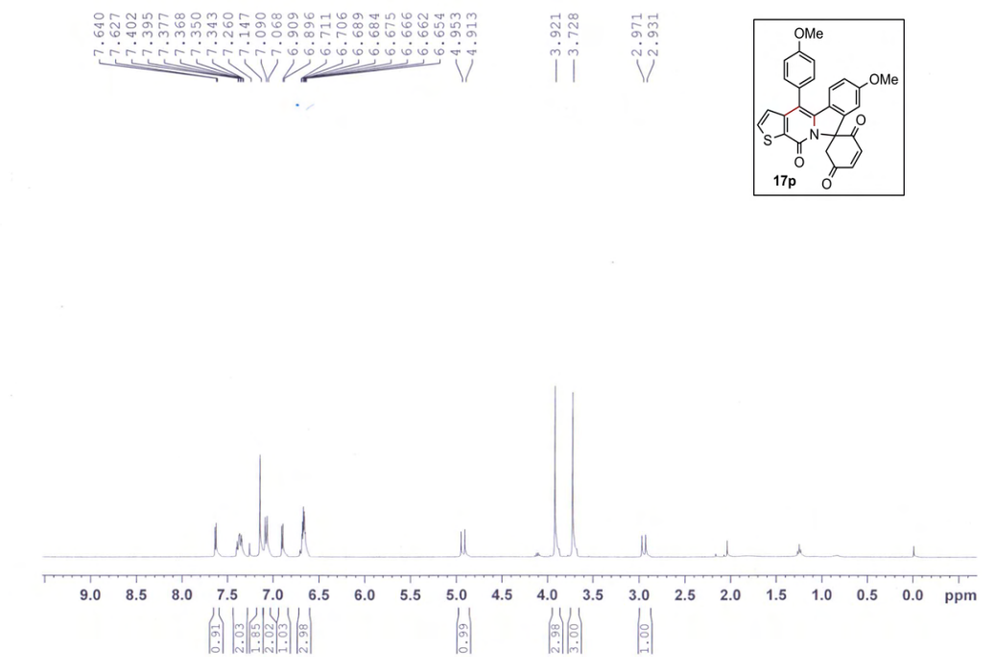
7.640
7.627
7.402
7.395
7.377
7.368
7.350
7.343
7.260
7.147
7.090
7.068
6.909
6.896
6.711
6.706
6.689
6.684
6.675
6.666
6.662
6.654
4.953
4.913
3.921
3.728
2.971
2.931
OMe
OMe
17p
9.0 8.5 8.0 7.5 7.0 6.5 6.0 5.5 5.0 4.5 4.0 3.5 3.0 2.5 2.0 1.5 1.0 0.5 0.0 ppm
0.91
2.03
1.85
2.02
1.03
2.98
0.99
2.98
3.00
1.00

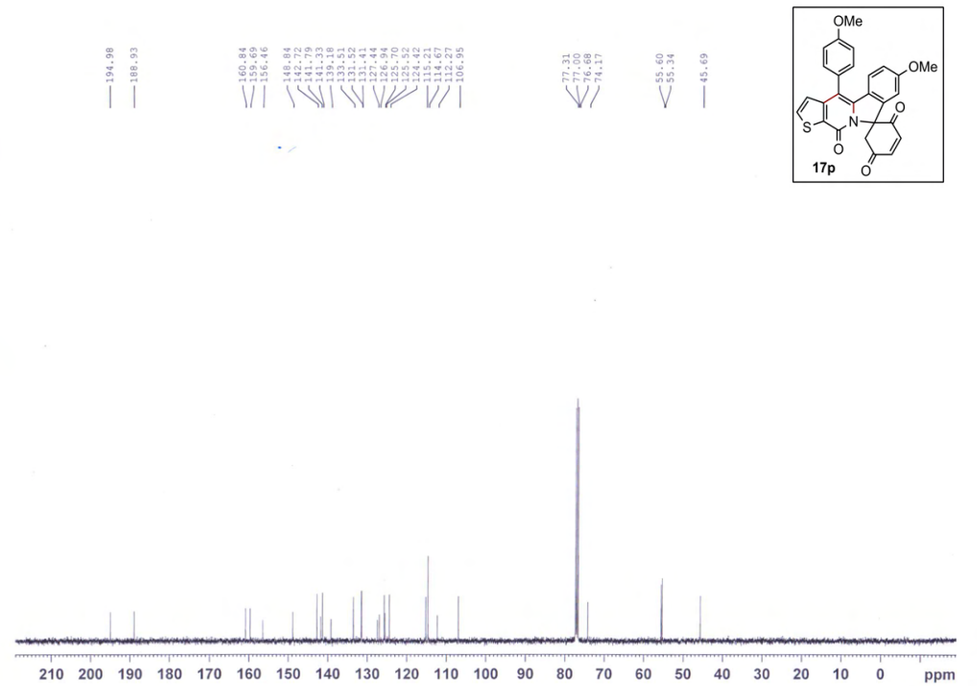
194.98
188.93
160.84
160.09
156.46
148.84
141.72
141.29
139.18
133.51
132.52
131.41
127.44
126.94
125.70
125.52
124.42
115.21
112.67
112.27
106.95
77.31
77.00
76.68
74.17
55.60
55.34
45.69
OMe
OMe
17p
210 200 190 180 170 160 150 140 130 120 110 100 90 80 70 60 50 40 30 20 10 0 ppm

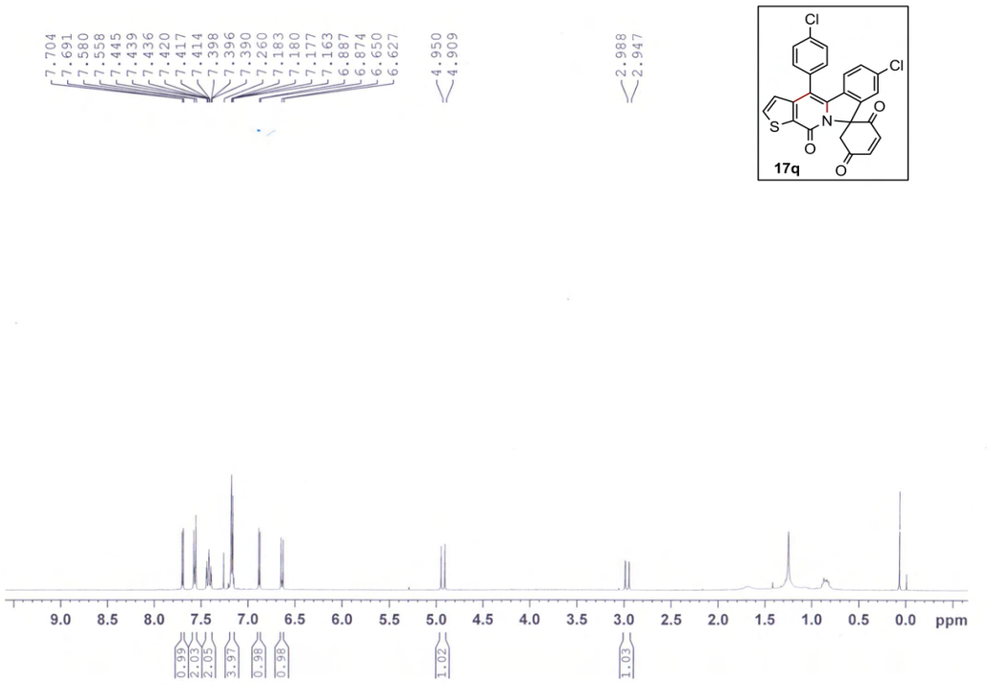
7.704
7.691
7.580
7.558
7.445
7.439
7.436
7.420
7.417
7.414
7.398
7.396
7.390
7.260
7.183
7.180
7.177
7.163
6.887
6.874
6.650
6.627
4.950
4.909
2.988
2.947
17q
9.0 8.5 8.0 7.5 7.0 6.5 6.0 5.5 5.0 4.5 4.0 3.5 3.0 2.5 2.0 1.5 1.0 0.5 0.0 ppm
0.99
2.03
2.05
3.97
0.98
0.98
1.02
1.03

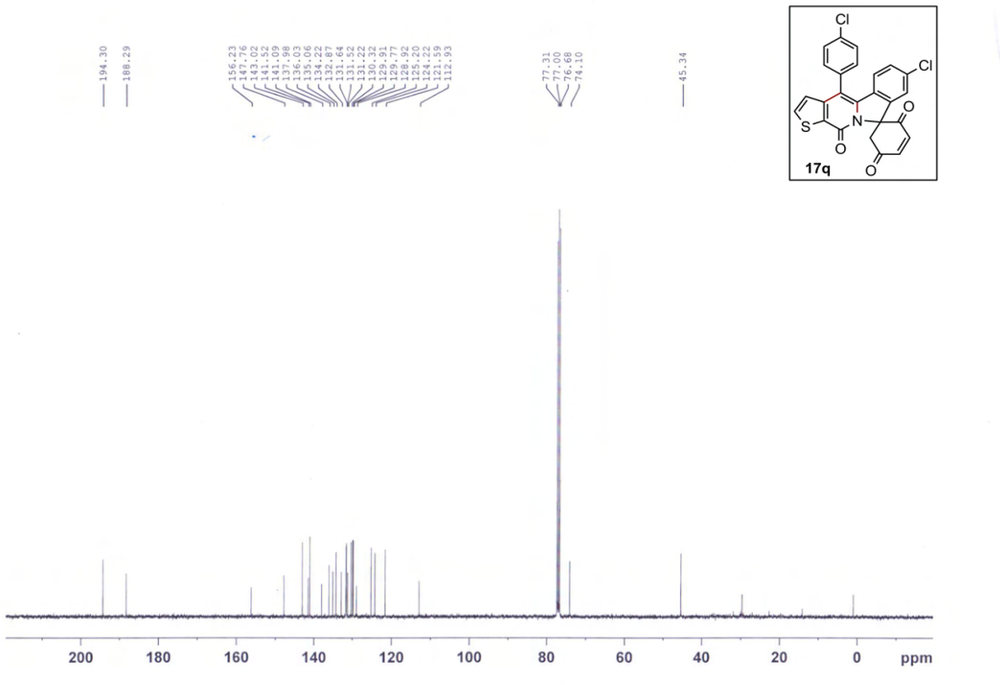
194.30
188.29
156.23
147.76
143.02
141.52
141.09
137.98
136.13
135.06
134.22
132.87
131.64
131.22
130.32
129.91
129.77
128.92
125.20
124.22
123.59
112.93
77.31
77.00
76.68
74.10
45.34
17q
200 180 160 140 120 100 80 60 40 20 0 ppm

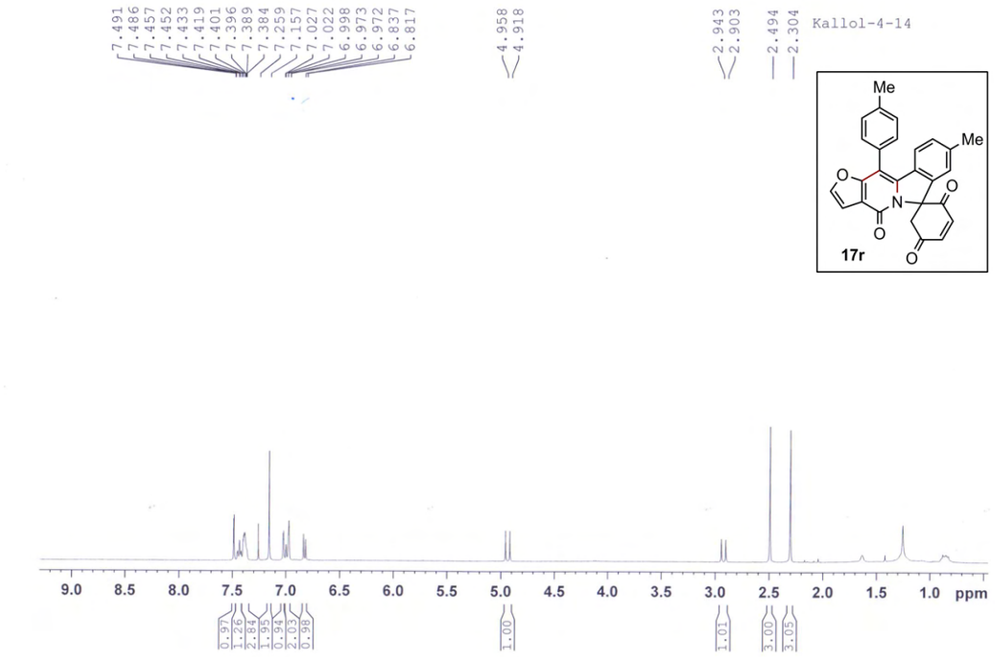
7.491
7.486
7.457
7.452
7.433
7.419
7.401
7.396
7.389
7.384
7.259
7.157
7.027
7.022
6.998
6.973
6.972
6.837
6.817
4.958
4.918
2.943
2.903
2.494
2.304
Kallol-4-14
17r
9.0 8.5 8.0 7.5 7.0 6.5 6.0 5.5 5.0 4.5 4.0 3.5 3.0 2.5 2.0 1.5 1.0 ppm
0.97
1.26
2.84
1.95
0.94
2.03
0.98
1.00
1.01
3.00
3.05

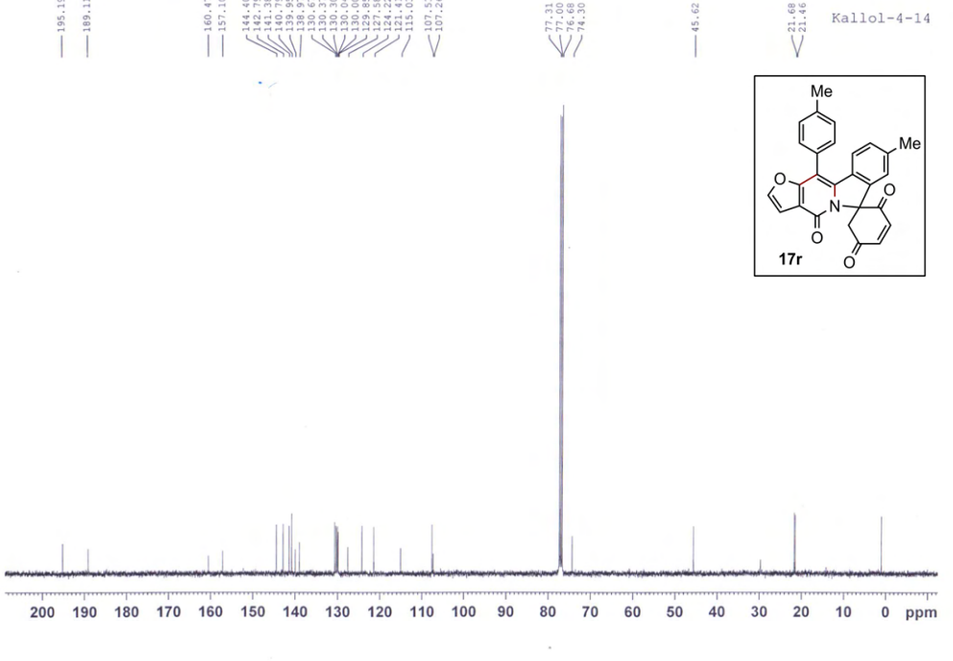
195.19
189.11
160.47
157.10
144.40
142.79
141.38
139.39
139.05
138.97
130.67
130.37
130.10
130.04
130.00
129.85
124.38
124.22
121.41
115.03
107.53
107.26
77.31
77.00
76.68
74.30
45.62
21.68
21.46
Kallol-4-14
17r
200 190 180 170 160 150 140 130 120 110 100 90 80 70 60 50 40 30 20 10 0 ppm

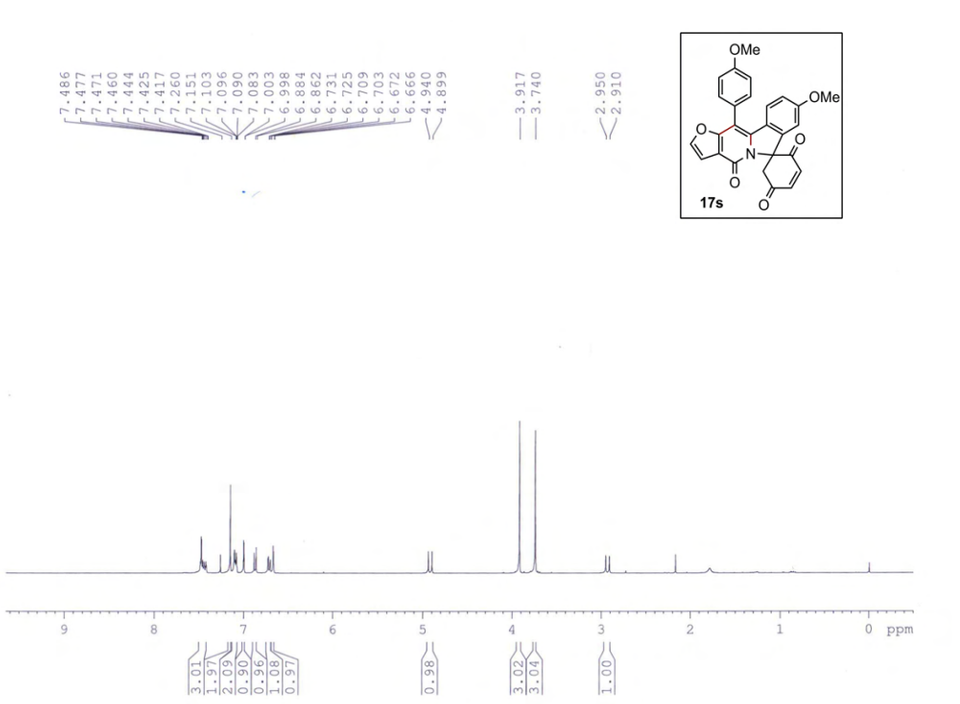
7.486
7.477
7.471
7.460
7.444
7.425
7.417
7.260
7.151
7.103
7.096
7.090
7.083
7.003
6.998
6.884
6.862
6.731
6.725
6.709
6.703
6.672
6.666
4.940
4.899
3.917
3.740
2.950
2.910
OMe
OMe
17s
9 8 7 6 5 4 3 2 1 0 ppm
3.01
1.97
2.09
0.90
0.96
1.08
0.97
0.98
3.02
3.04
1.00

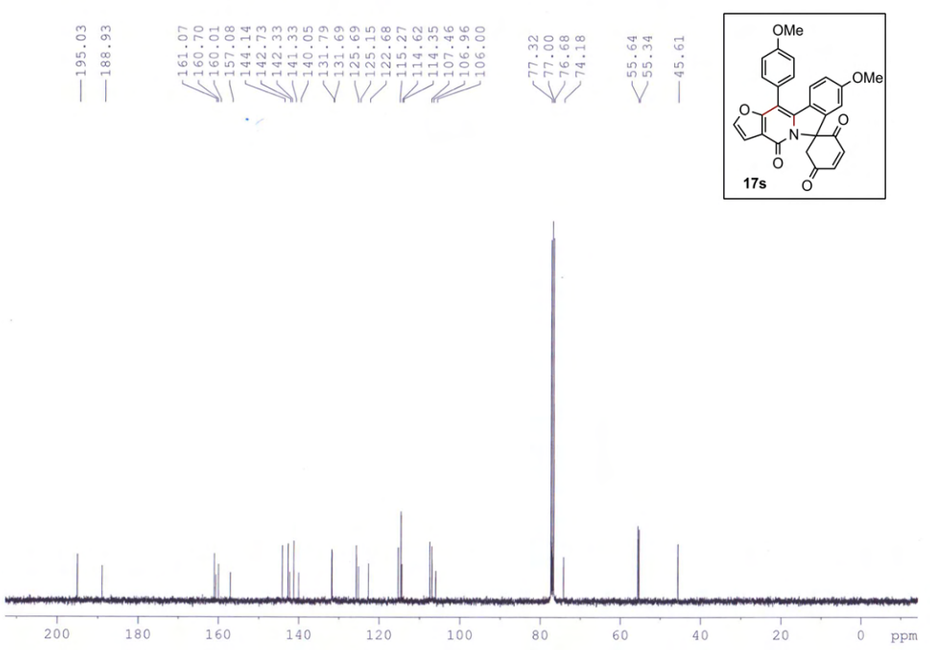
195.03
188.93
161.07
160.70
160.01
157.08
144.14
142.73
142.33
141.33
140.05
131.79
131.69
125.69
125.15
122.68
115.27
114.62
114.35
107.46
106.96
106.00
77.32
77.00
76.68
74.18
55.64
55.34
45.61
OMe
OMe
17s
200 180 160 140 120 100 80 60 40 20 0 ppm

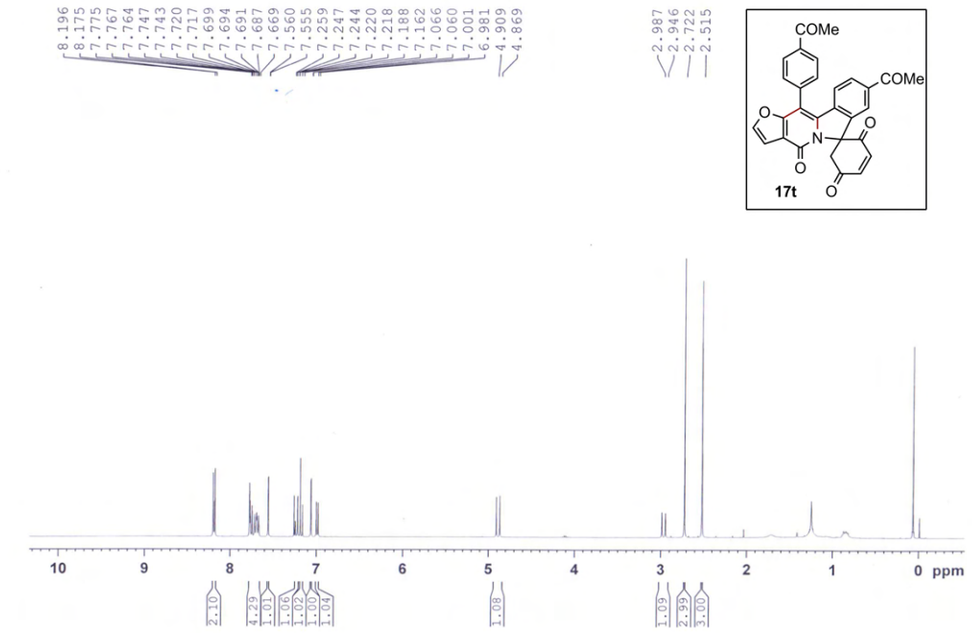
8.196
8.175
7.775
7.767
7.764
7.747
7.743
7.720
7.717
7.699
7.694
7.691
7.687
7.669
7.560
7.555
7.259
7.247
7.244
7.220
7.218
7.188
7.162
7.066
7.060
7.001
6.981
4.909
4.869
2.987
2.946
2.722
2.515
COMe
COMe
17t
10 9 8 7 6 5 4 3 2 1 0 ppm
2.10
4.29
1.01
1.06
1.02
1.00
1.04
1.08
1.09
2.99
3.00

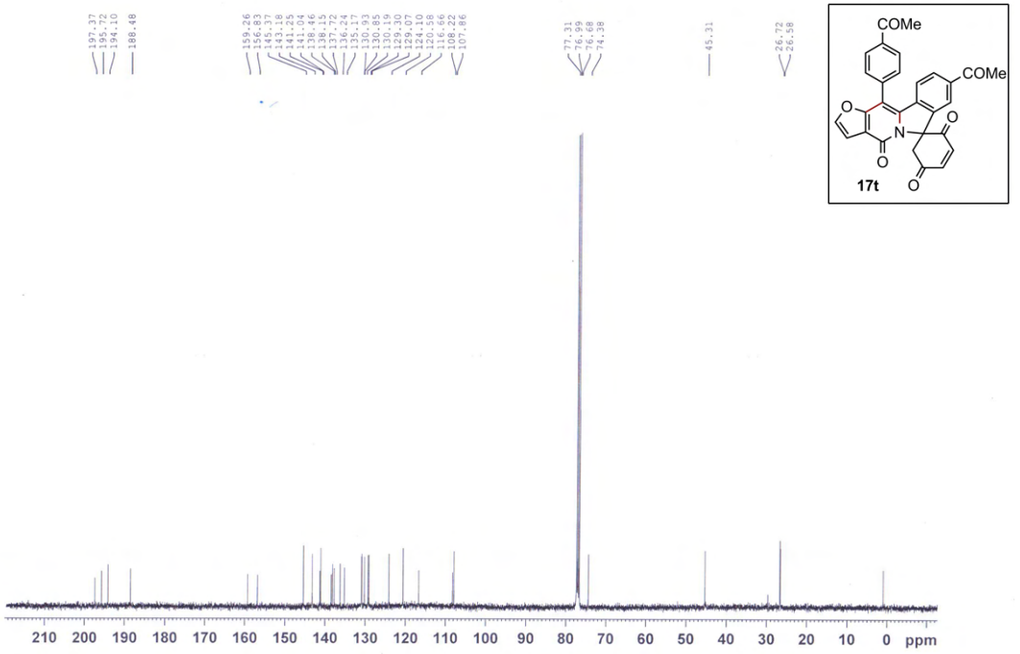
197.37
195.72
194.10
188.48
159.26
156.83
145.37
143.18
141.55
141.04
138.46
138.15
137.22
136.24
135.17
130.93
130.46
130.34
129.30
129.07
124.10
122.88
116.66
108.22
107.86
77.31
76.99
76.68
74.38
45.31
26.72
26.58
COMe
COMe
17t
210 200 190 180 170 160 150 140 130 120 110 100 90 80 70 60 50 40 30 20 10 0 ppm

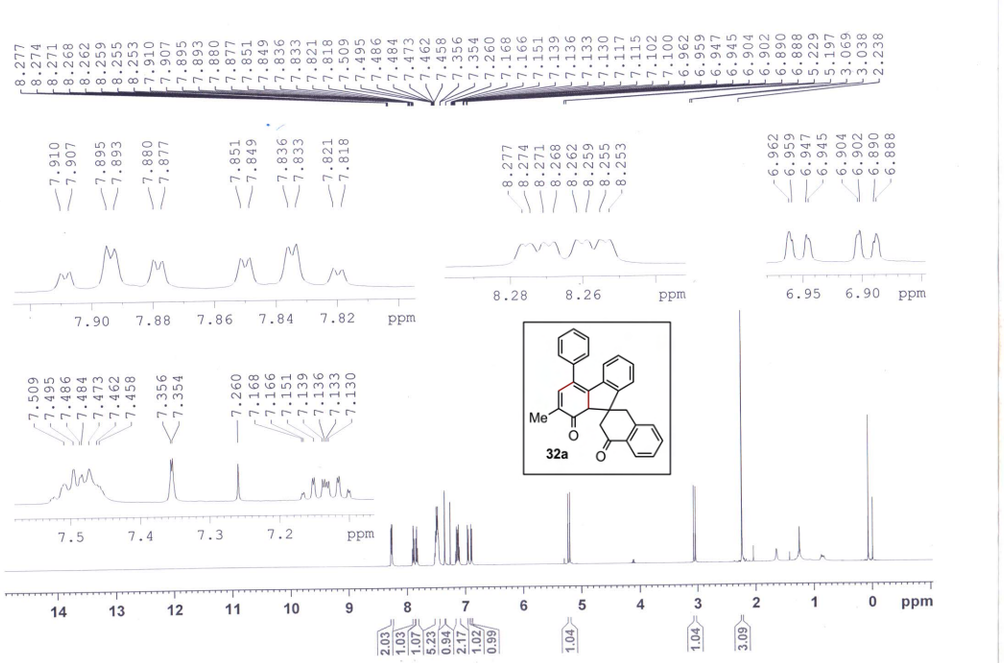
32a
ppm

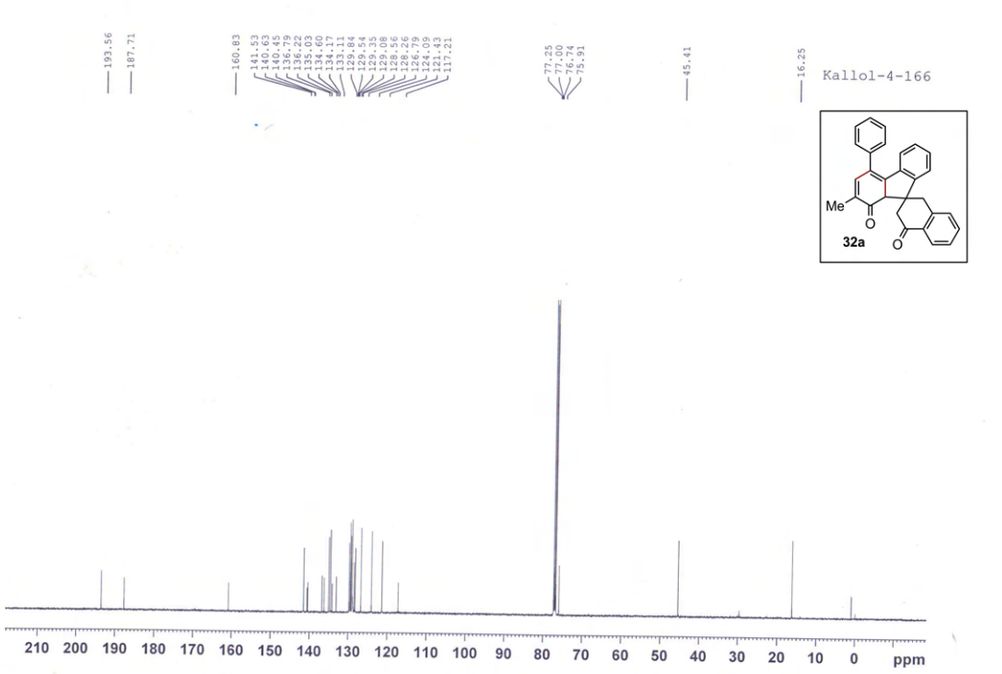
Kallol-4-166
32a
ppm

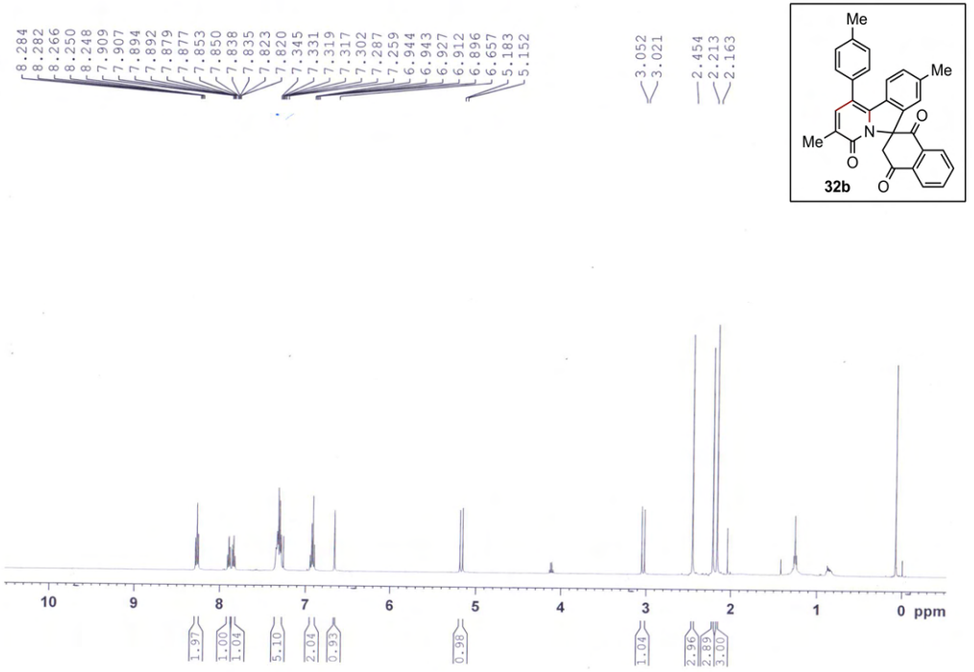
32b
ppm

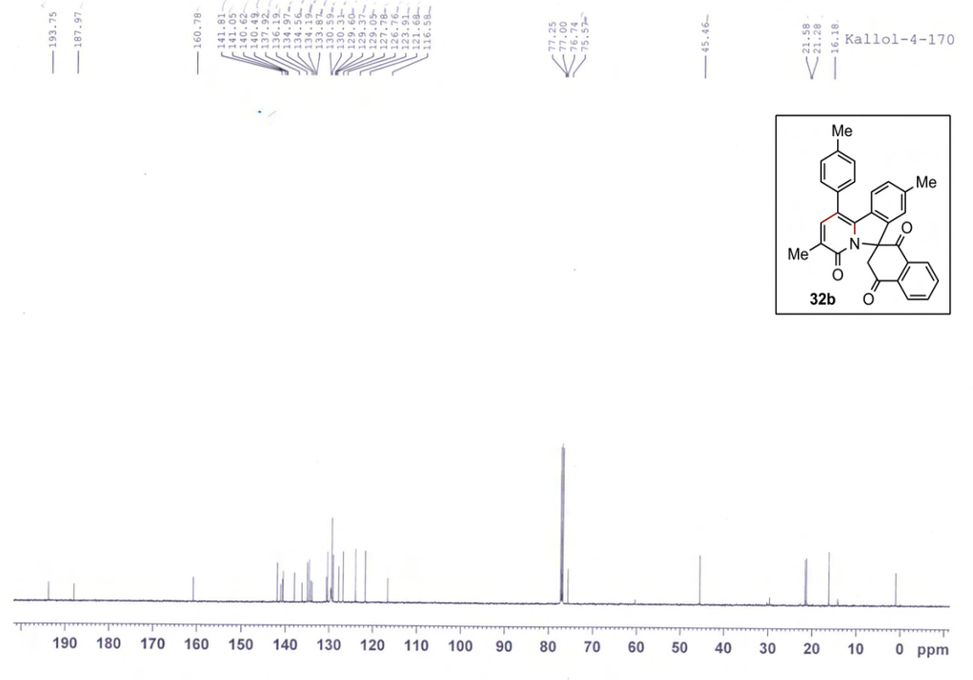
Kallol-4-170
32b
ppm

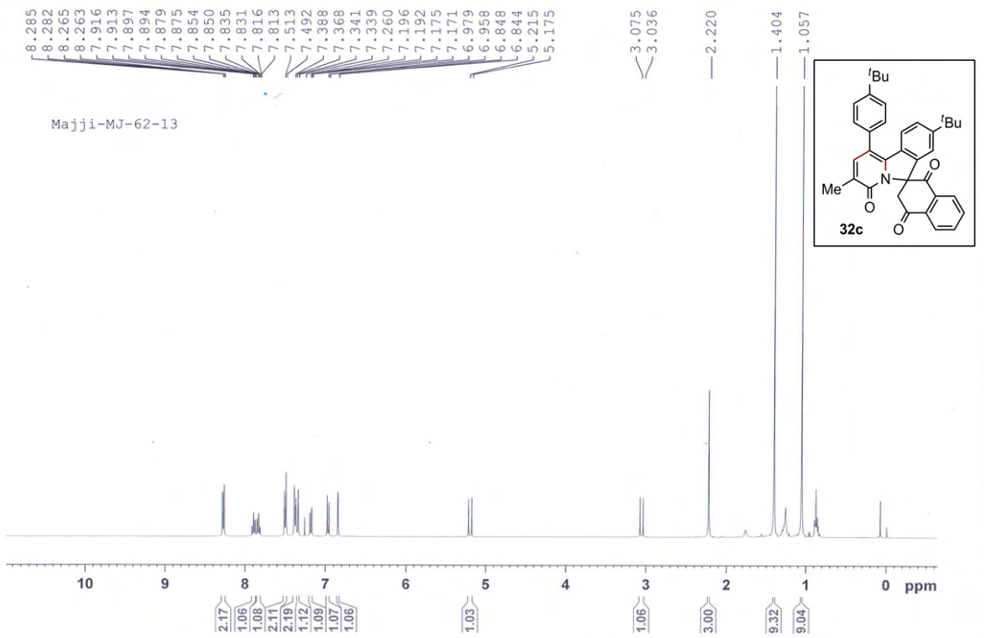
Majji-MJ-62-13
32c

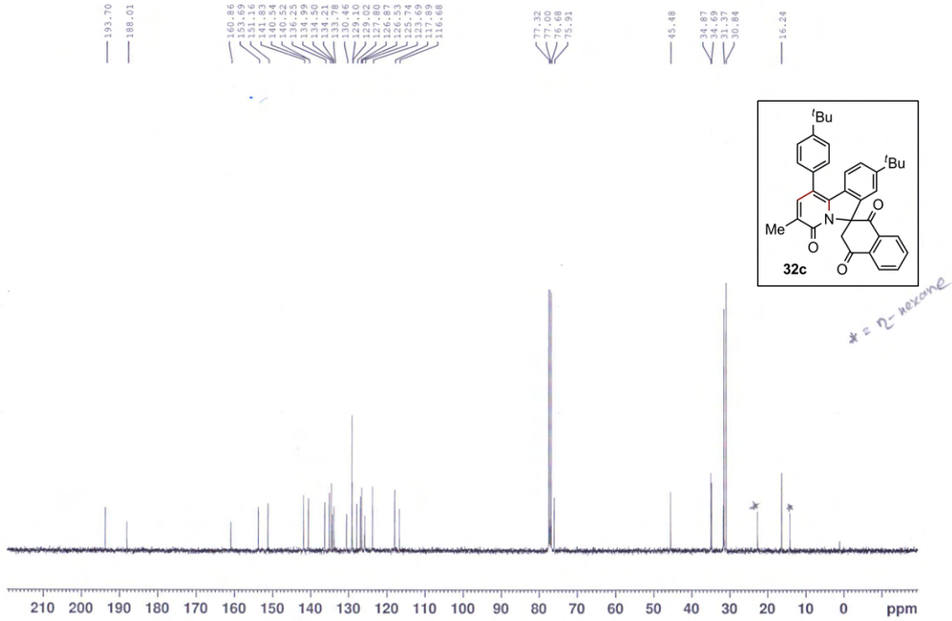
32c
* = n- hexane

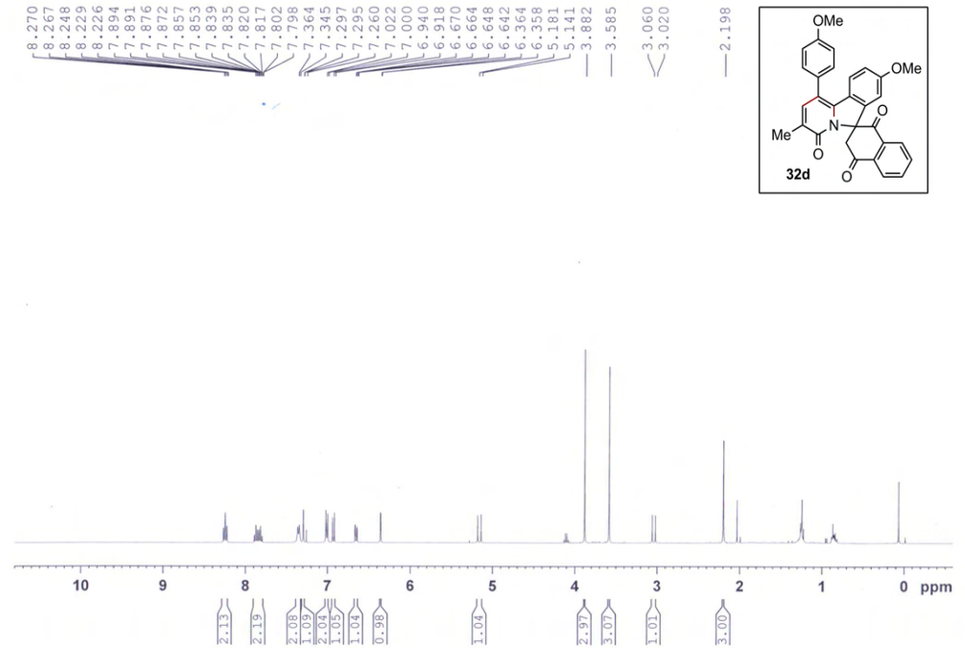
32d

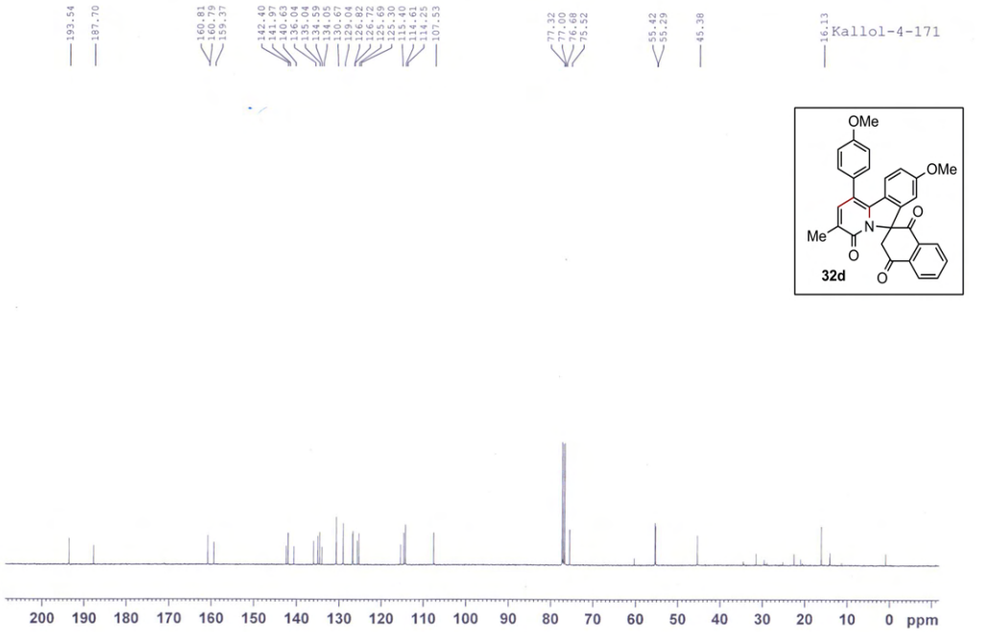
Kallol-4-171
32d

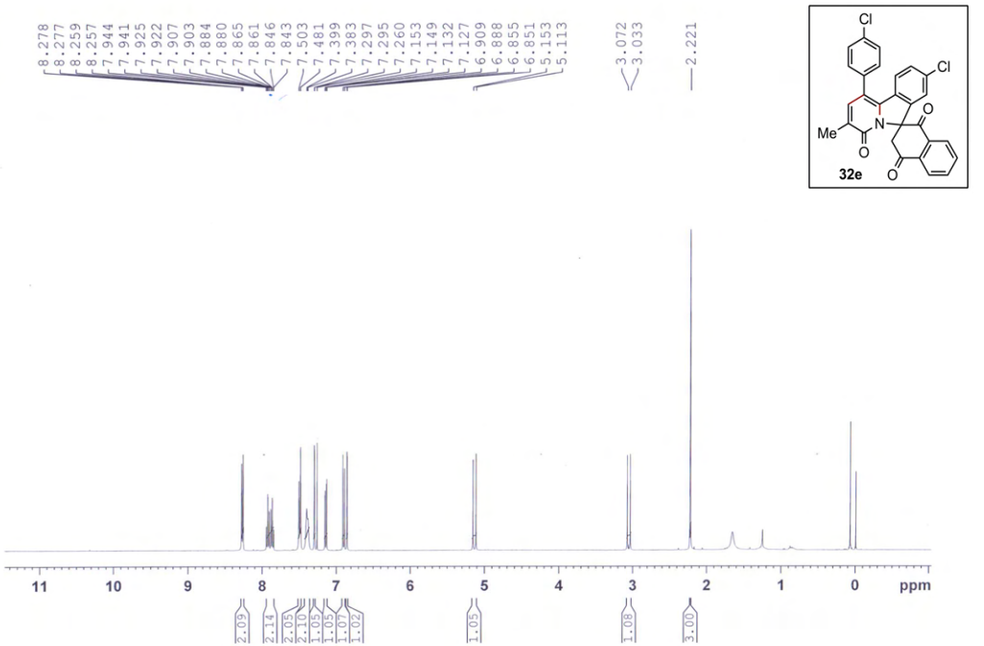
8.278
8.277
8.259
8.257
7.944
7.941
7.925
7.922
7.907
7.903
7.884
7.880
7.865
7.861
7.846
7.843
7.503
7.481
7.399
7.383
7.297
7.295
7.260
7.153
7.149
7.132
7.127
6.909
6.888
6.855
6.851
5.153
5.113
3.072
3.033
2.221
Cl
Cl
Me
O
N
O
O
32e
11 10 9 8 7 6 5 4 3 2 1 0 ppm
2.09 2.14 2.05 2.10 1.05 1.05 1.07 1.02 1.05 1.08 3.00

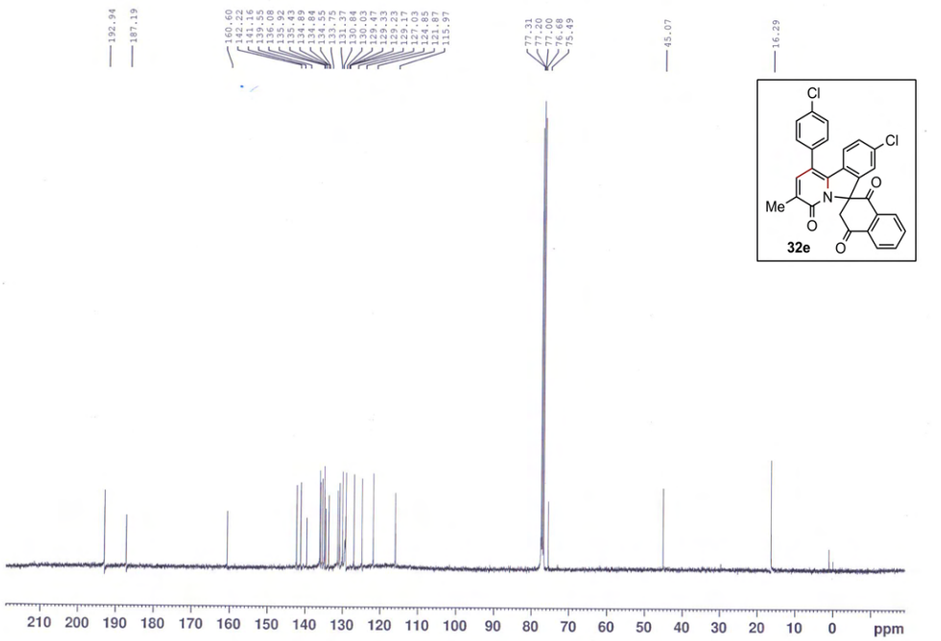
192.94
187.19
160.60
142.22
141.16
139.55
138.08
135.92
135.43
134.89
134.64
134.55
133.75
131.37
130.84
130.03
129.47
129.33
129.23
129.17
127.03
126.85
121.87
115.97
77.31
77.00
76.68
75.49
45.07
16.29
Cl
Cl
Me
O
N
O
O
32e
210 200 190 180 170 160 150 140 130 120 110 100 90 80 70 60 50 40 30 20 10 0 ppm

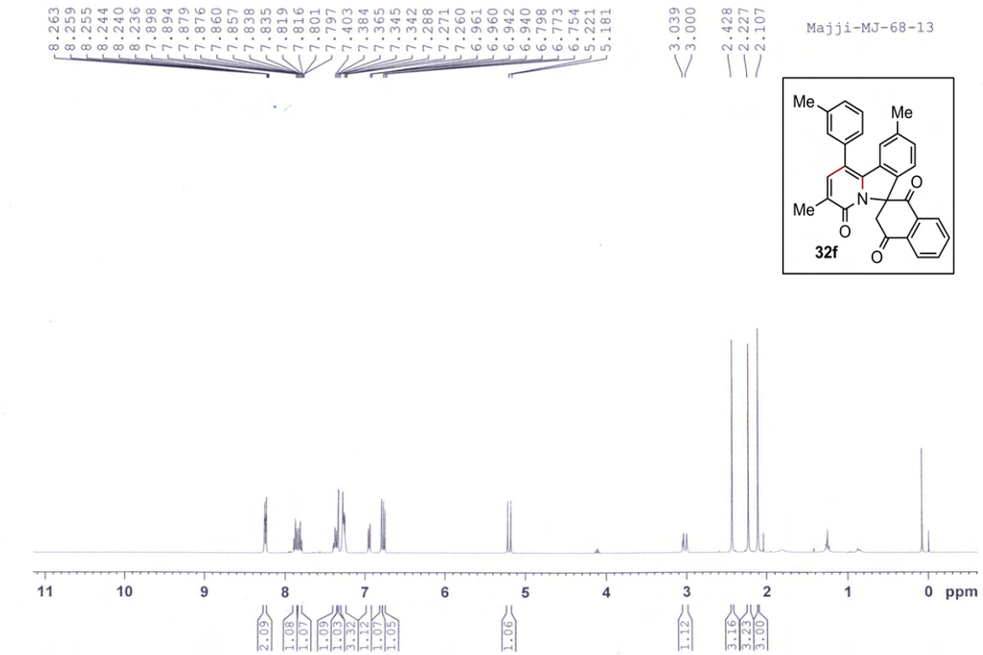
8.263
8.259
8.255
8.244
8.240
8.236
7.898
7.894
7.879
7.876
7.860
7.857
7.838
7.835
7.819
7.816
7.801
7.797
7.403
7.384
7.365
7.345
7.342
7.288
7.271
7.260
6.961
6.960
6.942
6.940
6.798
6.773
6.754
5.221
5.181
3.039
3.000
2.428
2.227
2.107
Majji-MJ-68-13
Me
Me
Me
O
N
O
O
32f
11 10 9 8 7 6 5 4 3 2 1 0 ppm
2.09 1.08 1.07 1.09 1.03 3.32 1.12 1.07 1.05 1.06 1.12 3.16 3.23 3.00

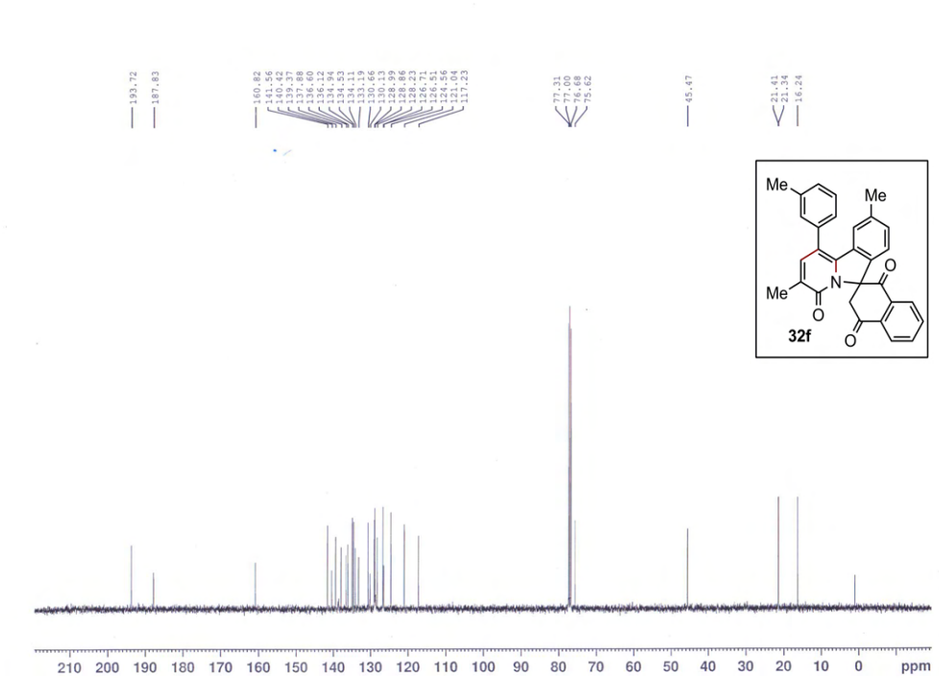
193.72
187.83
160.82
142.55
140.42
139.37
137.88
136.60
136.12
134.94
134.53
133.11
133.19
130.66
130.53
128.99
128.86
128.23
126.71
126.51
124.56
121.04
117.23
77.31
77.00
76.68
75.62
45.47
21.41
21.34
16.24
Me
Me
Me
O
N
O
O
32f
210 200 190 180 170 160 150 140 130 120 110 100 90 80 70 60 50 40 30 20 10 0 ppm

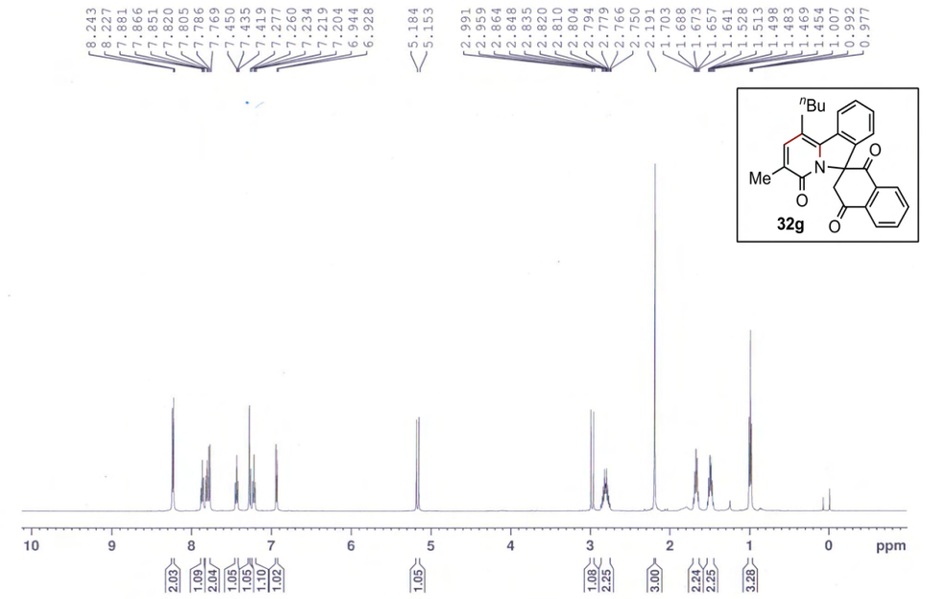
32g

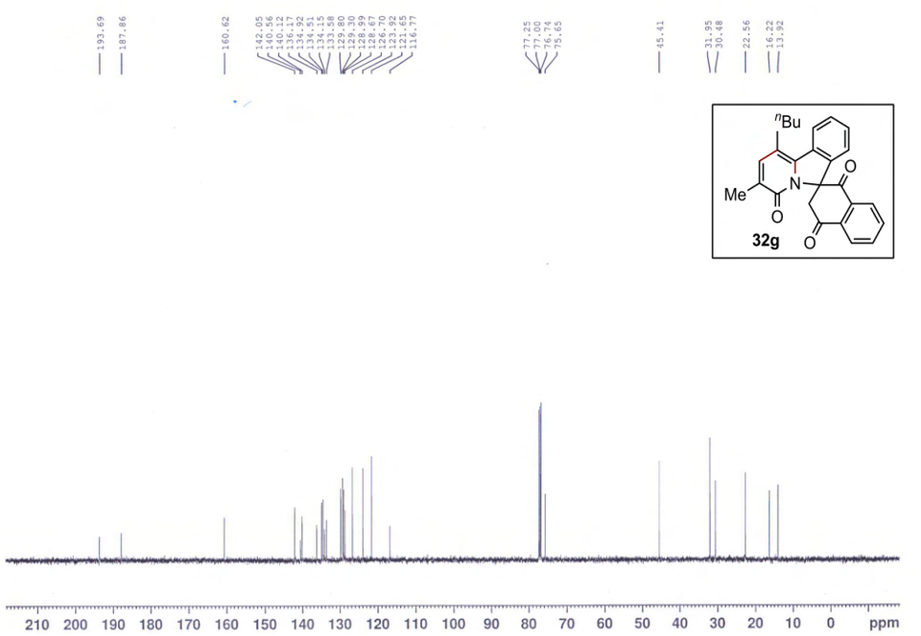
32g

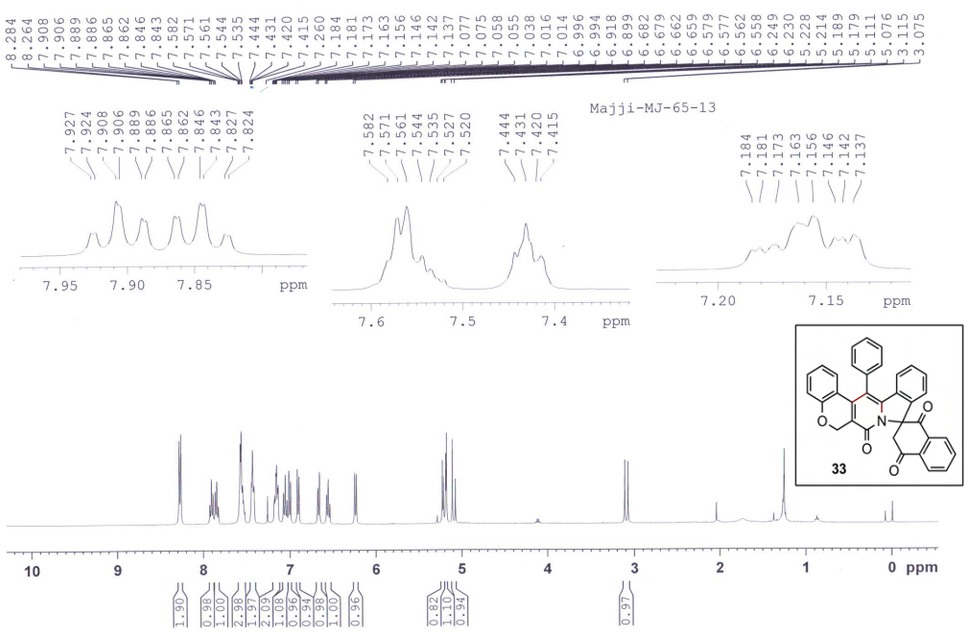
Majji-MJ-65-13
33

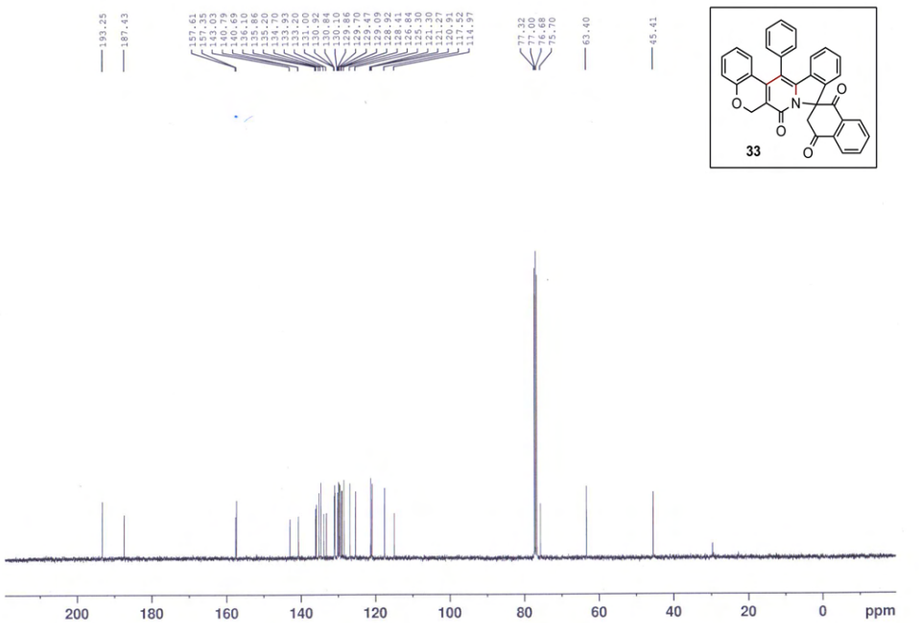
33

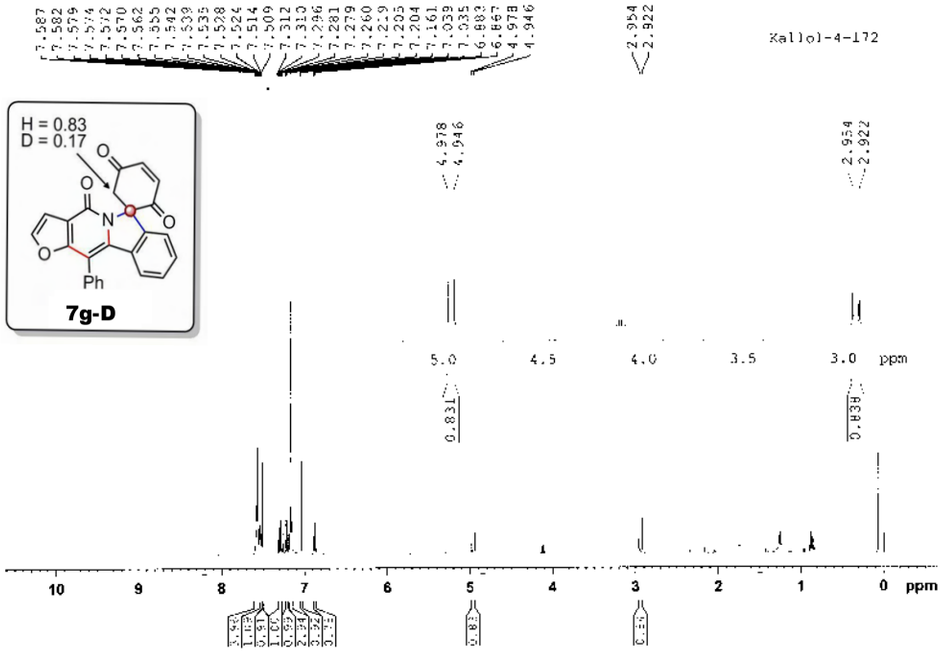
Kallol-4-172
H = 0.83
D = 0.17
Ph
7g-D
ppm

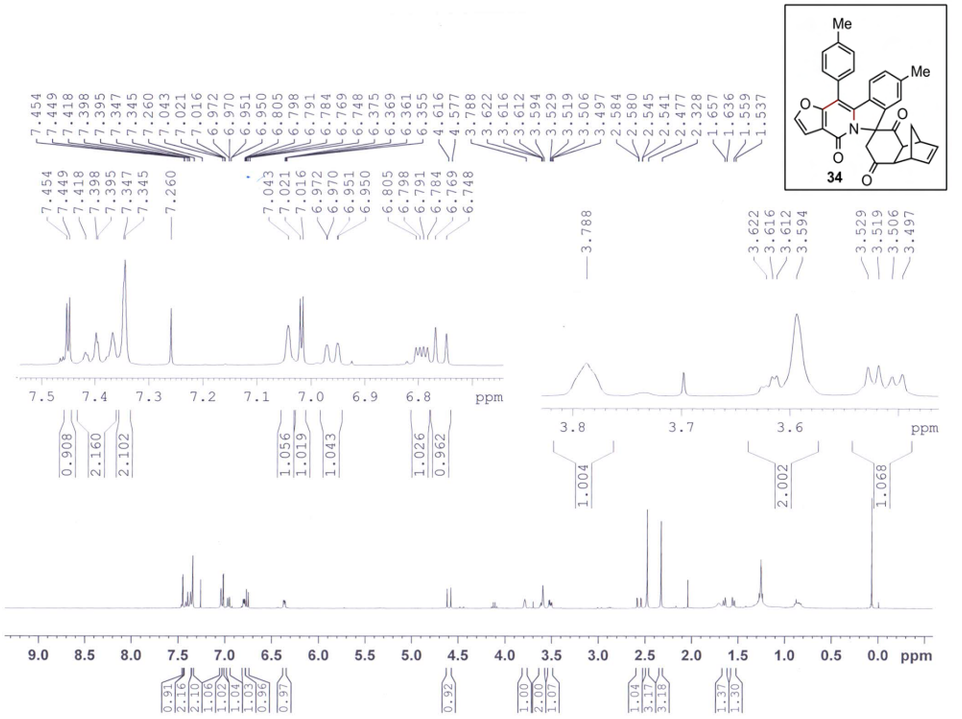
Me
Me
34
ppm

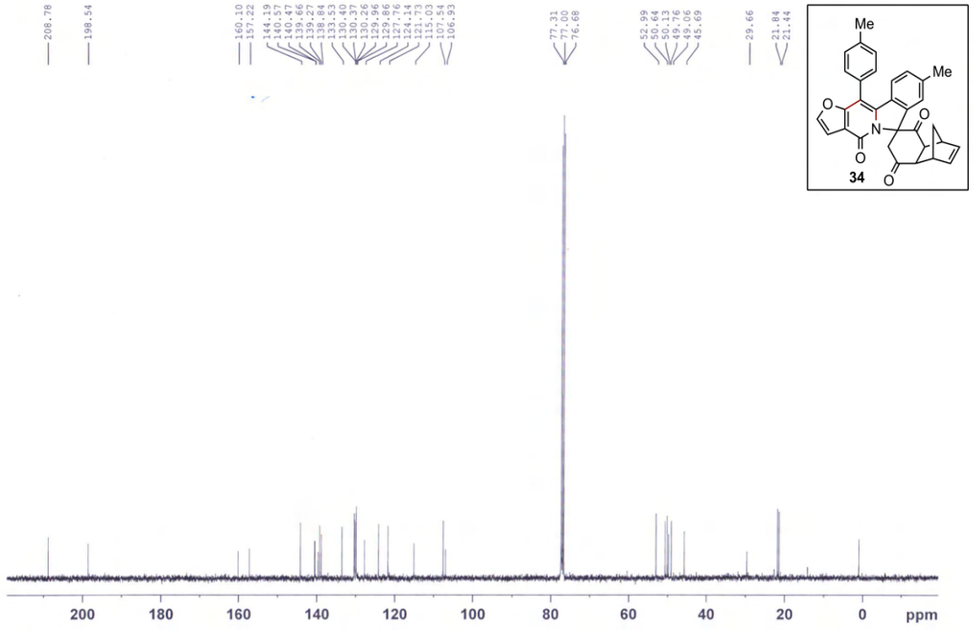
Me
Me
34
ppm

Chapter IV

Ruthenium Catalyzed Intramolecular Hydroarylation of Arenes with Olefins in Water Medium

Abstract

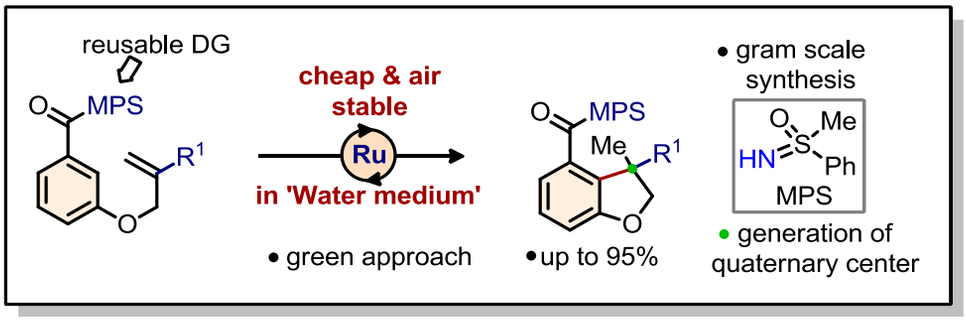

Presented herein the Ru-catalyzed intramolecular hydroarylation of arenes in water. With the aid of methyl phenyl sulfoximine or amide directing group, this atom efficient hydroarylation of arenes ensues dihydrobenzofuran derivatives. Sequential double hydroarylation of arene motif results highly peripheral decorated heterocycles. Deuterium scrambling studies and control experiments offer valuable informations in understanding the reactivity and the mechanistic data.

Reference:

Kallol Mukherjee, E. Ramesh, Koushik Ghosh, and Akhila K. Sahoo
Asian J. Org. Chem. **2018**, *7,* 1380.

IV.1. Introduction

Water is highly-abundant, non-toxic, non-flammable, and most importantly an essential commodity largely available and Green. Thus, development of a chemical reaction in environmentally benign "water" solvent draws significant attention; as the reactions in water allow easy work up and separation.[1] The direct functionalization of ubiquitous C–H bonds fulfils one such criteria of being a "Green" synthetic method, as this strategy does not primarily need the pre-functionalized compound, obviously regulating the formation of undesired waste. Notably, the transition-metal catalyzed activation of inert C–H bond has been emerged as a potential synthetic platform to construct complex molecular template of broad applications covering from the natural products synthesis to the molecules of pharmaceutical importance, and material science.[2–5] Given the challenges of organic substrates are immiscible in water and the reactive catalytic species are incompatible with water, the realization of a novel synthetic manifestation of C–H activation in water is thus a worthwhile endeavour. Moreover, the transition metal salts with small pK_h are readily hydrolysed, while the water-stable-metal salts with large pK_h exhibits less catalytic activity.[1b] Furthermore, the transition-metal catalyzed organic transformations occur both in-water and on-water modes in the interfaces of bulk-water layer.[1c,d]

IV.2. Known synthetic methods for transition metal-catalyzed hydroarylation reactions

IV.2.1. Previous strategies of Rh-catalyzed hydroarylation:

In 2001, Bergman and Ellman reported a proficient route of imine-directed Rh-catalyzed C–H activation and hydroarylation reaction sequence of **1** for the synthesis of indane, dihydroxybenzofuran, tetralane, and dihydroindole derivatives (**2a**–**d**, **Scheme IV.1**).[6] This cyclization modules constructs bicyclic scaffolds with high level of selectivity. The substrate scope is broad. The O-/N-tethered olefins with different chain length

smoothly underwent reaction. Instead of simple alkene, variety of substituted alkene were also participated in this transformation.

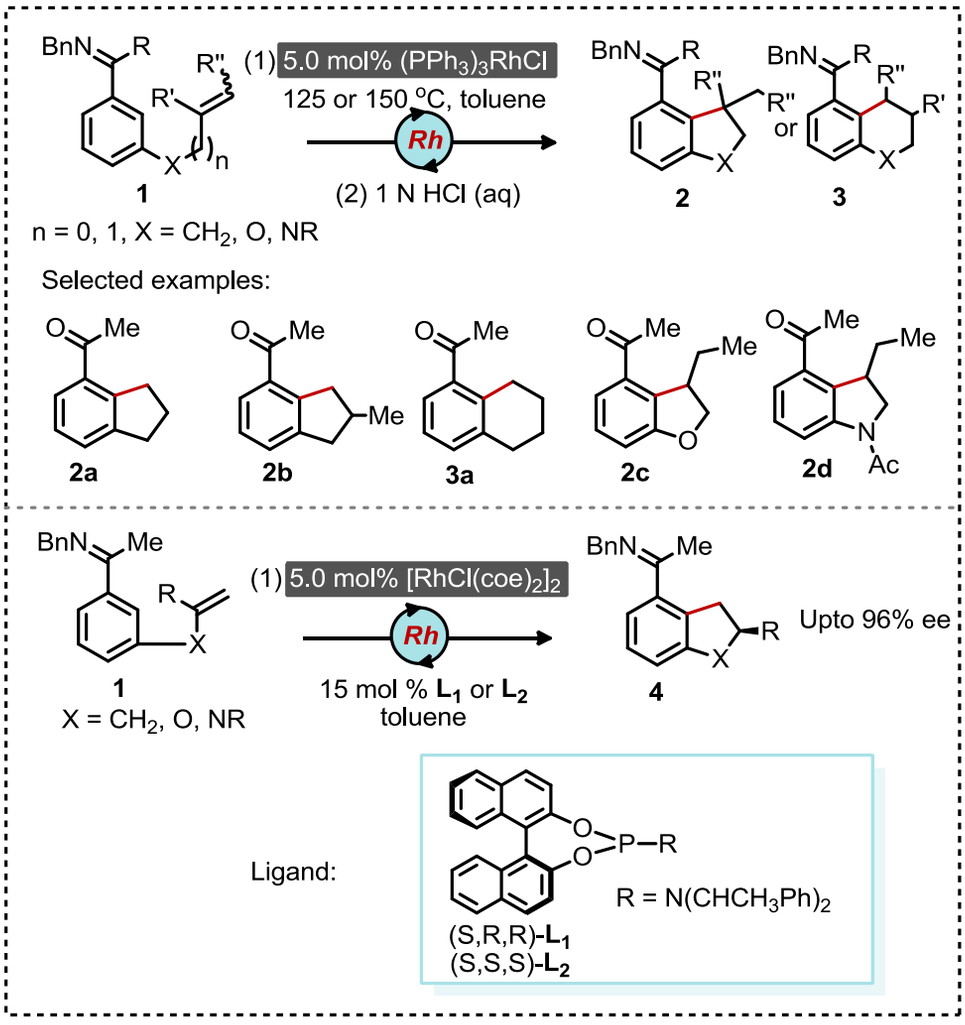

Scheme IV.1: Rh(II)-catalyzed imine-directed C–H hydroarylation

In 2004, the identical strategy has been extended for the asymmetric variant of intramolecular C–H hydroarylation. The chiral ligand enabled Rh-catalytic system play vital in the enantioselective variant of C(sp^2)–H bond activation (**Scheme IV.1**).[6c]

In addition, the asymmetric variant of hydroarylation strategy has been applied for the synthesis of biologically relevant (+)-lithospermic acid moiety **7**. The target compound was achieved in 10 steps and with 5.9% overall yield. Hence, C–H activation strategy is useful for the efficient construction of natural product **7** (**Scheme IV.2**).[6e]

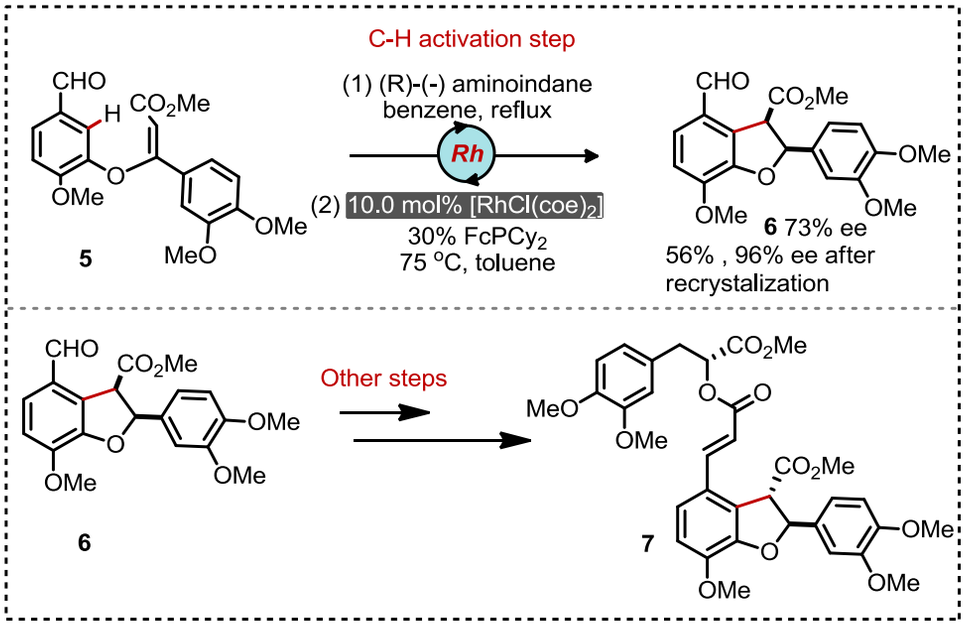

Scheme IV.2: Synthetic strategy of (+)-lithospermic Acid

Based on the use of amides, three hydroarylation variants in the presence of Rh-catalysts have been discovered by the Rovis group in 2013 (**Scheme IV.3)**.[7a] A direct hydroarylation product **9** was accessed when di-alkyl protected amide DG employed in the hydroarylation reaction. Whereas the N-methoxy protected amide containing arenes underwent hydroarylation followed by Heck-type reaction to give the olefin bearing hydroarylation product **10**. In case of N-pivaloyl protected amide derivatives, a multiple C–H functionalizations that involves hydroarylation and C–N bond coupling delivered intramolecular amidoarylation product **11** (**Scheme IV.3**).

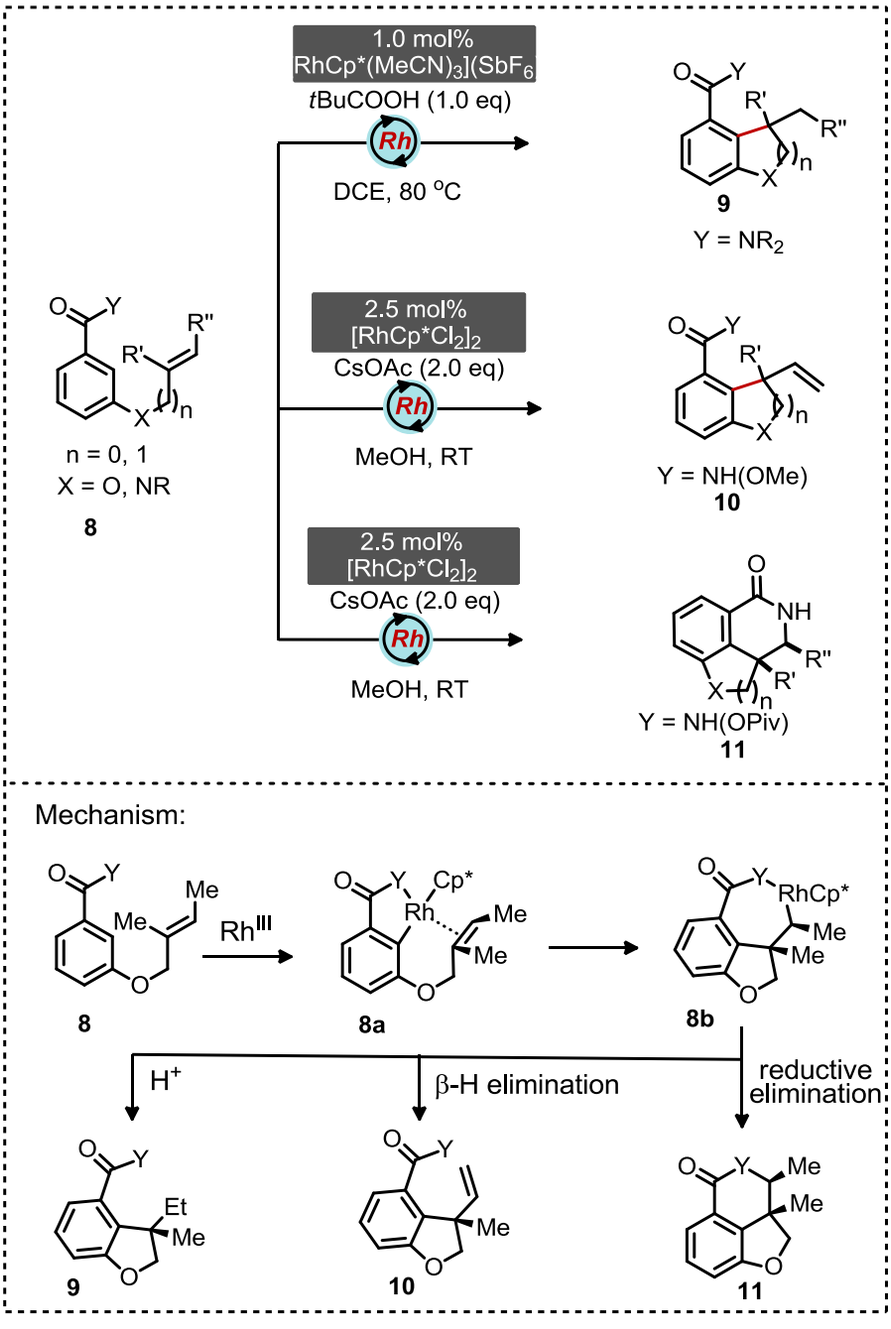

Scheme IV.3: Rh(III)-catalyzed hydroarylation, Heck-type reaction and amidoaryl -ation

IV.2.2. Known synthetic methods for the Co-catalyzed hydroarylation:

In 2013, Yoshikai group for the first time used a combination of cobalt-NHC catlalytic system for the hydroarylation of indole systems having N-tethered olefin to prepare respective fused-indole skeletons tetrahydropyridoindole **13** and dihydropyrroloindole

14. The construction of bicyclo[3.3.1] skeleton as well as formation of quarternary centre are the main features of this transformation (**Scheme IV.4**).[8]

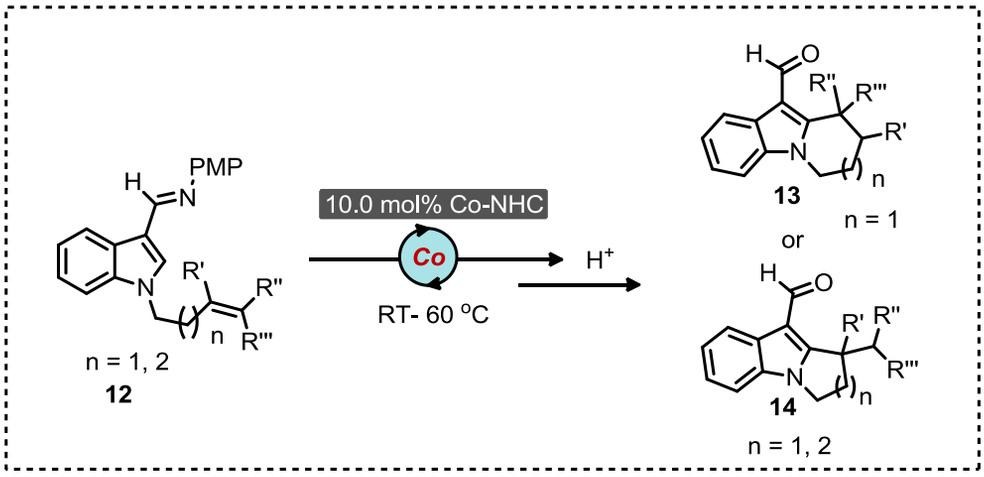

Scheme IV.4: Co-NHC catalyzed hydroarylation of indole derivatives

IV.2.3. Known synthetic methods for the Ru-catalyzed of hydroarylation:

In 2012, our group revealed an air stable Ru-catalyzed intramolecular hydroarylation strategy for the first time. Methylphenylsulfoximine (MPS) coupled carboxylate with O-tether and N-tether alkene undergoes intramolecular hydroarylation to deliver dihydrobenzofuran, indolines and double hydroarylated product **16/17**; interestingly, the reaction was successfully carried out at room temperature in 1,2-DCE (**Scheme IV.5**).[9a] Moreover, one-pot multiple C–H functionalizations involving subsequent C–C/C–C and C–C/C–N were also showcased for the first time (**18/19**).

A plausible mechanistic cycle is sketched in **Scheme IV.5**. First step is the formation of active catalyst **A** from the reaction of [{$RuCl_2$(p-cymene)}$_2$], $AgSbF_6$, and $Cu(OAc)_2$. This active catalyst coordinates with the MPS and activates the proximal *ortho*-C–H bond of **15** to form the five membered cyclometalated complex **15a**. Subsequent intramolecular alkene insertion of **15a** followed by protodemetalation of **15c** delivers the product **16**.

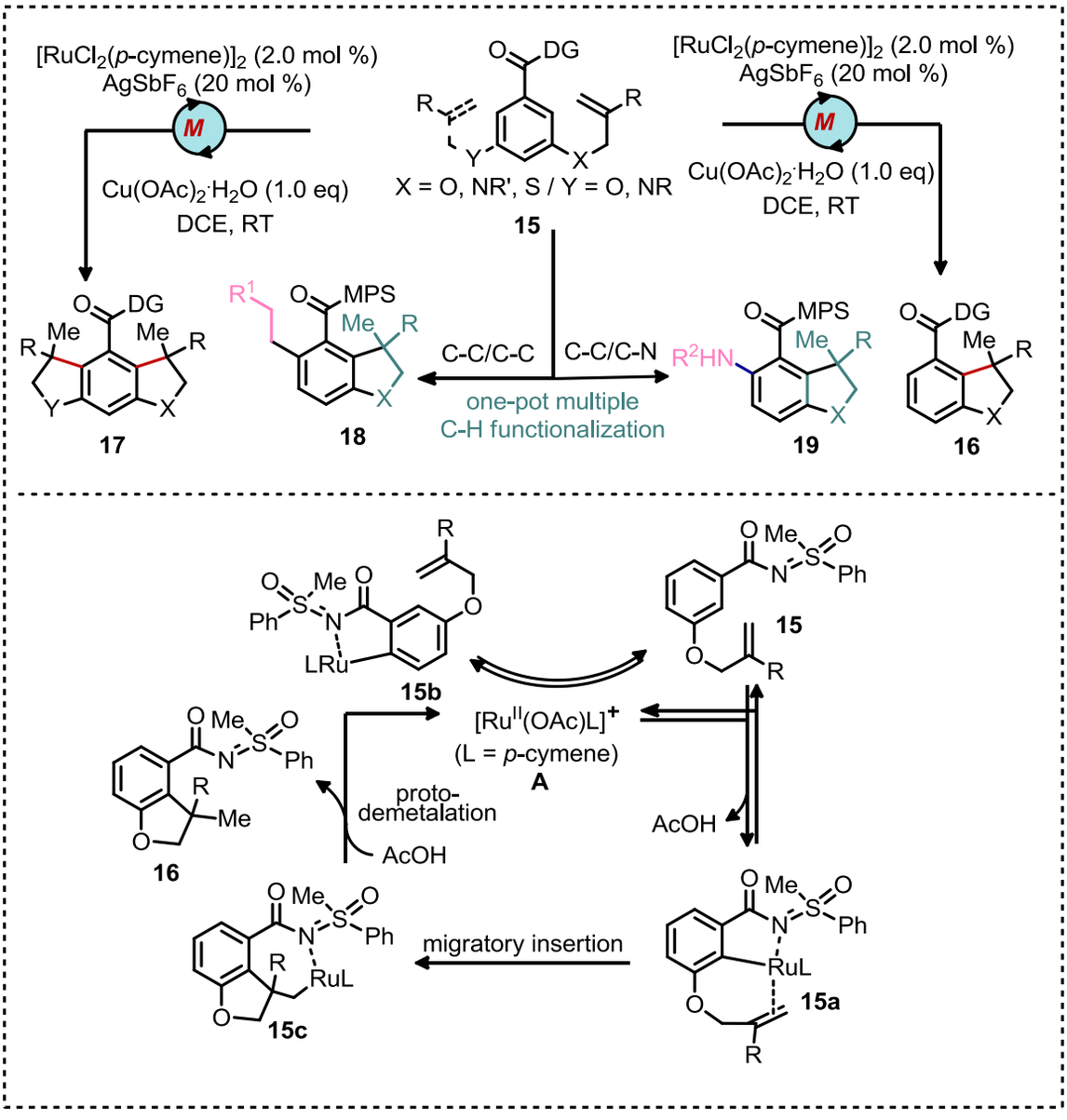

Scheme IV.5: MPS directed Ru-catalyzed hydroarylation

The same hydroarylation strategy was further extended towards amide directed hydroarylation for the synthesis of dihydrobenzofuran, chroman, and indoline derivatives **21–23**. The main features of this protocol are the atom-efficiency, broad substrate scope and excellent yield (**Scheme IV.6**).[9b]

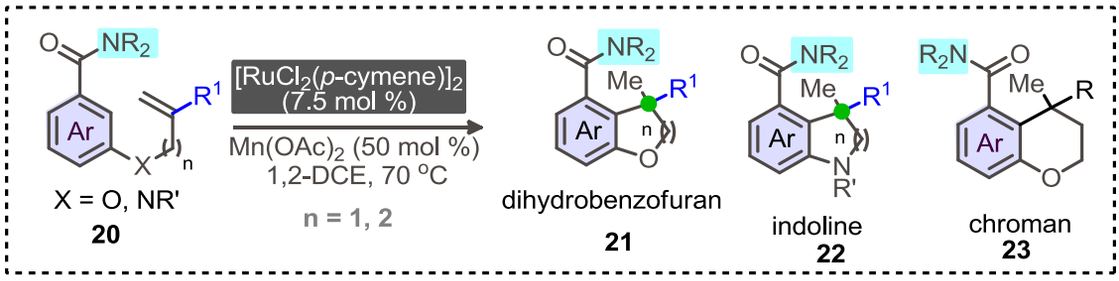

Scheme IV.6: Amide directed Ru-catalyzed hydroarylation

IV.3. Motivation and Design for Double Annulation

The transition-metal-catalyzed intramolecular hydroarylation of O-tethered olefin-bearing arene directly constructs dihydrobenzofuran skeleton, which is widely found in the molecules of various natural products.[5] A notable imine-directed Rh-catalyzed hydroarylation of arenes was at first demonstrated by Ellman and Bergman's group (**Scheme IV.7**).[6] Subsequently, Rh-, Co-, Ru-, and Ir- catalysts have independently been used for the identical transformations (**Scheme IV.7**).[7–10] Most of these transformations were successfully executed in organic solvents (toluene / 1,2-dichloroethane / 1,4-dioxane) (**Scheme IV.7**). By contrast, no such intramolecular hydroarylation of arenes in water is known till 2016. Whereas the cost-effective and air-stable Ru-catalysts have been used for the directed functionalization of arene C–H bonds in/on water.[11–12]

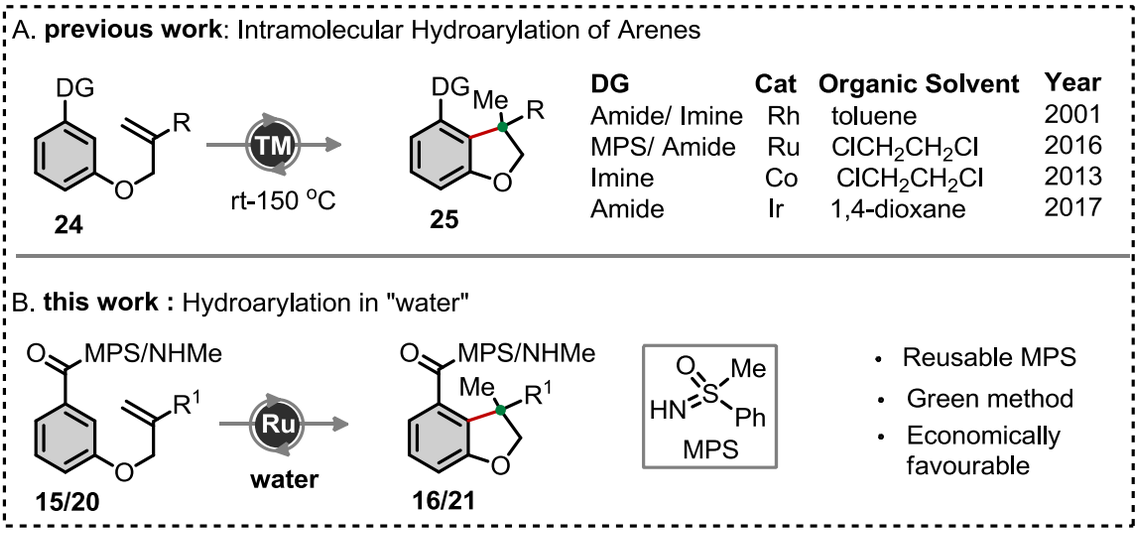

Scheme IV.7: Hydroarylation in water medium

Inspired from these studies, we herein developed the methyl phenyl sulfoximine (MPS)/ NHMe-directed Ru-catalyzed intramolecular hydroarylation of O-tethered olefin bearing benzoic acid derivatives **15/20** in water for the synthesis of wide arrays of dihydrobenzofurans **16/21**. The sequential unsymmetrical C–H functionalization of dihydrobenzofuran was also investigated.

IV.4. Results and Discussion

IV.4.1. Synthesis of precursors

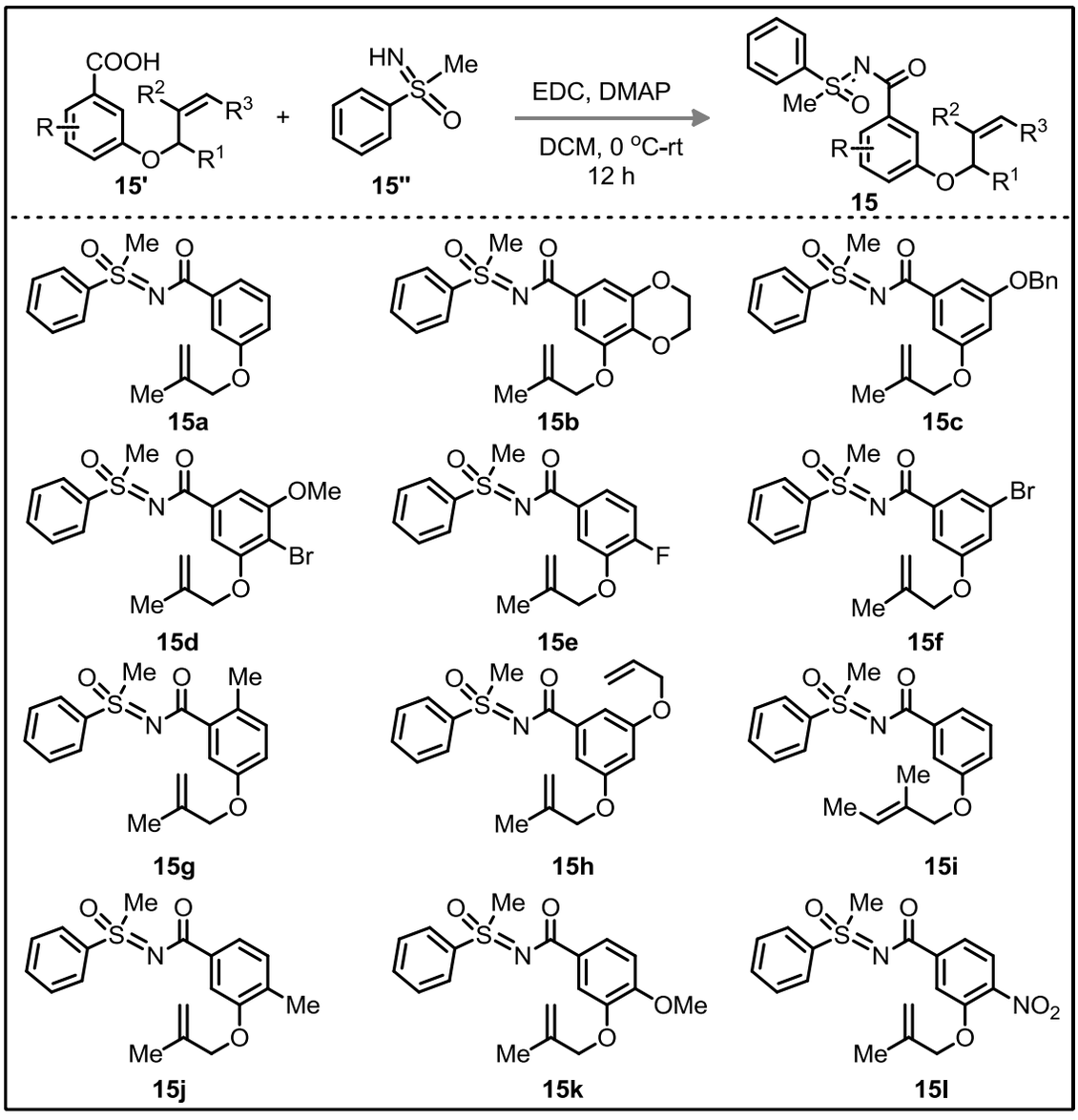

Scheme IV.8: Preparation of N-heteroaroyl sulfoximine derivatives

A library of starting materials MPS-enabled O-tethered olefin bearing benzoic acid derivatives has been synthesized using the known procedure, which are shown in **Scheme IV.8**.[9] The EDC.HCl mediated coupling between O-tethered olefin bearing benzoic acid derivatives **15′** and methyl phenyl sulfoximine **15″** led to the precursors **15** in good overall yields.

IV.4.2. Optimization studies

Encouraged from our recent demonstration of the MPS assisted Ru-catalyzed intramolecular hydroarylation of arenes,[9a] we envisaged probing the identical transformation in water. To start with, the hydroarylation of [3-(2-methylallyloxy)benzoyl] methylphenyl sulfoximine (**15a**) was investigated under Ru-catalyst in water (**Table IV.1**). Gratifyingly, the desired hydroarylation compound **16a** was formed in 28% yield, when the reaction was conducted under the catalytic system

Table IV.1: Optimization of Reaction Parameters[a]

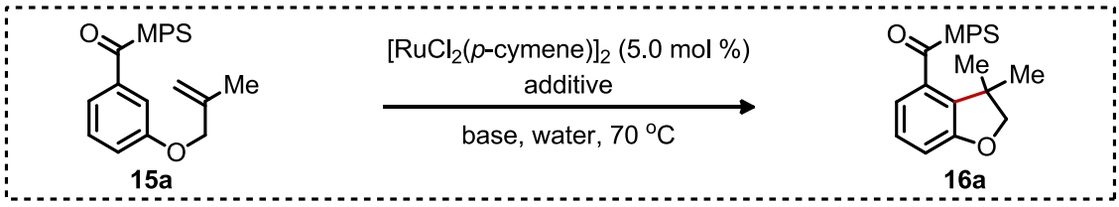

entry	additive (20 mol %)	Base (1.0 equiv)	time (h)	yield of **16a** (%)[b]
1	$AgSbF_6$	$Cu(OAc)_2 \cdot H_2O$	12	28
2	–	$Cu(OAc)_2 \cdot H_2O$	24	nr
3[c]	$AgBF_4$	$Cu(OAc)_2 \cdot H_2O$	12	39
4	$NaPF_6$	$Cu(OAc)_2 \cdot H_2O$	12	47
5	KPF_6	$Cu(OAc)_2 \cdot H_2O$	12	67
6	KPF_6	$Mn(OAc)_2$	12	49
7	KPF_6	NaOH	12	nr
8	KPF_6	KOH	12	nr

9	KPF_6	AcOH	12	22
10[d]	KPF_6	$Cu(OAc)_2 \cdot H_2O$	12	97
11[e]	KPF_6	$Cu(OAc)_2 \cdot H_2O$	12	93
12[f]	KPF_6	$Cu(OAc)_2 \cdot H_2O$	12	38

[a] Reactions were carried out using **15a** (0.2 mmol), $[RuCl_2(p\text{-cymene})]_2$ (5.0 mol %), base (0.2 mmol), additive (20 mol %) in water (1.0 mL) at 70 C. [b] Isolated yields. [c] ^1H NMR yield. [d] 100 °C. [e] $[RuCl_2(p\text{-cymene})]_2$ (3.0 mol %) and KPF_6 (12 mol %) was used at 100 °C. [f] The reaction was performed in neat at 100 °C.

comprising {$[RuCl_2(p\text{-cymene})]_2$ (5.0 mol %), $AgSbF_6$ (20 mol%), and $Cu(OAc)_2 \cdot H_2O$ (1.0 equiv)} in water at 70 C (entry 1). Perhaps the formation of active cationic Ru complex, obtained in-situ from Ru- and Ag salt, is hampered in water, which eventually affects activation of arene *o*-C–H bond. By contrast, the reaction in the absence of $AgSbF_6$ did not yield **16a** (entry 2); thus, an additive (responsible forming the respective chloride salts from Ru-catalyst) is indispensable. The use of various chloride trapping agents is therefore envisioned. Among the additives $AgBF_4$, $NaPF_6$, and KPF_6 screened (entries 3–5), KPF_6 worked better affording 67% of **16a** (entry 5). Presumably the water soluble KCl salt facilitates the formation of cationic Ru-species, which helps in the activation of the arene *o*-C–H bond. The use of $Mn(OAc)_2$ instead of $Cu(OAc)_2$ did not work better (entry 6). The Ru(OH)R complex, generated in-situ from the base promoted water mediated Ru-catalyzed reaction, is probably responsible for the activation of arene C–H bond through the internal electrophilic substitution (IES) type mechanism.[13] Not even a trace of the product **16a** was detected when the reaction was conducted in presence of NaOH or KOH even at harsh conditions (140 C) (entries 7 and 8), thus refuting the participation of IES-type mechanism.[13] While the reaction in presence of acetic acid yielded 22% **16a** (entry 9). Pleasingly, **16a** was isolated in 97% yield when the identical reaction in entry 5 heated at 100 C (entry 10). The use of less amount of Ru-catalyst (3.0 mol%) did not affect the reaction outcome (entry 11). Thus, reaction of **15a** under the

catalytic conditions {[$RuCl_2$(*p*-cymene)]$_2$ (3.0 mol%), KPF_6 (12 mol%), $Cu(OAc)_2 \cdot H_2O$ (1.0 equiv) in H_2O at 100 °C for 12 h} furnished **16a** in 93% yield (entry 11). Interestingly, **16a** (38%) was obtained when the reaction performed in neat (entry 12); presumably the interaction of substrate with catalyst in molten state is responsible for product formation. We therefore believe that the reaction in water medium can enhance dispersion of the organic oily-phase of the reactants.[1c,d]

IV.4.3. Reaction scope-I

We next surveyed the generality of this MPS-assisted hydroarylation of arenes in water under the optimized condition shown in entry 11, **Table IV.1**. The compound **16a** was isolated from **15a** (0.3 mmol) in 95% yield; even the identical transformation worked well in 1.5 mmol scale affording 94% **16a**. The MPS-enabled electron-rich arenes [dihydrobenzo[*b*][1,4]dioxine / *m*-OBn / *p*-Br-*m*-OMe] reacted smoothly to provide the corresponding **16b** (82%), **16c** (81%), and **16d** (79%). The transformable halo groups (F/Br) on the arene motifs were survived, accessing **16e** and **16f** in 89% and 54% yield, respectively. The sterically encumbered *o*-Me arene derivative underwent hydroarylation to yield the respective 5-Me-bearing dihdrobenzofuran **16g** in 67% yield. Whereas *m,m'*-di-O-allyl MPS-bearing carboxylate under the catalytic conditions exclusively provided the mono-hydroarylation product **16h** (82%); the dihydroarylation did not occur even the reaction conducted for longer time. The intramolecular hydroarylation of tri-substituted olefin bearing substrate delivered the corresponding 3,3-methyl-ethyl bearing dihdrobenzofuran **16i** in 33% yield. Disappointingly, the *p*-Me / *p*-OMe / *p*-NO_2 substituted arene derivatives failed to provide the respective hydroarylation products **16j**–**16l** (**Scheme IV.9**); presumably, the respective substrates **15j**–**15l** did not miscible in water even at higher temperature, which eventually obstructs the hydroarylation reactions in water medium.

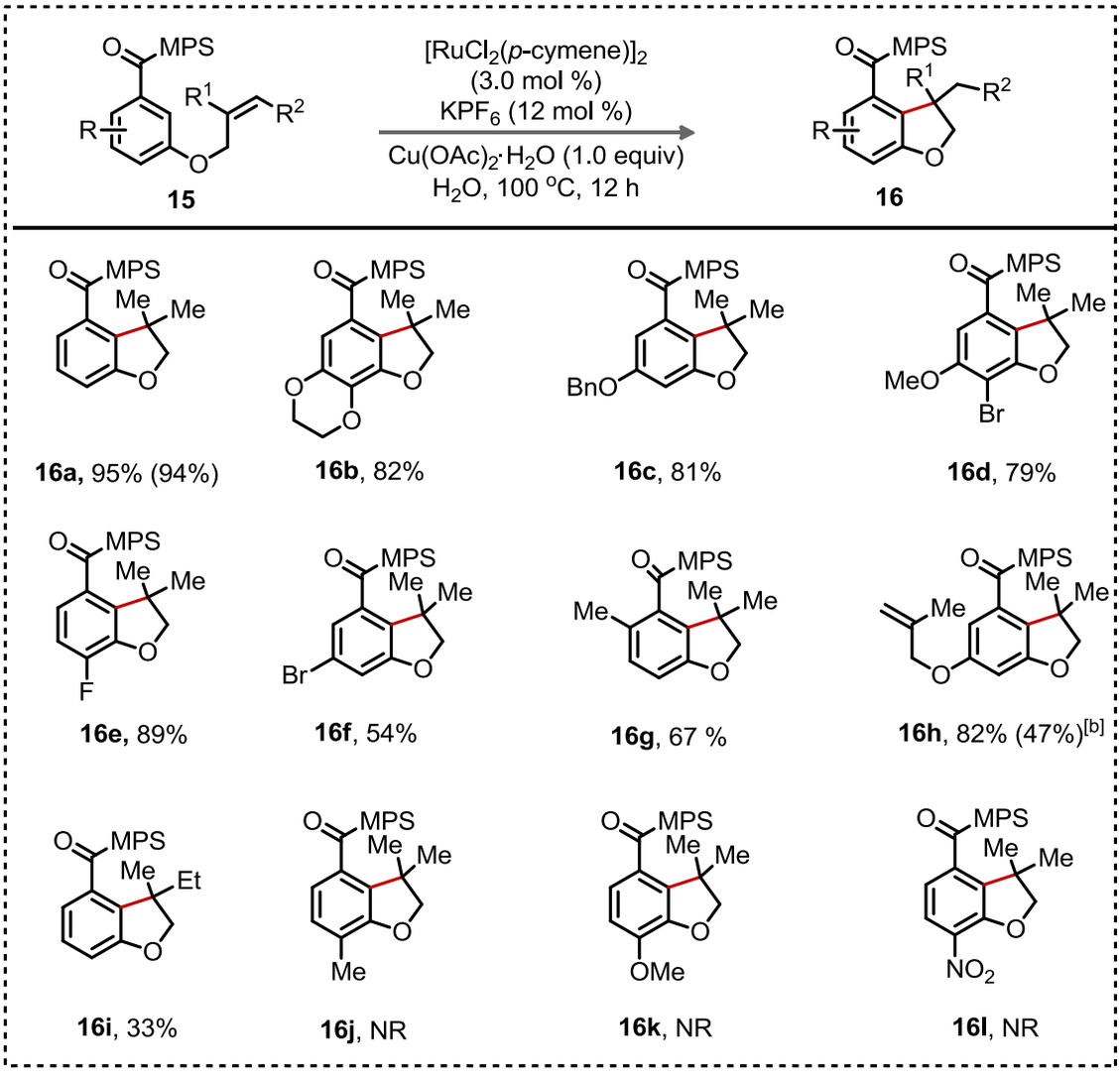

Scheme IV.9: Substrate scope-I

IV.4.4. Reaction scope-II

Interestingly, the amide-NHMe directed hydroarylation of *p*-OMe / *p*-NO_2 substituted arene derivatives **20a** and **20b** under the Ru-catalyzed catalytic conditions of entry 11, **Table IV.1** along with $AgSbF_6$ in water independently provided **21a** and **21b**, respectively albeit in moderate yield [Eq 1 and Eq 2, **Scheme IV.10**]. We presumably believe that the amide bearing substrate **20a** and **20b** forms the corresponding salts in the presence of acetate base and provokes the reaction to occur at an elevated temperature in water medium.

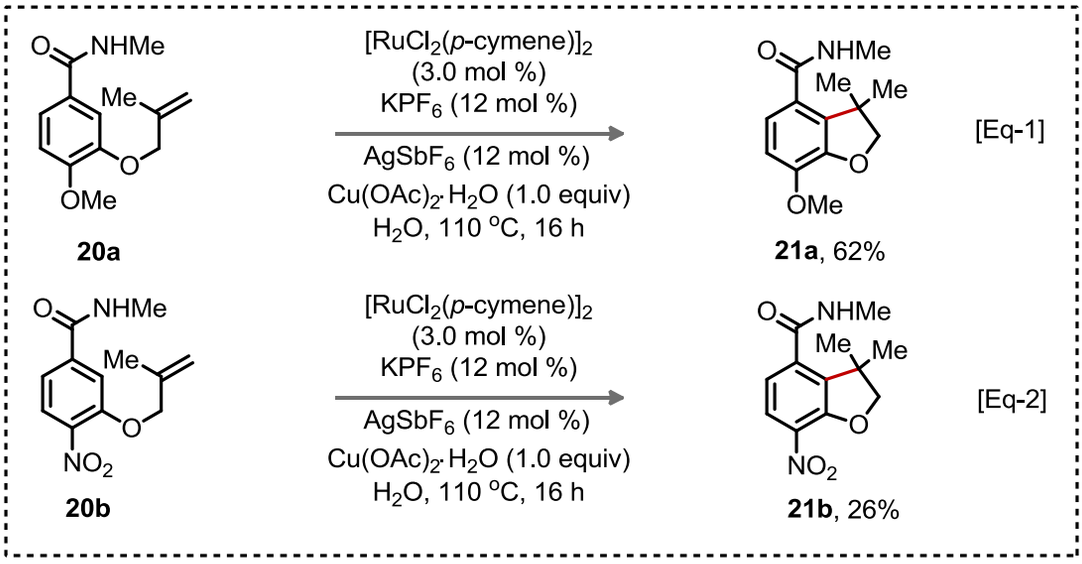

Scheme IV.10: Substrate scope-II

Encouraged with the directing group aided hydroarylation of arenes in water (**Scheme IV.9** and **Scheme IV.10**, Eq 1–2), the hydroarylation of aryl *o*-C–H bond of dihydrobenzofuran derivative **16h** with the spatially configured olefin was examined. Pleasingly, the dicyclization product **17** was isolated in 65% yield, when **16h** was exposed to the optimized catalytic conditions (**Scheme.IV.11).**

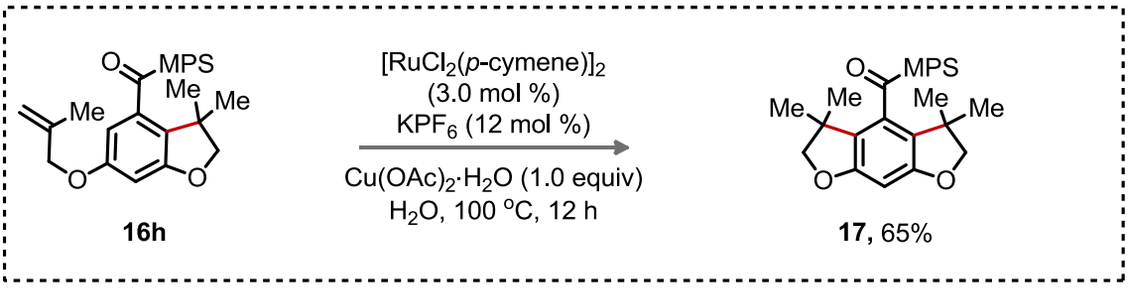

Scheme.IV.11: Substrate scope-III

IV.4.5. Gram-scale:

Next, the scalability of this reaction was tested through a gram scale hydroarylation in water. Gratifyingly, the hydroarylation of **15a** (1.0 g) was successfully carried out even in presence of 1.0 mol % Ru-catalyst in water to furnish **16a** (0.92 g; 92%)

(**Scheme.IV.12**). This demonstration truly validates the importance of MPS-DG and efficacy of Ru-catalysis in this hydroarylation in water. By contrast, the notable other intramolecular hydroarylation strategies invariably requires more amount of catalyst.[6–10]

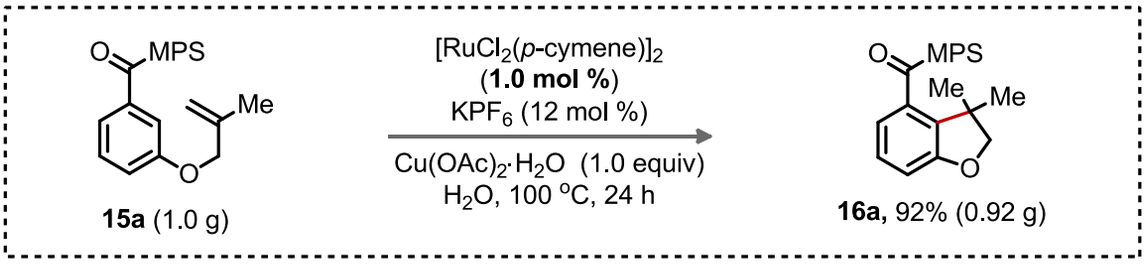

Scheme.IV.12: Gram-scale synthesis

IV.4.6. Control Experiments

To understand the path of the reaction in water, various control experiments were envisaged (**Scheme.IV.13)**. The reaction in presence of TEMPO provided 80% isolated yield of **16a**; thus, the cyclization does not involve radical intermediate [Eq 1]. The reaction in D_2O provided 12 % deuterium incorporation in the *o*-C–H bond of **15g** [Eq 2]; thus, the *o*-C–H bond activation via concerted metalation-deprotonation (CMD) path is reversible.[9a] While the identical transformation of **15a** in D_2O delivered 55% and 15% deuterium incorporation in the *o*-C–H and the newly generated 3-methyl moiety of dihydrobenzofuran in **16a-H/D**, respectively; thus, the reaction involves protodemetalation [Eq 3].[9a] The 85% protonation of the 3-methyl moiety in dihydrobenzofuran suggests that the proton source of AcOH (obtained in-situ via the acetate assisted activation of C–H bond by CMD) is superior over D_2O [Eq 3].[9a] A competitive experiment among **15a** (1,1′-di-substitued alkene) and **15i** (1,1′,2-trisubstituted alkene) under the optimized conditions in 1 h led to **16a** (88%) and **16i** (12%) [Eq 4]; thus, steric bulkiness of olefin affects the reactivity as well the productivity.

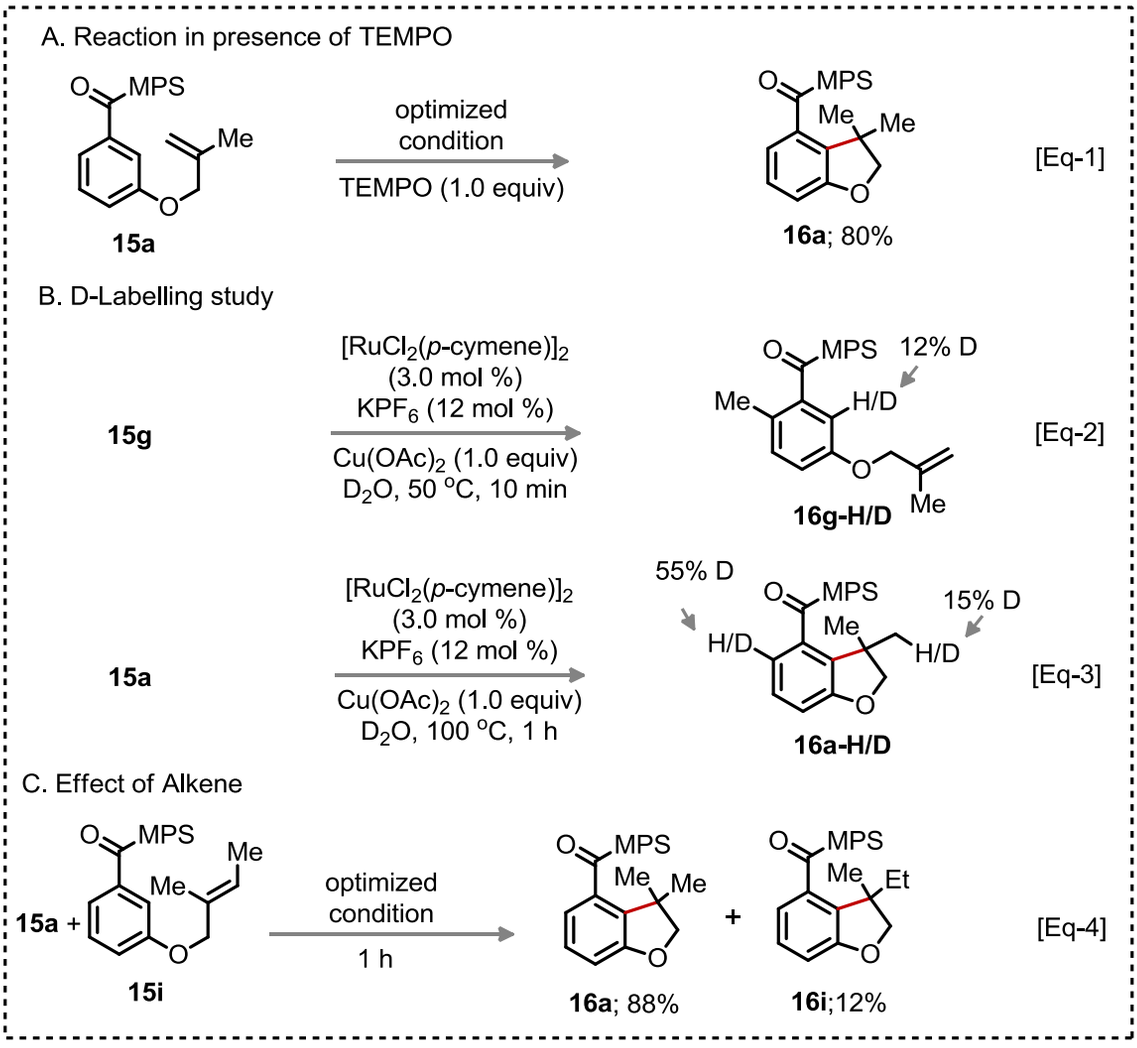

Scheme.IV.13: Control Experiments

IV.4.7. Mechanistic Cycle

A plausible reaction pathway for this hydroarylation reaction is sketched in **Scheme.IV.14**. The reaction begins with the formation of active Ru-catalyst from $[RuCl_2(p\text{-cymene})]_2$, KPF_6, and $Cu(OAc)_2 \cdot H_2O$. Next, the coordination of active Ru-species to the MPS-DG promotes *o*-C–H bond activation to produce cyclometalated complex **15a/20a**. The migratory insertion of **15a/20a** then leads to **15c/20c**. Finally, proto-demetalation of **15c/20c** affords the desired product **16/21** with the regeneration of active catalyst (**Scheme.IV.14**).

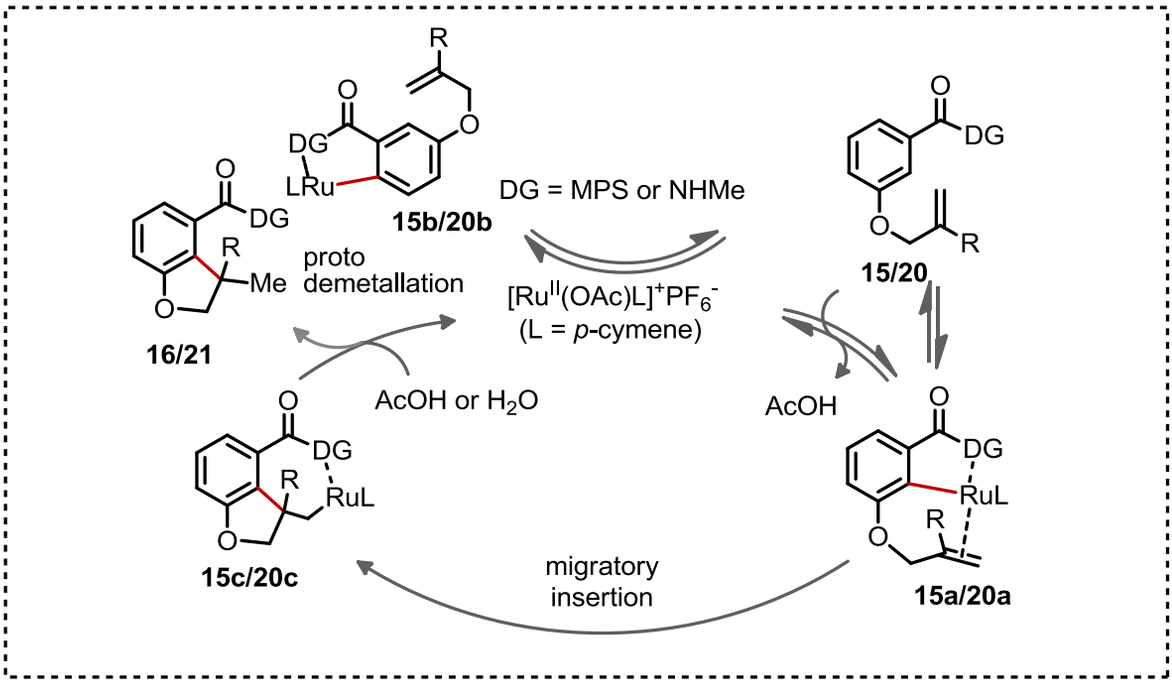

Scheme.IV.14: Proposed Mechanistic Profile

IV.4.8. Application

Multiple functionalization of readily accessible arene motif builds highly peripheral decorated novel molecular scaffold. Thus, further functionalization of *o*'-C–H bond of the MPS-enabled dihydrobenzofuran derivative was envisaged, despite the electronic and steric biasness of the molecular scaffold. To check the feasibility of next functionalization, the Ru-catalyzed MPS-assisted *o*'-C–H acetoxylation, bromination, and/or annulation of dihydrobenzofuran derivative was then surveyed. Pleasingly, annulation between **16a** and 1,2-diphenyl acetylene under the Ru-catalysis provided an unusual dihydrofuran-fused-isoquinolone framework **26** in 62% yield (**Scheme.IV.15**).[14a] The *o*'-C–H bromination and acetoxylation were independently performed on **16a** under the respective catalytic conditions [NBS (1.5 equiv), $Pd(OAc)_2$ (15 mol%), AcOH (2.5 equiv) in DCE at 100 °C] and [$Pd(OAc)_2$ (10 mol%), $K_2S_2O_8$ (2.0 equiv) in $CHCl_3$:AcOH (3:5) at 100 °C] to afford **27** (72%) and **28** (67%), respectively (**Scheme.IV.15**).[14b,c] Thus, the sequential intramolecular hydroarylation followed by

C–C, C–O, and C–Br bond formations of *o*-C–H bonds of arene motifs build novel molecules with various functionalities.

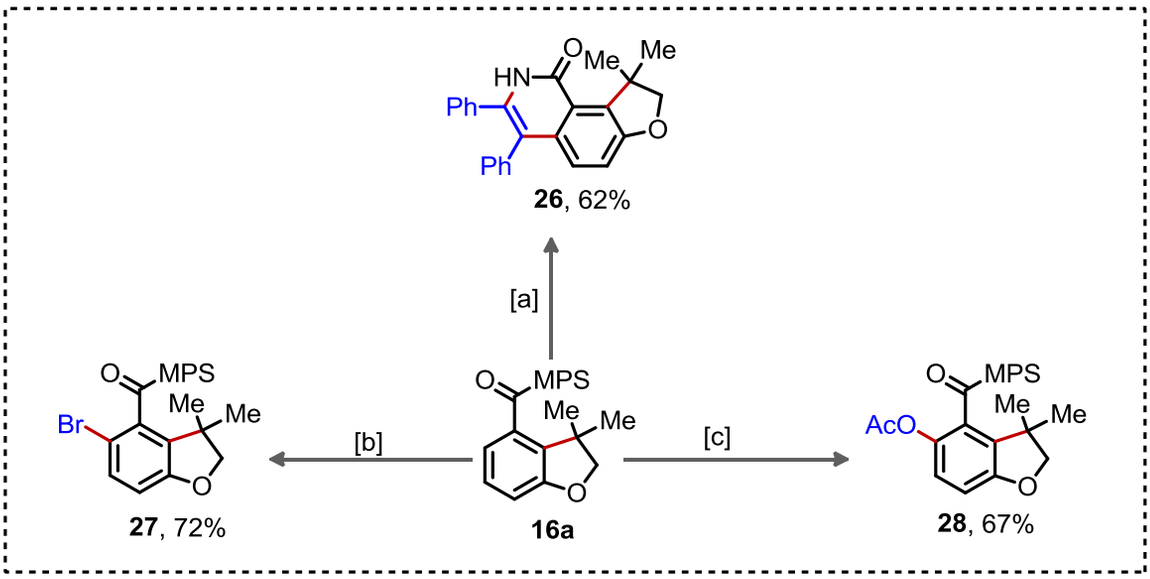

[a] **16a** (100 mg, 0.3 mmol), 1,2-diphenyl acetylene (64 mg, 0.36 mmol), $[RuCl_2(p\text{-cymene})]_2$ (5.0 mol %), $AgSbF_6$ (20 mol %), and AcOH (0.3 mmol) in 1,4-dioxane (2.0 mL) at 120 C for 24 h. [b] **16a** (0.3 mmol), $Pd(OAc)_2$ (15 mol %), NBS (0.45 mmol), AcOH (2.5 equiv), $ClCH_2CH_2Cl$ (3.0 mL) at 100 °C for 12 h. [c] **16a** (0.3 mmol), $Pd(OAc)_2$ (10 mol %), $K_2S_2O_8$ (0.6 mmol), and AcOH/$CHCl_3$ (3:5, 2.0 mL) at 100 °C for 12 h.

Scheme.IV.15: Application

IV.5. Conclusion

In summary, the MPS/amide group directed Ru-catalyzed hydroarylation of arenes in water is developed. To the best of our knowledge, hydroarylation of arenes in water is the first report. This method directly constructs dihydrobenzofuran derivatives from commercially available 3-hydroxy benzoic acids. Despite the challenges, the current synthetic manifestation exhibits moderate scope; thus, to unravel novel and effective synthetic method in this regard remains an attractive endeavor. Sequential unsymmetrical functionalization of unactivated multiple C–H bonds of arene

derivatives through hydroarylation–annulation/ hydroarylation-acetoxylation, and hydroarylation-halogenation builds novel molecular skeletons. The cleavage and recovery of the MPS moiety from the products and the gram-scale hydroarylation in water make the current synthetic method viable.

IV.6. Experimental

IV.6.1. General Experimental Information

All the reactions were performed in an oven-dried Schlenk flask. Commercial grade solvents were distilled prior to use. Column chromatography was performed using either 100-200 Mesh or 230-400 Mesh silica gel. Thin layer chromatography (TLC) was performed on silica gel GF254 plates. Visualization of spots on TLC plate was accomplished with UV light (254 nm) and staining over I_2 chamber.

Proton, carbon, and fluorine nuclear magnetic resonance spectra (^{1}H NMR, ^{13}C NMR and ^{19}F NMR) were recorded based on the resonating frequencies as follows: (^{1}H NMR, 400 MHz; ^{13}C NMR, 101 MHz; ^{19}F NMR, 376 MHz) and (^{1}H NMR, 500 MHz; ^{13}C NMR, 126 MHz; ^{19}F NMR, 470 MHz) having the solvent resonance as internal standard (^{1}H NMR, $CDCl_3$ at 7.26 ppm; ^{13}C NMR, $CDCl_3$ at 77.0 ppm). Few cases tetramethylsilane (TMS) at 0.00 ppm was used as reference standard. Data for ^{1}H NMR are reported as follows: chemical shift (ppm), multiplicity (s singlet; bs broad singlet; d doublet; bd broad doublet, t triplet; bt broad triplet; q quartet; m multiplet), coupling constants, *J*, in (Hz), and integration. Data for ^{13}C NMR, ^{19}F NMR were reported in terms of chemical shift (ppm). IR spectra were reported in cm^{-1}. LC-MS spectra were obtained with ionization voltage of 70ev; data was reported in the form of *m/z* (intensity relative to base peak 100). Elemental (C, H, N) analysis were carried out using FLASH EA 1112 analyzer. High resolution mass spectra were obtained in ESI mode. Melting points were determined by electro-thermal heating and are uncorrected. X-ray data was collected at 293 K using graphite monochromated Mo-K radiation (0.71073 Å).

Materials: Unless otherwise noted, all the reagents and intermediates were obtained commercially and used without purification. Dichloromethane (DCM), 1,2-dichloroethane (DCE), and chloroform were distilled over CaH_2. THF was freshly distilled over sodium/benzophenone ketyl under dry nitrogen. $[RuCl_2(p\text{-cymene})]_2$, $AgSbF_6$, $AgBF_4$, $NaPF_6$, KPF_6 were purchased from Sigma Aldrich Ltd, and used as received. Bases such as $Cu(OAc)_2{\cdot}H_2O$, $Mn(OAc)_2$, NaOH, KOH were purchased from Aldrich Ltd. and used as received. Analytical and spectral data of all those known compounds are exactly matching with the reported values.

IV.6.2: General Procedure for the Hydroarylation of O-Tethered Compounds (15)

The hydroarylation reactions were conducted in a 50 mL Schlenk tube having high pressure valve and side arm. The tube was charged with (**15**, 0.3 mmol), $[RuCl_2(p\text{-cymene})]_2$ (6.0 mg, 3.0 mol %), and $Cu(OAc)_2{\cdot}H_2O$ (60 mg, 0.3 mmol). Subsequently, the additive KPF_6 (7.0 mg, 12 mol %) was introduced to the flask in a glove box. Water (H_2O) (2.0 mL) was added to the mixture and the resulting mixture was stirred at 100 °C for 12 h. The reaction mixture was filtered through a small plug of Celite and washed with dichloromethane (3 × 5.0 mL). The solvents were evaporated under the reduced pressure and the crude material was purified using column chromatography on silica gel.

Following this procedure, compounds **16a–16i** were prepared. Analytical and spectral data of these compounds are exactly matching with the reported values.[2]

***N*-[3,3-Dimethyl-2,3-dihydrobenzofuran-4-carboxyl]-*S*-methyl-*S*-phenylsulfoximine (16a):**[9a]

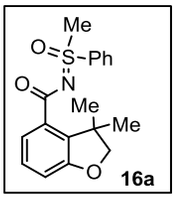

16a (93 mg, 95%) as colourless solid; ^{1}H NMR (400 MHz, $CDCl_3$) δ (d, J 8.0 Hz, 2H), 7.67 (bt, J 7.2 Hz, 1H), 7.62–7.55 (m, 2H), 7.53 (d, J 7.6 Hz, 1H), 7.14 (t, J 7.8 Hz, 1H), 6.88 (d, J 8.0 Hz, 1H), 4.18–4.10 (m, 2H), 3.40 (s, 3H), 1.47 (s, 3H), 1.38 (s, 3H); ^{13}C NMR (101 MHz, $CDCl_3$) δ , 160.4, 138.7, 135.4, 134.1, 133.7, 129.6, 127.5, 127.1, 122.7, 112.6, 85.3, 44.3, 43.3, 25.5, 25.2.

_N_-[7,7-Dimethyl-2,3,7,8-tetrahydrobenzofuro[6,7-*b*][1,4]dioxine-6-carboxyl]-_S_-methyl-_S_-phenylsulfoximine (16b):[9a]

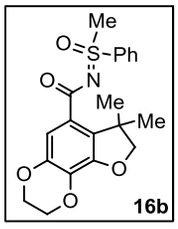

16b (95 mg, 82%) as colorless solid; ^{1}H NMR (400 MHz, $CDCl_3$) δ 8.02 (d, J 7.2 Hz, 2H), 7.66 (bt, J 7.2 Hz, 1H), 7.58 (t, J 7.4 Hz, 2H), 7.27 (bs, 1H), 4.34–4.29 (m, 2H) 4.28–4.24 (m, 2H), 4.24–4.21 (m, 2H), 3.38 (s, 3H), 1.46 (s, 3H), 1.37 (s, 3H); ^{13}C NMR (101 MHz, $CDCl_3$) δ 174.2, 148.3, 142.6, 138.9, 133.6, 132.1, 130.0, 129.6, 127.1, 125.2, 112.5, 87.0, 64.8, 64.3, 44.4, 43.8, 25.7, 25.5.

_N_-[6-(Benzyloxy)-3,3-dimethyl-2,3-dihydrobenzofuran-4-carboxyl]-_S_-methyl-_S_-phenylsulfoximine (16c):[9a]

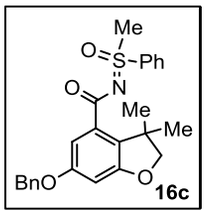

16c (106 mg, 81%) as colourless solid. ^{1}H NMR (400 MHz, $CDCl_3$) δ (d, J 7.6 Hz, 2H), 7.73–7.64 (m, 1H), 7.63–7.57 (m, 2H), 7.47–7.30 (m, 5H), 7.20 (d, J 2.4 Hz, 1H), 6.56 (d, J 2.4 Hz, 1H), 5.05 (s, 2H), 4.20–4.12 (m, 2H), 3.40 (s, 3H), 1.45 (s, 3H), 1.37 (s, 3H); ^{13}C NMR (101 MHz, $CDCl_3$) δ 175.2, 161.7, 158.7, 138.7, 136.9, 134.2, 133.8, 129.6, 128.5, 127.9, 127.5, 127.2, 109.2, 100.1, 86.1, 70.4, 44.4, 42.9, 25.8, 25.6.

_N_-[7-Bromo-6-methoxy-3,3-dimethyl-2,3-dihydrobenzofuran-4-carboxyl]-_S_-methyl-_S_-phenylsulfoximine (16d):[9a]

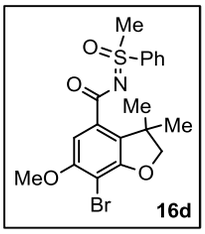

16d (104 mg, 79%) as colourless viscous liquid; ^{1}H NMR (400 MHz, $CDCl_3$) δ (d, J 7.4 Hz, 2H), 7.72 (t, J 7.2 Hz, 1H), 7.65 (t, J 7.2 Hz, 2H), 7.11 (s, 1H), 4.30 (d, J 8.0 Hz, 1H), 4.27 (d, J 8.0 Hz, 1H) 3.93 (s, 3H), 3.45 (s, 3H), 1.48 (s, 3H), 1.38 (s, 3H); ^{13}C NMR (101 MHz, $CDCl_3$) δ 174.6, 158.8, 155.5, 138.5, 133.9, 132.6, 129.7, 129.2, 127.1, 105.8, 96.6, 86.3, 56.6, 44.4, 44.2, 25.9, 25.4.

_N_-[7-Fluoro-3,3-dimethyl-2,3-dihydrobenzofuran-4-carboxyl]-_S_-methyl-_S_-phenylsulfoximine (16e):[9a]

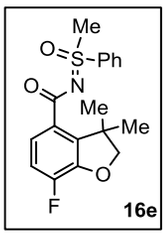

16e (93 mg, 89%) as colourless solid; ^{1}H NMR (400 MHz, $CDCl_3$) δ 8.04 (d, *J* 8.0 Hz, 2H), 7.69 (bt, *J* 7.2 Hz, 1H), 7.66–7.55 (m, 3H), 6.93 (t, *J* 9.2 Hz, 1H), 4.34–4.19 (m, 2H), 3.41 (s, 3H), 1.50 (s, 3H), 1.40 (s, 3H); ^{13}C NMR (101 MHz, $CDCl_3$) δ 174.4, 149.6 (d, *J* 250 Hz), 147.0 (d, *J* = 9 Hz) 139.8, 138.7, 133.8, 129.7, 127.1 (d, *J* = 14 Hz), 124.3 (d, *J* 6.1 Hz), 114.6 (d, *J* 17 Hz), 86.7, 44.4, 25.4, 25.1. ^{19}F NMR (376 MHz, $CDCl_3$) δ –134.25.

_N_-[6-Bromo-3,3-dimethyl-2,3-dihydrobenzofuran-4-carboxyl]-_S_-methyl-_S_-phenylsulfoximine (16f):[9a]

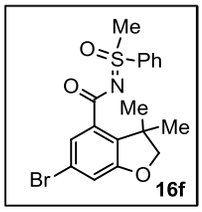

16f (66 mg, 54%) as colourless solid. m.p. 167–170 C; R_f 0.49 (6:4 hexane/EtOAc); ^{1}H NMR (500 MHz, $CDCl_3$) δ – (m, 2H), 7.70 (tt, *J* 7.5, 1.5 Hz, 1H), 7.66 (d, *J* 2.0 Hz, 1H), 7.63 (t, *J* 7.5 Hz, 2H), 7.03 (d, *J* 2.0 Hz, 1H), 4.17 (d, *J* 8.0 Hz, 1H), 4.15 (d, *J* 8.0 Hz, 1H), 3.41 (s, 3H), 1.45 (s, 3H), 1.36 (s, 3H); ^{13}C NMR (101 MHz, $CDCl_3$) δ 174.0, 161.4, 138.4, 135.2, 135.0, 133.9, 129.7, 127.1, 125.3, 120.3, 115.8, 85.9, 44.4, 43.1, 25.4, 25.1; IR (KBr) $_{max}$ 2927, 1632, 1217, 748 cm^{-1}; **HRMS (ESI)** for $C_{18}H_{18}BrNNaO_3S$: (M+Na)+: calcd. 430.0083, found 430.0079.

_N_-[3,3,5-Trimethyl-2,3-dihydrobenzofuran-4-carboxyl]-_S_-methyl-_S_-phenylsulfoximine (16g):[9a]

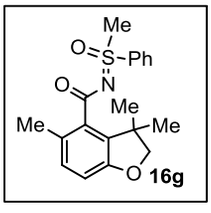

16g (80 mg, 67%) as colorless solid; ^{1}H NMR (400 MHz, $CDCl_3$) δ 8.07 (d, *J* 8.0 Hz, 2H), 7.70 (t, *J* = 7.4 Hz, 1H), 7.62 (t, *J* = 7.4 Hz, 2H), 6.92 (d, *J* 8.0 Hz, 1H), 6.67 (d, *J* 8.0 Hz, 1H), 4.15 (d, *J* = 8.4 Hz, 1H), 4.12 (d, *J* = 8.4 Hz, 1H), 3.49 (s, 3H), 2.33 (s, 3H), 1.46 (s, 3H), 1.40 (s, 3H); ^{13}C NMR (101 MHz, $CDCl_3$) δ 177.7, 157.8, 138.6, 135.6, 134.0, 131.5, 129.8, 129.6, 127.1, 125.5, 109.9, 85.0, 44.3, 43.0, 26.1, 25.8, 18.7.

_N_-[6-(2-Methylallyl)oxy)3,3-dimethyl-2,3-dihydrobenzofuran-4-carboxyl]-_S_-methyl-_S_-phenylsulfoximine (16h):

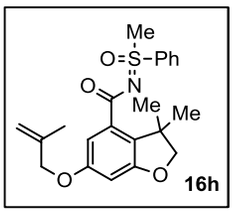

16h (99 mg, 82%) as colourless viscous liquid; R_f 0.39 (6:4 hexane/EtOAc); ^{1}H NMR (400 MHz, $CDCl_3$) δ 8.05 (t, J 6.6 Hz, 2H), 7.75–7.65 (m, 1H), 7.64–7.58 (m, 2H), 7.35 (d, J 2.4 Hz, 1H), 7.29–7.26 (m, 1H), 5.09 (s, 1H), 4.98 (s, 1H), 4.44 (s, 2H), 4.13 (s, 2H), 3.58–3.47 (m, 3H), 1.82 (s, 3H), 1.41 (s, 3H), 1.38 (s, 3H); ^{13}C NMR (101 MHz, $CDCl_3$) δ 160.1, 159.6, 140.7, 134.1, 129.65, 129.58, 127.2, 127.1, 123.3, 112.8, 108.1, 106.3, 93.7, 85.7, 71.9, 43.9, 42.6, 26.2, 26.1, 19.4; IR (Neat) $_{max}$ 2924, 1590, 1223, 755 cm^{-1}; **HRMS (ESI)** for $C_{22}H_{25}NNaO_4S$ $(M+Na)^+$: calcd. 422.1397, found 422.1406.

***N*-[3-Ethyl-3-methyl-2,3-dihydrobenzofuran-4-carboxyl]-*S*-methyl-*S*-phenylsulfoximine (16i):**[9a]

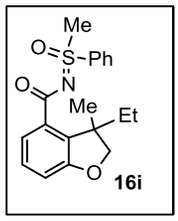

16i (35 mg, 33%) as colourless viscous liquid; the compound was obtained as inseparable mixture with the unreacted precursor **2i**; ^{1}H NMR (400 MHz, $CDCl_3$) (representative peaks of **3i**) δ 8.03 (d, J 7.6 Hz, 2H), 7.66 (t, J 7.4 Hz, 1H), 7.63–7.51 (m, 3H), 7.14 (t, J 7.8 Hz, 1H), 6.86 (d, J 8.0 Hz, 1H), 4.32 (d, J 8.4 Hz, 1H), 4.06 (d, J 8.4 Hz, 1H), 3.39 (s, 3H), 2.17–2.04 (m, 1H), 1.72–1.65 (m, 1H), 1.35 (s, 3H), 0.75 (t, J 7.6 Hz, 3H); ^{13}C NMR (101 MHz, $CDCl_3$) (representative peaks of **3i**) δ 175.5, 160.9, 138.8, 134.5, 133.8, 133.7, 129.6, 127.6, 127.1, 122.6, 112.3, 82.3, 47.3, 44.3, 30.6, 24.3, 9.1.

IV.6.3: General Procedure for Hydroarylation of O-Tethered Compounds (20)

The hydroarylation reactions were conducted in a 50 mL Schlenk tube having high pressure valve and side arm. The tube was charged with (**20**, 0.3 mmol), $[RuCl_2(p\text{-cymene})]_2$ (6.0 mg, 3.0 mol %), and $Cu(OAc)_2 \cdot H_2O$ (60 mg, 0.3 mmol). Subsequently, the additive KPF_6 (7.0 mg, 12 mol %) and $AgSbF_6$ (7.0 mg, 12 mol %) was introduced to the flask in a glove box. Water (H_2O) (2.0 mL) was added to the mixture and the resulting mixture was stirred at 110 C for 16 h. The reaction mixture was filtered through a small plug of Celite and washed with dichloromethane (3 × 5.0 mL). The solvents were

evaporated under the reduced pressure and the crude material was purified using column chromatography on silica gel.

Following this procedure, compounds **21a** and **21b** were prepared. Analytical and spectral data of these compounds are exactly matching with the reported values. [3]

7-Methoxy-N-3,3-trimethyl-2,3-dihydrobenzofuran-4-carboxamide (21a): [9b]

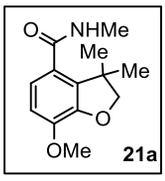

21a (44 mg, 62%) as colorless solid; ^{1}H NMR (400 MHz, CDCl3) δ 6.86 (d, *J* = 8.4 Hz, 1H), 6.69 (d, *J* = 8.0 Hz, 1H), 5.87 (bs, 1H), 4.24 (s, 2H), 3.87 (s, 3H), 2.95 (s, 3H), 1.45 (s, 6H); ^{13}C NMR (101 MHz, $CDCl_3$) *δ* 169.4, 148.4, 146.2, 135.4, 126.0, 120.1, 110.4, 86.0, 55.9, 43.7, 26.6, 25.8.

N-3,3-Trimethyl-7-nitro-2,3-dihydrobenzofuran-4-carboxamide (21b):[9b]

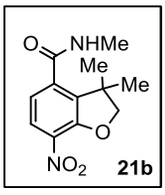

21b (19 mg, 26%) as pale yellow solid; ^{1}H NMR (400 MHz, $CDCl_3$) *δ* 7.90 (d, *J* = 8.4 Hz, 1H), 6.90 (d, *J* = 8.4 Hz, 1H), 5.95 (bs, 1H), 4.44 (s, 2H), 3.01 (d, *J* 4.4 Hz, 3H), 1.48 (s, 6H); ^{13}C NMR (101 MHz, $CDCl_3$) *δ* 167.6, 155.3, 138.85, 138.80, 133.6, 124.3, 119.0, 87.2, 42.7, 26.7, 25.7.

IV.6.4: General Procedure for the Dual Hydroarylation Reaction From mono-Hydroarylated product 16h

The dual hydroarylation reaction was conducted in a 50 mL Schlenk tube having high pressure valve and side arm. The tube was charged with **16h** (0.3 mmol), [$RuCl_2$(*p*-cymene)]$_2$ (6.0 mg, 3.0 mol %), and $Cu(OAc)_2 \cdot H_2O$ (60 mg, 0.3 mmol). Subsequently, the additive KPF_6 (7 mg, 12.0 mol %) was introduced to the flask in a glove box. Water (H_2O) (2.0 mL) was added to the mixture and the resulting mixture was stirred at room temparature for 12 h. The reaction mixture was filtered through a plug of Celite and washed with CH_2Cl_2 (3 × 5.0 mL). The solvents were evaporated under the reduced

pressure and the crude material was purified using column chromatography on silica gel (30– 0% *n*-hexane/EtOAc eluent) to give the desired product **17**.

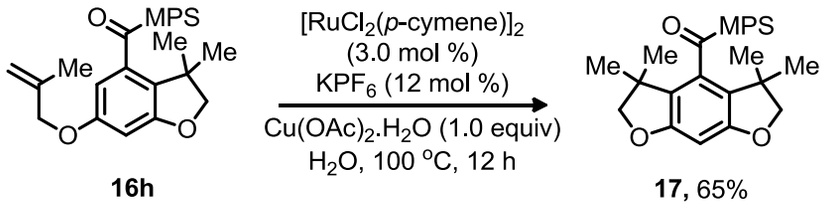

16h **17,** 65%

_N_-[3,3,5,5-Tetramethyl-2,3,5,6-tetrahydrobenzo[1,2-*b*:5,4-*b*']difuran-4-carboxyl]-_S_-methyl-_S_-phenylsulfoximine (17):[9a]

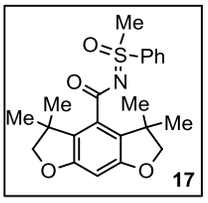

17 (79 mg, 65%) as colourless crystalline solid; ^{1}H NMR (400 MHz, $CDCl_3$) δ 8.06 (d, J 7.6 Hz, 2H), 7.70 (t, J 7.4 Hz, 1H), 7.62 (t, J 7.6 Hz, 2H), 6.26 (s, 1H), 4.13 (s, 4H), 3.56 (s, 3H), 1.40 (s, 6H), 1.37 (s, 6H); ^{13}C NMR (101 MHz, $CDCl_3$) δ 176.4, 160.1, 138.4, 134.1, 131.9, 129.6, 127.1, 123.3, 93.7, 85.7, 43.9, 42.5, 26.2, 26.1.

IV.6.5: General Procedure for the Annulation of Dihydrobenzofuran 16a with 1,2-Diphenyl acetylene

The annulation reactions were conducted in a 50 mL Schlenk tube having high pressure valve and side arm. The tube was charged with **16a** (100 mg, 0.3 mmol), 1,2-diphenyl acetylene (64 mg, 0.36 mmol), $[RuCl_2(p\text{-cymene})]_2$ (9.0 mg, 5.0 mol %), and AcOH (0.3 mmol). Subsequently, the additive $AgSbF_6$ (20 mg, 20 mol %) was introduced to the flask in a glove box. 1,4-Dioxane (2.0 mL) was added to the mixture and the resulting mixture was stirred at 120 °C for 24 h. The reaction mixture was filtered through a plug of Celite and washed with dichloromethane (3 × 5.0 mL). The solvents were evaporated under reduced pressure and the crude material was purified using column chromatography on silica gel (20–30% *n*-hexane/EtOAc eluent) to give the desired product.

9,9-Dimethyl-3,4-diphenyl-8,9-dihydrofuro[2,3-*h*]isoquinolin-1(2H)-one (26):

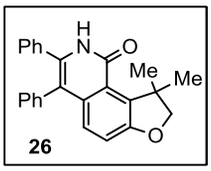

26 (68 mg, 62%) as colorless crystalline solid; ^{1}H NMR (400 MHz, $CDCl_3$) δ 9.79 (bs, 1H), 7.30–7.24 (m, 3H), 7.22 (bs, 5H), 7.18 (d, *J* 8.8 Hz, 1H), 7.16–7.11 (m, 2H), 7.05 (d, *J* 8.8 Hz, 1H), 4.31 (s, 2H), 1.54 (s, 6H); ^{13}C NMR (101 MHz, $CDCl_3$) δ 159.4, 136.7, 135.2, 134.5, 134.2, 131.9, 129.2, 128.30, 128.26, 128.1, 127.5, 127.1, 117.6, 116.1, 86.4, 44.6, 29.7, 26.7.

IV.6.6: General Procedure for the Unsymmetrical Two-fold C–H Functionalization (*Intramolecular Hydroarylation & Intermolecular Bromination*) Reaction

The twofold C–H functionalization reaction was conducted in a 50 mL Schlenk tube having high pressure valve and side arm. The tube was charged with **16a** (100 mg, 0.3 mmol), NBS (80 mg, 0.45 mmol), $Pd(OAc)_2$ (11.0 mg, 15 mol %), and AcOH (0.75 mmol). 1,2-Dichloroethene (DCE) solvent (3.0 mL) was added to the mixture and the resulting mixture was stirred at 100 ^{o}C for 12 h. The reaction mixture was filtered through a plug of Celite and washed with dichloromethane (3 × 5.0 mL). The solvents were evaporated under reduced pressure and the crude material was purified using column chromatography on silica gel (35–50% *n*-hexane/EtOAc eluent) to give the desired product.

N-[5-Bromo-3,3-dimethyl-2,3-dihydrobenzofuran-4-carboxyl]-*S*-methyl-*S*-phenylsulfoximine (27):

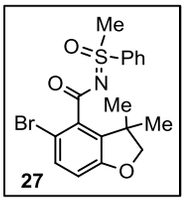

27 (88 mg, 72%) as colourless solid. ^{1}H NMR (400 MHz, $CDCl_3$) δ (d, *J* 7.6 Hz, 2H), 7.69 (t, *J* 7.4 Hz, 1H), 7.61 (t, *J* 7.6 Hz, 2H), 7.30–7.24 (m, 1H), 6.64 (d, *J* 8.4 Hz, 1H), 4.18 (d, *J* 8.4 Hz , 1H), 4.14 (d, *J* 8.4 Hz , 1H), 3.55 (s, 3H), 1.46 (s, 3H), 1.39 (s, 3H); ^{13}C NMR (101 MHz, $CDCl_3$) δ 175.2, 159.1, 138.0, 136.8, 134.1, 134.0, 132.0, 131.9, 129.6, 111.4, 108.8, 85.2, 44.0, 43.3, 26.4, 25.4.

IV.6.7: General Procedure for the Unsymmetrical Two-fold C–H Functionalization (*Intramolecular Hydroarylation & Intermolecular Acetoxylation*) Reaction

The two fold C–H functionalization reaction was conducted in a 50 mL Schlenk tube having high pressure valve and side arm. The tube was charged with **16a** (100 mg, 0.3 mmol), $Pd(OAc)_2$ (7.0 mg, 10 mol %), $K_2S_2O_8$ (162 mg, 0.6 mmol) and $AcOH/CHCl_3$ (3:5, 2.0 mL) were added to the mixture and the resulting mixture was stirred at 100 °C for 12 h. The reaction mixture was filtered through a plug of Celite and washed with dichloromethane (3 × 5.0 mL). The solvents were evaporated under reduced pressure and the crude material was purified using column chromatography on silica gel (35-50% *n*-hexane/EtOAc eluent) to give the desired product.

_N_-[5-Actoxy-3,3,-dimethyl-2,3-dihydrobenzofuran-4-carboxyl]-_S_-methyl-_S_-phenylsulfoximine (28):

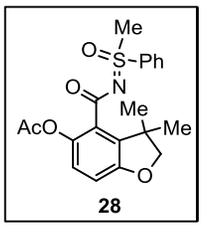

28

28 (78 mg, 67%) as colourless solid. m.p. 222 C; R_f 0.40 (6:4 hexane/EtOAc); ^{1}H NMR (400 MHz, $CDCl_3$) δ 8.08–8.02 (m, 2H), 7.74–7.66 (m, 1H), 7.65–7.58 (m, 2H), 6.84 (d, J 8.8 Hz, 1H), 6.77 (d, J 8.8 Hz, 1H), 4.17 (s, 2H), 3.42 (s, 3H), 2.12 (s, 3H), 1.45 (s, 3H), 1.40 (s, 3H); ^{13}C NMR (101 MHz, $CDCl_3$) δ 173.7, 169.9, 157.5, 141.0, 138.3, 134.0, 133.8, 129.7, 128.7, 127.2, 122.3, 110.6, 85.5, 44.2, 43.4, 25.7, 25.5, 20.9; IR (Neat) $_{max}$ 2927, 1632, 1217, 748, 494 cm^{-1}; **HRMS (ESI)** for $C_{20}H_{21}NNaO_5S$ $(M+Na)^+$: calcd. 410.1033, found 410.1039.

IV.6.8: General Procedure for the Hydrolysis of Hydroarylated Product

Compound **16b** (0.25 mmol) was dissolved in NaOH in H_2O and MeOH solution (1:1, 2.0 mL) and stirred at 70 °C for 6 h. The reaction mixture was extracted with Et_2O, dried over Na_2SO_4, and concentrated under vacuum to give 7,7-dimethyl-2,3,7,8-tetrahydrobenzofuro[6,7-*b*][1,4]dioxine-6-carboxylic acid (**29**). The basic aqueous-layer was acidified with dil. HCl and extracted with CH_2Cl_2. The CH_2Cl_2 layer was washed with brine, dried over Na_2SO_4, and concentrated under vacuum to give the methylphenylsulfoximine (**15''**).

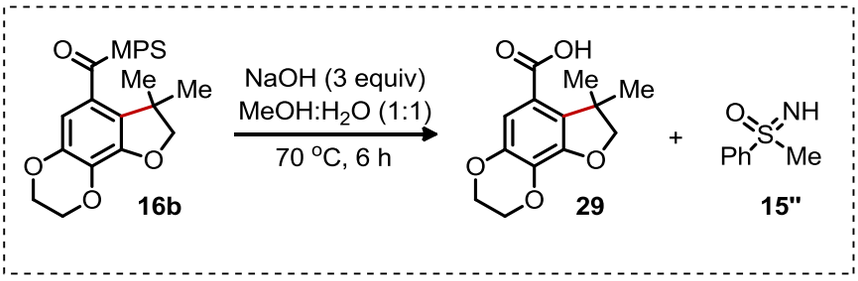

7,7-Dimethyl-2,3,7,8-tetrahydrobenzofuro[6,7-*b*][1,4]dioxine-6-carboxylic acid (29):

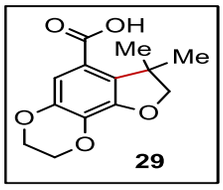

29 (52 mg, 81%) as colourless solid. ^{1}H NMR (400 MHz, $CDCl_3$) δ (s, 1H), 4.42–4.27 (m, 6H), 1.53 (s, 6H); ^{13}C NMR (101 MHz, $CDCl_3$) δ 171.1, 148.7, 143.0, 133.7, 131.5, 117.7, 113.5, 87.0, 64.8, 64.2, 44.1, 25.6.

IV.7. References

(1) a) C. I. Herrerías, X. Yao, Z. Li, C.-J. Li, *Chem. Rev*. **2007**, *107*, 2546; b) T. Kitanosono, K. Masuda, P. Xu, S. Kobayashi, *Chem. Rev*. **2018**, *118, 679;* c) R. N. Butler, A. G. Coyne, Org. Biomol. Chem., **2016**,*14*, 9945; d) S. Narayan, J. Muldoon, M. G. Finn, V. V. Fokin, H. C. Kolb, K. B. Sharpless, Angew. Chem., Int. Ed. **2005**, *44*, 3275.

(2) Selected reviews on C–H activation: a) R. G. Bergman, *Nature.* **2007**, *446*, 391; b) I. V. Seregin, V. Gevorgyan, *Chem. Soc. Rev*. **2007**, *36*, 1173; c) X. Chen, K. M. Engle, D.–H. Wang, J –Q. Yu, *Angew. Chem., Int. Ed.* **2009**, *48*, 5094; d) D. A. Colby, R. G. Bergman, J. A. Ellman, *Chem. Rev*. **2010**, *110*, 624; e) T. W. Lyons, M. S. Sanford, *Chem. Rev.* **2010**, *110*, 1147; f) L. C. M. Castro, N. Chatani, *Chem. Lett*. **2015**, *44*, 410; g) B. Liu, F. Hu, B –F. Shi, *ACS Catalysis* **2015**, *5*, 1863.

(3) C–H activation in synthesis: a) K. Godula, D. Sames, *Science* **2006**, *312*, 67; b) D. Y.-K. Chen, S. W. Youn, *Chem.-Eur. J.* **2012**, *18*, 9452.

(4) DG in C–H activation: a) G. Rouquet, N. Chatani, *Angew. Chem., Int. Ed.* **2013**, *52*, 11726; b) S. D. Sarkar, W. Liu, S. I. Kozhushkov, L. Ackermann, *Adv. Synth. Catal.* **2014**,

356, 1461; c) M. R. Yadav, R. K. Rit, M. Shankar, A. K. Sahoo, *Asian. J. Org. Chem.* **2015**, *4*, 846.

(5) a) G. Zammit, M. Erman, S. Wang-Weigand, S. Sainati, J. Zhang, T. Roth, *J. Clin. Sleep Med.* **2007**, *3*, 495; b) T. Ito, H. Endo, H. Shinohara, M. Oyama, Y. Akao, A. Iinuma, *Fitoterapia* **2012**, *83*, 1420.

(6) a) R. K. Thalji, K. A. Ahrendt, R. G. Bergman, J. A. Ellman, *J. Am. Chem. Soc.* **2001**, *123*, 9692; b) K. A. Ahrendt, R. G. Bergman, J. A. Ellman, *Org. Lett.* **2003**, *5*, 1301; c) R. K. Thalji, J. A. Ellman, R. G. Bergman, *J. Am. Chem. Soc.* **2004**, *126*, 7192; d) R. K. Thalji, K. A. Ahrendt, R. G. Bergman, J. A. Ellman, *J. Org. Chem.* **2005**, *70*, 6775; e) S. J. O'Malley, K. L. Tan, A. Watzke, R. G. Bergman, J. A. Ellman, *J. Am. Chem. Soc.* **2005**, *127*, 13496; f) A. Watzke, R. M. Wilson, S. J. O'Malley, R. G. Bergman, J. A. Ellman, *Synlett* **2007**, 2383.

(7) a) T. A. Davis, T. K. Hyster, T. Rovis, *Angew. Chem., Int. Ed.* **2013**, *52*, 14181; b) B. Ye, P. A. Donets, N. Cramer, *Angew. Chem., Int. Ed.* **2014**, *53*, 507; c) T. A. Davis, C. Wang, T. Rovis, *Synlett.* **2015**, *26*, 1520.

(8) Z. Ding, N. Yoshikai, *Angew. Chem., Int. Ed.* **2013**, *52*, 8574.

(9) a) K. Ghosh, R. K. Rit, E. Ramesh, A. K. Sahoo, *Angew. Chem., Int. Ed.* **2016**, *55*, 7821; b) R. K. Rit, K. Ghosh, R. Mandal, A. K. Sahoo, *J. Org. Chem.* **2016**, *81*, 8552;

(10) D. F. Fernández, M. Gulías, J. L. Mascareñas, F. López, *Angew. Chem., Int. Ed.* **2017**, *56*, 9541.

(11) Recent ruthenium-catalyzed transformations in water; see: a) P. B. Arockiam, C. Fischmeister, C. Bruneau, P. H. Dixneuf, *Angew. Chem., Int. Ed.* **2010**, *49*, 6629. b) L. Ackermann, S. Fenner, *Org. Lett.* **2011**, *13*, 6548 c) B. Li, K. Devaraj, C. Darcel, P. H. Dixneuf, Tetrahedron. **2012**, *68*, 5179; d) L. Ackermann, J. Pospech, H. Potukuchi, *Org. Lett.* **2012**, *14*, 2146; *e)* L. Ackermann, L. Wang, R. Wolfram, A. V. Lygin, *Org. Lett.* **2012**, *14*, 728. f) A. Tlili, J. Schranck, J. Pospech, H. Neumann, M. Beller, *Angew. Chem., Int. Ed.* **2013**, *52*, 6293; g) P. B. Arockiam, C. Fischmeister, C. Bruneau, P.

H. Dixneuf, *Green Chem.* **2013,** *15 , 67; h) L. A. Adrio, J. Gimeno, C. Vicent, Chem. Commun.* **2013**, *49,* 8320; i) B. Li, C. B. Bheeter, C. Darcel, P. H. Dixneuf, *Top Catal.,* **2014**, *57,* 833; j) J. Pospech, A. Tlili, A. Spannenberg, H. Neumann, M. Beller, *Chem. Eur. J.* **2014**, *20*, 3135; k) A. Tlili, J. Schranck, J. Pospech, H. Neumann and M. Beller, *ChemCatChem.* **2014**, *6,* 1562; l) K. S. Singh, S. G. Sawant, P. H. Dixneuf, *ChemCatChem.* **2016**, *8,* 1046; m) C. Binnani, D. Tyagi, R. K. Rai, S. M. Mobin, S. K. Singh, *Chem. Asian J.* **2016**, *11,* 3022; n) P. Nareddy, F. Jordan, M. Szostak, *Org. Lett.* **2018**, *20,* 34; o) G. Zhang, F. Jia, L. J. Gooßen, *Chem. Eur. J.* **2018**, *24*, 4537; p) W. –J. Han, F. Pu, C. –J. Li, Z. –W. Liu, J. Fan, X –Y. Shi, *Adv. Synth. Catal*, **2018**, *360*, 1358.

(12) For a recent review on transition-metal-catalyzed C(sp^2)–H bond functionalization in water, see: a) B. Li, P. H. Dixneuf, *Chem. Soc. Rev*. **2013**, *42*, 5744. b) L. Ackermann, *Chem. Rev.* **2011**, *111*, 1315.

(13) J. Oxgaard, W. J. Tenn, R. J. Nielsen, R. A. Periana, W. A. Goddard, *Organometallics.* **2007**, *26*, 1565. b) T. R. Cundari, T. V. Grimes, T. B. Gunnoe, *J. Am. Chem. Soc.* **2007**, *129*, 13172.

(14) a) M. R. Yadav, R. K. Rit, M. Shankar, A. K. Sahoo, *J. Org. Chem*. **2014**, *79*, 6123. b) R. K. Rit, M. R. Yadav, K. Ghosh, M. Shankar, A. K. Sahoo, *Org. Lett.* **2014**, *16*, 5258. c) M. R. Yadav, R. K. Rit, A. K. Sahoo, *Chem. Eur. J*. **2012**, *18*, 5541.

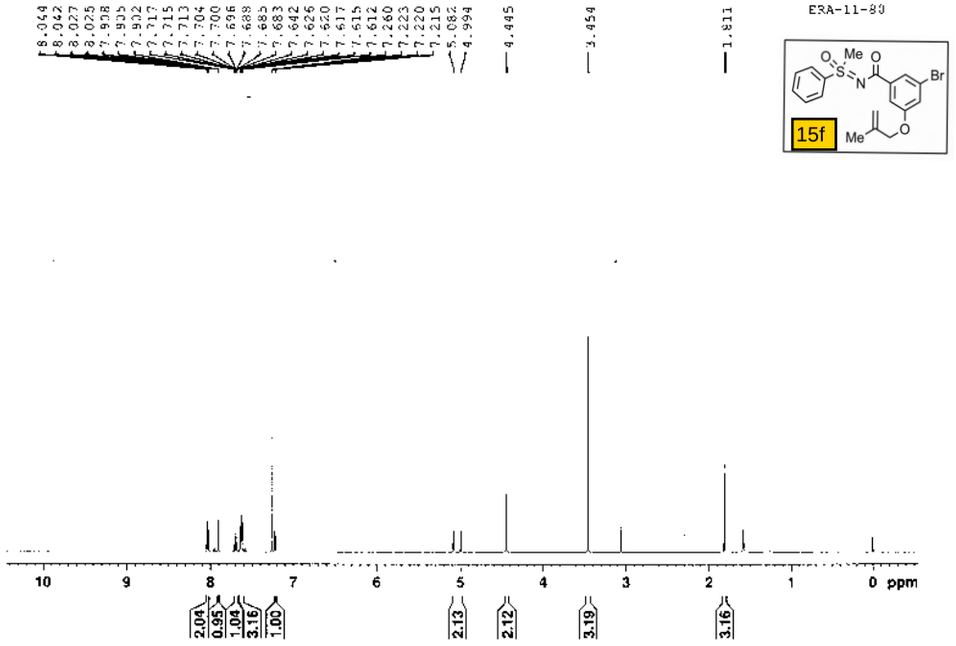
ERA-11-80
15f

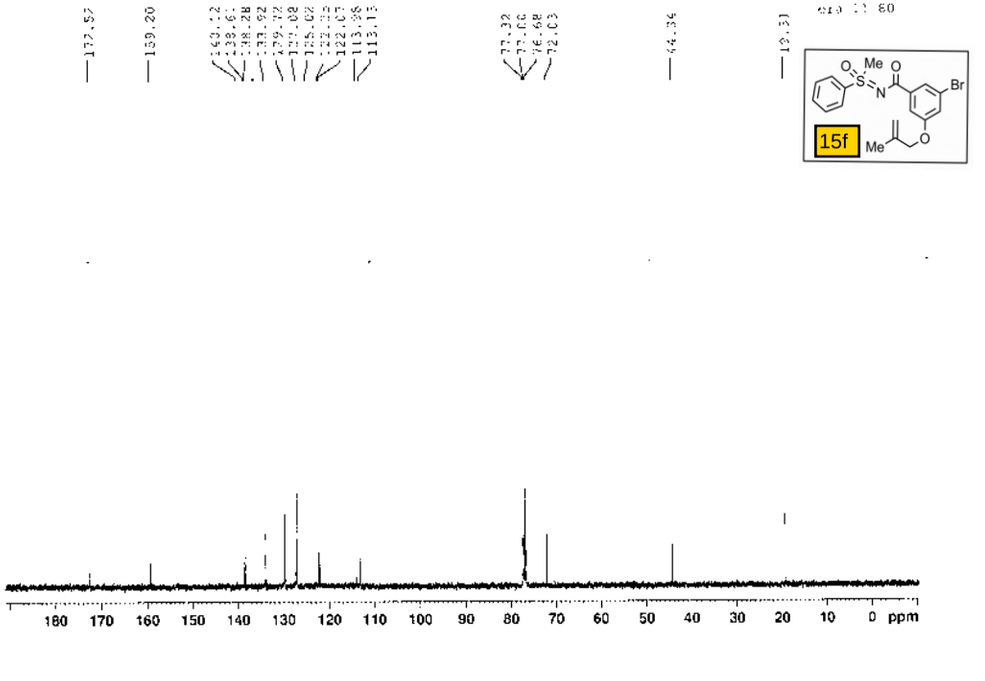
15f

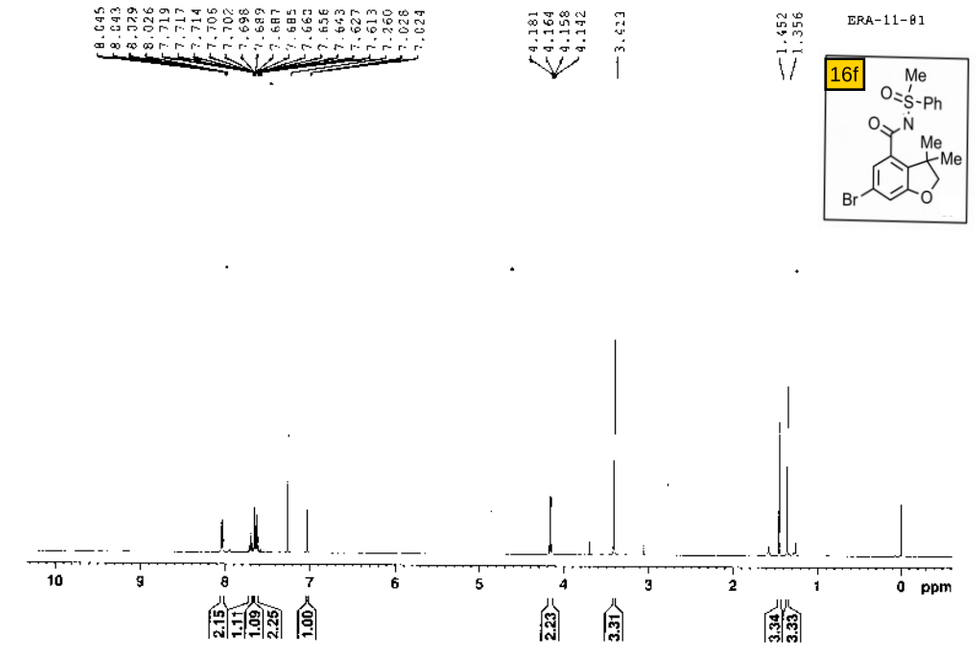
ERA-11-81
16f

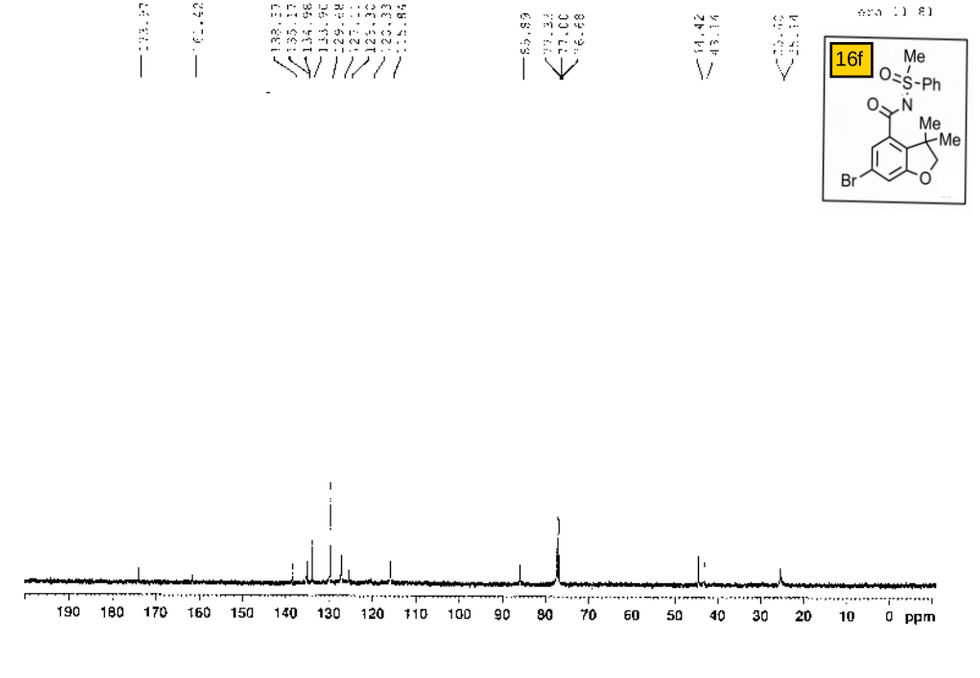
16f

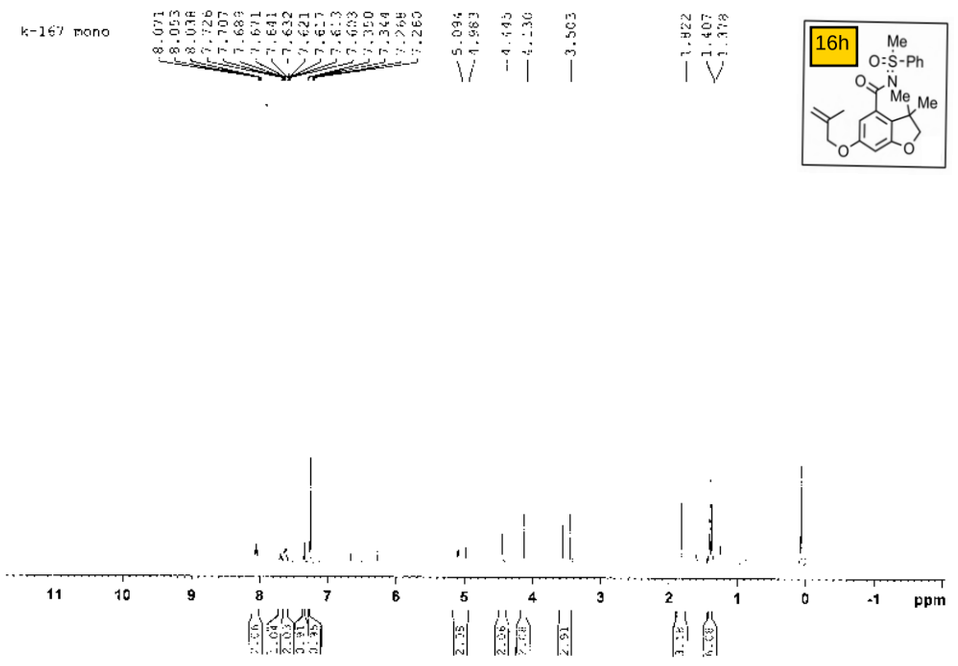
k-167 mono
16h
Me
O=S-Ph
N
Me
Me
Me
O
O

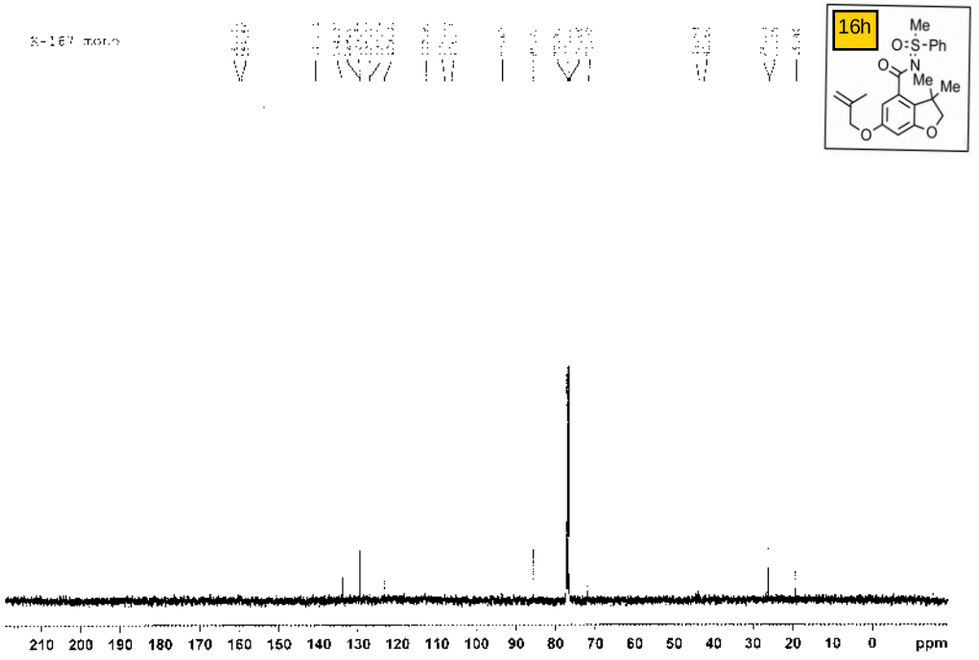
16h
Me
O=S-Ph
N
Me
Me
Me
O
O

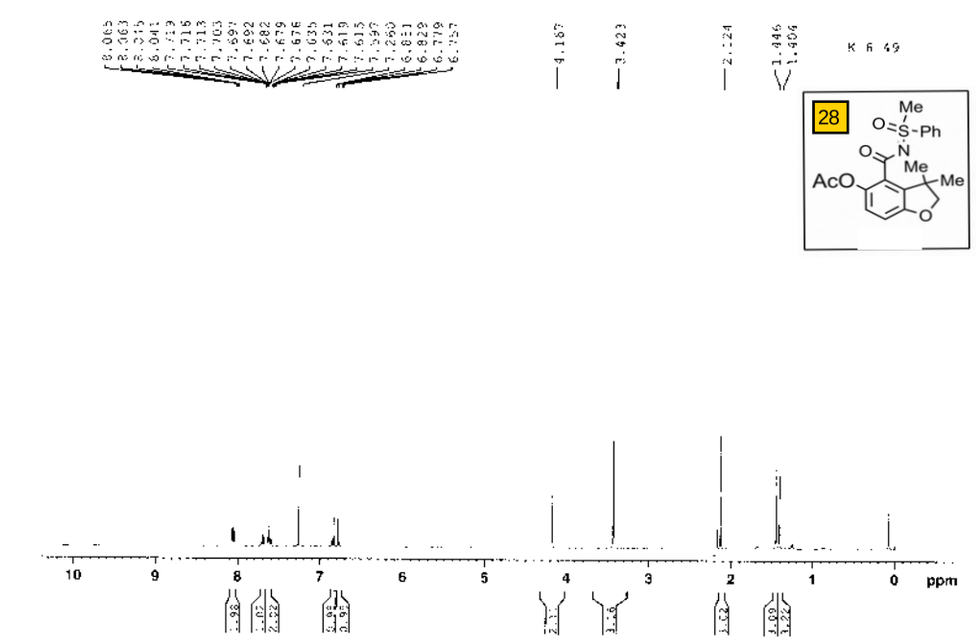
K 6 49
28
Me
O=S-Ph
N
Me
AcO
Me
Me
O

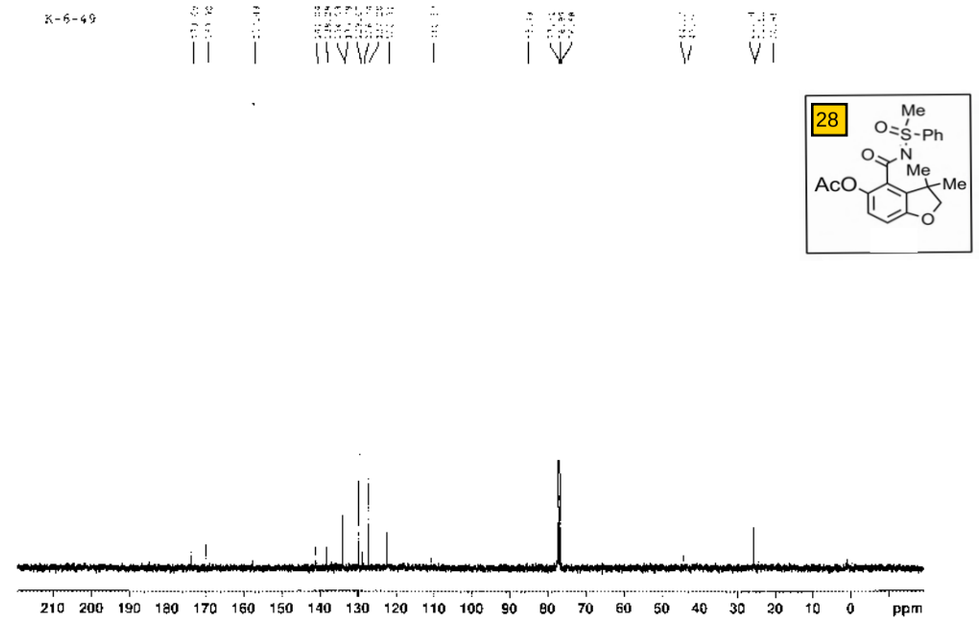
K-6-49
28
Me
O=S-Ph
N
Me
AcO
Me
Me
O

15g-H/D
MPS 12% D
ERA-1-101
8.044
8.026
8.023
7.673
7.655
7.639
7.632
7.619
7.616
7.603
7.600
7.260
7.095
7.074
6.923
6.916
6.903
6.895
5.091
4.978
4.438
3.413
2.505
1.021
ppm

ERA--11 67
8.063
8.047
7.704
7.690
7.675
7.663
7.629
7.616
7.579
7.260
7.162
7.147
6.904
6.889
4.174
4.157
4.152
4.135
3.428
1.485
1.394
ppm

List of Publications

1. Kinetic Resolution of Sulfur-Stereogenic Sulfoximines by Pd(II)-MPAA Catalyzed C–H Olefination and Arylation (*Communicated*)
Kallol Mukherjee, Nicolas Grimblat, Somratan Sau, Koushik Ghosh, Majji Shankar, Vincent Gandon and Akhila K. Sahoo*

2. Directing Group Assisted Unsymmetrical Multiple Functionalization of Arene C− H Bonds
Koushik Ghosh, Raja K. Rit, Majji Shankar, **Kallol. Mukherjee** and A. K. Sahoo* *The Chemical Record*, **2020**, *20*, 1017

3. Sulfoximine Assisted Unsymmetrical Two-fold C–H Functionalization of Arenes
Koushik Ghosh, Arghadip Ghosh, **Kallol Mukherjee**, Raja. K. Rit and Akhila K. Sahoo* *J. Org. Chem*. **2020**, *85*, 8618

4. Double Annulation of ortho-and peri-C−H Bonds of Fused (Hetero) Arenes to Unusual Oxepino-Pyridines
Akhila K. Sahoo*, Majji Shankar, Raja K. Rit, Somratan Sau, **Kallol Mukherjee** and Vincent Gandon *Chem. Sci*. **2020**, *11*, 10770

5. One-Pot Unsymmetrical {[4 + 2] and [4 + 2]} Double Annulations of o/o′-C–H Bonds of Arenes: Access to Unusual Pyranoisoquinolines
Majji Shankar, Koushik Ghosh, **Kallol Mukherjee**, Raja. K. Rit and Akhila. K. Sahoo* *Org. Lett*. **2018**, *20*, 5144-5148

6. Ruthenium-Catalyzed Intramolecular Hydroarylation of Arenes with Olefins in Water
Kallol Mukherjee, E. Ramesh, Koushik Ghosh and Akhila K. Sahoo* *Asian J. Org. Chem*. **2018**, *7*, 1380

7. An Orchestrated Unsymmetrical Annulation Episode of C(sp^2)–H Bonds with Alkynes and Quinones: Access to Spiro-isoquinolones
Kallol Mukherjee, Majji Shankar, Koushik Ghosh and Akhila K. Sahoo* *Org. Lett*. **2018**, *20*, 1914.

8. Ru-Catalyzed One-Pot Di-Annulation of Heteroaryls: Direct Access to -Conjugated Polycyclic Amides
Majji Shankar, Koushik Ghosh, **Kallol Mukherjee**, Raja K. Rit, and Akhila K. Sahoo* *Org. Lett*. **2016**, *17*, 6416.

Conference Attended

1. **Kinetic Resolution of Sulfoximine via alkenylation and Annulation Episode of C(sp^2 –H Bonds with Alkynes and Quinones**

   Kallol Mukherjee and Akhila K. Sahoo*

   Oral and Poster Presentation at "**Chem Fest-2020**" held at School of Chemistry, University of Hyderabad, Hyderabad, India on **February, 2020**.

2. **Unsymmetrical Cyclization Episode of C(sp^2 –H Bonds with Alkynes and Quinones: Ruthenium Catalyzed Hydroarylation in Water**

   Kallol Mukherjee and Akhila K. Sahoo*

   Oral Presentation at "**XV J-NOST-2019**" held at Delhi University, Delhi, India on **Oct, 2019**.

3. **An Orchestrated Cyclization Episode of C(sp^2)-H Bonds with Alkynes and Quinones:Access to Spiro-Quinolinones**

   Kallol Mukherjee and Akhila K. Sahoo*

   Poster Presentation at "**ICCHD-2018**" held at Kolkata, India on **Dec, 2018**.

4. **Ru-Catalyzed One-Pot Di-Annulation of Heteroaryls: Direct Access to –Conjugated Polycyclic Amides**

   Kallol Mukherjee and Akhila K. Sahoo*

   Poster Presentation at "**Chem Fest-2017**" held at School of Chemistry, University of Hyderabad, Hyderabad, India on **February, 2017**.

Biographical Sketch

Kallol Mukherjee was born in Paligram (village), Guskara Burdwan (dist), West Bengal, India on 13th Aug, 1991. He did primary schooling in Paligram B. S. Vidyamandir (10th standard), D. Gonapaputtuga. He finished Intermediate education at the Bikna K. P. S. Vidyapith, Bankura. Then he received B. Sc degree from Visva-Bharati University, Shantiniketan, West Bengal in 2012 where he gained some interest in chemistry. He obtained Master's degree in Chemistry (Organic chemistry) in 2014 from the same University. In December-2013 and June-2014 he cleared CSIR-JRF (70 and 36 rank) and GATE (278 rank) Examination. In Jan-2015, he started the research work at the School of Chemistry, University of Hyderabad under the guidance of Prof. Akhila Kumar Sahoo. His research interest deals with the development of "Stereoselective C–H Functionalization and Unsymmetrical Multiple C–H Annulations".

Metal-Catalyzed Stereoselective C-H Functionalization Mediated Kinetic Resolution of Sulfoximines and Unsymmetrical Multiple C-H Annulations

by Kallol Mukherjee

Submission date: 28-Jun-2021 03:14PM (UTC+0530)
Submission ID: 1613238663
File name: Thesis_Kallol.pdf (9.69M)
Word count: 15299
Character count: 83822

Chapter 1

Stereoselective C–H Bond Activation and Annulation: An Introduction

Abstract

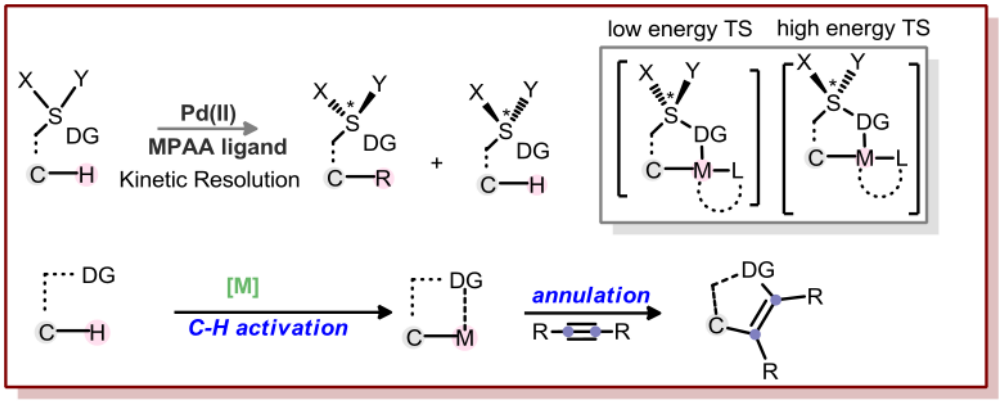

C–H activation strategy has been employed for the introduction of chirality in molecules as well as the construction of complex molecular scaffolds through unsymmetrical multiple C–H annulations. In the first part of this chapter, a brief introduction of C–H activation along with various mechanisms of C–H activation are discussed. The second part enumerates the concept of kinetic resolution of substrates through C–H functionalization. The origin of stereoselectivity and the use of chiral amino acid ligand in combination with transition metal catalyst is briefed. The coordination of sulfoximine pyridyl-motif with Pd(II)-catalyst and mono-protected chiral amino acid (MPAA) ligand for the enantio-determining C(aryl)–H activation is narrated. The last part of this chapter covers unsymmetrical multiple annulations and hydroarylation 'in water' that involves C–H activation.

I.1. Introduction:

Inert C–H bonds are undoubtedly ubiquitous. Hence, direct conversion of C–H bonds to carbon-carbon (C–C), carbon-heteroatom (C–X) bonds has had a significant impact enriching the synthetic potential. Along this line, direct functionalization of C–H bond could reliably be used making complex molecular scaffolds with ease. Thus, the development of novel synthetic method linked to the functionalization of inert C–H bonds always appealing. The transition-metal (TM) catalyzed cross-coupling reactions offered a synthetically alternative plan for making diverse ranges of bond formations; however, these methods primarily require pre-functionalized precursors, which are prepared from readily available materials by multi-step synthesis, and generate a large amount of waste by-products during the reaction. In this connection, an unconventional TM-catalyzed activation and functionalization of inert C–H bond has provided a synthetically alternative greener pathway by not only discovering new reactions but also making novel chemical space with diversity. Despite the tremendous synthetic potential, selective activation of a particular C–H bond in organic molecules by combining the inherent stereo- and regio-selectivity issues is always challenging.

I.1.1. Transition metal-catalyzed cross-coupling reaction

Transition metal catalyzed cross-couplings are the trustworthy approaches for the introduction of complexity in the molecule.[1] In this case, an organometallic reagent (main group metal), in the presence of a group 8 or group 10 metal catalysts in combination with an organic electrophile allows making C–C and C–heteroatom bonds (**Scheme I.1**).[2] Since the early discoveries in this field by Kumada, Suzuki , Kochi, Corriu, and Murahashi; many organometallic reagents, such as organoboron, organosilicon, organotin, and organozinc have proved to be very useful coupling partner for cross-coupling reactions. Diversity of coupling partners and electrophiles made these process key tools for organic synthesis, resulting a plethora of synthetic methods towards pharmaceuticals and natural products.[3] The overall catalytic cycle of the cross-coupling reaction is depicted in **Scheme I.2**. In general, the cross-coupling

reaction mainly involves oxidative addition of electrophile to metal centre, followed by transmetalation, and finally, reductive elimination (**Scheme I.2**).

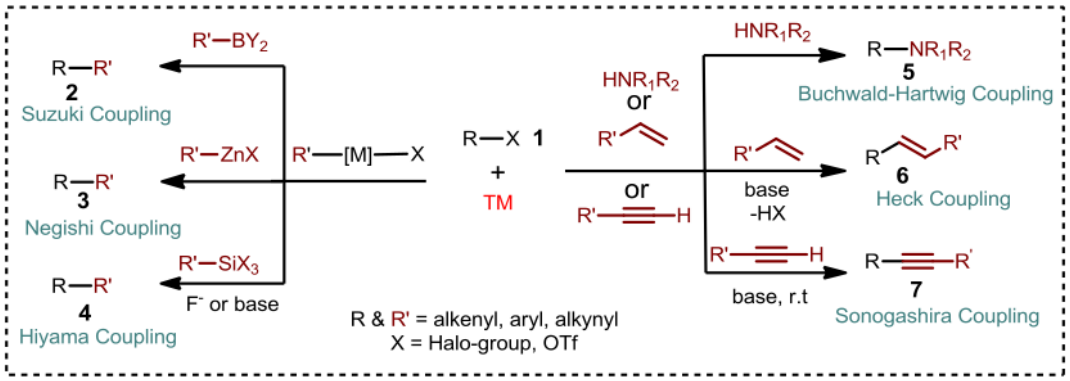

Scheme I.1: General overview of metal-catalyzed cross-coupling reaction

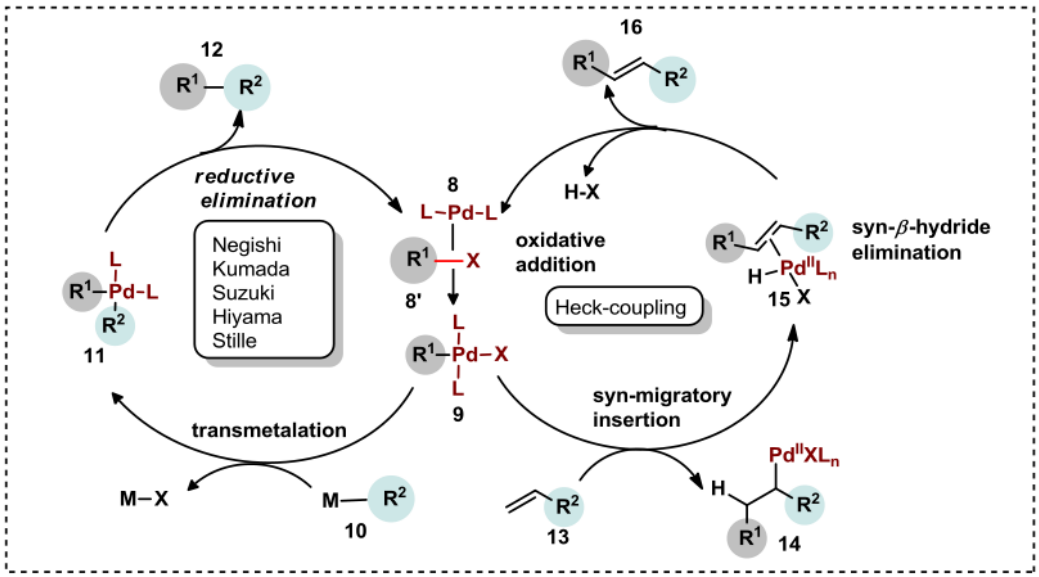

Scheme I.2: Pathways of various cross-coupling reactions

However, most of the cross-coupling reactions often associated with requirement of pre-functionalized starting materials (electrophiles, organometallic reagents, and nucleophiles), which make this process synthetically lengthy and cumbersome.[4]

Therefore, development of an alternate straightforward, atom-economical, and greener method for the synthesis of complex molecules from readily accessible precursors always draws significant attention to the synthetic community.

I.2. The C–H Bond Activation/ Functionalization

The C–H activation is a chemical process that functionalizes the inert C–H bond by increasing its reactivity. In organometallic point of view, C–H activation refers to a process where metal interacts with the inert C–H bond of **17** and directly forms a metal-carbon intermediate **18**. Next, interaction of an electrophile or nucleophile to **18** then makes C-C and C-heteroatom bonds in **19**.[5] The first step in generally a C–H activation and the second step is the functionalization. Thus, C–H activation can be termed as C-H functionalization, whereas C–H functionalization is not always considered as C–H activation. The formation of direct metal-carbon intermediate is the main feature of C–H activation (**Scheme I.3**).

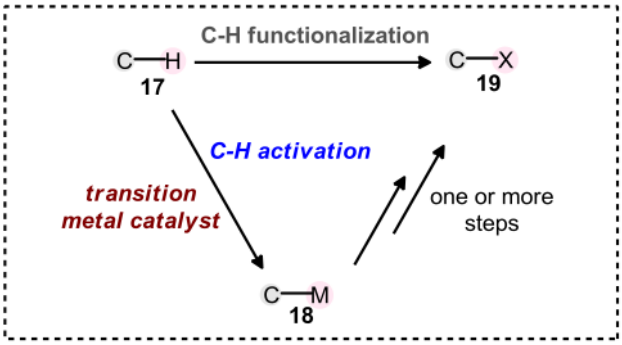

Scheme I.3: C–H bond activation/C–H functionalization

I.3. Mechanistic Pathway Overview of C–H Activation

The C–H activation or functionalization process occurs in two different ways. One involves outer-sphere mechanism, where C–H bond at first inserts into the ligated transition metal (TM) species (see **20**, **Scheme I.4**). While the other 'inner-sphere' mechanism encompasses a direct coordination of TM to the C–H bond that in-situ

forms a C–M or C–M–H intermediate (see **21**, **Scheme I.4**). Although "C-H functionalization" and "C-H activation" terminologies are often mixed up and created confusion in the chemical society, however, the term "C-H activation" is widely confined to inner-sphere mechanism.[6a]

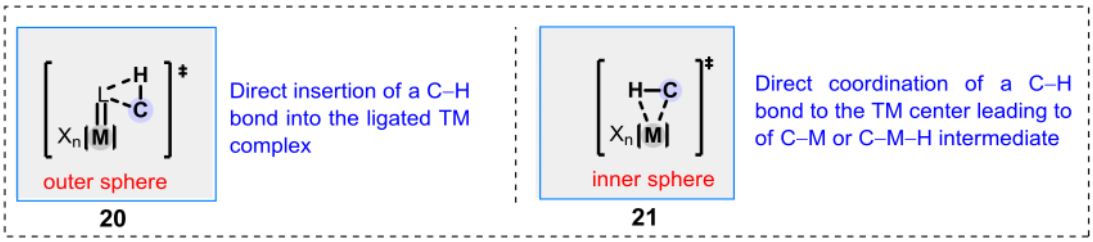

Scheme I.4: inner-sphere and outer-sphere mechanism

I.3.1. Insights of outer-sphere mechanism

In case of outer-sphere mechanism: no direct interaction of the C–H bond with the active metal catalyst occurs; instead, the ligand attached with the TM-species reacts with the C–H bond. The ligated-TM-species can either abstracts a hydrogen radical followed by recombination with organic radical or the ligand can directly insert into the inert C–H bond (**23** or **26**; **Scheme I.5**). Thus, the outer-sphere mechanism usually occurs with the insertion of high oxidation state metal containing reactive oxo, carbene, or nitrene species to the C–H bond.

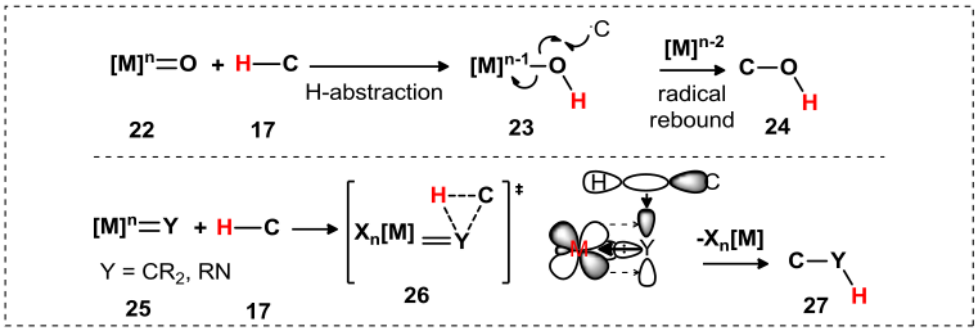

Scheme I.5: Outer-sphere mechanism

I.3.2. Insights of inner-sphere mechanism: nucleophilic vs electrophilic character [6]

Inner-sphere mechanism in C–H bond functionalization comprises with the coordination of C–H bond with the active metal complex to provide a metal-carbon intermediate.[Error! Bookmark not defined.,Error! Bookmark not defined.] Thus, interaction of TM-coordinated aryl or alkyl species with the external electrophile/nucleophile or the ligand attached with the metal itself can trigger the functionalization. Based on the mechanistic insights, the inner-sphere mechanism occurs in three ways. They are typified as: (i) electrophilic activation, (ii) σ-bond metathesis, and (iii) oxidative addition. However, the exact pathways of inner sphere C–H activation has become so far unclear. With respect to the charge transfer direction, the inner-sphere C–H activation process is being simplified and broadly classified into two main categories: (i) reverse charge transfer from metal dπ orbital to the σ* orbital of the coordinated C–H bond and (ii) forward charge transfer (CT) from filled σ orbital of C–H bond to an empty dσ orbital of metal.[6b] The electron deficient metal complex as well as cationic late transition metal complex having low energy dπ and dσ orbitals participate in forward CT over reverse CT; the overall process is thus electrophilic (**Scheme I.6**, right). On the other hand, electron-rich transition metals having high energy dπ and dσ orbitals participate in reverse CT and therefore the pathway is nucleophilic (**Scheme I.6**, left).

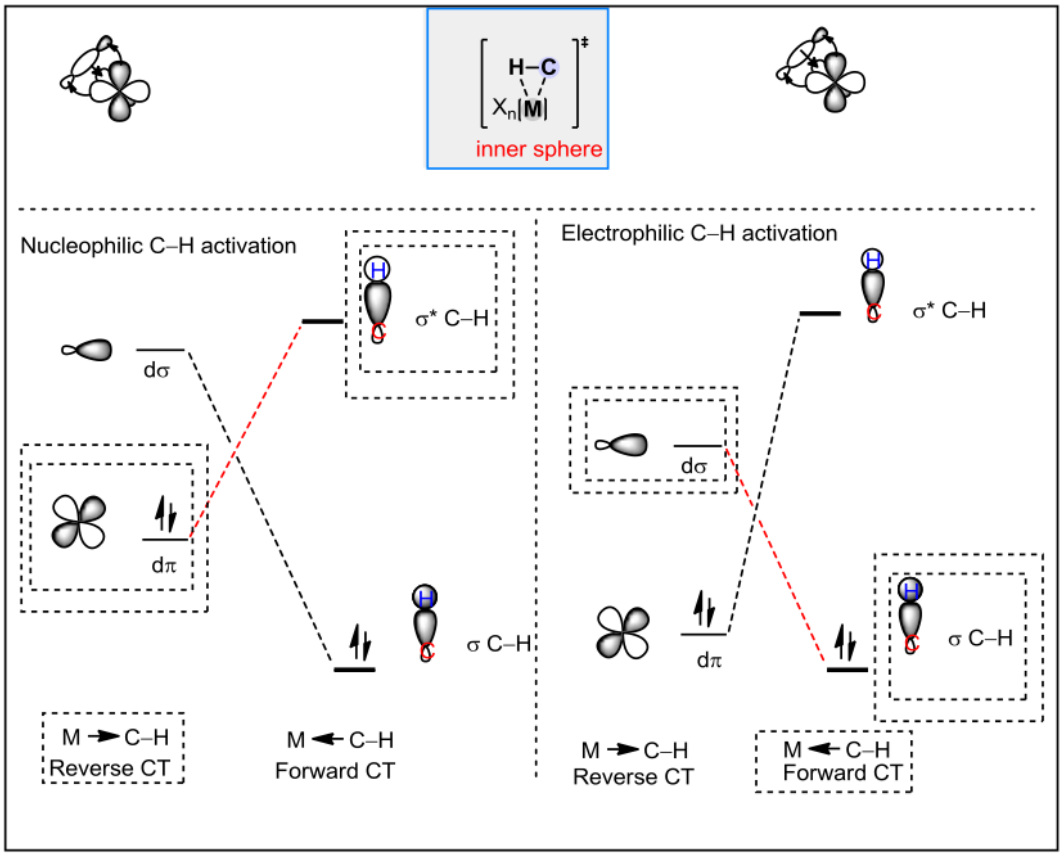

Scheme I.6: Nucleophilic vs electrophilic C–H activation

I.3.2.1. Oxidative addition

The electron-rich, nucleophilic, low-valent d^8 second- and third-row late transition metal complexes mostly involve oxidative addition pathways for the C–H activation. In this case, a balanced enthalpy change among C–H bond breakage and the M–C and M–H bonds formation is maintained. The transformation initiates with the metal coordination to C–H bond and then electron density transfer to the LUMO of C–H bond (σ*).

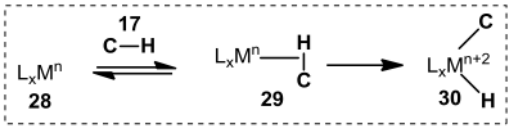

Scheme I.7: oxidative addition mechanism

The gradual accumulation of electron density in the LUMO could decrease the C–H bond order and therefore is ease to

cleave. Eventually oxidative addition of a nucleophilic moiety could increase the oxidation state of TM. To get a qualitative idea of oxidative addition, the respective molecular diagram is sketched in **Scheme 1.8**.

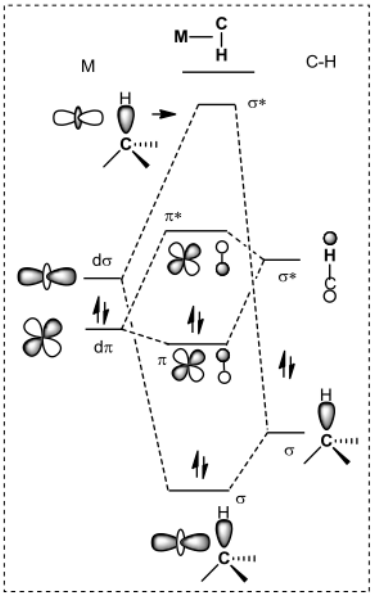

***Scheme I.8**: MO diagram of oxidative addition*

I.3.2.2. Sigma-bond metathesis

The early TM with d^0 electronic configuration and high oxidation state is not amenable to undergoing oxidative addition. Such species can react with a particular C–H bond via σ-bond metathesis (σ-BM). This mechanism involves four centered kite-like transition state **34** that takes place without changing oxidation state of the metal (**Scheme I.9**). Mainly, the group-III metals (scandium lanthanides and actinides) along with few group-IV and V TM are amenable to this mechanism.

A qualitative MO diagram for s-bond metathesis is shown in **Scheme I.10.** the absence of d-electrons thus precludes the π-interaction.

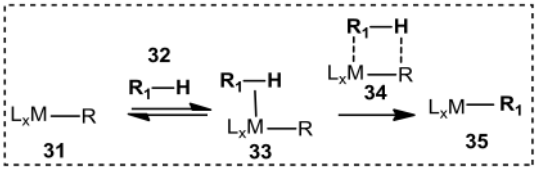

Scheme I.9: Sigma-bond metathesis mechanism

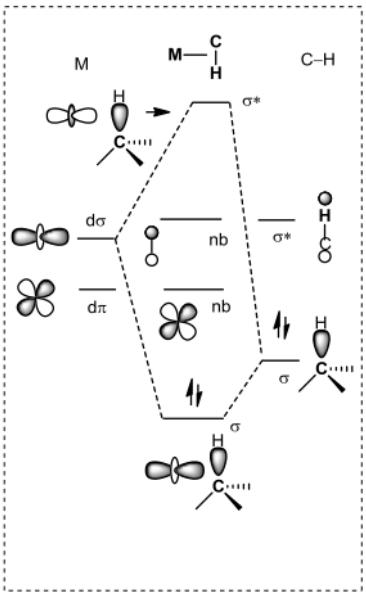

***Scheme I.10**: MO diagram of sigma-bond metathesis*

I.3.2.3. Electrophilic C–H activation:

The electron-deficient high oxidation state late transition metal complexes, such as Pd(II), Ru(II), Ir(III) and Pt(II) mostly participate in the electrophilic activation. In such cases, the coordination of C–H bond to metal complex starts with strong σ-donation and weak π-back-donation (**Scheme I.11 and Scheme I.12**). In case of aromatic system, electrophilic addition of TM species into the arene moiety at first forms a wheland type intermediate **36**. Next, the base mediated loss of proton forms a metal-carbon intermediate **37**.

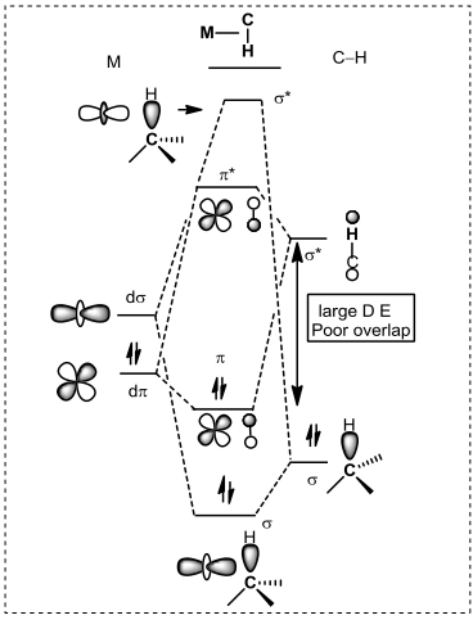

Scheme I.11 MO diagram of electrophilic C–H activation

A qualitative molecular orbital diagram is sketched in **Scheme I.11**. The mechanism involves an interaction of energetically viable TM d-orbital (dσ) with the C–H bond (σ).

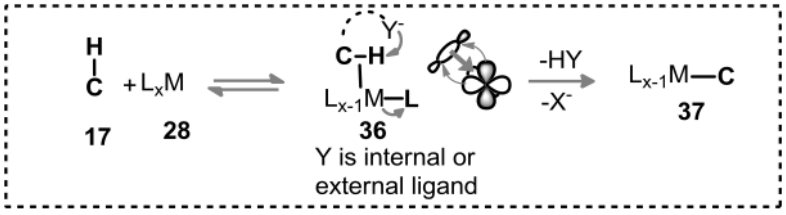

Scheme I.12 Electrophilic mechanism

I.3.2.4. Ambiphilic concerted mechanism: [7,8]

The inner-sphere mechanism that involves an intramolecular H–abstraction by an internal ligand, such as an alkoxy or an halide anion, or a bridging heteroatom based species (for example: carboxylate anion) via a concerted cyclic mechanism (**Scheme I.13)**. This mechanism can be classified as: internal electrophilic substitution (IES),

ambiphilic metal-ligand activation (AMLA), or concerted metalation deprotonation (CMD). In these cases, a significant H-bond between ligand lone pair with the corresponding C–H bond increases the electron density of C–H σ-bond, which eventually facilitates the agostic interaction(**38**→**40**→**37** or **39**→**41**→**37**) (**Scheme I.13**).

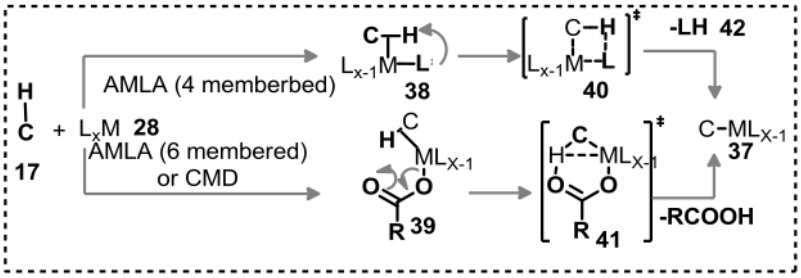

Scheme I.13 Ambiphilic concerted mechanism

I.3.2.5. 1,2-addition:

An alternate 1,2-addition involves a sigma bond metathesis of C–H bond **17** to the double bonded metal- nonmetal (M=X) species **43** via a concerted four membered transition state **44**. The newly formed H–X species remain attached to the metal complex **45** (**Scheme I.14**).

Scheme I.14 1,2-addition

I.4. Different Methods of C–H Functionalization

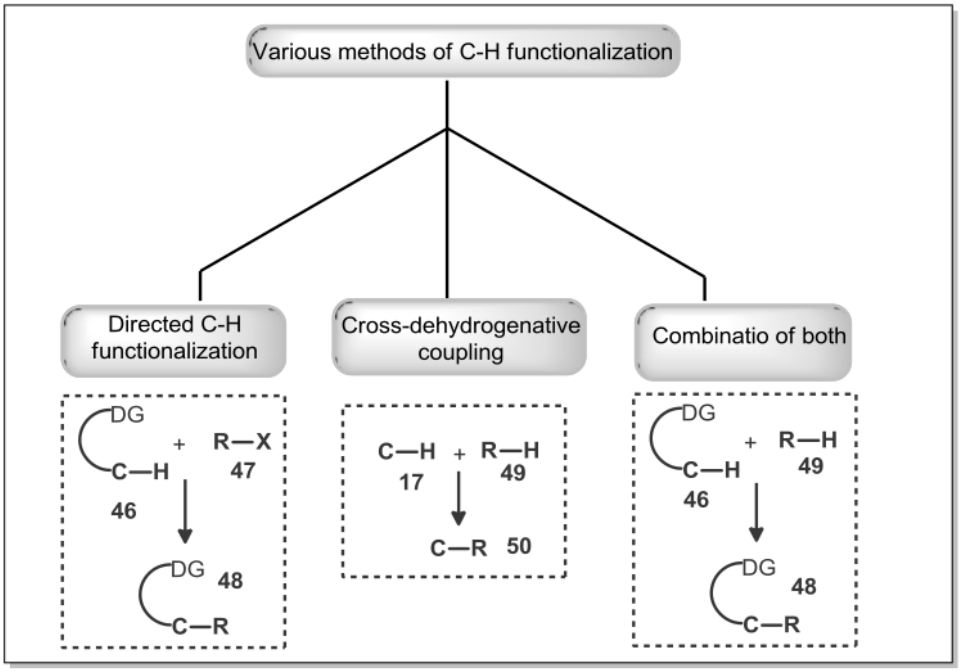

Scheme I.15 Different methods of C–H activation/functionalization

The transition-metal catalyzed C–H activation/functionalization can be categorised into three main classes (**Scheme I.15**):

1) **Directed activation**: The directing group (DG) assisted C–H activation initiates with the coordination of DG with the TM complex, which activates the C–H bond close proximity to the TM-species. The transformation is therefore highly regioselective. By tuning the DG, the C–H activation can be made –*ortho*, -*meta*, or –*para* selective.

2) **Cross-dehydrogenative or non-directed activation**: Cross-dehydrogenative C–H activation generally happens with the most acidic C–H bond. Thus, the process is non-regioselective.[13]

3) **DG assisted cross-dehydrogenative coupling**: This process involves the combination of the above two pathways.

This thesis primarily based on "Directing Group Assisted C-H Bond Activation" principle. The contents of this thesis aims in the development of TM catalyzed kinetic resolution of sulfoximine through C–H functionalization, synthesis of spiro-fused heterocycles through multiple C–H annulations, and hydroarylation 'in water'.

I.5. Transition Metal Catalyzed Stereoselective C–H Activation:

In the past few decade, the TM-catalyzed C−H bond functionalization has gained a great amount of attention for development of versatile synthetic methods that functionalizes inert C–H bonds to –OH, $–NH_2$, halide, and aryl or alkyl groups and the synthesis of complex molecules.[9] Among various TMs employed for the C–H activation domain, palladium (Pd) catalysts have been widely used as further functionalization of palladium−carbon intermediate is ease and well-studied.[10] Significant efforts on Pd-catalyzed C–H functionalization are mostly linked to racemic transformations. Moreover, ligands play significant in facilitating cleavage of C–H bond and enhancing the overall reactivity for the formation of C−C/C−X bonds.[3] The ligand coordination with Pd-species can lower energy barrier of elementary steps involved in C–H activation and also modulate facial selectivity (regio- as well stereoselectivity). [11]

In this section, a brief historical background in the development of bifunctional mono-N-protected amino acid (MPAA) ligands for discovering Pd-catalyzed stereoselective C–H functionalization is discussed. The conceptual imprints for the kinetic resolution of molecular scaffolds in presence of MPAA ligand and Pd-catalyst is also enumerated.

I.5.1 Historical background and discovery of MPAA ligand towards stereoselective C–H functionalization:

I.5.1.1 Background: In 1969 Werneke group has attempted performing cyclopalladation of (dimethylamino)methylferrocene **51** with K_2PdCl_4 but ended up with only amine ligation species **52** (**Scheme I.16**).[12a]

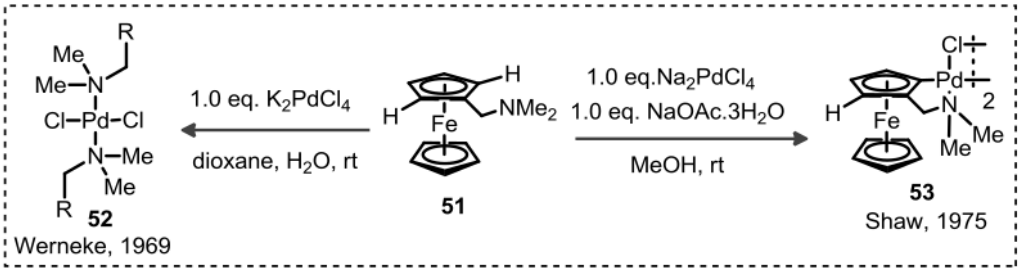

Scheme I.16: Acetate anion-mediated cyclopalladation

In 1975, the Shaw group successfully demonstrated the synthesis of desired cyclopalladation complex **53** from (dimethylamino)methylferrocene **51** when carried out in presence of stoichiometry amount sodium acetate (**Scheme I.16**).[12b] This is one of the earliest examples of acetate mediated cyclopalladation of C(sp^2)–H bond.[13]

In 1979, Sokolov proposed an alternate mechanism for the Dg assisted acetate anion mediated C(aryl)−H deprotonation in combination with Pd(II) catalyst. The Pd–carbon bond formation occurs through a six-membered cyclic transition state **55** following concerted metalation deprotonation (CMD) pathway (**Scheme I.17**).[14]

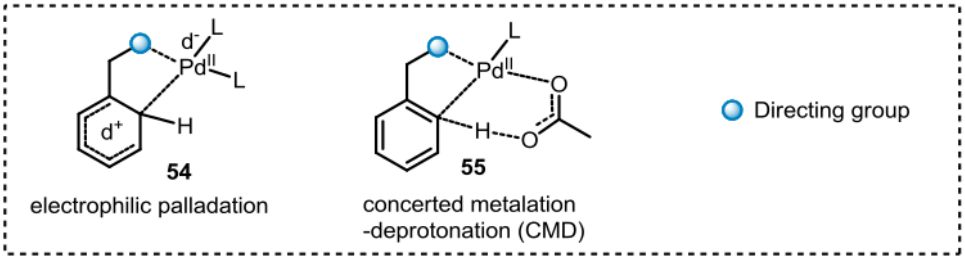

Scheme I.17: Topology of CMD process

One of the earliest reports on stereoselective cyclopalladation has been showcased by Sokolov in 1977. The reaction of a (dimethylamino)methylferrocene **56** containing α-amine chiral center with 1.0 equivalent of Na_2PdCl_4 and sodium acetate has led to a diastereoselective cyclopalladation (**57:58)** with d.r. 85:15 (**Scheme I.18**).[15]

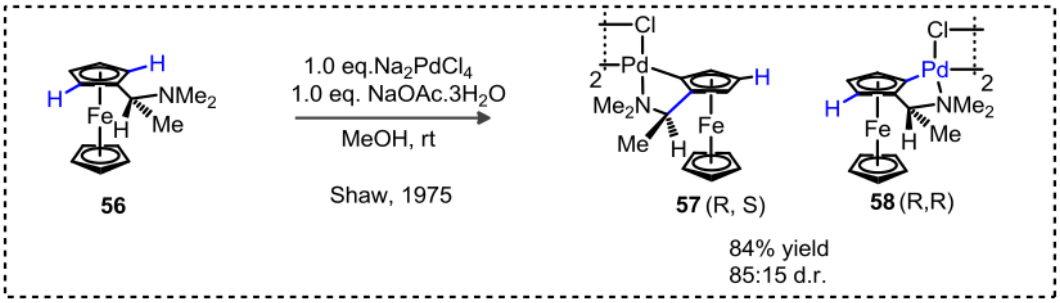

Scheme I.18: Substrate controlled diastereoselective cyclopalladation

I.5.1.2 Discovery of MPAA ligand:

In 1979, Sokolov hypothesized that instead achiral carboxylic acid in CMD mediated cyclopalladation, the use of chiral amino acid as carboxylate source **60** could bring chiral induction in cyclopalladation step from **59** to **61** (**Scheme I.19**).[14]

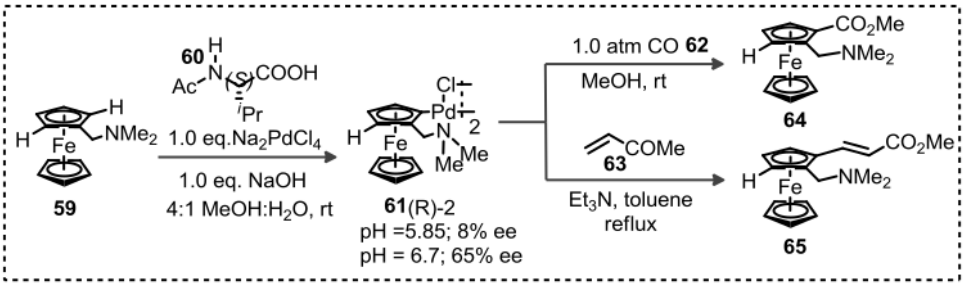

Scheme I.19: Substrate controlled diastereoselective cyclopalladation

I.5.2. Selective examples for the synthesis of C-stereogenic molecules via C(sp²)–H functionalization:

The Yu group developed Pd/MPAA catalyzed desymmetrization strategy for the construction of stereogenic C–C via C–alkylation/C–alkenylation and intramolecular C–O bond formation **66**–**68** (**Scheme I.20**). Identical strategy has been expanded further to the synthesis of various chiral amine derivatives **69–71** (**Scheme I.20**).[16,17]

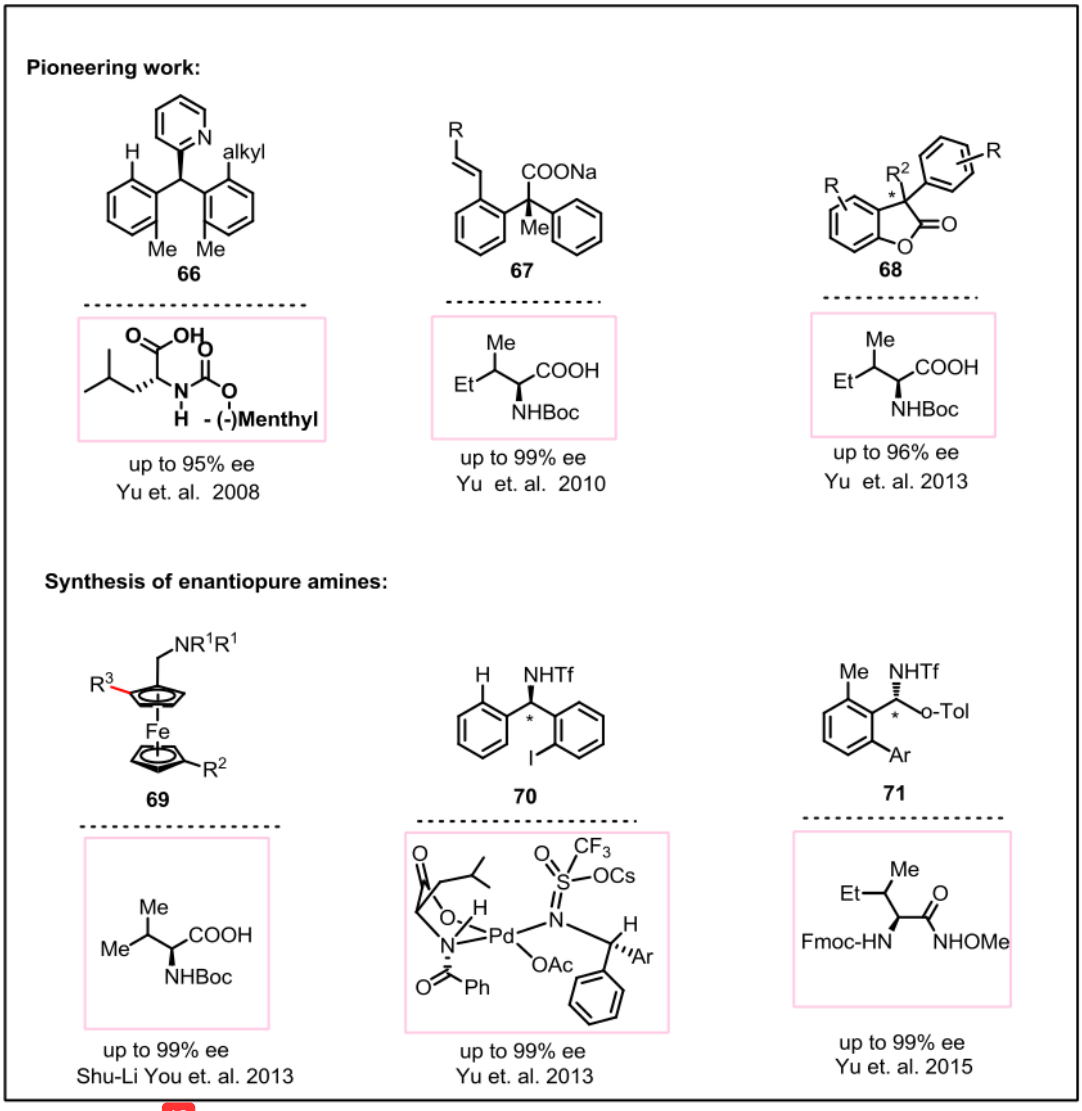

Scheme I.20: Synthesis of C-stereogenic molecules via C(sp^2)–H functionalization

I.5.3 Selective example of the synthesis of C-stereogenic molecules via C(sp^3)–H functionalization:

In **2014** and **2015**, Yu group revealed an early example of Pd/MPAA catalyzed enantioselective C(sp^3)–H arylation via desymmetrization of cyclobutyl (**72**), acyclic amide **73** and cyclopropyl **75** derivatives (**Scheme I.21**). [18a-b]

In **2016**, the same group reported the discovery of N-acetyl-protected chiral aminoethyl quinoline ligands enabled enantioselective functionalization of β-methylene C–H bonds for the generation of C-stereogenic aliphatic amides **74** with high enantioselectivity (**Scheme I.21**).[18c]

In continuation, the amino acid transient DG can facilitate enantioselective arylation of β-methylene C–H bonds of benzyl carbon of **76** (**Scheme I.21**).[18d]

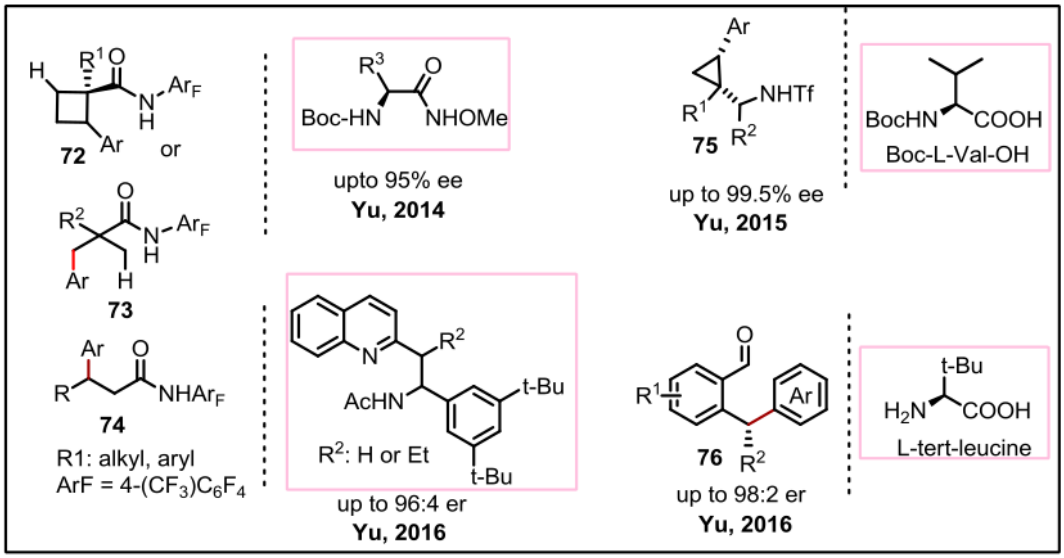

Scheme I.21: Selected example of C-stereogenic molecules via C(sp^3)–H functionalization

I.5.4 Synthesis of C-stereogenic molecules via *m*-selective C(sp^2)–H functionalization:

In **2018**, Yu group reported a challenging enantioselective *m*-C–H activation using a catalytic amount of chiral norbornene [(+)-NBE-CO2Me] transient mediator (**Scheme I.22**).[19] This method has been used for the enantioselective *meta*-C–H arylation of benzylamine derivatives **77**.

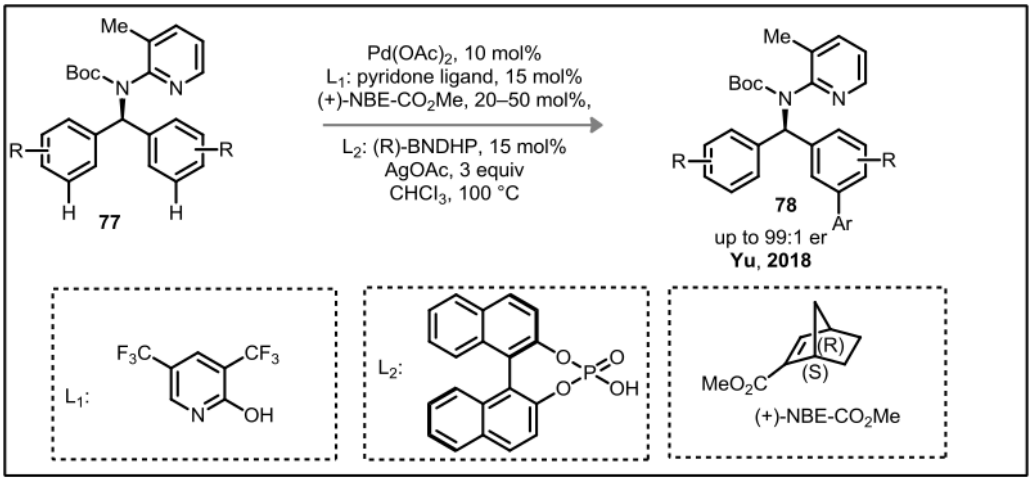

Scheme I.22: Desymmetrization via *meta*-selective functionalization

I.5.5 Synthesis of heteroatom centered stereogenic molecules via C(sp²)–H functionalization:

Related examples of Pd/Rh/Ir-catalyzed enantioselective C(sp²)–H functionalization for the generation of stereogenic heteroatom center are listed in **Scheme I.23**.[20]

The Yu and Wang group independently reported Pd/MPAA catalyzed enantioselective C(sp²)–H functionalization for the construction of stereogenic P (**79**) and S-centered (**80**) molecules, respectively (**Scheme I.23**).

In **2017**, the Cramer group demonstrated chiral Rh/Ir catalyzed enantioselective C(sp²)–H functionalization for the construction of stereogenic P-centered annulation product **81** and C–N bod forming compound **82**, respectively (**Scheme I.23**).[R]

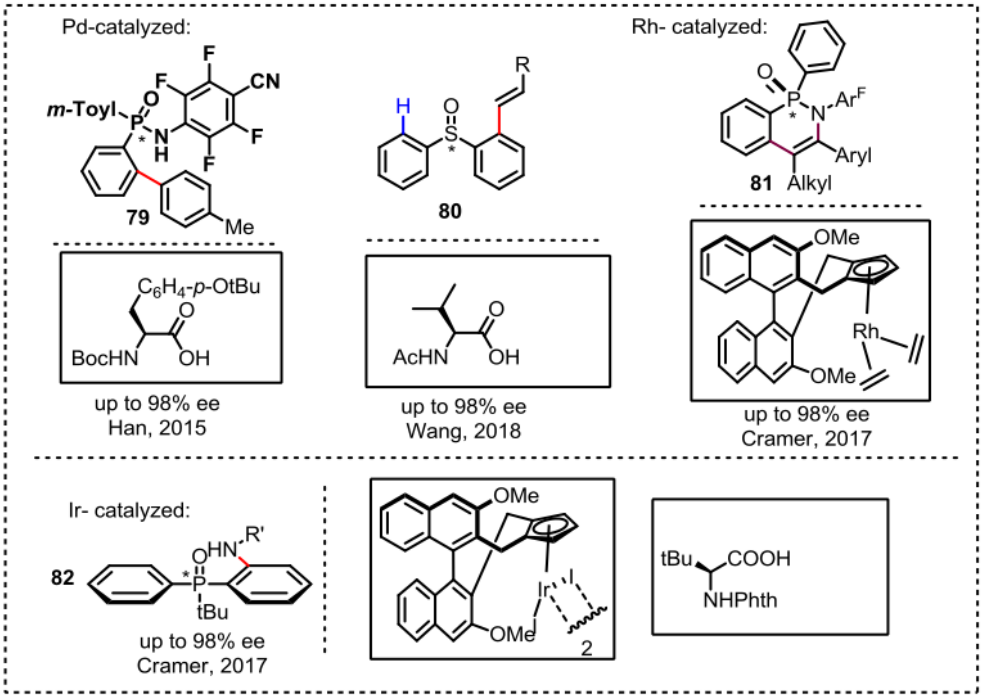

Scheme I.23: Selected example of metal catalyzed formation of stereo heteroatom center

I.5.6. Palladium Catalyzed Kinetic Resolution, Motivation, Hypothesis, and Planning

A notable effort [31] has been made in the past decade in the enantioselective C–H functionalization by desymmetrization strategies and among these approaches, palladium catalyzed desymmetrization of prochiral [42] C–H bond has been successfully implemented for the construction of stereogenic carbon, phosphorus and sulfur center. However, requirement of two enantiotropic group in the compound limits the desymmetrization method synthetically practical. At this point, the kinetic resolution (KR) method could easily address these inherent drawbacks. Thus, Yu's discovery on Pd-catalyzed KR of benzyl amine and aryl acetic acid via arylation and alkenylation is undoubtedly a breakthrough (**Scheme I.24A**). In spite of this success, the related strategy of Pd-catalyzed heteroatom centred KR of arenes remains unknown, although exceedingly appealing (**Scheme I.24B**).

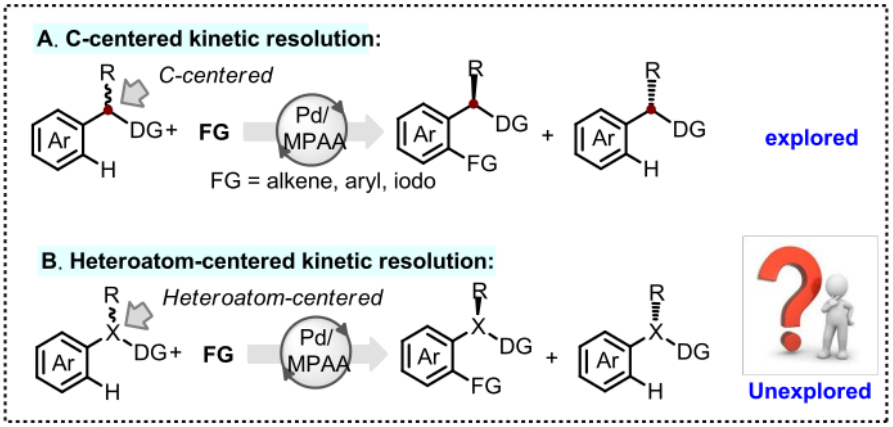

Scheme I.24: Palladium catalyzed kinetic resolution via C(sp^2)–H activation and motivation

With this intention, we devised a Pd-catalyzed KR of 2-pyridylaryl sulfoximines using a commercially available Pd(II) catalyst and a simple chiral amino acid (MPAA) ligand, via C(aryl)–H arylation and olefination (Fig 1B), which remains unexplored (**Scheme I.25**).[21] The concept relies on kinetically regulated CMD step of C(aryl)–H activation (k_1>>k_2, **Scheme I.25**) through preferred coordination of pyridine over imine to Pd-MPAA and ligand geometry **$CMD_{Pyr\text{-}DS}$** over **$CMD_{Pyr\text{-}DR}$** (**Scheme I.25**). *A transformation is therefore developed and discussed in Chapter II.*

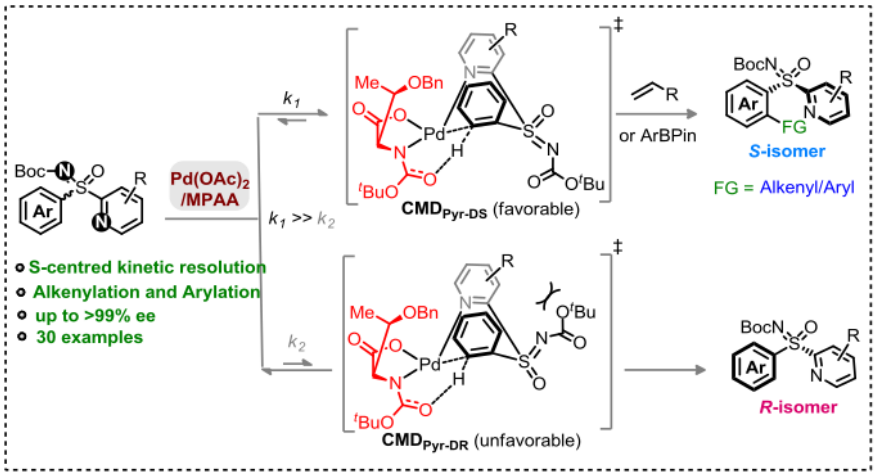

Scheme I.25: Kinetic resolution of phenyl pyridyl sulfoximine

I.6 Transition Metal Catalyzed Annulation Reaction

The TM-catalyzed annulation approaches have been widely implemented for the construction of variety of heterocyclic compounds. In 1991 and 1995, Larock group reported palladium catalyzed annulation of substituted aryl halides **93** with a wide range of internal alkynes **94** (**Scheme I.26**).[22] This method showed a straightforward pathway for the construction of benzofurans, indoles, benzopyrans, and isocoumarins. However, pre-functionalized precursors required in this process limits synthetic utility of this transformation. A probable solution to this would be TM-catalyzed annulation via direct C–H activation.

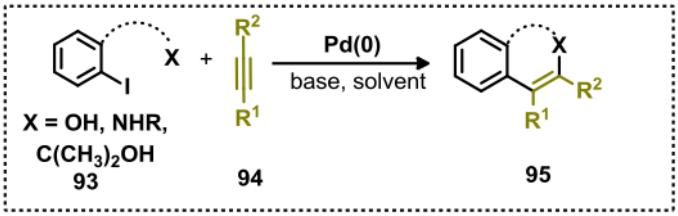

Scheme I.26: Larock annulation of aryl halide with alkynes

I.6.1 Transition metal-catalyzed oxidative annulation via C–H activation

The DG enabled TM-catalyzed oxidative annulation of aromatic C–H bond with alkenes/alkynes offers an atom-economical pathway for the construction of highly conjugated heteroarenes from readily accessible precursors.[23] Few the most recent demonstration of TM-catalyzed oxidative annulations are showcased in **Scheme I.27**. In 2007, Miura group showed a Rh(III)-catalyzed oxidative C–H annulation of easily accessible benzoic acids with alkyne derivatives for the synthesis of highly substituted lactones.[27] Subsequently, Rh(III), Ru(II), and Co(III) catalysts have been employed for the discovery of DG assisted annulations with alkynes and unsaturated systems for the synthesis of wide arrays of novel N/O-bearing heterocycles; a brief snapshots for the construction of new heterocycles is depicted in **Scheme I.27**.[23-27]

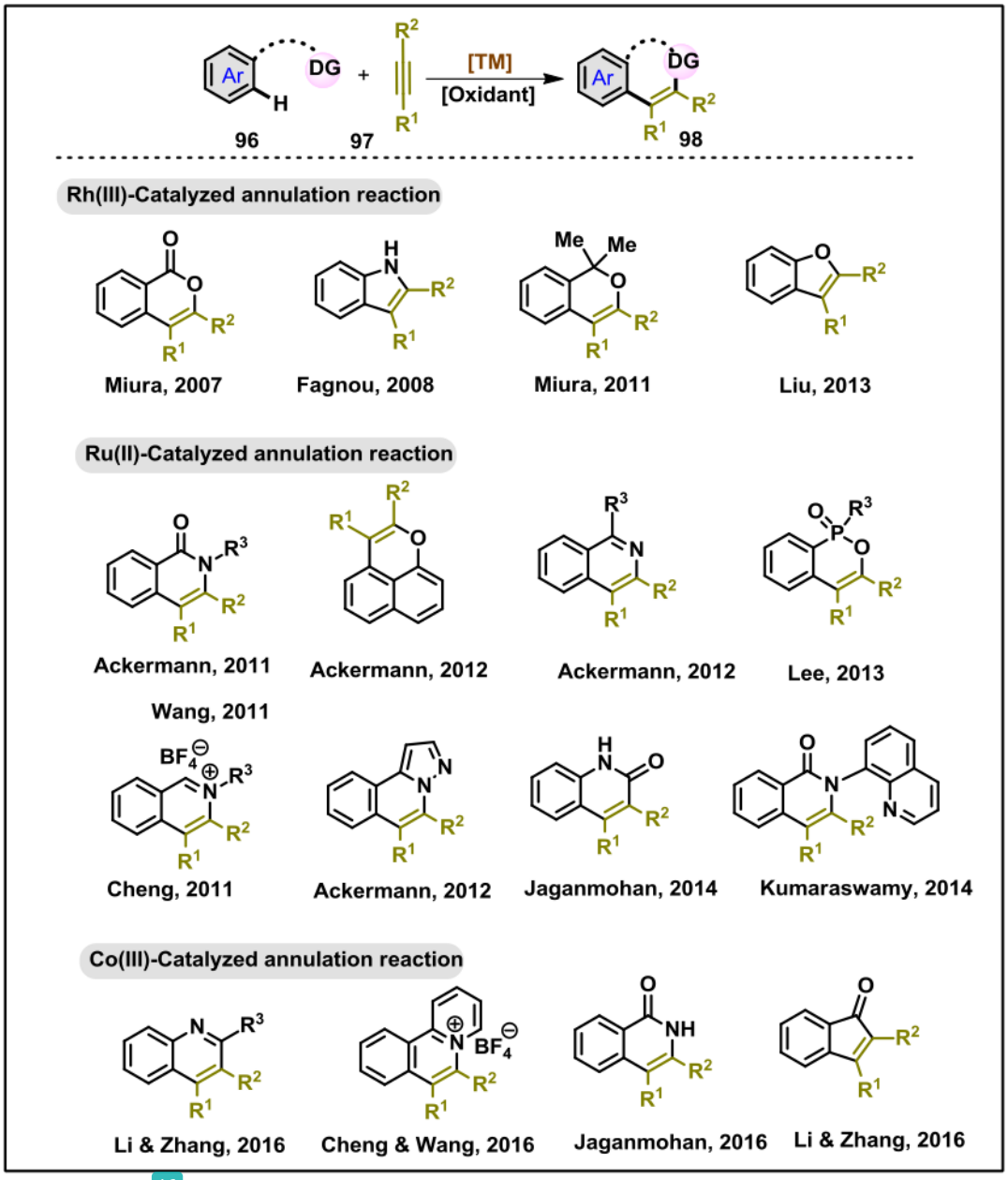

Scheme I.27: Selected examples of transition-metal catalyzed annulations [16]

I.6.2 Mechanism of transition-metal catalyzed oxidative annulation [16]

A representative mechanistic cycle for the DG mediated annulation reaction with alkyne is shown in **Scheme I.28** (Path-I: non-oxidizable DG; Path-II: Oxidizable DG). The transformation initiates with the coordination of TM with DG to form the respective metallacycle A or I.

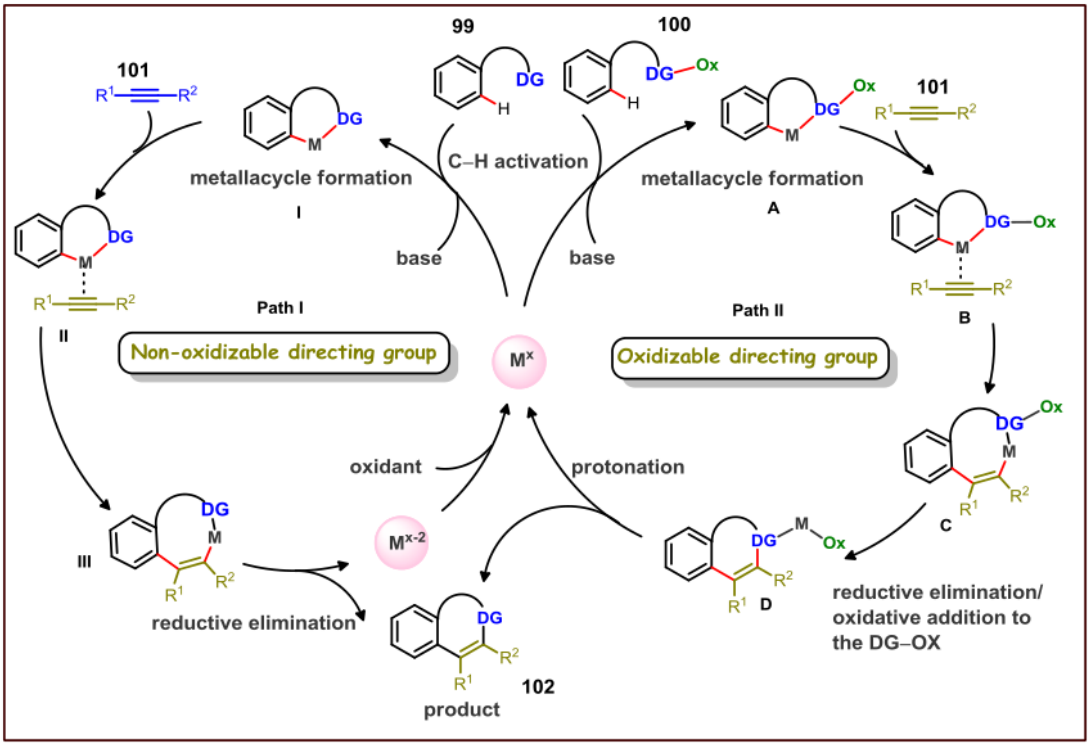

Scheme I.28: Metal catalyzed oxidative annulation

Next, the alkyne insertion to **A** or **I** give metallacycle **C** and **III** via **B** and **II**, respectively. The formation of 7-membered metallacycle **C**/**III** is quite common for both the methods (Path I and II). In case of Path-I, reductive elimination of **Int-III** delivers the corresponding mono-annulation product **102** with the reduction of TM species to M^{x-2}. Thus, external oxidant is necessary to re-oxidise the catalyst M^{x-2} to M^{x} for further reaction (**oxidant enabled; Path-I).** Whereas in Path-II, reductive elimination of **C** and simultaneous oxidative insertion of metal complex across the DG-Ox bond and protodemetalation of **D** delivers the annulation product **102** along with active catalyst M^{x} (**oxidant free; Path-II**).[26]

I.6.3. Transition metal-catalyzed multiple C–H activation

Over the time, numerous efforts have been devoted in the development of synthetic methods for the activation and functionalization of multiple C–H bonds. However, these transformations mostly dealt with mono-functionalized C–H bond followed by the introduction of second functional group in the other C–H bond. Simultaneous introduction of distinct functionalities in multiple C–H bonds remain challenging.

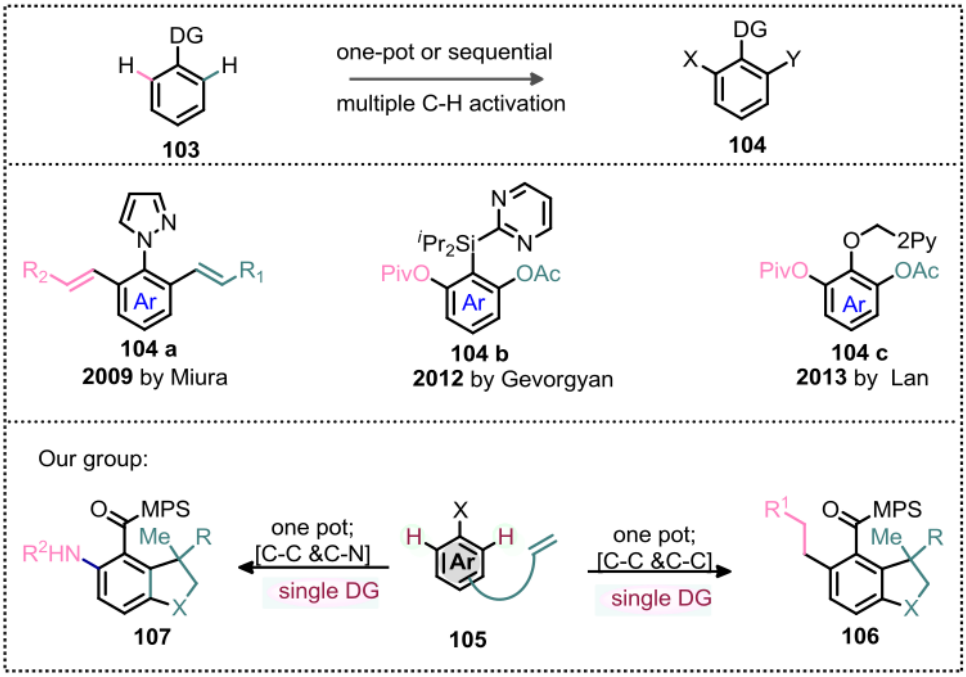

Scheme I.29: Selected examples of multiple C–H functionalization

In 2009, Miura and co-workers reported pyrazolyl group directed unsymmetrical di-alkenylation of arenes (**104a**; **Scheme I.29**).[28]

In 2012, Gevorgyan group showcased a sequential acetoxylation followed by pivoxylation of two *ortho*-C(arene)–H bonds. The multiple unsymmetrical C–O bond formations were viable in one-pot in the presence of a pyrimidyl-DG (**104b**; **Scheme I.29**).[29]

Similar kind of sequential olefination of two ortho-C–H bonds was demonstrated by Lan and co-worker using 2-pyridylmethyl as a removable directing group. (**Scheme I.29**).

In 2012, our group demonstrated methylphenyl sulfoximine directed intramolecular *o*-C–H hydroarylation followed by intermolecular *o'*-C–N and C–C bond formation for the synthesis of peripheral substituted dihydrobenzofuran derivatives **(106, 107; Scheme I.29)**. Interestingly, both steps are performed in one-pot.[30]

I.6.4. Motivation, Hypothesis, and Planning

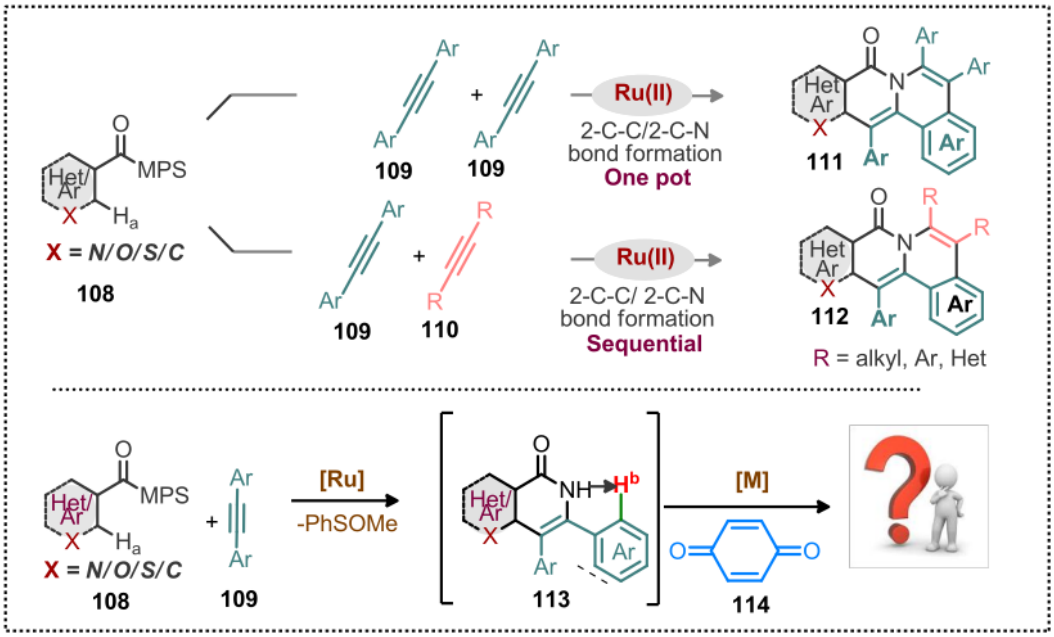

Scheme I.30: Motivation and hypothesis of multiple cyclization

Our group has recently showcased a Ru-catalyzed sulfoximine directed one-pot symmetrical double annulation of arenes with alkyne to construct π-extended poly-fused heterocycles **111** (**Scheme I.30**). The identical transformation can also be applied for the unsymmetrical linear-type double annulations with different alkynes to make **112** (**Scheme I.30**).

Inspired from these demonstrations of double annulations, we envisaged performing a sequential double annulation with alkyne and a quinone moiety in an orchestrated manner. This process could lead to either a π-extended poly-fused heterocycles **111** by stitching two molecules of alkyne or the annulation process could bind both alkyne and quinone simultaneously (**Scheme I.30**). *A transformation in this line is therefore developed and discussed in Chapter III.*

The TM-catalyzed DG enabled intramolecular hydroarylation of arenes with olefins have been well-studied (**Scheme I.31**).[30] The transformations are successful when carried out in organic solvents, such as: toluene, 1,2-dichloroethane, 1,4-dioxane etc (**Scheme I.31**). We hypothesized that the hydroarylation reaction may be possible in water medium instead of organic solvent. Thus, amide directed hydroarylation strategy in water medium is envisaged (**Scheme I.31**). *The Ru-catalyzed intramolecular hydroarylation transformation is therefore developed and discussed in Chapter IV.*

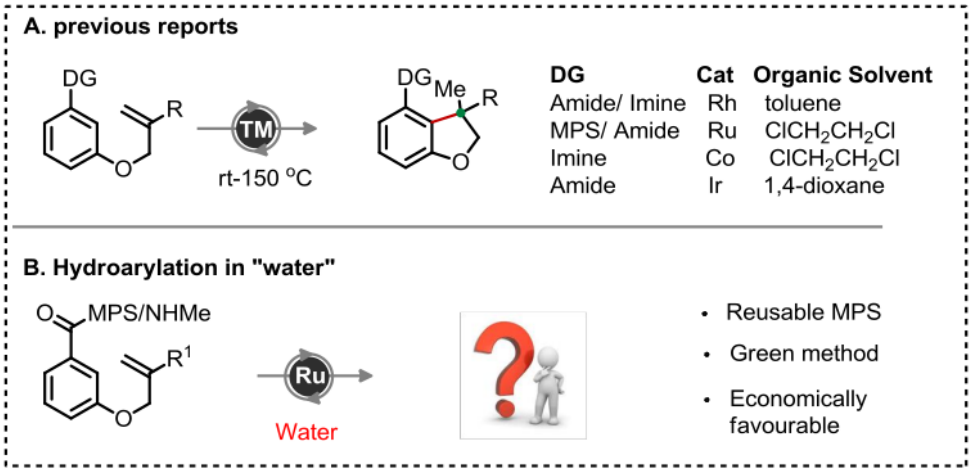

Scheme I.31: Intramolecular hydroarylation 'in water'

Chapter II

Kinetic Resolution of Sulfur-Stereogenic Sulfoximines by Pd(II)-MPAA Catalyzed C–H Olefination and Arylation

Abstract

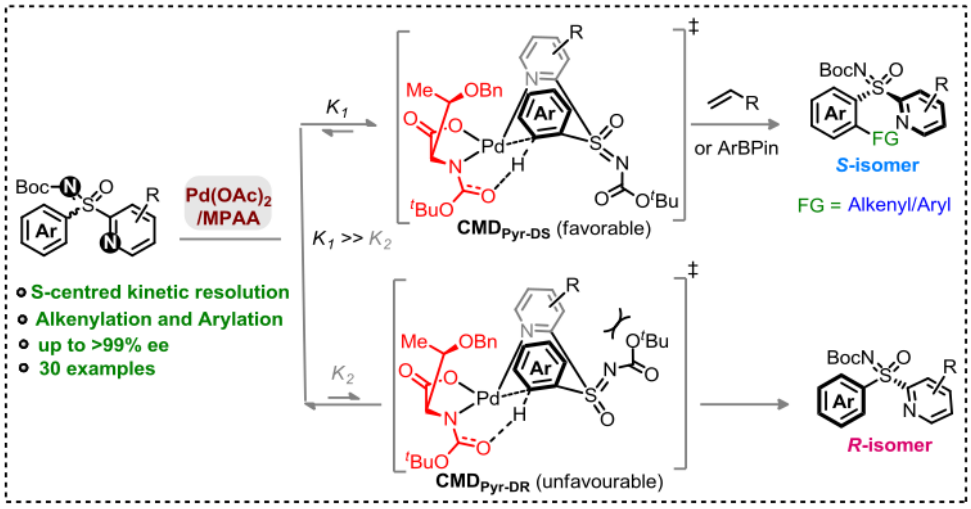

A direct Pd(II)-catalyzed kinetic resolution of heteroayl-enabled sulfoximines through an *ortho*-C–H alkenylation/arylation of arenes has been developed for the first time. The coordination of sulfoximine pyridyl-motif with Pd(II)-catalyst and chiral amino acid MPAA ligand helps the enantio-determining C(aryl)–H activation. This method provides access to a wide range of enantiomerically enriched aryl-pyridyl-sulfoximine precursors and the C(aryl)–H alkenylation/arylation adducts in good yields with high enantio-selectivity (up to >99% ee), and selectivity factor up to >200; which are otherwise inaccessible by the conventional methods. The directing group (DG) preference, ligand effect, geometry constraints, and the transient six-membered concerted-metalation-deprotonation (CMD) species displays indomitable resilience in the stereoselectivity origin; DFT studies validate this outcome.

Reference:

Kallol Mukherjee, Nicolas Grimblat, Somratan Sau, Koushik Ghosh, Majji Shankar, Vincent Gandon and Akhila K. Sahoo*

II.1. Introduction

The directing group (DG) assisted desymmetrization of prochiral C–H bond provides an impeccable entry to construct functionalized chiral molecules. This strategy has led to making stereogenic carbon, phosphorus, silicon and sulfur centered species through selective functionalization of prochiral C–H bonds.[1–3] However, essential requirements of two enantiotopic groups limits synthetic potential of desymmetrization processes. At this juncture, kinetic resolution (KR) of C–H bonds is undoubtedly an attractive alternative (**Scheme II.1A**). In this regard, the Yu's DG assisted chiral amino acid enabled palladium (Pd)-catalyzed carbon centred KR of arene C–H bonds through alkenylation, arylation, and/or iodination is undoubtedly a breakthrough constructing highly functionalized

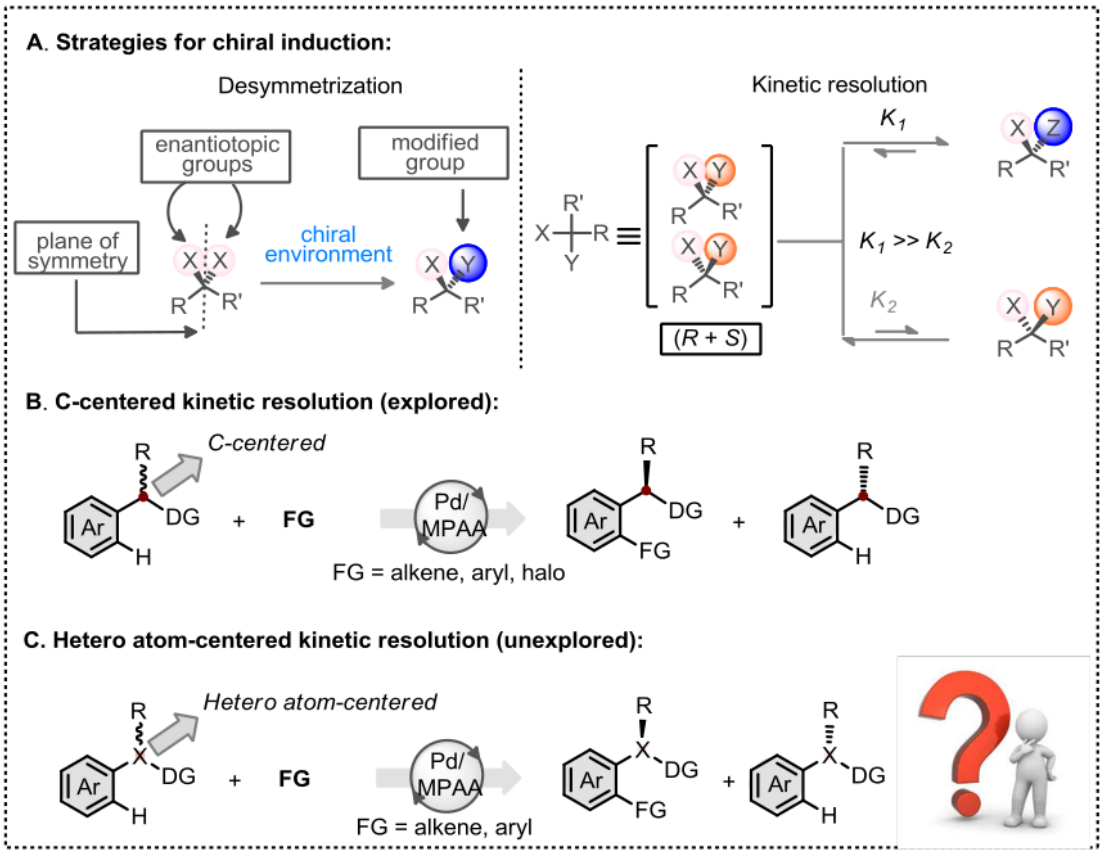

Scheme II.1: Kinetic resolution for the generation of stereogenic hetero atom centre chiral entities. (**Scheme II.1B**).[4] However, these strategies are limited to C-centred resolution while related strategy for heteroatom centered KR of arene is obscure (**Scheme II.1C**).

II.2. Previous strategies for Pd/MPAA catalyzed desymmetrization

In **2008**, Yu group reported a desymmetrization method for the Pd(II)/ monoprotected amino acids (MPAA)-catalyzed enantioselective activation of C(sp²)–H bond. This process is successful for making chiral C-stereogenic centre. Monoprotected α-amino acid ligands are found essential in this process. The mechanistic feature is sketched in **Scheme II.2**.[2a]

The transformation begins with the in-situ formation of Pd/MPAA-complex **3**. Next,

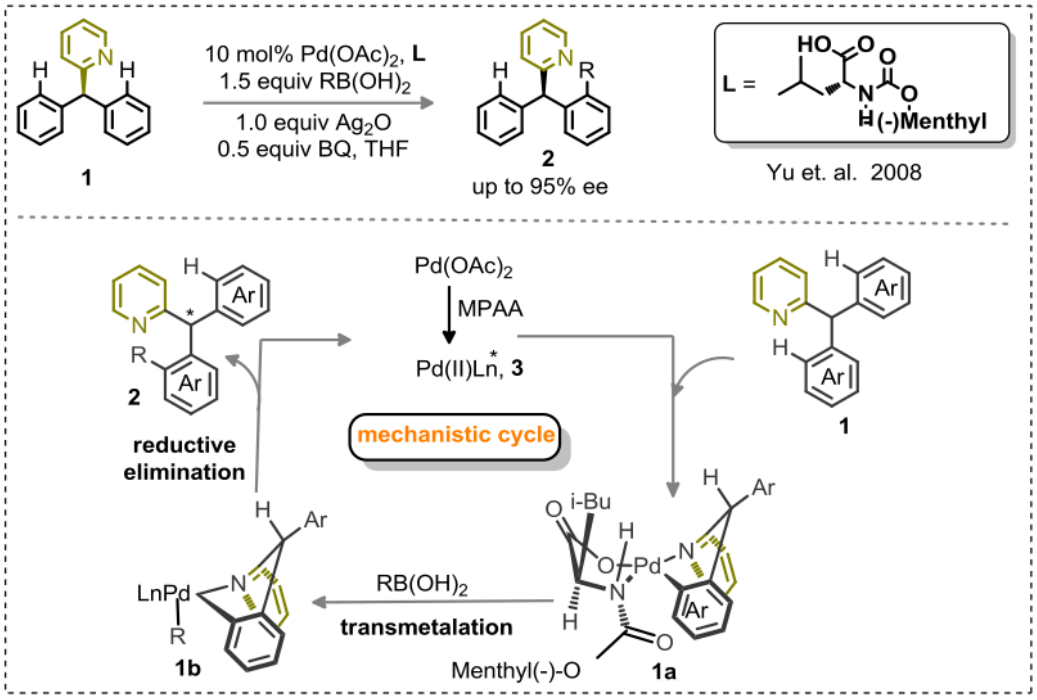

Scheme II.2: Pd(II)/MPAA-catalyzed enantioselective C(sp²)–H functionalization via alkylation

the reaction of **3** with **1** proceeds with enantio-determining C–H activation to deliver 6-membered palladacycle **1a**. The transmetalation of **1a** with the boronic acid counterpart then provides **1b**. Finally, reductive elimination of **1b** gives the final product **2** (**Scheme II.2**).

In **2010**, the identical strategy has been extended for the enantioselective C–H activation of carboxylic acids **4**. Monoprotected α-amino acids are once again found effective for the enantio-determining C–H insertion of **4** to enable **4a** (**Scheme II.3**).[2c]

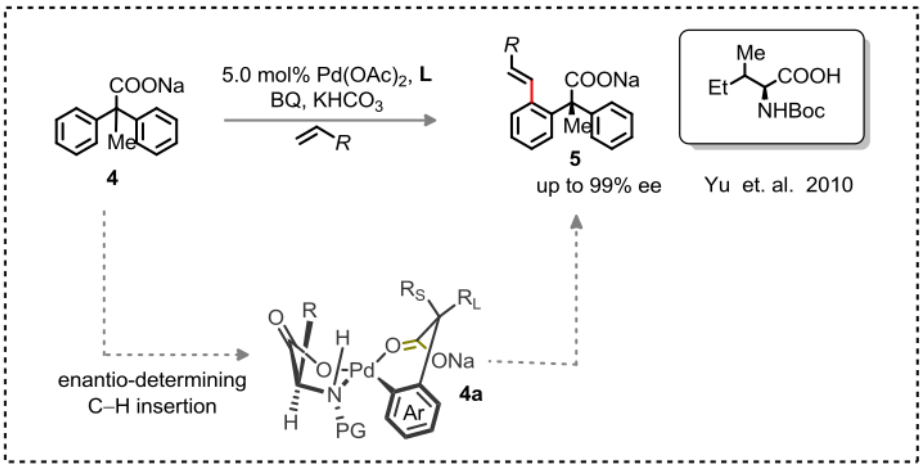

Scheme II.3: Enantioselective C–H activation reactions of carboxylic acid

In **2013**, the same group developed Pd(II)/MPAA catalyzed enantioselective C(sp^2)–H activation and simultaneous intramolecular C–O bond formation to deliver chiral benzofuranones **7** with up to 96% ee. This is the first example of enantioselecctive C–H functionalization which involves Pd(II)/Pd(IV) catalysis (**Scheme II.4**).[2e]

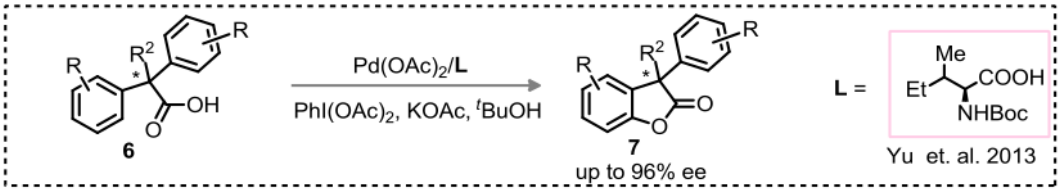

Scheme II. 4: Enantioselective C(sp^2)–H activation and synthesis of chiral benzofuranones

In same year, the You group revealed Pd/MPAA catalyzed stereoselective C–H functionalization of aminomethylferrocene derivatives **8** for the construction of planar-chiral ferrocenes derivatives **9** with high enantioselectivity. Commercially available N-Boc-protected amino acids are being successfully used for the chiral induction. Moreover, the reaction occurs in the presence of air as external oxidant, which makes the current synthetic method practical (**Scheme II.5**).[2g]

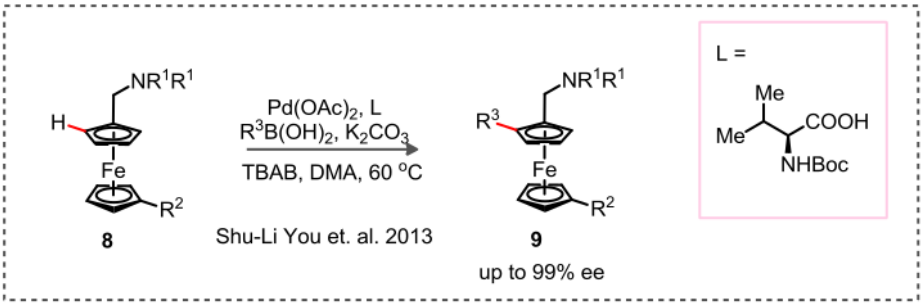

Scheme II.5: Stereoselective C–H functionalization of aminomethylferrocene

In **2013**, a first example of an Pd-catalyzed enantioselective C(sp²)−H iodination of (diarylmethyl)amine **10a** has been demonstrated by the Yu group. This strategy

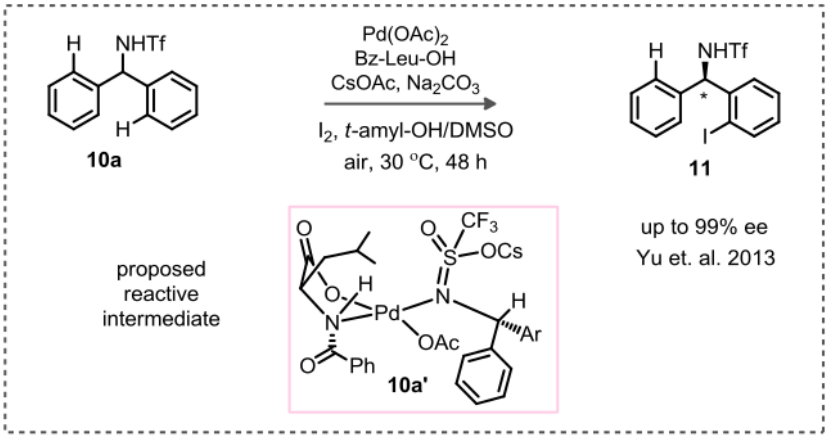

Scheme II.6: Pd(II)/MPAA-catalyzed enantioselective C(sp²)–H iodination

provides a useful access to functionalized chiral (diarylmethyl)amine derivatives **11**. The commercially available mono-N-protected amino acid ligand (MPAA) along with

the inexpensive halogenating agent I_2 are used in this transformation making the method synthetically workable (**Scheme II.6**).[2f] A neutral σ-donor directing group helps the formation of reactive intermediate **10a'**.

In **2015**, a stereoselective C(sp^2)–H functionalization of nosyl-protected diarylmethylamines **10b** with ArBpin has been developed by the the same group. Once again, the MPAA ligand has been found effective to deliver the respective arylated chiral diarylmethylamine derivatives **12** (**Scheme II.7**).[2i]

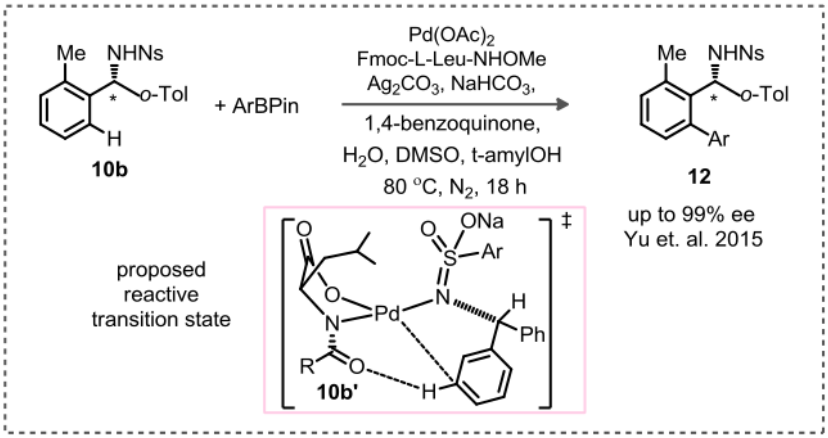

Scheme II.7: Pd(II)/MPAA-catalyzed enantioselective C(sp^2)-H functionalization via arylation

Although the known desymmetrization strategies are viable in making C–H functionalized chiral molecules, prochiral C–H bonds are essential for all these transformations.[2] While kinetic resolution (KR) of C–H bonds offers booming advantages for making functionalized chiral molecules.

II.3. Motivation and Design of Kinetic Resolution

In this regard, Yu's pioneering routes on DG assisted chiral amino acid enabled palladium (Pd)-catalyzed carbon centred KR of arene C–H bond through alkenylation, arylation, and/or iodination is undoubtedly a breakthrough (**Scheme II.8**).[4] Despite the

successes, related strategy for the *Pd-catalyzed heteroatom centered KR of arene* remains obscure although exceedingly appealing (**Scheme II.8**).

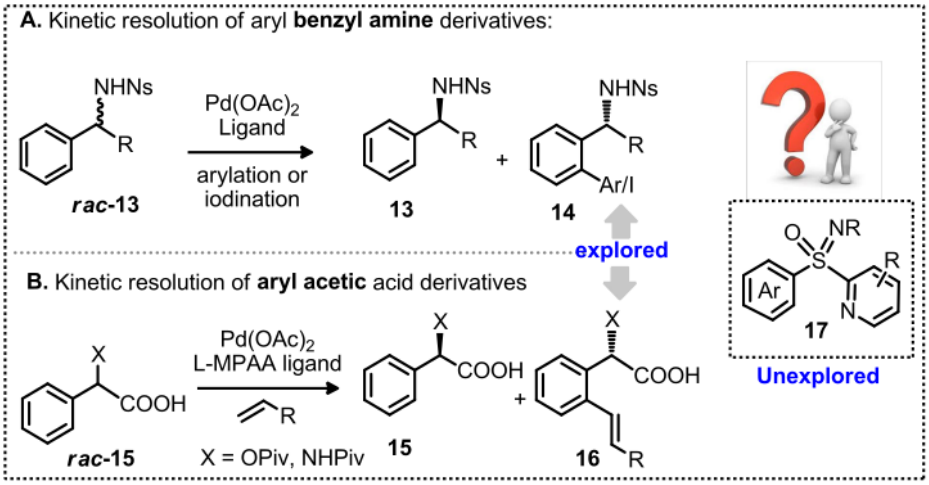

Scheme II.8: Kinetic resolution for the generation of stereogenic C-centre

On the other hand sulfoximines, configurationally stable motif with *S*-stereogenicity, have been found in the molecules of medicinal importance and agrochemicals.[5] Notably, sulfoximines have emerged as chiral auxiliary and DG for C–H functionalizations.[6] These benefits have enabled facile access to diverse range of sulfoximines. Whereas syntheses of enantioenriched sulfoximines have invariably rely on resolution techniques, stereoselective imination and oxidation.[7,8] Elegant enantioselective and KR routes to sulfoximines have been independently developed by Cramer and Li group, but all these approaches rely on Rh -catalyzed [4+2] annulation of diazoesters and aryl-sulfoximines in presence of specially designed ligands (**Scheme II.9**).[9] Mechanistically, this transformation proceeds with the coordination of the sulfoximine **18/19** to the Rh(III) center which initiates *ortho*-C–H activation via a CMD pathway. Then coordination and insertion of the diazo species **21** with **18b** leads to the formation of carbenoid intermediate **18c**, which in turn undergoes protonation to produce ketone **22**. Finally an off-cycle cyclocondensation offers desired product **20a** or **20b**.

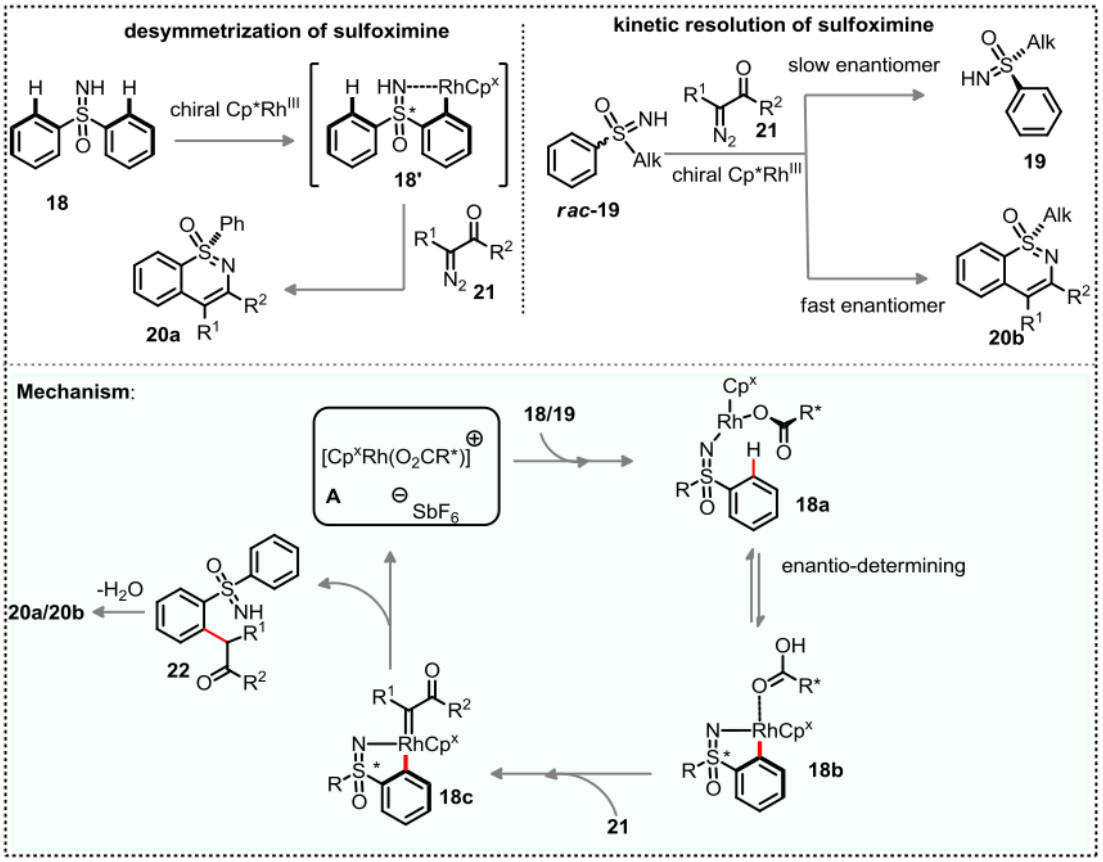

Scheme II.9: Desymmetrization and kinetic resolution of sulfoximines through annulation

To this end, we devised a Pd-catalyzed C–H functionalization method for KR of 2-pyridylaryl sulfoximine using commercially available Pd(II) catalyst and chiral amino acid (MPAA) ligand via C(aryl)–H arylation and olefination (**Figure II.1A**), which is unexplored. The concept relies on kinetically regulated concerted-metalation-deprotonation (CMD) step of C(aryl)–H activation (K_1>>K_2, **Figure II.1A**), coordination of pyridine over imine to Pd-MPAA and the ligand geometry **CMD$_{Pyr\text{-}DS}$** over **CMD$_{Pyr\text{-}DR}$** (**Figure II.1B**). These factors might influence the selectivity (*S* over *R*; **Figure II.1A**).

(Detailed explaination is given in section **II.4.7**) The transformation is general constructing wide arrays of enantiomerically enriched C-olefinated/arylated aryl-pyridyl-*S*-sulfoximines, which are otherwise inaccessible by other routes.

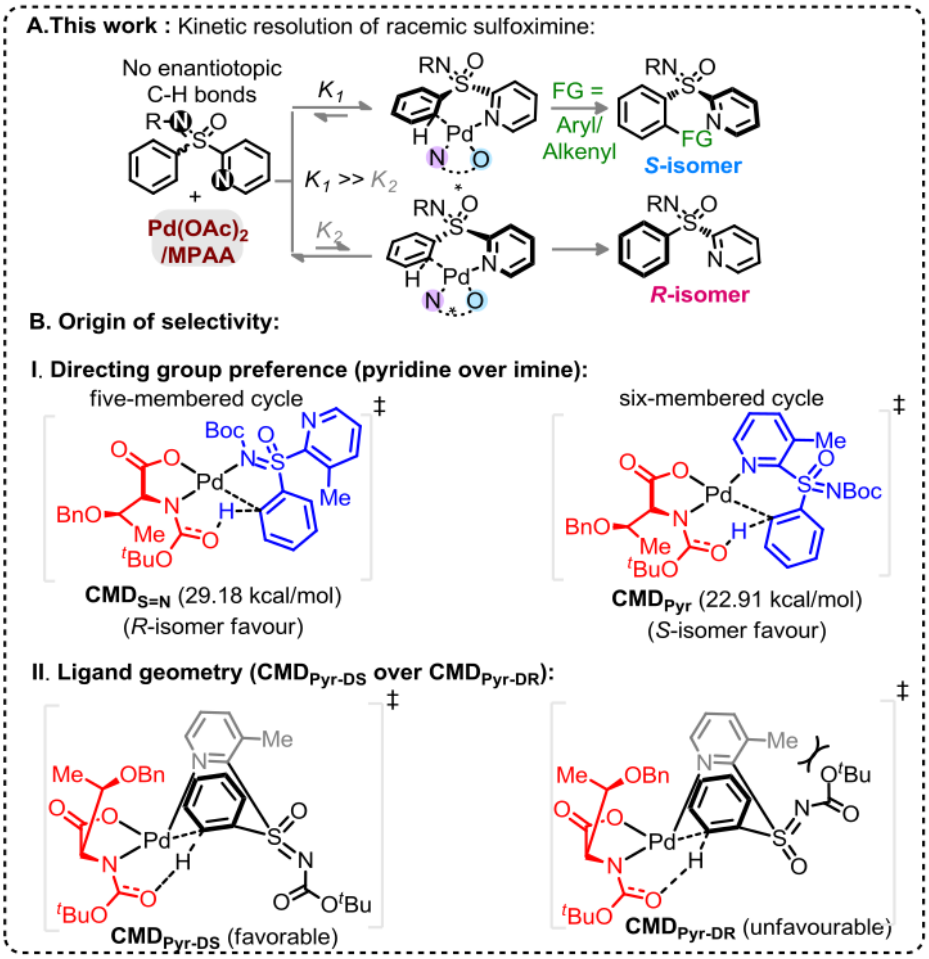

Figure II.1: Kinetic resolution of sulfoximine

II.4. Results and Discussion

II.4.1. Synthesis of precursors

General procedure for the synthesis of racemic (rac) 27a–27l (GP-1):[10]

To pursue our hypothesis, diverse range of N-Boc protected aryl-pyridyl-sulfoximine precursors are prepared using the known synthetic procedures. Coupling of thiols with pyridines followed by $PhI(OAc)_2/(NH_4)_2CO_3$ mediated imination and oxidation gives sulfoximine. Finally Boc-protection gives the N-Boc protected aryl-pyridyl-sulfoximine precursors (Detailed procedure is given in experimental section). A list of aryl-pyridyl-sulfoximine derivatives are shown in **Scheme II.10**.

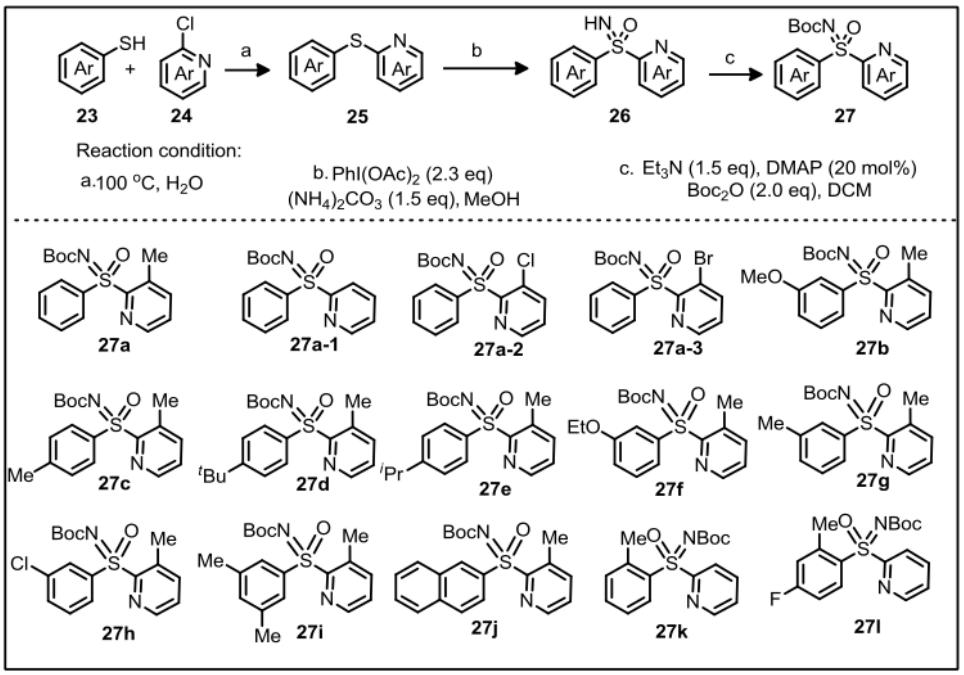

Scheme II.10: List of sulfoximine precursors synthesized

Thiols (**23**) and pyridines (**24**) are purchased from commercially available source and used; the molcules are listed in **Scheme II.11**.

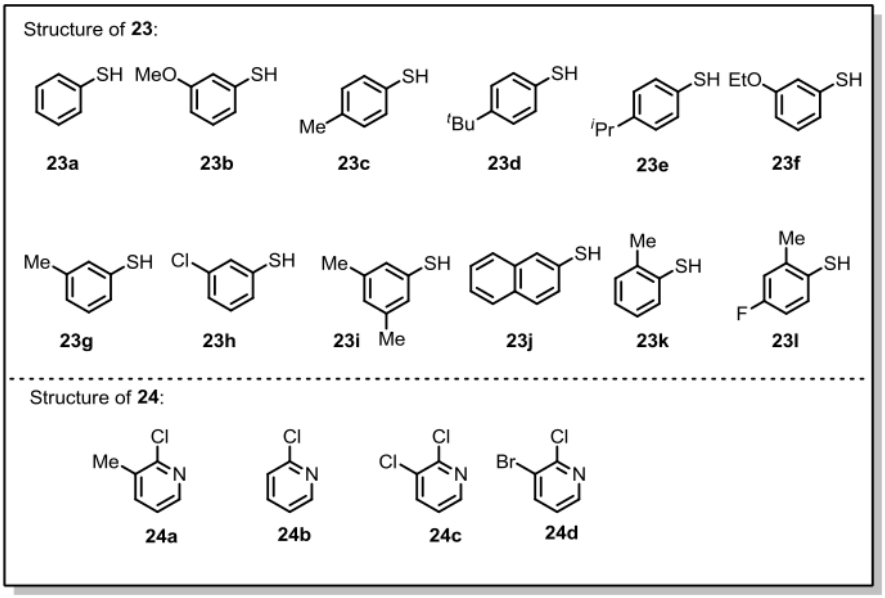

Scheme II.11: List of thiols and pyridines used for sulfoximine synthesis

II.4.2. Synthesis of Chiral Ligands (GP-2):[11]

All mono protected amino acids ligands **L1**–**L8** and **L11** were purchased from commercial sources or synthesized following the known procedures.[2] Ligands **L9** and **L10** are prepared and presented in **Scheme II.12**.

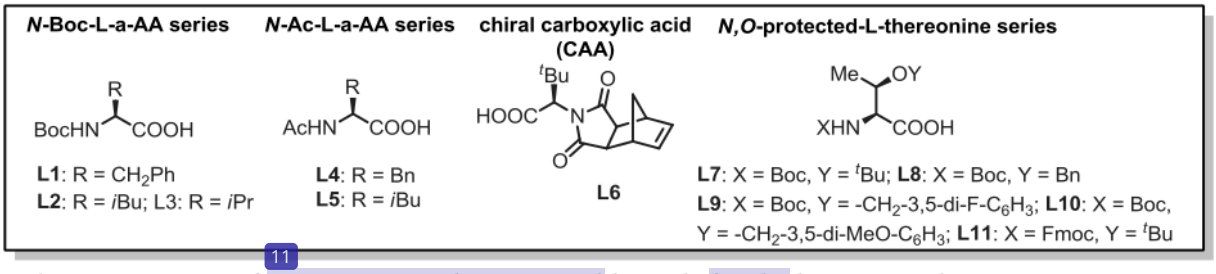

Scheme II.12: List of mono protected amino acid ligands for the kinetic resolution

II.4.3. Optimization studies

II.4.3.1. Optimization of reaction conditions for C–H alkenylative kinetic resolution:

The study was initiated in the non-substituted N-Boc-phenyl-2-pyridyl sulfoximine (*rac*-**27a-1**) with ethyl acrylate (**28a**; 0.6 equiv) in presence of $Pd(OAc)_2$ (10 mol%), Boc-L-Phe-OH (**L1**; 30 mol%), Ag_2CO_3 (2.0 equiv) in $ClCH_2CH_2Cl$ (1,2-DCE) at 75 °C (**Table II.1**). The desired C2-alkenylation product (*S*)-**29a-1** (18%, conversion after 3 days) along with

Table II.1. Ligands Screening [a]

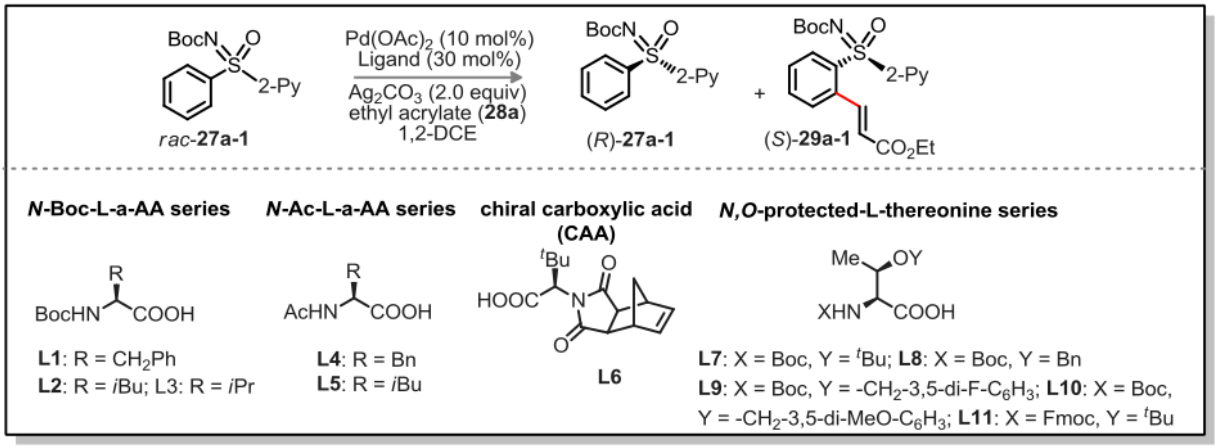

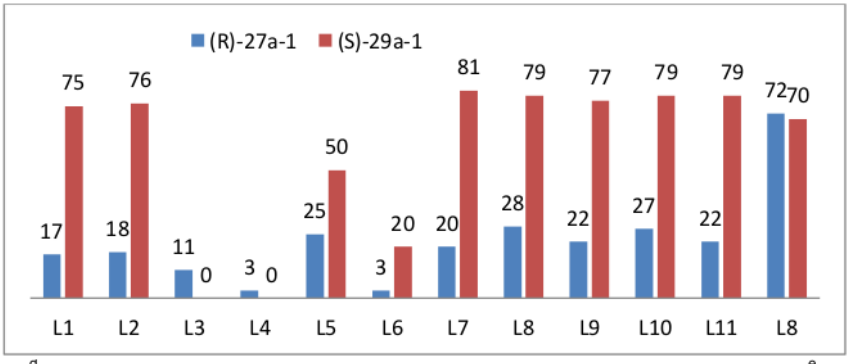

[a]Reaction conditions: ***rac*-27a-1** (0.1 mmol), ethyl acrylate **28a** (0.6 equiv), $Pd(OAc)_2$ (10 mol%), ligand (30 mol%), Ag_2CO_3 (2.0 equiv), 1,2-DCE (1.0 mL), N_2, 75 °C, 3 days. [b]Calculated conversion, C = eeSM/(eeSM + eePR). [c]Determined by chiral HPLC analysis. [d]Selectivity factor (s) = ln[(1 − C)(1 − eeSM)]/ln[(1 − C)(1 + eeSM)]. [e]Ethyl acrylate (2.0 equiv) was used.

the precursor (*R*)-**27a-1** were obtained in 75% ee and 17% ee, respectively, exhibiting a low selectivity factor (*s*) of 8. This encouraging result unfolded our curiosity examining the effect of other ligands. None of the N-Boc-, N-acetyl-, and N-imide-protected commercially available α-amino acid ligands (**L2**–**L6**) with distinct side chains were effective. Assuming the additional coordination ability of easily modifiable –OH group in threonine, various N, O-protected threonine ligands were tested.

The reaction *s* factor was improved a little for (*S*)-**29a-1** 81% ee and 79% ee, when Boc-L-Thr(ᵗBu)-OH (**L7**) and Boc-L-Thr(Bn)-OH (**L8**) were used, respectively. Electronic perturbation in O-benzyl moiety does not have any impact on enantioselectivity (**L9** and **L10**). The use of **28a** (2.0 equiv) in presence of ligand **L8** could found effective improving the conversion (50%) with (*S*)-**29a-1** (70% ee).

Table II.2. Solvent screening [a]

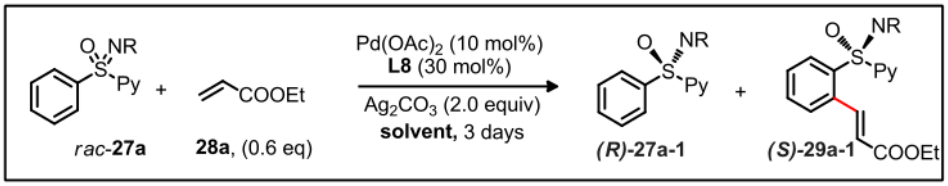

Entry	solvent	Conversion[b]	*ee* [%][c]		*s*[d]
			(R)-27a-1	*(S)*-29a-1	
1	THF	trace	–	–	–
2	CH_3CN	trace	–	–	–
3	1,4-dioxane	trace	–	–	–
4	HFIP	trace	–	–	–
5	toluene	12.76	12	82	11
6	TFT	24.78	28	85	16
7	2-chloro toluene	16.33	16	82	12
8	3-methoxy anisole	27.27	30	80	12
9	1,2-dimethoxy propane	9.9	09	82	11
10	4-Cl-TFT	17	17	83	13
11	TFE	trace	–	–	–
12	2-methoxy propane	trace	–	–	–
13	2-methyl anisole	20.75	24	84	14

[a]Reaction conditions: ***rac*-27a-1** (0.1 mmol), ethyl acrylate **28a** (0.6 equiv), $Pd(OAc)_2$ (10 mol%), **L8** (30 mol%), Ag_2CO_3 (2.0 equiv), solvent (1.0 mL), N_2, 75 °C, 3 days. [b]Calculated conversion, C = eeSM/(eeSM + eePR). [c]Determined by chiral HPLC analysis. [d]Selectivity factor (*s*) = ln[(1 − C)(1 − eeSM)]/ln[(1 − C)(1 + eeSM)].

A number of solvents were tested. None of them was found effective in increasing the conversion of the desired product **29a-1** (**Table II.2**).

To enhance sulfoximine resolution enantioselectivity by maintaining conversion (~50%; **Table II.1**), we scrutinized the co-oxidant effect (**Table II.3**). 2-chlorobenzoquinone (2-Cl-BQ) was found best providing 77% ee of (*S*)-**29a-1** (39% conversion, *s* factor of 13; entry-2, **Table II.3**).

Table II.3. Additive screening [a]

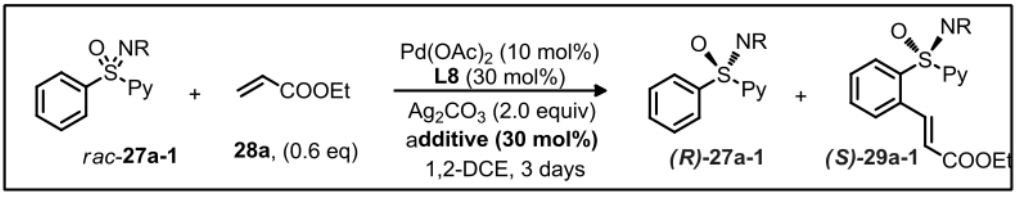

Entry	Additive	Conversion[b]	*ee* [%][c]		*s*[d]
			(*R*)-27a-1	(*S*)-29a-1	
1	BQ	18	17	78	10
2	2-chloro BQ	39	50	77	13
3	2, 5-dichloro BQ	35	40	75	10

[a]Reaction conditions: **rac-27a-1** (0.1 mmol), ethyl acrylate **28a** (0.6 equiv), $Pd(OAc)_2$ (10 mol%), L8 (30 mol%), Ag_2CO_3 (2.0 equiv), additives (0.3 equiv), 1,2-DCE (1.0 mL), N_2, 75 °C, 3 days. [b]Calculated conversion, C = eeSM/(eeSM + eePR). [c]Determined by chiral HPLC analysis. [d]Selectivity factor (*s*) = ln[(1 − C)(1 − eeSM)]/ln[(1 − C)(1 + eeSM)].

Next, we unravelled scrutinizing DG effect (**Table II.4**). Thus, various substituted 2-pyridyl containing sulfoximines were independently subjected to **2a**. Upon various trials, 3-methyl pyridyl DG was found superior affording alkenylation resolution species (S)-**29a** (96% ee) with s factor of 58, although conversion was confined to 17% (entry 1). While 3-Cl/Br substituted pyridyl DG were unsuccessful (entries 2 and 3). The reaction conversion was improved to 22% when **28a** (2.0 equiv) was employed

under the reaction shown in entry 4. The identical transformation with methyl acrylate (**28b**, 2.0 equiv) could enhance the conversion to 27% (entry 5). Finally, loading of 2-Cl-BQ 50 mol% led to (S)-**29b** (96% ee, s factor of 85 with 34% conversion; entry 6, **Table II.4**) and found optimum.

Table II.4. Directing group screening [a]

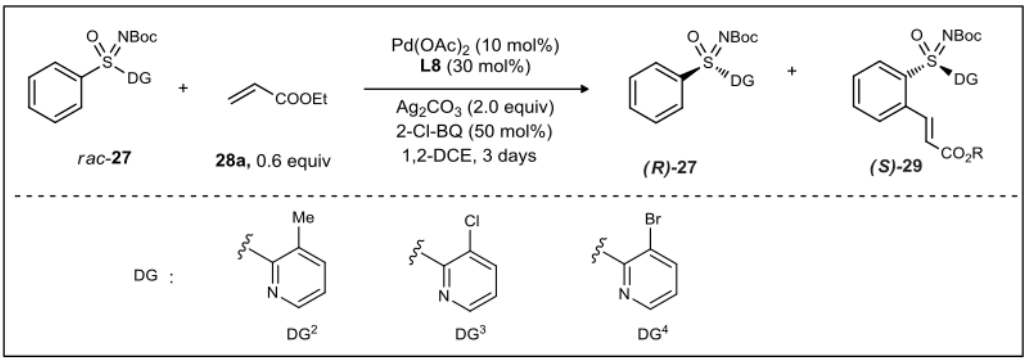

Entry	DG	Conversion[b]	*ee* [%][c]		*s*[d]
			(R)- 27	*(S)*-29	
1	DG^2	17	20	96	58
2	DG^3	nr	–	–	–
3	DG^4	nr	–	–	–
4[e]	DG^2	22	27	95	48
5[f]	DG^2	27	35	94	44
6[f,g]	DG^2	34	50	96	85

[a]Reaction conditions: **rac-27** (0.1 mmol), acrylate **28** (0.6 equiv), $Pd(OAc)_2$ (10 mol%), **L8** (30 mol%), Ag_2CO_3 (2.0 equiv), additives (0.3 equiv), 1,2-DCE (1.0 mL), N_2, 75 °C, 3 days. [b]Calculated conversion, C = eeSM/(eeSM + eePR). [c]Determined by chiral HPLC analysis. [d]Selectivity factor (s) = ln[(1 − C)(1 − eeSM)]/ln[(1 − C)(1 + eeSM)]. [e]Ethyl acrylate (2.0 equiv) was used. [f]Methyl acrylate instead ethyl acrylate. [g]2-Cl-BQ (50 mol%) was used.

II.4.3.2 Optimization of reaction conditions (arylation):

Next, we investigated the feasibility of Pd-catalyzed C–H arylative KR of sulfoximines (**Table II.5–Table II.8**). The reaction of N-Boc-3-methoxyphenyl-2-(3-methylpyridyl) sulfoximine (**27b**) with (4-CF_3)Ph-Bpin (**31a**; 2.0 equiv) was performed under the catalytic conditions of **Table II.5**. Pleasingly, the desired product (*S*)-**30a** was obtained

in 94% ee with *s* factor of 39 along with the recovery of (*R*)-**27b** in 20% ee and 18% conversion (entry 1, **Table II.5**). The oxidant Ag_2O played a vital role; conversion was increased to 51% (entry 2, **Table II.5**). Carrying out the reaction at 60 °C enhanced the *s* factor to 50 (entry 4, **Table II.5**). The s factor was raised to 64 with reaction conversion 41% and 94% ee of (*S*)-**30a**, when trifluorotoluene (TFT) was used (entry 1, **Table II.6**). Performing the reaction with 20 mol% of **L8** improved the outcome (entry 3, **Table II.7**). Importantly, reaction concentration from 0.1 M to 0.067 M led to (*S*)-**30a** (94% ee) and (*R*)-**27b** (88% ee) with 48% conversion and *s* factor of 95 (entry 3, **Table II.8**).

Table II.5. Oxidant screening[a]

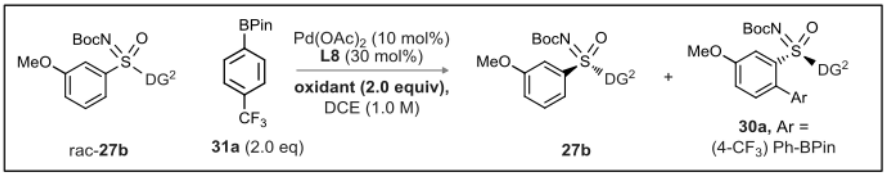

Entry	Oxidant	Conversion (c)[b]	*ee* [%][c]		*s*[d]
			(R)-1b	*(S)*-5a	
1	Ag_2CO_3	18	20	94	39
2	Ag_2O	51	88	86	38
3	AgOAc	12	12	90	21
4[e]	Ag_2O	43	70	92	50

[a]Reaction conditions: *rac*-**27b** (0.1 mmol), **31a** (2.0 equiv), $Pd(OAc)_2$ (10 mol%), **L8** (30 mol%), oxidant (2.0 equiv), 2-Cl-BQ (0.5 equiv), 1,2-DCE (1.0 mL), N_2, 75 °C, 3 days. [b]Calculated conversion, C = eeSM/(eeSM + eePR). [c]Determined by chiral HPLC analysis. [d]Selectivity factor (*s*) = ln[(1 − C)(1 − eeSM)]/ln[(1 − C)(1 + eeSM)]. [e]Reaction is performed in 60 °C.

Table II.6. Solvent screening[a]

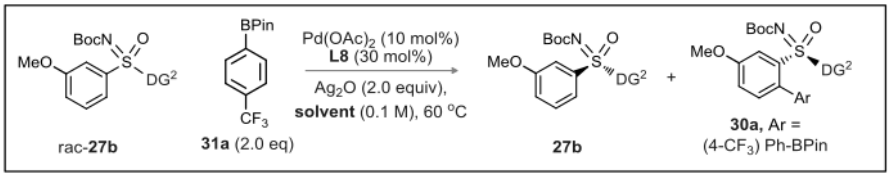

Entry	Solvent	Conversion	*ee* [%][c]	*s*[d]

		(c)[b]	(*R*)-1b	(*S*)-5a	
1	TFT	41	66	94	64
2	THF	31	44	96	75
3	*t*-Amyl-OH	36.0	54	96	84

[a]Reaction conditions: *rac*-**27b** (0.1 mmol), **31a** (2.0 equiv), $Pd(OAc)_2$ (10 mol%), **L8** (30 mol%), Ag_2O (2.0 equiv), 2-Cl-BQ (0.3 equiv), 1,2-DCE (1.0 mL), N_2, 75 °C, 3 days. [b]Calculated conversion, C = eeSM/(eeSM + eePR). [c]Determined by chiral HPLC analysis. [d]Selectivity factor (*s*) = ln[(1 − C)(1 − eeSM)]/ln[(1 − C)(1 + eeSM)].

Table II.7. Screening of ligand loading[a]

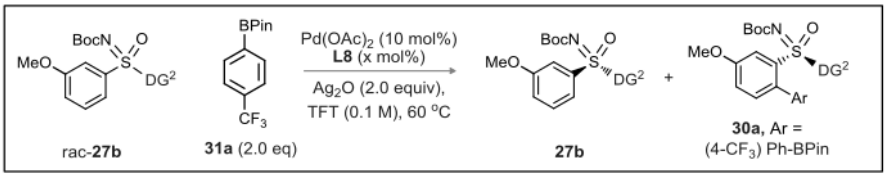

Entry	Ligand loading (x mol%)	Conversion (c)[b]	*ee* [%][c]		*s*[d]
			(*R*)-1b	(*S*)-5a	
1	10 mol%	41	64	94	62
2	15 mol%	42	68	94	66
3	20 mol%	46	80	94	79
4	40 mol%	40	62	94	61

[a]Reaction conditions: *rac*-**27b** (0.1 mmol), **31a** (2.0 equiv), $Pd(OAc)_2$ (10 mol%), **L8** (x mol%), Ag_2O (2.0 equiv), 2-Cl-BQ (0.3 equiv), 1,2-DCE (1.0 mL), N_2, 75 °C, 3 days. [b]Calculated conversion, C = eeSM/(eeSM + eePR). [c]Determined by chiral HPLC analysis. [d]Selectivity factor (*s*) = ln[(1 − C)(1 − eeSM)]/ln[(1 − C)(1 + eeSM)].

Table II.8. Screening of solvent loading[a]

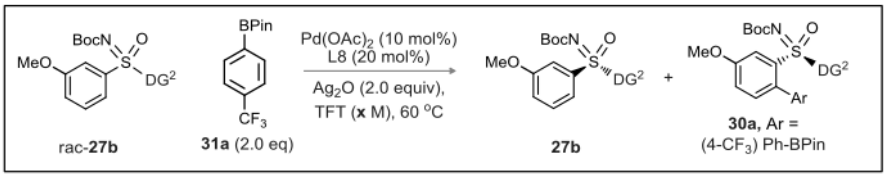

Entry	Molarity	Conversion	*ee* [%]c	s[d]

		(c)[b]	*(R)*-1b	*(S)*-5a	
1	0.2 M	41	64	94	62
2	0.13 M	41	66	94	64
3	0.067 M	48	88	94	95
4	0.05 M	47	84	94	86

[a]Reaction conditions: *rac*-**27b** (0.1 mmol), **31a** (2.0 equiv), $Pd(OAc)_2$ (10 mol%), **L8** (20 mol%), Ag_2O (2.0 equiv), 2-Cl-BQ (0.3 equiv), 1,2-DCE (x M), N_2, 75 °C, 3 days. [b]Calculated conversion, C = eeSM/(eeSM + eePR). [c]Determined by chiral HPLC analysis. [d]Selectivity factor (*s*) = ln[(1 − C)(1 − eeSM)]/ln[(1 − C)(1 + eeSM)].

II.4.4. Reaction scope-I

The reaction generality of Pd-catalyzed C–H alkenylative KR of sulfoximines was then surveyed (**Table** II.9).[10] Compound **29b** (98.2:1.8 er) was isolated in 26% yield. The alkenylation occurred at the less-hindered arene C–H bond and the chiral sulfoximines **29c** and **29d** were obtained with *s* factors of 162 and 140, respectively. The catalytic system was compatible with common functional groups, such as ketone, sulfone and phosphate in the alkene, providing access to **29e** (95.6:4.4 er), **29f** (94.6:5.4 er) and **29g** (97.6:2.4 er). *Notably, the reaction of methyl vinyl sulfone with* ***27b*** *displayed an exceptional s factor of >200 for compound* ***29h***. The reaction of *p*-(Me/^{t}Bu/^{i}Pr)-substituted aryl sulfoximines with **28b/** vinyl-ketone (**28c**)/ vinyl-sulfone (**28f**) smoothly delivered **29i**–**m** in excellent enantioselectivity and *s* factor of 55 to >200. The *m*-substituted electron donating (OEt, Me) and chloro bearing aryl-sulfoximines underwent olefination with **28b** to give the desired products **29n**–**p** with *s* factor of 24 to 111. The low yield of **29p** (22%; 94.4:5.6 er) is justified by a conversion of 28%, which can be attributed to electron deactivation by the halo group and the possibility for the formation of cross-coupled side product. Even the sterically hindered *m*,*m*'-dimethyl substituted aryl sulfoximine **27i** reacted well, yielding **29q** (36%, 97.9:2.1 er, *s* factor of 107).

Table II.9. Scope of C–H alkenylative kinetic resolution of sulfoximines[a],[c]

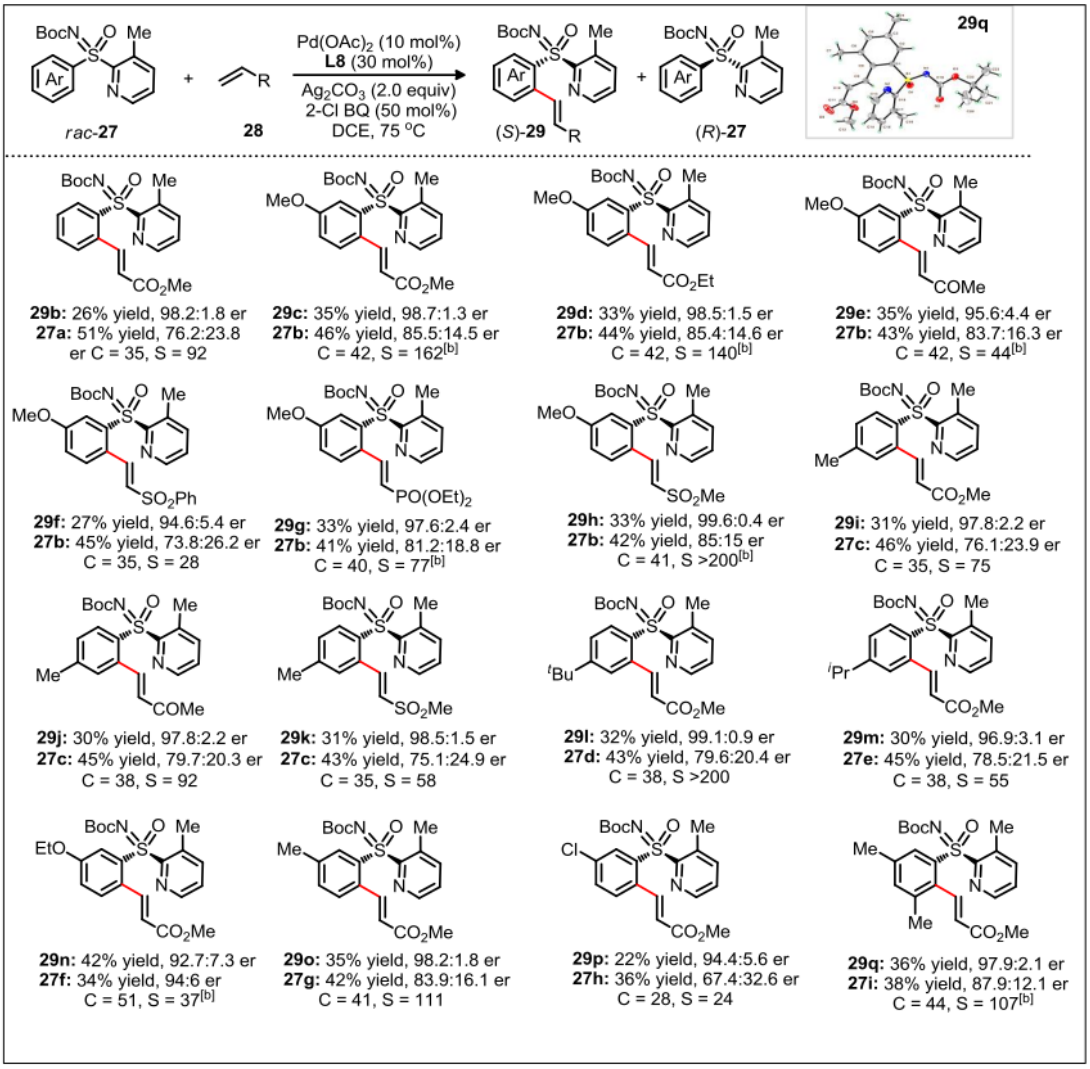

[a]Reaction conditions: **rac-27** (0.25 mmol), olefin (2.0 equiv), $Pd(OAc)_2$ (10 mol%), **L8** (30 mol%), Ag_2CO_3 (2.0 equiv), 2-Cl-BQ (0.5 equiv), 1,2-DCE (2.5 mL), 75 °C, 3 days. [b]Olefin (1.8 equiv) was used. [c]Yield of the isolated olefinated product. Calculated conversion, C = eeSM/(eeSM + eePR). enantiomeric ratio (er) was determined by chiral HPLC analysis. Selectivity factor (*s*) = ln[(1 − C)(1 − eeSM)]/ln[(1 − C)(1 + eeSM)].

II.4.5. Reaction scope-II

We next probe sulfoximines KR via enantioselective C−H arylation with arylpinacol boronate esters (**Table** II.10).

Table II.10. Scope of C–H arylative kinetic resolution of sulfoximines[a],[b]

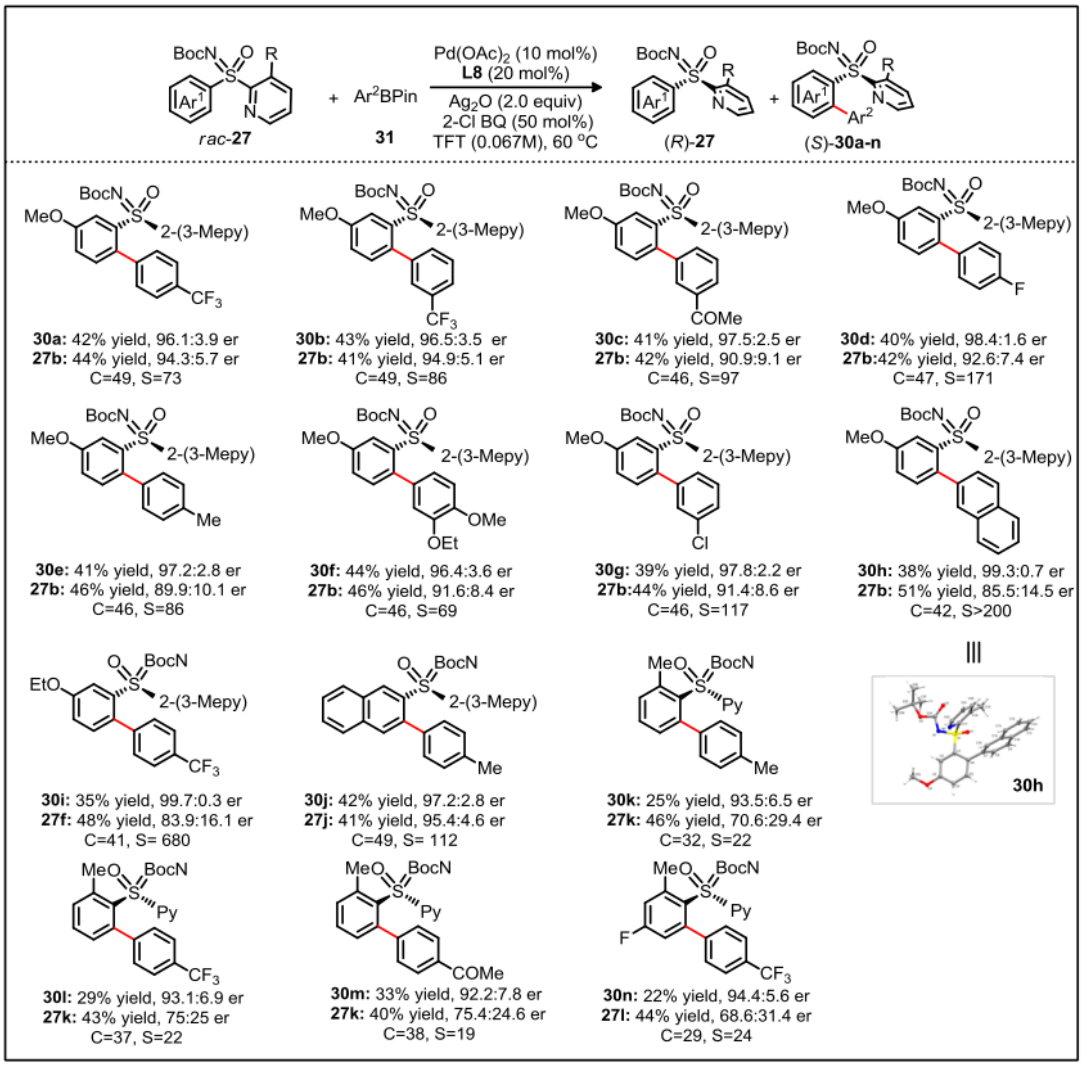

[a]Reaction conditions: *rac*- **17** (0.2 mmol), **31** (2.0 equiv), $Pd(OAc)_2$ (10 mol%), **L8** (20 mol%), Ag_2O (2.0 equiv), 2-Cl-BQ (0.5 equiv), TFT (3.0 mL), 60 °C, 3 days. [b]Yield of the isolated arylation product. Calculated conversion, C = eeSM/(eeSM + eePR); Enantiomeric ratio (er) was determined by chiral HPLC analysis;. Selectivity (s) = ln[(1 − C)(1 − eeSM)]/ln[(1 − C)(1 + eeSM)]

At first, the reaction of **17b** with various arylpinacol boronate esters having electron withdrawing groups [*p*-CF_3 (**31a**), *m*-CF_3 (**31b**), *m*-COMe (**31c**) and *p*-F (**31d**)], electron donating groups [*p*-Me (**31e**), and *p*-OMe-*m*-OEt (**31f**))] at the aryl motif independently

led to the arylative resolution products **30a** (96.1:3.9 er, 42%), **30b** (96.5:3.5 er, 43%), **30c** (97.5:2.5 er, 41%), **30d** (98.4:1.6 er, 40%), **30e** (97.2:2.8 er, 41%), and **30f** (96.4:3.6 er, 44%), respectively, with *s* factor of 69–171 and conversion 46–49%. Moreover, the precursor (*R*)-**17b** was isolated in 41–46% yield with good enantioselectivity. The labile –Cl group was tolerated under the Pd-catalytic system, making **30g** (97.8:2.2 er, 39%) with an *s* factor of 117. Notably, π–conjugated naphthyl-enabled sulfoximine resolution product **30h** (99.0:1.0 er, *s* factor of >200) was reliably accessed. *The arylation of m-OEt-phenyl bearing sulfoximine* ***1c*** *with* ***31a*** *provided* ***30i*** *(>99% ee) with s factor of >200.* Likewise, **30j** (97.2:2.8 er, *s* factor of 112) was made from the arylation of 2-naphthyl containing sulfoximine **17j** with **31e**. The steric bulkiness in aryl-motifs exerts influence on C–H functionalizations. Despite the challenges, *o*-tolyl enabled sulfoximines, **17k** and **17l**, were successful in undergoing arylation with **31a/31c/31e** to afford **30k–n** in good enantioselectivity; the moderate *s* factor of 19–24 and conversion (*c* = 29–38%) is considered suitable.

II.4.6. DFT studies

We performed a theoretical study to unveil the reaction mechanism (**Figure II.2**).[12,13] The MPAA ligand coordination to the metal center lowers the energy barrier of the CMD step, forming a semi planar five membered ring.[12] The coordination of both nitrogen atoms in sulfoximine **27a** forms **int-0** with the displacement of acetic acid, where the *S*-configuration at sulfur is 1.0 kcal/mol more stable than the *R* one. Prior to deprotonation, a *cis* coordination of aryl group to the *N*-protected moiety of the MPAA-ligated intermediate occurs. This assists the CMD process by establishing the absolute configuration of the sulfur motif. This calculation fully complies with the experimental observations of the resolution selectivity (calc. 98:2, exp. 98:2; **Figure II.2**a-III).

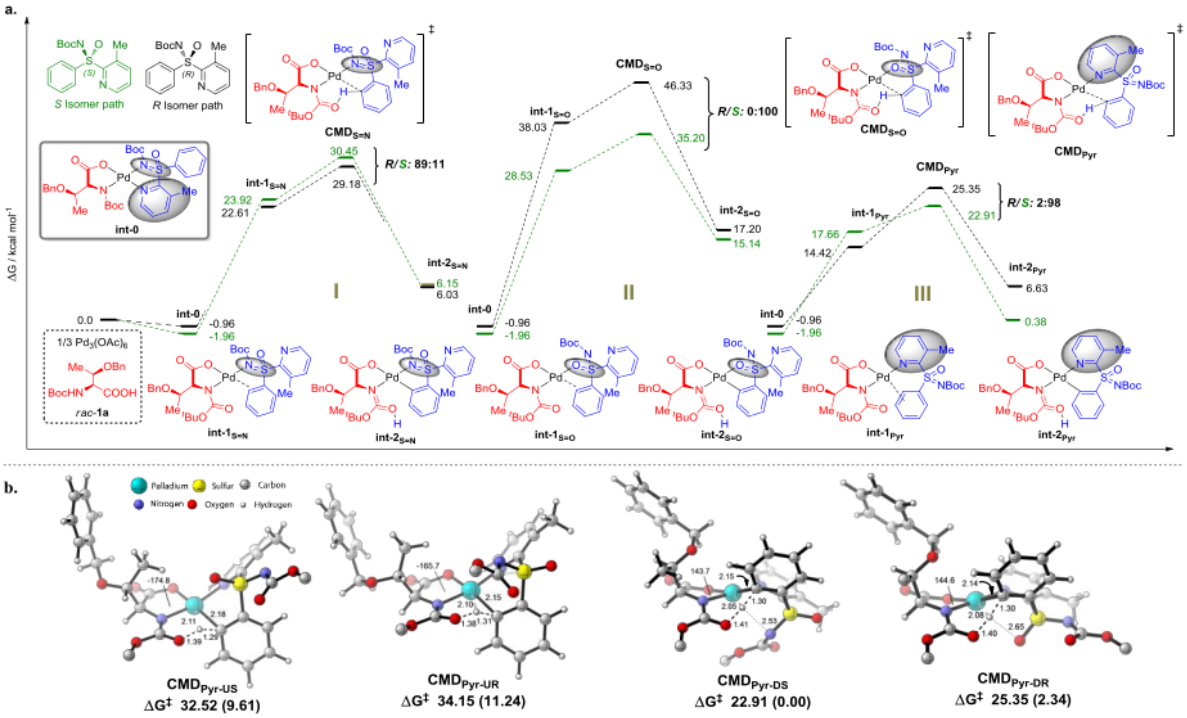

Figure II.2. [a]Free enegy profile, [b]Transition structures for each **CMD$_{Pyr}$** approach. *tert*-Butyl group from NBoc removed from all models to simplify visualization. Free energies in kcal/mol, distances in Å. Free energies at 343.15 K in DCE in kcal/mol. Relative free energies in parenthese.

Notably, the experimentally observed ***S*-int-2$_{Pyr}$** is thermodynamically favored over ***R*-int-2$_{Pyr}$** isomer by 6 kcal/mol. In retrospect, the CMD transition states of **int-1$_{S=N}$** (**Figure II.2a-I**) and **int-1$_{S=O}$** (**Figure II.2a-II**) lie much higher than **int-1$_{Pyr}$** (**Figure II.2a-III**), and their respective $\Delta\Delta G^{\neq}$ do not coincide with the experimental findings. We believe the CMD step could be responsible for the kinetic resolution. This hypothesis has been previously validated by Cheng *et al*, who also focused their study on the CMD as determining step.[12] Based on their findings, and considering the plane defined by the coordination of MPAA to the Pd, the bulky α–side chain of the ligand (above the plane) pushes the N-Boc moiety down to avoid steric hindrance (**Figure II.2b** and **Figure II.1-B**). Thus, sulfoximine phenyl group coordination complex with Pd-MPAA can point upward (U) or downward (D) on the plane, with *R* or *S* configurations. This translates

to four possible CMDs: **CMD$_{Pyr\text{-}UR}$**, **CMD$_{Pyr\text{-}US}$**, **CMD$_{Pyr\text{-}DR}$** and **CMD$_{Pyr\text{-}DS}$**. The CMDs adopt a 6-membered palladacycle with twisted boat conformation. In case of upward phenyl group linkage (**CMD$_{Pyr\text{-}UR}$** and **CMD$_{Pyr\text{-}US}$**), the sulfur atom and its substituents are located above the plane; while these substituents are below the plane for **CMD$_{Pyr\text{-}DR}$** and **CMD$_{Pyr\text{-}DS}$**. In agreement with Cheng's observations,[12] the C1-N2-Pd-O3 dihedral angle for **CMD$_{Pyr\text{-}UR}$** and **CMD$_{Pyr\text{-}US}$** is *ca* 170°, which generates a high steric interaction when compared with the *ca* 140° for **CMD$_{Pyr\text{-}DR}$** and **CMD$_{Pyr\text{-}DS}$**. These latter are favored by hydrogen bond interactions, making the combination of steric and electronic effects accounting for a difference of nearly 10 kcal/mol in each enantiomer. The preference for the *S* configuration by ~2.5 kcal/mol over the *R* isomer, lies in a steric clash of the NBoc group with the methyl group from the pyridine moiety and in consequence with the phenyl group, causing an energetically demanding arrangement.

Based on the literature, which included experimental observations, it is known that insertion/elimination steps come right after the CMD.[12] To corroborate our selectivity findings, we studied the mechanism for the insertion step in the Pyr and N=O series. Analysis of the transition states revealed that, as in the CMD case, pyridine acting as a directing group provides the lowest energy barriers (24.28 kcal/mol for the *S* isomer and 28.67 kcal/mol for the *R* isomer). The study of this step confirms the selectivity observed at the CMD and shows the irreversibility of the reaction.

II.4.7. Application

The synthetic potential of chiral sulfoximine was next probed (**Scheme II.13**). The trifuloroacetic acid (TFA) mediated *N*-Boc deprotection of (*R*)-**27b** provided chiral sulfoximine (*R*)-**32** (95% ee). Next, reduction of (*R*)-**32** led to chiral sulfoxide (*R*)-**33** (90% ee) when exposed to *t*-BuNO$_2$ at rt for 2 h; chiral integrity of S-motif is preserved. The N-Boc deprotection and intramolecular Michael cyclization to the activated olefin-moiety of (*S*)-**29c** was smooth delivering **34** (as a single diastereomer) in 95% ee. A one-

pot TFA assisted N-Boc deprotection and oxidative intramolecular C–N bond formation of (*S*)-**30d** furnished (*S*)-**35** (93% ee, 62% yield).

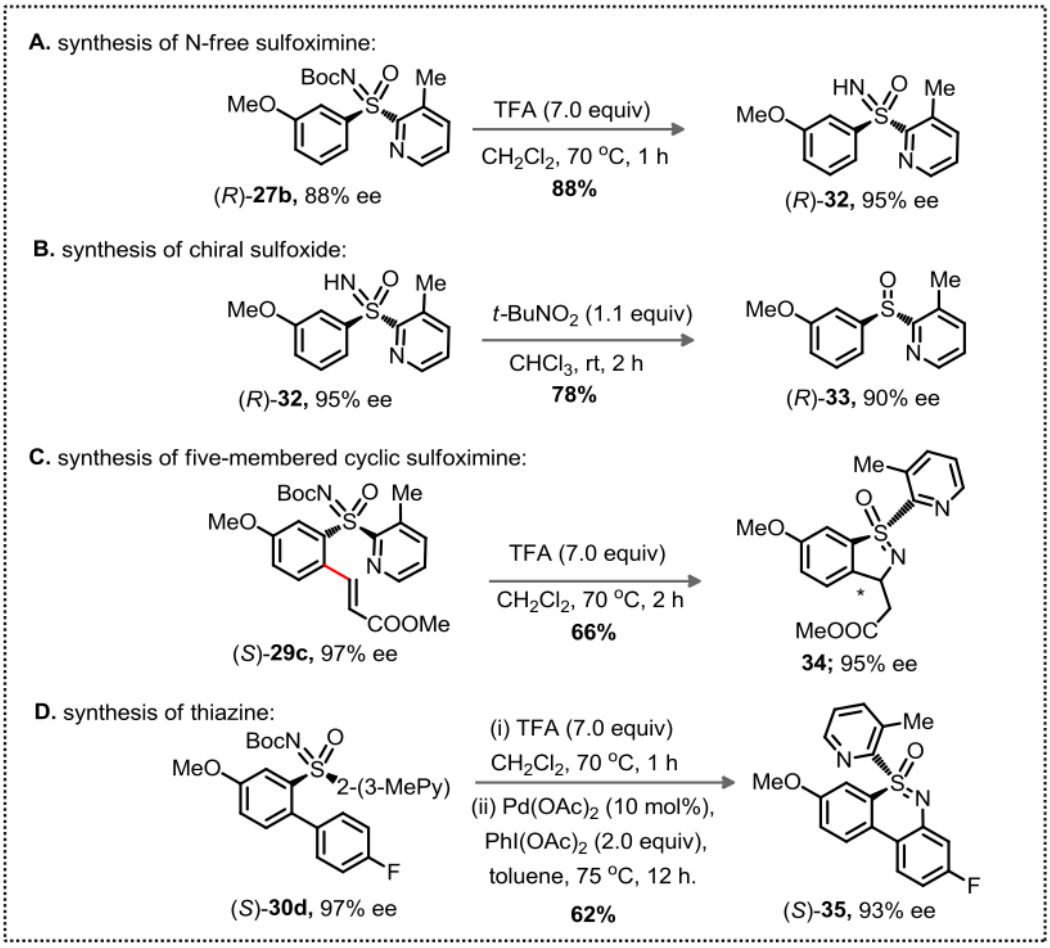

Scheme II.13: Derivatization of Chiral Product

II.5. Conclusion

In summary, a Pd(II)-catalyzed pyridyl substituted KR of sulfoximines through C(aryl)–H alkenylation and arylation has been revealed for the first time. The transformation addresses the inherent challenges in the KR of coordinatively active pyridyl-enabled sulfoximines (highly susceptible to TM-catalyst quenching) with no

prochiral center in the presence of chiral amino acid MPAA ligands and Pd(II)-catalyst. The common functional groups were tolerated under Pd-catalysis exhibiting good substrate scope for C–H alkenylative and arylative sulfoximines KR products in high enantioselectivity with *s* factor up to >200. In-depth DFT studies uncover the salient features of coordination selectivity of pyridyl-group over sulfoximine imine.

Chapter III

Unsymmetrical Annulation of C(sp²)–H Bonds with Alkynes and Quinones: Access to Spiro-Isoquinolones

Abstract

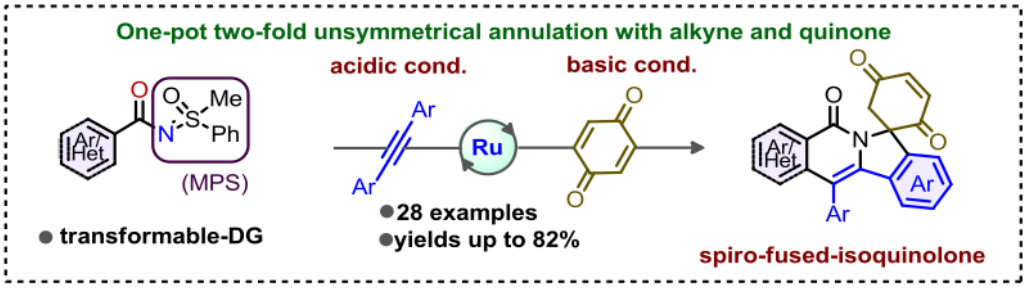

A non-trivial Ru-catalyzed one-pot sequential oxidative coupling of a (hetero)arene/vinylic/chromene system with alkyne and quinone is presented; the methyl phenyl sulfoximine (MPS) directing group is vital. This cyclization forms four (two C–C and two C–N) bonds in a single operation and produces unusual spiro-fused-isoquinolones with a broad scope. The release of phenyl methyl sulfoxide makes the MPS group transformable. A deuterium scrambling study sheds light on the reaction path.

Reference:

Kallol Mukherjee, Majji Shankar, Koushik Ghosh, and Akhila K. Sahoo
Org. Lett. **2018**, *20*, 1914–1917.

III.1. Introduction

The synthetically validated annulation tool has had a profound impact in chemistry, as this method reliably transforms the readily accessible less-functionalized compounds to structurally complex molecules.[1] In this regard, the transition-metal (TM)-catalyzed and directing group (DG) supported activation, functionalization, and annulation of inert C–H bonds are incomparable.[2–5] Obviously, the functionalization of environmentally different C–H bonds with distinct coupling partners results in structurally diverse molecular scaffolds.[6] A viable synthetic example of this is the directed double functionalization of proximal C–H bonds with identical functional groups.[7] By contrast, the chelation-assisted unsymmetrical functionalization of C–H bonds is often nonselective, uncontrolled, and unproductive;[8] however, a sequential two-step synthetic process under divergent DGs and/or different catalytic conditions is implemented for the construction of novel molecular scaffolds.[9]

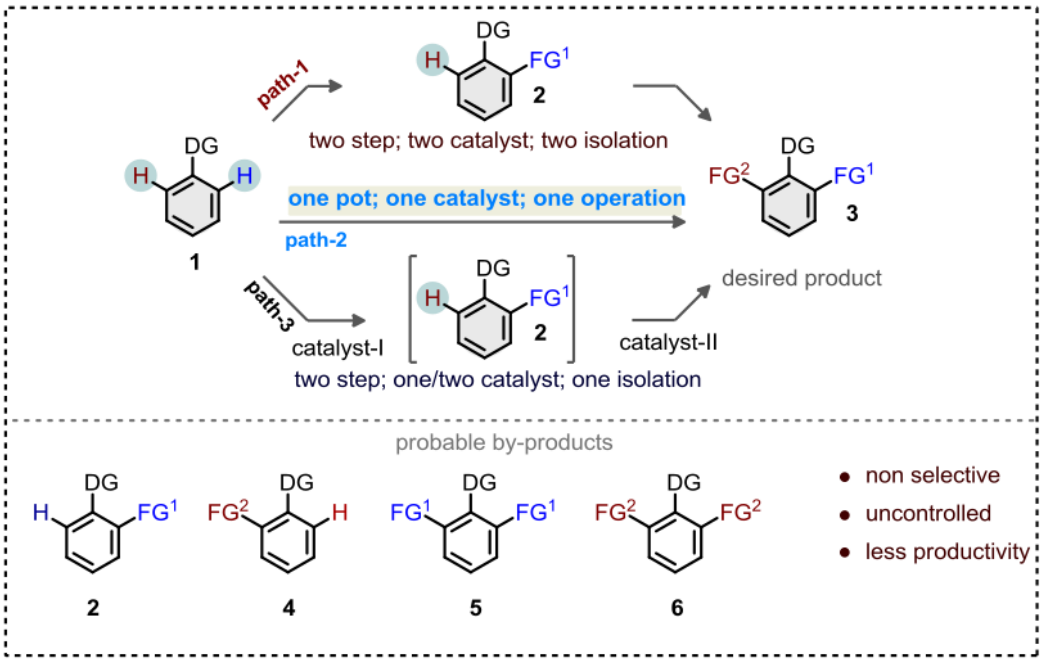

Scheme III.1: Multiple C–H functionalization and challenges

III.2. Previous strategies for annulation

III.2.1. Previous strategies of Ru-catalyzed mono-annulation:

In 2010 Ackermann group reported oxidative mono-annulation strategy for N–Me benzamide derivatives **7** with internal alkyne **8** for the synthesis of isoquinoline moieties **10** (**eq 1**, **Scheme III.2**). This method involves the inexpensive and air stable Ru(II) catalyst. The functionalization of N-Me benzamide dervivatives essentially requires an external oxidant. The external oxidant re-oxidizes the catalyst at the end of the cycle and makes the catalytic system active. Later the same protocol has been extended towards N–OMe benzamide substrate **9** (**eq 2**, **Scheme III.2**).[10, 11] The N–OMe moiety acts as an internal oxidant and thus, the synthetic method does not need external oxidant. Thus, the synthetic method is atom-economic and green. The mechanistic features of both the methods have been sketched in **Scheme III.2**.

Mechanistic cycles starts with the in-situ formation of active Ru(II)-complex [RuL(OAc)$_2$] **A**. The reaction of **A** with **7** or **9** provides 5-membered ruthenacycle **7a or 9a** via simultaneous N–H and C–H bond activation. Next, the alkyne insertion to **7a** or **9a** intermediate gives a 7-membered metallacycle **7b** or **9b.** Formation of 7-membered metalycycle is common for both the methods. Next, reductive elimination of **7b** delivers the corresponding mono-annulation product **10** along with the formation of inactive Ru(0) system. External oxidant is therefore necessary to re-oxidize Ru(0) to Ru(II) catalytic system, which helps the reaction to proceed further; thus, the transformation is ***oxidant enabled*** (**Scheme III.2**). While in case of **9b**, reductive elimination followed by oxidative insertion of Ru(II) complex across the N–OMe bond and protodemetalation of **9c** delivers isoquinoline derivative **11** along with active catalyst; thus, the transformation is ***oxidant free*** (**Scheme III.2**).

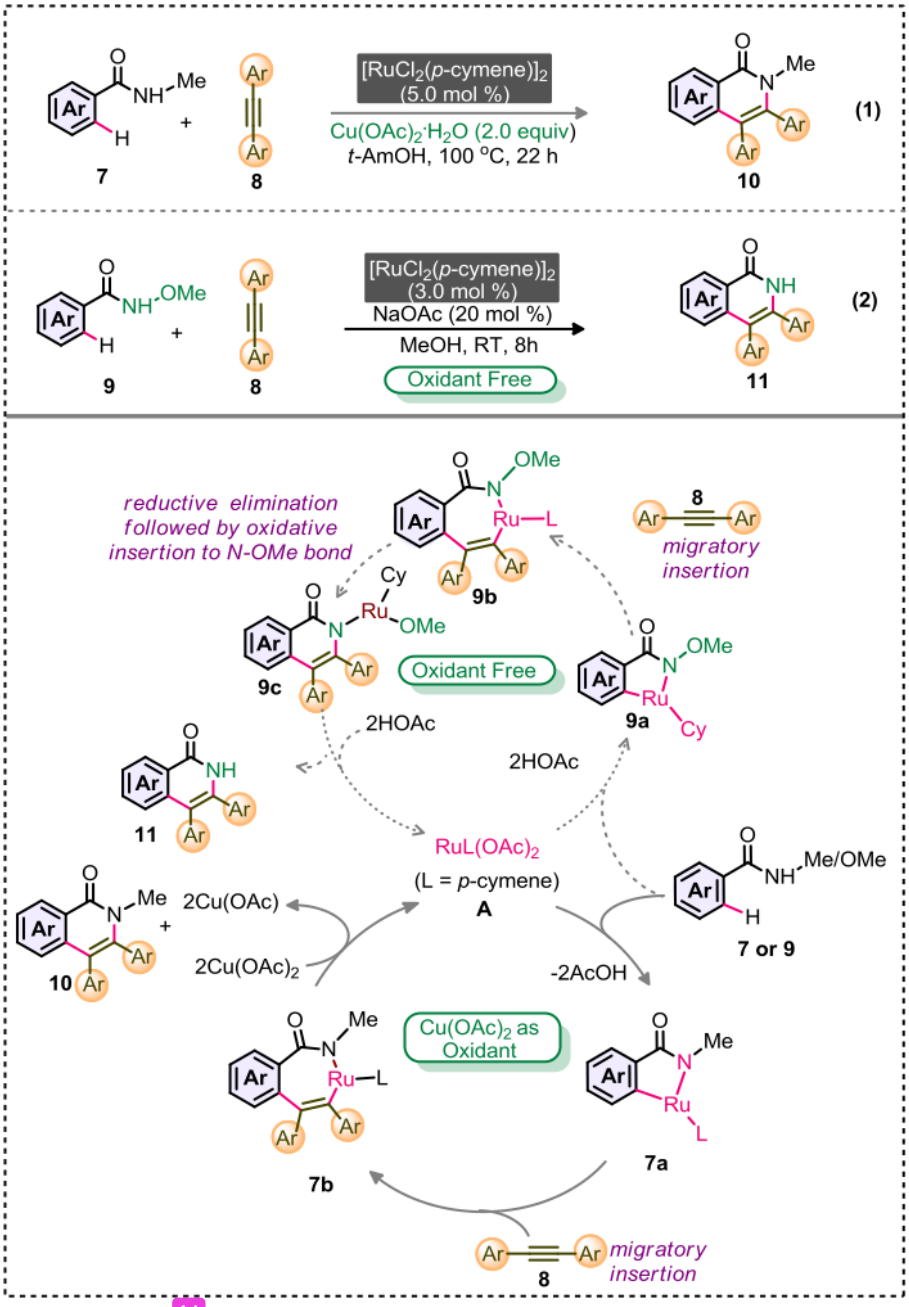

Scheme III.2: Ru(II)-catalyzed annulation of N–Me benzamide and N-OMe with alkyne and plausible mechanism

In 2011, identical strategy has been further extended for the construction of bio-active isoquinolones motifs in water medium (**Scheme III.3**). The N-methoxybenzamides **9** and/or hydroxymic acid derivatives **12** have been successfully employed for the reaction. Interestingly, Ru(II)-carboxylate, obtained in-situ from $[RuCl_2(p\text{-cymene})]_2$ and $MesCO_2K$ was essential for the reaction chemoselectivity.[12,13]

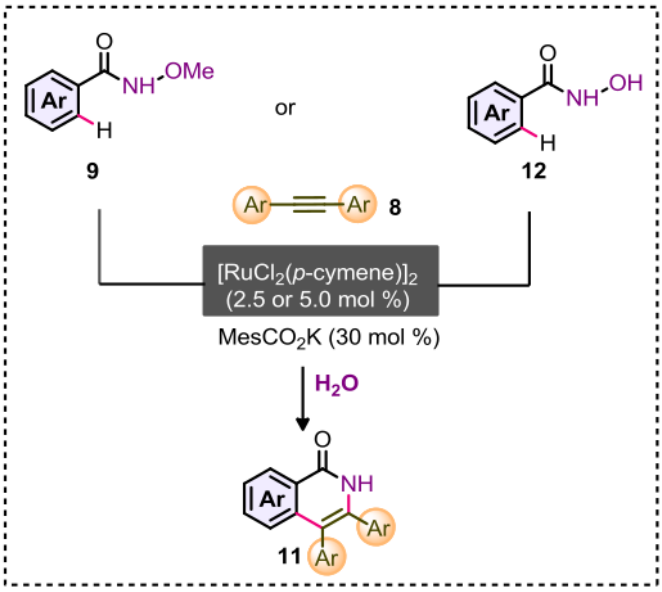

Scheme III.3: Ru(II)-catalyzed oxidative annulation in water medium

In **2014**, our group showcased a sulfoximine directing group assisted oxidative mono-annulation of MPS-coupled carboxylate **13** with internal alkyne. The sulfoximine moiety behave as an internal oxidant. The reaction proceeds without any external oxidant as sulfur (+6) of sulfoximine moiety is reduced to sulfoxide (+4; **14**) and Ru(0) gets reoxidized to Ru(II) (**Scheme III.4**).[14]

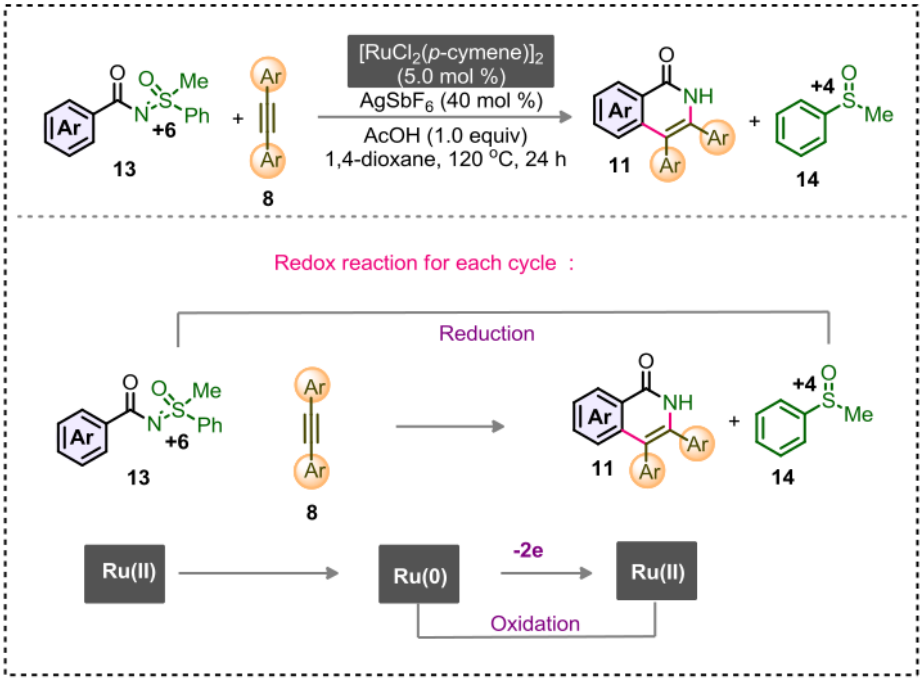

Scheme III.4: MPS directed Ru(II) catalyzed oxidative annulation of arenes

III.2.2. Known strategies of metal-catalyzed mono to di-annulation reactions:

The mono-annulation product isoquinolones **11** has been further used for the oxidative annulation with alkynes to form C–C and C–N bonds. This process leads to highly π-conjugated dibenzo[a,g]quinolizin-8-one derivatives with broad substrate scope. (**Scheme III.5**).[15]

The key intermediates **11a**, **11b**, and **11c** are isolated and the structures are determined by X-ray crystallographic analysis. These informations provide insights in understanding the mechanistic details of the reaction. Thus, the mechanistic cycle involves a Ru(II)-Ru(0)-Ru(II) catalytic system (**Scheme III.5**). The sandwich Ru(0) complex **11c** can be reoxidized by external oxidant $Cu(OAc)_2$.

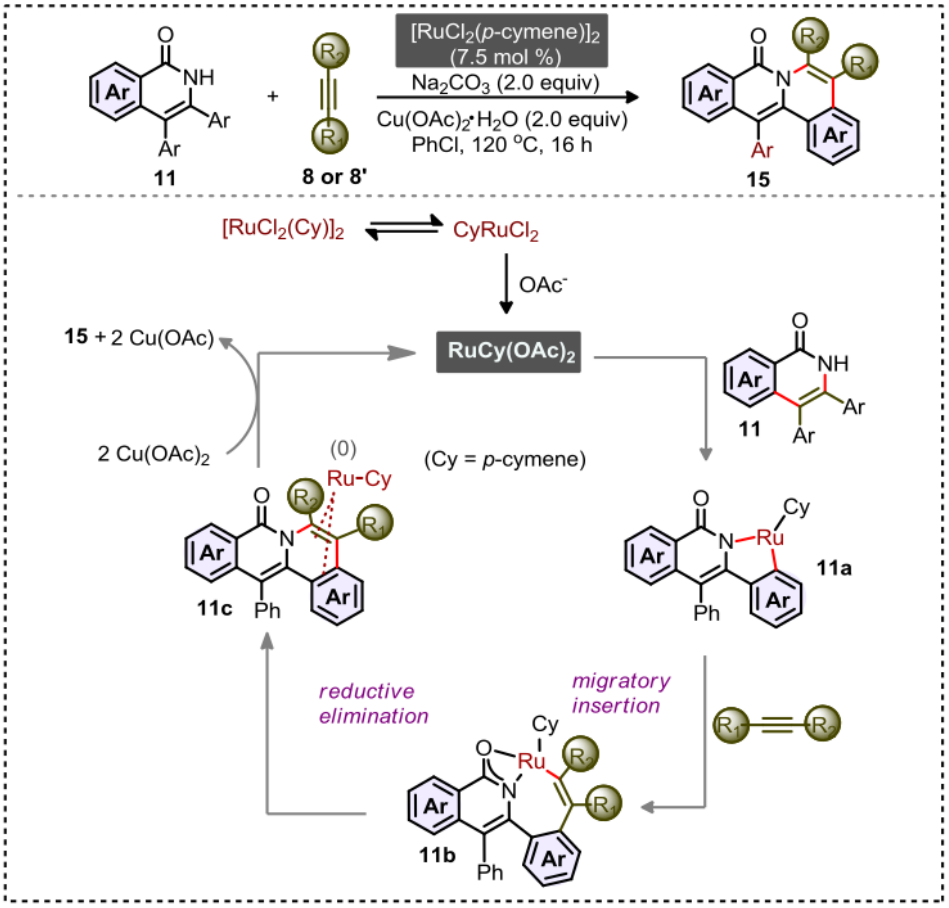

Scheme III. 5: Mechanism for the formation of polycyclic amides

In 2015, Wang group revealed an interesting Ir-catalyzed oxidative coupling of quinone with isoquinolones **11**. This process leads to the structurally complex spiro-derivatives. (**Scheme III.6**).[16a] In the same year Miura group developed Cu-catalyzed spirocyclization of benzamide with maleimide to make spiro-fused product **19** (**Scheme III.6**).[16b]

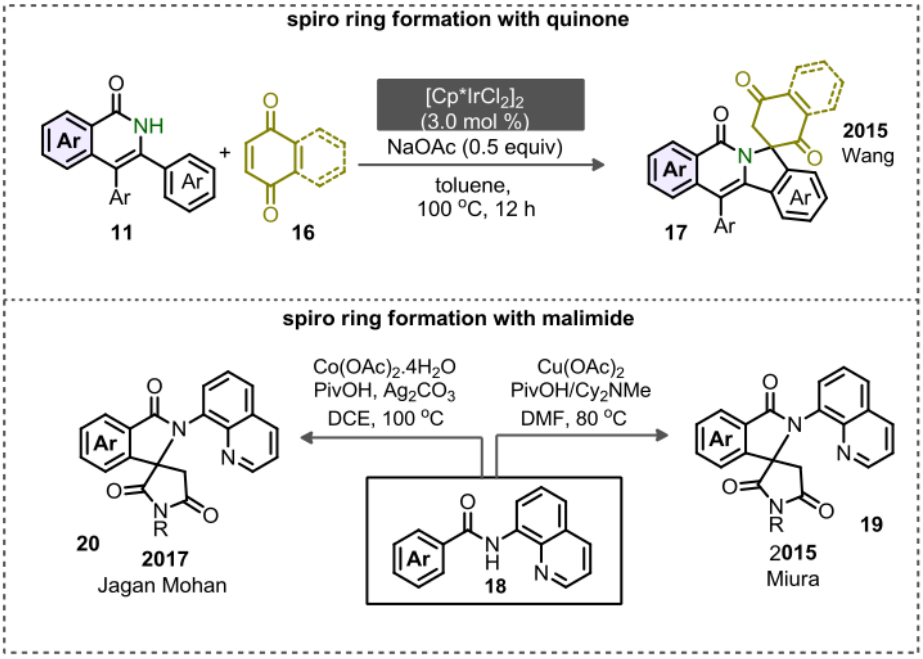

Scheme III.6: Ir(III)-catalyzed mono-annulation with quinone

In 2017 the same methodology was further extended for the Co-catalyzed annulation of **18** with succinimide for the synthesis of isoindolone spirosuccinimides **20** (**Scheme III.6**)[16c].

III.2.3. TM-Catalyzed of (One-pot/two-pot) symmectrical and un-symmetrical di-annulation.

In 2010, Miura and Satoh reported a Rh-catalyzed one-pot symmetrical di-annulation of benzamide derivatives when reacted with two molecules of alkyne.[17] At first, coupling of benzamide with one molecule alkyne leads to mono-annulation product **11**. Next, second C–H activation of the arene motif, proximity to the isoquinolone to provide **Int-B**. Finally, insertion of alkyne to **Int-B** leads to the symmetrical di-annulation product **15**. The same kind of di-annulation strategy were also revealed by Li group to access π-conjugated scaffolds.[18] The overall process involves two C–C & C–N bond formation in one pot (**Scheme III.7**).

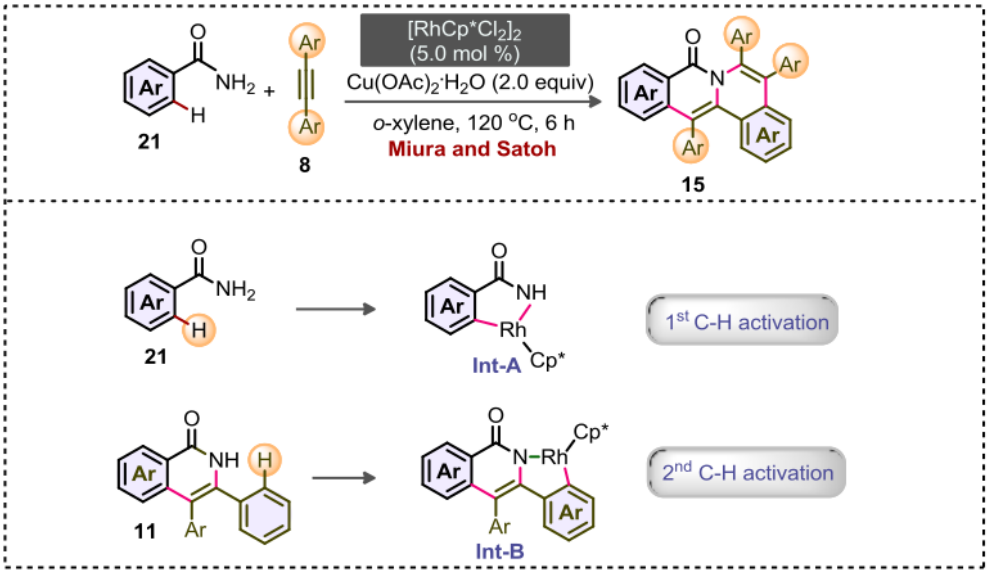

Scheme III.7: Symmetrical di-annulation between benzamides and alkynes

Later, Ru-catalysts have been used for the development of identical strategy. Thus, Dong group demonstrated a Ru-catalyzed one-pot symmetrical di-annulation of benzamide **21** derivatives with two alkyne molecules. However, the limited substrate scope and poor products yield of the diannulation products are the major drawbacks (**Scheme III.8**).[19]

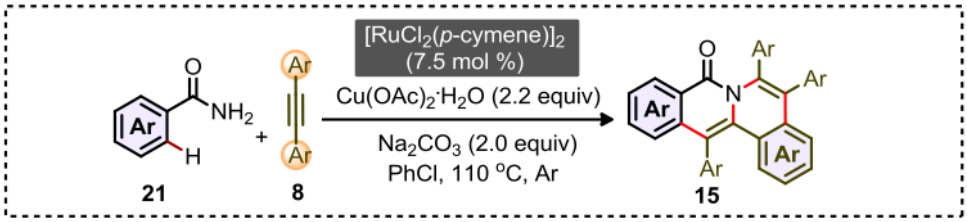

Scheme III.8: Double annulation between benzamides and diphenyl acetylene

In 2016, our group disclosed an interesting Ru-catalyzed symmetrical di-annulation of methyl phenyl sulfoximine (MPS) coupled heteroarenes **13** with two molecules of similar alkynes to deliver **15** (**Scheme III.9**). Next, the identical strategy has been used for the unsymmetrical difunctionalization of arenes with two distinct alkynes to afford **15′** (**Scheme III.9**).[20]

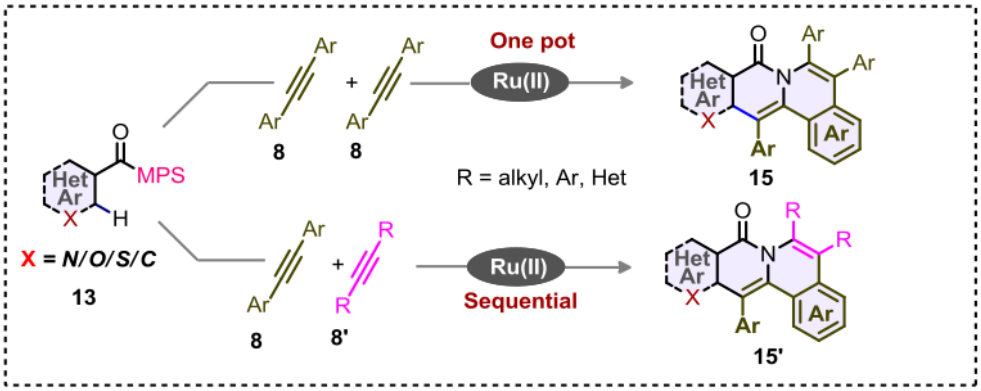

Scheme III.9: Double annulations of MPS-enabled (hetero)arenes

III.3. Motivation and Design for Double Annulation

A one-pot, single DG-enabled unsymmetrical tandem *o*-C–H di-functionalization of arenes has recently been presented via the intramolecular *o*-C–H hydroarylation and intermolecular *o*′-C–C/C–N bond formations,[21a] and also, the *o*-C–H alkylation and *o*′-C–H amidation of *N*-phenoxyacetamide.[21b]

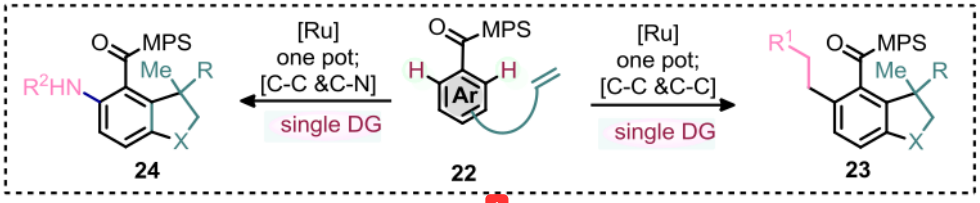

Scheme III.10: One-pot intermolecular hydroarylation and intermolecular *o*′-C–C/C–N bond formations

Two synthetic steps are essential to realize a cascade two-fold annulation of arenes with different coupling partners; hence, stitching of distinct functional groups (FG^1/FG^2) requires different catalytic conditions (**Scheme III.11**).[9b-c]

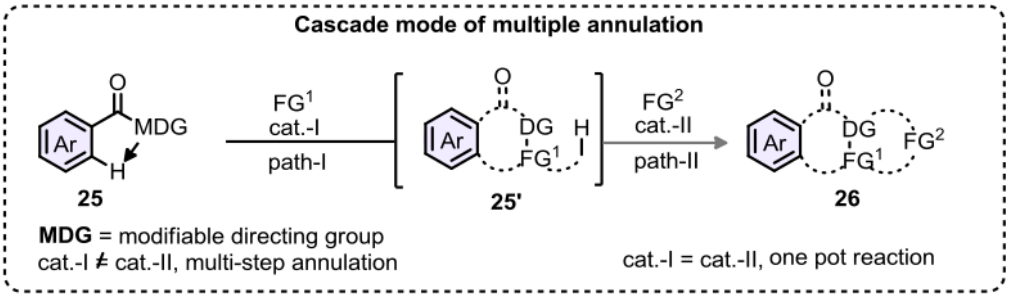

Scheme III.11: Mutiple annulation

We have recently demonstrated a direct double annulation of transformable methylphenyl sulfoximine (MPS)-DG-aided C(sp^2)–H bonds with different alkynes.[22] Thus, the one-pot, two-fold unsymmetrical C–H di-annulation of (hetero)arenes with distinct coupling partners (alkyne and olefin) in the presence of a single DG under single catalytic conditions is a worthwhile endeavor, which has so far not been reported. We propose that alkyne over olefin can undergo multiple annulation with C(sp^2)–H bonds and generate **11** (mono-annulation) and **15** (di-annulation) products,[22a] which eventually obstructs the formation of the projected unsymmetrical di-annulation compound **27/17** (**Scheme III.12**).

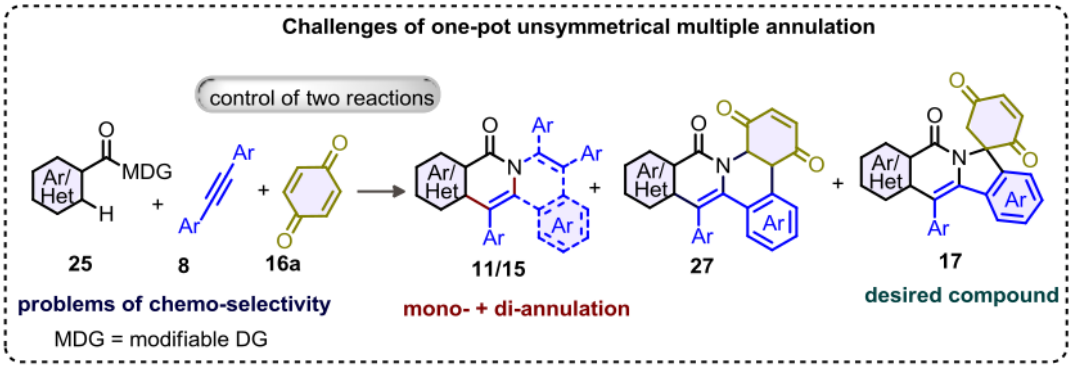

Scheme III.12: Challenges of mutiple annulation

Moreover, the quinone moiety is an effective Michael acceptor and is susceptible to Heck coupling; thus, α,α′-difunctionalization of the quinone motif to install a spiro-

skeleton is possible, although challenging.[23] However, the Ir-catalyzed oxidative coupling of isoquinolone with benzoquinone is feasible for constructing novel spiro-fused heteroarenes.[16a] Thus far, there have been no reports on the respective one-pot unsymmetrical multiple annulations of heteroarene/vinylic system from a simple carboxylate precursor.

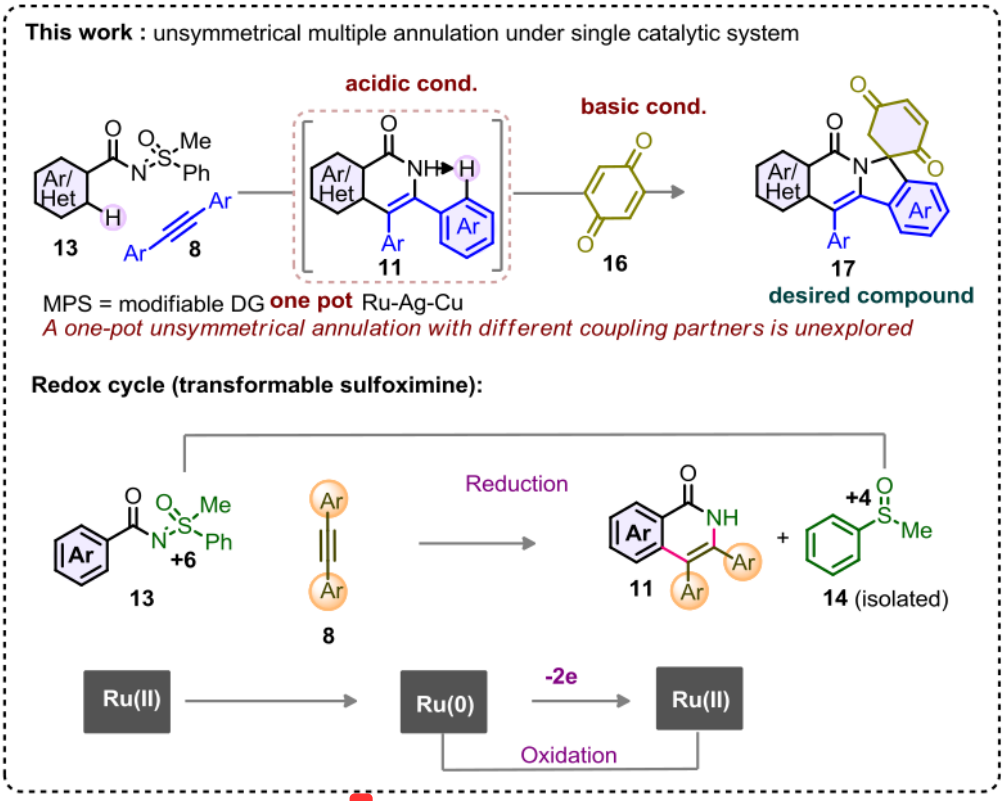

Scheme III.13: Orchestrated annulation of C(sp²)–H bonds with alkyne and quinone

On the basis of our preliminary understanding of the MPS-DG assisted annulation of hetero(arene)/vinylic systems, we herein invent a tunable one-step synthetic technique for the divergent annulation of C(sp²)–H bonds with alkyne and quinone (**Scheme III.13**). The strategy involves mono-annulation of proximal C–H bond of MPS-DG bearing amide and alkyne under cost-effective, air-stable Ru catalyst in presence of acid source.[24] The in-situ formation of isoquinolone/pyridone through protodemetalation restrict further di-annulation with alkyne and the oxidizable MPS-DG helps

regeneration of active catalyst. Next, the base-promoted annulation with quinone delivers the synthetically promising unusual spiro-fused-isoquinolones of pharmaceutical and material importance.[25] The isolation of methylphenyl sulfoxide, the sole precursor of MPS, endorses MPS-DG as transformable (**Scheme III.13**).[26]

(draw separately about the concept)

III.4. Results and Discussion

III.4.1. Synthesis of precursors

For achieving the goal, a library of starting materials has been synthesized using the known synthetic procedure and shown in **Scheme III.14.** [20,27]

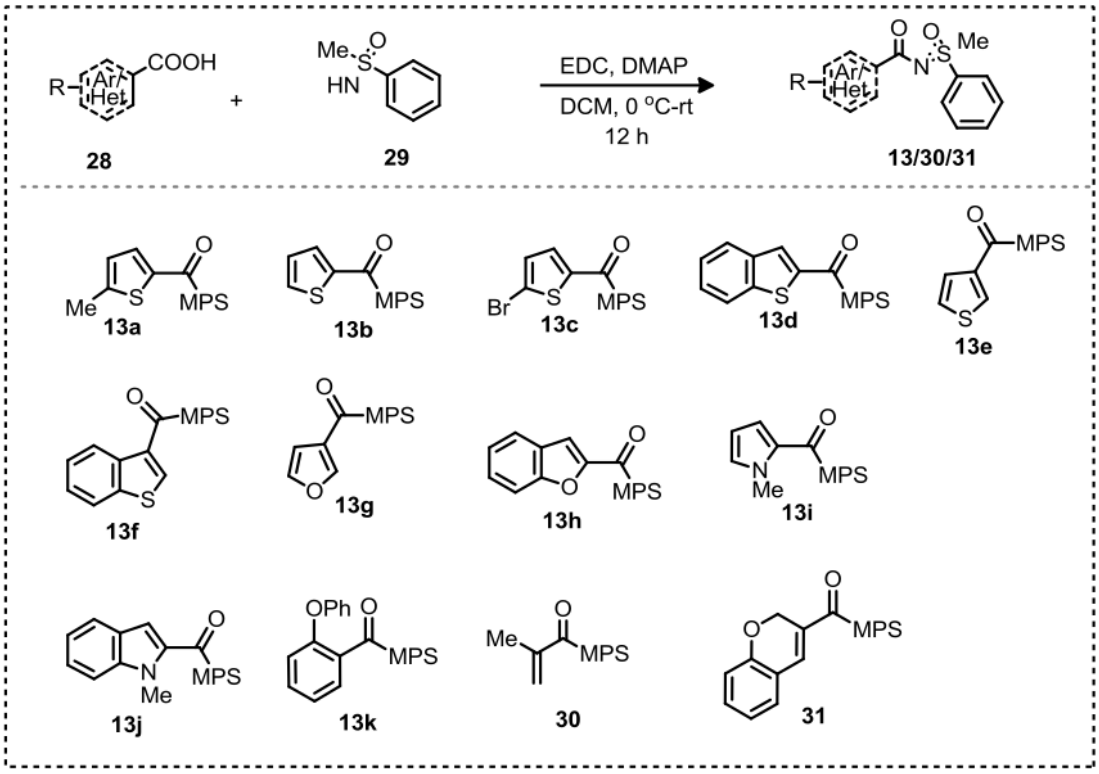

Scheme III.14: Preparation of N-heteroaroyl sulfoximine derivatives

Symmetrical and unsymmetrical alkynes were synthesized following the reported procedure.[28] Analytical and spectral data of these compounds are exactly matching with the reported values.

The symmetrical alkynes **8a**, **8b**, **8c**, **8d**, **8e**, **8f** and **8h** were prepared (**Scheme III.15**).[28] Diphenyl acetylene (**8a**) and phenyl N-butyl acetylene (**8g**) were purchased from comercially available source and used.

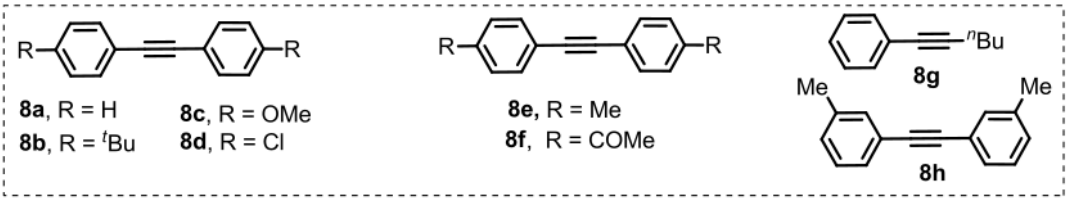

Scheme III.15: List prepared of symmetrical and unsymmetrical alkynes

Benzoquinone (BQ; **16a**), naphthaquinone (**16b**), and chloroquinone (**16c**) were purchased from commercially available source and used.

III.4.2. Optimization studies

The feasibility of the one-pot three component cascade annulations (envisaged in **Scheme III.13**) is probed by subjecting MPS coupled 5-methyl-thiophene-2-carboxylate (**13a**) with diphenylacetylene (**8a**) and benzoquinone (**16a**) in the presence of Ru-catalysts (Table III.1). Pleasingly, the predicted product **17a** (20%) and di-annulation compound **15** (35%; from **13a** and **8a**) formed when the reaction was executed under the catalytic conditions [Ru-catalyst (10 mol %), $AgSbF_6$ (40 mol %), and $Cu(OAc)_2 \cdot H_2O$ (1.0 equiv) in 1,2-dichloroethane (DCE) at 120 °C for 10 h] (entry 1). This result is particularly noteworthy; as MPS-bearing heteroarenes and alkynes are amenable to annulation, which occurs even at 60 °C.[22a]

To realize better turnout of **17a**, the annulation episode among **13a**, **8a**, and **16a** was conducted at 60 °C (where alkyne undergoes cyclization) and 120 °C (where quinone

commences annulation) in a single pot under one catalytic condition; pleasingly, **17a** was isolated in 35% yield (entry 2). This information encouraged us to survey the reaction by turn wise addition of **8a** and **16a**. Thus, the entire transformation was performed accordingly [the reaction was at first carried out at 60 °C in presence of 1.2 equiv of **8a** for 10 h, subsequently **16a** was introduced and the mixture was then heated at 120 °C for 10 h]; this process resulted 45% of **17a** along with the diannulation product

Table III.1: Optimization of reaction conditions

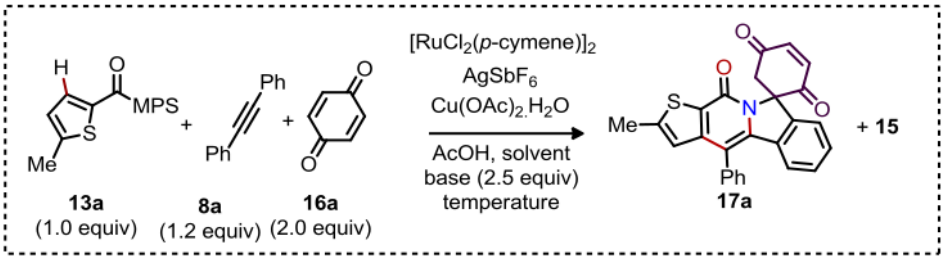

Entry	additive (2.0 equiv)	base (2.5 equiv)	temperature (°C)	yield of **17a** (%)
1	–	–	120	20 (35)[b,c]
2	–	_	60/120	35 (21)[b,c]
3	–	_	60/120	45 (18)
4	AcOH	_	90/120	26 (11)
5	AcOH	$NaHCO_3$	90/120	62 (07)
6	AcOH	Na_2CO_3	90/120	40 (10)
7	AcOH	K_2CO_3	90/120	39 (10)
8	AcOH	K_3PO_4	90/120	61 (06)
9	AcOH	KH_2PO_4	90/120	66 (05)
10	AcOH	KH_2PO_4	90/120	50 (15)[d]
11	AcOH	KH_2PO_4	90/120	72 (04)[e]
12	AcOH	KH_2PO_4	90/120	35 (40)[f,g]
13	AcOH	KH_2PO_4	90/120	39 (16)[h]
14	AcOH	KH_2PO_4	90/120	35 (0)[i]

[a]Reaction conditions: [a]Conditions: **13a** (0.18 mmol, 1.0 equiv), **8a** (1.2 equiv), Ru-catalyst (10 mol %), $AgSbF_6$ (40 mol %), $Cu(OAc)_2 \cdot H_2O$ (1.0 equiv), additive (2.0 equiv), DCE (1.5 mL) at 90 °C for 10 h; then BQ (2.0 equiv), base (2.5 equiv) and 1,4-dioxane (1.5 mL), at 120 °C for 10 h; yield

of **15** (di-annulation with alkyne) is shown in the parenthesis. [b]All the reactants in one-pot. [c]**8a** (1.0 equiv). [d]1,4-dioxane instead of DCE. [e]Addition of 1,4-dioxane (1.5 mL) after first cyclization. [f]In the absence of $Cu(OAc)_2 \cdot H_2O$. [g]Yield of **11** (mono-annulation with alkyne) is shown in the parenthesis. [h]O_2 as oxidant. [i]CuBr2 as oxidant.

15 (18%) (entry 3). Interestingly, annulation between **13a** and **8a** in presence of 2 equiv AcOH restricted the formation of **15** to 11%; meanwhile, delivery of **17a** was affected (entry 4), a consequence of ineffective binding of Ru to the NH-moiety of mono-annulation product in acid medium. Interestingly, addition of $NaHCO_3$ base, along with **16a** helped the production of **17a** (62%), endorsing the requirement of base after first cyclization (entry 5). Encouraged by the observation, various bases (Na_2CO_3, K_2CO_3, K_3PO_4, and KH_2PO_4) were screened (entries 6–9); KH_2PO_4 was found optimum yielding 66% of **17a** (entry 9). Although the overall reaction in 1,2-DCE was better over 1,4-dioxane (entries 9 and 10), the use of mixture of solvents in this two-fold cyclization strategy [1,2-DCE for the first annulation and subsequent addition of 1,4-dioxane in the second annulation] led to 72% **17a** (entry 11). This transformation in the absence of $Cu(OAc)_2 \cdot H_2O$ provided **17a** in only 35% yield, along with 40% of the mono-annulation compound **11** (entry 12) suggesting the oxidant indispensable; as it helps the regeneration of active catalyst after second annulation. Moreover, the reactions in presence of oxidant O_2 or $CuBr_2$ were not effective (entry 13 and entry 14). Thus, the one-pot synthetic avenue for the unsymmetrical annulation of **13a** with **8a** and **16a** under the optimized catalytic conditions (entry 11, **Table III.1**) smoothly provided unusual spiro-fused isoquinolone **17a**.

III.4.3. Reaction scope-I

The synthetic generality of this unprecedented two successive unsymmetrical annulation is validated by examining MPS-assisted cyclization of C(sp^2)–H bonds of challenging heteroarene/vinylic/chromene systems with alkynes and quinones (Scheme III.16). Thus, the MPS-coupled thiophene-2-/benzothiophene-2-carboxylate

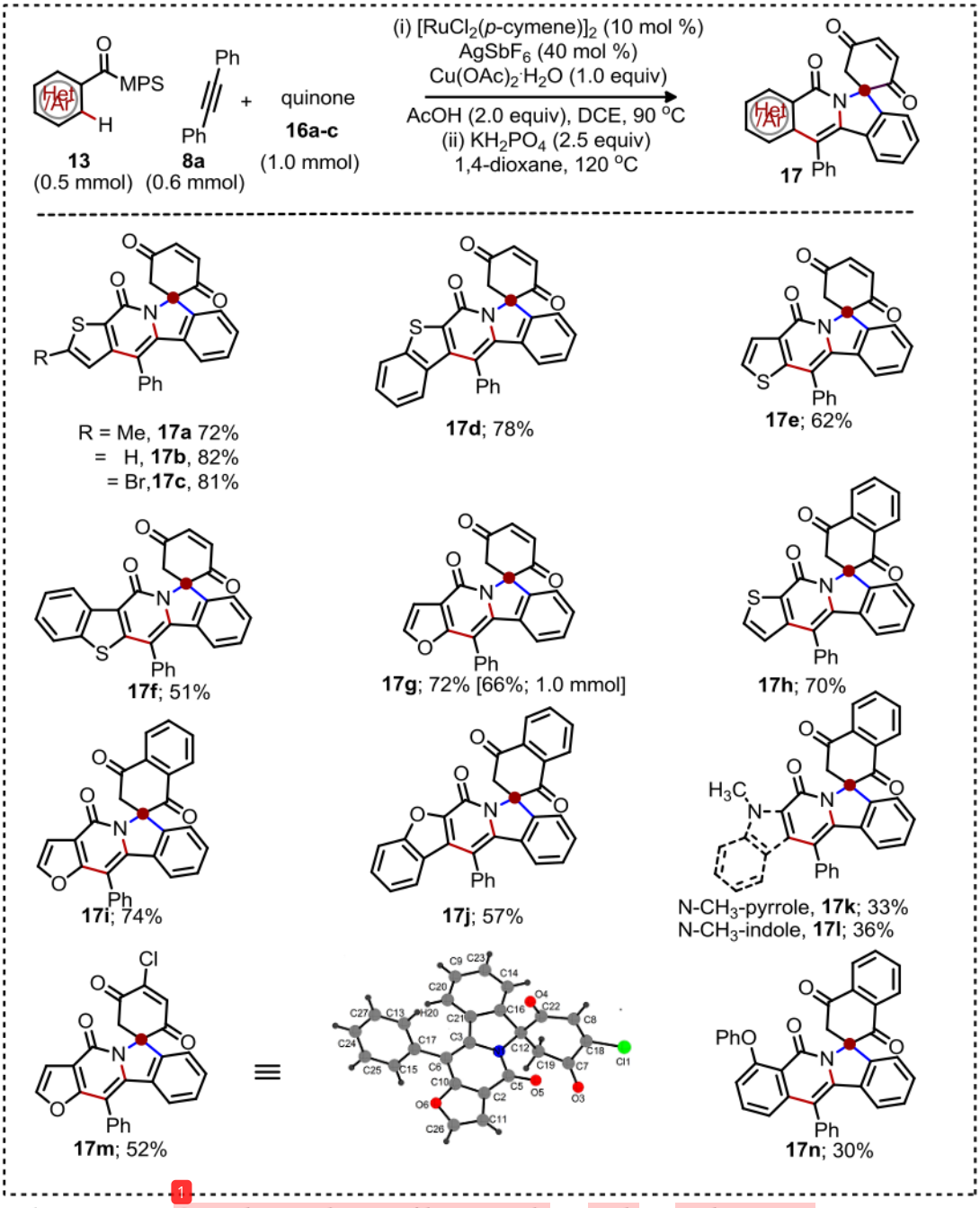

Scheme III.16: Cascade annulation of heteroaryls **13** with **8a** and quinone **16** (**13a**–**d**) were reacted with **8a** and **16a** to afford the desired spiro-products **17a**–**17d** (72–82%); the modifiable Br-group survived to provide **17c**. The thiophene-3-

/benzothiophene-3-carboxylates were also participated, delivering **17e** (62%) and **17f** (51%). Likewise, the spiro-product from oxygen bearing heteroarene **17g** (72%) was readily isolated from the cyclization cascade of MPS-bearing furan-3-carboxylate (**13g**) with **8a** and **16a**.

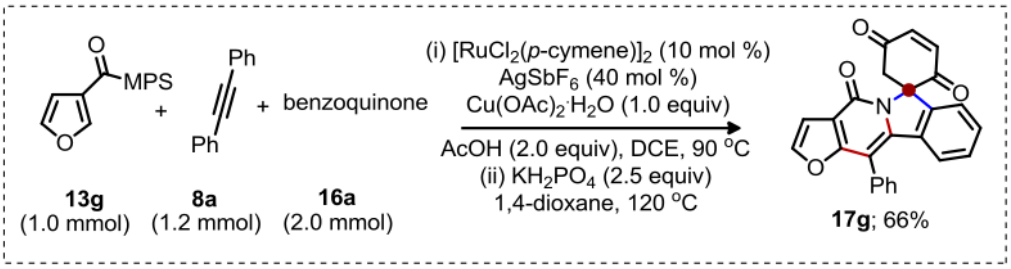

Scheme III.17: 1 mmol scale reaction

The identical reaction in 1.0 mmol scale; resulted 66% of **17g (Scheme III.17)**. The naphthaquinone (**16b**) also took part in the cascade cyclization episode with **13b**/**13g**/**13h** and **8a** to deliver **17h** (70%), **17i** (74%), and **17j** (57%), respectively (**Scheme III.16**). Moreover, the N-bearing heterocycles pyrrole and indole skeleton were stitched with **8a** and **16b** accessing the poly-fused spiro-skeletons **17k** and **17l**, albeit in moderate yield. The product **17m** was isolated from the annulations of **13g** with **8a** and 2-chloro-benzoquinone (**16c**); X-ray analysis confirms the structure **17m**. Annulations of challenging *o*-substituted arene motif with **8a** and **16b** delivered **17n**.

III.4.4. Reaction scope-II

We next probed the alkyne scope in this one-pot two-successive annulation of MPS-bearing heteroarene and quinone (**Scheme III.18**). Pleasingly, 1,2-diarylacetylenes {having *para*-substituents on the arene moiety, electron-donating [-^{t}Bu (**8b**)/-OMe (**8c**)] or -Cl (**8d**) group} smoothly reacted with **13b** and **16a** under the optimized procedure to afford spiro-fused enlarged isoquinolones **17o** (75%), **17p** (67%), and **17q** (69%). Likewise, the furan-enabled spiro-isoquinolone products **17r** (68%), **17s** (66%), and **17t**

(67%) were undeniably accessed when **13g** coupled with **8e** (*p*-Me-)/**8c** (*p*-MeO-) /electron-withdrawing (*p*-COMe) group containing alkyne (**8f**) and **16a**, respectively.

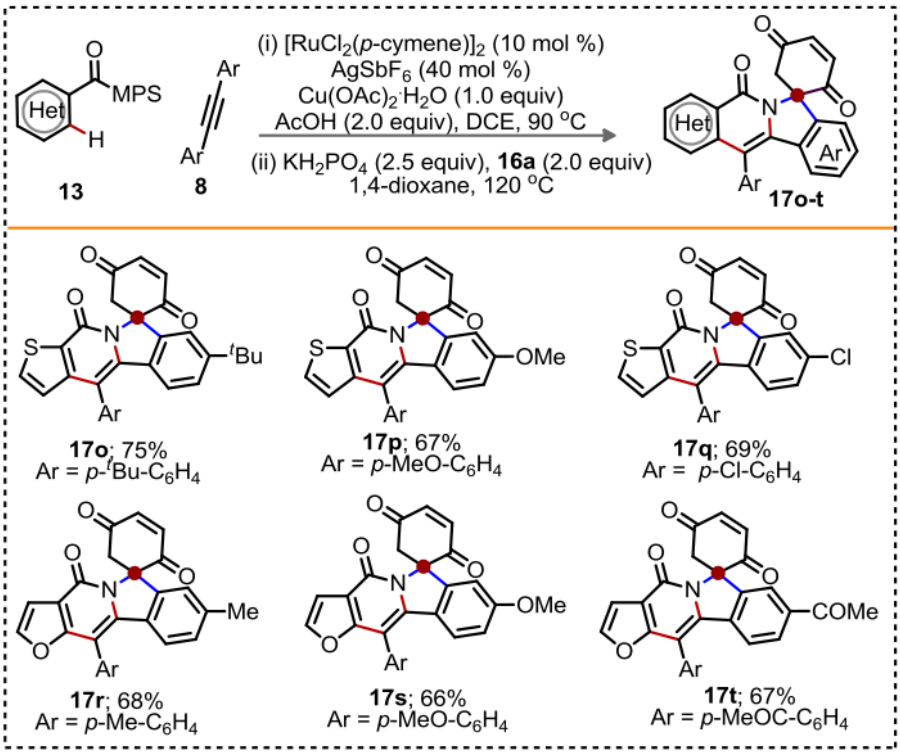

Scheme III.18: Cascade annulation of heteroaryls **13** with alkynes (**8**) and **16a**

III.4.5. Reaction scope-III

Inspired from the unsymmetrical di-annulation of heteroaryls with alkynes and quinones (**Scheme III.16** and **Scheme III.18**), the identical reaction in the challenging vinylic system was next surveyed (**Scheme III.19**); as vinylic systems tend to polymerize under the oxidative conditions and also are effective Michael acceptors.[18] Gratifyingly, the reaction of *N*-(methacryloyl)-MPS (**30**) with **8a** and **16b** under the optimized catalytic conditions in entry 11, **Table III.1** delivered **32a** in 62% yield. To further authenticate the synthetic viability of this two-fold annulations of acrylamides,

the reaction between **30**, the electron-rich (Me/^{t}Bu/OMe) group containing *para*-substituted 1,2-diarylacetylenes, and **16b** delivered the desired spiro-fused novel heterocycle manifolds **32b** (61%), **32c** (70%), and **32d** (62%).

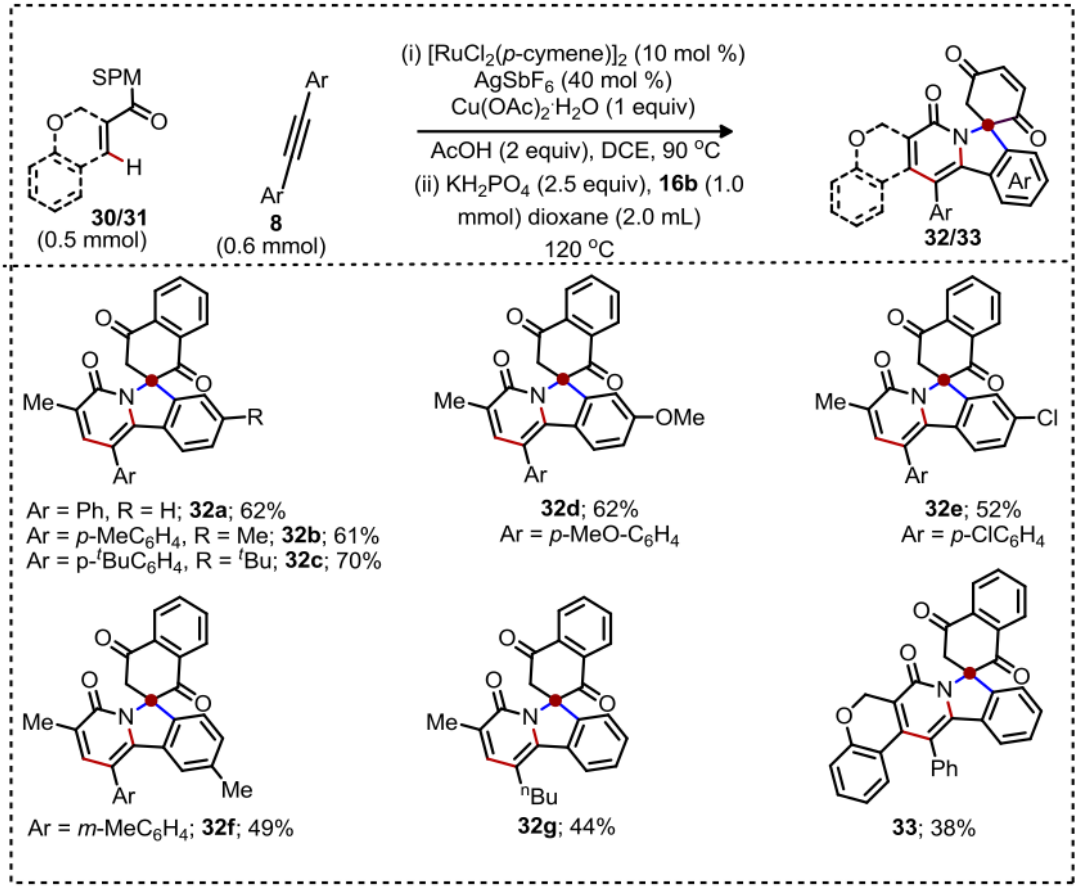

Scheme III.19: Cascade annulation of vinyl/chromenes **30/31** with alkynes (**8**) and **16b**

The product **32e** with the labile chloro group in the periphery was also constructed. The *meta*-Me bearing 1,2-diarylalkyne participated in the cascade annulation, accessing **32f**. The spiro compound **32g** was isolated from the annulation of **30**, unsymmetrical *n*-butyl-phenyl alkyne **8g**, and **16b**; the regioselective mono-annulation of **30** with **8g** makes this process feasible. The 2H-chromene-3-carboxylate derivative **31** successfully

underwent annulations with **8a** and **16b** to deliver the conjugated spiro species **33** in 38% yield.

III.4.6. Control Experiments

To understand the possible reaction pathway, a few control experiments have been performed (**Scheme III.20**). The reaction in the absence of oxidant $Cu(OAc)_2$ led to mono-annulation product (69%); the reductive cleavage of MPS group herein helps oxidation of Ru-catalyst and keeps the catalytic cycle active (eq 1). However, the reaction of **11b** with benzoquinone under the optimized condition led to 35% of the desired product **17b** (eq 1).

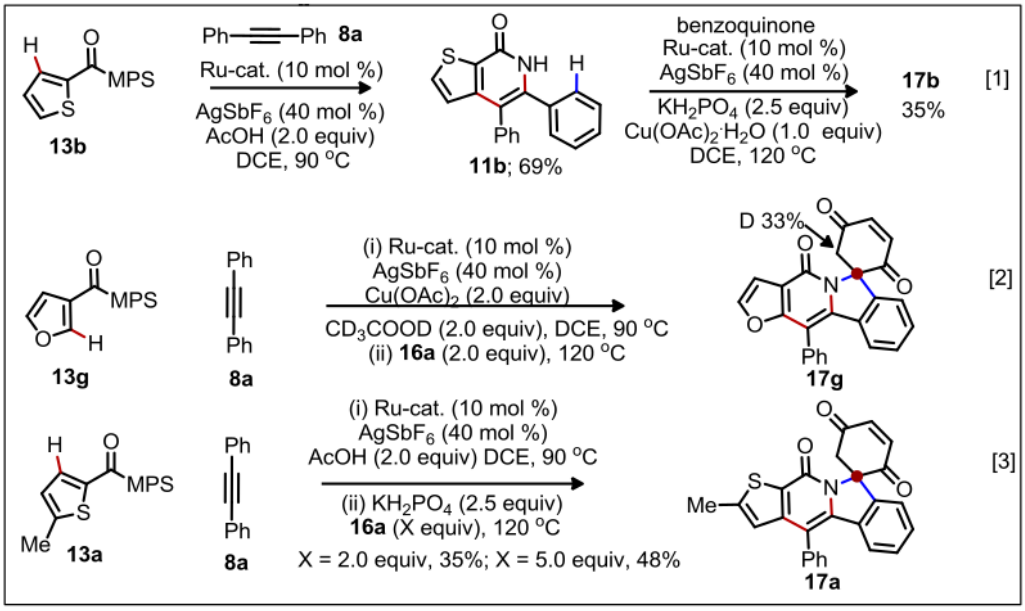

Scheme III.20. Control Experiments

Product **17g** with 33% deuterium incorporation in the quinone moiety was detected when the reaction exhibited in CD_3CO_2D (eq 2), reflecting the occurrence of protodemetalation in the transformation.[19] Hence, formation of the desired spiro-product is possible through the metalation of acidic $C(sp^3)$–H bond, followed by C–N reductive elimination (see the Mechanistic Cycle in **Scheme III.21**). Interestingly, the reaction in presence of 2.0 and 5.0 equiv of BQ produced 35% and 48% of **17a**,

respectively (eq 3); thus, the weak oxidant BQ is incapable in carrying out the transformation. Consequently, the oxidant $Cu(OAc)_2$ plays vital retaining the catalytic cycle alive via revival of active Ru(II) species.[5]

III.4.7. Mechanistic Cycle

Based on the precedence and the current observation, the plausible reaction pathway is outlined in **Scheme III.21**.[3,5] The reaction initiates with the coordination of MPS to the active Ru-species forming the ruthenacycle **13-I** via chelation-assisted C−H metalation.

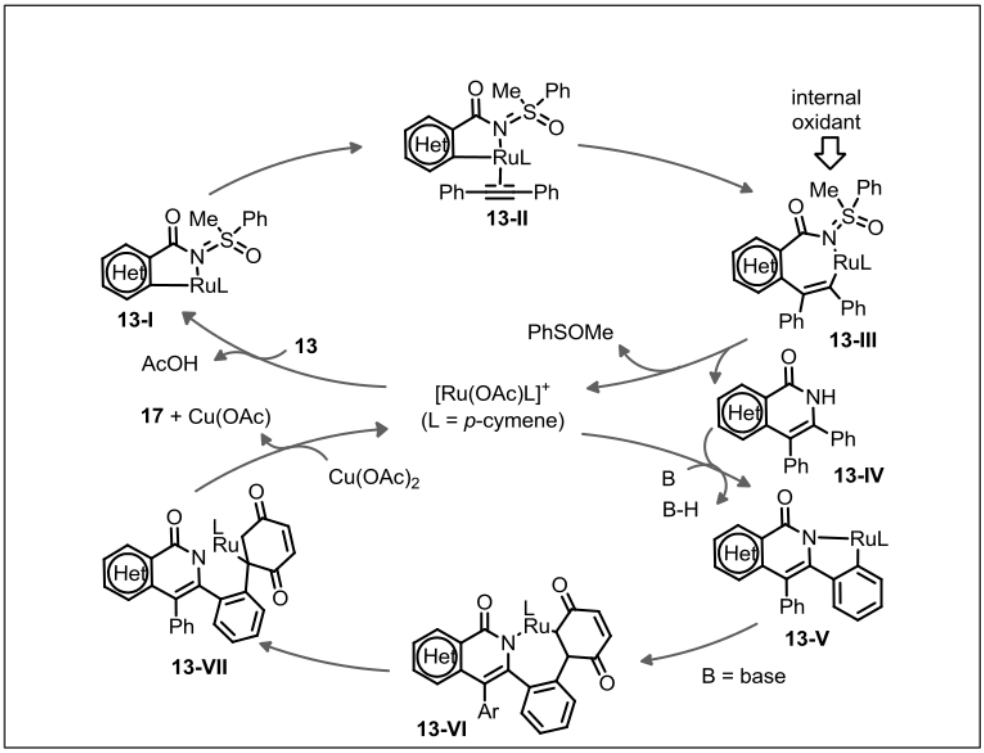

Scheme III.21: Proposed mechanistic profile

Subsequent alkyne coordination-insertion to **13-I** provides seven membered ruthenacycle **13-III** through **13-II**. Next, synergistic C−N reductive elimination and N−S cleavage affords **13-IV** in-situ, which simultaneously undergoes proximal C−H metalation to deliver **13-V**. Insertion of benzoquinone to **13-V** gives 7-membered ruthenacycle **13-VI**; protodemetalation of **13-VI** (eq 2, **Scheme III.20**) followed by

metalation of acidic C(sp^3)–H generates more stable 6-memberd ruthenacycle **13-VII**. Reductive elimination of **13-VII** finally leads to spiro-fused-isoquinolone **17**. The $Cu(OAc)_2$ helps regenerating the active Ru-catalyst.[29]

III.4.8. Application

The synthetic manipulation of peripheral olefin moiety in the spiro-isoquinolone scaffold was further elaborated by performing [4+2] cycloaddition of **17g** with cyclopentadiene resulting in complex molecular entity **34** (**Scheme III.22**).

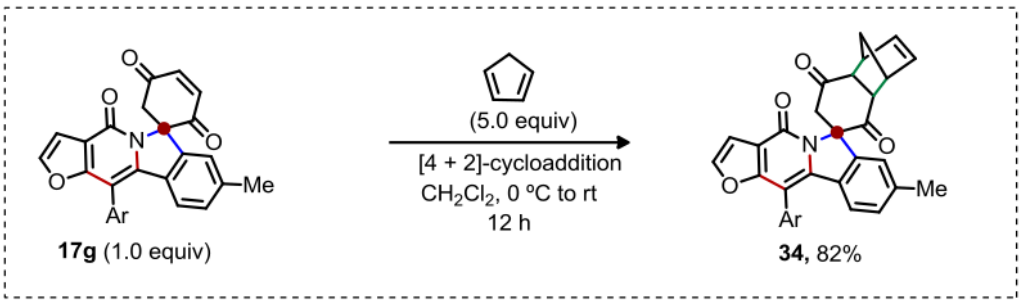

Scheme III.22. Application

III.5. Conclusion

In summary, we have revealed for the first time a Ru-catalyzed MPS-assisted two-fold unsymmetrical cyclization of heteroarenes/vinylic systems with different coupling partners (first with the alkynes and then with the quinones); both these annulations are realized via one-pot synthesis resulting in four bonds (two C–C and two C–N). These highly orchestrated cyclization techniques are largely suitable for the fabrication of un-natural spiro-isoquinolinones.

Recently, Ru-catalyzed C–H annulation strategy has been implemented for the synthesis of various spiro-fused heterocycles shown in **Scheme III.23.**

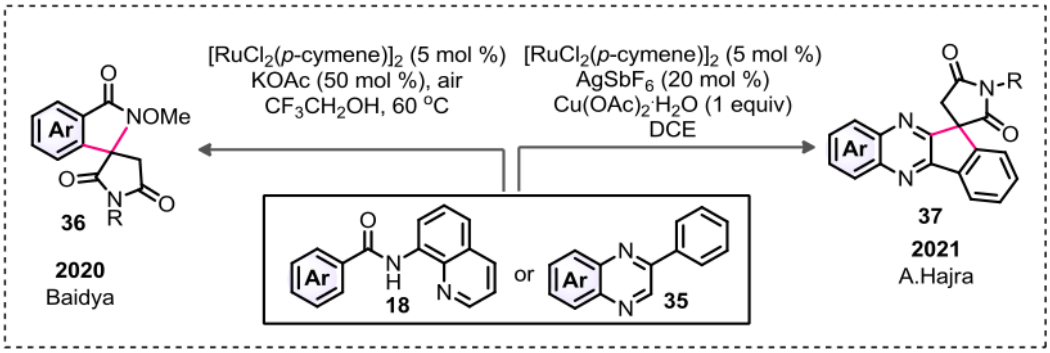

Scheme III.23: Synthesis of spiro-fused heterocycles

Chapter IV

Ruthenium Catalyzed Intramolecular Hydroarylation of Arenes with Olefins in Water Medium

Abstract

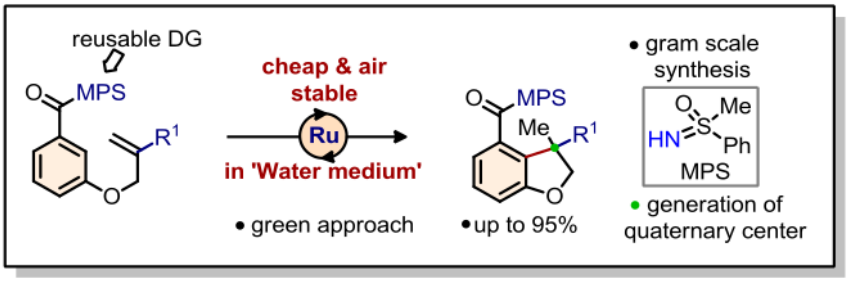

Presented herein the Ru-catalyzed intramolecular hydroarylation of arenes in water. With the aid of methyl phenyl sulfoximine or amide directing group, this atom efficient hydroarylation of arenes ensues dihydrobenzofuran derivatives. Sequential double hydroarylation of arene motif results highly peripheral decorated heterocycles. Deuterium scrambling studies and control experiments offer valuable informations in understanding the reactivity and the mechanistic data.

Reference:

Kallol Mukherjee, E. Ramesh, Koushik Ghosh, and Akhila K. Sahoo
Asian J. Org. Chem. **2018**, *7*, 1380.

IV.1. Introduction

Water is highly-abundant, non-toxic, non-flammable, and most importantly an essential commodity largely available and Green. Thus, development of a chemical reaction in environmentally benign "water" solvent draws significant attention; as the reactions in water allow easy work up and separation.[1] The direct functionalization of ubiquitous C–H bonds fulfils one such criteria of being a "Green" synthetic method, as this strategy does not primarily need the pre-functionalized compound, obviously regulating the formation of undesired waste. Notably, the transition-metal catalyzed activation of inert C–H bond has been emerged as a potential synthetic platform to construct complex molecular template of broad applications covering from the natural products synthesis to the molecules of pharmaceutical importance, and material science.[2–5] Given the challenges of organic substrates are immiscible in water and the reactive catalytic species are incompatible with water, the realization of a novel synthetic manifestation of C–H activation in water is thus a worthwhile endeavour. Moreover, the transition metal salts with small pK_h are readily hydrolysed, while the water-stable-metal salts with large pK_h exhibits less catalytic activity.[1b] Furthermore, the transition-metal catalyzed organic transformations occur both in-water and on-water modes in the interfaces of bulk-water layer.[1c,d]

IV.2. Known synthetic methods for transition metal-catalyzed hydroarylation reactions

IV.2.1. Previous strategies of Rh-catalyzed hydroarylation:

In 2001, Bergman and Ellman reported a proficient route of imine-directed Rh-catalyzed C–H activation and hydroarylation reaction sequence of **1** for the synthesis of indane, dihydroxybenzofuran, tetralane, and dihydroindole derivatives (**2a–d**, **Scheme IV.1**).[6] This cyclization modules constructs bicyclic scaffolds with high level of selectivity. The substrate scope is broad. The O-/N-tethered olefins with different chain length

smoothly underwent reaction. Instead of simple alkene, variety of substituted alkene were also participated in this transformation.

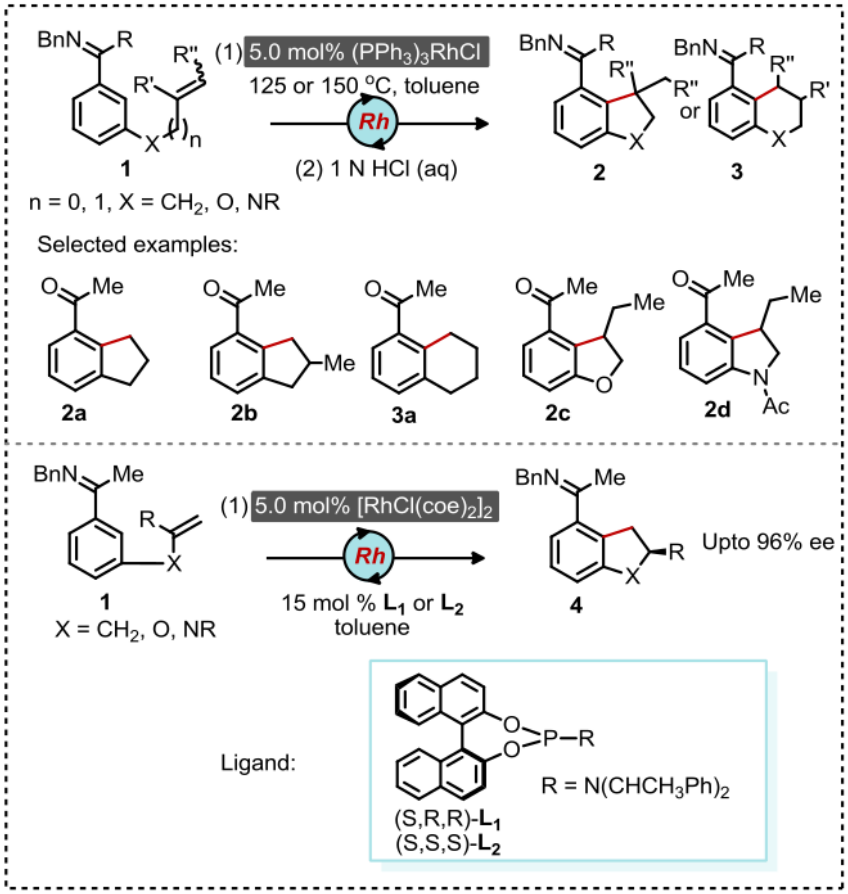

Scheme IV.1: Rh(II)-catalyzed imine-directed C–H hydroarylation

In 2004, the identical strategy has been extended for the asymmetric variant of intramolecular C–H hydroarylation. The chiral ligand enabled Rh-catalytic system play vital in the enantioselective variant of C(sp^2)–H bond activation (**Scheme IV.1**).[6c]

In addition, the asymmetric variant of hydroarylation strategy has been applied for the synthesis of biologically relevant (+)-lithospermic acid moiety **7**. The target compound was achieved in 10 steps and with 5.9% overall yield. Hence, C–H activation strategy is useful for the efficient construction of natural product **7** (**Scheme IV.2**).[6e]

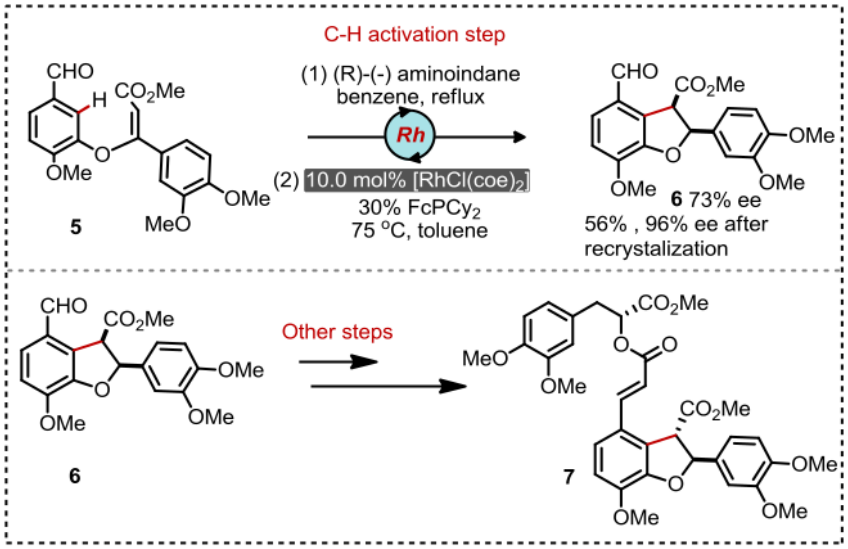

Scheme IV.2: Synthetic strategy of (+)-lithospermic Acid

Based on the use of amides, three hydroarylation variants in the presence of Rh-catalysts have been discovered by the Rovis group in 2013 (**Scheme IV.3**).[7a] A direct hydroarylation product **9** was accessed when di-alkyl protected amide DG employed in the hydroarylation reaction. Whereas the N-methoxy protected amide containing arenes underwent hydroarylation followed by Heck-type reaction to give the olefin bearing hydroarylation product **10**. In case of N-pivaloyl protected amide derivatives, a multiple C–H functionalizations that involves hydroarylation and C–N bond coupling delivered intramolecular amidoarylation product **11** (**Scheme IV.3**).

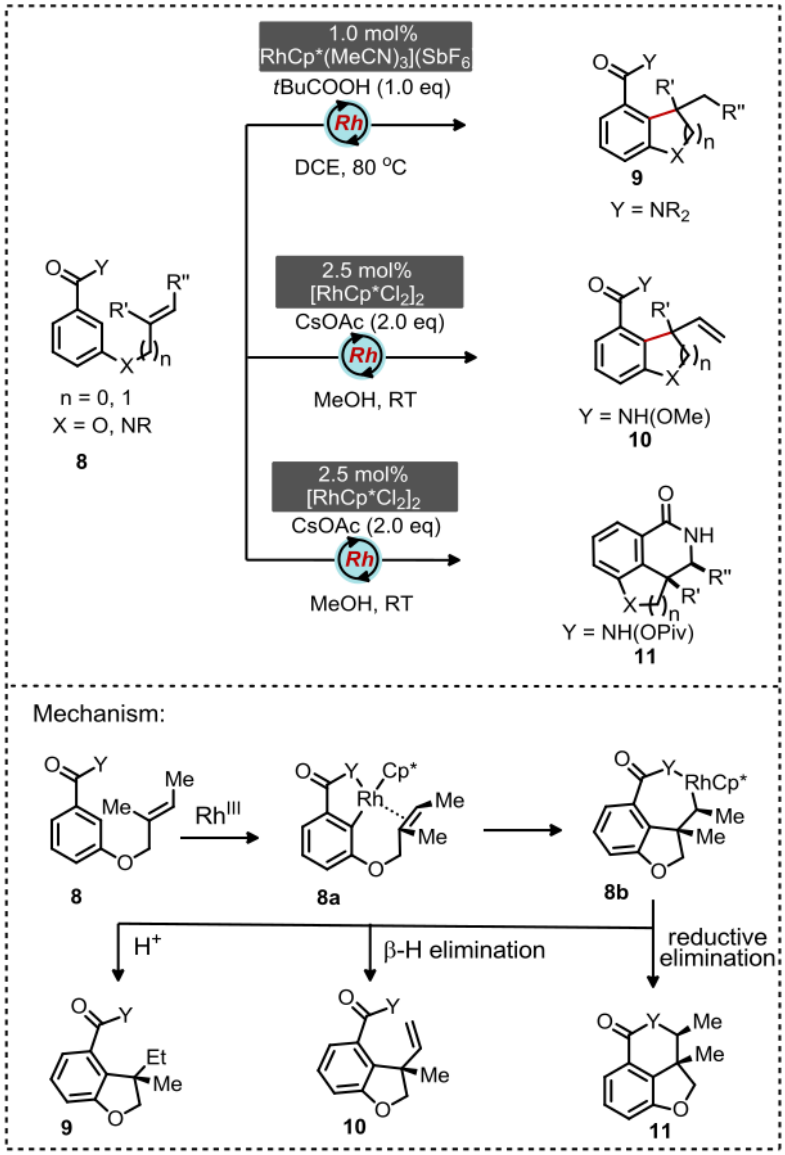

Scheme IV.3: Rh(III)-catalyzed hydroarylation, Heck-type reaction and amidoaryl -ation

IV.2.2. Known synthetic methods for the Co-catalyzed hydroarylation:

In 2013, Yoshikai group for the first time used a combination of cobalt-NHC catlalytic system for the hydroarylation of indole systems having N-tethered olefin to prepare respective fused-indole skeletons tetrahydropyridoindole **13** and dihydropyrroloindole

14. The construction of bicyclo[3.3.1] skeleton as well as formation of quarternary centre are the main features of this transformation (**Scheme IV.4**).[8]

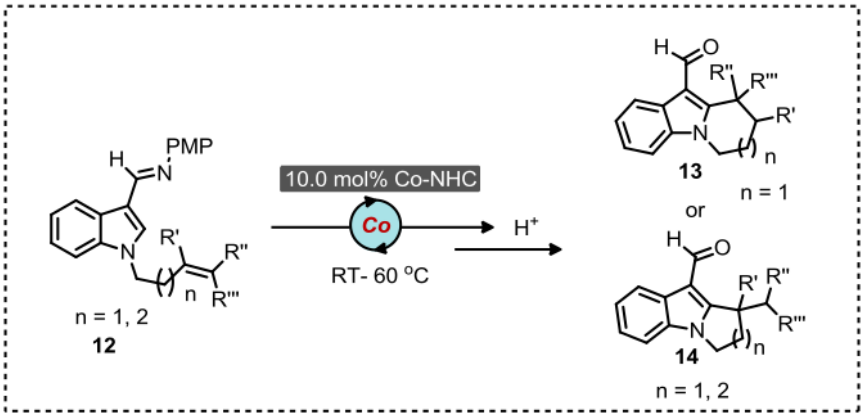

Scheme IV.4: Co-NHC catalyzed hydroarylation of indole derivatives

IV.2.3. Known synthetic methods for the Ru-catalyzed of hydroarylation:

In 2012, our group revealed an air stable Ru-catalyzed intramolecular hydroarylation strategy for the first time. Methylphenylsulfoximine (MPS) coupled carboxylate with O-tether and N-tether alkene undergoes intramolecular hydroarylation to deliver dihydrobenzofuran, indolines and double hydroarylated product **16/17**; interestingly, the reaction was successfully carried out at room temperature in 1,2-DCE (**Scheme IV.5**).[9a] Moreover, one-pot multiple C–H functionalizations involving subsequent C–C/C–C and C–C/C–N were also showcased for the first time (**18/19**).

A plausible mechanistic cycle is sketched in **Scheme IV.5**. First step is the formation of active catalyst **A** from the reaction of [{$RuCl_2$(p-cymene)}$_2$], $AgSbF_6$, and $Cu(OAc)_2$. This active catalyst coordinates with the MPS and activates the proximal *ortho*-C–H bond of **15** to form the five membered cyclometalated complex **15a**. Subsequent intramolecular alkene insertion of **15a** followed by protodemetalation of **15c** delivers the product **16**.

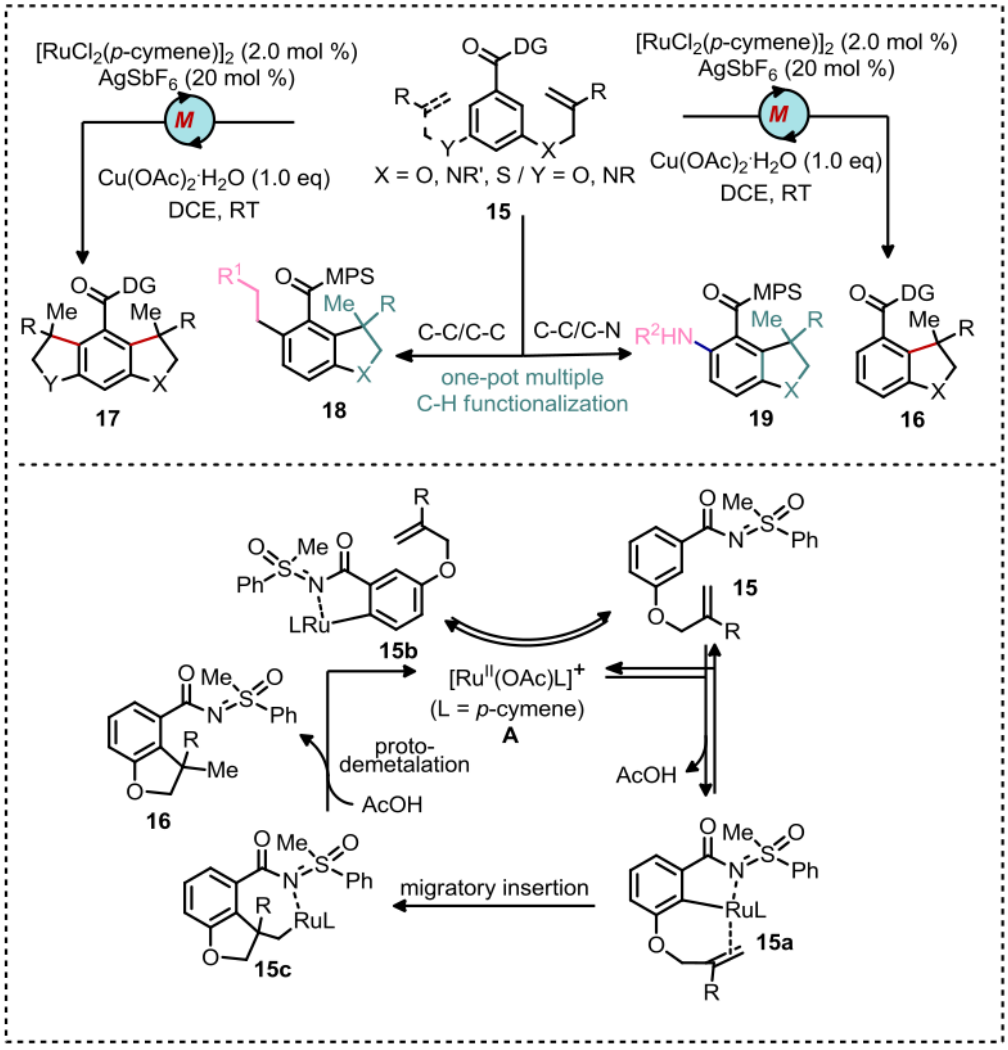

Scheme IV.5: MPS directed Ru-catalyzed hydroarylation

The same hydroarylation strategy was further extended towards amide directed hydroarylation for the synthesis of dihydrobenzofuran, chroman, and indoline derivatives **21–23**. The main features of this protocol are the atom-efficiency, broad substrate scope and excellent yield (**Scheme IV.6**).[9b]

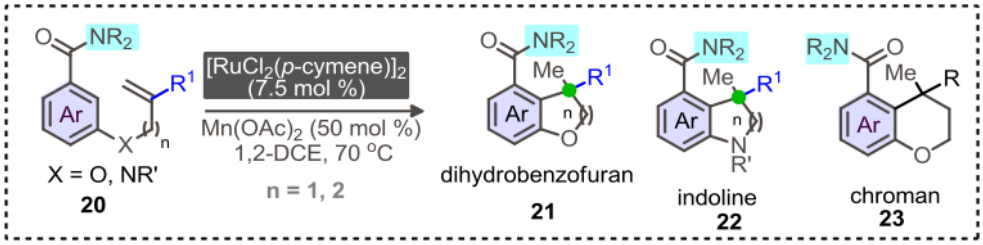

Scheme IV.6: Amide directed Ru-catalyzed hydroarylation

IV.3. Motivation and Design for Double Annulation

The transition-metal-catalyzed intramolecular hydroarylation of O-tethered olefin-bearing arene directly constructs dihydrobenzofuran skeleton, which is widely found in the molecules of various natural products.[5] A notable imine-directed Rh-catalyzed hydroarylation of arenes was at first demonstrated by Ellman and Bergman's group (**Scheme IV.7**).[6] Subsequently, Rh-, Co-, Ru-, and Ir- catalysts have independently been used for the identical transformations (**Scheme IV.7**).[7–10] Most of these transformations were successfully executed in organic solvents (toluene / 1,2-dichloroethane / 1,4-dioxane) (**Scheme IV.7**). By contrast, no such intramolecular hydroarylation of arenes in water is known till 2016. Whereas the cost-effective and air-stable Ru-catalysts have been used for the directed functionalization of arene C–H bonds in/on water.[11–12]

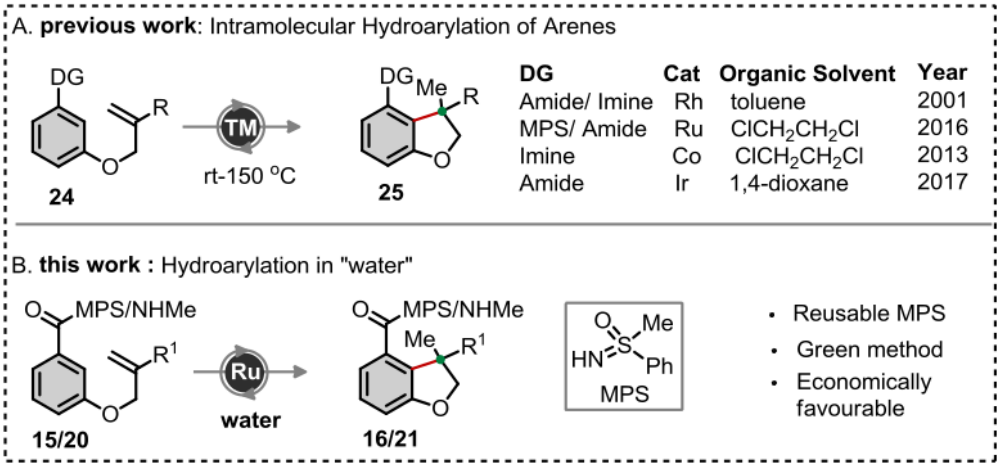

Scheme IV.7: Hydroarylation in water medium

Inspired from these studies, we herein developed the methyl phenyl sulfoximine (MPS)/ NHMe-directed Ru-catalyzed intramolecular hydroarylation of O-tethered olefin bearing benzoic acid derivatives **15/20** in water for the synthesis of wide arrays of dihydrobenzofurans **16/21**. The sequential unsymmetrical C–H functionalization of dihydrobenzofuran was also investigated.

IV.4. Results and Discussion

IV.4.1. Synthesis of precursors

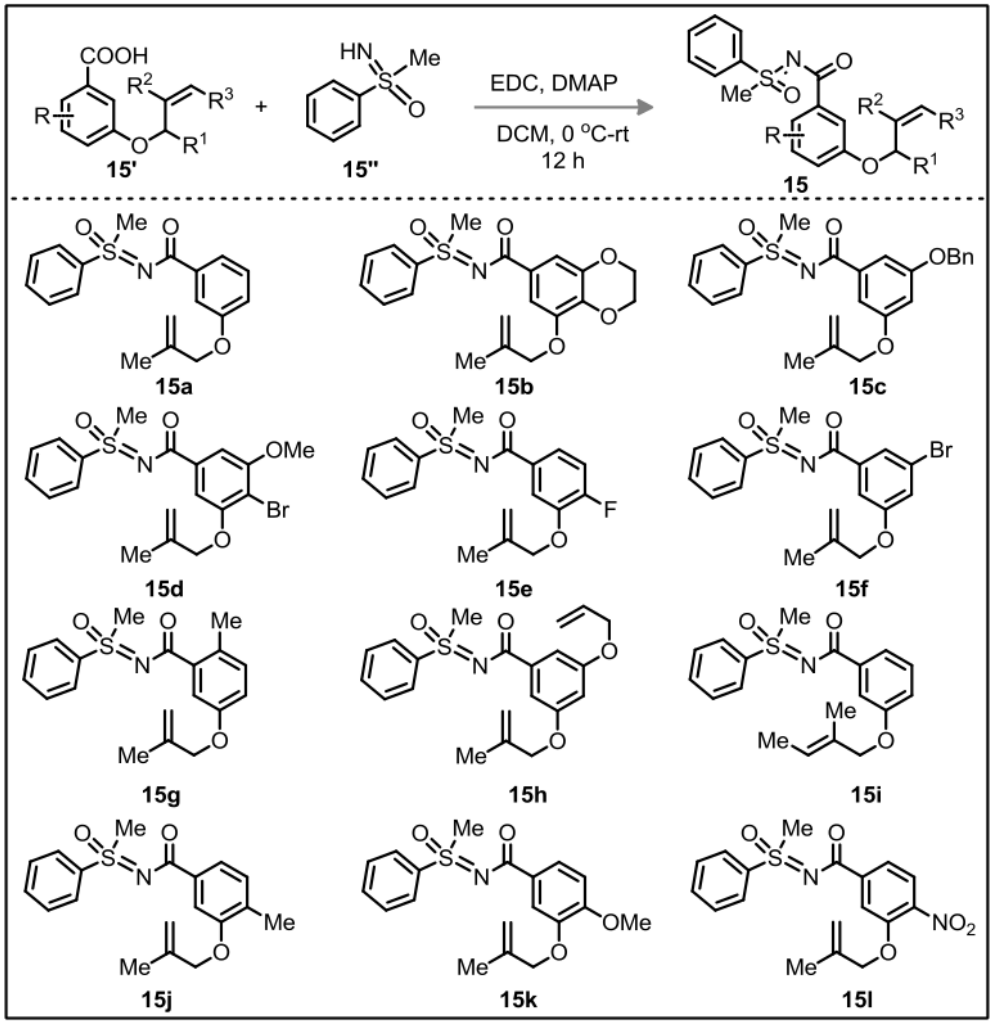

Scheme IV.8: Preparation of N-heteroaroyl sulfoximine derivatives

A library of starting materials MPS-enabled O-tethered olefin bearing benzoic acid derivatives has been synthesized using the known procedure, which are shown in **Scheme IV.8**.[9] The EDC.HCl mediated coupling between O-tethered olefin bearing benzoic acid derivatives **15′** and methyl phenyl sulfoximine **15″** led to the precursors **15** in good overall yields.

IV.4.2. Optimization studies

Encouraged from our recent demonstration of the MPS assisted Ru-catalyzed intramolecular hydroarylation of arenes,[9a] we envisaged probing the identical transformation in water. To start with, the hydroarylation of [3-(2-methylallyloxy)benzoyl] methylphenyl sulfoximine (**15a**) was investigated under Ru-catalyst in water (**Table IV.1**). Gratifyingly, the desired hydroarylation compound **16a** was formed in 28% yield, when the reaction was conducted under the catalytic system

Table IV.1: Optimization of Reaction Parameters[a]

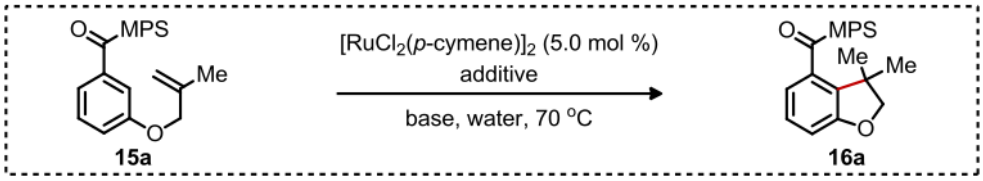

entry	additive (20 mol %)	Base (1.0 equiv)	time (h)	yield of **16a** (%)[b]
1	$AgSbF_6$	$Cu(OAc)_2 \cdot H_2O$	12	28
2	–	$Cu(OAc)_2 \cdot H_2O$	24	nr
3[c]	$AgBF_4$	$Cu(OAc)_2 \cdot H_2O$	12	39
4	$NaPF_6$	$Cu(OAc)_2 \cdot H_2O$	12	47
5	KPF_6	$Cu(OAc)_2 \cdot H_2O$	12	67
6	KPF_6	$Mn(OAc)_2$	12	49
7	KPF_6	NaOH	12	nr
8	KPF_6	KOH	12	nr

9	KPF_6	AcOH	12	22
10[d]	KPF_6	$Cu(OAc)_2 \cdot H_2O$	12	97
11[e]	KPF_6	$Cu(OAc)_2 \cdot H_2O$	12	93
12[f]	KPF_6	$Cu(OAc)_2 \cdot H_2O$	12	38

[a] Reactions were carried out using **15a** (0.2 mmol), $[RuCl_2(p\text{-cymene})]_2$ (5.0 mol %), base (0.2 mmol), additive (20 mol %) in water (1.0 mL) at 70 °C. [b] Isolated yields. [c] ^1H NMR yield. [d] 100 °C. [e] $[RuCl_2(p\text{-cymene})]_2$ (3.0 mol %) and KPF_6 (12 mol %) was used at 100 °C. [f] The reaction was performed in neat at 100 °C.

comprising {$[RuCl_2(p\text{-cymene})]_2$ (5.0 mol %), $AgSbF_6$ (20 mol%), and $Cu(OAc)_2 \cdot H_2O$ (1.0 equiv)} in water at 70 °C (entry 1). Perhaps the formation of active cationic Ru complex, obtained in-situ from Ru- and Ag salt, is hampered in water, which eventually affects activation of arene *o*-C–H bond. By contrast, the reaction in the absence of $AgSbF_6$ did not yield **16a** (entry 2); thus, an additive (responsible forming the respective chloride salts from Ru-catalyst) is indispensable. The use of various chloride trapping agents is therefore envisioned. Among the additives $AgBF_4$, $NaPF_6$, and KPF_6 screened (entries 3–5), KPF_6 worked better affording 67% of **16a** (entry 5). Presumably the water soluble KCl salt facilitates the formation of cationic Ru-species, which helps in the activation of the arene *o*-C–H bond. The use of $Mn(OAc)_2$ instead of $Cu(OAc)_2$ did not work better (entry 6). The Ru(OH)R complex, generated in-situ from the base promoted water mediated Ru-catalyzed reaction, is probably responsible for the activation of arene C–H bond through the internal electrophilic substitution (IES) type mechanism.[13] Not even a trace of the product **16a** was detected when the reaction was conducted in presence of NaOH or KOH even at harsh conditions (140 °C) (entries 7 and 8), thus refuting the participation of IES-type mechanism.[13] While the reaction in presence of acetic acid yielded 22% **16a** (entry 9). Pleasingly, **16a** was isolated in 97% yield when the identical reaction in entry 5 heated at 100 °C (entry 10). The use of less amount of Ru-catalyst (3.0 mol%) did not affect the reaction outcome (entry 11). Thus, reaction of **15a** under the

catalytic conditions {[$RuCl_2$(*p*-cymene)]$_2$ (3.0 mol%), KPF_6 (12 mol%), $Cu(OAc)_2 \cdot H_2O$ (1.0 equiv) in H_2O at 100 °C for 12 h} furnished **16a** in 93% yield (entry 11). Interestingly, **16a** (38%) was obtained when the reaction performed in neat (entry 12); presumably the interaction of substrate with catalyst in molten state is responsible for product formation. We therefore believe that the reaction in water medium can enhance dispersion of the organic oily-phase of the reactants.[1c,d]

IV.4.3. Reaction scope-I

We next surveyed the generality of this MPS-assisted hydroarylation of arenes in water under the optimized condition shown in entry 11, **Table IV.1**. The compound **16a** was isolated from **15a** (0.3 mmol) in 95% yield; even the identical transformation worked well in 1.5 mmol scale affording 94% **16a**. The MPS-enabled electron-rich arenes [dihydrobenzo[*b*][1,4]dioxine / *m*-OBn / *p*-Br-*m*-OMe] reacted smoothly to provide the corresponding **16b** (82%), **16c** (81%), and **16d** (79%). The transformable halo groups (F/Br) on the arene motifs were survived, accessing **16e** and **16f** in 89% and 54% yield, respectively. The sterically encumbered *o*-Me arene derivative underwent hydroarylation to yield the respective 5-Me-bearing dihdrobenzofuran **16g** in 67% yield. Whereas *m,m'*-di-O-allyl MPS-bearing carboxylate under the catalytic conditions exclusively provided the mono-hydroarylation product **16h** (82%); the dihydroarylation did not occur even the reaction conducted for longer time. The intramolecular hydroarylation of tri-substituted olefin bearing substrate delivered the corresponding 3,3-methyl-ethyl bearing dihdrobenzofuran **16i** in 33% yield. Disappointingly, the *p*-Me / *p*-OMe / *p*-NO_2 substituted arene derivatives failed to provide the respective hydroarylation products **16j**–**16l** (**Scheme IV.9**); presumably, the respective substrates **15j**–**15l** did not miscible in water even at higher temperature, which eventually obstructs the hydroarylation reactions in water medium.

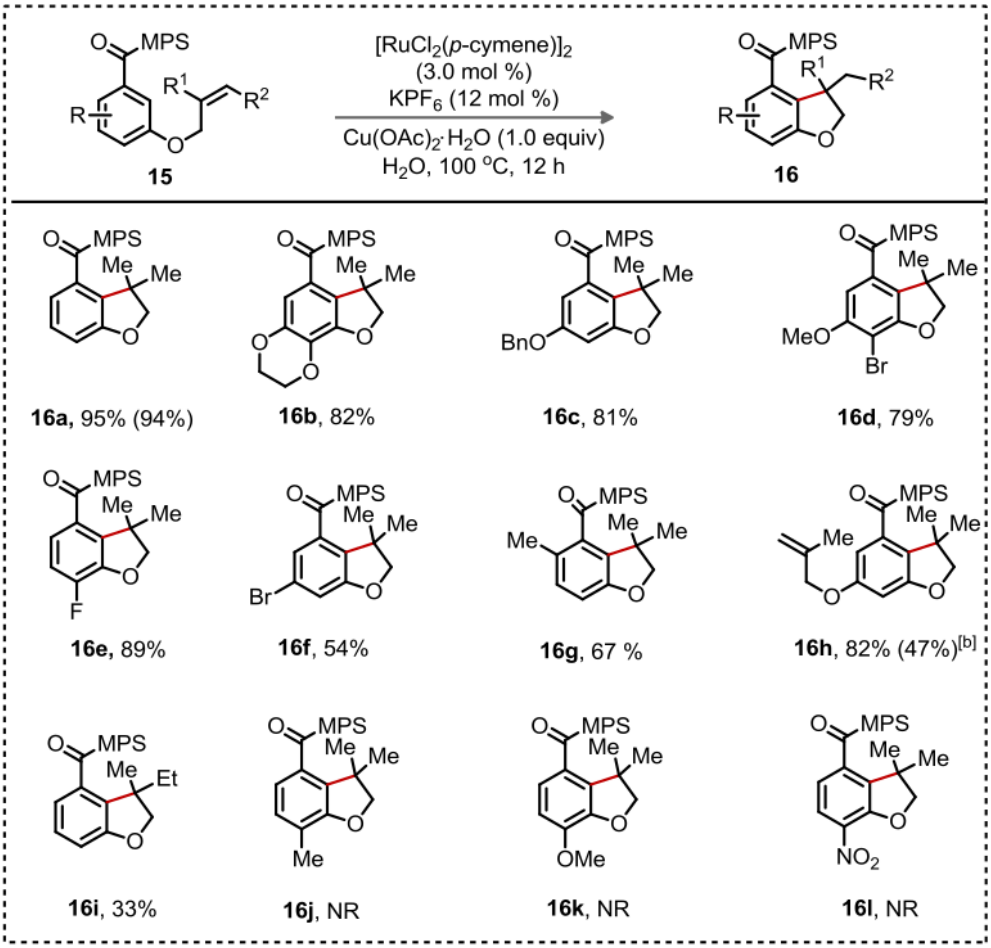

Scheme IV.9: Substrate scope-I

IV.4.4. Reaction scope-II

Interestingly, the amide-NHMe directed hydroarylation of *p*-OMe / *p*-NO_2 substituted arene derivatives **20a** and **20b** under the Ru-catalyzed catalytic conditions of entry 11, **Table IV.1** along with $AgSbF_6$ in water independently provided **21a** and **21b**, respectively albeit in moderate yield [Eq 1 and Eq 2, **Scheme IV.10**]. We presumably believe that the amide bearing substrate **20a** and **20b** forms the corresponding salts in the presence of acetate base and provokes the reaction to occur at an elevated temperature in water medium.

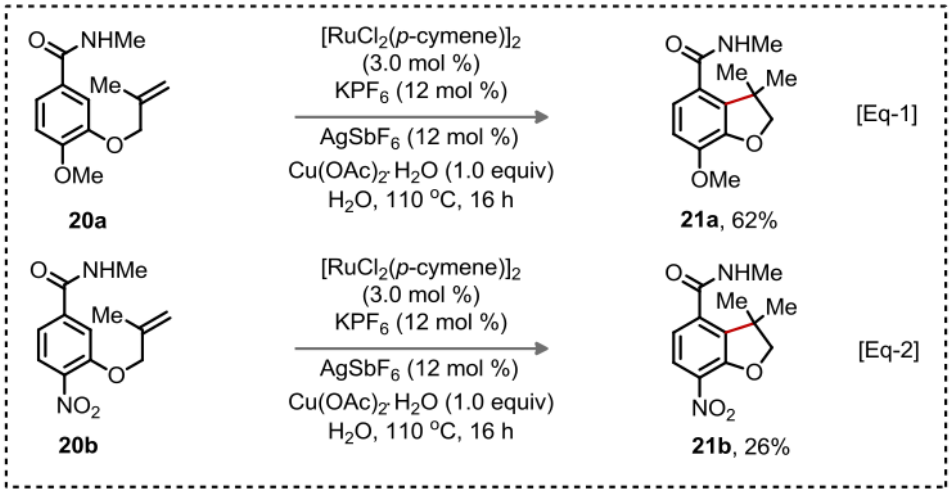

Scheme IV.10: Substrate scope-II

Encouraged with the directing group aided hydroarylation of arenes in water (**Scheme IV.9** and **Scheme IV.10**, Eq 1–2), the hydroarylation of aryl *o*-C–H bond of dihydrobenzofuran derivative **16h** with the spatially configured olefin was examined. Pleasingly, the dicyclization product **17** was isolated in 65% yield, when **16h** was exposed to the optimized catalytic conditions (**Scheme.IV.11).**

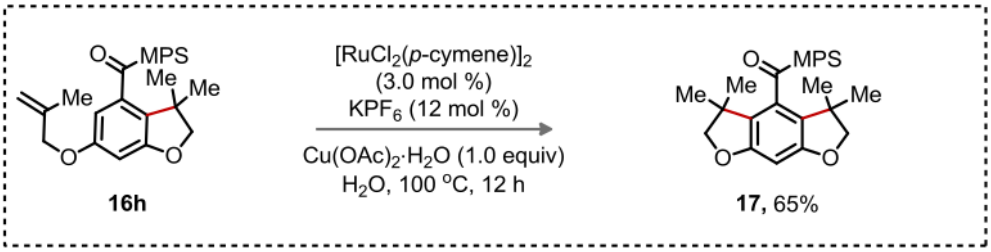

Scheme.IV.11: Substrate scope-III

IV.4.5. Gram-scale:

Next, the scalability of this reaction was tested through a gram scale hydroarylation in water. Gratifyingly, the hydroarylation of **15a** (1.0 g) was successfully carried out even in presence of 1.0 mol % Ru-catalyst in water to furnish **16a** (0.92 g; 92%)

(**Scheme.IV.12**). This demonstration truly validates the importance of MPS-DG and efficacy of Ru-catalysis in this hydroarylation in water. By contrast, the notable other intramolecular hydroarylation strategies invariably requires more amount of catalyst.[6–10]

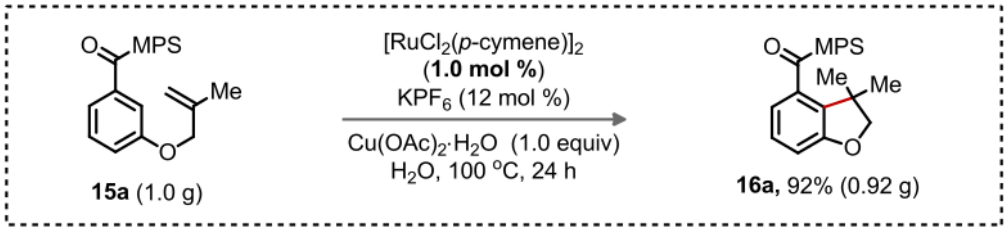

Scheme.IV.12: Gram-scale synthesis

IV.4.6. Control Experiments

To understand the path of the reaction in water, various control experiments were envisaged (**Scheme.IV.13**). The reaction in presence of TEMPO provided 80% isolated yield of **16a**; thus, the cyclization does not involve radical intermediate [Eq 1]. The reaction in D_2O provided 12 % deuterium incorporation in the *o*-C–H bond of **15g** [Eq 2]; thus, the *o*-C–H bond activation via concerted metalation-deprotonation (CMD) path is reversible.[9a] While the identical transformation of **15a** in D_2O delivered 55% and 15% deuterium incorporation in the *o*-C–H and the newly generated 3-methyl moiety of dihydrobenzofuran in **16a-H/D**, respectively; thus, the reaction involves protodemetalation [Eq 3].[9a] The 85% protonation of the 3-methyl moiety in dihydrobenzofuran suggests that the proton source of AcOH (obtained in-situ via the acetate assisted activation of C–H bond by CMD) is superior over D_2O [Eq 3].[9a] A competitive experiment among **15a** (1,1′-di-substitued alkene) and **15i** (1,1′,2-trisubstituted alkene) under the optimized conditions in 1 h led to **16a** (88%) and **16i** (12%) [Eq 4]; thus, steric bulkiness of olefin affects the reactivity as well the productivity.

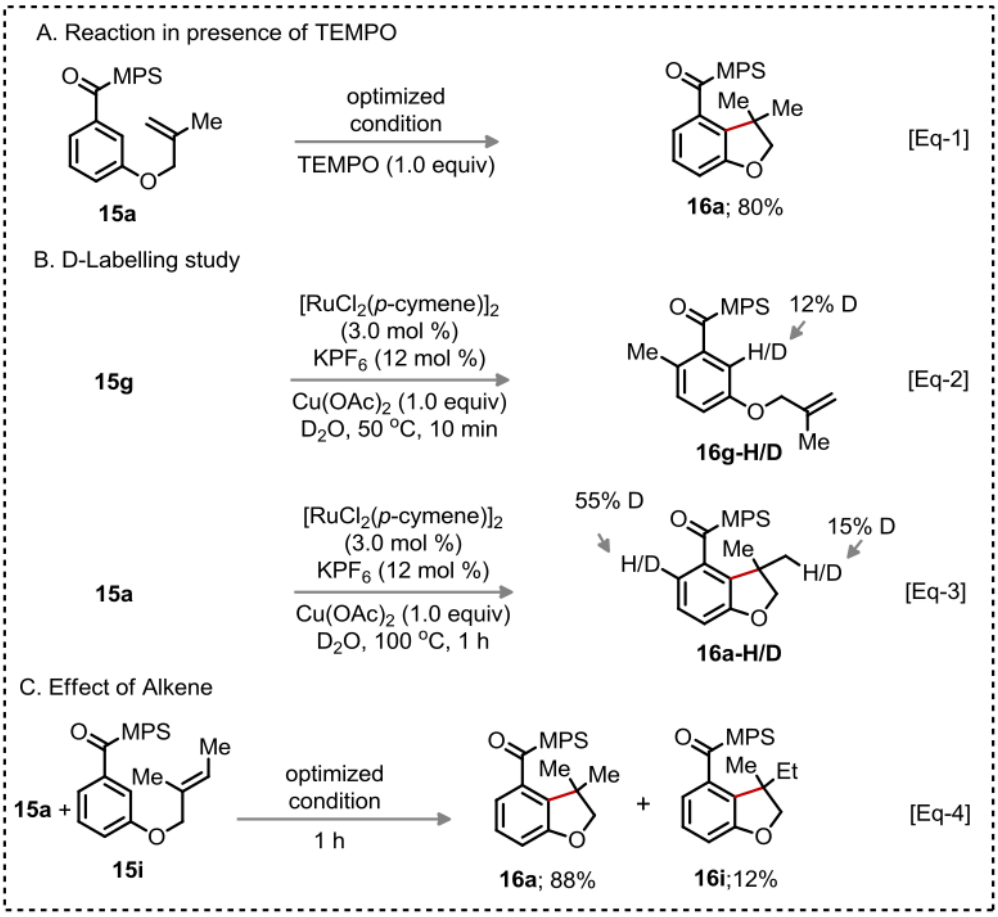

Scheme.IV.13: Control Experiments

IV.4.7. Mechanistic Cycle

A plausible reaction pathway for this hydroarylation reaction is sketched in **Scheme.IV.14**. The reaction begins with the formation of active Ru-catalyst from $[RuCl_2(p\text{-cymene})]_2$, KPF_6, and $Cu(OAc)_2 \cdot H_2O$. Next, the coordination of active Ru-species to the MPS-DG promotes *o*-C–H bond activation to produce cyclometalated complex **15a/20a**. The migratory insertion of **15a/20a** then leads to **15c/20c**. Finally, proto-demetalation of **15c/20c** affords the desired product **16/21** with the regeneration of active catalyst (**Scheme.IV.14**).

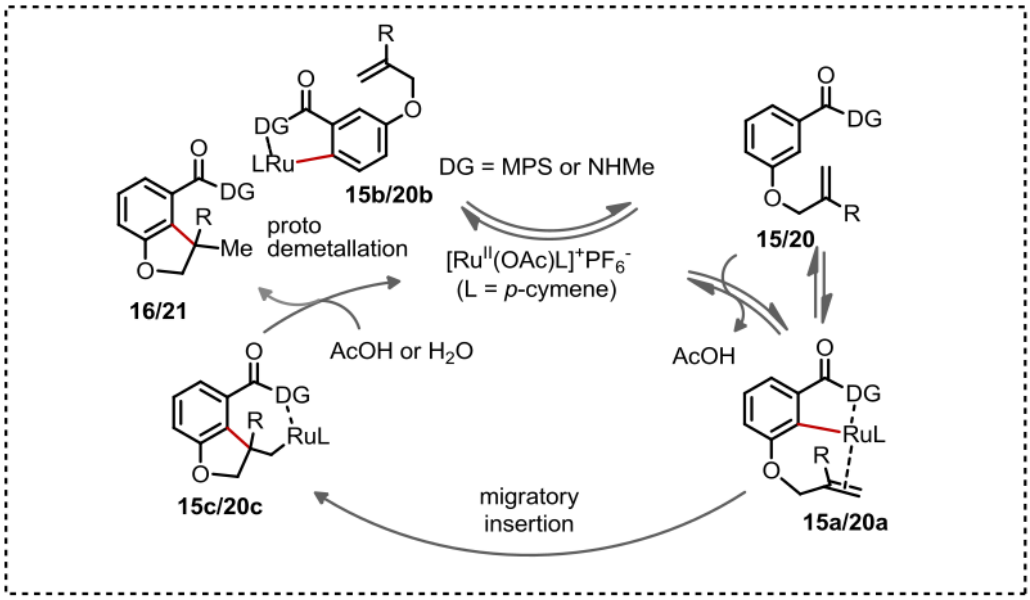

Scheme.IV.14: Proposed Mechanistic Profile

IV.4.8. Application

Multiple functionalization of readily accessible arene motif builds highly peripheral decorated novel molecular scaffold. Thus, further functionalization of *o*'-C–H bond of the MPS-enabled dihydrobenzofuran derivative was envisaged, despite the electronic and steric biasness of the molecular scaffold. To check the feasibility of next functionalization, the Ru-catalyzed MPS-assisted *o*'-C–H acetoxylation, bromination, and/or annulation of dihydrobenzofuran derivative was then surveyed. Pleasingly, annulation between **16a** and 1,2-diphenyl acetylene under the Ru-catalysis provided an unusual dihydrofuran-fused-isoquinolone framework **26** in 62% yield (**Scheme.IV.15**).[14a] The *o*'-C–H bromination and acetoxylation were independently performed on **16a** under the respective catalytic conditions [NBS (1.5 equiv), $Pd(OAc)_2$ (15 mol%), AcOH (2.5 equiv) in DCE at 100 °C] and [$Pd(OAc)_2$ (10 mol%), $K_2S_2O_8$ (2.0 equiv) in $CHCl_3$:AcOH (3:5) at 100 °C] to afford **27** (72%) and **28** (67%), respectively (**Scheme.IV.15**).[14b,c] Thus, the sequential intramolecular hydroarylation followed by

C–C, C–O, and C–Br bond formations of *o*-C–H bonds of arene motifs build novel molecules with various functionalities.

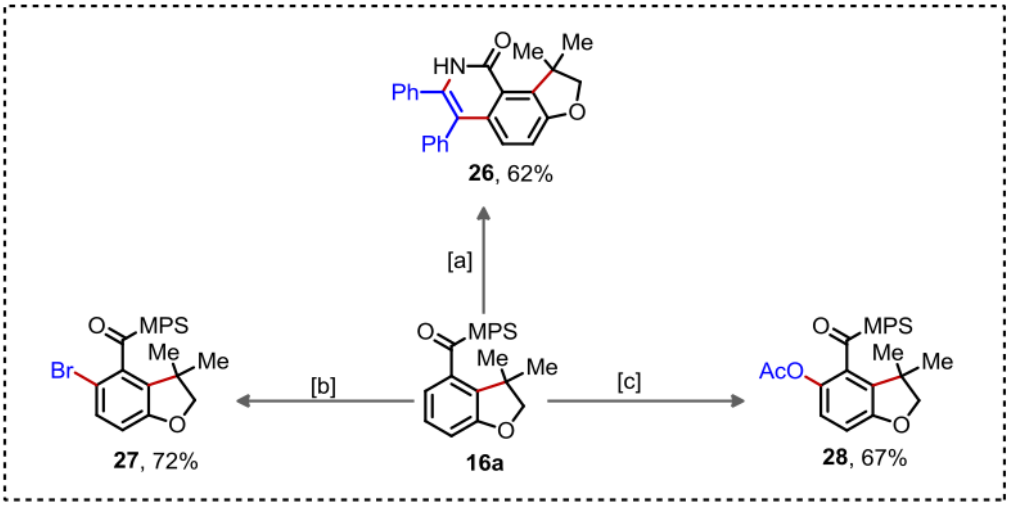

[a] **16a** (100 mg, 0.3 mmol), 1,2-diphenyl acetylene (64 mg, 0.36 mmol), $[RuCl_2(p\text{-cymene})]_2$ (5.0 mol %), $AgSbF_6$ (20 mol %), and AcOH (0.3 mmol) in 1,4-dioxane (2.0 mL) at 120 °C for 24 h. [b] **16a** (0.3 mmol), $Pd(OAc)_2$ (15 mol %), NBS (0.45 mmol), AcOH (2.5 equiv), $ClCH_2CH_2Cl$ (3.0 mL) at 100 °C for 12 h. [c] **16a** (0.3 mmol), $Pd(OAc)_2$ (10 mol %), $K_2S_2O_8$ (0.6 mmol), and AcOH/$CHCl_3$ (3:5, 2.0 mL) at 100 °C for 12 h.

Scheme.IV.15: Application

IV.5. Conclusion

In summary, the MPS/amide group directed Ru-catalyzed hydroarylation of arenes in water is developed. To the best of our knowledge, hydroarylation of arenes in water is the first report. This method directly constructs dihydrobenzofuran derivatives from commercially available 3-hydroxy benzoic acids. Despite the challenges, the current synthetic manifestation exhibits moderate scope; thus, to unravel novel and effective synthetic method in this regard remains an attractive endeavor. Sequential unsymmetrical functionalization of unactivated multiple C–H bonds of arene

derivatives through hydroarylation–annulation/ hydroarylation-acetoxylation, and hydroarylation-halogenation builds novel molecular skeletons. The cleavage and recovery of the MPS moiety from the products and the gram-scale hydroarylation in water make the current synthetic method viable.

Metal-Catalyzed Stereoselective C-H Functionalization Mediated Kinetic Resolution of Sulfoximines and Unsymmetrical Multiple C-H Annulations

ORIGINALITY REPORT

38%	7%	38%	2%
SIMILARITY INDEX	INTERNET SOURCES	PUBLICATIONS	STUDENT PAPERS

PRIMARY SOURCES

1	Kallol Mukherjee, Majji Shankar, Koushik Ghosh, Akhila K. Sahoo. " An Orchestrated Unsymmetrical Annulation Episode of C(sp)–H Bonds with Alkynes and Quinones: Access to Spiro-isoquinolones ", Organic Letters, 2018 Publication	13%
2	Akhila Kumar Sahoo, Kallol Mukherjee, E Ramesh, Koushik Ghosh. "Ruthenium Catalyzed Intramolecular Hydroarylation of Arenes with Olefins in Water Medium", Asian Journal of Organic Chemistry, 2018 Publication	9%
3	Kallol Mukherjee, E. Ramesh, Koushik Ghosh, Akhila K. Sahoo. "Ruthenium-Catalyzed Intramolecular Hydroarylation of Arenes with Olefins in Water", Asian Journal of Organic Chemistry, 2018 Publication	5%
4	pubs.acs.org Internet Source	2%

Our publication

Prof. AKHILA K. SAHOO
School of Chemistry
University of Hyderabad
Central University P.O.
Hyderabad, INDIA.

Our publication

Prof. AKHILA K. SAHOO
School of Chemistry
University of Hyderabad
Central University P.O.
Hyderabad, INDIA.

Our publication

Prof. AKHILA K. SAHOO
School of Chemistry
University of Hyderabad
Central University P.O.
Hyderabad, INDIA.

footnotes of reaction condition

Prof. AKHILA K. SAHOO
School of Chemistry
University of Hyderabad
Central University P.O.
Hyderabad, INDIA.

5	Parthasarathy Gandeepan, Thomas Müller, Daniel Zell, Gianpiero Cera, Svenja Warratz, Lutz Ackermann. "3d Transition Metals for C–H Activation", Chemical Reviews, 2018 Publication	1 %
6	Submitted to University of Hyderabad, Hyderabad Student Paper	1 %
7	Fares Roudesly, Julie Oble, Giovanni Poli. "Metal-catalyzed CH activation/functionalization: The fundamentals", Journal of Molecular Catalysis A: Chemical, 2017 Publication	<1 %
8	Chu, L., K.-J. Xiao, and J.-Q. Yu. "Room-temperature enantioselective C-H iodination via kinetic resolution", Science, 2014. Publication	<1 %
9	Qian Shao, Qing-Feng Wu, Jian He, Jin-Quan Yu. " Enantioselective γ-C(sp)–H Activation of Alkyl Amines via Pd(II)/Pd(0) Catalysis ", Journal of the American Chemical Society, 2018 Publication	<1 %
10	Wenjun Lu, Lihong Zhou. "Oxidation of C—H Bonds", Wiley, 2017 Publication	<1 %

11	Christopher G. Newton, Shou-Guo Wang, Caio C. Oliveira, Nicolai Cramer. "Catalytic Enantioselective Transformations Involving C–H Bond Cleavage by Transition-Metal Complexes", Chemical Reviews, 2017 Publication	<1 %
12	David Balcells, Eric Clot, Odile Eisenstein. "C—H Bond Activation in Transition Metal Species from a Computational Perspective", Chemical Reviews, 2010 Publication	<1 %
13	"C‐H Activation for Asymmetric Synthesis", Wiley, 2019 Publication	<1 %
14	Joshua R. Hummel, Jeffrey A. Boerth, Jonathan A. Ellman. "Transition-Metal-Catalyzed C–H Bond Addition to Carbonyls, Imines, and Related Polarized π Bonds", Chemical Reviews, 2016 Publication	<1 %
15	onlinelibrary.wiley.com Internet Source	<1 %
16	Tirumaleswararao Guntreddi, Majji Shankar, Nagarjuna Kommu, Akhila K. Sahoo. " Construction of Pyranoisoquinolines via Ru(II)-Catalyzed Unsymmetrical Double Annulation of -Methoxybenzamides with Unactivated	<1 %

Alkynes ", The Journal of Organic Chemistry, 2019
Publication

17	www.ncbi.nlm.nih.gov Internet Source	<1%
18	Koushik Ghosh, Raja K. Rit, E. Ramesh, Akhila K. Sahoo. "Ruthenium-Catalyzed Hydroarylation and One-Pot Twofold Unsymmetrical C−H Functionalization of Arenes", Angewandte Chemie, 2016 Publication	<1%
19	Gui-Juan Cheng. "Mechanistic Studies on Transition Metal-Catalyzed C–H Activation Reactions Using Combined Mass Spectrometry and Theoretical Methods", Springer Science and Business Media LLC, 2017 Publication	<1%
20	Kelvin S. L. Chan, Hai-Yan Fu, Jin-Quan Yu. "Palladium(II)-Catalyzed Highly Enantioselective C–H Arylation of Cyclopropylmethylamines", Journal of the American Chemical Society, 2015 Publication	<1%
21	Daniel H. Ess, William A. Goddard, Roy A. Periana. "Electrophilic, Ambiphilic, and Nucleophilic C−H Bond Activation: Understanding the Electronic Continuum of	<1%

C−H Bond Activation Through Transition-State and Reaction Pathway Interaction Energy Decompositions", Organometallics, 2010
Publication

---

22 Charles S. Yeung, Vy M. Dong. "Catalytic Dehydrogenative Cross-Coupling: Forming Carbon−Carbon Bonds by Oxidizing Two Carbon−Hydrogen Bonds", Chemical Reviews, 2011 <1 %
Publication

---

23 Chen, Zhengkai, Binjie Wang, Jitan Zhang, Wenlong Yu, Zhanxiang Liu, and Yuhong Zhang. "Transition metal-catalyzed C–H bond functionalizations by the use of diverse directing groups", Organic Chemistry Frontiers, 2015. <1 %
Publication

---

24 Denise A. Colby, Robert G. Bergman, Jonathan A. Ellman. "Rhodium-Catalyzed C−C Bond Formation via Heteroatom-Directed C−H Bond Activation", Chemical Reviews, 2010 <1 %
Publication

---

25 Ling Zhu, Yuan-Ye Jiang, Xia Fan, Peng Liu, Bao-Ping Ling, Siwei Bi. "Mechanism of Palladium-Catalyzed Alkylation of Aryl Halides with Alkyl Halides through C–H Activation: A Computational Study", Organometallics, 2018 <1 %
Publication

26	David L. Davies, Stuart A. Macgregor, Claire L. McMullin. "Computational Studies of Carboxylate-Assisted C–H Activation and Functionalization at Group 8–10 Transition Metal Centers", Chemical Reviews, 2017 Publication	<1 %
27	www.science.gov Internet Source	<1 %
28	Kai-Jiong Xiao, David W. Lin, Motofumi Miura, Ru-Yi Zhu, Wei Gong, Masayuki Wasa, Jin-Quan Yu. " Palladium(II)-Catalyzed Enantioselective C(sp)–H Activation Using a Chiral Hydroxamic Acid Ligand ", Journal of the American Chemical Society, 2014 Publication	<1 %
29	doi.org Internet Source	<1 %
30	"Organic Reaction Mechanisms · 2016", Wiley, 2020 Publication	<1 %
31	Kai-Jiong Xiao, Ling Chu, Jin-Quan Yu. "Enantioselective C−H Olefination of α-Hydroxy and α-Amino Phenylacetic Acids by Kinetic Resolution", Angewandte Chemie International Edition, 2016 Publication	<1 %

32	Percia Beatrice Arockiam, Christian Bruneau, Pierre H. Dixneuf. "Ruthenium(II)-Catalyzed C–H Bond Activation and Functionalization", Chemical Reviews, 2012 Publication	<1 %
33	Qian Shao, Qing-Feng Wu, Jian He, Jin-Quan Yu. "Enantioselective γ-C(sp3)–H Activation of Alkyl Amines via Pd(II)/Pd(0) Catalysis", Journal of the American Chemical Society, 2018 Publication	<1 %
34	Bin Liu, Ye-Qiang Han, Fang Hu, Bing-Feng Shi. "Palladium-Catalyzed Directed Arylation of Unactivated C(sp 3) H Bonds", Elsevier BV, 2017 Publication	<1 %
35	Brandon E. Haines, Jin-Quan Yu, Djamaladdin G. Musaev. "Enantioselectivity Model for Pd-Catalyzed C–H Functionalization Mediated by the Mono-N-protected Amino Acid (MPAA) Family of Ligands", ACS Catalysis, 2017 Publication	<1 %
36	Majji Shankar, Koushik Ghosh, Kallol Mukherjee, Raja K. Rit, Akhila K. Sahoo. "Ru-Catalyzed One-Pot Diannulation of Heteroaryls: Direct Access to π-Conjugated Polycyclic Amides", Organic Letters, 2016 Publication	<1 %

37	edoc.ub.uni-muenchen.de Internet Source	<1 %
38	Nikolaos V. Tzouras, Ioannis K. Stamatopoulos, Argyro T. Papastavrou, Aggeliki A. Liori, Georgios C. Vougioukalakis. "Sustainable metal catalysis in C H activation", Coordination Chemistry Reviews, 2017 Publication	<1 %
39	Peng-Xiang Shen, Liang Hu, Qian Shao, Kai Hong, Jin-Quan Yu. " Pd(II)-Catalyzed Enantioselective C(sp)–H Arylation of Free Carboxylic Acids ", Journal of the American Chemical Society, 2018 Publication	<1 %
40	Pradeep Nareddy, Frank Jordan, Michal Szostak. "Recent Developments in Ruthenium-Catalyzed C–H Arylation: Array of Mechanistic Manifolds", ACS Catalysis, 2017 Publication	<1 %
41	Shun-Ichi Murahashi. "C–H Transformation at Functionalized Alkanes", Handbook of C–H Transformations, 08/08/2005 Publication	<1 %
42	Yan Qin, Lihui Zhu, Sanzhong Luo. "Organocatalysis in Inert C–H Bond Functionalization", Chemical Reviews, 2017 Publication	<1 %

43	Thomas W. Lyons, Melanie S. Sanford. "Palladium-Catalyzed Ligand-Directed C−H Functionalization Reactions", Chemical Reviews, 2010 Publication	<1 %
44	Vadim P. Boyarskiy, Dmitry S. Ryabukhin, Nadezhda A. Bokach, Aleksander V. Vasilyev. "Alkenylation of Arenes and Heteroarenes with Alkynes", Chemical Reviews, 2016 Publication	<1 %
45	ikcoc14.org Internet Source	<1 %
46	Vern L. Schramm, David C. Baker. "Spontaneous epimerization of (S)-deoxycoformycin and interaction of (R)-deoxycoformycin, (S)-deoxycoformycin, and 8-ketodeoxycoformycin with adenosine deaminase", Biochemistry, 2002 Publication	<1 %
47	Zhang, Y.-H., G.-F. Shi, and J.-Q. Yu. "3.23 Carbon–Carbon σ-Bond Formation via CH Bond Functionalization", Comprehensive Organic Synthesis II, 2014. Publication	<1 %

Exclude quotes On Exclude matches < 14 words

Exclude bibliography On